

Cy 2

ANL-5719

INL Technical Library



210435

**Argonne National Laboratory**

**HAZARD SUMMARY REPORT**  
**EXPERIMENTAL BREEDER REACTOR II**  
**(EBR-II)**

**PLEASE RETURN  
TO THE INL  
RESEARCH LIBRARY**

**PDF Available**

**KEEP - Site Related**

Digitized  
09-08-09

*copy per  
Hale C.  
8-9-2010*

ARGONNE NATIONAL LABORATORY  
P. O. Box 299  
Lemont, Illinois

HAZARD SUMMARY REPORT  
EXPERIMENTAL BREEDER REACTOR II (EBR-II)

by

L. J. Koch, H. O. Monson, D. Okrent, M. Levenson, W. R. Simmons  
J. R. Humphreys, J. Haugsnes, V. C. Jankus, W. B. Loewenstein

May, 1957

Operated by The University of Chicago  
under  
Contract W-31-109-eng-38

## FOREWORD

This report describes the present conceptions of the Experimental Breeder Reactor-II as well as the safety procedures and precautions which are currently anticipated for its operation. Undoubtedly as further ideas are investigated and as construction proceeds, modifications will be introduced. The basic concepts and design, however, are essentially stabilized; it is anticipated that any alterations will be of a minor nature in comparison with the principles incorporated. Although final approval for operation of the reactor has not yet been obtained, this report is being issued at this time since no gains or benefits to those who can utilize the information contained herein will be obtained by postponing publication.

## ACKNOWLEDGEMENTS

Acknowledgement is made of major contributions to the preparation of this report by the following people:

T. R. Bump	R. W. Seidensticker
J. P. Burelbach	T. R. Spalding
E. Hutter	F. Verber

The advice and assistance of the following people are also acknowledged:

R. Avery	A. D. Rossin
A. H. Barnes	H. A. Sandmeier
Leslie Burris, Jr.	C. H. Scheibelhut
J. C. Carter	J. H. Schraidt
I. G. Dillon	O. S. Seim
S. H. Fistedis	A. B. Shuck
J. R. Ginder	J. R. Simanton
M. Grotenhuis	M. R. Sims
R. A. Hartfield	F. A. Smith
R. A. Jaross	K. F. Smith
K. D. Kuczen	E. S. Sowa
A. E. McArthy	T. E. Sullivan
R. L. Ramp	F. Tebo
M. B. Rodin	H. J. Wheeler

# TABLE OF CONTENTS

	<u>Page</u>
I. INTRODUCTION . . . . .	1
II. SUMMARY . . . . .	3
III. DESCRIPTION OF EBR-II FACILITY. . . . .	10
A. Primary System. . . . .	11
1. Reactor . . . . .	13
2. Primary Cooling System . . . . .	22
3. Shutdown Cooling System . . . . .	25
4. Neutron Shield . . . . .	27
5. Counters, Chambers, and Instrument Thimbles . . . . .	29
6. Control and Safety Drive Systems . . . . .	30
7. Fuel Handling System . . . . .	34
8. Primary Tank and Biological Shield. . . . .	37
9. Disassembly Cell . . . . .	41
10. Sodium Cleanup System . . . . .	42
11. Inert Gas System . . . . .	43
12. EBR-II Working Model . . . . .	44
B. Secondary System. . . . .	45
C. Steam System . . . . .	46
D. Process System . . . . .	47
IV. EBR-II PLANT OPERATION AND PERFORMANCE . . . . .	53
A. Control and Instrumentation of the Power System. . . . .	53
1. General . . . . .	53
2. Nuclear System . . . . .	57
3. Primary System. . . . .	63
4. Secondary System. . . . .	67
5. Steam System . . . . .	68
6. Electrical System. . . . .	69
B. Normal Steady State Operation . . . . .	75
1. Flux Distributions . . . . .	75
2. Reactor Heat Generation Distributions . . . . .	78
3. Reactor Temperature Distribution. . . . .	79
4. Power Cycle Operating Conditions. . . . .	84

## TABLE OF CONTENTS

	<u>Page</u>
C. Steady-State Operation at Three-Fourths Power . . . . .	86
1. Flux Distributions . . . . .	88
2. Reactor Heat Generation Distributions . . . . .	88
3. Reactor Temperature Distributions . . . . .	88
4. Power Cycle Operating Conditions . . . . .	90
D. Preoperational Testing and Experiments . . . . .	90
E. Normal Startup . . . . .	91
1. System Conditions Prior to Startup . . . . .	91
2. Startup Procedure . . . . .	92
F. Normal Shutdown . . . . .	93
G. Fast Shutdown (Scram) . . . . .	93
1. Primary Pumps Operative . . . . .	94
2. Only Auxiliary Pump Operative . . . . .	94
H. Shutdown Cooling . . . . .	94
1. Removal of Heat from Reactor . . . . .	95
2. Removal of Heat from Bulk Sodium . . . . .	95
I. Reactivity Coefficients . . . . .	95
1. Isothermal Temperature Coefficient . . . . .	96
2. Power Coefficient of Reactivity . . . . .	97
3. Reactivity Coefficients During a Zero Flow Accident . . . . .	99
J. Fuel Loading and Unloading . . . . .	99
K. Fuel Recycle . . . . .	101
1. Fuel Processing . . . . .	101
2. Pin Fabrication . . . . .	102
3. Fuel Element Assembly . . . . .	103
4. Subassembly Fabrication . . . . .	104
V. ENUMERATION AND EVALUATION OF POSSIBLE HAZARDS . . . . .	105
A. Safety Features of Mechanical Design . . . . .	105
B. Safety Features of Nuclear and Control Design . . . . .	106
C. Nuclear Accidents . . . . .	106
D. Consequences of Pump Failure . . . . .	108

## TABLE OF CONTENTS

	<u>Page</u>
E. Possible Consequences of Core Meltdown . . . . .	109
F. Consequences of Sodium Chemical Reactions . . . . .	111
G. Radiation Hazard to the Surrounding Area from a Hypothetical Reactor Disaster . . . . .	112
H. Conclusions . . . . .	113

### APPENDICES

A. Effects of Operational Abnormalities . . . . .	197
B. Doppler Effect . . . . .	275
C. Maximum Credible Nuclear Accidents . . . . .	281
D. Possible Sodium Chemical Reactions . . . . .	297
E. Containment of Possible Accidents . . . . .	323
F. The Radiation Hazard to the Surrounding Area from a Hypothetical Reactor Disaster . . . . .	343
G. Hydrology, Seismology, and Meteorology . . . . .	371

## LIST OF TABLES

<u>No.</u>	<u>Title</u>	<u>Page</u>
I	EBR-II Data . . . . .	5-9
II	Subassembly Composition . . . . .	15
III	Comparison of Reference Fissium Alloys . . . . .	50
IV	Physical Properties of Uranium and Uranium Alloys . . . . .	50
V	Physical Properties of Reference Fissium Alloy B. . . . .	51
VI	Irradiation Stability of Reference Fissium Alloys A and B . . . . .	52
VII	System Abnormalities Causing Scram and/or Alarm. . . . .	58-60
VIII	Uncertainty Factors Used in Thermal Analysis of Fuel and Blanket Elements. . . . .	80
IX	Summary of Thermal Analysis Results for Maximum Temperature Region of Core and Blankets (No Uncertainty Factors Included). . . . .	81
X	Summary of Thermal Analysis Results for Maximum Temperature Regions of Core and Blankets (Including Uncertainty Factors). . . . .	82
XI	Summary of Thermal Analysis Results for Maximum Temperature Regions of Core and Blanket (No Un- certainty Factors Included) . . . . .	89
XII	Summary of Thermal Analysis Results for Maximum Temperature Regions of Core and Blanket (Including Uncertainty Factors). . . . .	89
XIII	Isothermal Temperature Coefficients. . . . .	96
A-I	Reactivity Effects of Changes in Material Density . . . . .	198
C-I	Maximum Reactivity Rise and Average Energy Developed for Various Reactivity Insertion Rates. . . . .	291
D-I	ANL Experimental Data. . . . .	302
D-II	Test Data for Sodium to Oxygen Ratio Variation. . . . .	307
D-III	Reaction Product Data. . . . .	311
F-I	Parameters Used in Estimating Internal Radiation Hazards . . . . .	362
F-II	Total Integrated Dose & Relative Ground Concentration Downwind for Unit Source . . . . .	363
F-III	Annual Summary of Low Level Temperature Soundings, Two-year Period: September, 1950 through August, 1952 . . . . .	364
F-IV	External Beta-Dose (rep) and Gamma-Dose (roentgens) from Airborne Fission Product Activity. . . . .	365
F-V	External Radiation Hazard from Activity Deposited on the Ground . . . . .	366
F-VI	Amount of Radioisotope which could be Accumulated in Critical Organ by Inhalation Under Daytime Conditions (Microcuries). . . . .	367
F-VII	Amount of Radioisotope which could be Accumulated in Critical Organ by Inhalation Under Nocturnal Conditions (Microcuries) . . . . .	368

LIST OF TABLES

<u>No.</u>	<u>Title</u>	<u>Page</u>
F-VIII	Radiation Hazard from Inhaled Airborne Activity . . . . .	369
F-IX	Internal Radiation Hazard from Activity Deposited on the Ground . . . . .	370
G-I	Summary of Temperature Inversions for the Year August, 1950 to July, 1951 (NRTS - Central Facilities) . . .	376
G-II	Number of Cases that Pronounced Wind Directions Shifts Occurred Near Indicated Levels - June, 1950 - May, 1951 . . . . .	377

## LIST OF FIGURES

<u>No.</u>	<u>Title</u>	<u>Page</u>
1	Simplified Flow Diagram . . . . .	115
2	Temperature-Enthalpy Diagram . . . . .	116
3	Artist's Conception of EBR-II Site. . . . .	117
4	Plant Arrangement Plot Plan . . . . .	118
5	Reactor Plant Plans and Elevation. . . . .	119
6	National Reactor Testing Station Site Plan . . . . .	120
7	Primary System. . . . .	121
8	Reactor Arrangement . . . . .	122
9	Reactor . . . . .	123
10	Core Subassembly . . . . .	124
11	Core Subassembly Elements. . . . .	125
12	Inner Blanket and Outer Blanket Subassemblies . . . . .	126
13	Control Subassembly. . . . .	127
14	Safety Subassembly. . . . .	128
15	Reactor Vessel Assembly . . . . .	129
16	Reactor Support Grid . . . . .	130
17	Schematic of Primary Coolant System . . . . .	131
18	Instrument Flow Sheet. . . . .	132
19	Shutdown Cooler. . . . .	133
20	Neutron Shield . . . . .	134
21	Nuclear Instrument Thimble Locations. . . . .	135
22	Chamber Thimble. . . . .	136
23	Subassembly Gripper Mechanism . . . . .	137
24	Control Gripper Actuating Device and Mechanical Interlock for Support Platform. . . . .	138
25	Control Drive and Latch Mechanism . . . . .	139
26	Control Rod Performance Characteristics . . . . .	140
27	Control and Safety Rod Drive System . . . . .	141
28	Fuel Handling System . . . . .	142
29	Reactor Cover Hold Down . . . . .	143

## LIST OF FIGURES

<u>No.</u>	<u>Title</u>	<u>Page</u>
30	Subassembly Transfer (from Reactor Proper) . . . . .	144
31	Subassembly Transfer (to Transfer Arm) . . . . .	145
32	Primary Tank Support Structure . . . . .	146
33	Typical Column Detail for Primary System Support Structure . . . . .	147
34	Shield Cooling Air System Schematic Diagram . . . . .	148
35	Sodium Cleanup System Flow Diagram . . . . .	149
36	Primary Inert Gas System Flow Sheet . . . . .	150
37	EBR-II Working Model . . . . .	151
38	Primary Sodium System: EBR-II Working Model . . . . .	152
39	Simplified Block Diagram of Control System . . . . .	153
40	Rod Insertion vs Fraction of Total Rod Worth Effective. . . . .	154
41	Control Rod Displacement vs Time After Start of Rod Movement . . . . .	155
42	Fraction of Total Control Rod Worth Effective vs Time After Start of Rod Movement . . . . .	156
43	Safety Rod Displacement vs Time After Start of Rod Movement . . . . .	157
44	Fraction of Total Safety Rod Worth Effective vs Time After Start of Rod Movement . . . . .	158
45	Nuclear Instrument Channels . . . . .	159
46	Nuclear Instrument Range . . . . .	160
47	Primary and Secondary Sodium Flow Rates and Temperatures vs Reactor Power. . . . .	161
48	Primary Coolant Flow Rate vs Time with Auxiliary Pump Only in Operation (on Battery) . . . . .	162
49	Single Line Electrical Diagram. . . . .	163
50	Reactor Model for Two-Dimensional, Two-Group Analysis . . . . .	164
51	Radial Group I Neutron Flux Distribution (Two-Dimensional Analysis)(Z = 0.0 cm to Z = 27.3 cm) . . . . .	165
52	Radial Group I Neutron Flux Distribution (Two-Dimensional Analysis) (Z = 27.3 cm to Z = 54.5 cm) . . . . .	166

## LIST OF FIGURES

<u>No.</u>	<u>Title</u>	<u>Page</u>
53	Radial Group II Neutron Flux Distribution (Two-Dimensional Analysis) ( $Z = 0.0$ cm to $Z = 27.3$ cm) . . . . .	167
54	Radial Group II Neutron Flux Distribution (Two-Dimensional Analysis) ( $Z = 27.3$ cm to $Z = 54.5$ cm) . . . . .	168
55	Axial Group I Neutron Flux Distribution (Two-Dimensional Analysis) ( $r = 0.0$ cm to $r = 24.3$ cm) . . . . .	169
56	Axial Group I Neutron Flux Distribution (Two-Dimensional Analysis) ( $r = 24.3$ cm to $r = 45.9$ cm) . . . . .	170
57	Axial Group II Neutron Flux Distribution (Two-Dimensional Analysis) ( $r = 0.0$ cm to $r = 24.3$ cm) . . . . .	171
58	Axial Group II Neutron Flux Distribution (Two-Dimensional Analysis) ( $r = 24.3$ cm to $r = 51.3$ cm) . . . . .	172
59	Reactor Model for One-Dimensional, Ten-Group Analysis . . . . .	173
60	Radial Neutron Flux Distributions in $Z = 0$ Plane (One-Dimensional Analysis) . . . . .	174
61	Axial Neutron Flux Distributions at $r = 0$ (One-Dimensional Analysis) . . . . .	175
62	Radial Gamma Flux Distributions in $Z = 0$ Plane . . . . .	176
63	Axial Gamma Flux Distributions (Upward) at $r = 0$ . . . . .	177
64	Radial Power Density Distribution at Center Plane of Clean Reactor ( $Z = 0$ ) (Reactor Power = 62.5 mw) . . . . .	178
65	Axial Power Density Distributions in Clean Reactor (Reactor Power = 62.5 mw) . . . . .	179
66	Radial Temperature Distribution Through a Fuel Element at Point of Maximum Fuel Temperature (Reactor Power = 62.5 mw) . . . . .	180
67	Axial Temperature Distribution of Fuel Alloy and Coolant (Point A: $r = 0$ cm) (Reactor Power = 62.5 mw) . . . . .	181
68	Axial Temperature Distribution in Blanket Uranium and Coolant (Point B: $r = 24.2$ cm) (Reactor Power = 62.5 mw) . . . . .	182
69	Axial Temperature Distribution in Blanket Uranium and Coolant (Point C: $r = 34.9$ cm) (Reactor Power = 62.5 mw) . . . . .	183
70	Power Output per Subassembly in Clean Reactor (Reactor Power = 62.5 mw) . . . . .	184

## LIST OF FIGURES

<u>No.</u>	<u>Title</u>	<u>Page</u>
71	Coolant Flow Distribution in Clean Reactor (Reactor Power = 62.5 mw) . . . . .	185
72	Average Coolant Temperature Rise Through Each Subassembly (Reactor Power = 62.5 mw) . . . . .	186
73	Radial Temperature Distribution Through a Fuel Element at Point of Maximum Fuel Temperature (Reactor Power = 45 mw). . . . .	187
74	Axial Temperature Distributions in Fuel Alloy and Coolant (Point A: $r = 0$ cm) (Reactor Power = 45 mw) . . . . .	188
75	Axial Temperature Distribution in Blanket Uranium and Coolant (Point B: $r = 24.2$ cm) (Reactor Power = 45 mw) . . .	189
76	Axial Temperature Distribution in Blanket Uranium and Coolant (Point C: $r = 34.9$ cm) (Reactor Power = 45 mw) . . .	190
77	Various Reactor Temperatures During Scram vs Time After Scram Signal Reaches Control Rods (All Pumps Remain in Operation) (Rod Worth: 0.05; Initial Rod Insertion: 90%). . . . .	191
78	Various Reactor Temperatures During Scram vs Time After Failure of Both Main Pumps (Auxiliary Pump Continues in Operation). (Rod Worth: 0.05; Initial Rod Insertion: 90%). . . . .	192
79	Various Reactor Temperatures During Scram vs Time After Failure of Both Main Pumps (Auxiliary Pump Continues in Operation) (Rod Worth: 0.03; Initial Rod Insertion: 60%). . . . .	193
80	Approximate Reactor Conditions During the Long-Term (Natural Convection) Cooling Process . . . . .	194
81	Primary Tank Bulk Sodium Temperature vs Time after Shutdown . . . . .	195
A-1	Flux vs Time for Several Feedback Coefficients and Fixed Insertion Rate . . . . .	227
A-2	Excess Reactivity vs Time for Several Feedback Coefficients and Fixed Insertion Rate. . . . .	228
A-3	Flux Integral vs Time for Several Feedback Coefficients and Fixed Insertion Rate. . . . .	229
A-4	Flux vs Time for Several Insertion Rates and Fixed Feedback . . . . .	230

## LIST OF FIGURES

<u>No.</u>	<u>Title</u>	<u>Page</u>
A-5	Excess Reactivity vs Time for Several Insertion Rates and Fixed Feedback . . . . .	231
A-6	Flux Integral vs Time for Several Insertion Rates and Fixed Feedback . . . . .	232
A-7	Ratio of Integrated Power to Fractional Change in Fuel Length as a Function of Reactor Period with no Coolant Flow . . . . .	233
A-8	Flux and Power vs Time for Single Control Rod Insertion. . . . .	234
A-9	Excess Reactivity vs Time for Single Rod Insertion . . . . .	235
A-10	$\int_0^t n dt$ vs Time for Single Rod Insertion. . . . .	236
A-11	Flux Integral and Fuel Element Temperature Rise vs Time . . . . .	237
A-12	Flux and Power vs Time . . . . .	238
A-13	Flux and Power vs Time . . . . .	239
A-14	Excess Reactivity vs Time. . . . .	240
A-15	$n/(dn/dt)$ vs Time. . . . .	241
A-16	$n/(dn/dt)$ vs Time. . . . .	242
A-17	Flux Integral and Fuel Element Temperature Rise vs Time . . . . .	243
A-18	Excess Reactivity vs Time. . . . .	244
A-19	$n/n_0$ and Power vs Time . . . . .	245
A-20	Flux vs Time. . . . .	246
A-21	Excess Reactivity vs Time. . . . .	247
A-22	$\int_0^t n dt$ vs Time . . . . .	248
A-23	Primary System Coolant Flow Rate vs Time after Cessation of all Pumping Power (Based on 100% initial Reactor Power and Coolant Flow Rate). . . . .	249
A-24	Control Rod Displacement vs Time after Start of Rod Movement (Based on High Scram Assist Pressure ~100 psi) . . . . .	250
A-25	Total Reactor Power vs Time after Start of Rod Movement During Scram . . . . .	251

## LIST OF FIGURES

<u>No.</u>	<u>Title</u>	<u>Page</u>
A-26	Various Reactor Temperatures During Scram vs Time after Cessation of all Pumping Power (Rod Worth: 0.03; Initial Rod Insertion, 60%) (Scram Delay Time: 0.0 sec) . . .	252
A-27	Various Reactor Temperatures During Scram vs Time after Cessation of all Pumping Power (Rod Worth: 0.03; Initial Rod Insertion, 60%) (Scram Delay Time: 0.20 sec). . .	253
A-28	Total Reactor Power vs Time after Start of Rod Movement During Scram . . . . .	254
A-29	Various Reactor Temperatures During Scram vs Time after Cessation of all Pumping Power (Rod Worth: 0.05; Initial Rod Insertion: 90%; Scram Delay Time: 0.0 sec) . . .	255
A-30	Various Reactor Temperatures During Scram vs Time after Cessation of all Pumping Power (Rod Worth: 0.05; Initial Rod Insertion, 90%; Scram Delay Time: 0.20 sec) . . .	256
A-31	Maximum Fuel Temperature Occurring During Transient vs Time Delay Between Start of Scram and Cessation of all Pumping Power . . . . .	257
A-32	Various Reactor Temperatures vs Time after Cessation of all Pumping Power Subsequent to Scram (Rod Worth: 0.03; Initial Rod Insertion, 60%) . . . . .	258
A-33	Various Reactor Temperatures vs Time after Cessation of all Pumping Power Subsequent to Scram (Rod Worth: 0.05; Initial Rod Insertion, 90%) . . . . .	259
A-34	Reactor Temperatures vs Time after Loss of all Pumping Power (Without Scram) . . . . .	260
A-35	Maximum Temperature Difference ( $\Delta t_M$ ) Across Opposite Flats of a Fifth Row Subassembly During a Power Excursion (For the Case of Full Coolant Flow) . . . . .	261
A-36	Maximum Temperature Difference ( $\Delta t_M$ ) Across Opposite Flats of a Fifth Row Subassembly During a Power Excursion (For the Case of no Coolant Flow). . . . .	262
A-37	Assumed Initial Position of Core Subassemblies (Most Pessimistic Case) . . . . .	263
A-38	Assumed Initial Position of Core Subassemblies (Most Probable Case) . . . . .	264
A-39	Bowing of a Fifth Row Subassembly (With Coolant Flow and Most Pessimistic Initial Position) (Free Movement of Top of Subassembly: 0.022 in.) . . . . .	265

## LIST OF FIGURES

<u>No.</u>	<u>Title</u>	<u>Page</u>
A-40	Bowling of a Fifth Row Subassembly (with Coolant Flow and Most Pessimistic Initial Position)(Free Movement of Top of Subassembly: 0.090 in.) . . . . .	266
A-41	Equivalent Change in Core Radius vs Maximum Temperature Difference Across Opposite Flats of a Fifth Row Subassembly (with Coolant Flow and Most Pessimistic Initial Position) . . . . .	267
A-42	Bowling of a Fifth Row Subassembly (with no Coolant Flow and Most Pessimistic Initial Position) (Free Movement of Top of Subassembly: 0.022 in.) . . . . .	268
A-43	Bowling of a Fifth Row Subassembly (with no Coolant Flow and Most Pessimistic Initial Position) (Free Movement of Top of Subassembly: 0.090 in.) . . . . .	269
A-44	Equivalent Change in Core Radius vs Maximum Temperature Difference Across Opposite Flats of a Fifth Row Subassembly (with no Coolant Flow and Most Pessimistic Initial Position) . . . . .	270
A-45	Bowling of a Fifth Row Subassembly (with Coolant Flow and Most Probable Initial Position). . . . .	271
A-46	Equivalent Change in Core Radius vs Maximum Temperature Difference Across Opposite Flats of a Fifth Row Subassembly (with Coolant Flow and Most Probable Initial Position) . . . . .	272
A-47	Bowling of a Fifth Row Subassembly (with no Coolant Flow and Most Probable Initial Position) . . . . .	273
A-48	Equivalent Change in Core Radius vs Maximum Temperature Difference Across Opposite Flats of a Fifth Row Subassembly (with no Coolant Flow and Most Probable Initial Position) . . . . .	274
C-1	Reactivity Reduction vs Time . . . . .	294
C-2	Energy Developed for Given Excess Reactivity . . . . .	295
D-1	Experimental Reaction Vessel . . . . .	314
D-2	Combinations of Ejection Equipment Reservoirs and Ignition Chambers . . . . .	315
D-3	High-Speed Pressure Recording Instrumentation . . . . .	316
D-4	Sketch of Thermocouple Used to Measure Temperature of Wall Deposits. . . . .	317

## LIST OF FIGURES

<u>No.</u>	<u>Title</u>	<u>Page</u>
D-5	Peak Pressure and Temperature vs Quantity of Sodium Explosively Ejected into Experimental Reaction Vessel. . . .	318
D-6	Typical Experimental Pressure Profiles . . . . .	319
D-7	Reaction Product Fallout on Vessel Bottom Flange. . . . .	320
D-8	Peak Pressure and Temperature vs Quantity of Sodium Explosively Ejected into EBR-II Reactor Building . . . . .	321
E-1	Primary Containment System "Pressure Vessel". . . . .	340
E-2	Pressure Time Plot for Top of Tank . . . . .	341
E-3	Distance Time Diagram for Primary Tank . . . . .	342
G-1	Annual Wind Rose for the 20-ft Wind Level. . . . .	378
G-2	Lapse and Inversion Wind Roses for Year June 1950 Thru May 1951. . . . .	379
G-3	Frequency of Northeasterly vs Southwesterly Winds . . . . .	380
G-4	Wind Roses for 0300 and 1500 hrs for Year May 1950 Thru April 1951. . . . .	381
G-5	Precipitation Wind Rose for Period May 1950 Thru December 1951 . . . . .	382
G-6	Annual Lapse and Inversion Wind Roses for the 500-ft Level . . . . .	383
G-7	Annual Lapse and Inversion Wind Roses for the 5000-ft Level. . . . .	384

HAZARD SUMMARY REPORT  
EXPERIMENTAL BREEDER REACTOR II (EBR-II)

by

L. J. Koch, H. O. Monson, D. Okrent, M. Levenson,  
W. R. Simmons, J. R. Humphreys, J. Haugsnes, V. C. Jankus

I. INTRODUCTION

Argonne National Laboratory proposes to construct an Experimental Fast Power Reactor at the National Reactor Testing Station in Idaho, as a part of the Atomic Energy Commission's program for the development of power reactors.

The Experimental Breeder Reactor II (EBR-II) is an unmoderated, heterogeneous, sodium-cooled reactor and power plant with a power output of 62.5 megawatts (mw) of heat. The energy produced in the reactor is converted to 20 mw of electricity through a conventional steam cycle. The reactor is fueled with  $U^{235}$  or plutonium, and the plant includes an integral fuel processing facility where the irradiated fuel is processed, fabricated, and assembled for return to the reactor.

Although provisions are being made for subsequent loading of the reactor with uranium-plutonium fuel, the descriptions and analyses presented in this report pertain only to an enriched uranium loading. Some preliminary data relating to uranium-plutonium alloys are presented, and reference is made to the adaptability of the fuel element design and the fuel process cycle to these alloys. The uranium-plutonium alloy development program will continue, including the probable use of EBR-II as an irradiation facility and for engineering scale fuel processing and fabrication experiments. In addition, systems and kinetics analyses will be made similar to those presented in this report for the enriched uranium-fueled reactor. It is planned to present these data in a supplement to this report prior to the preparation of a plutonium-uranium fuel loading.

The separations process employed permits the buildup of certain fission products; operation of the plant will determine the effect of buildup of these fission products, as well as the buildup of the higher isotopes of uranium and plutonium.

The EBR-II is primarily an engineering facility to determine the feasibility of this type of reactor for central station power plant application. Major emphasis has been placed on achieving high thermal performance at high temperatures, and high fuel burnup with a fast and economical fuel processing system. The thermal performance of the reactor and the size of

the system components are such as to permit direct extrapolation to central station application. The plant has been designed to permit a maximum of experimental operational flexibility by separation of the plant systems, and yet permit extrapolation to a commercial plant which would not require the same degree of separation.

The EBR-II is a high performance reactor with a maximum power density in the core in excess of 1300 kw/liter of core volume. Associated with this high thermal performance are high temperature differences in the fuel and coolant, and coolant velocities as high as 26 fps. The determination of reactor performance at these operating conditions, and the investigation of the effects of operating variables, are a significant part of the experimental program.

The plant will be located at Site 16 at the National Reactor Testing Station to permit maximum operational flexibility of the reactor system, and because of the limited information available pertaining to power reactor operation with plutonium fuel. The same design philosophy has been employed, however, as would apply if the reactor were to be constructed in a populated area, and the reactor system will be housed in a gastight "containment shell." It is recognized that although the NRTS is an "isolated location" with respect to population density, high-priority facilities in the nation's reactor development programs are located there.

## II. SUMMARY

The EBR-II reactor consists of an enriched core surrounded on all sides by a fertile blanket of depleted uranium. The fuel elements which comprise the core section of the reactor consist of small diameter cylindrical pin assemblies. The design of the fuel element is influenced by the desire for high thermal performance, high burnup, and simplicity of construction. The fuel pin is a loose fit in a thin-walled tube which provides a clearance annulus between the pin and the tube wall. This annulus is filled with static sodium to provide a heat transfer bond between the fuel and fuel tube. Heat is removed from the fuel element by the primary sodium flowing along the outside of the fuel tube.

The fuel element lends itself to fabrication by remote control methods as required by the particular fuel process selected. Of particular significance is the fact that complete decontamination of the fuel is not obtained. Certain fission product elements, notably molybdenum and ruthenium, are not removed, and because of the high fission yield of these elements, they tend to build up in significant concentration in the fuel alloy. The fuel alloy to be employed in the EBR-II, therefore, is established by the fuel process; fortunately, it appears to exhibit excellent irradiation damage stability and thermal cycling stability. To avoid large changes in alloy composition with each fuel cycle, the reactor will be loaded initially with a synthetic alloy approximating the equilibrium composition, and consisting of enriched uranium plus approximately 5% (by weight) of synthetic fission products. (Provisions are made to permit subsequent loading of the reactor with plutonium-uranium alloys. The fuel process and fabrication cycle is adaptable to this fuel system and the addition of fission products appears to enhance the stability and fabricability of the alloy.)

The EBR-I has exhibited certain operational instabilities which as yet are not completely explained. It is believed that these instabilities are, at least in part, due to mechanical instability in the reactor, notably bowing of the fuel elements. In the EBR-II, every effort has been made to achieve a very rigid, close-packed arrangement of the fuel and, in addition, to produce preferential bowing such as to effect a probable bowing coefficient which is essentially zero or negative.

The reactor operates with a maximum power density in the core of approximately 1370 kw/liter with a maximum coolant velocity of 26 fps, and reactor coolant temperatures of 700F inlet and 900F outlet. Reactor control is effected by the movement of fuel into and out of the reactor core. This is accomplished by 12 modified moveable fuel subassemblies which move vertically and are located at the outer edge of the core.

Heat is removed from the reactor by the primary sodium coolant system and transferred to the secondary sodium system in a shell-and-tube heat exchanger. The secondary system transfers the heat to the steam generator where superheated steam is produced to drive a conventional turbine-generator.

The reactor and the entire primary coolant system, including heat exchanger, are contained in a large vessel (primary tank) and operate completely submerged in the coolant. This provides a high degree of reliability of containment of the primary coolant and of operation of the cooling system.

The large volume of sodium in the primary system provides a reliable source of constant temperature coolant to the reactor. Inlet sodium is pumped from the bulk sodium directly to the reactor. Because of the large heat capacity of the primary sodium, the temperature of the sodium entering the reactor remains essentially constant irrespective of changes in reactor power or reactor coolant outlet temperature or of temperature changes in the secondary system or steam system.

Shutdown cooling of the reactor is accomplished by natural convection of the primary sodium through the reactor. The relative elevation of the reactor and heat exchanger provides natural convection of the coolant even though heat is not removed from the primary sodium in the heat exchanger. If the secondary sodium system is inoperative, the heat is delivered to the bulk volume of sodium in the primary tank. It is removed by shutdown coolers in the primary sodium, which operate by natural convection and transfer the heat to the atmosphere.

The bulk volume of sodium in the primary tank is also employed as the coolant during reactor unloading. The entire loading and unloading operations are carried out with the subassemblies submerged in the sodium and with the fission product decay heat being removed by natural convection of the sodium. The irradiated subassemblies are permitted to cool in the primary sodium system for 15 days before removal for processing.

The reactor, primary coolant system, and all associated equipment are contained in a building in the form of a gastight cylindrical steel shell designed to withstand a static internal pressure of approximately 25 psig (with a normal safety factor of approximately four). Pressure developed within this container may be the result of energy released in a nuclear accident, energy released in a sodium-air reaction, or a combination of the two. These two potential sources of accidental energy release are treated separately. The primary tank structure in conjunction with the biological shield is designed as a primary container to withstand the energy released in a nuclear accident. It is estimated that the structure will easily contain a nuclear accident equivalent to the detonation of 300 lb of TNT in the center

of the reactor, and probably could contain an accident several times this large. Although the primary system is expected to contain the nuclear energy release, some primary sodium may be expelled into the building atmosphere. The maximum pressure which may develop as a result of the sodium-oxygen reaction is a function of the rate and manner in which the sodium is exposed to the atmosphere. Experimental work described in this report indicates that pressures as high as 80 psig can be obtained under very idealized conditions; such peak pressures, however, being of very short duration. In an accidental expulsion of sodium into the EBR-II reactor building, it does not appear possible that pressures of this magnitude could be developed. It is not expected that pressure due to sodium-oxygen reaction could exceed the static pressure rating of the building shell-25 psig. If the pressure rating were exceeded, however, it is probable that the containment shell would not fail. No water or appreciable quantities of hydrocarbons are employed in the reactor building, thus eliminating possibility of other types of chemical reactions with sodium.

As a convenient reference, the major design and operating features of the EBR-II plant are summarized in Table I.

Table I

EBR-II DATA

General

Heat Output	mw	62.5
Gross Electrical Output	mw	20
Primary Sodium Temperature, to reactor	F	700
Primary Sodium Temperature, from reactor	F	900
Primary Sodium Flow Rate, through reactor	gpm	8200
Primary Sodium Maximum Velocity, in core	fps	26
Primary System Sodium Capacity	gal	86,000
Secondary Sodium Temperature, to heat exchanger	F	610
Secondary Sodium Temperature, from heat exchanger	F	880
Secondary Sodium Flow Rate	gpm	6050
Steam Generator		
Output	lb/hr	248,000
Steam Temperature	F	850
Steam Pressure	psig	1300
Feed-Water Temperature	F	550
Turbine Throttle Conditions		
Steam Flow	lb/hr	198,000
Steam Temperature	F	850
Steam Pressure	psig	1250

Table I (Cont'd.)

Reactor Data

Core Dimensions		
Equivalent Diameter	in.	19.04
Height	in.	14.22
Total Volume	liters	66.3
Upper and Lower Blanket Dimensions		
Equivalent Diameter	in.	19.04
Length (each end)	in.	18
Inner Blanket Dimensions		
Equivalent O.D.	in.	27.46
Length	in.	55.0
Radial Thickness	in.	4.21
Outer Blanket Dimensions		
Equivalent O.D.	in.	61.5
Length	in.	55.0
Radial Thickness	in.	17.02
Core Composition		
Fuel Alloy	vol-%	31.8
Stainless Steel (Type 304)	vol-%	19.5
Sodium	vol-%	48.7
Control and Safety Rod Composition (Fuel Section)		
Fuel Alloy	vol-%	21.3
Stainless Steel (Type 304)	vol-%	20.8
Sodium	vol-%	57.9
Upper and Lower Blanket Composition		
Uranium (depleted)	vol-%	32
Stainless Steel (Type 304)	vol-%	20.4
Sodium	vol-%	47.6
Inner and Outer Blanket Composition		
Uranium (depleted)	vol-%	60
Stainless Steel (Type 304)	vol-%	17.6
Sodium	vol-%	22.4
Subassemblies		
Core		47
Control (Rod and Thimble)		12
Safety (Rod and Thimble)		2
Inner Blanket		66
Outer Blanket		510
Total		637
Configuration		hexagonal
Dimension across flats ( <i>outside</i> )	in.	2.290
Hexagonal Tube Thickness	in.	0.040
Structural Material		304 SS
Lattice Spacing (Pitch)	in.	2.320 <i>implies 4.66 in sq in</i>

*or 30.08 sq cm per S/A*

area of extension of hex can = 4.54 cm<sup>2</sup> = 27.29 cm<sup>2</sup>  
 Area of interior of hex can = 4,230 in<sup>2</sup> = 27.29 cm<sup>2</sup>  
 Area of tubes + spacer wires (.0490) in driver S/A: 2.336 in<sup>2</sup>: 15.07 cm<sup>2</sup>  
 Area of flowing Na in 91 pin driver = 1.894 in<sup>2</sup>: 12.22 cm<sup>2</sup> (within the hex tube)  
 R to inside of hex flat 2.82 cm  
 R to inside of hex corner 3.25 cm  
 Heat transfer area, tubes plus spacers, = 6.52 sq ft per 91 pin S/A (not including hex cans)

Table I (Cont'd.)

	Clearance between subassemblies	in.	0.030
Mk II	Fuel Elements (Pin-Type, Sodium Bonded)	Mk I	
0.130	Fuel Pin Diameter	.01627 in <sup>2</sup> section	0.144
14. + (?)	Fuel Pin Length	Mk I A = 68.2 gm alloy = 69.8 gm total U per pin	14.22
0.174	Fuel Tube O.D.	5900 gm total U per S/A	0.174
0.012	Fuel Tube Wall Thickness		0.009
0.010	Thickness Na Bond Annulus		0.006
91	Elements per subassembly		91
	Upper and Lower Blanket Elements (Pin-Type, Sodium Bonded)		
	Blanket Pin Diameter	in.	0.3165
	Blanket Pin Length (Total)	in.	18
	Blanket Tube O.D.	in.	0.376
	Blanket Tube Wall Thickness	in.	0.022
	Thickness Na Bond Annulus	in.	0.008
	Blanket Elements per subassembly (each end)		19
	Control and Safety Rods		
	Configuration		hexagonal
	Dimension across flats	in.	1.908
	Fuel Elements		same as core subassembly
	Fuel Elements per rod		61
	Inner and Outer Blanket Elements (Pin-Type, Sodium Bonded)		
	Blanket Pin Diameter	in.	0.433
	Blanket Pin Length (Total)	in.	55
	Blanket Tube O.D.	in.	0.493
	Blanket Tube Wall Thickness	in.	0.018
	Thickness Na Bond Annulus	in.	0.012
	Blanket Elements per Subassembly		19 <sup>3.62 gm in or 23.37</sup> (77% rods) (85.7% to maintain of hex can)
	Fuel Alloy (Enriched U-fissium)		
	Total Core Loading	kg	363
	U <sup>235</sup> Enrichment	%	49
	Critical Mass - U <sup>235</sup>	kg	170
	Fuel Alloy Composition: (fissium)		
	Uranium	wt-%	95.0
	Zirconium	wt-%	0.2
	Molybdenum	wt-%	2.5
	Ruthenium	wt-%	1.5
	Rhodium	wt-%	0.3
	Palladium	wt-%	0.5
	Fertile Blanket Material (depleted uranium)		
	Total Blanket Loading	kg	28,100

Nuclear Data

Total Fissions per cc/sec, at center of core 4.4 x 10<sup>13</sup>

Table I (Cont'd.)

Neutron energy distribution at center of core			
Flux above 1.35 MEV	n/(cm <sup>2</sup> )(sec)		0.8 x 10 <sup>15</sup>
Flux below 1.35 MEV	n/(cm <sup>2</sup> )(sec)		2.9 x 10 <sup>15</sup>
Total Neutron Flux	n/(cm <sup>2</sup> )(sec)		3.7 x 10 <sup>15</sup>
Prompt Neutron Life Time	sec		8 x 10 <sup>-8</sup>

Reactor Control

## Power Coefficients:

0 - 22.5 mw	( $\Delta k/k$ )/mw		-3.2 x 10 <sup>-5</sup>
22.5 - 62.5 mw	( $\Delta k/k$ )/mw		-6.0 x 10 <sup>-5</sup>
Doppler Effect - Average	( $\Delta k/k$ )/C		+0.04 x 10 <sup>-5</sup>
Isothermal Temperature Coefficient	( $\Delta k/k$ )/C		-3.6 x 10 <sup>-5</sup>
Total Reactivity (worth)			
12 Control Rods	$\Delta k/k$		0.06
2 Safety Rods	$\Delta k/k$		0.015-0.020
Control Rod			
Total			12
Operating Drive (each rod)			rack & pinion
Velocity	in./min		5
Total Movement	in.		14
Scram Drive			pneumatic
Safety Rod			
Total			2
Operating Drive			rack & pinion
Velocity	in./min		2
Total Movement	in.		14
Scram Drive			gravity
Long-term Reactivity Effects (From Clean to 2% burnup)			
Burnup of U <sup>235</sup> in Core	$\Delta k/k$		-0.02
Buildup of Pu in Core	$\Delta k/k$		+0.002
Buildup of Pu in Blanket	$\Delta k/k$		+0.0072
Buildup of Fission Products	$\Delta k/k$		-0.002
Irradiation Growth of Fuel (4% growth)	$\Delta k/k$		-0.011

Heat Transfer

## Heat Generation in Reactor

Core, Control and Safety Subassemblies	mw		53.3
Upper and Lower Blanket	mw		1.2
Inner Blanket	mw		5.2
Outer Blanket	mw		2.6
Neutron Shield	mw		0.2

## Heat Generation in Core

Radial Maximum to Average Power			
Density at Reactor Center Plane	ratio		1.33

Table I (Cont'd.)

Axial Maximum to Average Power Density at Reactor Center Line	ratio	1.17
Power Density, Average	mw/liter	0.89
Power Density, Maximum	mw/liter	1.37
Power Density, Maximum to Average	ratio	1.53
Specific Power	mw/kg	0.314
Fuel Elements, surface area	sq ft	231
Control Elements, surface area (in active zone)	sq ft	32.4
Safety Elements, surface area	sq ft	6.6
Total	sq ft	270
Maximum Heat Flux	Btu/(hr)(ft <sup>2</sup> )	1,030,000
Average Heat Flux	Btu/(hr)(ft <sup>2</sup> )	680,000

### III. DESCRIPTION OF EBR-II FACILITY

The EBR-II Facility is comprised of four major, functional systems which may be defined briefly as follows:

- (1) The Primary System: the reactor and associated equipment, and the primary sodium cooling system.
- (2) The Secondary System: the intermediate sodium heat transfer system.
- (3) The Steam System: the steam-electric system.
- (4) The Fuel Process System: the system for decontaminating, fabricating, and assembling fuel elements.

The heat produced in the reactor is removed and transferred by the primary sodium system to the secondary sodium system in the heat exchanger. From the secondary system, the heat is transferred in the steam generator to produce superheated steam which is delivered to a conventional condensing turbine at 850F and 1250 psig. A simplified flow diagram of the power system is shown in Fig. 1. A temperature-enthalpy diagram is included as Fig. 2.

The irradiated fuel is processed by a high-temperature oxidative slagging process (to remove the greater portion of the fission products), fabricated, assembled into new fuel elements, and recycled through the reactor. These operations are carried out remotely in a large, high-irradiation level, inert atmosphere, hot lab facility.

The EBR-II Facility consists of five plants and miscellaneous supporting facilities and structures (Figs. 3 and 4). The plants are designated as follows:

- (1) The Reactor Plant (Fig. 5), includes the reactor system, the reactor primary sodium cooling system, the disassembly cell, and pertinent services to these facilities. The reactor building is a cylindrical gastight steel shell, constructed of 1 in. thick steel plate, and, designed to withstand an internal pressure of approximately 25 psi with "normal safety factors." Air locks, and service connections also meet this rating.
- (2) The Power Plant includes the turbine-generator and associated equipment, the control room for the reactor and power plants, and the major personnel facilities for the entire Facility. The building is of conventional construction.

(3) The Sodium Plant includes the pumping, purification, and storage facilities for the secondary sodium system. It also includes a receiving station for the sodium. It is of simple construction, containing only the minimum facilities required for operation. The building normally will not be occupied by operating personnel.

(4) The Boiler Plant houses the steam generator. It is somewhat isolated, with sodium lines linking it to the Sodium Plant, and steam and condensate lines linking it with the Power Plant. It is of extremely simple construction, containing only the minimum facilities required for operation. The building normally will not be occupied by operating personnel.

(5) The Process Plant includes the fuel process cell and supporting facilities, the inert gas storage facilities, the sodium equipment cleanup cell, and exhaust ventilation equipment for the Process Plant and Reactor Plant. The building is of conventional construction.

An additional building (Laboratory and Service Building) located adjacent to the EBR-II Facility provides supporting analytical facilities and personnel facilities, particularly for control of the fuel process cycle. The EBR-II Facility will be located at Site 16 of the National Reactor Testing Station in Idaho, as indicated in Fig. 6. Site data are presented in Appendix G.

#### A. The Primary System

The EBR-II primary system consists of the following:

- Reactor
- Primary Cooling System
- Shutdown Cooling System
- Neutron Shield
- Control and Safety Drive Systems
- Fuel-Handling System
- Primary Tank and Biological Shield
- Disassembly Cell
- Sodium Cleanup System
- Inert Gas System

The reactor, the primary sodium pumps and piping, the heat exchanger, and the fuel handling system are contained in the "primary tank," submerged in sodium, as shown in Fig. 7. Coolant is pumped directly from the bulk sodium in the primary tank to the reactor, and after flowing through the reactor, passes through the heat exchanger and back to the bulk sodium. This "submerged concept" is employed for the following reasons:

(1) The arrangement contributes significantly to the reliability of the primary coolant system. A very high degree of integrity can be constructed into the primary tank, since it is of relatively simple design (essentially, an unmodified right circular cylinder). As added safety measures, double-wall construction is used on the tank, and no external connections below the liquid sodium level are permitted. Because the entire coolant system is flooded with sodium (to a level approximately 10 ft above the top of the reactor), loss of reactor coolant is virtually impossible. (Even if both primary tank walls were to fail, the free volume between the inner tank and the liner of the biological shield is sufficiently small to maintain the sodium level above the top of the reactor.) In addition, the arrangement is ideally suited to natural convection cooling, providing extremely reliable shutdown cooling in the event of loss of forced convection.

(2) Since the reactor is to demonstrate the method of operation to be employed in a central station power plant, the replacement of fuel must be accomplished in a short time. Shortly after reactor shutdown, the heat generation in the fuel is high, and reliable cooling must be provided. This is accomplished by unloading and transferring the fuel elements while they are submerged in sodium. They are cooled by natural convection of the sodium, and unloading preparation can begin immediately after shutdown. The fuel elements are transferred to a fuel storage rack within the primary tank where they continue to cool, by natural convection of the sodium, until removed for processing.

(3) The need for leak tightness of the primary coolant system piping is eliminated. Small amounts of leakage are permissible, since the leakage is internal. (A small amount of leakage actually does occur at the connections between the pumps and the reactor, between the reactor tank and the reactor tank cover, and around subassembly nozzles.).

(4) The heat capacity of the very large mass of bulk sodium (approximately 620,000 lb) provides considerable "thermal inertia" to the primary system. It prevents rapid temperature transients in the primary sodium coolant reactor inlet temperature, and it adds reliability to the shutdown cooling system.

(5) A maximum of integrity is provided with regard to containment of radioactive sodium. The entire radioactive coolant system (with the exception of the single, small, sodium cleanup circulation circuit) is confined within the primary tank.

(6) Essentially all of the radioactivity in the plant is confined to the primary tank and, therefore, only the primary tank (and the single circuit referred to under (5) above) requires shielding. Shielded equipment cells and pipe galleries are eliminated.

(7) Auxiliary heating of the primary system sodium (to prevent freezing) is simplified, since the entire system is heated as a unit. The individual components and pipes, etc., are in an "atmosphere" of sodium, and the entire system is at one temperature.

## 1. Reactor

### a. Reactor Arrangement

The reactor is divided into three main zones: core, inner blanket, and outer blanket (Fig. 8). Twelve control rods are located at the outer edge of the core, and two safety rods are located within the core, as shown. Each zone is comprised of a number of right hexagonal subassemblies 2.29 in. across flats of the hexagon. All subassemblies are of identical size; their numerical distribution being as follows:

Core	47
Safety	2
Control	12
Inner Blanket	66
Outer Blanket	<u>510</u>
Total	637

The construction of the subassemblies and elements will be described later.

The core, including the control and safety rods, has an equivalent radius of 9.52 in. (24.17 cm) and a height of 14.22 in. (36.12 cm); a total core volume of 66.3 liters.

Division of the annular blanket surrounding the core into two separate zones, the inner blanket and the outer blanket, is necessitated by the wide variation in power generation across this region.

The 12 control rods and the 2 safety rods consist of modified movable fuel subassemblies. The rods, plus their stationary thimbles, comprise the control and safety subassemblies. The external dimensions of the thimbles are identical to the core and blanket subassemblies, and the lattice spacing for all units is identical. Reactor control is effected by moving the control rods in their thimbles (in a vertical direction) and thus moving fuel into, or out of, the core. Slow speed is provided for operating control, and high speed is provided for reactor shutdown (scram).

The safety rods are operative only during normal reactor shutdown, when fuel-loading operations are performed and the control rods are disconnected from their drives. The safety rods are not a

part of the normal reactor operational control system. The construction of the control rods and safety rods are described in Sections f and g.

Each subassembly is located and supported at the bottom by a combination support grid and inlet coolant plenum (Fig. 9). In addition, each subassembly makes contact with adjacent subassemblies by means of "buttons" formed in the hexagonal subassembly tubing, as described in Section b.

The heat generated in the fuel (or blanket) material is removed by sodium flowing up through the subassemblies and around the fuel and blanket elements. In order to accommodate the very large range of flow rates required, two parallel flow systems are employed. One system supplies the core and the inner blanket (a high-pressure system); the other supplies the outer blanket (a low-pressure system). The two systems have separate inlet plenum chambers and a common outlet plenum chamber, as described in Section h.

Because the inner blanket is included in the core-cooling system, experimental enlarging or reshaping of the core by substitution of core-type subassemblies within the inner blanket is possible. The largest experimental core contemplated includes the inner row of the inner blanket. It also will be possible to operate the reactor with this row partly filled with core subassemblies. This is the procedure which will be employed to adjust criticality of the reactor if the enrichment is not accurately established by critical experiments. (The ability to vary the size of the reactor core also permits variation in enrichment of the fuel alloy and thereby the investigation of such variables as Doppler coefficient as a function of enrichment over a limited range.)

#### b. Subassemblies

A single subassembly size is employed throughout the reactor, resulting in a close-packed reactor geometry. The hexagonal subassembly tube is 2.290 in. across external flats with a 0.040-in. wall thickness. The subassemblies are spaced on a triangular pitch of 2.320 in. center distance. A nominal clearance of 0.030 in. between each subassembly permits removal of the units from the reactor. Each face of the core and inner blanket subassembly hexagonal tubes contains a "button" (3/8 in. dia. by 0.014 in. high) which is formed by "dimpling" the tube wall. The function of these buttons is described in Appendix A.

The upper end of each subassembly is identical, and all subassemblies are accommodated by the same handling and transfer devices. The lower adapters are of different size to differentiate the three types of subassemblies, and are of different configuration to accommodate the two coolant systems. The subassembly-reactor grid relationship is described in Section h.

Each subassembly contains a number of fuel elements, and/or blanket elements, of size and shape appropriate to the particular type of subassembly. Approximate composition of each type of subassembly is shown in Table II. The composition is based on the volume of a unit lattice, and the sodium volume includes the static sodium in the reactor.

Table II

SUBASSEMBLY COMPOSITION

Subassembly Type	Volume - per cent			
	Fuel Alloy	Uranium	Steel	Sodium
Core - Fuel Section	31.8	0	19.5	48.7
Core - Blanket Section	0	32.0	20.4	47.6
Control and Safety - Fuel Section	21.3	0	20.8	57.9
Inner and Outer Blanket	0	60.0	17.6	22.4

c. Core Subassembly

The core subassembly (Fig. 10) is comprised of three "active" sections: upper blanket, core, and lower blanket. The core section consists of 91 cylindrical fuel elements spaced on a triangular lattice by a single, helical rib on the outside of each element. The elements are supported within the subassembly by fastening their lower ends to a support grid. The fuel elements (Fig. 11) are "pin type," consisting of a right circular cylinder (pin) of fuel alloy (0.144 in. dia. by 14.22 in. long) fitted into a thin-walled, stainless steel tube. The coolant flows along the outside of the element tube.

Each fuel pin is precision cast to size and consists of "equilibrium fissium alloy." Initially, the fissionable constituent will be  $U^{235}$ ; while later  $Pu^{239}$  will be employed. The composition of the fissium alloy varies with the fissionable isotope employed because of the difference in fission product yields. The method of fabrication of the fuel pin, and the composition of the fissium alloys, are described in Section III-D.

The fuel pin is contained in a stainless steel tube 0.009 in. wall thickness by 0.174 in. O.D. The resultant annulus between the pin and the inside of the tube (0.006 in.) is filled with static sodium to provide a thermal bond. The sodium bond extends a nominal 0.6 in. above the top of the fuel pin. An inert gas space (2.35 in.) is provided above the sodium to accommodate expansion of the sodium. The fuel element tube is welded closed at each end. The details of construction, assembly, and test of the fuel element are described in Section III-D.

The individual fuel elements are contained within the hexagonal subassembly tube. They are fastened to the subassembly at their lower end by hooking to a parallel strip grid, as shown in Fig. 10. The upper ends of the fuel elements are unrestrained, to permit free axial expansion of the fuel element. Mechanical attachment of the fuel elements in the subassembly is dictated largely by considerations of remote assembly and disassembly.

The upper and lower blanket sections are identical in construction and each consists of 19 pin-type elements also spaced on a triangular lattice. The unalloyed depleted uranium pins are 0.3165 in. dia. and total 18 in. long. They are similar in geometry to the fuel elements, being a loose fit in the blanket element tube which is 0.376 in. O.D. by 0.022 in. wall thickness. The 0.008 in. annulus is filled with sodium to provide the necessary thermal bond. The details of the upper and lower blanket elements are shown in Fig. 11.

The blanket elements are positioned in the subassembly by a parallel strip grid similar to that employed for the fuel elements. In addition to being fixed at the lower ends to the grid strips, the upper ends are also positioned by grid strips which permit axial expansion but no other movement. Since the blanket elements are positioned at each end, no spacer provisions are made along the length of the blanket elements.

The "lower adapter" of the subassembly engages the reactor grid, and contains slots through which the coolant enters the subassembly from the high pressure inlet coolant plenum chamber. The reactor grid, and the relationship with the subassembly adapter, are described in Section h.

#### d. Inner Blanket Subassembly

The inner blanket subassembly (Fig. 12) is comprised of 19 cylindrical blanket elements spaced on a triangular pitch and contained in the hexagonal subassembly.

The "active" blanket section consists of depleted uranium cylinders (0.433 in. dia.) totaling 55 in. in length. They are contained in a stainless steel tube 0.493 in. O.D. with a 0.018 in. wall thickness. The resultant 0.012 in. annulus is filled with static sodium to provide a thermal bond. The sodium extends a nominal 2.0 in. above the top of the uranium, with a 4.0-in. argon gas expansion region above the sodium. The end closures are welded to provide a sealed unit.

The lower adapter of the subassembly is similar to, but smaller in diameter than, the core subassembly. The inner blanket subassemblies engage the high-pressure inlet coolant plenum chamber in the reactor grid, as described in Section h.

e. Outer Blanket Subassembly

The outer blanket subassembly differs with the inner blanket subassembly in the design of the lower adapter. The lower adapter is arranged to engage the reactor grid in the low-pressure inlet plenum chamber. The two different lower adapters employed in the subassemblies are shown in Fig. 12; their function is described in Section h.

f. Control Subassembly

The control subassembly (Fig. 13) consists of a control rod and a guide thimble. The guide thimble is hexagonal in cross section and of the same dimensions as the subassembly tubes. Each thimble, therefore, occupies a unit lattice identical to those occupied by the various subassemblies.

Twelve identical control rods are employed to provide the required operational control for the reactor. The control rod consists of a modified core subassembly with a core section comprised of 61 cylindrical fuel elements identical to those employed in the core subassembly. The control rod is encased in a hexagonal tube 1.908 in. across flats, which is smaller than the hexagonal thimble tube by the equivalent of one row of fuel elements. The control rod does not contain an axial blanket. A void section equivalent in height to the reactor core is provided above the core section. During operation this void section is filled with sodium. Reactor control is effected by vertical movement of the control rod, adjusting the proportion of fuel or void (sodium) in the core region of the reactor. A reflector section of solid steel (except for flow passages for the coolant), is located immediately above the void section. The upper end of the control rod is equipped with an adapter section identical to the subassemblies for attachment to the control drive unit or the fuel gripper unit for unloading. The lower end of the control rod below the fuel section consists of a cylindrical tube also containing a steel reflector section. Bearings are provided on this lower section which provide the guide between the control rod and the guide thimble.

The control rod is cooled in a similar manner to the core subassemblies by the high-pressure sodium coolant system. Sodium enters through slots in the lower end of the thimble, and through a second set of slots in the lower end of the control rod. The slots in the thimble section are above the lower bearing of the control rod throughout the control rod travel. The lower end of the thimble is open, and the lower control rod bearing serves as a flow restriction to prevent sodium leakage from the bottom of the thimble. The primary system sodium pressure acts across the lower end of the control rod, and therefore exerts a downward force on the control rod. This downward force opposes the lifting force due to the pressure drop of the coolant flowing through the control rod (similar to the arrangement in the core subassemblies).

The control rod is removed from the reactor by the fuel-handling system in the same manner as the various subassemblies. The same considerations of irradiation damage and fuel recycling apply to the control rod. The guide thimble is also removable from the reactor in the event of damage. It is locked in the lower reactor grid by a latch which is engaged by rotating the thimble. Rotation of the thimble is normally prevented by the six subassemblies which surround it. To remove or install a thimble it is necessary, therefore, to first remove the six adjacent subassemblies.

Since the vertical position of the control rods in the reactor is variable, the heat generation within the control rod is also variable. The coolant flow through the control rod must be established for the maximum heat generation, i.e., with the control rod fully inserted in the reactor. If a constant coolant flow is employed, the temperature rise in the coolant decreases as the control rod is lowered out of the reactor. This results in considerable degradation of the outlet sodium temperature from the reactor. The arrangement of the control rod and guide thimble coolant inlet slots permits the use of variable orificing proportional to the position of the control rod in the reactor. This can be accomplished by the relative size and locations of the coolant slots in the guide thimble and in the control rod. The requirements for this system will be established experimentally to approach a constant outlet sodium temperature from the control rods in all operating positions. The system described will not permit precise control of coolant temperature, and it will be necessary to overcool the control rods, but not to the extent that would result in a constant flow system.

g. Safety Subassembly

The safety subassembly (Fig. 14) consists of a safety rod and a guide thimble. The safety rod and thimble are essentially identical to the control subassembly except for modifications at the lower end. Two safety rods are incorporated in the reactor and located as shown in Fig. 8. The safety rods are not a part of the normal operational control system. They are fully inserted in the reactor (in their most reactive position) at all times during operation and shutdown. The purpose of the safety rods is to provide "available negative reactivity" during operations when the reactor is shut down and the control rods are disconnected from their drives. Their primary purpose is to provide a safety device during reactor loading and unloading operations.

The safety rods are attached to a common drive unit extending below the reactor structure. The unit is driven by two shaft extensions outside the fuel transfer system and therefore is unaffected by fuel transfer operations. The drive unit is described in Section III-A-6.

The guide thimble is locked to the lower reactor grid structure in a similar manner to that described for the control rod guide thimble. The safety rod is engaged to the driving mechanism by a rotational locking mechanism. Inadvertent disengagement of the safety rod is prevented by a hexagonal-shaped collar on the upper end of the safety rod. This normally engages the inside of the thimble, preventing rotation of the safety rod. To connect or disconnect the safety rod for loading purposes, the safety rod must be raised 1 in. above its normal "up position" by the safety rod drive mechanism.

The safety rod upper adapter is identical to the control rod and the subassemblies, and is handled in the normal manner by the fuel transfer system. The guide thimble is removable in the same manner as the guide thimble in the control subassemblies.

Cooling of the safety rod is accomplished in the same manner as the control rod, but since it is a one-position device, no provisions are made for variable flow. The safety rods must be in an up position before the reactor can be made critical.

#### h. Reactor Vessel Assembly

The reactor vessel assembly (Fig. 15) consists of the reactor vessel, the grid assembly, and the top cover. It contains the reactor -- core and blanket subassemblies, and control and safety rods -- and provides the proper orientation of these units. The assembly is located and supported at the bottom and on the centerline of the primary tank; it is supported on the structural members which reinforce the bottom of the primary tank inner shell.

The vessel assembly is surrounded on all sides by the neutron shield and is submerged beneath approximately 10 ft of sodium.

The vessel assembly consists of three major units: the grid-plenum assembly, the vessel, and the top cover. To insure accurate alignment, the vessel is fastened to the grid assembly by bolts, which are tack-welded to insure a permanent connection. The vessel cover serves as a neutron shield as well as a closure. It is clamped to the vessel flange by means of three hold-down clamps. When the cover is closed, it forms the upper reactor coolant plenum chamber from which the coolant flows to the heat exchanger. Within the plenum chamber the coolant is at an average temperature of 900F and a pressure of 18 psig. The cover separates this sodium from the ambient bulk sodium in the tank. The sodium seal is formed between the vessel flange and the cover. When it is desired to unload fuel or blanket subassemblies, the hold-down clamps are released and the cover is elevated to the top of the primary tank to allow the fuel handling system to unload and transfer the fuel to the storage rack.

### Reactor Vessel

The reactor vessel is a cylindrical tank with flanged ends. The upper plenum of the vessel, as well as the coolant nozzle, is lined with a thermal baffle. The function of this baffle is to lower the temperature difference across the vessel wall and also the coolant outlet nozzle wall. Below the plenum region the vessel contains a laminated steel thermal shield. The vessel wall is "insulated" from the bulk sodium in which it is submerged by a second steel shell which is vented, and therefore contains static sodium. This shell-and-static-sodium combination provides sufficient thermal insulation with acceptable thermal stresses in the vessel wall.

### Grid-Plenum Assembly

The grid-plenum assembly is a combination grid structure which supports and locates the subassemblies and incorporates the coolant inlet plenum chambers. It consists of two 4 in. thick stainless steel plates containing the locating holes for the lower adapters of the subassemblies. The subassemblies are supported by the upper plate and extend through the lower plate. The subassemblies are supported by a spherical shoulder on the subassembly which engages a conical seat in the upper grid plate to provide a seal. This arrangement minimizes the leakage flow of coolant along the outside surfaces of the subassemblies.

The high-pressure coolant plenum chamber -- supply for the core and inner blanket -- is formed between the two grid plates. The low-pressure coolant plenum chamber -- supply for the outer blanket -- consists of an annular chamber immediately below the lower grid plate. The grid-plenum chamber arrangement and coolant flow arrangement are shown in Fig. 16. The upper and lower grid plates are interconnected by tubes welded to each plate in the outer blanket zone. This prevents short-circuiting of the high-pressure coolant through the outer blanket. It also provides the structural system required to support the entire reactor load on the upper plate. The high-pressure coolant flows between these tubes into the core and inner blanket region where it enters the subassemblies. The lower nozzles of the core and inner blanket subassemblies contain slots located between the upper and lower grid plates. The coolant enters the subassembly through these slots and flows upward through the subassembly. The lower end of the subassembly nozzles is closed, forming a "hydraulic piston." The sodium in the high-pressure coolant plenum chamber is at a pressure of 61 psig, of which 8 psig is static head. The remainder gives a pressure difference of 53 psi acting across the piston. This provides a downward force of 148 lb. on the core subassemblies and 116 lb. on the inner blanket subassemblies. The upper surface of the lower grid plate is "stepped" in such a manner as to vary the cross-sectional area of the slots in the subassemblies. This provides orificing of the flow through the subassemblies to match the heat generation rate.

The low-pressure coolant enters the low-pressure plenum chamber at 22 psig, and enters the lower nozzles of the outer blanket subassemblies through openings at the bottom. Because the pressure drop through the outer blanket subassemblies is much smaller and the weight of these units is larger, it is unnecessary to provide "hydraulic hold-down."

Three different hole diameters are employed in the grid plate, i.e., the core section has the largest diameter hole, the inner blanket section has a smaller diameter hole, and the outer blanket section has the smallest diameter hole. This prevents a fuel subassembly from being placed inadvertently in an inner blanket position or an outer blanket position, and likewise, an inner blanket subassembly cannot be placed in an outer blanket position. To prevent the interchange of subassemblies in the other direction, the subassembly orientation bars are used. These bars provide proper angular orientation of the subassemblies during loading. They are fastened to the underside of the lower grid plate as shown in Fig. 16 and engage slots in the subassemblies. There are three thicknesses of bars: the core subassemblies engage the thickest, the inner blanket subassembly slots are thinner, and the outer blanket subassembly slots are thinnest. If an inner blanket subassembly is inadvertently placed in a fuel position, the slot in the inner blanket subassembly tip is too narrow to engage the bar. This prevents engagement of the subassembly at least 2 in. short of its normal position in the grid, which is easily detected by the loading mechanism. The same condition exists if an outer blanket subassembly is placed in an inner blanket position or a fuel position.

This arrangement of loading control was adopted, because a core subassembly inserted in either blanket zone introduces both a reactivity problem and a cooling problem, while a blanket subassembly introduced in the wrong zone introduces only a cooling problem. The lower grid is 19 in. deep, while the core is only 14 in. long. If a core subassembly cannot engage the grid in the wrong location, an error during loading does not permit the fuel section of the subassembly to enter the core region. In the reverse manner, a subassembly can engage the grid for approximately 17 in. of travel, but the error is detectable.

#### Top Cover

The top cover provides the closure of the upper end of the reactor vessel and forms the upper surface of the outlet plenum chamber. It also provides the upper portion of the neutron shield. The 12 control rod drive shafts operate through the top cover, and guide bearings are provided in the cover for these units. During the unloading operations, the fuel gripper mechanism also operates through an opening in the top cover. A small amount of leakage occurs through these various openings during reactor operation when a sodium pressure differential of

approximately 12 psi exists across the cover. This leakage flow is employed as a part of the neutron shield cooling system in this region.

The top cover is raised and lowered by two shafts penetrating the small rotating plug. It is fastened to the reactor vessel by three clamping mechanisms, and the raising and lowering mechanism is designed to permit free expansion of the lifting shafts. This arrangement avoids the large load due to internal pressure being transferred to the cover lifting mechanism, and also avoids problems associated with differential thermal expansion in the system.

The underside of the top cover is provided with "projections" on the same spacing as the core and inner blanket subassemblies. These pins are positioned directly above each subassembly adapter and provide approximately 1/4 in. of clearance between the adapter and the end of the pin. The pins prevent any appreciable lifting of the subassemblies in the event of failure of the hydraulic hold-down system.

Thermocouple wells are provided adjacent to some of these pins to measure the outlet sodium temperature in all regions of the reactor. The thermocouple leads are introduced through tubes which are brought out through the hollow cover lifting drive shafts. Inside the cover the tubes are manifolded to the various locations. The tubes are permanently installed in the assembly, but the thermocouple junctions and leads can be withdrawn from the system.

## 2. Primary Cooling System

The primary system component arrangement is shown schematically in Fig. 17. The reactor vessel is centrally located at the bottom of the primary tank. The pumps, heat exchangers, and connecting piping are disposed radially around the reactor vessel and elevated somewhat above it.

The coolant flow path in the primary cooling system is as follows:

a. The d-c electromagnetic primary coolant pumps take suction from the bulk sodium approximately 7 ft above the bottom of the primary tank. The physical configuration of the primary coolant pumps resembles an inverted "U," with the pumping section being horizontal. The coolant flow in each pump is upward through the suction leg and downward through the discharge leg.

b. The flow from each pump separates into two streams before entering the high-pressure and low-pressure reactor inlet plenum chambers. The inlet nozzles to each of the lower plenums are approximately diametrically opposite. The pump outlet line is connected to the

high-pressure inlet plenum chamber. A smaller line connected to the outlet line supplies the low-pressure plenum chamber through an orifice and valve.

c. Coolant flow in all regions of the reactor is upward through the fuel and blanket subassemblies and into a common upper plenum chamber with a single 14-in. outlet.

d. The 14-in. upper plenum outlet nozzle is located on the opposite side of the reactor vessel from the heat exchanger. The connecting pipe between these two components describes a helix-like spiral to accommodate thermal expansion. The auxiliary pump is located in this line.

e. The primary coolant flows downward through the shell side of the heat exchanger and discharges into the bulk sodium in the primary tank. The heat exchanger outlet is approximately  $7\frac{1}{2}$  ft above the centerline of the reactor. This arrangement assures an inherently reliable natural convection cooling system for shutdown cooling as discussed further in Section III-A-3.

Ball-seat type pipe disconnects are used in the lines between the main sodium pumps and the lower plenums of the reactor vessel. This allows removal of these pumps from the primary tank for maintenance. The sodium line between the upper plenum of the reactor vessel and the heat exchanger shell is permanently attached to these two components. The heat exchanger shell is permanently attached to the cover of the primary tank; however, the tube bundle, upper and lower plenums, secondary sodium inlet and outlet nozzles, and shield plug can be removed as a unit in a vertical direction.

When the reactor is in operation, coolant is supplied by the two "main" primary sodium, d-c electromagnetic pumps operating in parallel. At 100% power operation, each pump supplies approximately 4250 gpm of coolant at 60 psi head.

Imbalance between the rate of flow through each main pump does not cause serious maldistribution of flow through the reactor because there is a very large pressure differential (41 psi) between the upper and lower plenums as compared to the pressure differences (0.5 psi) within each of the lower plenum chambers.

Power is supplied to each pump by a separate metallic rectifier unit. Flow control of the primary cooling system is effected by regulation of the voltage output of these rectifier units over a 0 to 3-volt range. Voltage control over this entire range is continuous and smooth. Interlocks between pump power, flow, and reactor control prevent reactor startup if the pumps are not operative.

During shutdown conditions (reactor power of 1% or less), sufficient coolant flow is established by thermal convection to remove fission product decay energy within established fuel alloy temperature limitations. The relative elevations of the heat exchanger and reactor were established to insure thermal convection of the primary sodium without heat removal in the heat exchanger.

A detailed discussion of the shutdown cooling system arrangement is contained in Section III-A-3.

The primary purpose of the auxiliary pump is to augment thermal convection under certain conditions of reactor shutdown. These conditions occur as a result of system malfunctions which tend to "destroy" the temperature distributions necessary to maintain thermal convection. The auxiliary pump insures continuity of flow under these conditions and prevents undesirable temperature transients (as described in Section IV-G).

The auxiliary pump is a d-c electromagnetic pump located in the reactor outlet line, and operates in series with the main pumps. Its design capacity is approximately 500 gpm at 0.15 psi and 900F sodium temperature. The pumping section is incorporated in the 14-in. outlet pipe with no change in pipe cross section. This is done to maintain the integrity of the piping system (at the expense of pumping efficiency, which is not important).

The auxiliary pump electrical power is supplied from metallic rectifier units and storage batteries. The storage batteries, operating in parallel with the rectifier units, assure pump operation in the event of a complete power failure. During normal operation, these batteries float on the line and remain fully charged at all times. In the event of a sustained power failure, the pump operates until the battery is discharged, which results in a gradual decay of the flow rate and an ideal "transition" to thermal convection. Interlocks between the auxiliary pump and reactor controls prevent reactor startup unless the pump is connected and operating with the batteries fully charged.

The primary cooling system is instrumented to measure, indicate, record, and initiate safety controls on temperature, flow, pressure, and liquid level. The signals from these instruments are either recorded, indicated, or scanned. Figure 18 is a flow diagram of the primary circuit, indicating points of measurement of flow, pressure and temperature.

The primary system is filled from the sodium receiving facility in the Sodium Plant via the primary tank fill line and the primary sodium cleanup facility. To avoid thermal shock or local freezing of the

sodium, the entire primary system is "normalized" at the temperature of the incoming sodium. Upon completion of the filling operation, the fill line is disconnected and capped.

The system can be drained by reversing the filling procedure and by energizing the drain pump. Draining will require considerable time (days), which is consistent with the requirements for fission product decay cooling of the fuel, and considerations of radioactive decay of the sodium.

Reactor operation is restricted to a minimum primary sodium temperature of 580F. The bulk sodium is heated to this temperature electrically by immersion heaters. Expansion of the bulk sodium between 580F and the 700F normal operating temperature raises the sodium level approximately 4 in. An 18-in. argon gas blanket is maintained between the sodium surface and the primary tank cover at 700F (22 in. at 580F).

### 3. Shutdown Cooling System

Removing the fission product decay heat from the reactor fuel after shutdown involves: heat removal from the reactor by the sodium flowing through the reactor; and heat removal from the sodium.

After reactor shutdown, coolant flow through the reactor can be maintained in any of the following ways:

- a. Operation of one or both of the main pumps.
- b. Operation of the auxiliary pump.
- c. Natural convection flow.

Heat removal from the sodium leaving the reactor can be accomplished by two methods:

- a. The heat can be transferred to the secondary system.
- b. The heat can be transferred to the bulk sodium in the primary tank and then removed by the "shutdown coolers."

If the reactor cover is closed, coolant flow through the reactor, by any of the three methods described above, follows the "normal circuit": through the heat exchanger - to the bulk sodium. If the secondary system is operating, the heat is transferred in the heat exchanger to the secondary system sodium. The secondary system, in turn, transfers heat to the steam system in the steam generator. The heat leaves the steam system via the condenser, and is transferred to the atmosphere through the condenser water cooling tower.

If the secondary system is inoperative, the heat is transferred to the bulk sodium in the primary tank. The heated sodium leaving the reactor is mixed with the bulk sodium by discharging from either the secondary heat exchanger, or, if the reactor vessel cover is raised, from the top of the reactor. The heat is then removed from the bulk sodium by the shutdown coolers which, in turn, transfer the heat to the atmosphere through a finned-tube air heat exchanger. Since the primary system has a very large thermal capacity compared to the amount of fission product decay heat removed from the reactor, the temperature rise of the bulk sodium is slow, and fast response of the shutdown coolers is not necessary. The salient feature of this method of heat removal is the complete independence of any external power source. All fluid flow is due to natural convection.

The shutdown cooler (Fig. 19) is an immersion-type, bayonet heat exchanger. Basically, it consists of two concentric pipes approximately 26 ft long, the outer pipe being closed at the bottom. The inner pipe is thermally insulated from the annulus to provide a greater thermal head for natural convection. The cooler is positioned in a vertical thimble which is immersed in the bulk sodium of the primary tank, with a thermal bond of sodium provided in the space between the thimble and bayonet heat exchanger. This type of construction has a dual purpose:

- a. It provides a structural barrier between the primary tank sodium and the coolant in the bayonet cooler -- the coolant being the eutectic alloy of sodium and potassium (NaK).
- b. It reduces the thermal stresses in the bayonet cooler.

NaK enters the inner pipe of the bayonet cooler at the top and flows downward to the bottom of the inner pipe where it reverses direction and enters the annulus. The flow is then upward through the annulus, where heat transfer to the NaK occurs, to the top of the bayonet cooler. Leaving the bayonet cooler, flow is upward into a finned-tube air heat exchanger, which is located in a dampered air stack outside the reactor containment building. Here the heat is transferred to the atmosphere by natural convection of air. The cooled NaK then flows downward into the inlet of the bayonet cooler.

The rate of heat release from the system is controlled by the position of the stack dampers. Normally the dampers are actuated by automatic control; however, manual control is also incorporated in the event of failure of the automatic system. During reactor operation, the dampers are normally closed and a minimum flow of NaK occurs in the shutdown cooling system. This method of operation prevents the freezing of NaK in cold weather, provides for positive starting when the dampers are opened, and also reduces thermal shock on the system. When the

stack dampers are opened, the thermal head on both the NaK and air side is increased. This gives rise to increased flow of both fluids which, in turn, results in increased heat removal from the bulk sodium.

The NaK cooling system, external to the bayonet cooler, is instrumented with thermocouples and an electromagnetic flowmeter. An alarm system is interlocked with these measuring devices to annunciate and indicate abnormal conditions of flow and temperature.

The system is designed for maximum reliability and simplicity. The design of the bayonet coolers provides for minimum internal stresses over large temperature ranges and minimum obstructions in the flow circuit. All welded construction is used and no valves are included in the system. After the system is filled with NaK, the filling line (which contains a valve) is capped. The system can be drained (except the bayonet cooler) by connecting a storage tank to the fill line. This is done only if the reactor is to be shutdown for an extended period during cold weather.

#### 4. Neutron Shield

The neutron shield surrounds the outside of the reactor vessel on all sides and is submerged in the bulk sodium of the primary tank. The shielding material is graphite and graphite impregnated with 3% (by weight) of natural boron. To prevent the reaction and contamination of the graphite with sodium, it is canned in stainless steel.

For purposes of description, the shield can be separated into three sections: radial, top, and bottom as shown in Fig. 20. To facilitate fabrication, handling, and installation, the graphite and the borated graphite is canned in conveniently sized pieces which can be readily stacked and placed in position around the reactor vessel. All cans used for cladding are leak tested, loaded with graphite, and closed by welding. The cans are filled with helium to an absolute pressure of 10 in. Hg (at room temperature) to minimize the internal pressure at operating temperature (12 psia at 700F), and also to provide a heat transfer medium to conduct the heat generated in the graphite to the can wall. The helium generated by the  $(n,\alpha)$  reaction with boron, results in an increase in pressure of approximately 19 psi (at operating temperature) during the life of the reactor, assuming that all of the helium generated is released to the helium atmosphere. (The cans are designed for a positive internal pressure 50 psi greater than the external pressure.) They are cooled externally by natural convection flow of sodium.

##### a. Radial Shield

The radial shield is assembled from graphite blocks ( $4\frac{1}{8} \times 4\frac{1}{8} \times 18$  in. long) fitted in stainless steel cans ( $4\frac{7}{16} \times 4\frac{7}{16} \times \frac{3}{32}$  in. wall

thickness and approximately 13 ft long). The  $1/8$  in. clearance space between the can and the graphite is filled with helium.

The cans are placed in rows around the periphery of the reactor vessel, and each row is held in place by stainless steel bands. Clearance is provided between the cans to permit natural convection flow of sodium. Each row is staggered with respect to adjacent rows to minimize neutron streaming. Specially shaped shielding cans are used around the inlet and outlet sodium pipes of the reactor vessel.

The three inside rows of cans contain plain graphite, the fourth row contains borated graphite, the fifth row contains plain graphite, and the sixth row contains borated graphite. The total graphite thickness of the radial neutron shield is  $24\frac{3}{4}$  in., of which  $8\frac{1}{4}$  in. is borated and  $16\frac{1}{2}$  in. is plain graphite.

b. Bottom Shield

The bottom shield is assembled from rectangular cans of similar composition and size used in the radial shield except that the lengths are tailored to fit the space available. The staggering and spacing pattern of the cans are also similar. The first two layers of cans, adjacent to the bottom of the reactor vessel, contain plain graphite, the third layer contains borated graphite, the fourth layer contains plain graphite, and the fifth layer contains borated graphite. The total graphite thickness of the bottom shield is  $20\frac{5}{8}$  in., of which  $12\frac{3}{8}$  in. is plain and  $8\frac{1}{4}$  in. is borated graphite.

c. Top Shield

Because of the complex structure of the reactor vessel cover, the cans are of complex shape. They are stacked to prevent neutron streaming and to permit cooling. The cans in the center portion of the cover are cooled by the leakage of sodium from the upper plenum chamber, between the control rod drive shafts and guide bushings. The other cans are cooled by natural convection of the bulk sodium through openings in the periphery of the cover.

The cover contains six layers of cans filled with either 3% borated graphite or boron carbide. The total thickness of the top shield is  $24\frac{3}{4}$  in.

## 5. Counters, Chambers, and Instrument Thimbles

### a. Counters and Chambers

#### General

Two fission counters and eight compensated ion chambers comprise the detectors for the nuclear instrument channels. Since detectors of proven reliability for 700F operation are not available, conventional detectors are employed in cooled thimbles. For reliable operation, the temperatures of counters and chambers are maintained below 140F.

A description of the nuclear instrument channels is incorporated in Section IV-A-2.

#### Counters

Two U<sup>235</sup>-enriched fission counters detect thermal neutrons in the startup range of operation. These counters are located close to the reactor neutron shield, where gamma intensities approach  $10^6$  r/hr after prolonged full power operation. This type of counter is employed because the large pulses due to fission fragment ionization may be efficiently discriminated in the presence of unusually high gamma radiation.

#### Chambers

Six compensated ion chambers of the boron-coated type are located near the reactor neutron shield. In addition, two identical chambers operate as back-ups in the biological shield cooling annulus.

This type of chamber electrically cancels the chamber current component due to gamma radiation of reasonable intensities. Since the gamma component is not proportional to the instantaneous reactor power, it constitutes an error superimposed on the normal neutron current. In EBR-II, the gamma intensity near the neutron shield is unusually high, at times exceeding the compensation capacity of the chambers. Therefore, dense gamma shielding is incorporated in thimbles to increase effective chamber neutron sensitivities by factors of 10 to 100, depending upon the channel's function. For certain channels, additional sensitivity is gained by means of graphite beam holes through the neutron shield.

### b. Instrument Thimbles

#### General

Eleven instrument thimbles provide housing for ten counters and chambers. Of these, eight extend downward vertically through

the primary tank cover into the sodium. They are distributed along a periphery just outside of the reactor neutron shield, as shown in Fig. 21. Each thimble is designed to reduce the high ambient temperature and gamma intensities in the surrounding sodium to levels tolerable for the type and function of the detector housed.

The remaining three thimbles extend vertically downward into ducts of the biological shield cooling annulus, and are outside of the primary tank; one is a spare. These channels are employed for high-power reactor operation. The gamma level can be tolerated because the channel functions only over a small high-power range where the neutron level predominates sufficiently. Since this is a low-temperature region, simple, conventional thimbles are employed.

#### Thimble Design

Figure 22 shows the design of a typical thimble, which operates immersed in the 700F primary sodium. Shielding is placed directly around the bottom of the inner pipe. Annular bayonet-type ducts, which merge into a single divided duct at the bottom, maintain temperature below 120F at the detector.

Helium gas is used as the coolant because it does not activate, it is inert, and it has good heat transfer properties. Helium enters and leaves the top of each thimble through ducts spiralled through the thimble biological shield plug and connected to distribution headers.

To provide operational reliability, duplicate full-capacity, heat exchangers and blowers operate in parallel. In the event of power failure, auxiliary power is supplied by the emergency diesel-electric generating unit.

The thimble is insulated with stainless steel wool, which is stable under irradiation, to minimize the cooling load. (Tests will be conducted to determine the heat load experimentally, and to evaluate other insulations - including an evacuated annulus.)

### 6. Control and Safety Drive Systems

Operation of the reactor is controlled by 12 control rods, which are described in Section 1-f. Each rod is independently driven by an electrical-mechanical drive mechanism. The drives are identical and are so arranged that only one drive may be operated at a time (with the exception of "scram," when all twelve operate simultaneously). Operating control is achieved by a 14 in. vertical motion of the control rods which is provided by a rack and pinion type drive with constant speed electric motors; therefore, only one speed of movement is possible. The control

rods are disconnected from their drives during fuel loading operations. The disconnect is made with the control rods in their down or least reactive position. The control rods remain in this position during the unloading procedure.

Two safety rods are provided in the reactor in addition to the 12 operational control rods. The safety rods are not a part of the normal operational control system for the reactor. The safety rods are always in the reactor and they are designed to function when the control rods are disconnected from their drives. The primary purpose of the safety rods is to provide "available negative reactivity" when the reactor is shut down and the control rods are disconnected. They provide a safety factor during reactor loading operations. The safety rods are described in Section 1-g. The safety rod drive mechanisms are completely independent of the control drive systems and completely independent of the fuel handling systems. They are actuated by low level detectors separate from the normal operational control system.

a. Control Drive System

The control rod drive mechanism performs three major functions: the connection between the drive and the control rod, the slow-speed vertical motion (in both directions) for reactor control, and the high-speed downward motion for reactor scram. These operating functions are combined in a single unit and are appropriately interlocked to insure the proper sequence of operation.

The control rod drive mechanism is attached to the control rod by means of a "gripper." The gripper attaches to the conical top of the control rod adaptor (which is also used for unloading). The gripper consists of two jaws which engage the control rod adaptor and are operated by a cam incorporated in a sliding sleeve. Jaw operation is positive; the jaws are opened and closed by the cam, and are locked in position by the cam. The jaws operate through a funnel-shaped guide tube and upon opening, recede beyond the guide tube, providing a smooth interior surface. This eliminates the possibility of the control rod adaptor "hanging up" after the jaws are opened. The gripper also contains a "sensing device" which makes contact with the top of the control rod adaptor. It consists of a plunger which is made to move one-half inch in a vertical direction by the control rod adaptor during engagement and disengagement of the control rod from the gripper. It is spring loaded and the motion of the sensing plunger is transmitted to a position indicator. If necessary, it can also be used to forcibly eject the adaptor from the gripper. A third check is also provided to eliminate the very unlikely possibility of the control rod adaptor sticking to the sensing plunger. The relationship between the control rod adaptor, the sensing plunger, and the gripper jaws is such that after the control rod is released, and the plunger is in the down position,

the jaws will not close if the adaptor is still in contact with the sensing plunger. Closing the jaws after the control rod has been released provides a final check that release has actually been accomplished. The arrangement of the units comprising the gripper mechanisms is shown in Fig. 23.

The gripper device is attached to the main shaft which extends upward through the biological shield into the operating area above the primary system. The actuating mechanism for the gripper and the sensing mechanism are located above the operating floor and are easily accessible for inspection and maintenance. The necessary motions employed to actuate the gripper and to sense the operations are transmitted by shafts from the gripper to the operating stations. The actuating mechanism shown in Fig. 24, is constructed in such a way that the control rod cannot be released except when it is in the down position of the control stroke. The position of the jaw actuating device and the position of the sensing device are indicated by transducers and are suitably interlocked into the system. The actuating device must be in its proper position, and the sensing device must affirm that it is, before subsequent operations can be performed.

The control rod is actuated by a long shaft which extends through the upper biological shield with the control rod attached to its lower end and the drive mechanism at its upper end. The shaft is driven by a rack and pinion at a rate of 5 in./min by a constant speed, instantly reversible, polyphase motor. The rack gear teeth are cut on the outside of the tube through which the main drive shaft extends. The drive shaft is connected to the rack tube by a fast-acting magnetic latch. The latch consists of two rollers which engage notches in the shaft and are actuated by a magnetic clutch. The magnetic clutch is energized to engage the latch and thereby connect the shaft to the rack tube. The latch arrangement is shown in Fig. 25.

The main shaft extends upward through the rack tube and is attached to a piston in a pneumatic cylinder. The upper end of the cylinder contains compressed air at a pressure of approximately 50 psig. The lower end of the cylinder is open to the atmosphere. The pneumatic pressure is always acting against the piston, tending to drive the shaft, and thus, the control rod down. Motion is prevented by the latch connecting the shaft to the drive rack. Upon a scram signal, the magnetic clutch is de-energized, releasing the shaft from the drive rack and driving the control rod down (out of the reactor core). Scram can occur at any position in the operating stroke of the control rod and is automatically actuated by a power failure (which de-energizes the magnetic clutch). A release time of 0.008 second, including the time elapsed between actuating the scram signal and beginning of shaft motion, is expected. (Tests conducted on a prototype unit have shown release times of 0.003 to 0.007 second.) To insure the compressed air supply to the air cylinders, they are supplied from

accumulator tanks, which, in turn, are supplied by an air compressor. Check valves are provided in the connecting lines between the accumulator tanks and the air cylinders and between the air compressor and the accumulator tanks, to prevent loss of compressed air in the event of line failure. Pressure-actuated switches scram the reactor in the event of failure of the air supply. The compressed air available in the cylinder or in the accumulator tanks is sufficient to insure a "pressure assist" during a scram in addition to the force of gravity.

Deceleration of the scram stroke is accomplished by a hydraulic shock absorber connected to the air cylinder. The shock absorber is actuated during the lower 5 in. of travel. Approximate velocity-displacement and displacement-time curves assuming 100% initial displacement are shown in Fig. 26.

A mechanical stop is built into the system when the piston reaches the top of the air cylinder. If the limit switches on the rack driving pinion fail to stop the unit at the upper end of its travel, the drive shaft is stopped (including the control rod) and the rack continues to travel, moving away from the shaft and disengaging the latch. When this occurs, the shaft and the control rod are automatically scrambled by the disengagement of the latch. Over-travel of the control rods is prevented and is not dependent upon the operation of the limit switches.

The 12 control drive mechanisms are mounted on a platform which surrounds a central support structure. The platform can be raised 3 in. and lowered  $3/4$  in. from its normal operating position. The upward movement is required to raise the lower end of the drive mechanism, after disconnect from the control rods, to clear the subassembly adaptors during fuel handling operations. The bottom position of the normal control rod stroke holds the control rod  $3/4$  in. above its bottom seat in the guide sleeve. When released from the gripper, the rod drops and is supported by the guide sleeve. The downward movement of the platform is required to engage the control rods when they are in their down position.

The motion of the support platform is electrically interlocked with the gripper-actuating mechanism and the sensing mechanism to prevent raising the platform before disconnecting the control rods from the drive mechanisms. Two mechanical interlocks are provided as an additional safety feature. Two of the twelve individual gripper jaw-actuating devices operate two rotating stops for the support platform. The platform cannot be raised until these two gripper mechanisms have been opened. The platform can only be raised if all twelve electrical circuits are properly sequenced, and the two mechanical safety devices are also in their proper position. The mechanical arrangement is shown on Fig. 24.

### b. Safety Drive System

The two safety rods (Fig. 27) are connected beneath the reactor to a horizontal bar which is connected to two vertical shafts which extend upward through the biological shield. Each shaft is coupled to a rack tube by a magnetic clutch latch arrangement similar in design to one described above for the control rod drive. The rods are driven by synchronous motor drives and simply raise the system to the "cocked position." When the latch is released, the drive mechanism and the safety rods fall 14 in. under the force of gravity. A pneumatic shock absorber decelerates the mechanism during the last 5 in. of movement. All reactor operations, including actuation of the control system or actuation of the fuel-handling system, require the safety rods to be in the up position.

The safety rods are connected to the horizontal support bar by a bayonet-type lock, described in Section III-A-1-g. The entire system acts as a unit with both rods being "dropped" simultaneously.

### 7. Fuel Handling System

"Fuel handling" includes: removing the subassembly from the reactor, transferring it to the storage rack, and after a 15-day cooling period (for fission product decay), removing it to the disassembly cell. The fuel-handling system (Fig. 28) consists of the reactor gripper mechanism, the holddown mechanism, the transfer arm, the storage rack and the disassembly cell gripper mechanism. The reactor gripper mechanism, and the holddown mechanism are located in the small rotating plug which is in turn eccentrically located in the large rotating plug. Rotation of the two plugs is employed to position the gripper over the desired location in the reactor, and to position the gripper at the "transfer position." The reactor cover is also supported by the small plug, rotates with it, with the gripper mechanism and holddown mechanism operating through the cover.

After the reactor is shut down, the 12 control rods are released from their individual control rod drive mechanisms. The reactor cover holddown clamps which fasten the cover to the reactor tank are then released. The three cover holddown clamps are equally spaced about the circumference of the cover. Clamping is accomplished by a tube which slides over a fixed rod, as shown in Fig. 29. Sliding the clamping tubes upward provides clearance between the flange and the tubes permitting the cover to be raised by the two elevating columns. The columns are raised by two synchronized electric motor-driven lifting mechanisms located on the small rotating plug. In the raised position, the reactor cover engages pins extending from the underside of the rotating plug, to prevent swinging of the relatively heavy mass (approximately 17 tons) during plug rotation. The cover is raised 9 ft-8 in. to provide clearance below it for removal of subassemblies from the reactor. The control drive mechanisms are then raised 3 in. to clear the subassembly adapters.

The reactor is now prepared for unloading a subassembly. The rotating plugs must be rotated to the proper location to position the gripper over the desired subassembly. Both shield plugs are supported by roller bearings and rotated by electric motors. The plugs are sealed around their periphery by "freeze seals" employing a bismuth-tin alloy. The bismuth-tin alloy is contained in a trough around the plug while a baffle fastened to the plug dips into it. During reactor operation, the alloy is frozen (melting point 281F), forming a gastight, pressure-proof seal. During fuel-handling operations, the alloy is heated until it reaches the liquid state, allowing rotation of the plugs. In addition to the rotation of the two plugs to the required location, it is also necessary to rotate the gripper unit about its centerline to provide the correct angular orientation of the gripper head.

All operations involved in the fuel handling cycle include provisions for maintaining a "known" angular orientation of the subassembly. Three locations on the subassembly provide this orientation control: (1) the cone-shaped adapter is slotted and engages a blade in the gripper mechanisms; (2) the section below the collar is rectangular and engages the slotted arm of the transfer arm; and (3) the lower nozzles of the subassemblies are slotted and engage orientation bars in the reactor grid and the storage rack. Each of these "orientation controls" on the subassemblies are in the same plane. Control of angular orientation, and knowledge of angular orientation is maintained at all times during the fuel handling cycle.

The rotating plugs and gripper head are rotated to the proper position for the particular subassembly to be removed. (There is an angular position for each of these three units for each lattice position in the reactor.) The holddown mechanism consisting of a "funnel-shaped" sleeve is lowered by an electrically driven screw over the subassembly to be removed. It contacts the six adjacent subassemblies, spreads them slightly, and prevents them from moving as the subassembly is removed. This arrangement is shown in Fig. 30. The holddown sleeve also acts as a guide for the gripper mechanism.

The gripper head is lowered (through the holddown sleeve) and contacts the adapter on the subassembly. The gripper device on the lower end of the mechanism grips the subassembly adapter in the same fashion as the control drive gripper described in Section III-A-6. The orientating blade between the gripper jaws engages the slot in the conical shaped head. The sensing device also functions as described in Section III-A-6. The gripping mechanism is moved vertically by an electrically-driven screw drive and the gripper jaws are motor operated. Interlocks prevent the opening of the gripper jaws except when the gripper head is in the upper plenum chamber of the reactor, or at the transfer point between the gripper and transfer arm.

After the subassembly has been raised out of the reactor, the holddown tube is raised around the suspended subassembly and acts as a support during movement of the two rotating plugs.

The plugs are rotated to the transfer point, and the gripper head is rotated to the "transfer angle." The collar on the subassembly adapter fits into the U-shaped transfer arm-holding device as shown in Fig. 31. The rectangular section below the collar assures proper orientation. The collar of the subassembly adapter fits into a recess on the transfer holding device into which it is lowered by the gripper mechanism. The locking bar on the transfer arm holding device locks the subassembly positively to the transfer arm. The subassembly is released by the gripper and the holddown is lowered.

The transfer arm is rotated through a horizontal arc of about 80 deg. and positions the subassembly above any one of three concentric rows of storage locations in the storage rack. The transfer arm is operated manually and, "by feel," provides several checkpoints for the operator; for example: The physical contact between the transfer arm and subassembly at the transfer position is felt, the transfer arm cannot be moved while the subassembly is held by the gripper and holddown sleeve, and provides a check that the transfer has been made correctly. Similar checks can be made between the transfer arm and the storage rack.

The storage rack is a tank-shaped structure providing 70 storage locations in three concentric rows. The storage rack is suspended by a shaft extending through the disassembly cell, with its drive mechanism mounted on the ceiling of the disassembly cell. The storage rack can be rotated as well as raised to different levels in the primary tank. An empty storage location is positioned below the subassembly, which is suspended from the transfer arm, by rotation of the storage rack. By elevating the storage rack, the subassembly is inserted into a storage location and at the end of the upward movement, it is lifted from the holding device upon release of the transfer arm locking bar. To assure proper vertical movement of the storage rack, a transfer-indicating device is used. This is a sensing rod extending vertically from the disassembly cell ceiling directly to the transfer position. It is actuated by the upper adapter of the subassembly, which is raised when improper rotation of the storage rack would position an already occupied storage location below the subassembly or if the storage rack lifting mechanism accidentally overtravels its correct transfer level. In either case, the transfer-indicating device acts as an electrical safety stop. A further checkpoint exists here. As long as the subassembly is held jointly by the storage rack and the transfer arm, the transfer arm cannot be moved, indicating proper operation of both mechanisms. After subassembly transfer, the transfer arm is rotated to a neutral position while the storage rack is lowered.

After 15 days cooling, the subassembly is removed from the storage rack to the disassembly cell. The disassembly cell gripping device is similar to the fuel-handling gripper, with the addition of flow channels for inert gas, which is circulated through the gripper shaft and

through the subassembly to provide cooling during transfer operations. The gripping device mechanism is mounted in a rotating plug in the ceiling of the disassembly cell, which positions the gripper over the subassembly in the storage rack and after removal transfers it to the disassembly receiving station. The rotating plug is of similar construction and has an identical sealing arrangement as the two rotating plugs above the reactor.

The operations performed in the disassembly cell are described in Section III-A-9.

A subassembly is loaded into the reactor by reversing the sequence of operations.

#### 8. Primary Tank and Biological Shield

The primary tank, primary structure, and shield cooling system comprise an integrated system, which is designed to: meet static load requirements, maintain accuracy of alignment, and contain internal energy release. As shown in Fig. 7, the tank is surrounded by, and supported by, the primary structure which includes the biological shield.

The primary tank and the primary structure are completely independent of each other on all sides except the top. The primary tank is supported at the top and all units entering the primary tank do so through the top. Much of the equipment entering the primary system is large and heavy and must be adequately supported, as well as the total weight of the primary tank. The "low temperature top structure" is designed to support these loads.

The primary structure is also designed to contain the energy release associated with a "hypothetical" nuclear accident. For design purposes, an energy release equivalent to 300 lb of TNT at the center of the reactor was assumed. (The possible magnitudes of energy release are discussed in Appendix C.) Although the primary tank would be destroyed, the primary structure surrounding the tank has been designed to contain this energy release without failure (as described in Appendix E).

##### a. Primary Tank

The primary tank is of double wall construction (a tank within a tank) to provide maximum reliability of sodium containment. The tank is constructed of Type 304 stainless steel. The inner tank is 26 ft internal diameter and the outer tank wall is 26 ft-11 in. internal diameter. The side walls are constructed of 1/2 in. thick plates, while 1 in. thick plates are employed for the tank bottoms. The space between the two tanks is filled with an inert gas, which is monitored to detect leakage through either tank wall (sodium or air). The outside of the tank is insulated to minimize heat loss from the primary system.

The bottom of each of the tanks is stiffened with radial beams. A similar structure is used for the primary tank cover, which is 39 in. deep. (This depth is used for shielding material and thermal insulation.)

The inner tank bottom plate structure is designed to support the reactor tank, the subassemblies, neutron shield and the entire sodium load. This load is transferred by the tank wall to the top cover where the tank is supported. The outer tank structure is designed to carry only the sodium load in the event of a leak developing in the inner tank.

The criteria used in the bottom plate structure design are as follows:

(1) The inner tank bottom plate structure is designed to support the full load with a maximum deflection of  $1/4$  in. at a temperature of 750F. This small deflection was established to minimize misalignment between the reactor and the upper structure of the primary system.

(2) The outer tank bottom plate structure is designed to support the uniformly distributed sodium load with an allowable bending stress in the plates and beams of 14,700 psi. (Deflection does not affect equipment alignment.)

The primary tank and its contents, and those components which are connected to the primary tank top cover, are supported by six hangers welded to the top cover beams, which in turn transfer these loads to the top structure beams. Each hanger is pin-connected so that differential radial expansion between the top structure and the primary tank cover (due to large differences in operating temperatures) will not impose any additional stresses in the system.

The primary tank design and the method of support are arranged to provide radial expansion about the vertical centerline of the system. The most critical units, the reactor and the rotating plugs which locate the control drives and fuel unloading mechanisms, are located on the physical centerline of the system. Differential vertical expansion is avoided by the use of identical material for all equipment in the system, and maintaining it at the same temperature.

#### b. Primary Structure

The primary structure (Fig. 32) consists of a system of columns and beams which transmit the loads to the main internal building foundation. In combination with the biological shield, it forms a "pressure vessel" surrounding the primary tank. The bottom structure consists of six radial beams embedded in the heavily reinforced concrete with six columns connected to the beams. These columns are connected at the top to six radial beams which frame into a circular ring (6 in. thick) located

on the centerline of the system. This top structure with additional stiffening members provides the supporting structure for the primary tank and for the major primary system components supported external to the primary tank.

The material proposed for this structure is USS Carilloy T-1 plate steel, which has a yield point of 90,000 psi and a tensile strength of 105,000 psi at room temperature. Using American Welding Society E-12015 electrodes welded joint efficiencies of 100% are anticipated.

A ring of ordinary concrete (6 ft thick) provides the radial biological shield, the inside diameter of which is at essentially the same diameter as the inside of the six vertical columns. The shield alone provides sufficient strength to carry the static loads imposed on the top structure. The steel columns are required to provide the strength required to withstand the assumed internal energy release. The steel columns are not only required to carry the load resulting from the internal pressure against the top structure, but certain precautions must be taken to maintain the integrity of these columns from "blast damage."

c. Blast Shield

In order to preserve the integrity of the primary structure (in particular, the columns) and the radial biological shield in the event of an "explosion-type accident" in the reactor, a laminated and continuous blast shield (2 ft thick) is placed between the primary tank and the biological shield. The laminations consist of alternate layers of 1/2 in. thick carbon steel plate shells and 4 in. thick lightweight concrete (a foam type of concrete with a very low density), or glass wool. The blast shield serves as a cushion for most of the energy released, reducing the pressure acting on the structure to allowable limits. The mechanism of energy attenuation and absorption is the crushing of the low-density concrete and glass wool, and the stretching of the steel shells. An estimate of the effectiveness of the blast shield is included in Appendix E.

d. Biological Shield

The radial biological shield is constructed of ordinary concrete 6 ft thick. The concrete is reinforced with continuous hoops of reinforcing rods in such a manner so as to allow the shield to resist safely an internal pressure of 75 psig. (The estimated resultant pressure beyond the blast shield is only 5 psig.)

Figure 33 shows the detail of the primary structure columns in the radial biological shield. The inner steel form for the biological shield is permanent. The columns have been set back 2 in. from the inner face of the biological shield to avoid lateral loading of the columns in the event that the concrete tends to move outward.

The radial biological shield and structure is continuous except at an elevation near the top of the primary tank where it is penetrated by several horizontal offset holes (approximately 8 in. dia.) for the ventilation ducts required for shield cooling. The shield is heated by the heat loss from the primary system, and by energy absorbed in attenuating neutrons and gamma rays. The heat is removed to avoid overheating the steel plates and the concrete.

e. Shield Cooling System

The shield is cooled by forced circulation of air. It is essentially a re-circulation system; however, a fraction of the air is continuously drawn into the system and an equal amount is discharged from the building. The shield cooling system is a part of the building ventilation system and the air is exhausted from the building through the shield cooling system. The shield cooling system operates at a pressure slightly below that of the building atmosphere. This provides in-leakage and also simplifies certain areas in the shield which cannot be connected to a closed circulation system. The top structure and the shield plugs installed therein are cooled by air drawn from the building atmosphere. The radial shield and the structure below the primary tank are cooled primarily by recirculated air. Figure 34 is a simplified diagram describing the shield cooling system. Air from inside the building shell is drawn into the primary system through a duct system in the rotating plugs and in the primary top structure, and circulated around the top cover of the primary tank, through ducts in the biological shield into exhaust blowers. It joins air which has circulated through the radial shield and bottom shield air space. The air flow then is split into two paths, one to the exhaust stack in the Process Plant, and the other through coolers.

The heat that must be removed by the shield cooling system consists almost entirely of the heat loss from the primary system, the heating in the shield due to neutron and gamma ray attenuation being only a small fraction of the total heat load. The total heat load is approximately 430,000 Btu/hr, of which 415,000 Btu/hr is the heat loss from the primary tank, and approximately 15,000 Btu/hr is due to the neutron and gamma attenuation in the structure and shield.

An air-cooling system of 15,000 cfm capacity with a maximum air velocity of approximately 30 fps is required. Reliability of the system is achieved by auxiliary power supplies to the exhaust blowers and coolers. Because of the large heat capacity of the system, interruption of the cooling system is not critical.

## 9. Disassembly Cell

The disassembly cell is a sealed, shielded cell directly interconnected with the reactor primary system. The disassembly cell is actually a part of the Process Cell but is located in the reactor building to perform certain preliminary process operations.

All subassemblies entering the reactor system are transferred through the disassembly cell to the storage rack, and thence to the reactor. All subassemblies removed from the reactor follow a reverse pattern and, in addition, the core subassemblies, control rods, and safety rods are partially disassembled. These units which contain enriched fuel are permitted to cool, while submerged in sodium in the storage rack, for 15 days after removal from the reactor. After this cooling period, these units still require forced convection of inert gas through them to provide adequate cooling. To avoid the necessity for elaborate cooling facilities in the transfer coffins, these units are disassembled to the extent that forced convection cooling is not required. This consists of removing the hexagonal subassembly cans and separating the individual fuel elements. The subassembly cans are cut and separated from the internal sections of the subassembly in essentially the reverse manner of the assembly operations. The fuel elements are mechanically engaged to the grid in the subassembly and can be mechanically removed. After the individual fuel elements are removed from the cluster and separated, they will cool adequately in the atmosphere of the cell. The blanket sections of the core subassemblies and the blanket subassemblies do not introduce cooling problems and are not disassembled in the disassembly cell.

During the disassembly operations on the enriched units it is necessary to provide a continuous flow of inert gas through the units to extract heat from the cluster of fuel elements. This is accomplished in the disassembly cell with much more reliability than would be possible in the transport coffins required to transport this equipment to the Process Plant. Of particular importance is the fact that the coffins must be transferred through the reactor building air lock, with the attendant possibilities of malfunction of equipment, loss of forced cooling, and resultant melting of the fuel.

The process operations are also divided between the disassembly cell and the process cell with respect to fission product contamination. The operations in the disassembly cell involve the physical separation of the fuel elements from the core subassembly, but do not include any separation of the fuel element containers from the irradiated fuel. No appreciable fission product release is expected in the disassembly cell, and the primary contaminant in this cell is activated sodium. Gross fission product contamination is confined to the process cell.

## 10. Sodium Cleanup System

A recirculating cold trap system (Fig. 35) is used for continuous primary sodium purification. This system enables the maintenance of impurity concentrations at or near their greatly reduced solubility limits for temperatures just above the melting point of sodium. Cold trap precipitation is effective in maintaining low concentration of such impurities as sodium hydride, most fission products, and particularly sodium monoxide.

The cold trap consists of a 500-gallon tank filled with Type 304 stainless steel wire mesh to provide supplementary surface area to enhance sodium crystallization and deposition.

A regenerative heat exchanger is incorporated in the main sodium stream to reduce over-all heat losses in the cold trap system. The cold trap operational temperature of 350F is maintained by a secondary sodium cold trap coolant loop.

Two types of analytical devices are used to determine the sodium quality. A plugging indicator is mounted on the cold trap inlet line to monitor the oxygen concentration in the primary tank sodium. Two vacuum cup samplers are used to physically remove sodium samples for chemical or radiological analysis; samples may be taken from either the cold trap inlet or discharge line.

Parts of the cold trap circuit lie below the level of sodium in the primary tank. Since radioactive primary sodium is circulated in the cold trap system, it is essential to eliminate the possibility of an accident or equipment failure resulting in syphoning of primary tank sodium. To avoid this possibility, a surge tank is included in the cold trap inlet line at its highest point of elevation. An argon gas blanket pressure is maintained such that, under static conditions, the sodium level is just below the surge tank discharge opening. With the pump operating the level rises sufficiently to establish flow. The power supply to the pump is interlocked to a sodium vapor monitor at the cold trap floor level to cut out when a sodium leak is detected, thereby "breaking" the inlet sodium line at the surge tank. In addition, an argon gas line is provided for positive gas addition to insure breaking the sodium column in an emergency.

The cold trap discharge line empties into a splash sleeve in the gas phase of the primary tank, precluding any possibility of syphoning through the discharge line.

Five remotely controlled valves are placed in the cold trap circuit for use in isolating various sections of the system during emergencies and for any necessary repair work. The horizontal sections of both the cold trap inlet and discharge lines are pitched to drain back into the Primary Tank.

These provisions insure a minimum of sodium spillage in the event of system failure. Excluding failure of the cold trap tank proper, a rupture at any other place in the system can involve no more than the sodium inventory in the cold trap discharge line and in the vertical section of the inlet line.

#### 11. Inert Gas System

It is necessary to provide an inert gas blanket over the primary system sodium and an inert gas atmosphere within the disassembly cell. Of the noble gases, argon was chosen for this system because it is superior with respect to: pumping, heat transfer, sealing, and secondary effects on structural materials (such as nitriding). To maintain a low level of atmosphere contamination, a gas cleanup system (Fig. 36) is provided through which the argon can be continuously recirculated and purified. Continuous circulation is also desirable as a means of preventing excessive sodium aerosol buildup in the gas.

Although the disassembly cell and primary tank are interconnected, the two gas systems are essentially separated and the gas system is arranged to handle them independently (with a small leakage rate between the systems). Because the recirculation requirements for the two regions are different, the primary inert gas system provides independent control of the pressure and recirculation rate of the primary tank blanket gas and the disassembly cell atmosphere. During normal operation, the primary tank pressure and recirculation rate is respectively -3 in. H<sub>2</sub>O and 20 cfm and for the disassembly cell -2 in. H<sub>2</sub>O and 200 cfm. The purpose of a lower pressure in the primary tank is to minimize diffusion of sodium vapors from the primary tank to the disassembly cell. The blower discharge pressure and the capacity of the blower head tank are established such that, upon equalization, the pressure of the complete primary inert gas system would be less than 2 psig. Make-up gas is added to the primary circulating gas system, as needed, from the Process Plant argon gas supply system. Excess gas is vented directly through filters to the exhaust stack or to a retention tank for subsequent disposal.

An internal inert gas manifold within the disassembly cell supplies heated argon for drying fuel subassemblies upon their removal from the primary tank. This manifold also supplies coolant gas through flexible connections to the fuel subassemblies prior to and during their disassembly.

Argon vented to the stack is continuously monitored for activity. If the activity exceeds the tolerable level, the gas is pumped into a retention tank and held until it decays sufficiently for safe disposal.

## 12. EBR-II Working Model

In order to demonstrate the feasibility of the submerged primary system design concept, a working model of significant size was constructed. The working model (Fig. 37) duplicates all of the significant components of the parent design, appropriately scaled to function in this system. These include:

- a. The primary tank (approximately 11 ft. dia. by 8 ft deep), which contains approximately 5,000 gal of sodium. The sodium is heated electrically and maintained at approximately 750F, which approximates the ambient sodium temperature in the EBR-II system.
- b. A reactor mock-up of 61 "dummy fuel subassemblies."
- c. A prototype d-c, electromagnetic pump with a design capacity of 1,000 gpm at 40 psi head. The pump, piping, reactor, and instrumentation are interconnected in a manner similar to the EBR-II primary system. Since this is an isothermal experiment, the heat exchanger is omitted and a throttle valve is incorporated in its place. The arrangement of the flow system is shown schematically in Fig. 38.
- d. A by-pass circulation sodium purification system which includes a pump, regenerative heat exchanger, and cold trap for the continuous circulation of sodium and continuous removal of sodium oxide.
- e. A prototype shutdown cooler.

The operation of the system components has shown that the physical arrangement and the operational procedures are entirely feasible. Fuel-handling operations have been performed periodically; a total of approximately 80 loading and unloading operations have been completed. The pump has operated a total of 4500 hrs without difficulty. The continuous by-pass sodium purification system has demonstrated the feasibility of maintaining the sodium purity below 0.002 wt-% O<sub>2</sub>. This has been accomplished in a system in which the inert gas blanket leakage is higher than is expected in the EBR-II system. The shutdown cooler has operated very satisfactorily, and the heat removal capability has equalled that predicted.

Several minor modifications have been made in some of the operating mechanisms as a result of the experience obtained from the operation of the working model. These are also incorporated in the EBR-II system components, and even greater operational reliability is anticipated in the EBR-II system. An intangible asset has been the practical experience obtained from the operation of this unit and by the confidence in the system design which has resulted from this satisfactory operation. Particularly significant has been the comparative ease with which modifications

to the system have been made. Although there is no radioactivity present, these modifications have been made in the face of all of the "chemical problems" associated with the sodium. This experience has demonstrated that the maintenance problems which may be expected in the EBR-II can be suitably performed with the addition of adequate precautions to take into account the additional complexity associated with radioactive sodium.

Particularly significant experience was obtained from the system after abnormal contamination of the sodium with oxygen during certain maintenance operations. Comparable system contamination in small experimental loops and apparatus have caused considerable operational difficulties in the past. In the working model the system was quickly and easily purified, and normal operation resumed. This experience has minimized concern with respect to the problems associated with the inadvertent oxygen contamination of the sodium system. It also suggests that larger sodium systems are considerably more reliable than the small, experimental systems upon which the majority of previous experience has been based.

#### B. Secondary System

The secondary system is the non-radioactive sodium heat transfer loop between the radioactive primary system and the steam system. The principal function of this system is to transfer heat from the primary sodium system to the steam system in an efficient manner. The flow rate is  $2.58 \times 10^6$  lb/hr (approximately 6050 gpm). The heat exchanger inlet temperature is 610F and the outlet temperature 880F. The principal components of the secondary system in flow sequence, are the sodium circulating pump, the heat exchanger, the steam superheater and the steam evaporator.

The circulating pump is an a-c linear induction electromagnetic pump with a capacity of 6500 gpm at about 65 psi. Flow control down to 5% of nominal rating is achieved by providing a variable input alternating current voltage to the pump. This variable voltage is obtained from the output of a motor generator set, which is controlled to provide the required increments of flow.

The circulating pump is located in the Sodium Plant building which is about 50 ft from the Reactor Plant building. This single story building of fireproof construction also contains the secondary sodium purification system, sodium receiving facilities, and the sodium storage tank. The sodium storage tank is below floor level in this building, and the entire secondary system sodium, except that in the heat exchanger, can drain into this tank.

The surge tank, which is connected into the piping at the circulating pump inlet, maintains a constant head to the pump. The sodium purification system circulates 20 gpm from the storage tank and discharges

into the surge tank insuring constant level. The overflow returns to the storage tank through an internal overflow pipe in the surge tank. Argon gas at approximately 10 psi is provided as an inert gas atmosphere over the sodium in the surge and storage tanks.

The heat exchanger is located within the primary tank in the Reactor Plant. It is suspended from the primary tank cover, and is almost totally submerged in the primary sodium. It is a shell-and-tube-type exchanger with the secondary sodium on the tube side.

The Boiler Plant building is 100 ft from the Reactor Plant building. The steam generation equipment is located so as to insure drainage to the storage tank in the Sodium Plant. The secondary sodium passes through the superheater section and the evaporator section in series.

All piping in the secondary system is capable of absorbing thermal expansions due to temperature changes from ambient to 1000F. The sodium yard piping is carried on conventional concrete piers fitted with pipe guide or anchor frames as required. The yard piping is heated, insulated, and weatherproofed. Heating is accomplished by 60-cycle induction heating, and serves to maintain a temperature above the freezing point of sodium (208F).

### C. Steam System

The steam system serves as a "heat sink" for power generated in the reactor. Steam is generated at 1300 psig, 850F from the heat delivered by the secondary sodium system. At 62.5 mw reactor output, the steam generator will deliver 248,000 lb/hr steam to a 20 mw steam power plant of essentially conventional design. An induced draft cooling tower provides low-temperature heat rejection.

Certain features have been added to the system to improve reliability and to divorce the reactor from load fluctuations on the turbine.

A by-pass system operates in conjunction with the turbine to permit absorption of all energy produced in the reactor irrespective of electrical output. Normal plant operation consists of continuous by-pass of steam to absorb load variations in the steam system without affecting the reactor.

Steam conditions were selected to provide maximum stability to the heat transfer loops with respect to system temperatures. The saturation temperature of 1300 psig steam (580F) approximates the minimum temperature of the secondary system (610F). This results in a constant high temperature heat sink provided the steam pressure is maintained

constant, which can be readily accomplished. The temperature of the secondary sodium seen by the primary sodium coolant system is essentially constant under all conditions of operation.

Recent experience has indicated that reliability of the steam generator unit cannot be assured. High thermal stresses are known to have contributed to many of the failures. In an effort to minimize thermal stresses in the EBR-II steam generator, special feed-water temperature requirements have been included. In addition to feed-water heating by extraction from the turbine, feed-water temperature is raised further by an additional heater supplied with steam direct from the 1300 psig system. In this manner, the feed-water is heated to 550F over the entire load range resulting in a very small temperature difference between the feed-water and the evaporator water (580F).

Because of the questionable reliability of the steam generator at this stage of development, the EBR-II steam generator is located in a separate building adequately removed from the reactor, with "blow-out panels" designed to fail in a direction away from the reactor. The steam generator is also separated from the bulk of the sodium in the secondary system to minimize resultant damage if a serious failure occurs.

#### D. Process System

Although fuel processing is normally not covered in a discussion of reactor safety it is included here since it is an integral part of this reactor cycle. The EBR-II probably will be the first reactor in this country to operate directly on recycled fuel and hence face the entire problem of heavy isotope buildup.

Irradiated fuel from the reactor will be cooled for only 15 days prior to transfer to the process plant for decanning and processing. The processing facilities are contained in two shielded cells located in the Process Plant. The larger of these cells contains the equipment for decanning spent fuel and blanket elements, for processing them, and for fabricating the fuel into new elements. This cell is gastight and contains an inert atmosphere of high-purity argon. The second cell is a conventional shielded hot cell with an air atmosphere and is used for assembly of subassembly units as well as service work for the main cell.

Spent fuel elements are disassembled in the reactor building and the individual fuel pins (still canned in stainless steel) are transferred to the inert gas cell of the process plant. Here the pins are mechanically decanned. The bare pins are then charged to a furnace in 10-kilogram batches and melted in an environment deficient in oxygen. Under these conditions the volatile and noble gas fission products are released to the furnace atmosphere and those fission products whose oxides are more

stable than uranium oxide (cerium, rare earths) appear in the dross or slag. The ingot resulting from this melting operation contains uranium, plutonium, and the fission products Zr, Nb, Mo, Ru, Rh, Pd and presumably Tc. These elements reach an equilibrium value and it is the "estimated equilibrium" alloy that will be used for the EBR-II fuel (see end of section for discussion of "fissium" and its properties). The ingot produced by the processing furnace is remelted in an injection-casting furnace and new fuel pins are cast directly to size in expendable Vycor molds. The pins are then cut to length and inspected prior to reassembly into new elements.

In the reassembly area of the process plant new fuel cans containing the bottom fitting and spacer wire are cleaned and leak tested before being introduced into the fabrication facilities. The bond sodium is introduced into the can and the can is then transferred into the shielded portion of the cell. The refabricated pins are inserted into the cans which are then capped and welded. Each assembled pin is treated to ensure that the bond metal (sodium) wets both the pin and the can so that good heat transfer is assured, and each pin is leak tested to check the final seal weld. The final step in pin preparation is a bond-testing procedure which not only monitors the bonding treatment but also determines the sodium level within the can.

The finished pins are transferred from the argon atmosphere cell to the air cell where they are assembled into new subassemblies for return to the reactor.

"Fissium" is the name that has been applied to all alloys of uranium, plutonium, and fission products arising out of the work on pyrometallurgical processing. Most of the processes in this category do not completely remove the metallic fission products and as a result the concentration of these elements increases with fuel re-cycle until an equilibrium value is reached. This equilibrium value is a function of the fission yield of the isotopes involved, half-life, cooling time, cross section, and dragout via slag and processing losses. As a result there are many possible equilibrium alloys, depending upon: the ratios of the fissionable materials ( $U^{235}$ ,  $U^{238}$ ,  $Pu^{239}$ ), on process operating conditions, on reactor cycle, etc. Some of the variables are adjustable so that some control can be exercised over the composition of the recycled alloy.

The major fission products generated per cycle in  $U^{235}$  irradiated to 2% burnup are as follows:

<u>Element</u>	<u>wt-%</u>	<u>Element</u>	<u>wt-%</u>
Rubidium	0.021	Indium	0.001
Strontium	0.072	Tin	0.004
Yttrium	0.037	Tellurium	0.024
Zirconium	0.23	Iodine	0.012
Niobium	0.013	Xenon	0.25
Molybdenum	0.18	Krypton	0.027
Technetium	0.052	Cesium	0.22
Ruthenium	0.14	Barium	0.076
Rhodium	0.025	Total Rare Earths	0.60
Palladium	0.016	Silver + Antimony + Cadmium	0.006

If an appreciable per cent of the total fissions are due to  $U^{238}$  or  $Pu^{239}$ , the fission yield curve changes slightly to account for the extra three or four mass units and some of the concentrations change accordingly. In general, the metal atoms (Mo, Ru, Rh, Pd) re-cycle with the fuel, and the non-metallic atoms are removed in processing, with zirconium, niobium, and tellurium being partly removed. It is apparent that between pure uranium and the equilibrium fuel of infinite re-cycle there exists an infinite number of alloys.

The problems introduced by starting a reactor cycle on "pure" uranium and then processing and fabricating a slightly different alloy at every pass are tremendous. As a result, it is planned to load the reactor with an alloy approaching one of the equilibrium alloys. The change in composition per pass in this case is slight and changes in properties are expected to be negligible. This plan alleviates the effects of the ingrowth of all fission products except technetium but still leaves those problems arising from heavy element buildup. It is anticipated that the equilibrium alloy resulting from the operation of EBR-II with a uranium fuel loading may be as follows:

<u>Element</u>	<u>wt-%</u>
Zirconium	0.1 - 0.2
Niobium	0.01
Molybdenum	1.6 - 3.4
Technetium	0.5 - 1.0
Ruthenium	1.2 - 2.6
Rhodium	0.2 - 0.5
Palladium	0.1 - 0.3
Silver + Cadmium + Antimony	0.1

Since an infinite number of alloys are obviously possible in such a system a few reference alloys have been standardized on for testing. The first two reference alloys on which data are available are listed in Table III.

Table III

COMPARISON OF REFERENCE FISSIUM ALLOYS

<u>Element</u>	<u>Alloy A</u>	<u>Alloy B</u>
Uranium	95.0	69.2
Plutonium	-	20.0
Zirconium	0.2	0.5
Molybdenum	2.5	2.8
Ruthenium	1.5	4.3
Rhodium	0.3	0.7
Palladium	0.5	2.5

The properties of alloy A as determined by Saller<sup>1</sup> are listed in Table IV.

Table IV

PHYSICAL PROPERTIES OF URANIUM AND URANIUM ALLOYS

<u>Property</u>	<u>Temp., C</u>	<u>Alloy A</u>		<u>U-2 wt-% Zr</u>	<u>Uranium</u>
<u>Density, gm/cc</u>	20	17.95		18.6	19.1
	65	17.4		-	-
	640	-		-	18.4
	700	17.4		-	-
	720	-		-	18.1
	800	17.3		-	18.1
<u>Melting Range, C</u>		1002 - 1081		1150	1133
<u>Thermal Expansion, 10<sup>-6</sup>/C</u>		<u>Heat.</u>	<u>Cool.</u>		
	20 - 100	11.0	13.7		14.5
	20 - 200	12.5	14.4	15	
	20 - 300	13.6	15.1		16
	20 - 400	14.0	15.7		
	20 - 650	16.6	-		20.5
	20 - 700	16.6	23.3		
	20 - 800	16.8	23.4		
<u>Thermal Conductivity, cal/(cm<sup>2</sup>)(sec)(C)</u>		<u>BMI Data</u>		<u>ANL Data</u>	
	20	0.026	-		0.066
	100	0.034	-		0.068
	200	0.044	0.040	0.062	0.069
	300	0.053	0.048	0.067	0.074
	400	0.062	0.056	0.073	0.081
	500	0.071	0.063	0.080	0.088
	600	0.080	0.071		0.096
	700	0.088	-		0.105
	800	0.097			0.115
900	0.125			0.127	

<sup>1</sup>H. A. Saller, "Properties of a Fissium-Type Alloy," Battelle Memorial Institute, BMI-1123, August 23, 1956.

### Thermal Cycling Stability

Four specimens hot rolled at 675C, cycled 250 times from 150C to 750C grew 3 to 6% in length; however, this growth may be due to the rolling temperature being just above the alpha transformation.<sup>1</sup> Four specimens as cast, and four specimens wrought and gamma treated<sup>2</sup> cycled 200 times from 66 to 620C showed negligible growth and no surface roughening. Four other specimens cycled 200 times from 66 to 716C also showed negligible length change but showed some volume increase.

Properties of alloy B as determined at Argonne are given in Table V.

Table V

#### PHYSICAL PROPERTIES OF REFERENCE FISSIUM ALLOY B

<u>Property</u>	<u>Temp., C</u>	<u>Alloy B</u>
<u>Density, gm/cc</u>	Room Temp	16.5 - 16.6
<u>Thermal Expansion, 10<sup>-6</sup>/C</u>	20 - 100	12.1
	20 - 500	15.2

#### Thermal Cycling Stability

After 200 cycles from 25 - 500C there was no warping, no diameter distortion and only 0.07% growth.

Unlike the U-20% Pu binary, alloy B does not appear to be pyrophoric, and, in addition, has excellent radiation damage stability as indicated in Table VI.

---

<sup>2</sup>Reactor Engineering Division Quarterly Report - Section I, ANL-5571, July, 1956, p. 156.

Table VI

IRRADIATION STABILITY OF REFERENCE FISSIUM ALLOYS A AND B

<u>Specimen Identity</u>	<u>Approx.</u>	<u>Approx.</u>	<u>% Change</u>	
	<u>Burnup, %</u>	<u>Temp., C</u>	<u>Length</u>	<u>Diameter</u>
<u>Alloy A</u>				
CG-2, as cast	0.4	500	0.34	1.23
CG-5, as cast			0.86	0.86
CG-10, as cast			0.42	0.11
CG-45C } cast;			0.83	2.70
CG-47A } water quenched			1.86	2.70
CG-48B } from 850C			2.11	0.70
CG-46A } cast;			0.86	0.75
CG-47B } furnace cooled			0.87	0.88
CG-48C } from 850C			1.11	0.93
<u>Alloy B</u>				
CF-10, as cast	1.0	450	2.30	0.16
CF-12, as cast	1.0		0.88	0.40
CF-14, as cast	0.3		-	1.80
CF-15, as cast	0.3		0.57	0.89
CF-16, as cast	0.3		0.62	0.08

#### IV. EBR-II PLANT OPERATION AND PERFORMANCE

##### A. Control and Instrumentation of the Power System

###### 1. General

Control of the power system is centralized in a control room located in the Power Plant Building. Control, in general, is manual. Only the simplest of control functions, or those which might adversely affect facility safety if handled manually, are effected automatically. As examples, control of primary and secondary system coolant flow rates is manual; control of reactor power level is manual during raising or lowering of power, but is automatic at steady state; control of feed-water flow rate and steam pressure is automatic. A simplified block diagram of the control system is shown in Fig. 39.

In essence, the basic control philosophy for the EBR-II power system consists in providing: (1) control of reactor power level; (2) maintenance of balance between the rates of heat removal effected by each of the major thermal systems, from the cooling tower to the reactor; and, (3) maintenance of essentially complete isolation of the reactor from the effects of turbine-generator load variation. As with most thermal systems, the additional control requirements exist of maintaining desired system temperature and pressure levels and precluding excessively high rates of temperature change; e.g., as described earlier, throttle steam temperature and pressure are maintained constant at 850F and 1250 psi, respectively, at all reactor or turbine-generator loads.

###### a. Control of Reactor Power

Operational control of reactor power is afforded by vertical movement of the twelve control rods. The rods are of the fuel-bearing type, and are positioned symmetrically about the periphery of the core. The maximum speed of rod movement available for control purposes is limited mechanically to 5 in./min. For the purpose of scramming the reactor, however, a trip arrangement is incorporated in each rod which enables rapid downward movement (out of the core).

Changes in reactor power level are effected by manual adjustment of rod positions. Once stabilized operation at a given power level has been established by the operator, the power level is maintained at steady state by automatic control of regulating rod motion (the control being based on sensing of neutron flux level). Upon occurrence of any of the facility condition abnormalities (listed later) which initiate a reactor scram signal, all twelve rods automatically are ejected from the core at high speed to effect reactor scram.

A total of ten fission counters and ionization chambers are provided which enable sensing of reactor period, as well as of neutron flux level, throughout the range from source power to several times full power. From these detectors are derived the signals for measurement and control of reactor power and for initiation of reactor scram in the event of excessively short period or excessively high power. The detectors are located in vertical thimbles at various positions outside the reactor tank. Eight of the thimbles are immersed in the primary tank sodium and are positioned immediately adjacent to the outer surface of the radial neutron shield; two are located outside the primary tank, within the shield cooling air annulus.

b. Maintenance of Balance between Major Thermal Systems

The major thermal systems of the facility are the primary system, secondary system, and steam system (plus circulating water system). Heat generated within the reactor is removed by the primary system and delivered to the heat exchanger. From the exchanger, the heat is transferred by the secondary system to the steam generator (superheater and evaporator). From the steam generator, the heat is transported by the steam system to the turbine and the condenser. That heat absorbed by the turbine is converted to electrical power, and that released in the condenser is absorbed by the circulating water system which effects final dissipation to the atmosphere via the cooling tower. A simplified flow diagram for the major systems is shown in Fig. 1.

The rate of heat removal by the cooling tower is maintained equal to the rate of heat removal from the condenser by conventional control means identical to those employed in coal- or gas-fired plants. Similarly, conventional control is employed to maintain the rate of heat removal from the condenser (plus that effected by the turbine) equal to the rate of heat removal from the secondary system (by the steam generator). Balance between rate of heat removal from the secondary system and that from the primary system is obtained by employment of an evaporator of sufficiently large capacity to accommodate the maximum anticipated heat transfer load in conjunction with maintenance of constant evaporator water temperature (through automatic regulation of the main steam system pressure). The balance between rate of heat removal from the primary system and the rate of heat removal from the reactor requires a special control technique. Any imbalance of these two rates produces a continuous change in the primary tank bulk sodium temperature. In order to effect the proper balance, the following method of control is utilized:

(1) The primary system flow rate is regulated at any given power level so as to provide a predetermined reactor coolant outlet temperature, this temperature varying from 900F at full power to 850F at

very low power. This 50F variation in reactor coolant outlet temperature is employed in order to maintain a constant steam temperature of 850F at all power levels.

(2) Irrespective of reactor power level, the temperature of the cold leg of the secondary system automatically remains between 580 and 610F. This is because the temperature of the evaporator water is kept constant and the design and capacity of the evaporator are such as to effect a very small approach temperature at the sodium outlet end. Also irrespective of reactor power level, the temperature of the hot leg of the secondary system remains relatively constant, varying from about 880F at full power to about 850F at very low power (reflecting control of the reactor outlet coolant temperature). Consequently, the rates of heat removal from both the primary system and the secondary system become approximately proportional to the secondary system flow rate.

(3) Since the rate of heat removal from the primary system is a function of the secondary system flow rate, control of this flow rate is employed to maintain balance between the rate of heat removal from the primary system and that from the reactor.

c. Isolation of the Reactor From Effects of Load Variation

An important feature of the EBR-II in regard to reactor stability is the virtual isolation of the reactor from the effects of changes in power system conditions external to the reactor. This is accomplished by employing: (1) a method of control of reactor power level such that neither changes in electrical load demand nor in any operating condition of the power system are reflected as changes in reactor power demand; (2) a system design and method of control which eliminate any effect of change in electrical load upon reactor inlet coolant temperature; and, (3) a system design which minimizes the effect of change in any system condition (or existence of any abnormal system condition) upon reactor coolant inlet temperature.

Reactor power level is established by operator control only. No control link is provided to effect automatic adjustment of reactor power (other than scram) upon occurrence of change in electrical load demand or any power system operating condition. Consequently, with the further provision of achieving essentially complete stability of reactor inlet coolant temperature and reactor coolant flow rate as described below, optimum conditions for promotion of reactor stability are realized.

The steam system is designed to by-pass a certain amount of steam around the turbine-generator at all times. This by-pass steam flows directly from the steam generator to the condenser; the amount by-passed is automatically regulated to maintain the main steam line

pressure constant under all conditions. Operating procedure requires that the reactor power level exceed the maximum possible turbine-generator load under all circumstances. This is accomplished through operator adjustment of the turbine-admission-valve-stop to limit maximum steam flow (and, therefore, turbine-generator load) to a proper value dependent upon the desired reactor power operating level. With this method of operation, the reactor power (and, therefore, the steam generation rate) is continuously maintained at a level higher than that required by the turbine-generator load, and excess steam always is being by-passed to the condenser. Change in turbine-generator load, whether increase or decrease, automatically is accommodated by a corresponding change in the amount of excess steam being by-passed, with no change being effected in the steam generation rate or temperature in the steam generator. Since the only connection between the turbine-generator and the primary system is through the steam generation equipment (via the secondary system), this arrangement also eliminates any effect of change in turbine-generator (electrical) load upon reactor inlet coolant temperature.

With the submerged primary system design employed, the reactor inlet coolant temperature is identical with the bulk sodium temperature within the primary tank. The thermal capacity of the bulk sodium plus that of the submerged components is large (the bulk sodium volume is about 86,000 gal.). Accordingly, the rate of change of average bulk sodium temperature even at high rates of heat addition (or loss) is extremely low. The rate of heat addition is essentially a function of the degree of imbalance between reactor power level and rate of heat removal from the primary system. Accordingly, since heat removal from the primary system is accomplished almost entirely by the secondary system, mal-operation of the secondary system flow rate control or adventitious temperature excursions within the secondary system can have only negligible effect upon reactor coolant inlet temperature unless the abnormality exists for a very long time. Under any condition, the rate of change of reactor coolant inlet temperature, or bulk sodium temperature, is very small and is readily correctable either through manual control or through operation of interlocks on bulk sodium temperature or reactor coolant temperatures. For example if the reactor were operating at full power (62.5 mw) with no heat being removed from the primary tank, the rate of bulk sodium temperature rise would be only about 14F/min. Thus the system design renders the reactor coolant inlet temperature extremely insensitive to changes in any other system condition (or existence of any abnormal system condition).

#### d. Alarm and Scram Provisions

In addition to enabling control of the power system and providing indication and recording of sensings, the system instrumentation is designed to: (1) effect an alarm (annunciation and indication) in the control room when a condition in the system is abnormal; (2) indicate in the

control room which condition is abnormal; and, (3) effect automatic scram of the system when the abnormal condition is critical. Scram always includes the cutting off of main pump power in the secondary system as well as fast shutdown of the reactor. For certain types of abnormality, the magnitude of the abnormality may be the determining factor as to whether or not an immediate scram is required. In these cases, a pre-scram warning alarm (annunciation and indication) is provided at a magnitude of abnormality sufficiently low as to permit its existence without jeopardizing safety or equipment. This warning affords the operator opportunity to effect manual corrective action, and only if such action fails to prevent the magnitude of the abnormality from becoming critical does automatic scram result. Scram always is accompanied simultaneously by annunciation and indication.

A list of abnormalities of importance and the contemplated alarm and/or scram provisions for each is given in Table VII. All abnormalities intimately connected with reactor safety initiate reactor scram. The other abnormalities listed are not directly pertinent to reactor safety, but are included to describe the type of plant control contemplated. (The term "alarm" is used to mean both indication and annunciation.)

## 2. Nuclear System

### a. Control Rod Characteristics

Operational control of the reactor is accomplished through vertical movement of the twelve control rods. Movement of each rod is independently controlled from the control room, and the position of each rod is continuously indicated in the control room. The control rod locations within the reactor core are shown in Fig. 8. Construction of the rods is described in Section III.A.1.f; design and operation of the rod drive system are described in Section III.A.6. Drive speed (either up or down) is mechanically limited to 5 in./min. The approximate relation between rod insertion and fraction of total rod worth effective is indicated in Fig. 40. Since the total worth of each rod will not be more than  $0.006 \Delta k/k$ , the drive speed available restricts the maximum possible reactivity addition rate to less than  $0.00011 \Delta k/k$  per second (based on 2 rods).

Although the twelve control rods and drives are identical, during steady-state reactor operation eleven are used for shimming and one is used for regulating. The "regulating rod" is defined, for descriptive purposes, as the rod being controlled by the automatic control system; any of the twelve rods may be used as the regulating rod. During manual operation, either during change in reactor power level or steady-state operation, all twelve rods are defined as "shim rods." The power supply is arranged to supply power to only one shim rod drive unit at a

Table VII

## SYSTEM ABNORMALITIES CAUSING SCRAM AND/OR ALARM

Abnormality	Alarm Only	Pre-Scram Warning Alarm	Scram and Alarm
<u>Nuclear:</u>			
1. Reactor period too short. (For number of instrument channels employed and number of trips required as indication of abnormality, see Section IV-A-2-c)			X
2. Reactor power level, based on neutron flux level, too high. (For number of instrument channels employed and number of trips required as indication of abnormality, see Section IV-A-2-c)		X	X
3. Ionization chamber temperature too high	X		
<u>Primary System:</u>			
4. Loss of power to either main pump			X
5. Core inlet coolant flow rate too low			X
6. Blanket inlet coolant flow rate too low			X
7. Total reactor coolant flow rate, measured at reactor outlet, too low			X
8. Reactor tank cover unlocked			X
9. Coolant mean temperature in reactor upper plenum too high		X	X
10. Coolant temperature at selected reactor subassembly outlets too high		X	X
11. Coolant pressure in reactor upper plenum too high or too low		X	X
12. Temperature differential between heat exchanger outlet sodium and primary tank bulk sodium too high		X	X
13. Primary tank bulk sodium temperature too high or too low		X	X
14. Primary tank bulk sodium level too high or too low		X	X
15. Primary tank inert blanket gas pressure too high		X	X
16. Loss of power to auxiliary pump	X		
17. Core coolant pressure at reactor inlet too high or too low	X		
18. Blanket coolant pressure at reactor inlet high or low	X		
19. Primary tank inert blanket gas temperature (sensed inside primary tank) too high	X		
20. Sodium leakage into space between inner and outer walls of primary tank	X		
21. Sodium cleanup system flow rate too low	X		
22. Sodium temperature at outlet from cold trap too high or too low	X		
23. Leakage from sodium cleanup system	X		
24. Coolant air flow at outlet from biological shield too low	X		
25. Coolant air temperature at outlet from biological shield too high	X		
26. Selected temperatures of biological shield too high	X		
27. Coolant temperature in shutdown cooler too low.	X		
28. Differential in pressure between inside and outside of Reactor Building too high	X		
29. Rotating plug seal temperature too high	X		
<u>Secondary System:</u>			
30. Loss of power to sodium pump	X		
31. Sodium flow rate too low or changing too rapidly	X		
32. Sodium temperature at superheater inlet too high or too low	X		
33. Sodium temperature at evaporator outlet too high or too low	X		
34. Sodium pressure at evaporator inlet too high or too low	X		
35. Sodium level in surge tank too high or too low	X		
36. Sodium level in storage tank too high or too low	X		
37. Sodium flow rate too high	X		
38. Sodium cleanup system flow rate too low	X		
39. Sodium temperature at outlet from cold trap too high or too low	X		
40. Surge tank sodium overflow rate too low	X		
41. Radioactivity level of sodium too high	X		
42. Loss of power to auxiliary pump	X		

Table VII (Cont'd.)

Abnormality	Alarm Only	Pre-Scram Warning Alarm	Scram and Alarm
<u>Steam System:</u>			
43. Evaporator water level too high or too low	X		
44. Steam pressure at superheater inlet too high or too low	X		
45. Circulating water pressure drop across condenser too low	X		
46. Loss of power to condensate pumps	X		
47. Condensate pump discharge pressure too low	X		
48. Water level in deaerator feed-water heater too low	X		
49. Loss of feed-water flow	X		
50. Steam temperature at outlet of desuperheater No. 1 too high	X		
51. Feed-water pressure at feed-water pump outlet too low	X		
52. Feed-water temperature too high or too low	X		
53. Steam system main relief valve open	X		
54. Condenser pressure too high	X		
55. Cooling tower water level too low	X		
56. Cooling tower water temperature too low	X		
57. Turbine oil pressure too low	X		
58. Turbine bearing temperature too high	X		
<u>Electrical System:</u>			
59. Generator stator temperature too high	X		
60. Generator rotor temperature too high	X		
61. Generator hydrogen pressure too low	X		
62. Generator differential relay operation	X		
63. Generator bearing temperature too high	X		
64. Generator bearing oil pressure too low	X		
65. Turbine-generator vibration	X		
66. Generator breaker automatic trip	X		
67. Main power transformer No. 1 breaker automatic trip	X		
68. Main power transformer No. 2 breaker automatic trip	X		
69. Bus tie breaker automatic trip	X		
70. ARBOR feeder No. 1 breaker automatic trip	X		
71. ARBOR feeder No. 2 breaker automatic trip	X		
72. TREAT (and misc.) breaker automatic trip	X		
73. Main 2400-volt auxiliary power transformer 13.8-kv breaker automatic trip	X		
74. Reserve 2400-volt auxiliary power transformer 13.8-kv breaker automatic trip	X		
75. Main 2400-volt auxiliary power transformer 2.4-kv breaker automatic trip	X		
76. Reserve 2400-volt auxiliary power transformer 2.4-kv breaker automatic trip	X		
77. Main 480-volt auxiliary power transformer 13.8-kv breaker automatic trip	X		
78. Reserve 480-volt auxiliary power transformer 13.8-kv breaker automatic trip	X		
79. Main 480-volt auxiliary power transformer 480-volt breaker automatic trip	X		
80. Reserve 480-volt auxiliary power transformer 480-volt breaker automatic trip	X		
81. Main bus (13.8-kv) voltage high	X		
82. Main bus (13.8-kv) voltage low	X		
83. Main bus frequency low	X		
84. Reserve 2400-volt auxiliary power transformer temperature high	X		
85. Reserve 2400-volt auxiliary power transformer oil level low	X		
86. Reserve 480-volt auxiliary power transformer temperature high	X		
87. Reserve 480-volt auxiliary power transformer oil level low	X		
88. Main power transformer No. 1 temperature high	X		
89. Main power transformer No. 1 oil level low	X		

Table VII (Cont'd.)

Abnormality	Alarm Only	Pre-Scram Warning Alarm	Scram and Alarm
<u>Electrical System (Cont'd.)</u>			
90. Main power transformer No. 2 temperature high	X		
91. Main power transformer No. 2 oil level low	X		
92. Main 2400-volt auxiliary power transformer temperature high	X		
93. Main 2400-volt auxiliary power transformer oil level low	X		
94. Main 480-volt auxiliary power transformer temperature high	X		
95. Main 480-volt auxiliary power transformer oil level low	X		
96. 125-volt d-c bus ground	X		
97. Battery charging M-G set breaker auto-trip	X		
98. Lighting automatic transfer switch operation	X		
99. Diesel-generator set water temperature high	X		
100. Diesel-generator set oil pressure low	X		
101. Diesel-generator set failure to start	X		
102. Primary coolant pump No. 1 rectifier: temperature high	X		
103. Primary coolant pump No. 1 rectifier: liquid cooling system pressure low	X		
104. Primary coolant pump No. 2 rectifier: temperature high	X		
105. Primary coolant pump No. 2 rectifier: liquid cooling system pressure low	X		
106. Primary coolant auxiliary pump rectifier: temperature high	X		
107. Primary coolant auxiliary pump rectifier; cooling system pressure low	X		
108. Control M-G set: rectifier input supply de-energized	X		
109. Primary coolant auxiliary pump: rectifier input supply de-energized	X		
110. Secondary system pump 2400-volt feeder breaker automatic trip	X		
111. Secondary system pump 480-volt feeder breaker automatic trip	X		
112. Secondary system auxiliary pump rectifier feeder breaker automatic trip	X		
113. Boiler feed-water pump breaker automatic trip	X		
114. Circulating water pump No. 1 breaker automatic trip	X		
115. Circulating water pump No. 2 breaker automatic trip	X		
116. Circulating water pump No. 3 breaker automatic trip	X		
<u>General</u>			
117. Smoke in Reactor Plant			X
118. Smoke in Sodium Plant or Boiler Plant	X		
119. Radioactivity level in Reactor Plant too high	X		
120. Air stack radioactivity level too high	X		
121. Inert gas storage tank pressure too low	X		

time, restricting rod movement to one rod at a time. At steady-state reactor operation, with the regulating rod on automatic control, one shim rod can be moved to permit adjusting the position of the regulating rod in the reactor.

During scram, the twelve control rods are ejected (downward) from the core by air pressure plus gravity. Rod release time, or time between receipt of scram signal at the rod drive and start of rod movement, is 0.008 sec. Rod displacement versus time after start of rod movement during scram is shown in Fig. 41. The relation between fraction of total rod worth effective and time after start of rod movement is shown in Fig. 42 for various values of initial rod insertion. Initial rod insertion is expected to be greater than 80 per cent under normal operating conditions.

The total reactivity worth of a single control rod is expected to be approximately  $0.005 \Delta k/k$ , and of all twelve rods, approximately  $0.06 \Delta k/k$ .

#### b. Safety Rod Characteristics

The safety rod locations within the reactor core are shown in Fig. 8. Construction of the rods is described in Section III.A.1.g; design and operation of the rod drive system are described in Section III.A.6. The relation between rod insertion and fraction of total rod worth effective is similar to the control rods (Fig. 40). Rod displacement versus time after start of rod movement is shown in Fig. 43. The fraction of total rod worth effective versus time after start of rod movement is indicated in Fig. 44. It is anticipated that the rod release time will not exceed 0.015 sec.

The total reactivity worth of the two safety rods is expected to be in the range from  $0.015$  to  $0.020 \Delta k/k$ .

#### c. Description of Instrumentation

Reactor neutron flux measurements are accomplished through ten channels of instrumentation. These channels are operated from ten neutron detectors disposed about the reactor and provided with gamma shielding as described in Section III-A-5. Measurement of neutron flux is employed for three general purposes, as follows:

(1) Monitoring of flux level and reactor period from source level through the power range.

(2) Initiate automatic scram of control rods, or drop-out of safety rods, whenever the power level exceeds a preset value or the reactor period becomes excessively short.

(3) Monitoring of flux level in the power range to enable automatic control of reactor power level.

Figure 45 is a block diagram of the nuclear instrumentation. The reactor power range covered by each of the channels is indicated on Fig. 46.

The Startup Range is covered by two identical fission counter channels (1 and 2) which indicate neutron flux level and period based on measurement of neutron pulse counting rate. Both linear and logarithmic indication of this level is provided. Period measurement for trip is also made. The trips are arranged so that either may cause scram; they are disconnected when the flux level exceeds the top of the channel range.

The Log Power Range is covered by channels 3 and 4, which are logarithmic level channels employing measurement of current from ionization chambers. These are wide-range channels, the range of which overlaps the top of the counter channel range and extends to a decade beyond full power. Log level indication is provided for general monitoring of reactor power level. Period measurement is derived for period indication and safety trip. The trips are arranged so that either may cause scram; they remain operative over the entire reactor power range.

The Linear Power Range is covered by channels 5 and 6, which are linear wide-range d-c amplifier channels which measure current from ionization chambers. The wide range is obtained by manual range switching. These channels are used for accurate indication of reactor power level and for control of the regulating rod. Also, these channels provide high-flux level trip with automatic adjustment of the trip level integral with the range switching. The trips are arranged so that either may cause scram; they are made inoperative (by shorting out) above about 50% power level.

Channels 7, 8, 9, and 10 are identical in range and employ d-c amplifiers which measure current from ionization chambers. These channels are used in the high-power range and for high-flux level trip only. The trips are arranged so that two trips are required for scram.

The safety trip provisions may be summarized as follows: a single period trip effects scram at any power level; a single high-level trip effects scram at levels up to about 50% power; two high-level trips (out of four) effect scram in the high power range.

To assure maximum reliability and regulation of the electrical power source for the nuclear instrumentation, a special motor-generator set with a floating battery power supply is provided as described in Section IV. A.6.f.

### e. Neutron Source

The neutron source is contained in a specially designed subassembly which is positioned within the inner row of the inner blanket. This subassembly may be loaded into the reactor in the same manner as an inner blanket subassembly and may be periodically replaced by a similar one. The source is approximately equal in length to and is located at the same elevation as the reactor core. The source material consists of a solid right circular cylinder of activated antimony inserted into a cylindrical sleeve of beryllium metal.

The antimony-beryllium neutron source is designed so that the detector sees a flux of the least  $100 \text{ n}/(\text{cm}^2)(\text{sec})$ . Calculations indicate that, after irradiation in the MTR, the source produces the required flux at the detector for a period of 60 days of zero power EBR-II operation. Any extended period of high-power operation would tend to lengthen the cycle. Continuous operation of the reactor at full power (62.5 mw) would keep the source strength essentially constant. Calculations further indicate that after 60 days of zero power operation the source neutron emission rate is  $1.6 \times 10^{10} \text{ n}/\text{sec}$  if the initial source strength is  $4.3 \times 10^{10} \text{ n}/\text{sec}$ .

## 3. Primary System

### a. Primary Coolant Loop

The reactor coolant outlet temperature is controlled by primary coolant flow rate regulation at the temperature required to maintain a constant steam temperature of 850F. At a power level of 62.5 mw of heat, the reactor coolant outlet temperature is 900F. Figure 47 shows the relationship between primary coolant flow rate, coolant outlet temperature, and reactor power level for constant steam temperature to the turbine throttle. Control of total flow is achieved by regulation of pumping power to each main pump.

The use of two main pumps operating in parallel increases the reliability of the primary coolant loop. With each pump providing 50% of the required flow, complete failure of one pump reduces the steady-state coolant flow rate through the reactor to about 46% of nominal. Under these conditions, the operative pump capacity increases by approximately 149% (at a reduced head), and about 63% of the total flow short circuits through the inoperative pump to the bulk sodium in the primary tank. Steady-state operation of the reactor at full power (62.5 mw) with only one pump operating results in an increase of about 210F in the maximum fuel alloy temperature.

A pump failure, however, causes immediate scram, and is indicated by an abrupt decrease in the following: current flow to the pump (if caused by a power failure), as well as fluid flow from the pump, and pump discharge pressure (irrespective of cause of failure). A pump failure is also indicated by a change in the upper plenum sodium temperature; this change, however, occurs much less rapidly than the others.

The primary cooling system is designed to promote good natural circulation of the primary coolant. The coolant forced and thermal convection flow direction are the same throughout the primary system. The sodium flow is up through the reactor and down through the shell side of the heat exchanger, which are the hot and cold legs, respectively, of the system. The main primary sodium pumps supply coolant to both the core and blanket regions; consequently, no flow reversals occur within the system during transition from forced to thermal convection flow. Furthermore, the auxiliary pump assures a minimum flow rate of about 500 gpm immediately following shutdown of the main pumps.

If an abnormality causing reactor scram occurs which includes not only loss of main pump flow, but loss of rectifier power to the auxiliary pump, then the auxiliary pump receives power from connected batteries. These batteries, which float fully charged on the line in parallel with the auxiliary pump rectifier, are always ready to deliver power to the auxiliary pump. Under such circumstances, the auxiliary pump supplies a coolant flow of about 500 gpm to the reactor immediately subsequent to the power failure with a decreasing flow rate as battery power degenerates. A plot of flow rate versus time for the auxiliary pump operating only on battery power is shown in Fig. 48. This system results in an adequate coolant flow rate through the system. The maximum fuel alloy temperature never exceeds the value obtaining at the time of scram.

It is planned to monitor the loop system conditions at the points indicated in Fig. 18. As control instrumentation is detailed, it will be designed for fail-safe operation.

(1) Flow: Five electromagnetic flowmeters (permanent magnet, induced current devices which generate output voltage proportional to average flow rate with essentially an instantaneous time response) are installed in the loop. The principal flow-measuring device for the primary coolant loop, is located in the outlet pipe from the reactor. This total reactor coolant flow measurement is continuously indicated and recorded in the control room. The indicating instrument is provided with an adjustable low-limit switch for scram. The other four flowmeters are located in the two inlets to the high-pressure coolant plenum and the two inlets to the low-pressure coolant plenum. These flows also are indicated and recorded in the control room, with adjustable low limit switches for scram.

Five conventional orifice flowmeters are provided in positions similar to the above. These are employed for calibration and backup of the electromagnetic flowmeters. All are indicated and recorded in the control room.

(2) Pressure: Pressure is measured at eight locations in the primary coolant loop: at the two main pump outlets; at points in the main pump lines just downstream from the pump "disconnects;" in each of the two inlet plenums; in the outlet plenum; and the heat exchanger inlet. Pressures are measured by pneumatic null-balance transmitters. All pressures are indicated in the control room. The three plenum pressures are continuously recorded, the recorders being provided with high- and low-pressure contacts for alarm indication in the case of the inlet plenums and for scram in the case of the outlet plenum.

(3) Temperature: Temperatures are measured in many locations in the primary coolant loop, three of which are critical: reactor inlet coolant temperature, reactor outlet coolant temperature, and heat exchanger outlet temperature. These temperatures are measured and continuously recorded in the control room. The recorders are provided with high- and/or low-temperature contacts for alarm, and for scram.

In addition to measuring the average reactor outlet coolant temperature, numerous thermocouples are located in the upper plenum to sense sodium temperature at the outlets of various subassemblies. Selected temperatures are indicated and recorded in the control room, the recorders being provided with adjustable high contacts for alarm and for scram; the others are scanned, and temperatures of particular interest are indicated in the control room.

Additional thermocouples are located at various positions in the primary coolant loop; these are selection-indicated in the control room.

b. Primary Tank

The elements of the primary tank which involve instrumentation or control are the tank vessel and the shutdown coolers.

(1) Flow: An electromagnetic flowmeter is installed in the cold leg of each of the two shutdown coolers. The flow rates are indicated in the control room.

(2) Pressure: A pressure transmitter is installed in the primary tank inert gas blanket. The indicating instrument is provided with high and low adjustable contacts for alarm indication and an adjustable high contact for scram and alarm.

(3) Temperature: A thermal-sensing element is installed inside the tank in the inert gas blanket. In the remote event of high gas temperature resulting from fire inside the tank (caused by serious air leakage), indication and alarm are effected.

NaK temperatures are measured in the inlet and outlet legs of each shutdown cooler. The inlet leg temperatures are continuously indicated in the control room on indicating instruments provided with an adjustable low contact for alarm indication.

Numerous thermocouples are located throughout the tank vessel structure. About six of these temperatures are continuously indicated in the control room; another dozen are selection-indicated; the remainder are made available at a terminal block in the reactor building.

(4) Sodium Level: Two sodium level detectors are installed in the bulk sodium of the primary tank. The bulk sodium level measured by one of these detectors is continuously indicated and recorded in the control room. Indication only is provided by the other. Both instruments are provided with high and low contacts for alarm indication.

c. Biological Shield

(1) Flow: An air flowmeter is installed in the shield cooling system. The air flow rate is continuously indicated in the control room. Adjustable low contacts are provided for alarm indication.

(2) Temperature: A thermocouple well is installed at the outlet of the shield cooling duct. The outlet air temperature is continuously indicated in the control room. An adjustable high contact is provided for alarm indication.

Numerous thermocouples are located throughout the upper tank structure and the radial shield. Three of these are continuously indicated in the control room; adjustable high contacts are provided for alarm indication. The remainder are made available for selection-indication or at a terminal block in the reactor building.

d. Sodium Cleanup System

(1) Flow: An electromagnetic flowmeter is installed in the sodium cleanup recirculation line. The flow rate is continuously indicated in the control room. The indicator is provided with an adjustable low contact for alarm indication.

(2) Temperature: Temperature is measured at the outlet of the cold trap. This temperature is continuously indicated in the control room. The indicator is provided with adjustable high and low contacts for alarm indication.

#### 4. Secondary System

A description of the secondary system, is given in Section III-B; system conditions are measured at the points indicated in Fig. 18.

##### a. Flow

An electromagnetic flowmeter is installed in the pump discharge line. The sodium flow rate is continuously indicated and recorded in the control room. The indicating instrument is provided with high and low flow adjustable limit switches for alarm indication. An orifice-type flowmeter, with indication in the Sodium Plant Building, provides calibration and backup for the electromagnetic flowmeter.

Flow in the sodium cleanup system is continuously sensed and is indicated in the control room. Alarm is initiated by low flow condition.

##### b. Pressure

Pressure is sensed at nine locations in the secondary loop. Indication and alarm are provided locally and in the control room for pump inlet, pump discharge, differential across the pump, and gas blanket pressure. Recording, indication, and alarm are provided in the control room only for inlet and outlet of heat exchanger, superheater inlet, and inlet and outlet of evaporator.

Pressure of the sodium cleanup system is indicated locally, with alarm provision in the control room.

##### c. Temperature

Seven thermocouple wells are installed in the loop. The temperatures at the inlet and the outlet of the superheater, at outlet of the evaporator, and at the inlet and outlet of the heat exchanger are continuously recorded in the control room. The recorders for the superheater inlet and evaporator outlet temperatures are provided with adjustable high and low contacts for alarm indication.

The sodium cleanup system cold trap temperatures are continuously indicated in the control room with high and low contacts for alarm indication.

##### d. Sodium Level

Two sodium level detectors are installed, one in the surge tank at pump inlet and one in the storage tank. Both levels

are continuously indicated in the control room. The indicators are provided with adjustable high and low contacts for alarm indication.

## 5. Steam System

The steam system is designed to:

- (1) provide a reliable constant temperature heat sink for the power produced by the reactor;
- (2) provide certain special system features to enhance the reliability of the sodium-to-water steam generation equipment; and,
- (3) employ conventional steam system practice and to achieve reasonable thermal efficiency for the steam conditions available.

The steam generator provides a constant temperature heat sink by maintaining steam pressure constant under all conditions. Steam pressure is regulated by an automatic controller in the steam by-pass line as indicated on Fig. 1. The capacity of the steam by-pass system is equal to the capacity of the steam generator; the full-power steam production can be condensed independent of the turbine generator. The by-pass steam passes through pressure-reducing stations prior to entering the condenser.

To minimize thermal shock and thermal stresses in the evaporator section of the steam generator, the feed water is heated to a temperature of 550F (saturation temperature is 580F). Flexibility of operation of the steam system is provided to accomplish feed-water heating under the various available methods of plant operation. Feed-water heaters No. 1 and 3 are supplied with extraction steam from the turbine when it is operating at, or near, full load. Heater No. 4 receives steam direct from the main steam line to provide 550F feed water to the evaporator. Heater No. 2 (deaerator) is supplied from the auxiliary turbine drives boiler feed pump.

At low load or no load on the turbine, steam is supplied to heaters No. 1 and No. 3 from PRV-desuperheating stations or flash tanks. This system provides reasonable cycle efficiency under normal turbine operation, and essentially constant feed-water temperature at all loads irrespective of turbine operation.

To provide the degree of reliability desired in the steam system, it is arranged to isolate the reactor from turbine-generator load variations. The turbine generator normally will be electrically paralleled with the NRTS 138-kv loop; consequently, electrical load variations will be minimized. To provide available steam to absorb minor load variations,

a small quantity of steam is by-passed around the turbine at all times. The amount of by-pass steam required to absorb the maximum load variations must be determined by actual operational experience, but the by-pass system is capable of handling up to 100% of the steam generated. (For purposes of establishing a heat balance, a by-pass flow of 5,000 lb/hr was assumed at full load.)

Steam system conditions are monitored at the points indicated in Fig. 18.

a. Pressure

Steam pressure is measured at the turbine throttle and continuously indicated in the control room. The recorder is equipped with adjustable high- and low-pressure contacts for alarm indication. A signal from this pressure transmitter is also employed to regulate the steam by-pass control valve which maintains constant pressure in the main steam supply line. Pressure is also measured at the feed-water pump outlet and the condensate pump outlet. These pressures are indicated in the control room, with low-pressure contacts for alarm indication.

b. Flow

Feed-water flow is measured and indicated in the control room, with a low-flow contact for alarm indication. Water level in the deaerator feed-water heater and in the evaporator are also measured and indicated in the control room with high- and/or low-level contacts for alarm indication.

c. Temperature

Feed-water temperature is measured at the outlet of the feed-water heater No. 4, and is continuously recorded in the control room. The recorder is provided with high- and low-level contacts for alarm indication.

Various additional temperatures and pressures are measured in the steam system to permit satisfactory operation of this system. The more important of these are indicated in Table VII, and follow conventional steam system practice; they are provided with alarm indication, but are not critical to reactor operation.

6. Electrical System

a. General

The planned design features and the major electrical equipment and feeder arrangement comprising the EBR-II power generating

and distribution system are shown in Fig. 49. System details are included to better describe the type of plant control contemplated.

All equipment, apparatus, components, devices and materials incorporated in the design conform to the standards of the American Standards Association, the American Institute of Electrical Engineers and/or the National Electrical Manufacturers Association.

b. Main Operating Features of the Electrical System

The EBR-II Facility is arranged for parallel operation with the Utility Power System, with two (2) full-capacity ties to the National Reactor Testing Station (NRTS) 138-kv power loop. The 138-kv power loop is a normally closed loop; it is served from two Utility System transmission lines, one on each side of the 138-kv loop sectionalizing oil circuit breaker #10 in the EBR-II main outdoor substation. The main power transformers are of the load-ratio-control type, each with a 12,000/16,000 kva, OA/FA rating. Thus, two sources of 138-kv power supply will be available for the EBR-II, for two experimental reactor facilities (ARBOR and TREAT), and for other experimental facilities. When the EBR-II generator is operating in parallel with the Utility System, three sources of 13.8-kv power supply exist. A fourth source of power (for EBR-II only) is provided by an automatic starting 480-volt, 3-phase, 60-cycle emergency diesel-generator set for the operation of essential or critical auxiliary loads, such as the shield cooling exhaust blowers, inert gas circulating system, reactor fuel transfer system drives, sodium cold trap pumps, emergency lighting, instrument controls, etc. The emergency diesel generator set is arranged to operate only after there is sustained outage of the three aforementioned 13.8-kv sources of power supply. The rated total elapsed no-voltage time for the diesel-generator set to be started, come up to speed and take the load, is 15 to 20 seconds. (The diesel-generator set is equipped with its own starting battery.)

The EBR-II Facility has a generating capacity of approximately 20,000 kw. The estimated load distribution, based on estimated load requirements for planned Site 16 facilities, is approximately as follows:

EBR-II Auxiliaries	3500 kw		EBR-II Auxiliaries	3500 kw
ARBOR	7500		ARBOR (reduced	
TREAT	200	or	operation)	1350
Future Area Loads	800		TREAT (reduced	
Into 138-kv System	8000		operation)	100
			Future Area Loads	
Total	20,000 kw		(reduced operation)	500
			Into 138-kv System	14,550
			Total	20,000 kw

To provide a maximum of continuity of power supply, and to minimize the number of reactor scrams, particularly when EBR-II is operating without benefit of its generator being used, normal operation of the EBR-II Facility is to be with the bus tie breaker #105 closed. This provides continuity of power supply, without momentary interruption, on the various branch feeders of the 13.8-kv switchgear in the event one of the 138/13.8-kv tie circuits to the 138-kv power loop becomes disconnected.

Furthermore, normal operation of the EBR-II Facility is to be with the generator connected to the 138-kv loop. The design provides for this connection also to be maintained without momentary interruption through a disturbance on the 138-kv system, wherein the loop is faulted on one side of the loop sectionalizing breaker #10, resulting in the disconnection of one of the main power transformers from the 13.8-kv bus.

In the event both sides of the 138-kv loop are lost, breakers #104 and #106 both trip automatically to disconnect the 13.8-kv bus from the faulted loop. However, the generator breaker #100 remains closed to maintain operation of the EBR-II auxiliaries and other loads on the 13.8-kv bus. Assuming that power was being delivered from EBR-II to the 138-kv system when this occurred, an amount of steam corresponding to the power which was being delivered to the 138-kv system would be automatically by-passed to the condenser. On the other hand, if the load on the generator is increased appreciably as a result of separation of the two systems, the generator breaker would be tripped by an under-frequency relay on the 13.8-kv bus, unless the load were reduced in time to prevent tripping.

Normal operating procedure will be to deliver some power into the 138-kv system; therefore, in the majority of cases there will be a sufficiency of steam to accommodate the loads on the 13.8-kv bus.

In anticipation of possible severe operating conditions, wherein the nature of the experiments requires or results in erratic operation of the EBR-II generator and/or the ARBOR loads, advantage will be taken of the flexibility of control inherent in the 13.8-kv system. Accordingly, to minimize disturbances between EBR-II and ARBOR during such operation, the bus tie breaker #105 would be kept open; EBR-II would then be connected to the 138-kv loop through breaker #104 (breakers #101, #107 and #108 would be kept open). ARBOR and TREAT would be supplied from the 138-kv loop through breaker #106 and through breakers #109 and #110, respectively.

As indicated in Fig. 49, the 2400-volt and 480-volt auxiliary power requirements for the EBR-II Facility are furnished respectively through 13.8/2.4-kv and 13.8/0.48-kv full capacity auxiliary power transformers on either side of the bus tie circuit breaker in the 13.8-kv switchgear.

The lighting load is supplied from the 480/120-208-volt, 60-cycle, 3-phase, distribution transformer via the 120-208-volt bus of the a-c/d-c distribution cubicle. Lighting for the Process Plant is supplied locally from a separate 480/120-208-volt, 3-phase, 60-cycle distribution transformer.

Emergency lighting for the entire facility is supplied from the emergency 120-volt bus of the a-c/d-c distribution cubicle which is automatically transferred to the station battery upon failure of the normal a-c supply.

All motors rated less than 1/2 hp are for 110-volt, single-phase, 60-cycle operation or for 440-volt, 3-phase, 60-cycle operation. Motors rated 1/2 hp to 125 hp are for 440-volt, 3-phase, 60-cycle operation. All larger motors are for 2400-volt, 3-phase, 60-cycle operation. In general, motors are normal torque motors of the drip-proof type. Motors for outdoor service or for operation in moist atmospheres are of the totally enclosed, fan-cooled type. Drainage plugs are provided in the end shields of the totally enclosed motors.

In general, across-the-line starters are employed; 110-volt, single-phase, 60-cycle control is obtained from an individual unfused control transformer connected to the line side of each magnetic starter.

#### c. Generator and 13.8-kv Switchgear

The steam turbine driven generator is of conventional hydrogen-cooled, non-salient pole design, rated 20,000 kw, 13,800 volts, 3-phase, 60-cycle, 0.85 power factor, with a direct connected exciter. The generator is equipped with all standard auxiliaries and accessories, including an oil-lubrication system, hydrogen cooling system, turning gear, overspeed switch, tachometer, temperature detectors, etc.

A continuously acting automatic voltage regulator of the rotating regulator type is incorporated in the design.

The 13.8-kv metal clad switchgear consists of 1200-ampere, 3-P.S.T. circuit breakers with an interrupting capacity of 500,000 kva. The circuit-breaker-closing solenoids and shunt-tripping devices are for 125-volt d-c operation and are served from a station battery.

#### d. Station Battery

A 125-volt station storage battery of sufficient ampere-hour capacity is included to serve the various electrically-operated circuit breakers, certain instrumentation and indicating lights, and the emergency

lighting loads for the entire facility. A battery-charging motor-generator set is included for trickle charging and for equalizing charging of the battery and to relieve the battery of its load during sustained emergency lighting service.

e. Relay Protection for the Electrical System

A coordinated protective relaying system prevents excessive damage to the faulted or defective element and isolates it from the system with minimum disturbance to power supply. Included in the protective relaying system are the following features: (a) bus differential protection, (b) generator differential protection, (c) main power transformer differential protection, and (d) numerous other relays for the protection of the generator, the various transformers, feeders, etc., all in accordance with the best established practice for power plants and distribution systems.

f. Instrumentation and Control

The instrumentation and control for the electrical system, except for the 138-kv system, are centralized on panel boards in the Control Room (located in the Power Plant).

Power for control and instrumentation of the reactor and heat transfer systems is provided by a continuous power supply system consisting of a metallic rectifier, a standby (floating) battery and d-c motor-a-c generator M-G set.

g. Continuous Power Supply for the Primary Coolant System Auxiliary Pump

To assure maintained operation of the 500-gpm auxiliary d-c electromagnetic pump in the primary coolant system, a metallic rectifier and floating storage battery arrangement (Fig. 49) is provided. With loss of a-c power to the rectifier, the floating battery maintains uninterrupted operation of the pump (at a decreasing pump rate) for a period of approximately 30 min. It is unlikely, however, that the duration of battery-powered pump operation will exceed 15 or 20 seconds, since power supply to the rectifier should be restored with the automatic starting of the emergency diesel-generator set.

The knife switch shown in Fig. 49 is provided for disconnecting the battery from the auxiliary pump to protect the battery after the emergency operation period is completed.

For normal startup of the pump (from the rectifier) the knife switch is in its open position. After the pump is operating,

the knife switch is closed to "float" the battery on the line. An auxiliary contact is provided on the knife switch to prevent startup and operation of the reactor when the battery is disconnected.

h. Electrical Safety Features

The electrical system is designed to achieve simplicity of operation, ease of maintenance, and safety to equipment and personnel. The control circuits for related operations of equipment are interlocked, insofar as possible, to prevent improper sequence of operation due to human error. The safety features of the electrical system include the following listed items:

(1) All circuit breakers have adequate interrupting capacity and are trip-free.

(2) Provisions are made for padlocking the circuit breakers in the "test" position. The circuit breakers in the motor control centers have provision for padlocking same in the open position.

(3) An individual unfused control transformer is provided with each magnetic starter for 110-volt control.

(4) The position of operating handles, levers, etc., clearly indicate to the operator whether the breaker is open or closed.

(5) Cables for the 13.8-kv circuits have a 15-kv ungrounded neutral system voltage rating.

(6) Cables for 2400-volt circuits have a 5000-volt rating.

(7) Instruction nameplates are installed where specific instruction or precaution is essential.

(8) Complete ground bus systems are provided in each of the buildings for the convenient grounding of electrical equipment enclosures, motor frames, conduit systems, etc.

(9) Lightning protection for all buildings is provided in accordance with U.S. Department of Commerce "Code for Protection Against Lightning," Handbook 46.

## B. Normal Steady-State Operation

This section describes the full power (62.5 mw) operating conditions of the power system.

### 1. Flux Distributions

#### a. Neutron Flux

The neutron flux distribution is obtained on the basis of multigroup diffusion theory. Such a distribution determines the power and gamma-ray distributions throughout the system.

The reactor is an essentially heterogeneous system and contains many inherent asymmetries which are not easily adapted to rigorous analysis. To obtain a description of the nuclear behavior of the system, more than one model must be devised to represent realistically the system of interest. In all models, a virgin reactor is assumed, with no fission products or plutonium. The core loading employs enriched uranium; the blanket loadings employ depleted uranium.

#### (1) Two-Dimensional, Two-Group Analysis

Figure 50 describes the model used to perform a two-dimensional, two-energy group diffusion theory analysis of the system. This model does not include the minor axial asymmetries inherent in the design. Neither does it include the radial asymmetries due to the presence of control rods. Many of these geometric deviations have been approximately accounted for by a suitable averaging process. The analysis of the system shown in Figure 50 does give an over-all neutron flux distribution, especially throughout the blanket regions. The latter cannot be accurately obtained by simpler, one-dimensional analytical techniques.

In the analysis, the two-energy groups assumed are such that Group I represents neutrons above, and Group II represents neutrons below, the  $U^{238}$  fission threshold. This indicates that neutrons having energies greater than 1.35 Mev fall into Group I while all others fall into Group II.

Figures 51 and 52 give radial distributions for the high energy (Group I) flux for the indicated values of  $z$ , the axial distance from the center of the core. (The identification of the region is that corresponding to the plane  $z = 0$  or the line  $r = 0$ .) Figures 53 and 54 give radial distributions for the low energy (Group II) flux for the indicated values of  $z$ .

Figures 55 and 56 give axial distributions for the high-energy flux for the indicated values of  $r$ , the radial distance from the center of the core in  $z = 0$  plane. Figures 57 and 58 give axial distributions for the low-energy flux for the indicated values of  $r$ .

For this analysis, the following calculated parameters apply at the center of the core ( $z = 0, r = 0$ ).

Power Density	PD = 1.37 mw liter of core volume
Total Number of Fissions	$\int_E \Sigma_f \phi dE = 4.4 \times 10^{13}$ fissions/(cc)(sec)
High Energy Neutron Flux (above 1.35 Mev)	$\phi_1 = 0.8 \times 10^{15}$ n/(cm <sup>2</sup> )(sec)
Low Energy Neutron Flux (below 1.35 Mev)	$\phi_2 = 2.9 \times 10^{15}$ n/(cm <sup>2</sup> )(sec)
Total Neutron Flux	$\phi = 3.7 \times 10^{15}$ n/(cm <sup>2</sup> )(sec)

## (2) One-Dimensional, Ten-Group Analysis

In addition to the two-energy group analysis, a ten-energy group analysis using one-dimensional techniques is available to show the spatial behavior of the neutron flux, principally in the radial direction near the  $z = 0$  plane and axially near the line  $r = 0$ .

Figure 59 shows the reactor model which was analyzed with these techniques. One of the principal results found in this multi-group analysis which is not readily obtained on the basis of the two-group calculations is concerned with the spatial variation of the neutron spectrum.

For simplicity in graphical representation, the ten-energy groups have been combined so that only five groups of neutrons are shown in Figs. 60 and 61. These groups represent neutrons in the energy intervals tabulated below.

<u>Group</u>	<u>Energy Interval, Mev</u>
1	Above 1.35
2	0.5 to 1.35
3	0.18 to 0.5
4	0.07 to 0.18
5	0 to 0.07

Figure 60 shows the radial distribution of the neutron flux near the  $z = 0$  plane. Figure 61 shows the axial distribution of the

neutron flux near the line  $r = 0$ . It is to be noted that the spectrum is degraded appreciably along any traverse outward from the center of the core.

For the multigroup analysis, the predicted parameters for the center of the core ( $z = 0, r = 0$ ) are:

Power Density	PD = 1.37 mw/liter of core volume
Total No. of Fissions/(cc)(sec)	$\int_E \Sigma_f \phi dE = 4.4 \times 10^{13}$ fissions/(cc)(sec)
Neutron Flux (above 1.35 Mev)	$\phi_1 = 8.0 \times 10^{14}$ n/(cm <sup>2</sup> )(sec)
Neutron Flux (0.5 to 1.35 Mev)	$\phi_2 = 10.5 \times 10^{14}$ n/(cm <sup>2</sup> )(sec)
Neutron Flux (0.18 to 0.5 Mev)	$\phi_3 = 11.1 \times 10^{14}$ n/(cm <sup>2</sup> )(sec)
Neutron Flux (0.07 to 0.18 Mev)	$\phi_4 = 6.2 \times 10^{14}$ n/(cm <sup>2</sup> )(sec)
Neutron Flux (0 to 0.07 Mev)	$\phi_5 = 1.9 \times 10^{14}$ n/(cm <sup>2</sup> )(sec)
Total Neutron Flux	$\phi = 3.77 \times 10^{15}$ n/(cm <sup>2</sup> )(sec)

#### b. Gamma Flux

Figure 62 shows the gamma-ray flux distribution from the core edge radially outward through the concrete biological shield. This analysis is based on a twenty energy-group neutron flux calculation in spherical geometry. Similarly, Fig. 63 shows the gamma-ray flux distribution from the edge of the core axially upward through the upper biological shield in the rotating plug.

Heating due to gamma rays has been calculated at various points within the reactor. The points of interest are principally those where the contribution of such heating could represent an appreciable fraction of the total heat generation. The calculated parameters based on energy absorption coefficients associated with five energy groups are listed below. For comparison, the energy created at these points is also given.

	kw/liter	
	<u>Gamma Ray Heating</u>	<u>Local Fission Energy Release Rate</u>
Inner edge of inner blanket ( $z = 0$ )	37.0	132.0
Outer edge of inner blanket ( $z = 0$ )	5.7	18.4
Lower edge of upper blanket ( $r = 0$ )	31.0	32.5

The axial variation of the gamma-ray heat generation in the inner blanket adjacent to the core has been estimated. In general, this variation follows the axial power distribution in the core adjacent to the inner blanket.

## 2. Reactor Heat Generation Distributions

An approximate breakdown of power generation in the various zones of the "clean" reactor is given below.

<u>Zone</u>	<u>Power, mw</u>	<u>% of Total</u>
Core	53.3	85.4
Upper plus lower blanket	1.2	1.9
Inner blanket	5.2	8.3
Outer blanket	2.6	4.1
Neutron shield	.2	0.3
	<u>62.5</u>	<u>100.0</u>

The radial power density distribution at the center plane of the reactor is shown in Fig. 64. This distribution is based on 82% insertion of each of the twelve control rods and 100% insertion of the two safety rods. In the control rod and safety rod regions of Fig. 64, two power density distribution curves are presented. The dashed line shows the anticipated power densities in control or safety subassemblies; the solid line indicates the power densities expected in the core subassemblies within these regions.

The radial maximum to average power density ratio of the core at the reactor center plane is 1.33; the effective radial maximum to average ratio over the entire height of the core is 1.32.

The axial power density distributions at the centerline of the core, inner edge of the inner blanket, and inner edge of the outer blanket are shown in Fig. 65.

The axial maximum to average power density ratio at the inner edge of the inner blanket is 3.45; at the inner edge of the outer blanket, 2.84.

The axial maximum to average ratio at the centerline of the core for the core section only is 1.17. The effective axial maximum to average ratio over the entire radius of the core for the core section only is 1.16.

Maximum power density in the core is 1.37 mw/liter of core volume. Average power density in the core is 0.893 mw/liter. The ratio of maximum to average power density in the core is 1.53.

These power densities and distributions are based on the clean reactor; however, analysis indicates that only small changes in heat generation distribution are effected by core burnup and plutonium formation, and these changes have been allowed for in calculation of maximum fuel and blanket temperatures. They also include the contributions of local absorption of gamma rays noted in Section IV-B-1-b.

### 3. Reactor Temperature Distribution

The maximum mean reactor outlet coolant temperature achievable in a given reactor for specific maximum permissible fuel and blanket alloy temperatures is a function of various parameters; for example: reactor inlet coolant temperature, reactor power level, and the coolant distribution. In general, to attain high mean coolant outlet temperature at a practical coolant inlet temperature and high reactor power, it is necessary to orifice the coolant flow to certain of the subassemblies; that is, it is necessary to establish the proper coolant mass flow distribution. Achievement of this distribution in the EBR-II requires orificing of all subassembly rows except rows 1, 2, and 3 (numbered radially outward from the center of the core). In most cases, the various rows require orificing of different degrees, since different amounts of power per subassembly are generated in the various rows. The degree of orificing employed in each row is based on one or more of these limitations (depending upon the row): maximum permissible fuel alloy or blanket uranium temperature; maximum permissible coolant temperature at subassembly outlet; minimum acceptable orifice size.

In addition to flow distribution, another consideration affecting calculated temperature distributions within the reactor is the degree of uncertainty associated with each of the quantities (such as thermal conductivity value, heat transfer coefficient, power density level, etc.) entering into the temperature calculations. If each quantity is analyzed separately, a degree of uncertainty can be estimated and a factor assigned. The magnitude of this "uncertainty factor" expresses the degree of uncertainty associated with the magnitude of the quantity. The various calculated temperature differences are increased by multiplication by the appropriate uncertainty factors. For example, if the "uncertainty factor" associated with the heat transfer coefficient is 1.20, which means that the heat transfer coefficient cannot be predicted to better than  $\pm 20\%$ , the nominal film temperature drop,  $\theta$ , is increased by 20% to  $1.20 \theta$ . Thus, in many of the figures referred to in this section, two temperature curves for the same conditions are shown: one which includes the use of uncertainty factors in the calculations, and one which does not. The uncertainty factors employed are listed in Table VIII. The temperature distributions which involve the use of these factors are considered very conservative. The temperature distributions based on nominal calculations (without uncertainty factors) are those more representative of the average conditions expected to exist within the reactor.

Based on the above considerations, each type of fuel and blanket element is designed to cool under the most severe conditions to which that type of element is exposed. The most severe conditions within each major reactor zone occur in the first, sixth, and eighth subassembly rows (center line of core, inner edge of the inner blanket, and inner edge of the outer blanket, respectively). The axial power density distributions at these locations are shown in Fig. 65.

Radial temperature distributions through a fuel element at the point of maximum fuel alloy temperature in the reactor are shown in Fig. 66. The effect of uncertainty factors on temperature distribution is apparent.

Axial distributions of the maximum fuel alloy and blanket uranium temperatures and coolant temperatures are shown in Figs. 67, 68, and 69.

The power output per subassembly in each row is shown in Fig. 70. The coolant flow rate per subassembly distribution is shown in Fig. 71. The mixed mean coolant temperature rise through each subassembly is shown in Fig. 72.

Table VIII

UNCERTAINTY FACTORS USED IN THERMAL ANALYSIS OF FUEL AND BLANKET ELEMENTS

	$F_{\Delta T}$	$F_{\theta_f}$	$F_{\theta_c}$	$F_{\theta_b}$	$F_{\theta_u}$
<u>Nuclear and Mechanical Factors:</u>					
Precision in Neutron Flux Distribution	1.10	1.15	1.15	1.15	1.15
Precision of Total Coolant Flow Rate Through a Subassembly	1.03	1.00	1.00	1.00	1.00
Precision of Coolant Velocity Profile Within a Subassembly	1.05	1.00	1.00	1.00	1.00
Manufacturing Deviations from Nominal (Dimensions)	1.00	1.02	1.06	1.00	1.02
Manufacturing Deviations from Nominal (Fissionable Material Concentration)	1.00	1.02	1.02	1.02	1.02
<u>Thermal Factors:</u>					
Thermal Conductivity Value	1.00	1.00	1.10	1.10	1.15
Heat Transfer Coefficient	1.00	1.20	1.00	1.00	1.00
<u>Operational Factors:</u>					
Precision of Measurement of Power Level	1.02	1.02	1.02	1.02	1.02
Possible Transient Overload	<u>1.05</u>	<u>1.05</u>	<u>1.05</u>	<u>1.05</u>	<u>1.05</u>
<u>Total</u>	1.27	1.54	1.46	1.38	1.48
<u>2/3 Factor</u>	1.18	1.36	1.31	1.25	1.32

Table IX gives pertinent temperatures, heat fluxes, and coolant flow rates in subassemblies of rows 1, 6, and 8. Uncertainty factors are not included. Table X gives the same information as Table IX, but with uncertainty factors included.

Table IX

SUMMARY OF THERMAL ANALYSIS RESULTS FOR MAXIMUM TEMPERATURE  
REGION OF CORE AND BLANKETS

(No Uncertainty Factors Included)

(Reactor Power = 62.5 mw)

	Region			
	Core	Upper Blanket	Inner Blanket	Outer Blanket
<u>Coolant Flow in Maximum Power Subassembly</u>				
Flow Velocity, fps	25.8	25.2	10.4	2.6
Flow Rate, gpm	152.1	152.1	19.6	4.9
Estimated Pressure Drop, psi	23.0	9.0	24.2	1.7
<u>Maximum Heat Flux, Btu/(hr)(ft<sup>2</sup>)</u>	1,034,000	78,800	285,900	30,200
<u>Temperatures, F</u>				
Maximum Uranium	1189	974	1024	829
Coolant, at Outlet	923	925	884	829
Coolant, at Inlet	702	923	700	700
Coolant Temperature Rise, Inlet to Outlet	221	2	184	129
Coolant at Point of Maximum Uranium Temperature	863	923	824	829
Mixed Mean Coolant Outlet Temperature from Entire Region	918	921	845	790
<u>Temperature Difference at Point of Maximum Uranium Temperature, F</u>				
Through Uranium	183	31	142	0
Through Uranium-Sodium Interface	13	1	3	0
Through Sodium "Bond" Layer	14	1	7	0
Through Sodium-Clad Interface	11	1	3	0
Through Clad Layer	63	12	35	0
Through Coolant Film	42	5	10	0
Total Element Temperature Difference	326	51	200	0

The information given in Tables VIII, IX, and X and the power density distributions given in Figs. 64 and 65 are based on fuel and blanket elements as described in Sections III-A-1-c, d, and e, and shown in Figs. 10, 11, and 12. The following reactor conditions, thermal property values, and heat transfer assumptions are employed:

Reactor Conditions:

- (1) Total reactor power - 62.5 mw
- (2) Mean coolant outlet temperature - 900F
- (3) Coolant inlet temperature - 700F
- (4) Maximum pressure drop across subassemblies - 41 psi

Table X

SUMMARY OF THERMAL ANALYSIS RESULTS FOR MAXIMUM TEMPERATURE  
REGIONS OF CORE AND BLANKETS

(Including Uncertainty Factors)

(Power = 62.5 mw)

	Region			
	Core	Upper Blanket	Inner Blanket	Outer Blanket
<u>*Coolant Flow in Maximum Power Subassembly</u>				
Flow Velocity, fps	25.8	25.2	10.4	2.6
Flow Rate, gpm	152.1	152.1	19.6	4.9
Estimated Pressure Drop, psi	23.0	9.0	24.2	1.7
<u>*Maximum Heat Flux, Btu/(hr)(ft<sup>2</sup>)</u>	1,034,000	78,800	285,900	30,200
<u>Temperatures, F</u>				
Maximum Uranium	1320	1030	1100	852
Coolant, at Outlet	963	965	917	852
Coolant, at Inlet	702	963	700	700
Coolant Temperature Rise, Inlet to Outlet	261	2	217	152
Coolant, at Point of Maximum Uranium Temperature	892	963	842	852
<u>*Mixed Mean Coolant Outlet Temperature from Entire Region</u>	918	921	845	790
<u>Temperature Differences at Point of Maximum Uranium Temperature, F</u>				
Through Uranium	243	40	186	0
Through Uranium-Sodium Interface	13	1	3	0
Through Sodium "Bond" Layer	18	2	9	0
Through Sodium-Clad Interface	11	1	3	0
Through Clad Layer	84	16	45	0
Through Coolant Film	59	7	12	0
Total Element Temperature Difference	428	67	258	0

\*No uncertainty factors included.

Thermal Properties:

(1) Thermal conductivities (at operating temperature of hottest fuel element):

<u>Material</u>	<u>Btu/(hr)(ft)(F)</u>
Fuel alloy (5 wt-% fission) or blanket uranium, after 1 atom-% burnup	18.8
Stainless Steel, AISI Type 304	11.5
Bond Sodium	40.3

(2) Coolant thermal properties: from the Liquid-Metals Handbook, Sodium-NaK Supplement, 1 July 1955, AEC - Department of the Navy (TID-5277).

To be conservative, the thermal conductivity of the blanket uranium is assumed equal to that of the fission fuel alloy. The fuel alloy conductivity value is based on interpolation and extrapolation of data given in BMI-986, BMI-984, and a private communication from H. Deem of BMI to L. Basil of APDA. It appears that increasing the burnup to 2 atom per cent would affect this value only slightly. The thermal conductivity of stainless steel Type 304 is taken from the Metals Handbook, 1948 Edition, American Society for Metals.

Heat Transfer Assumptions:

(1) Sodium heat transfer coefficients are based on the relation suggested in "Comments on Liquid Metals as Coolants in High Power Density Power Reactors," by H. O. Monson (TID-7506, Part I, July, 1956). The relation is  $Nu = 2.3 + 0.23 Pe^{1/2}$ .

(2) All heat is generated within the fuel alloy or blanket uranium.

(3) Uniform rate of heat generation per unit volume exists throughout a given cross section of a fuel pin or blanket pin.

(4) Power densities within those subassemblies of the inner and outer blankets which experience the highest temperatures in their respective zones are assumed 7% higher than indicated in Section IV-B-2. This is to allow for the effects of plutonium buildup.

(5) Interfacial conductance between sodium bond and clad or fuel is 100,000 Btu/(hr)(ft<sup>2</sup>)(F).

- (6) No axial heat conduction occurs.
- (7) No radial heat conduction occurs between subassemblies.
- (8) Uniform coolant flow velocity exists within a sub-assembly.

#### 4. Power Cycle Operating Conditions

The contemplated steady-state operating temperatures and coolant flow rates in the principal heat transfer systems at full power are shown in Fig. 1, and described below.

##### a. Primary System

The primary sodium coolant flow rate through each of the main d-c electromagnetic pumps is approximately 4250 gpm; total flow is about 8500 gpm. The flow separates into two streams before entering the reactor lower plenum chambers; a high-pressure stream flows to the plenum supplying the core and inner blanket, and a very low-pressure stream (pressure reduction being effected by orificing of the inlet piping) flows to the plenum supplying the outer blanket. Flow through the reactor totals 8200 gpm, the remaining 300 gpm representing leakage back to the primary tank bulk sodium through the ball-seat disconnects and the sub-assembly hold-down devices. Of this total flow through the reactor, 6990 gpm flows from the high-pressure plenum through the core and inner blanket subassemblies, 710 gpm flows from the low-pressure plenum through the outer blanket subassemblies, and 500 gpm flows through the clearance spaces between subassemblies.

The two coolant flows from the lower plenums, after passing through their respective groups of subassemblies, merge within a common upper plenum. The mixed mean primary coolant temperature in this plenum is 900F. The coolant enters the shell side of the shell-and-tube, counter-flow heat exchanger at approximately 900F, since the heat loss between the reactor and heat exchanger is very small. After passing through the heat exchanger, the coolant returns to the bulk sodium with a temperature slightly different from that of the bulk sodium. This small temperature difference is required to maintain the bulk sodium temperature constant at 700F, because of extraneous heat losses and heat gains by the bulk sodium; viz., gains due to gamma heating of the bulk sodium and coolant leakage past the control drives in the reactor tank cover, and losses due to the sodium coolers and to the shield cooling air.

Primary system coolant pressure drop from pump outlet to the high-pressure plenum is 4 psi; across the subassemblies in the high pressure stream, from lower to upper plenum, 41 psi (across the subassemblies in the low-pressure stream, only about 2 psi); from upper reactor plenum to the heat exchanger, 5 psi; through the heat exchanger, 7 psi;

and approximately 3 psi of static head. Total pressure drop of the primary flow system is 60 psi. Since the primary tank blanket gas is at a pressure only a few inches of water above atmospheric, the maximum pressure in the primary cooling system is less than 65 psig.

b. Secondary System

A secondary system flow rate of 6050 gpm is provided by the main a-c linear electromagnetic pump located in the Sodium Plant Building. The coolant flows from the pump to the tube side of the heat exchanger, entering the exchanger at 610F and leaving at 880F. It then flows to the superheater, and because the heat loss in the connecting piping is small, enters at approximately 880F. The coolant leaves the superheater at 807F and, after passing through the evaporator, returns to the main pump at 610F.

Pressure drop through the heat exchanger is 7 psi, and through the superheater plus evaporator, about 29 psi. Approximate pressure drop through all connecting piping and fittings is 29 psi. Total pressure drop in this system is approximately 65 psi. Since the inlet side of the pump is maintained at a pressure of 10 psig by the argon blanket gas in the secondary system sodium expansion tank, maximum pressure in the secondary system is 75 psig.

c. Steam System

Feed water at 550F is supplied to the evaporator at a rate of 268,000 lb/hr. Saturated steam is generated within the evaporator at 580F and 1300 psig. This steam flows through the separator and then through the superheater from which it leaves at 850F. Turbine throttle steam conditions are 850F and 1250 psig. About 198,000 lb/hr are used by the turbine-generator; the remaining steam (50,000 lb/hr) is employed for direct feed-water heating, for the feed-water pump turbine, and for maintenance of the by-pass flow around the turbine to the condenser.

The turbine exhausts 146,000 lb/hr of steam (moisture content, 14%) to the turbine deaerating condenser operating at  $1\frac{1}{2}$  in. Hg pressure.

The feed-water heating system consists of a blowdown cooler, two feed-water heaters employing steam extracted from the turbine, one deaerating heater which utilizes steam from the exhaust of the feed-water pump turbine, and a high pressure heater using steam supplied directly from the main steam line.

The blowdown cooler reduces the temperature of 13,700 lb/hr of evaporator blowdown from 338F to 102F and increases the feed-water temperature from condenser hot well temperature 92F to 110F.

Feed-water heater #1 uses 18,100 lb/hr of 5 psig steam from the turbine #1 extraction point to raise the feed-water temperature to 210F. Feed-water heater #2, the deaerating heater, uses 20,500 lb/hr of exhaust steam from the feed-water pump turbine at a pressure of 100 psig, and raises the feed-water temperature to 338F. Feed-water heater #3 uses 33,800 lb/hr of 635 psig steam extracted from the turbine #2 extraction point to raise the feed-water temperature to 480F. Feed-water heater #4 uses 24,500 lb/hr of steam from the main steam line, and raises the feed-water temperature to its final temperature of 550F.

The steam by-pass flow around the turbine to the condenser is 5,000 lb/hr.

The condenser employs a circulating water flow rate of 23,600 gpm at 70F and 82F inlet and outlet temperatures, respectively.

### C. Steady-State Operation at Three Fourths Power

The maximum power level at which the reactor may be safely operated is primarily dependent upon the maximum permissible core fuel alloy temperature. Blanket uranium temperatures in the EBR-II, as described in Section IV-B-3., are maintained lower than the core fuel temperatures and, therefore, are not controlling.

Probably the most commonly applied criterion in establishment of maximum permissible fuel temperature is the resistance of the fuel to thermal cycling damage. In the case of suitably fabricated unalloyed uranium, for example, damage due to thermal cycling within the alpha range (up to about 1220F) has been found to be minor compared to the rather severe damage sustained in thermal cycling through the alpha-beta transition temperature into the beta range. With such material, therefore, a maximum operating temperature of about 1200F is indicated. Similarly, the uranium-low zirconium alloys suffer increased damage from thermal cycling above about the same temperature, and an approximate limit of 1200F is applicable.

Radiation, or burnup damage also is temperature dependent. In addition to the usual irradiation damage observed with relatively low burnup, at the high burnups contemplated for the EBR-II fuel (1 to 2 atom-%), a tendency exists for the fuel to swell or puff, as a result of internal pressure exerted by the large amounts of accumulated fission product gases. At relatively low temperatures, this tendency appears to be negligible. There is evidence, however, that at high temperatures (where the fuel alloy strength is appreciably reduced, say at 1500 or 1600F) prohibitively extensive swelling occurs. In the extreme, such swelling could seriously stress or even rupture the fuel element clad.

In fuel elements employing stainless steel clad, the uranium-iron eutectic melting point represents an additional criterion. Since it is probable that, at least in local regions, the fuel alloy of EBR-II fuel elements will come into intimate contact with the steel clad, melting of the element could occur if the temperature at the point of contact were to reach the eutectic melting point.

There also exist certain considerations which bear only indirectly on determination of maximum permissible operating fuel temperature. For example, the higher mechanical strength of the fuel at lower temperatures is considered an advantage (apart from the swelling aspect). A special circumstance in which this may be of importance is that of a reactor excursion on a very short period, in which reduction of fuel axial expansion by inertial forces is minimized by the higher strength. Also, the greater the difference between normal operating temperature and fuel alloy melting temperature, the more severe may be the reactor excursion which just effects incipient melting. Finally, the lower the operating temperature (by reduction of power), the lower are the fuel alloy thermal stresses.

Tests performed on EBR-II prototype fuel elements show that the 5 wt-% fissium alloy is considerably superior to either unalloyed uranium or uranium-low zirconium alloys under thermal cycling. It is expected that negligible damage to the fissium alloy would result from thermal cycling incurred during operation of the EBR-II at maximum fuel temperatures up to about 1350F. Several irradiation tests on EBR-II type fuel elements have been conducted employing both uranium-low zirconium alloys and fissium alloys. The testing times were of several months each, with burnups up to 1 atom-%. Maximum fuel temperatures in most cases were relatively low, but in one uranium-low zirconium case exceeded 1200F and in one 5 wt-% fissium case exceeded 1300F. The maximum damage observed attributable to irradiation was limited to a uniform swelling of the fuel in the amount of several per cent change in cross-sectional area. Since the prototype fuel elements incorporate a sodium bond annulus equivalent in area to more than 16% of the fuel area, it is estimated that EBR-II fuel elements (5 wt-% fissium) can accommodate at least 2 atom-% burnup at a maximum operating temperature of 1300F without significant increase in clad stress due to exertion of pressure by the fuel. The uranium-iron eutectic melting temperature is 1340F. The maximum fuel-to-clad interface temperature in the EBR-II, if operated with maximum fuel temperature of 1320F is approximately 1050F (full power, all uncertainty factors included, as indicated in Fig.66), a temperature well below the eutectic melting point.

To be conservative in respect to the above considerations, initial operation of the EBR-II will be confined to power levels of 45 mw or less, with consequently reduced fuel element operating temperatures. During this operation, frequent removal of subassemblies for examination of fuel elements at various degrees of burnup is contemplated. In subsequent operation,

the power level will be gradually increased to permit evaluation of the effect of increased temperatures. It is expected that this testing procedure on temperature and burnup effects (and, indirectly, on degree of manifestation of uncertainty factors) will enable eventual operation at full power.

This section describes the contemplated operating conditions of the power system at 45 mw, or approximately three-fourths full power.

1. Flux Distributions

Neutron flux distributions are the same as described in Section IV-B-1 for the full-power case, except that all magnitudes are reduced in the ratio of 45 to 62.5 mw.

2. Reator Heat Generation Distributions

Heat generation distributions are the same as described in Section IV-B-2 for the full-power case, except that all power and power density magnitudes are reduced in the ratio of 45 to 62.5 mw.

3. Reactor Temperature Distributions

The primary coolant flow rate assumed in calculating reactor temperature distributions at 45 mw is  $45/62.5$  of that employed at full power. The actual flow rate intended to be used, however, is somewhat higher than this (Fig. 47). Consequently, the maximum temperatures actually anticipated are lower (by about 20 or 30F) than those presented herein.

Radial temperature distributions through a fuel element at the point of maximum fuel alloy temperature in the reactor is shown in Fig. 73. The effect of uncertainty factors on temperature distribution is apparent.

Axial distributions of the maximum fuel alloy and blanket uranium temperatures and coolant temperatures are shown in Figs. 74, 75, and 76.

The power output and the coolant flow rate per subassembly in each row are the same as indicated in Figs. 70 and 71, respectively, except reduced in magnitude in the ratio of 45 to 62.5 mw. The mixed mean coolant temperature rise through each subassembly is the same as shown in Fig. 72.

Table XI gives pertinent temperatures, heat fluxes, and coolant flow rates in subassemblies of rows 1, 6, and 8. Uncertainty factors are not included. Table XII gives the same information as Table XI, but with uncertainty factors included.

Table XI

SUMMARY OF THERMAL ANALYSIS RESULTS FOR MAXIMUM TEMPERATURE  
REGIONS OF CORE AND BLANKET

(No Uncertainty Factors Included)

(Power = 45 mw)

	Region			
	Core	Upper Blanket	Inner Blanket	Outer Blanket
<u>*Coolant Flow in Maximum Power Subassembly</u>				
Flow Velocity, fps	18.6	18.1	7.5	1.9
Flow Rate, gpm	109.5	109.5	14.1	3.5
Estimated Pressure Drop, psi	12.0	4.6	12.6	0.9
<u>*Maximum Heat Flux, Btu/(hr)(ft<sup>2</sup>)</u>	744,500	56,700	205,800	21,700
<u>Temperatures, F</u>				
Maximum Uranium	1098	961	968	829
Coolant, at Outlet	923	925	884	829
Coolant, at Inlet	702	923	700	700
Coolant Temperature Rise, Inlet to Outlet	221	2.0	184	129
Coolant, at Point of Maximum Uranium Temperature	863	923	824	829
<u>*Mixed Mean Coolant Outlet Temperature from Entire Region</u>	918	921	845	790
<u>Temperature Differences at Point of Maximum Uranium Temperature F</u>				
Through Uranium	132	22	103	0
Through Uranium-Sodium Interface	9	1	2	0
Through Sodium "Bond" Layer	10	1	5	0
Through Sodium-Clad Interface	8	1	2	0
Through Clad Layer	46	9	25	0
Through Coolant Film	30	4	7	0
Total Element Temperature Difference	235	38	144	0

\*No uncertainty factors included.

Table XII

SUMMARY OF THERMAL ANALYSIS RESULTS FOR MAXIMUM TEMPERATURE  
REGIONS OF CORE AND BLANKET

(Including Uncertainty Factors)

(Reactor Power = 45 mw)

	Region			
	Core	Upper Blanket	Inner Blanket	Outer Blanket
<u>*Coolant Flow in Maximum Power Subassembly</u>				
Flow Velocity, fps	18.6	18.1	7.5	1.9
Flow Rate, gpm	109.5	109.5	14.1	3.5
Estimated Pressure Drop, psi	12.0	4.6	12.6	0.9
<u>*Maximum Heat Flux, Btu/(hr)(ft<sup>2</sup>)</u>	744,500	56,700	205,800	21,700
<u>Temperatures, F</u>				
Maximum Uranium	1200	1011	1027	852
Coolant, at Outlet	963	965	917	852
Coolant, at Inlet	702	963	700	700
Coolant Temperature Rise, Inlet to Outlet	261	2	217	152
Coolant, at Point of Maximum Uranium Temperature	892	963	842	852
<u>*Mixed Mean Coolant Outlet Temperature from Entire Region</u>	918	921	845	790
<u>Temperature Difference at Point of Maximum Uranium Temperature F</u>				
Through Uranium	175	29	134	0
Through Uranium-Sodium Interface	9	1	2	0
Through Sodium "Bond" Layer	13	1	6	0
Through Sodium-Clad Interface	8	1	2	0
Through Clad Layer	61	11	32	0
Through Coolant Film	42	5	9	0
Total Element Temperature Difference	308	48	185	0

\*No uncertainty factors included.

#### 4. Power Cycle Operating Conditions

The steady-state operating temperatures and coolant flow rates in the principal heat transfer systems are shown in Fig. 1.

##### D. Preoperational Testing and Experiments

Prior to operation of the reactor and power system, the equipment and components will be inspected and tested. This will include leak testing, pressure testing, and circuitry tests. It will also include "dry runs" on the mechanical components - control and safety drives, fuel handling, and disassembly equipment. Particular attention will be given to the components which will be difficult to service after operation has begun.

A broad range of experiments is planned for the EBR-II as part of the initial start-up program. These experiments are planned to explore the critical and dynamic characteristics of the reactor, characteristics of the nuclear instrumentation, and fluid flow performance of the heat transfer systems.

Two series of experiments defined as "dry" experiments and "wet" experiments are scheduled. The dry experiments will be conducted without sodium in the primary system and at "zero power" level. The wet experiments will be run with the primary system filled with sodium.

The primary purpose of the dry critical experiments is to check the nuclear instrumentation system. Because of the physical arrangement of thimbles inside the primary tank, modification of the design or location of the thimbles after power operation of the reactor will be difficult. It will also be relatively simple to provide special startup instrumentation within the reactor during the dry criticals. Fission counters will be temporarily installed in one or more of the control rod locations. These counters will be located across the core from the neutron source in a zone of maximum sensitivity to flux level change.

During the dry criticals, the leakage through the neutron shield will be determined so that modification can be made if necessary.

Additional tests are planned to provide physics data of interest. The "dry critical mass" will be available to compare with the "wet critical mass," and thus determine the reactivity effect of the sodium. In addition, it is planned to determine the "dry isothermal temperature coefficient" by heating the reactor system. This information will permit the determination of the reactivity effect of change in sodium density.

The "wet experiments" will include zero power criticals in static sodium, repeating the dry type critical experiments. Isothermal

temperature coefficient measurements will be made at various temperatures. The reactivity worth of the control and safety rods, as well as the fuel and blanket subassemblies, will be measured. The effects (if any) of sodium flow through the reactor will be determined.

The preoperational experimental program will also include experiments at various power levels: evaluation of instrumentation and control; determination of the "power coefficient" (and correlation with the isothermal temperature coefficient); and determination of the kinetic characteristics of the reactor system, including mechanical oscillation tests. Full-range performance calibration will be made of the instruments in all systems. The reactor and power system will be calibrated at various power levels. An investigation will be made of the kinetic effects on the reactor and heat transfer loops of power level changes and reactor "scram."

Other kinetic experiments and reactivity measurements may be required to provide additional comprehensive performance data. Of primary importance is the determination of the validity of various kinetic experiments in predicting the kinetic characteristics of the reactor. This phase of the experimental program will incorporate the experimental techniques developed for EBR-I and may be considered an adjunct to the Laboratory's fast reactor safety program.

#### E. Normal Startup

Normal startup includes bringing the reactor and power systems to "operating conditions" from the "shutdown condition." The process involves the reactor, the primary system, the secondary system, the steam system (including cooling water), and the turbine-generator and electrical system.

##### 1. System Conditions Prior to Startup

The system shutdown conditions prior to startup vary depending upon the duration of shutdown and the purpose of the shutdown. The reactor is subcritical, and the primary system is at a temperature between 580 and 700F. The secondary sodium "cold leg" is at a temperature of approximately 580F, and the "hot leg" is between 580 and 700F. The steam system is at 1250 psig pressure and essentially at saturation temperature (574F). The temperature differences existing in the respective heat transfer systems, and the amount of steam being generated are dependent upon the amount of heat being generated in the reactor (fission product decay heat).

During a routine shutdown for fuel unloading, etc., the system temperatures will be maintained as closely as possible to the normal operating temperatures. The primary system temperature will be maintained at a temperature approaching 700F. The rate of heat removal from

the primary system will be maintained approximately equal to the fission product decay heat generation rate to avoid degrading system temperatures. Heat will be removed by the secondary system and dissipated in the steam generator by evaporating water. Heat is also removed from the primary system by the auxiliaries, including the shield air cooling system, the thimble cooling system, the sodium cleanup system, and the two shutdown coolers. The shutdown coolers are not employed during a short routine shutdown when the normal heat transfer systems are operative. They are normally used when the secondary system is unable to remove the fission product decay heat from the primary system, or for long term shutdown. As described in Section IV-H., the shutdown coolers remove a small amount of heat, even when in "shutdown condition." The heat removed from the primary system by these auxiliaries is approximately 350 kw.

## 2. Startup Procedure

The following startup procedure is contemplated. Preliminary to the startup of the reactor and power system components, the system interlocks are checked and annunciation points are reset. The flow rates of the primary pumps are set at the required flow for the power level at which the reactor will be operated. Since the power level, due to fission product heating, is quite small (2% or less), there is little temperature rise in the primary system, and the entire primary system is at essentially isothermal conditions.

The reactor is made critical, and the power level is slowly raised. The secondary flow rate is adjusted to correspond approximately to the power level of the reactor. If the primary sodium temperature is below 700F, the secondary system flow rate is established somewhat below the corresponding reactor power level to create a small imbalance between the rate of heat generation and the rate of heat removal from the primary system. This imbalance is continued until the primary system temperature reaches 700F. The rate at which the power level is increased and the secondary system flow rate is varied is limited by the maximum temperature change desired in the sodium systems (probably about 1F/min.).

During this entire period, steam is being generated at constant pressure and is being condensed. In the process, the steam system is gradually heated to operating temperatures. The steam being generated continues to be bypassed until the reactor and power system are at power and stabilized. The steam is then slowly diverted through the turbine in accordance with standard power plant operating procedures, and the turbine is brought up to speed. The generator, which operates in parallel with the NRTS 138-kv system, is then connected. The load applied to the generator is established at a level below the steam generation rate to permit bypassing steam.

If the turbine-generator is not operated, the startup procedure does not include the operation of this unit and the steam flow through the by-pass system.

#### F. Normal Shutdown

Normal shutdown is defined as a programmed shutdown of the reactor and power cycle during which the reactor power is gradually reduced and the heat transfer systems are simultaneously adjusted to accommodate the change in power level. Under normal operating conditions, the primary, secondary, and steam systems maintain a 700F primary bulk sodium temperature and steam at 1250 psig and 850F at the turbine throttle. The required temperatures and flow rates of the primary and secondary sodium systems to maintain these two system parameters at different reactor power levels are described in Section IV-A-3. The alternator may or may not be delivering electrical energy to the NRTS 138-kv system.

The first step in the normal contemplated shutdown procedure consists of dropping the load on the alternator, disconnecting it from the NRTS 138-kv system, and closing the turbine stop valve. The excess steam not required for turbine operation is delivered to the condenser via the steam by-pass system. The turbine-generator is shut down in accordance with normal power plant practice. The steam system continues to operate in the normal manner employed for "by-pass operation."

The reactor power level is slowly decreased and the secondary sodium flow rate is continually adjusted to maintain the primary bulk sodium temperature at 700F and 1250 psig steam at the turbine throttle. The rate at which the reactor power level and the secondary system flow rate are reduced, is limited by the desired maximum temperature changes in the sodium systems. The reactor power level is decreased until the reactor is subcritical and in the shutdown condition. The primary coolant flow rate is then gradually reduced until the pumping power is provided by the auxiliary pump (approximately 500 gpm).

The secondary system flow rate is adjusted to maintain the desired 700F bulk sodium temperature by controlling the evaporation rate of water in the steam generator at the controlled 1250 psig pressure.

#### G. Fast Shutdown (Scram)

Reactor scram is effected by certain primary system abnormalities, as listed in Table VII. Scram consists of fast shutdown of the reactor (by ejection of the control rods) and the cutting off of power to the secondary system pump. The primary system main pumps remain in operation during the scram process and are later shut down manually by the

operator. In this section, the calculated reactor temperature distributions obtaining during this type of scram and also during a scram initiated by primary system main pump failure are examined.

### 1. Primary Pumps Operative

This case represents the usual type of scram: both primary main pumps remain in operation. An initial condition of full reactor power is assumed, since at this level the temperature transients occurring are the most severe. A total control rod worth of  $0.05 \Delta k/k$  and an initial rod insertion of 90% are assumed.

Figure 77 indicates temperature variations as a function of time. The coolant temperature at outlet from the upper plenum is the most critical, in that it is indicative of the thermal shock potential effected at the upper plenum outlet nozzle and in the pipe leading to the heat exchanger. The temperature falls 150F in 10 sec at a maximum rate of about 38F/sec. This shock potential is exceeded only by certain cases of postulated accidents treated in the appendices. Ample thermal barrier protection is provided in the upper plenum nozzle and in the outlet piping to preclude significant shock even under these conditions.

### 2. Only Auxiliary Pump Operative

This case represents a scram initiated by loss of primary system pumping due to pump failure or to loss of electrical power. The primary auxiliary pump continues in operation (even in the event of loss of electrical power, since its power supply is backed up by a floating battery).

Figure 78 shows the same reactor temperatures as considered above as a function of time. Figure 79 shows the same temperatures for the conservative values of rod worth of  $0.030 \Delta k/k$  and initial insertion of 60%. In neither case does a potential thermal shock problem exist.

## H. Shutdown Cooling

The method of removing fission product decay heat from the reactor and effecting its dissipation to the atmosphere is described in detail in Section III-A-3. Briefly, the heat is removed by the primary sodium flowing through the reactor and either transferred to the secondary system or dumped (by mixing) to the primary tank bulk sodium. If transferred to the secondary system the heat is dissipated to the atmosphere via the steam system and circulating water system. If transferred to the bulk sodium the heat is rejected to the atmosphere by the two shutdown coolers provided for the purpose and by various extraneous systems which effect parasitic loss.

## 1. Removal of Heat from Reactor

After normal reactor shutdown, flow through the reactor is maintained either by operation of the auxiliary pump alone or by low-power operation of one or both of the main pumps, any of these flow sources being sufficient to cool the reactor readily. In the case of reactor scram, flow normally is maintained by operation of the auxiliary pump or by high-power operation of both main pumps (until manually reduced or cut out), with resulting reactor temperatures as discussed in Section IV-G. In the remote event that a reactor scram occurs concurrently with failure of all primary system pumps, the primary system is so designed that natural convection maintains sufficient flow to cool the reactor properly. This case is discussed in Sections 2-a and 2-b of Appendix A, and the various reactor temperatures existing in the short-term period immediately after scram are indicated. Approximate fission product decay power, flow rates, and temperatures existing during long-term natural convection cooling (after several hundred seconds following scram) are indicated in Fig. 80.

## 2. Removal of Heat from Bulk Sodium

The heat dumped to the primary tank bulk sodium is dissipated, at least in part, as parasitic losses to the room, to the instrument thimble cooling system, and to the biological shield cooling system. These losses are essentially constant at a given primary tank temperature, and are estimated to total about 130 kw for the normal tank temperature 700F. All decay heat in excess of this amount is dissipated to the atmosphere by the two shutdown coolers. Rate of heat removal by the coolers is varied by regulation of dampers on the air stack housing the air-fin cooling coils. Control of these dampers is automatic (with manual over-ride) and is based on primary tank temperature. Each cooler has a total capacity of 250 kw.

Because of the very large total thermal capacity of the bulk sodium and submerged components, any failure or maloperation of the shutdown coolers produces only an extremely small rate of change of primary tank (bulk sodium) temperature. Consequently, ample time is available for corrective action, even under the worst conditions. In Fig. 81, bulk sodium temperature is shown as a function of time after shutdown from full power with two, one, and none of the shutdown coolers in operation.

### I. Reactivity Coefficients

Two main reactivity coefficients are considered: the isothermal temperature coefficient, and the power coefficient of reactivity. In addition, some consideration is given to the reactivity coefficients applicable in a startup accident.

### 1. Isothermal Temperature Coefficient

The isothermal temperature coefficient is calculated by assuming that the entire reactor, including the structure, heats up uniformly. Expansions and changes of density are computed and translated into reactivity effects. The results are listed in Table XIII. There is no bowing effect, since the temperature distribution is isothermal. The Doppler effect has been assigned for a temperature of 700F, assuming a room temperature effect of  $1.5 \times 10^{-6}/C$ , as discussed in Appendix B. The resultant over-all isothermal temperature coefficient is calculated to be  $-3.6 \times 10^{-5} (\Delta k/k)/C$ .

Table XIII

#### ISOTHERMAL TEMPERATURE COEFFICIENTS

##### Core

Axial growth of fuel	$-0.39 \times 10^{-5} (\Delta k/k)/C$
Radial growth of fuel (displacement of Na)	$-0.09 \times 10^{-5}$
Axial growth of structure (density change)	$-0.039 \times 10^{-5}$
Density change of coolant	$-0.87 \times 10^{-5}$
Radial growth of supporting structure	$-0.97 \times 10^{-5}$
Doppler effect	$+0.04 \times 10^{-5}$ (average)
Bowing	0

##### Gaps

Density change of coolant	$-0.38 \times 10^{-5}$
Density change of structure	$-0.036 \times 10^{-5}$

##### Upper and Lower Blanket

Density change of coolant	$-0.21 \times 10^{-5}$
Radial growth of uranium and jacket	$-0.016 \times 10^{-5}$
Axial growth of blanket uranium	$-0.024 \times 10^{-5}$
Axial growth of jacket	$-0.021 \times 10^{-5}$

##### Inner Blanket

Density change of coolant	$-0.2 \times 10^{-5}$
Axial growth of blanket uranium	$-0.066 \times 10^{-5}$
Axial growth of jacket	$-0.022 \times 10^{-5}$
Radial growth of uranium and jacket	$-0.04 \times 10^{-5}$
Radial growth of supporting structure	$-0.17 \times 10^{-5}$
Bowing	0

##### Outer Blanket

Density change of coolant	$-0.017 \times 10^{-5}$
Axial growth of blanket uranium	$-0.014 \times 10^{-5}$
Axial growth of jacket	$-0.003 \times 10^{-5}$
Radial growth of supporting structure	-0.034

## 2. Power Coefficient of Reactivity

This coefficient is a function of flow rate and other operating conditions. It is calculated herein for the case of full flow, an average value being assigned for the coefficient between startup power (isothermal conditions at 700F) and full reactor power of 62.5 mw. At full power and full flow, and with an inlet sodium temperature of 700F, the following average temperatures are obtained at various points in the reactor.

	<u>Average Temperature (at Full Power), F</u>	<u>Temperature Increase (from 700F), C</u>
Core Coolant	810	61
Core Uranium	975	153
Core Cladding	862	90
Upper Gap	919	122
Lower Gap	702	1
Upper Blanket	924	124
Lower Blanket	705	3
Inner Blanket	780	44
Outer Blanket	745	25
Supporting Structure	700	0

Converting these temperature increases into reactivity changes, a total reactivity change of  $-0.0020 \Delta k/k$  is obtained. This reactivity change does not take into account bowing of the fuel assemblies which will be considered later. The effective power coefficient at full flow, and neglecting bowing, therefore, is:

$$\frac{-0.0020}{62.5} = -3.2 \times 10^{-5} (\Delta k/k)/\text{Megawatt} .$$

Bowing of the fuel assemblies under various conditions is estimated in Appendix A; it is also shown that the reactivity effects associated with bowing are particularly difficult to determine analytically, and that the results given in this report probably may be considered overestimates. It is shown that bowing is expected to be small and that it reverses in direction, with a resultant reversal in reactivity effect. Between zero power and 17 mw, maximum effective core radii changes of only about +0.001 in. and -0.004 in. are expected; the reactivity changes associated with these dimensional changes are relatively small, the -0.004 in. change amounting to about +0.0003  $\Delta k/k$ . Between 17 mw and 62.5 mw, the effective core radius is expected to increase by about +0.010 in. due to bowing. The latter change is estimated to be equivalent to a reactivity change of  $-0.0007 \Delta k/k$ . The expected average power coefficients, therefore, are:

From 0 to 17 mw,

$$-3.2 \times 10^{-5} + \frac{0.0003}{17} = -1.5 \times 10^{-5} \Delta k/k(\text{mw})$$

From 17 to 62.5 mw,

$$-3.2 \times 10^{-5} - \frac{0.0007}{(62.5 - 17)} = -4.8 \times 10^{-5} \Delta k/k(\text{mw})$$

If bowing were to take its most pessimistic course, however, the power coefficient would be affected appreciably. It is estimated that under the worst conditions, viz., a highly abnormal initial disposition of subassemblies, the core radius can be reduced 0.019 in. due to bowing, corresponding to a reactivity change of about 0.0014  $\Delta k/k$ . It is further calculated that for full flow conditions maximum bowing would take place between 9 and 28 megawatts, after which the direction of bowing would reverse. During the 9 to 28 megawatt transition, the power coefficient due to bowing alone would then be

$$\frac{0.0014}{(28 - 9)} = +7.4 \times 10^{-5} \Delta k/k(\text{mw}) .$$

Thus, if these bowing conditions were to prevail, the net power coefficient would also be positive, namely  $+4.2 \times 10^{-5} \Delta k/k$  per megawatt for this power range. Between 28 mw and 62.5 mw, the motion is reversed, and the bowing coefficient in this range would be about  $\frac{-0.0006}{(62.5 - 28)} = -1.7 \times 10^{-5}$ , and the over-all power coefficient would be  $-4.9 \times 10^{-5} \Delta k/k$  per megawatt.

Of course, this behavior is not expected. The positive bowing coefficient described above is based upon the most pessimistic conditions existing in the reactor. These conditions are developed in Appendix A as "possible," but no mechanism can be developed to produce them.

It is interesting to note that even under these abnormal conditions, the effective power coefficient above 28 mw is the same as the expected power coefficient. The rate of power change in the higher power range (28 to 62.5 mw) is, of course, more significant with respect to system temperature changes and associated engineering problems.

Generally speaking, at lower flows the behavior of the reactor should be identical to that at full flow, except that similar temperature rises will occur for lower powers, hence the power coefficient in units of  $\Delta k/k$  per megawatt will change proportionately.

*corresponds to 3 inch per mile*

### 3. Reactivity Coefficients During a Zero Flow Accident

Several hypothetical accidents of this nature have been examined in detail in Appendix A. For each case the appropriate time constants of the various reactivity effects are considered and an effective reactivity feedback effect estimated. Generally speaking, it is found that for power excursions on a period greater than a millisecond, the reactivity feedback coefficient is fairly constant. For the very long periods, a local equilibrium between fuel and sodium is reached, and the over-all core coefficient applies, roughly. As the periods get shorter and approach a millisecond, less heat is transferred to the core sodium, and it produces a smaller reactivity effect, but the greater axial expansion of the fuel elements balances this loss, approximately. Of course, for very short periods inertial effects come into play, reducing the shutdown mechanism.

#### J. Fuel Loading and Unloading

Preliminary to unloading operations, the control rods are driven out of the reactor and disconnected from their drives. At the time these rods are disconnected, the automatic scram interlocks are shifted from operation of the control rods to operation of the safety rods. With the 12 control rods out of the reactor, it is sub-critical by approximately  $0.05 \Delta k/k$  at operating temperature (approximately  $0.04 \Delta k/k$  at the melting temperature of sodium (208F)). The two safety rods represent an additional  $0.015$  to  $0.020 \Delta k/k$  of negative reactivity available.

Normal operation of the unloading system consists of removing a subassembly, transferring it to the storage rack, selecting its replacement from the storage rack and transferring it to the reactor. The process consists of an interchange of a new assembly for an irradiated assembly. One subassembly is handled at a time and the maximum change in reactivity normally expected consists of the difference between an irradiated and an unirradiated fuel subassembly. At 2% burnup of the fuel alloy, approximately 4% of the  $U^{235}$  is consumed. For a central fuel subassembly, this should produce a  $\Delta k/k$  of less than 0.001; for the other locations the change is smaller.

The above described "normal operation" is achieved partly by the inherent arrangement of the unloading system and also by management control. The unloading system is capable of handling only one subassembly at a time. It is impossible to remove or insert more than one subassembly in the reactor at a time. It is, however, possible to remove, in sequence, several subassemblies and then to install, in sequence, several subassemblies. This mode of operation is prevented by management; however, an inherent characteristic of the system tends to encourage the "normal process." Loading and unloading are a reversible process and the operator achieves maximum efficiency by following the normal mode of operation described above. The possible alternate method is less efficient because

it involves "returning empty-handed" which lengthens the cycle appreciably. It is important to note that there is no incentive for performing this task in the undesirable fashion.

There are two types of "mistakes" which must be considered: the introduction of a fuel assembly of higher enrichment in the core, and the introduction of a fuel assembly in the inner blanket. As discussed in Section IV-K, an incredible combination of errors is required to produce a fully enriched subassembly. It becomes even more incredible to produce a sufficient quantity of these assemblies to make the reactor critical in the "shutdown condition."

The substitution of a fuel subassembly for an inner blanket subassembly at the edge of the core represents a reactivity increase of approximately  $0.0027 \Delta k/k$ , which is more than an order of magnitude less than the shut down  $\Delta k$ . An accidental insertion of 15 or more core subassemblies for inner blanket subassemblies must occur for the reactor to reach delayed critical during loading operations. Standard core subassemblies are not interchangeable with inner blanket subassemblies as described in Section III-A-1-h. Special core subassemblies which fit the inner blanket zone are to be available, however, to provide loading flexibility in the system. These units will be under special management control and it is proposed to limit the number of such assemblies available in the plant. Also, these units will be stored in the vault, not in the storage rack. They will be introduced into the reactor system through the disassembly cell individually as required, which will differ from the normal loading procedure. If a special core subassembly is required for loading into the inner blanket, it will be transferred to the system through the disassembly cell, inserted in the storage rack, removed from the storage rack, and transferred to the reactor. To insert a second such unit will require repeating the procedure, which although not foolproof, is very adaptable to special management control. Again, an incredible combination of errors is required to make the reactor critical in its "shutdown condition."

For these reasons, the kinetic studies included in Appendix A for postulated accidents during unloading are basically academic. It should not be possible for these incidents to occur, for in addition to the incredible operator lapse required to permit these cumulative errors, it is necessary for these errors to go unobserved on the instruments which constantly monitor multiplication.

The unloading of a control rod represents a special case of fuel unloading. The control rod is unloaded in the same fashion as a core subassembly; however, it is unloaded from its "down position" and the fuel section of the control rod passes through the reactor core during the process. This represents a reactivity addition to the system of approximately  $0.005 \Delta k/k$ , and reduces the margin of shutdown during this period by about

10%. Since the unloading mechanism speed is only 6 in./min during the bottom 24 in. of travel, reactivity is added only slightly faster than the control rod drive itself normally adds reactivity.

The average rates of reactivity addition which apply to the unloading operation are as follows:

Central fuel element	$1.5 \times 10^{-4} \Delta k/k$ per second.
Control rod	$0.4 \times 10^{-4} \Delta k/k$ per second.
Safety rod	$0.7 \times 10^{-4} \Delta k/k$ per second.

After the fuel subassembly (or control rod) has been lifted 24 in., rate of travel is increased to 72 in./min. to permit the unloading operations to be performed in a reasonable time.

## K. Fuel Recycle

For purposes of operational control and quality control, the fuel cycle is divided into four phases: fuel processing, pin fabrication, fuel element fabrication, and the assembly of the fuel subassembly. Each operation is discussed briefly here with emphasis on those items that pertain to quality control rather than on the chemistry of the process or the details of the machinery used for the various operations.

### 1. Fuel Processing

The spent fuel is removed from the reactor as subassemblies containing approximately six kilograms of fuel alloy. The disassembly of such units is done in the disassembly cell mechanically on a unit basis so that the identity of each batch of 91 fuel elements is retained. Only the outer "hex" tube and the end blankets are removed at this point; the fuel alloy remains enclosed in its stainless steel can together with its sodium bond. The fuel elements are then transferred to the process plant, where they are individually fed through a decanning machine which first scores the stainless steel cans and then strips the can from the pin. If this operation does not break up the fuel pin it is broken up upon leaving the machine. This is done to provide samples and to facilitate subsequent handling. The pins are segregated into batches ranging from 1 kg to 10 kg and stored until analysis of the samples confirms the calculated composition (burnup, etc.) of the alloy. After sufficient operating experience has been obtained, the batch size will probably be one subassembly (approximately six kilograms) but initially it will be somewhat smaller so that distributions and variations in composition along the length and across the diameter of a subassembly may be determined. [There are available in the Laboratory Building being built in conjunction with EBR-II complete analytical facilities for use in connection with this work. These facilities consist of six shielded analytical junior caves, two regular wet radiochemistry laboratories, two counting rooms, and an instrument laboratory. This equipment permits element analysis, radiochemical analysis, and mass analysis.] When the

results of the sample analyses are made available, the batch of pins is transferred to the melt refining area.

The nominal batch size to be processed in the melt refining operation is ten kilograms. This is composed of spent pins, recycled scrap and make-up material. The material required to re-enrich the fuel alloy is added at the beginning of the melt refining operation for two reasons, as follows. During melt refining, the alloy is held in the molten state for a period in excess of two hours, while during the injection casting operation the metal is molten only for a period of minutes. Adding the enriching material ( $U^{235}$  or Pu) before the long holding time ensures the formation of a more homogenous alloy. Secondly, it allows a confirmatory analysis before the metal is sent on for fabricating. After the liquation period of the melt refining operation is over, the fuel alloy is cast into a cold metal mold. The resulting ingot is sampled and then stored until the results of the analyses indicate its composition is correct; it is then sent on to the fabricating area. At design conditions of 2% fuel burnup the maximum amount of enriching material to be added to a batch (ten kilograms of spent fuel, no recycle scrap) is 200 gm of  $U^{235}$ . The maximum error probable during this operation is the addition of the enriching material to a 10 kg charge consisting entirely of recycle scrap. This would produce an ingot having an enrichment of 51% instead of the nominal 49%. Since recycle scrap will not be segregated and will not be allowed to collect into such large batches, the probability of such an occurrence is unlikely. Should it occur at this point it would be detected upon analysis of the ingot before the metal had gone on to fabrication. The inadvertent casting of a fully enriched ingot is of even smaller probability, since enriching material is to be batched at the vaults into 100-gram to 200-gram batches. To charge a furnace with 10 kilograms of enriched material would require the confusion of kilogram-size batches of broken pins with 100-gram batches of make-up alloy, not once, but 100 times. In addition, this represents make-up material requirements for three to four months, while only a three- to four-day supply is available to the operating personnel at any one time.

## 2. Pin Fabrication

The pin-fabrication procedure consists of the vacuum remelting of an ingot received from the processing area and the injection casting of the fuel pins directly to size. A weighed, analyzed ingot is melted in the casting furnace and held under vacuum long enough to outgas the last traces of the inert gases, and the magnesium metal (introduced by the magnesium oxide crucible used in the melt refining step). At the end of the outgassing period, a batch of closed end Vycor molds are plunged into the melt at the same time that the furnace is vented to a gas storage tank. The in-rushing inert gas drives the molten metal up into the evacuated molds. Batches of 100 pins have been cast in a single operation. However, because of the fission product heating obtained in high-burnup, short-cooled fuel, and the problems of dissipating this heat from a close-packed bundle of 100 tubes, actual plant operation probably will be limited to about 50 pins, or 3 batches per 10-kilogram ingot.

The finished pin diameter is a function of the mold diameter so that all molds are inspected for size before being inserted into the process cell. An air gage comparator will be used to insure that all the Vycor tubing used is actually within the size tolerances established. The molds are simply 16- to 18-inch lengths of precision bore Vycor tubing, closed at one end, and coated internally with a graphite-ceramic wash. After the casting operation is complete, the Vycor, which is a high silica glass, is broken up and discarded. A set of cobbled rolls and powered wire brushes are used to remove the mold from the pin.

The finished castings are viewed with an inspection periscope and any obviously defective ones are removed and recycled to the melting operation. The approved castings, which are normally of the correct diameter but always too long, are cut to finished length. The pin is grasped in the center by a collet device and both ends are cut simultaneously by a "double tool chuck." In this way no precision operation is required within the cell. The accurate determination of the pin length is established by the tool spacing which is done exterior to the cell during the assembly of the tool holder. The chips from this operation serve as a sample for a final check on the composition of the finished fuel pin. Thus, from the time that the fuel is reconstituted in the melt refining furnace, each batch is checked twice to insure that the original charge was correct.

All finished fuel pins are inspected. Each pin is weighed on an analytical balance mechanism, calipered for length, and gaged for diameter. In addition, every pin passes under an inspection periscope through which it is examined for defects in contour and for porosity and other surface defects. The inspection procedure imposes no operating problems since even at the full reactor power of 62.5 mw only of the order of 50 pins per day need be produced. The finished, inspected pins are stored in racks until their composition is confirmed by analysis of the cut-off chips and are then transferred to the element assembly area.

### 3. Fuel Element Assembly

The fuel element tubes as delivered to the process cell have been inspected and tested; the bottom fitting and the spiral spacer wire have been welded on; the entire unit has been leak-tested, cleaned and dried; and, the correct amount of sodium metal has been loaded into each can. These operations are all normal direct ones (no radioactivity present) and the usual methods of quality control are used except that, again, 100% inspection and testing is used rather than sample inspection. The first step in assembly is the insertion of an inspected, finished fuel pin (received from the fabrication area) into the element can. The cap is inserted and the element is welded closed by inert gas arc welding. Providing the inert gas atmosphere which is essential for good welds is greatly simplified since the cell environment is inert gas. The elements are visually inspected for large weld defects and helium leak checked for small ones.

The mere filling of the annulus between the fuel pin and the fuel can with molten sodium does not ensure a good thermal bond; therefore, a "bonding" procedure is necessary. The most reliable procedure appears to be a combination of heat treatment and centrifuging. The ability of sodium to "wet" stainless steels and uranium alloys increases with temperature so that heating the assembled pins enhances the bond. Centrifuging the elements removes any small amounts of entrapped gas. Since the ability of sodium to "wet" metals increases with the temperature, the bond produced is "self-healing." However, it is not assumed that the bonding procedure produces good bonds and every pin is tested.

The bond-testing procedure (cyclograph) monitors the effectiveness of the bonding procedure and determines the sodium level within the can. It is important that the fuel pin be completely submerged in sodium for cooling purposes and that gas space remains for thermal expansion of the sodium. Those fuel elements meeting the specifications of leak tightness, bond integrity and sodium level are transferred to the subassembly fabrication area; those failing to pass are decanned and recycled through the assembly procedure; if they break in decanning, they are recycled to the casting furnace.

#### 4. Subassembly Fabrication

The major part of the subassembly is prefabricated external to the process cell; only the actual insertion of the fuel elements is done remotely. The subassembly is prefabricated in two units. The lower unit consists of the "lower adapter," the lower blanket section, and the fuel element grid. This unit is brought into the cell and positioned in the assembly fixture. The fuel elements are then individually threaded onto the grid. The upper prefabricated unit consists of the hexagonal subassembly shroud, the upper blanket and the "upper adapter" or handle. When the fuel elements have all been threaded onto the grid, the upper prefabricated unit is lowered over the fuel elements. The end of the hexagonal shroud tube is welded to the "lower adapter" and the fuel subassembly is then complete. It is transferred through the roof of the cell into a shielded coffin which is used to transfer the subassembly back to the reactor. The only probable error in assembly is that too few fuel pins may be placed in a subassembly; it is not possible to add more than the specified number. Administrative procedures will be used to reduce the possibility of a fuel subassembly containing less than the required number of fuel elements. There will be batched numbers of elements and a final check of the threaded grid will be made by the supervisor before the hexagonal shroud tube is lowered over the fuel elements.

## V. ENUMERATION AND EVALUATION OF POSSIBLE HAZARDS

### A. Safety Features of Mechanical Design

The mechanical design is such as to rule out many accidents which might ordinarily be considered as possibilities. The triple tank feature of the sodium system and the submerged design concept removes the loss of coolant accident from the list. The submerged design and coolant pump inlet features renders impossible the rapid addition of moderator to the core via the reactor cooling system. Further, the immense volume (and effective heat capacity) of bulk sodium from which the reactor inlet coolant is drawn renders impossible any sudden change in coolant inlet temperature with its attendant reactivity changes.

The shutdown cooling problem is resolved by the use of two electromagnetic pumps for the primary cooling system, the availability of an auxiliary pump backed by battery power, the upward flow through the reactor, and the arrangement of components within the primary tank, provided that any one of a number of scram circuits shuts down the reactor in the event of power or pump failure.

The control drive mechanism design is such as to prevent a rod from being raised above core level or from failing to unlatch without knowledge of the operator. The design also makes it impossible inadvertently to raise all rods as a unit. The unloading mechanism is limited to one core subassembly or blanket subassembly. Furthermore, subassemblies of normal design will fit only in preassigned regions (core, inner blanket, or outer blanket).

In addition to the twelve control rods, which are fail-safe, two safety rods are provided so that  $1.5 - 2\% \Delta k/k$  is available for shutdown during loading and unloading operations, should gross mismanagement and operational errors combine to make the reactor critical at this time. Actually, the number of special, experimental subassemblies will be carefully controlled so that such an incident should be impossible.

Perhaps the most vulnerable feature of the cooling system, the sodium-to-water heat exchanger (evaporator plus superheater) has been placed in a separate building, so that even a major accident from this source cannot jeopardize the reactor. Also, a special emergency heat removal system, employing natural convection alone, makes impossible an overheating of the core due to the loss of electric power.

Building construction is such as to prevent any anticipated earthquake activity from providing a source of difficulty.

## B. Safety Features of Nuclear and Control Design

Each control rod will be worth less than  $0.006 \Delta k/k$  for a full stroke of 14 in. Hence, the single drive speed of 5 in./min will limit reactivity addition rates from this source to less than  $0.00006 \Delta k/k$  per sec. The unloading mechanism introduces subassemblies into the core area at the rate of six inches per minute. Even for a central core subassembly, this results in a maximum reactivity addition rate of not more than  $0.0002 \Delta k/k$  per sec. A third type of drive mechanism is used for the two safety rods. This drive moves both rods as a unit at a speed of 2 in./min, and should add reactivity at a rate less than  $0.0001 \Delta k/k$  per sec.

Of the three types of drives mentioned above only a control rod drive is expected to be operated when the reactor is in the vicinity of delayed critical. But even at the maximum rate of  $0.0002 \Delta k/k$  per sec during fuel loading, there would be 30 to 40 sec between delayed and prompt critical for the operator to notice the error, and 10 to 15 sec before prompt critical within which the period scram instrumentation should note the excursion, stop the drive, and scram the safety rods. Thus, the reactivity addition rates have been chosen conservatively. In addition, the core design has been chosen to assure negative feedback effects due to heating of the core in an excursion. One-piece fuel pins insure that the enriched section will grow longer upon heating, losing reactivity. The buttons on the subassembly make bowing inconsequential at lower powers, and productive of negative reactivity at high powers. While the Doppler effect is fixed for a given enrichment, and may be positive for EBR-II, recent measurements plus theoretical developments indicate that it should be an inconsequential effect compared to other reactivity effects. (See Appendices A and B.)

In addition to a host of alarm signals, fail-safe, automatic scram actuation is effected by abnormalities in critical reactor variables, i.e., coolant temperatures, reactor period, power level, etc. Hence, any potentially dangerous abnormal operation results in immediate reactor shutdown.

The quality control provided in the Process Plant will prevent improper enrichment of fuel elements; however, the chance introduction of a fully enriched subassembly would not make the reactor critical during loading operations, unless this error was preceded by several incredible errors in loading.

## C. Nuclear Accidents

To evaluate further the inherent safety characteristics of the reactor, several hypothetical nuclear accidents have been assumed and their consequences determined. (See Appendix A.) The accidents considered were as follows:

Case 1.

Assume the reactor is at delayed critical and at zero power conditions (8 watts and 600F) with the safety rods out. These rods are then driven into the reactor in an uncontrolled fashion at their normal speed of two inches per min.

Case 2.

Assume the reactor is at delayed critical and zero power conditions with the central fuel subassembly removed. This element is then loaded at regular speed of 6 in. per min for the last 24 in. of motion.

Case 3.

Assume the reactor is at delayed critical and zero power conditions and a single control rod is driven into the reactor in an uncontrolled manner at 5 in. per min.

Case 4.

Same as Case 3., except that the excursion begins at operating power and full flow.

Case 5.

Assume the reactor is at delayed critical and zero power conditions with the central fuel subassembly being loaded. It is dropped and falls into the reactor. This is an accident where reactivity is added rapidly. Two subcases are considered: first, where the subassembly is dropped from just above the core, and second, where the subassembly falls the full length of the reactor.

Case 6.

Same as Case 2., except that the core subassembly is driven all the way in at the high speed of 72 in./min. (The high speed is employed normally after the subassembly has been raised 24 in.)

The first four cases involve low rates of reactivity addition; the last two, relatively large rates. In each of the first three cases, all for initial power equal to source level and with no coolant flow, either the period scram or a power level scram set for 1000 watts would easily terminate the excursion with no appreciable powers being developed. If no scram were operative, a sub-prompt-critical burst of power would develop in each of these cases, resulting in melting of the fuel elements in each of the first two cases. The melting point would be reached during the period in which

$\Delta k/k$  has swung negative, however. In the case of uncontrolled insertion of a control rod, it is possible that the entire rod may be inserted without quite melting the core. However, to assume the scrams nonoperative, in addition to the many abnormalities required to initiate the incident, is believed to be too unrealistic and pessimistic to be considered as productive of a "credible accident."

In Case 4., where a control rod is inserted at full power and full flow conditions, both the power level scram and the exit coolant temperature scram would be effective in preventing melting of the fuel elements.

Of the two high-reactivity-addition rate incidents, Case 6. would be terminated by the period scram practically before the accident got underway. In Case 5., however, where a central fuel subassembly is assumed to have been dropped into a just critical reactor, with only the safety rods available to shut down the reactor, the outcome is somewhat in doubt. If the rod is dropped from just above the core, and the period scrams are operative, it is likely that the safety rods will move in time to prevent melting. However, if it were possible for the accident to occur wherein the central subassembly was dropped from the top of the reactor, falling freely under gravity into its most reactive position, and the reactor had been just subcritical at the beginning of the accident, the safety rods would not be adequate to prevent melting. However, it is felt that too many coincidences are required to warrant considering this accident as "credible." In particular, the reactor should always be so far subcritical during any loading operation that the complete insertion of the assembly will still leave it 3 or 4%  $\Delta k/k$  subcritical.

Hence, it appears that even the hypothetical nuclear accidents treated in Appendix A are unlikely to produce any serious damage to the reactor.

#### D. Consequences of Pump Failure

One type of operational abnormality is represented by the sudden cessation of all primary system pumping power. This requires either (1) simultaneous mechanical failure of all three pumps in the system, or (2) loss of both building power supply and auxiliary pump battery supply.

In Appendix A, three assumed modes of losing all pumping power are treated:

- (1) Loss of all pumping power occurs, reactor scram follows immediately.
- (2) Reactor scram occurs, loss of pumping power occurs soon afterward.

- (3) Loss of all pumping power occurs, all control rods remain fixed in their initial positions.

In Case 1, analysis shows that overheating does not occur. However, if in addition to complete pumping power loss, an appreciable fraction ( $1/4$  to  $1/2$ ) of the control rods were to fail to operate, overheating would occur to the extent that maximum fuel temperature would rise to about 120F above normal, full-power operating temperature.

Similarly, in Case 2, overheating does not occur due solely to a reactor scram followed by loss of all pumping power. Only if this incident were accompanied by failure of one-fourth to one-half of the control rods and the loss of pumping power were to occur within approximately 30 sec after scram, would maximum fuel temperature exceed the normal full power operating temperature (and in the worst circumstances, by not more than about 150F).

Case 3 is considered as academic because of the combination of assumptions made (see Appendix A). The reactor would necessarily exhibit negative reactivity addition as a consequence of temperature increase, and therefore would become more and more subcritical as overheating progresses, at least up until the time at which melting commenced. The time required for melting to start under these circumstances is approximately three sec.

#### E. Possible Consequences of Core Meltdown

An attempt has been made to evaluate the possible effects of a reactor core meltdown. It is assumed that the integrity of the coolant tanks is maintained in advance of the accident, so that sodium is present everywhere at its inception. Then, in the event of a meltdown beginning at full power following extended operation at full power, the molten uranium will freeze inside the plenum below the lower blanket, should it drop that far. It seems more likely that any molten uranium will freeze in traversing the lower blanket, before reaching the lower plenum. The role that boiling sodium in the core might play in preventing or augmenting displacement of the fuel alloy from the core has not been considered, but it should not affect the conclusions on the limit of downward travel.

Without implying any credence to same, an attempt has been made to calculate the maximum possible nuclear explosion resulting from a core collapse under gravity. The following pessimistic set of hypotheses were made:

- (1) The sodium has boiled away from the center of the reactor.

(2) The uranium from the middle of the core has trickled down into the lower part of the core and is retained there, producing a region abnormally dense in enriched uranium at the core bottom, with a large gap at the core center.

(3) At the worst possible moment, the upper portion of the core falls as a single unit, producing a prompt critical configuration at the highest possible insertion rate.

With these assumptions, one calculates a maximum reactivity insertion rate in the vicinity of \$600/sec. The rate can be increased to 800 or \$1,000/sec if it is assumed also that the controls were initially withdrawn, leaving the reactor further subcritical and allowing the upper portion to gain more speed in falling.

The calculations in Appendix C show that for a \$1,000/sec accident in EBR-II, the total nuclear energy yield of  $2.4 \times 10^9$  joules =  $5.8 \times 10^8$  calories. Of this, approximately 80% is expected to be available as explosive energy, or  $4.8 \times 10^8$  calories, which is equivalent energywise to about 1050 lb TNT. (Pressures similar to those of TNT probably would be developed.)

For an incident involving smaller reactivity rates, say \$600/sec, the yield would be proportionately smaller, the explosive energy now being equivalent to about 660 lb of TNT, while an explosive energy of only about 280 lb of TNT was calculated for the \$200/sec case.

While no definitive statements can be made at this time, the circumstances attending the 600 and \$1,000/sec accidents require so many coincidences of timing and coordinated motion of fuel, that a much smaller rate must be assigned to the gravity-induced accident, if any semblance to realism is to be maintained. Hence, at least for the gravity-induced accident, an explosive energy of about 300 lb of TNT appears like a reasonable upper limit.

The EBR-II reactor has been provided with a double containment system (Appendix E). The primary containment system surrounds the primary tank in which the reactor is submerged. Its function is to contain the effects of the nuclear energy release without breaching. The secondary containment system surrounds the primary containment system and the Reactor Plant. The function of this system is to localize within the reactor building the effects of a possible sodium-air energy release, and to contain any fission gases which might escape the primary system.

Detailed analyses have been made of the primary containment system assuming a nuclear energy release in the center of the core equivalent to the detonation of 300 lb of TNT. Further, the time scale for this

energy release was chosen as that which made the explosion most difficult to contain. The analysis shows that the system can withstand such a blast, and perhaps a much stronger one without breaching. Furthermore, the missile shielding provided as part of the secondary containment should readily stop the worst missile which might be propelled upward through the top closure in such an explosion.

#### F. Consequences of Sodium Chemical Reactions

Sodium exposure to the atmosphere could occur in three broad categories: stagnant pool, pressurized spray, and as an explosive ejection. From the stagnant pool, combustion of the air in the building would take several hours; the heat would be largely lost by convection and conduction to the building wall, and only small pressure increase would arise for the secondary containment shell to withstand, as is discussed in Appendix D.

The sodium spray exposure has been examined both experimentally and theoretically, and peak pressures as high as 38 psig have been obtained in test chambers. The third category, that of explosive ejection is the most severe accident, however. In experiments at Argonne, momentary peak pressures of about 80 psig have been obtained in test chambers. This pressure represents the maximum resulting from a wide range of experiments in a fairly large test chamber, in which hot sodium was explosively ejected as a fine spray into an air volume. In all cases, the pressures obtained were considerably lower than the ideal theoretical calculation would predict. When thorough mixing of near stoichiometric quantities was not obtained, considerably lower peak pressures were obtained.

Extrapolation of these experiments to EBR-II, assuming that the volume of sodium spray required to achieve equal pressure increases linear with volume, an explosive ejection of from 14,000 to 23,000 lb of sodium, with ejection energies of from  $9 \times 10^4$  to  $14 \times 10^4$  kcal (equivalent to 180 to 310 lb of TNT) would be required. A considerably more powerful explosion would be required to breach the primary container and impart these energies to the sodium. However, it is doubtful even then that the fine degree of sodium dispersion achieved in the experiments would result within the reactor shell.

The building shell itself is designed for 24 psig, with a safety factor of four for maximum stress. Hence, there is a distinct possibility it would contain the maximum pressure achieved experimentally; it should definitely contain a more realistic pressure, two or three times smaller than this maximum. Of course, with the external shell intact, the oxygen would be consumed, and the reaction would cease.

G. Radiation Hazard to the Surrounding Area from a Hypothetical Reactor Disaster

To obtain some estimate of the potential hazard of EBR-II to communities in the vicinity of NRTS, a hypothetical container-rupturing disaster of  $10^{20}$  fissions was assumed to occur after the reactor had been operating at 60 mw for 135 days with no fuel element removal. To evaluate the hazard of plutonium, it was arbitrarily assumed the core contained 125 kg of Pu<sup>239</sup>.

It is immediately found that the hazard (except for the immediate vicinity of the reactor plant) is due almost exclusively to the long-lived fission products, which have been built up by long operation at high power. It is further found that the plutonium represents little additional hazard, assuming the existence of this high-level fission product activity.

The external radiation hazard from airborne activity does not appear to be serious. Under the variety of good and bad diffusion conditions considered in Appendix F, the estimated maximum external dose is less than the 300-roentgen exclusion radius dose at distances greater than 11 miles. The maximum external dose is less than 100 r at distances greater than 35 miles. During average daytime diffusion conditions, the maximum external dose is less than 200 r at all distances greater than 0.6 mile. With the exception of Atomic City there are no public population groups closer than 11 miles to the reactor. The other sites at NRTS are more than 12 miles distant. With the exception of Arco, and a few other communities with populations of the order of 100, the surrounding communities are more than 35 miles distant. Moreover, the prevailing winds under inversion conditions, when things are the worst, are such as to direct a concentrated cloud away from the nearest centers of heavy population.

During precipitation conditions the calculated maximum external radiation hazard is somewhat greater. There are mitigating factors, however. First precipitation conditions are relatively uncommon at NRTS and the probability of total instantaneous washout is particularly low. Secondly, the porous top soil and underlying lava would permit much of the activity to sink below ground level, sharply reducing the  $\beta$  dose, which is the major effect. Furthermore, the radius of the affected area, when high-dose rates are calculated, is a small one, and it would be relatively simple for one to escape the contaminated area.

While the effects thereof are perhaps harder to ascertain, the internal radiation hazard danger seems greater when compared with accepted tolerance levels. Particularly under nocturnal conditions, one could suffer a severe dose at distances as great as 60 miles.

Again there are mitigating factors. Cross wind movements would reduce the dose. Prevailing winds under the worst conditions are away from population centers. It is not likely that the stable conditions conducive to high doses will exist long enough for a large concentration of activity to travel more than 30 miles. And for this hazard, as well as in those mentioned previously, the assumption that the reactor will contain so many fission products, and that 50% would escape into the cloud and remain therein is highly pessimistic.

#### H. Conclusions

The conclusions might best be summed up in a pro and con type of presentation. In favor of the over-all safety we have the following:

(1) The unique reactor design supplies many inherent safety features.

(2) To the best of current knowledge, the reactor will have negative reactivity coefficients, prompt, slow, power and isothermal.

(3) Reactivity addition rates are carefully controlled and the instrumentation is adequate to handle many times the maximum possible drive rate.

(4) The mechanical design makes major loading errors rather incredible; a safety rod system is available for such errors in any event.

(5) Even fairly unrealistic loading and operating accidents involving the addition of reactivity should give no trouble, providing the instrumentation is operative.

(6) The cooling system is adequate to prevent serious overheating and fuel alloy melting in the unlikely advent of complete pump failure, unless all of several scram indicators fail to operate.

(7) While there is no indication fuel alloy melting would definitely result in a prompt critical assembly, pessimistic assumptions on a gravity-induced accident of this nature suggest 300 lb of TNT as a reasonable upper limit.

(8) The primary containment system is estimated to be able to contain easily a nuclear accident equivalent to the detonation of 300 lb of TNT in the center of the reactor without breaching, and probably could contain an accident considerably larger.

(9) The secondary containment system would probably contain the maximum possible sodium-air explosion. It should certainly contain

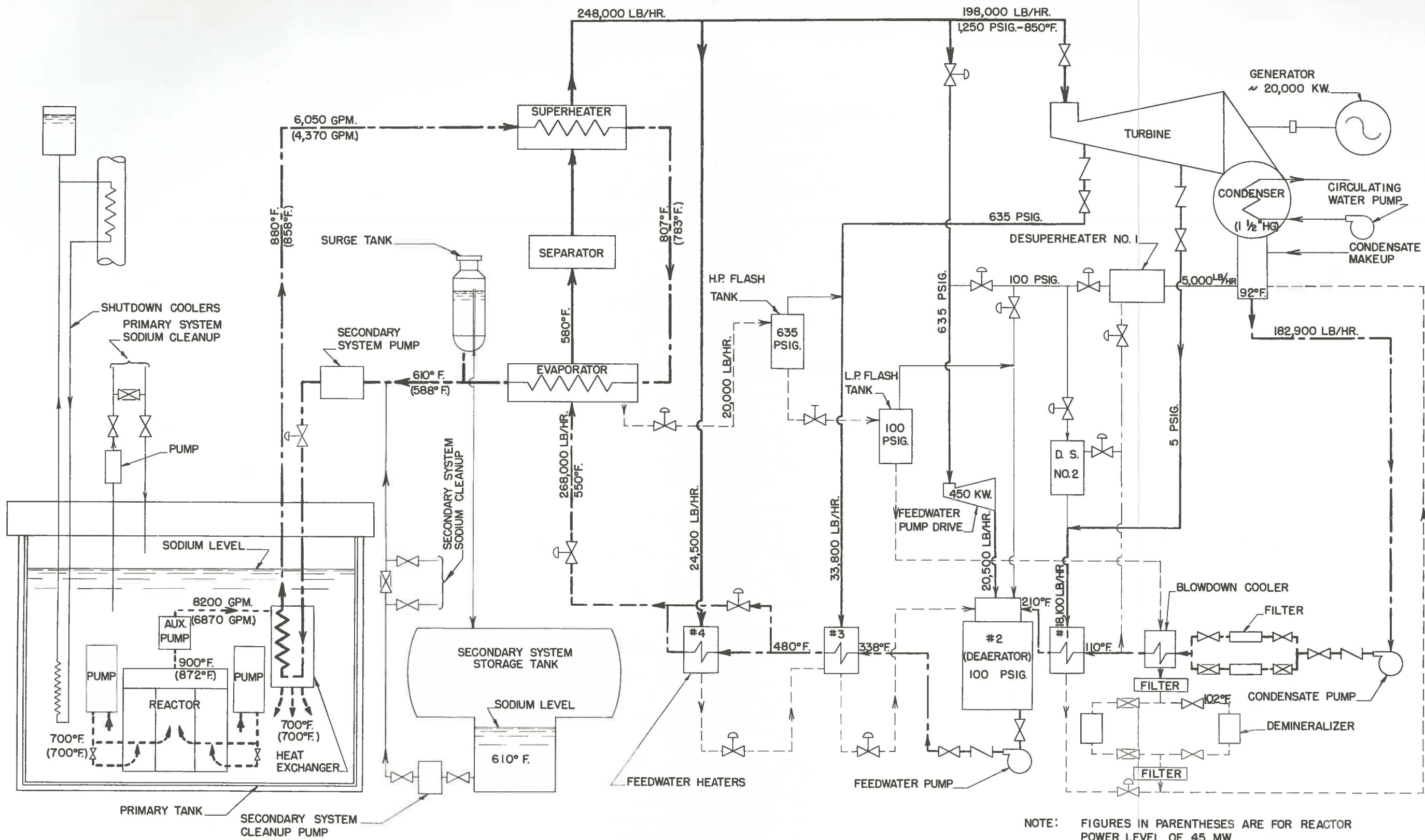
a more realistic interaction, reduced in magnitude by a factor of two or three. Further, it would take an extremely violent nuclear explosion to produce the fine sodium dispersion necessary for such a violent chemical interaction.

(10) The reactor will be located at NRTS, 35 miles from a large community. The prevailing winds are away from populated centers. High-radiation hazards at great distances from the reactor would exist over a fairly localized area in the advent of a disaster.

The qualifications which need to be mentioned in connection with the public safety are the following:

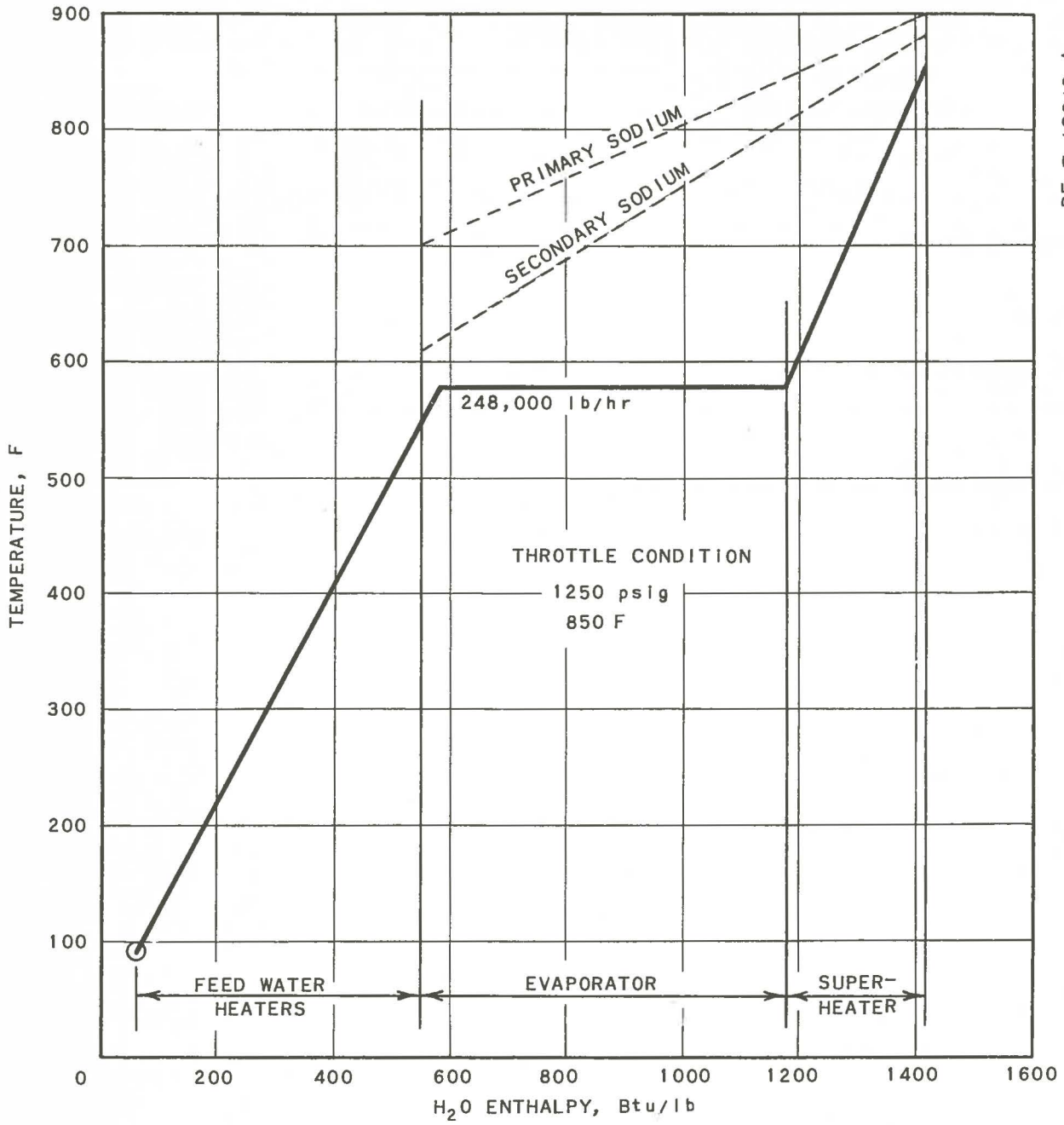
(1) This is an experimental reactor. Furthermore, complete understanding of past performance difficulties in EBR-I remains to be demonstrated, as well as a quantitative prediction of the EBR-II nuclear performance. Current investigations at the ANL, ZPR-III, Fast Neutron Critical Facility are yielding much information concerning the basic nuclear parameters of such systems.

(2) While a fairly pessimistic set of assumptions were made to calculate the maximum possible nuclear explosion induced by gravity following meltdown, this analysis does not pretend to cover all presently imagined circumstances of reactor assembly under core meltdown conditions.



NOTE: FIGURES IN PARENTHESES ARE FOR REACTOR POWER LEVEL OF 45 MW.

FIG. 1  
SIMPLIFIED FLOW DIAGRAM



RE-7-19646-A

FIG. 2  
TEMPERATURE-ENTHALPY DIAGRAM

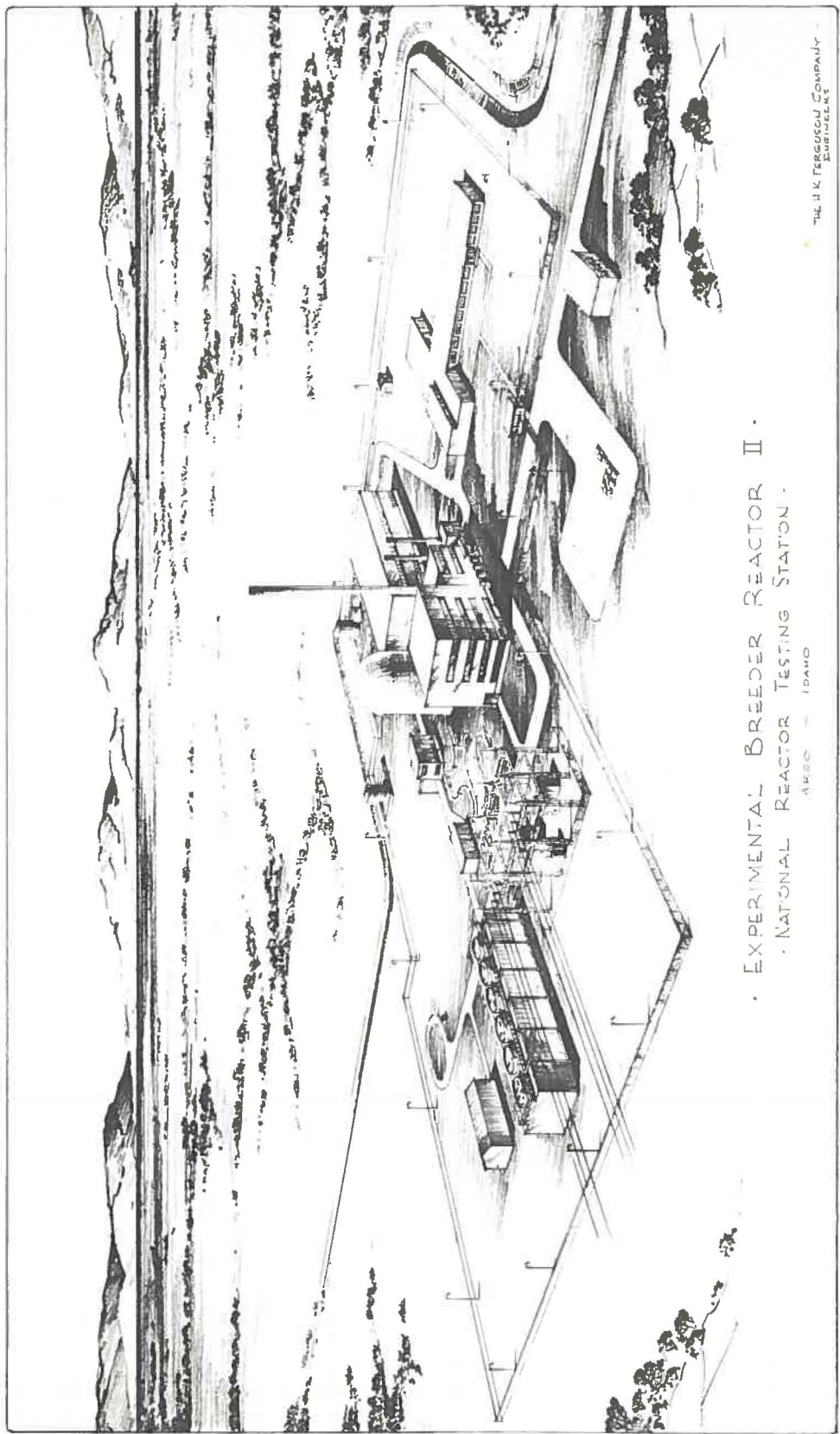


FIGURE 3

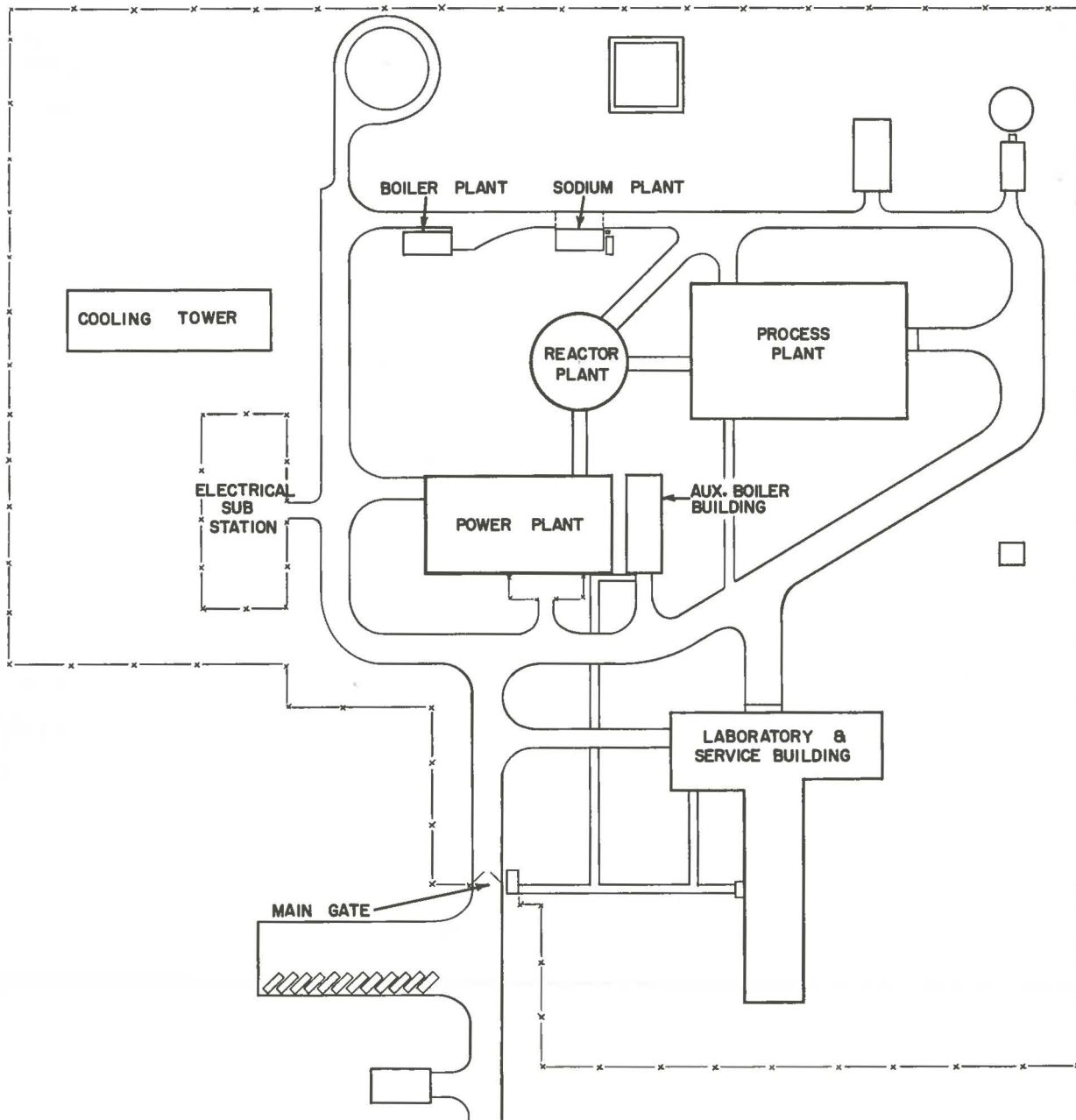


FIG 4  
PLANT ARRANGEMENT PLOT PLAN

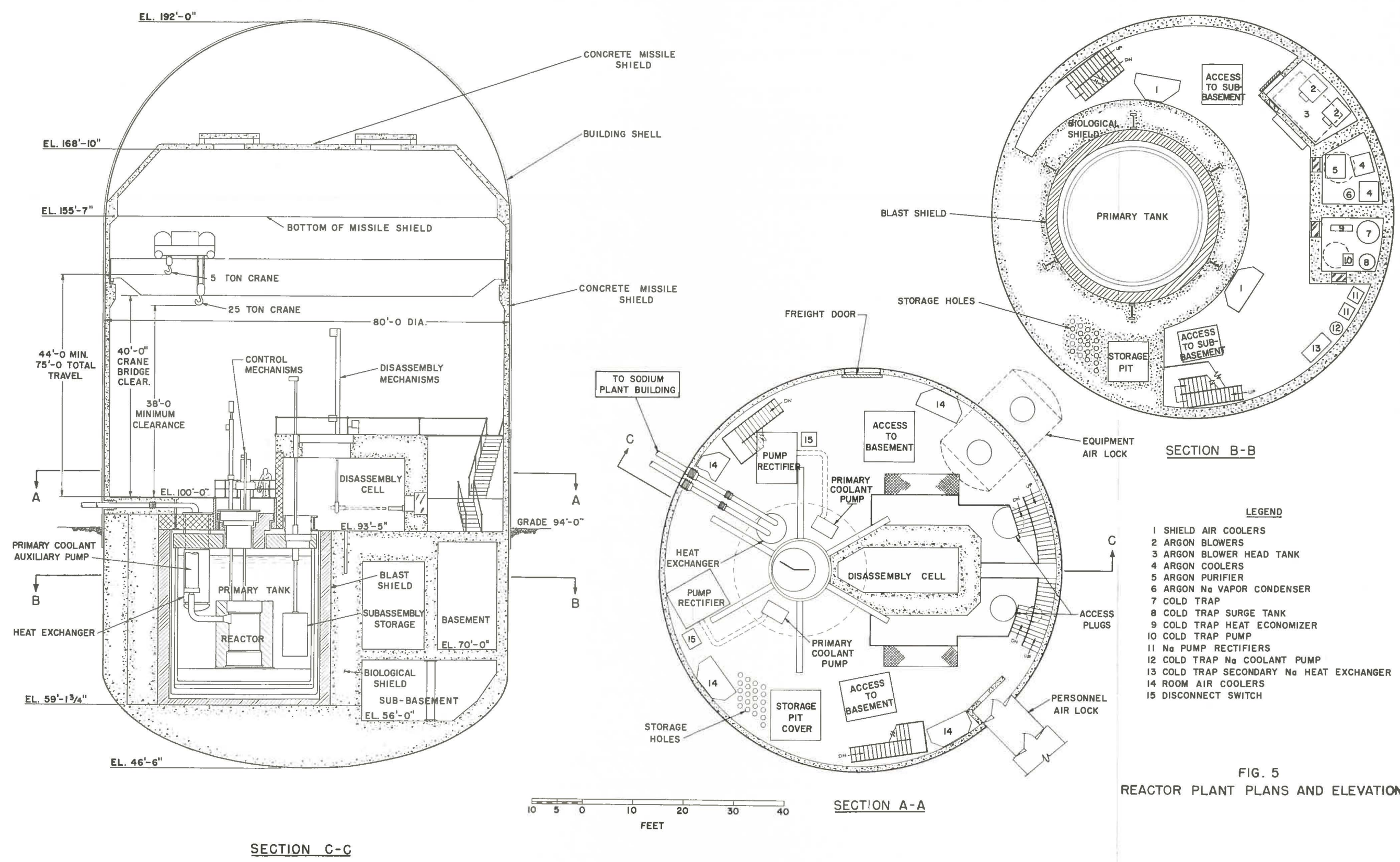
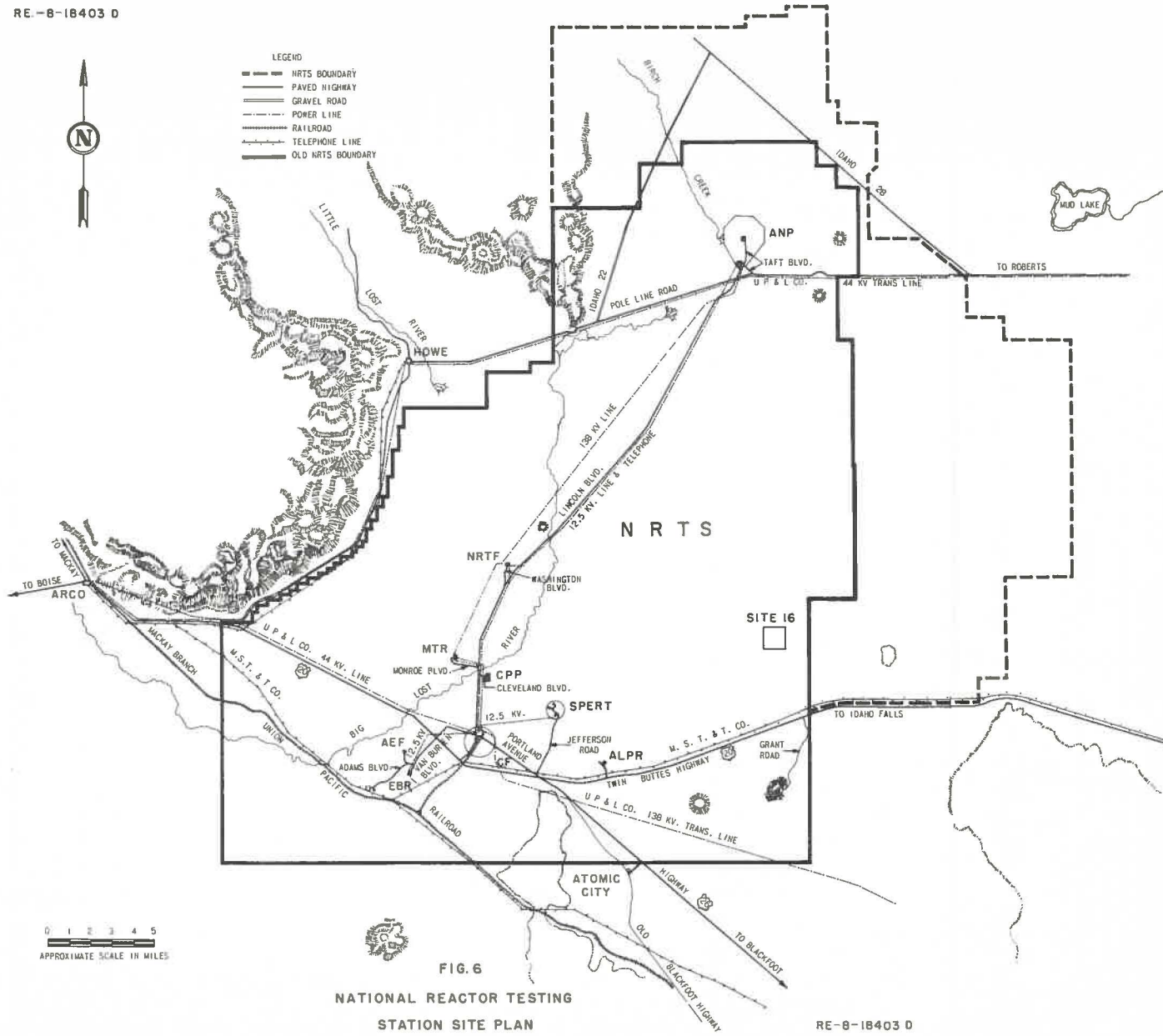


FIG. 5  
 REACTOR PLANT PLANS AND ELEVATION

RE-8-18403 D



0 1 2 3 4 5  
APPROXIMATE SCALE IN MILES

RE-8-18403 D

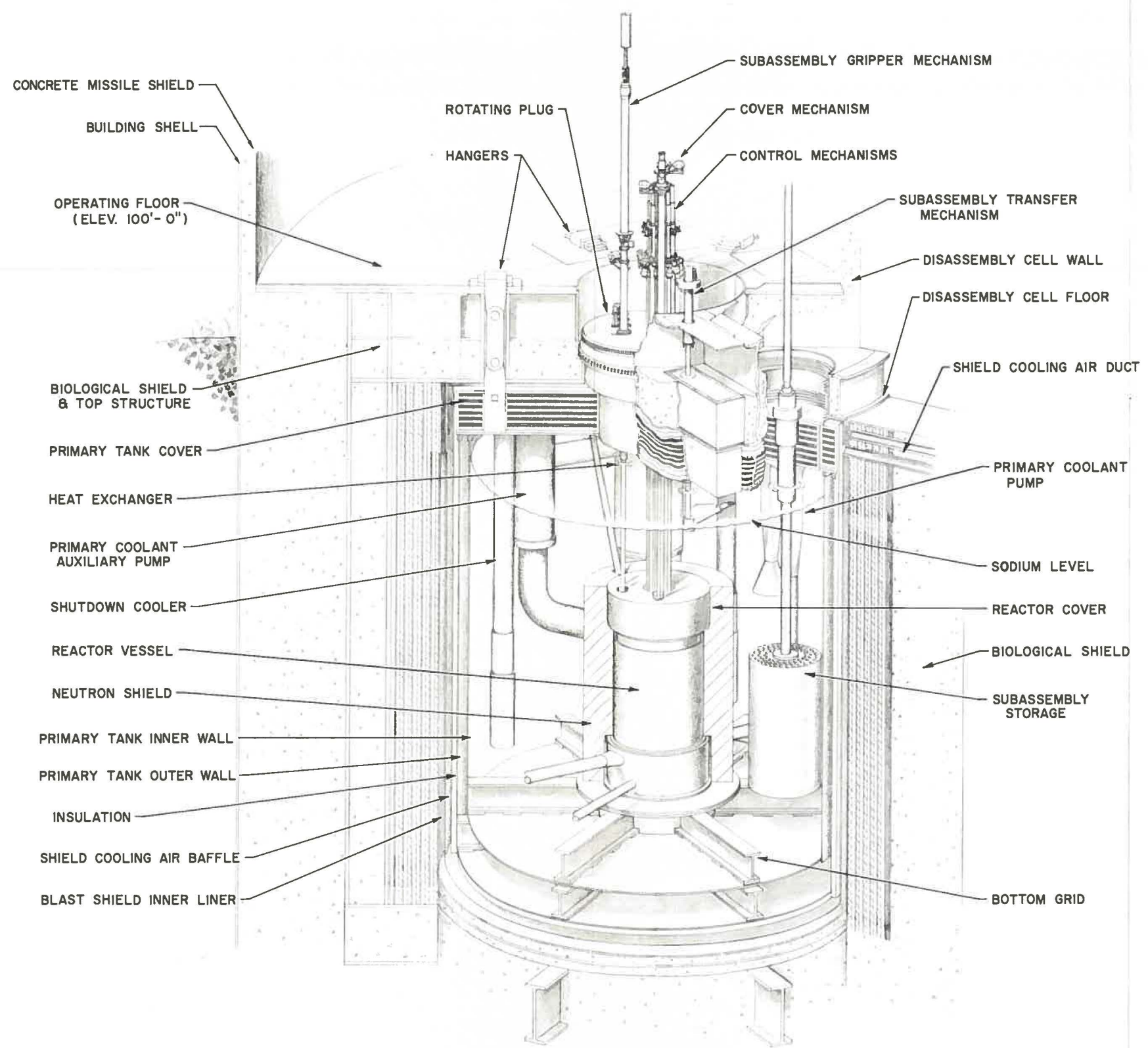


FIG. 7  
EBR II PRIMARY SYSTEM

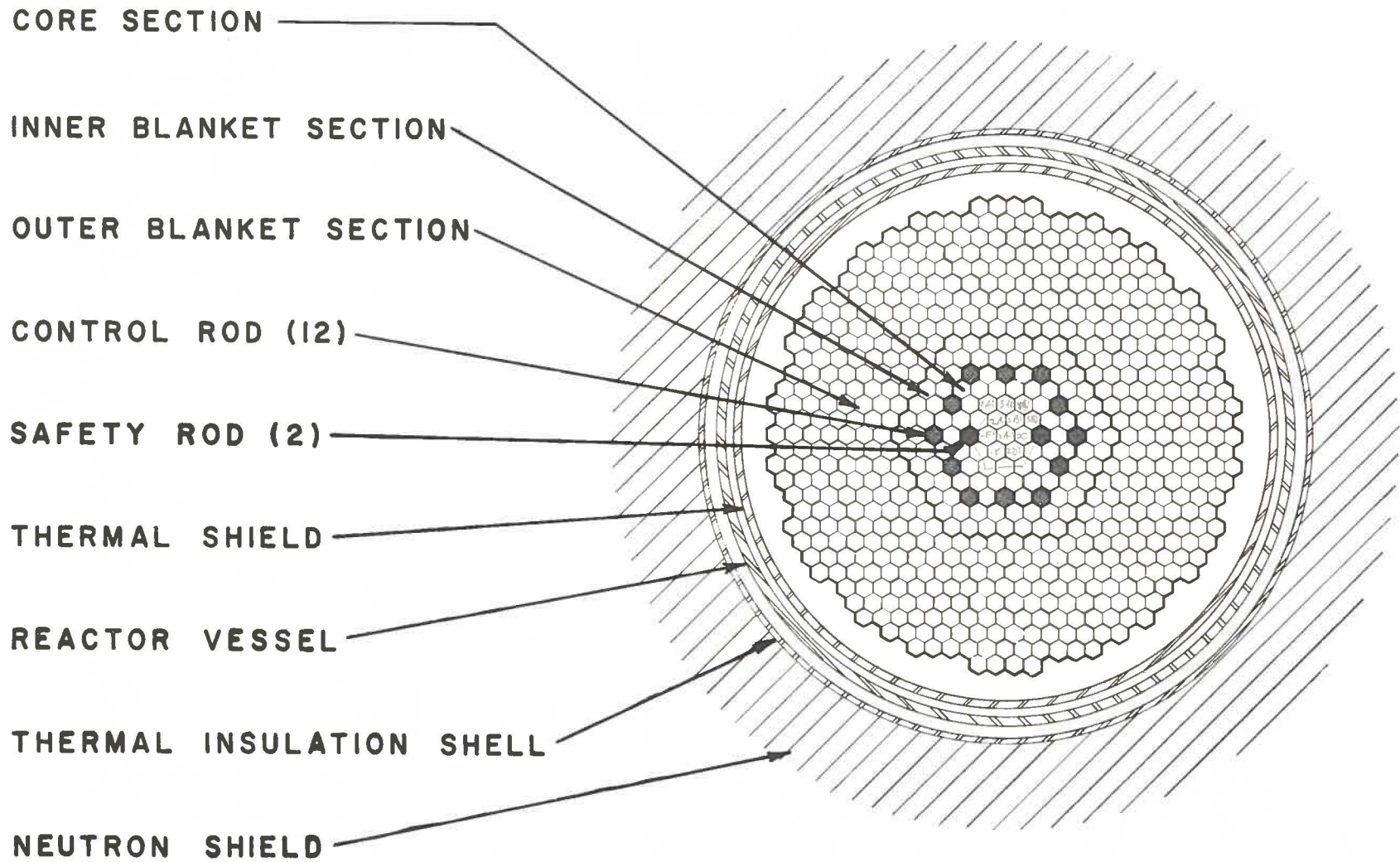


FIG. 8  
REACTOR ARRANGEMENT

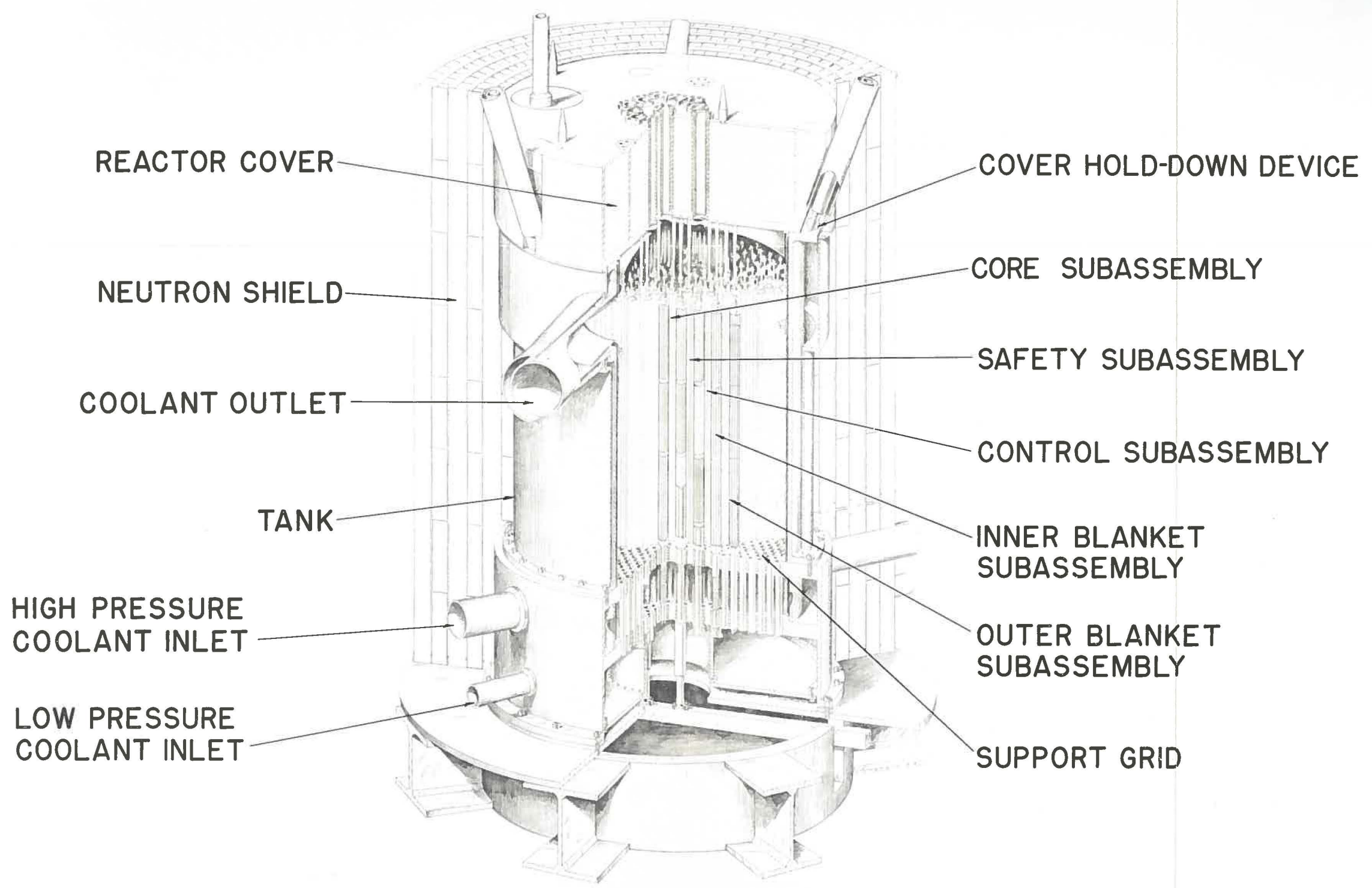


FIG. 9  
EBR II REACTOR

RE-6-20043+0  
E. J. MITTER G. G., 3-27-57

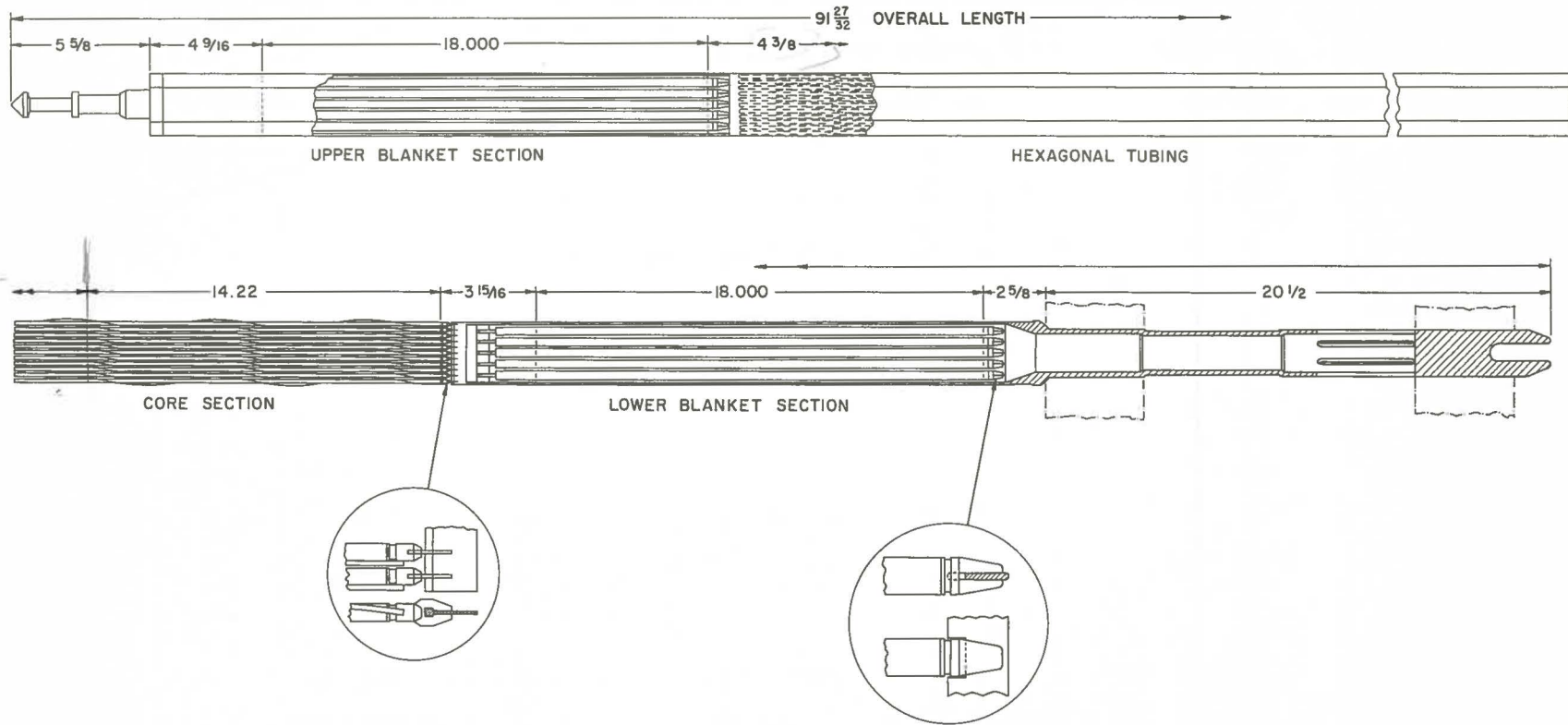


FIG. 10  
EBR-II CORE SUBASSEMBLY

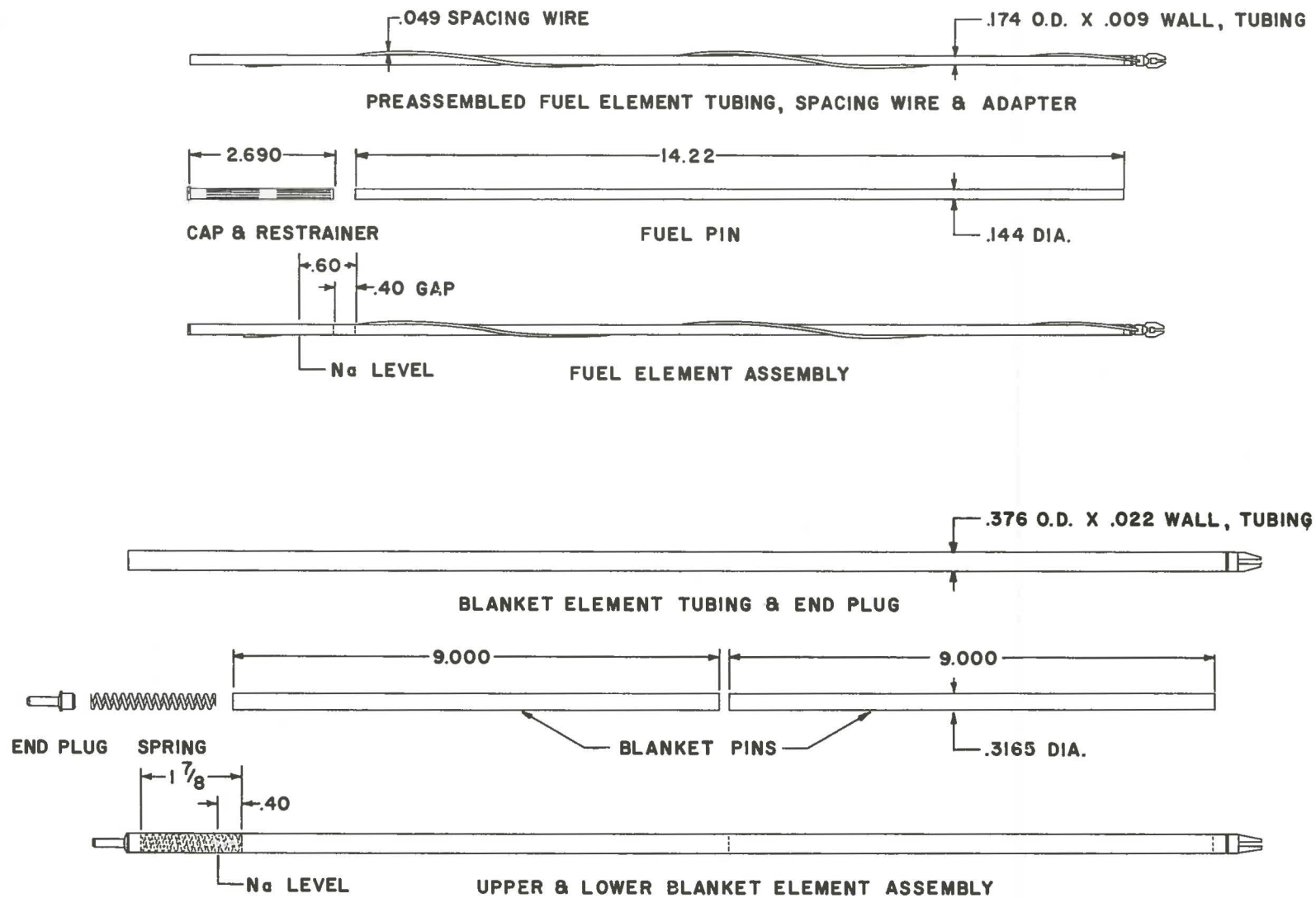


FIG. II  
CORE SUBASSEMBLY ELEMENTS

RE-6-20049-D  
E. RITTER: G. G., 3-27-57

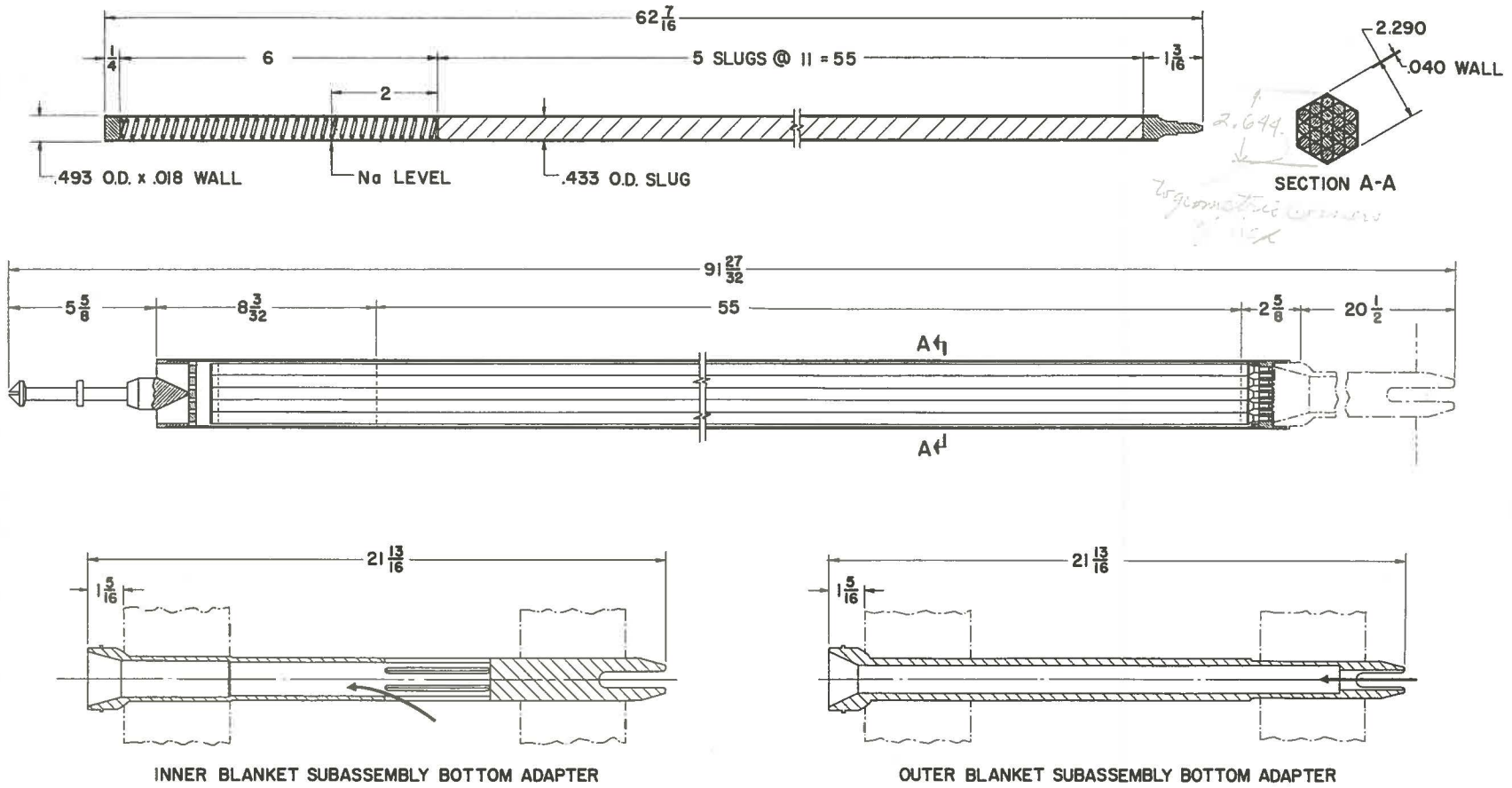


FIG. 12  
EBR II INNER BLANKET & OUTER BLANKET SUBASSEMBLIES



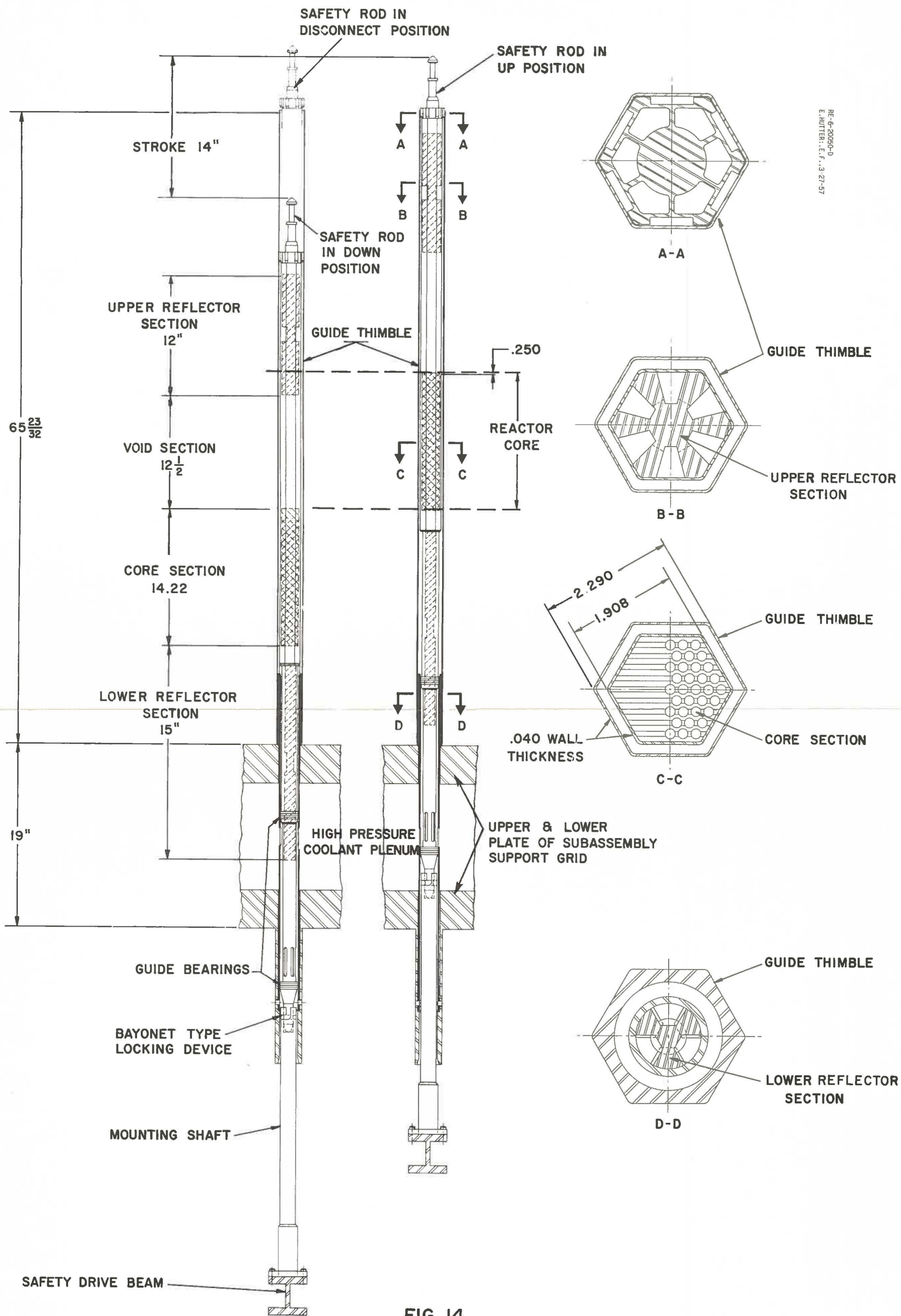


FIG. 14  
SAFETY SUBASSEMBLY

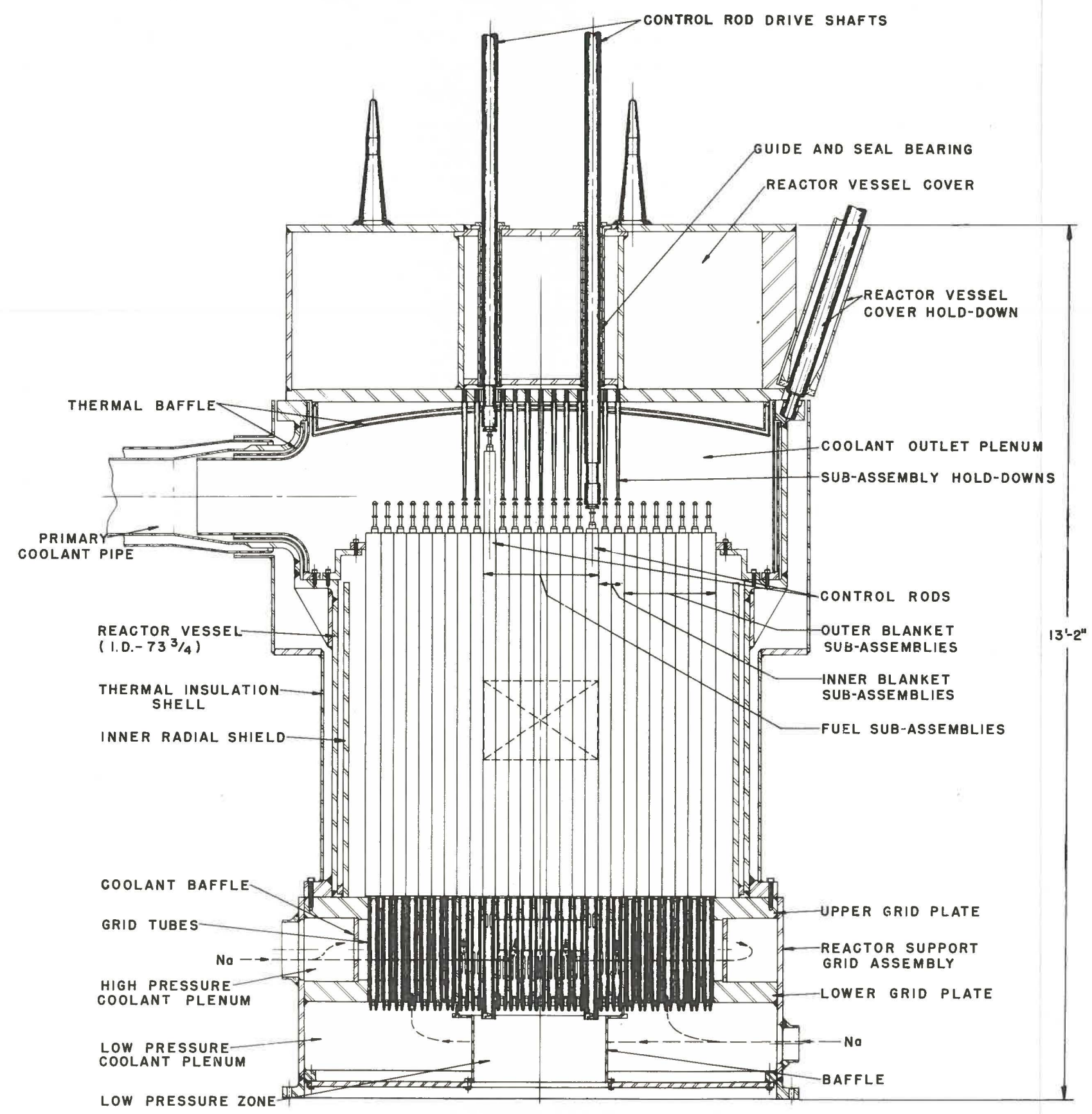


FIG. 15  
REACTOR VESSEL ASSEMBLY

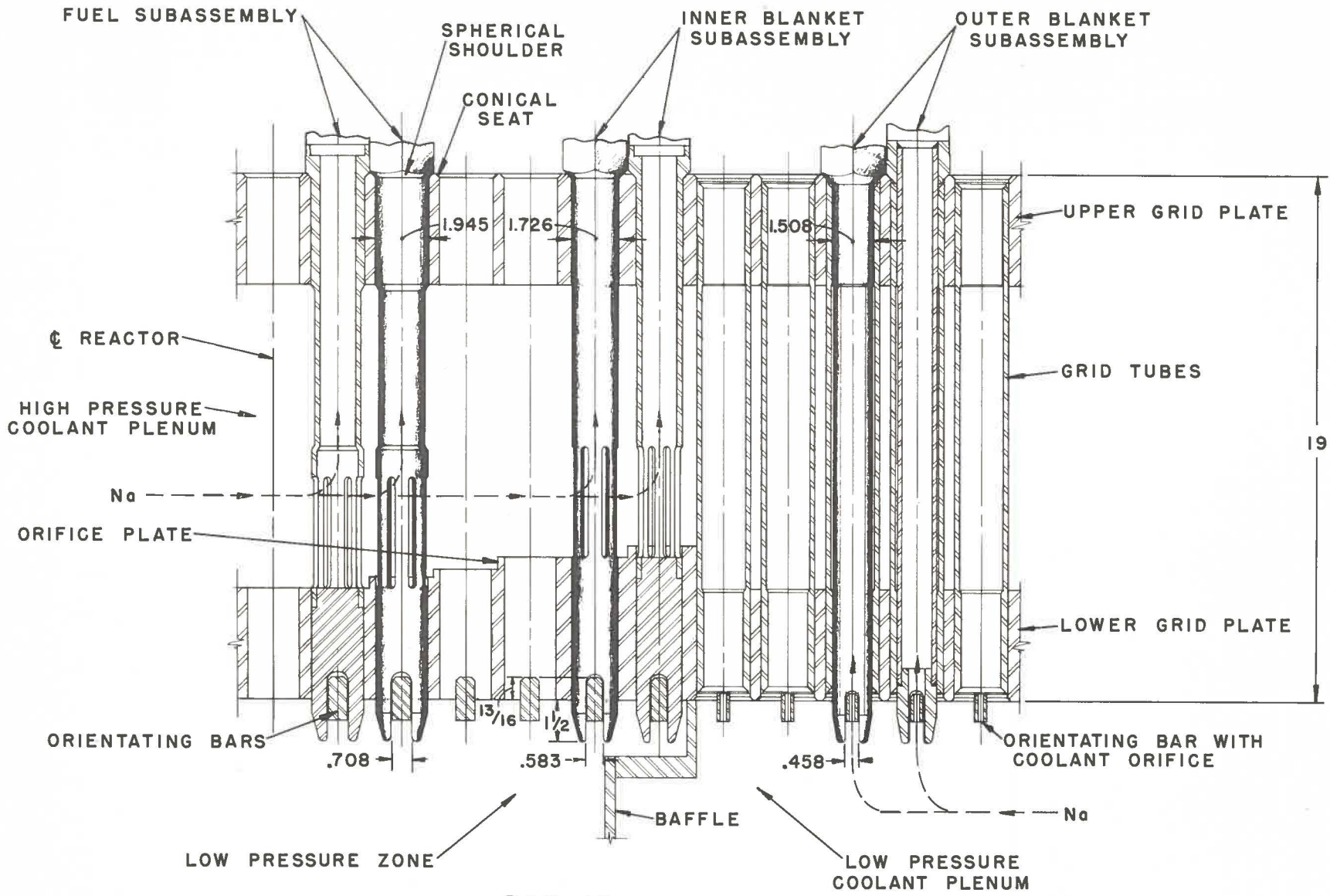


FIG. 16  
REACTOR SUPPORT GRID

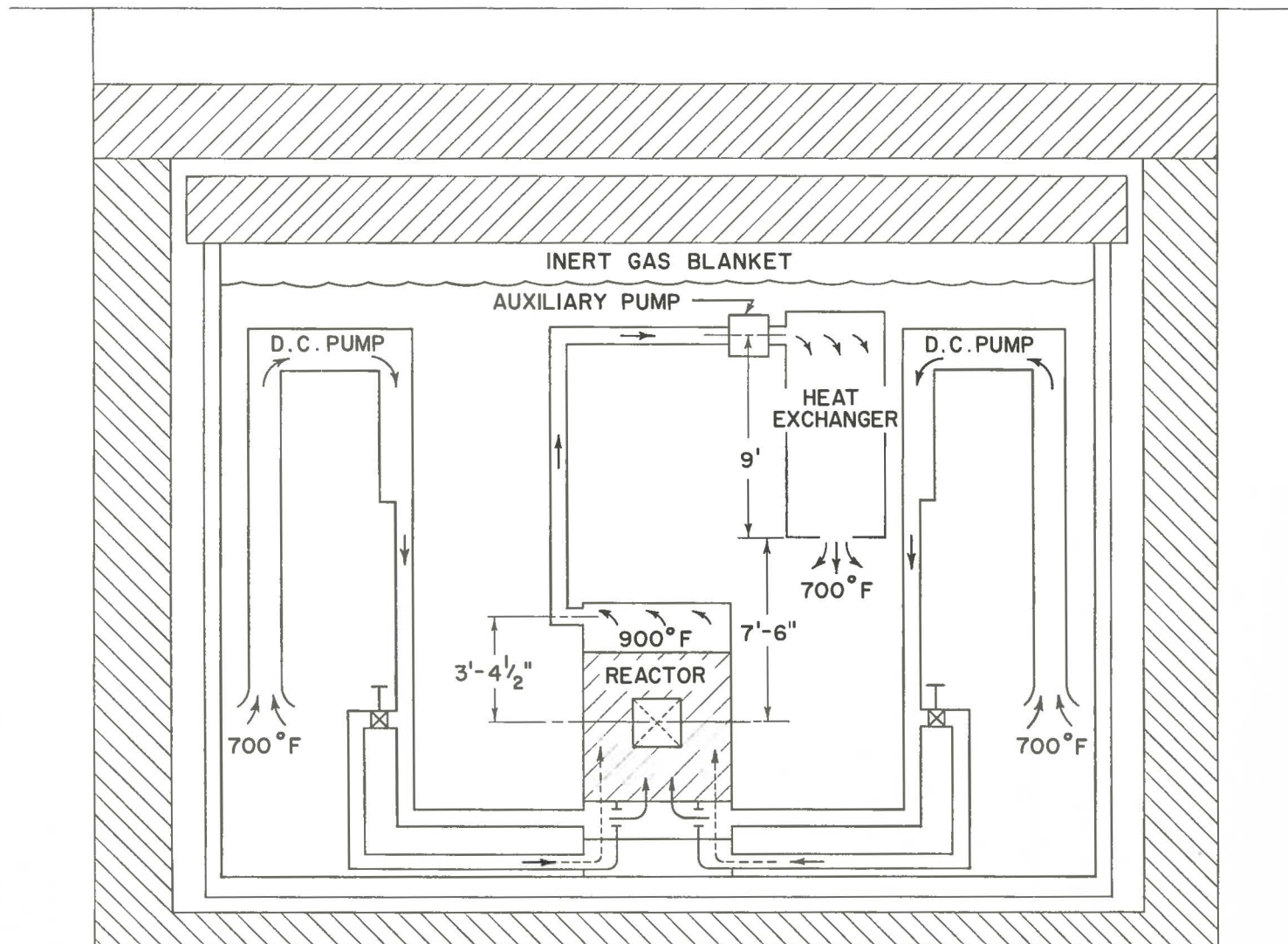


FIG. 17  
SCHEMATIC OF PRIMARY  
COOLANT SYSTEM

LEGEND	PREFIX NO	
PRIMARY SYSTEM	1	—————
SECONDARY SYSTEM	2	-----
STEAM SYSTEM	3	-----
SHUT DOWN COOLING	4	-----
FEEDWATER	5	-----
ARGON SYSTEM	6	-----
COOLING TOWER	7	-----
SHIELD AIR COOLING	8	-----

INSTRUMENT & SYMBOLS	
REMOTE READING	○
VALVE-REMOTE OPERATING	○/□
VALVE-REGULATING	□
TEMPERATURE	T
FLOW	F
PRESSURE	P
LIQUID LEVEL	L

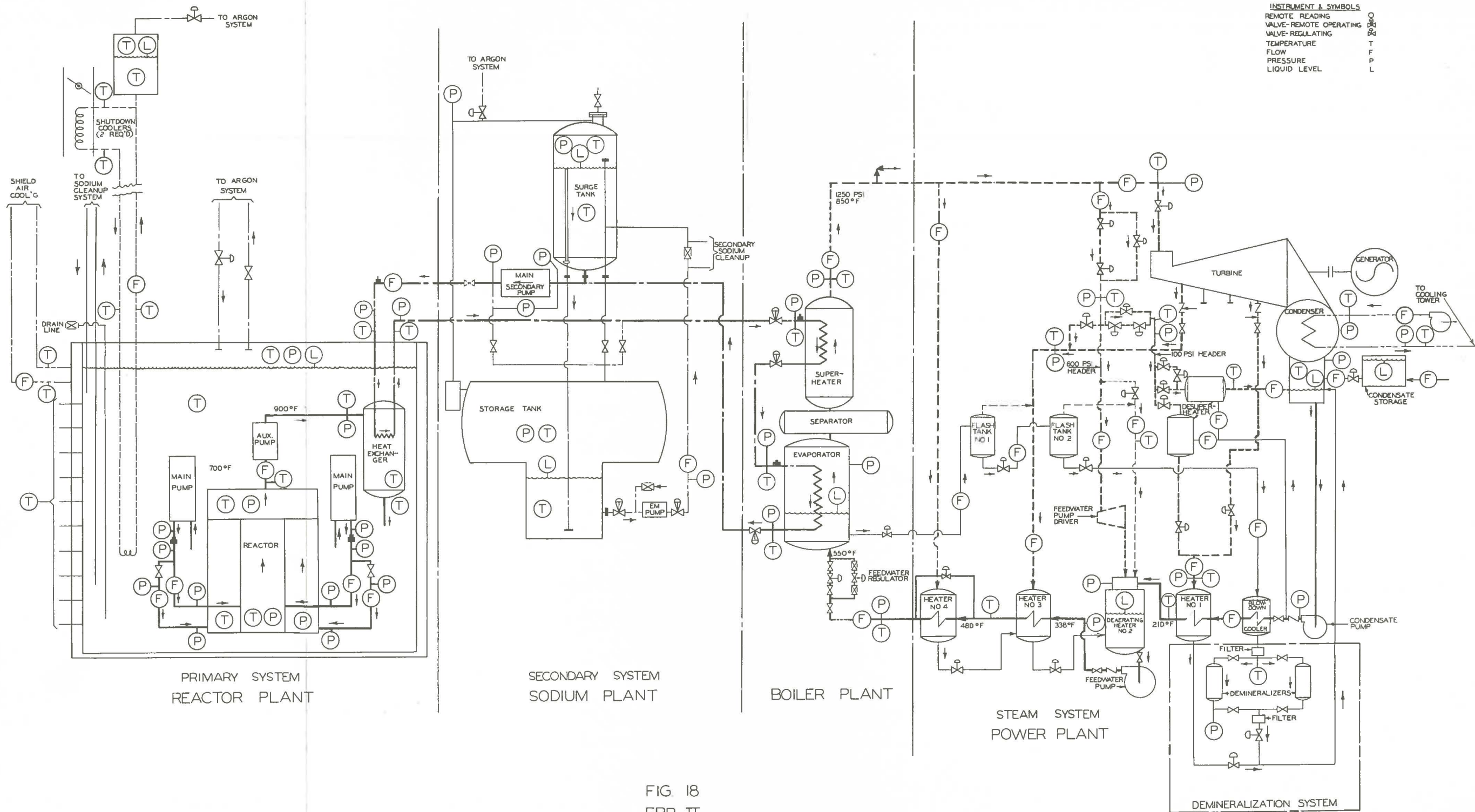
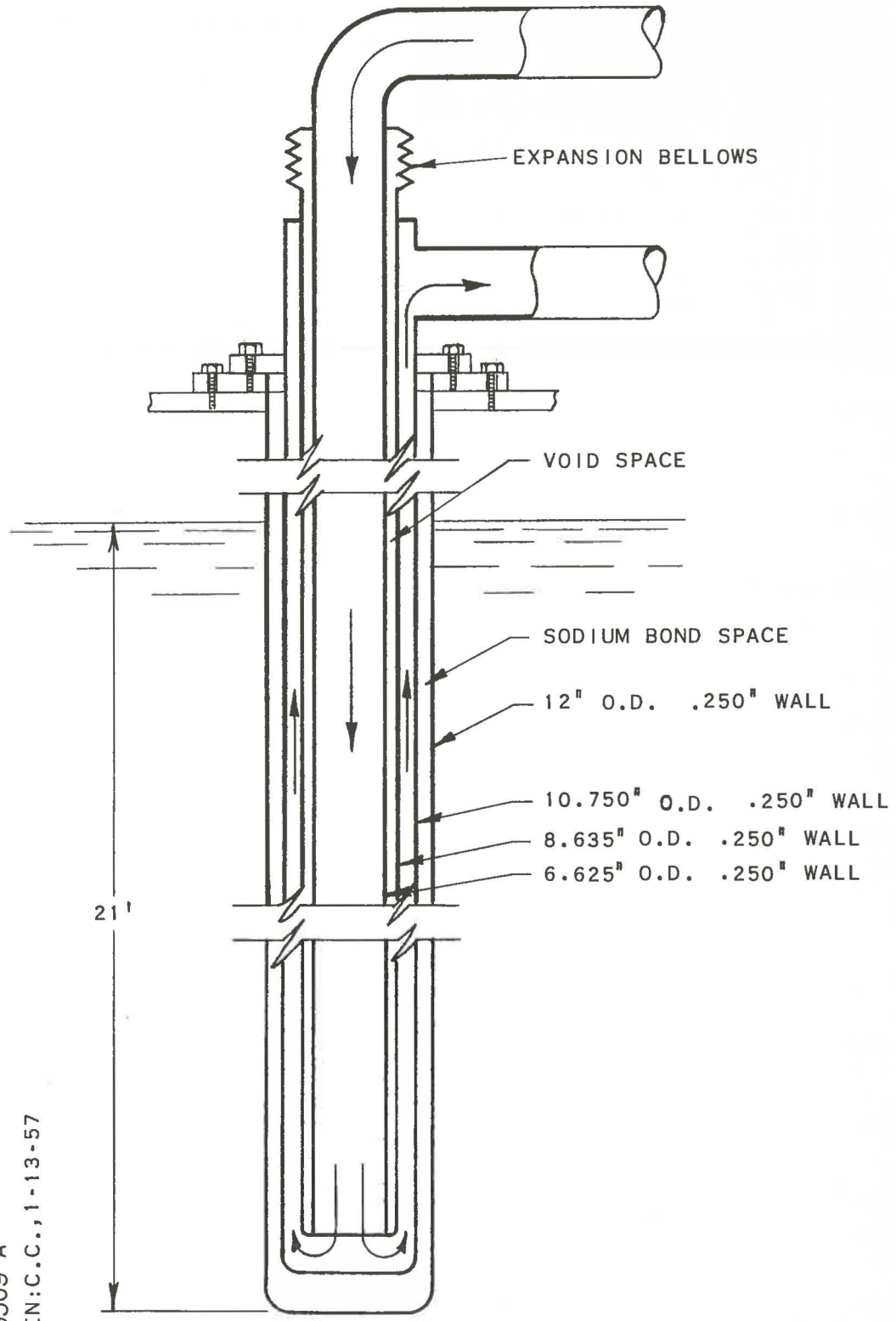


FIG 18  
EBR II  
INSTRUMENT FLOW SHEET



RE-8-19509-A  
K. KUCZEN: C.C., 1-13-57

FIG. 19  
SHUT-DOWN COOLER

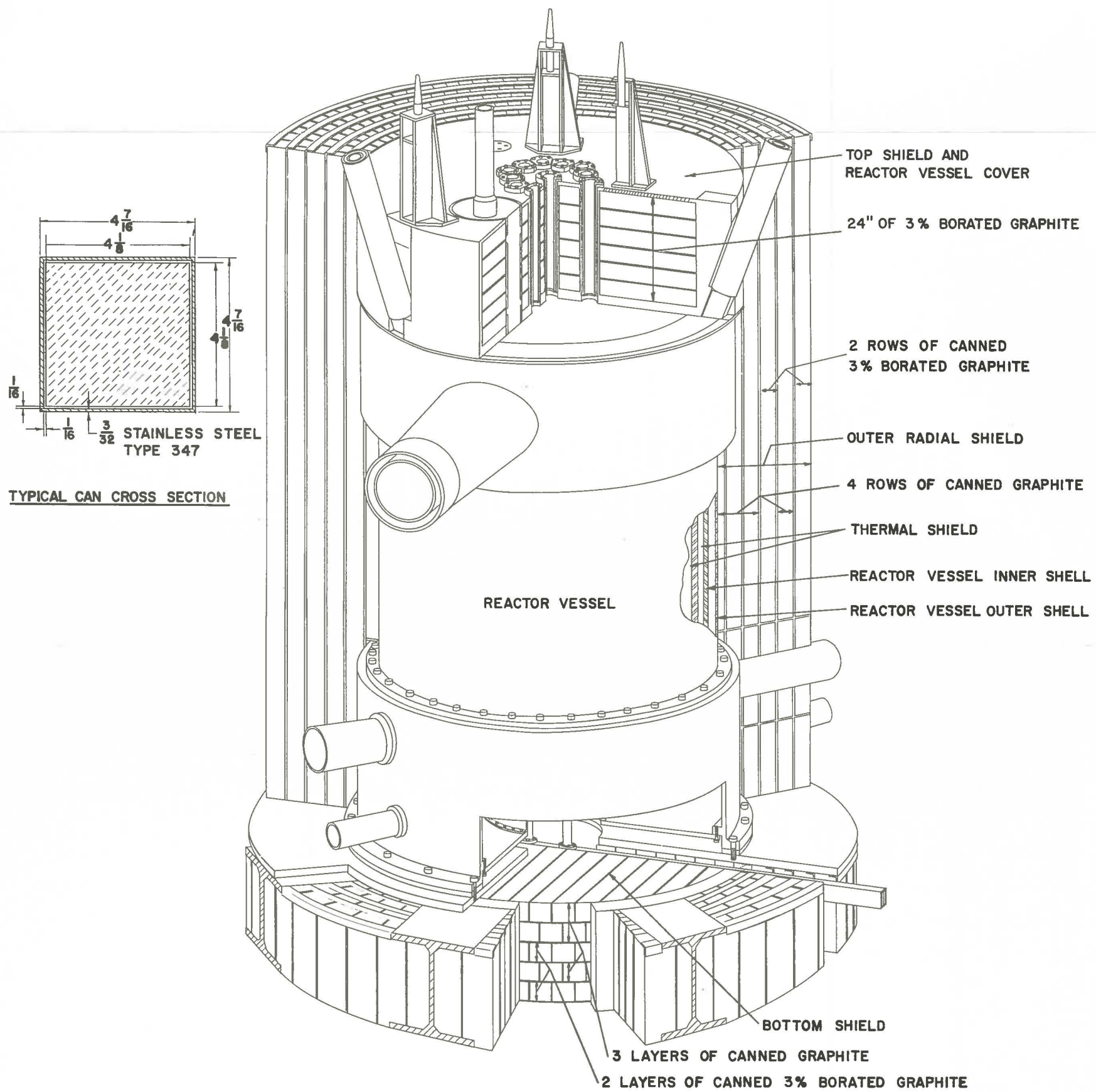


FIG. 20  
NEUTRON SHIELD

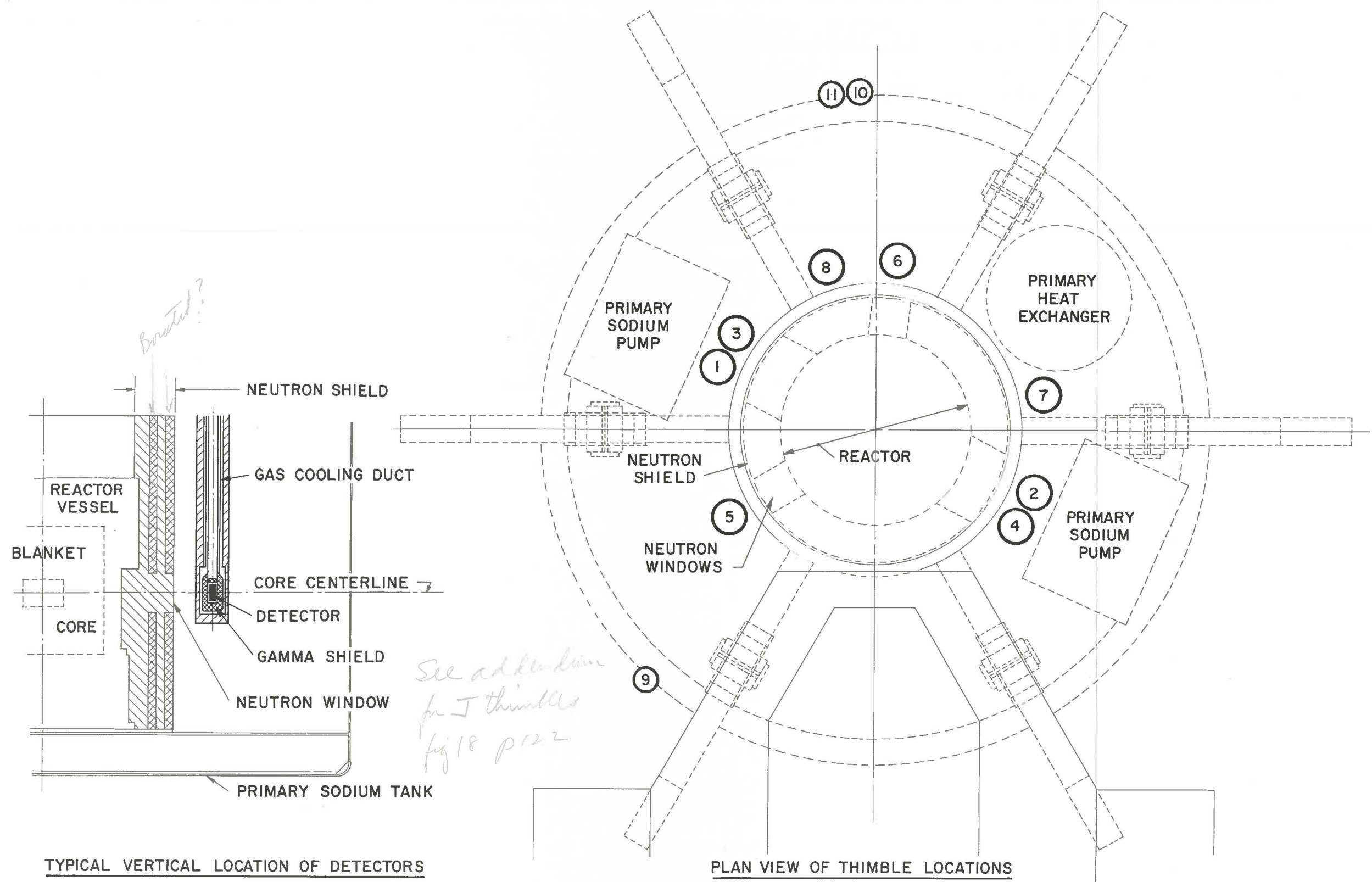


FIG. 21  
NUCLEAR INSTRUMENT THIMBLE LOCATIONS

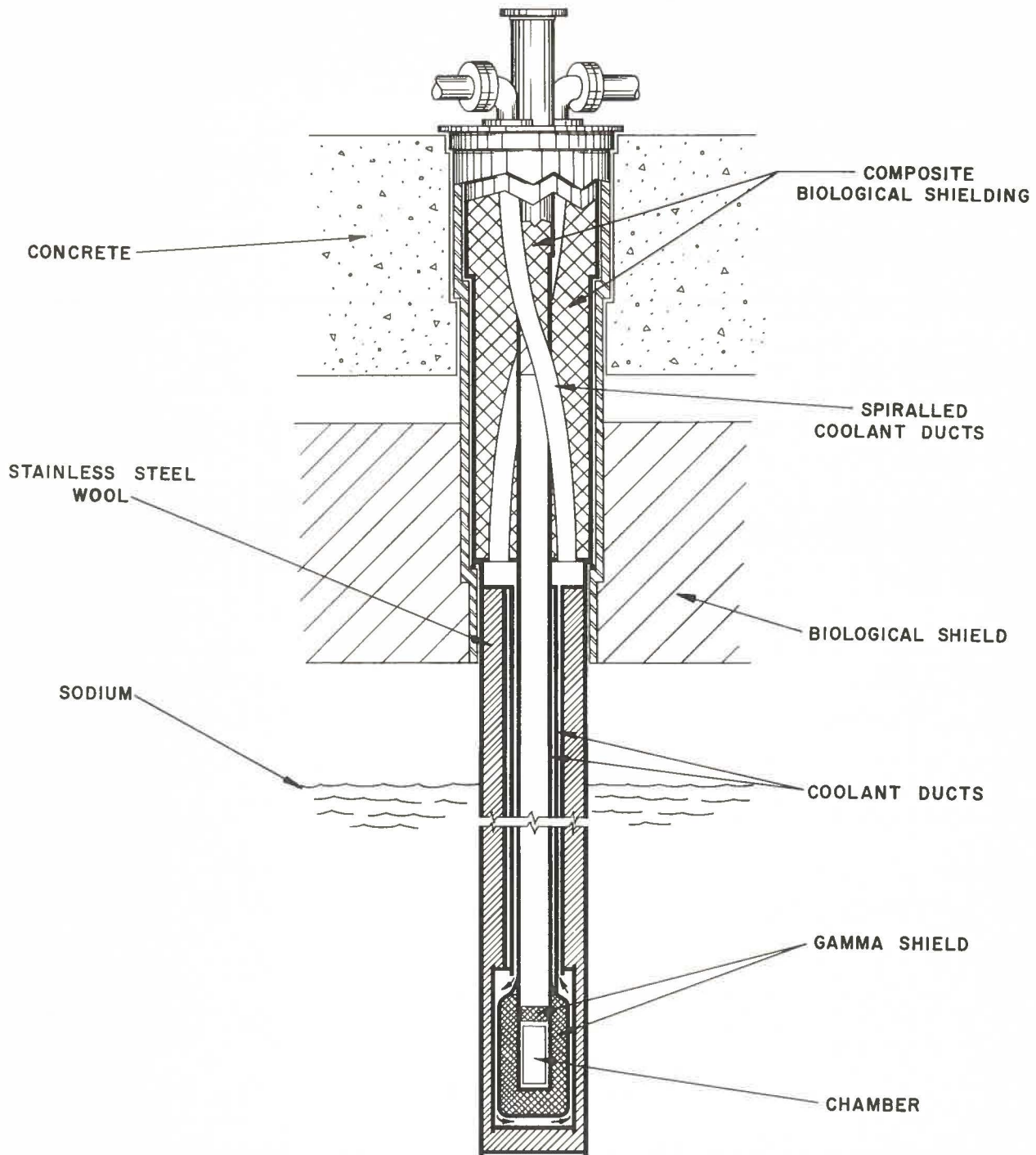


FIG. 22  
CHAMBER THIMBLE

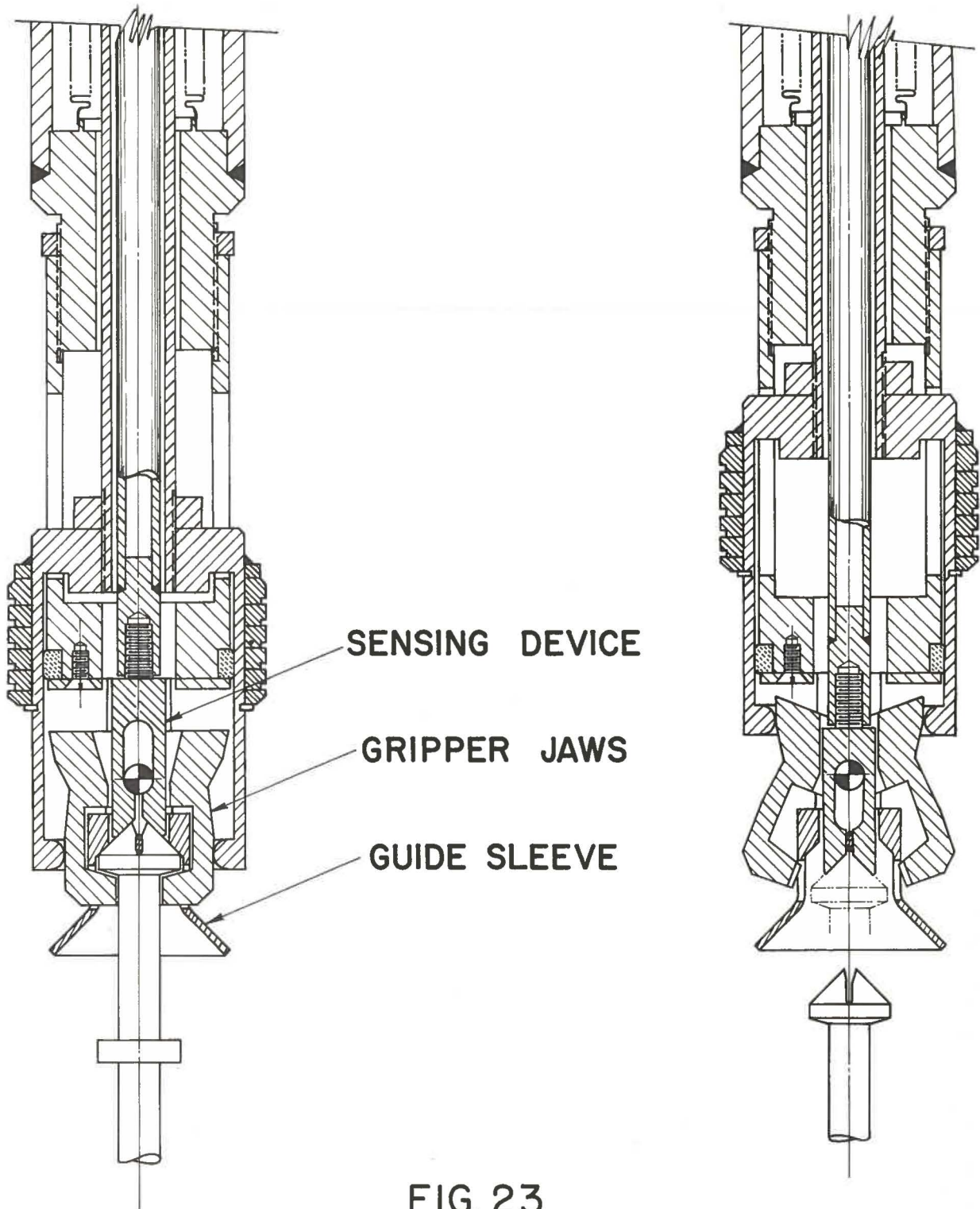
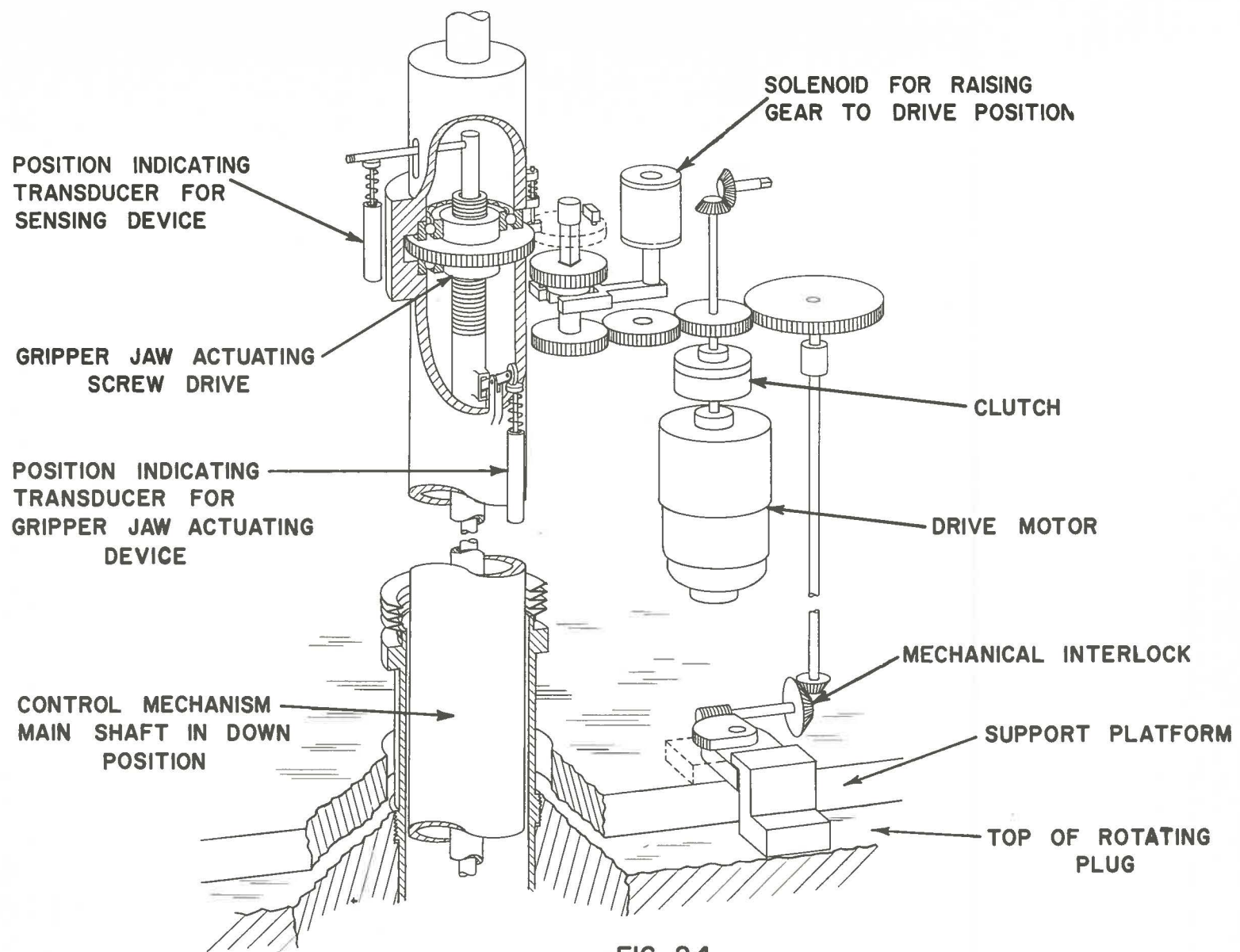


FIG. 23  
GRIPPER MECHANISM



**FIG. 24**  
**CONTROL GRIPPER ACTUATING DEVICE AND**  
**MECHANICAL INTERLOCK FOR SUPPORT PLATFORM**

RE-6-20046-C

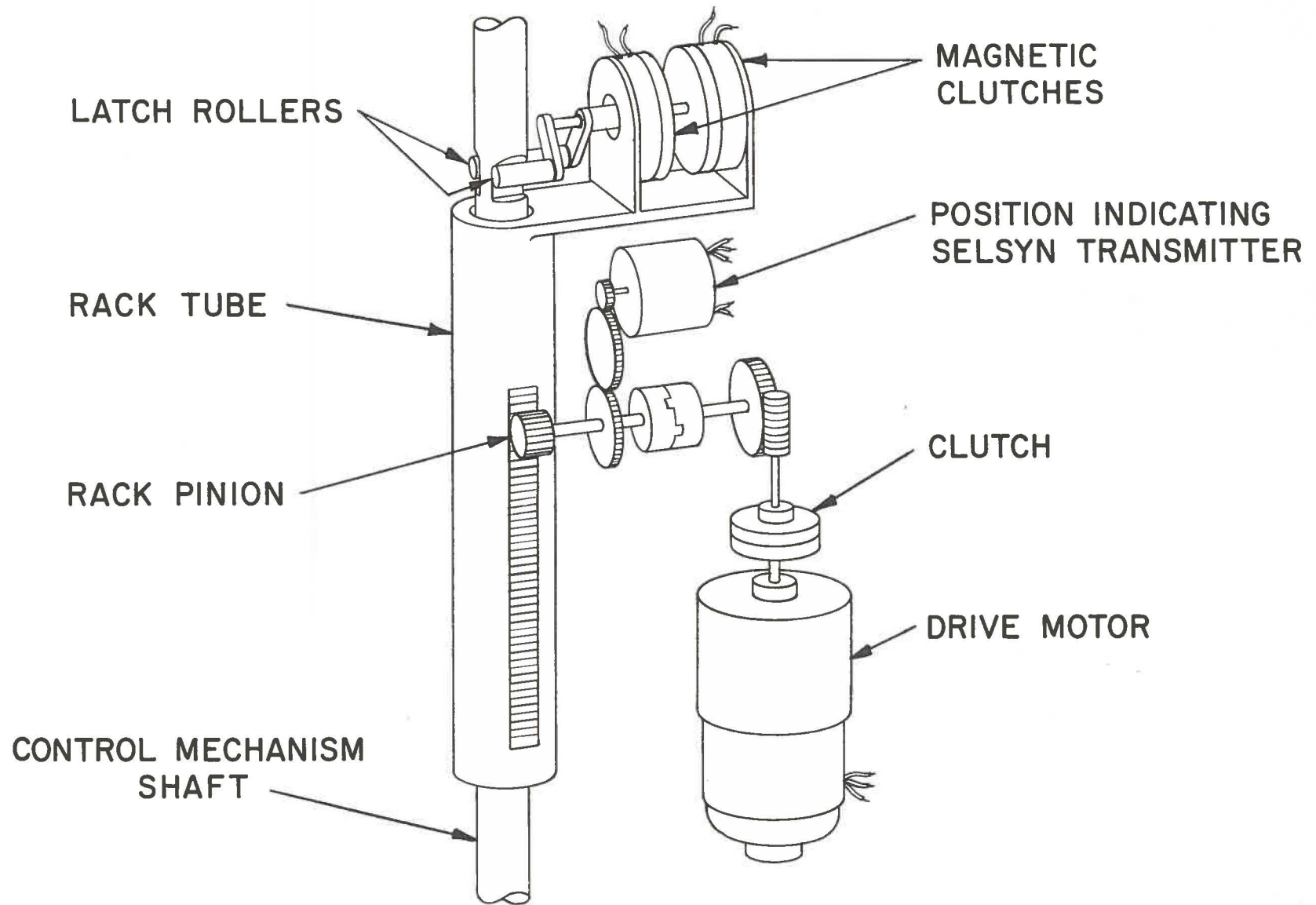
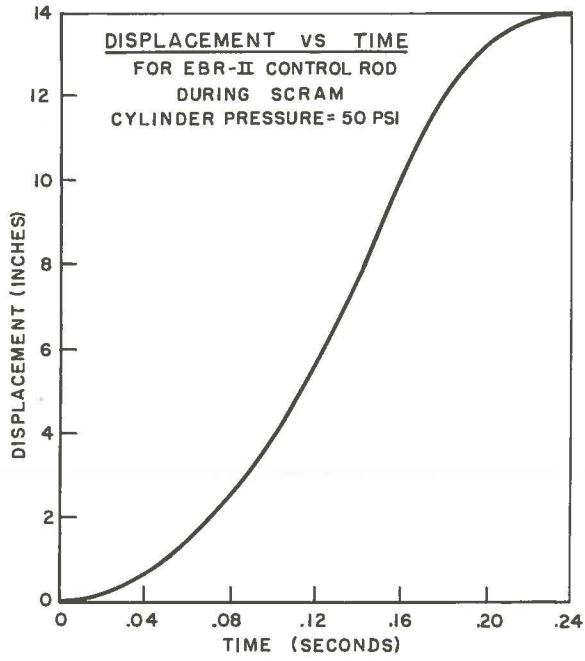
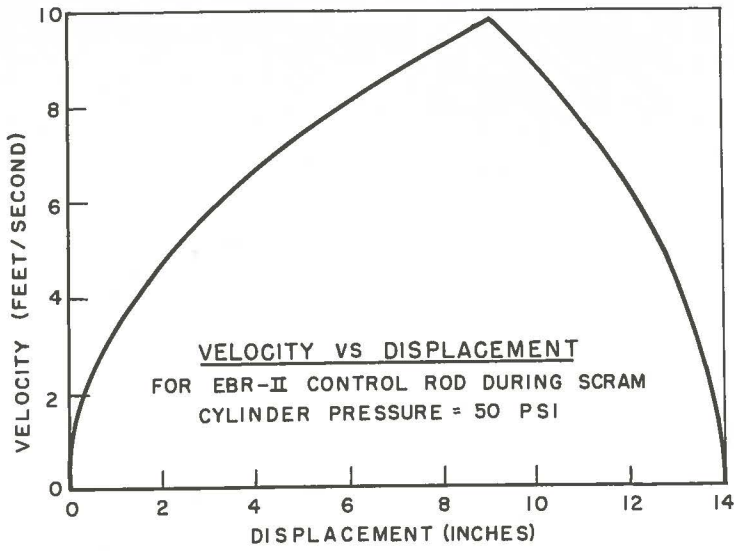


FIG. 25  
 CONTROL DRIVE AND LATCH MECHANISM



**FIGURE 26**  
**CONTROL ROD PERFORMANCE CHARACTERISTICS**

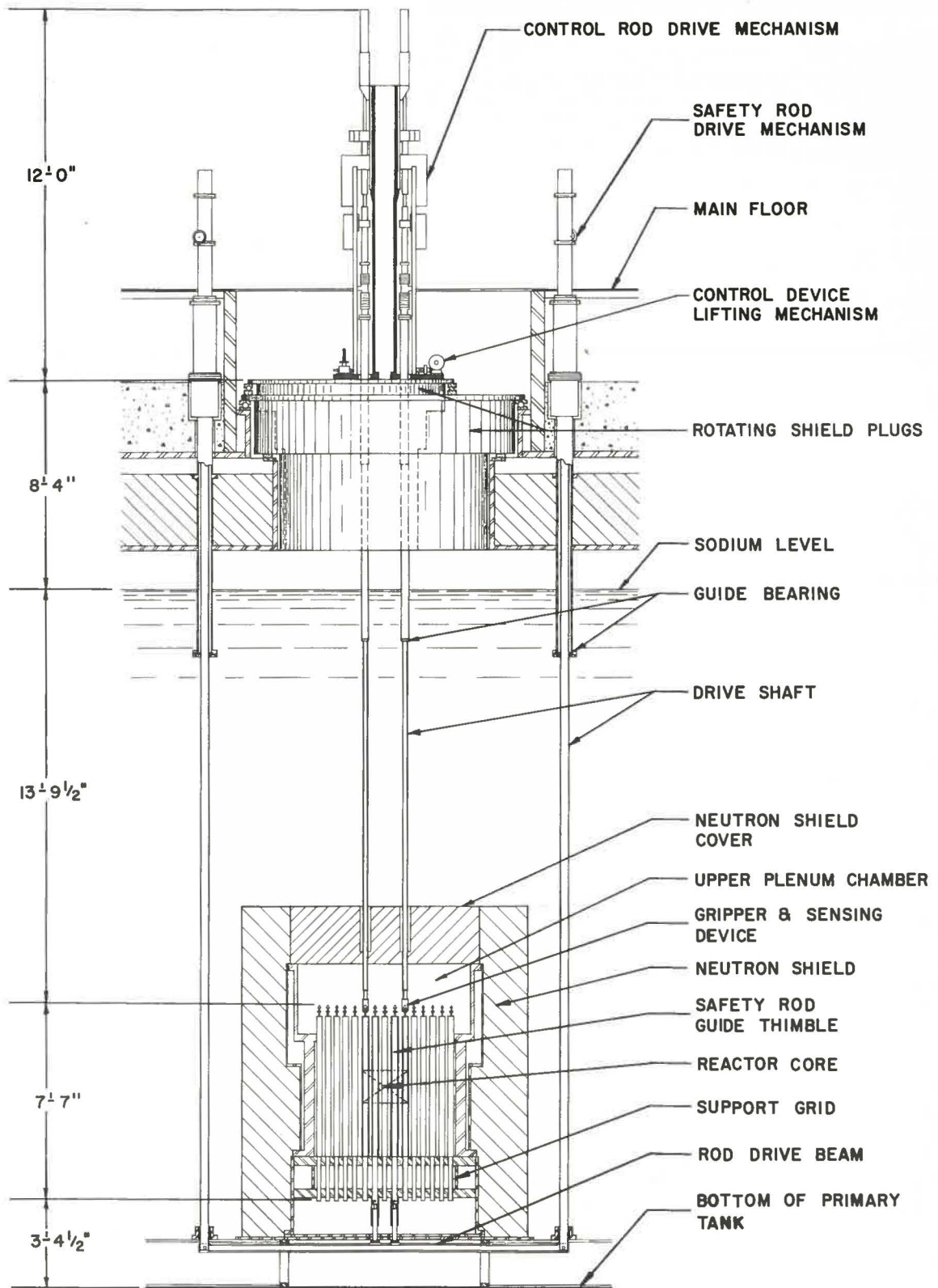


FIG. 27  
EBR II CONTROL & SAFETY ROD DRIVE SYSTEM

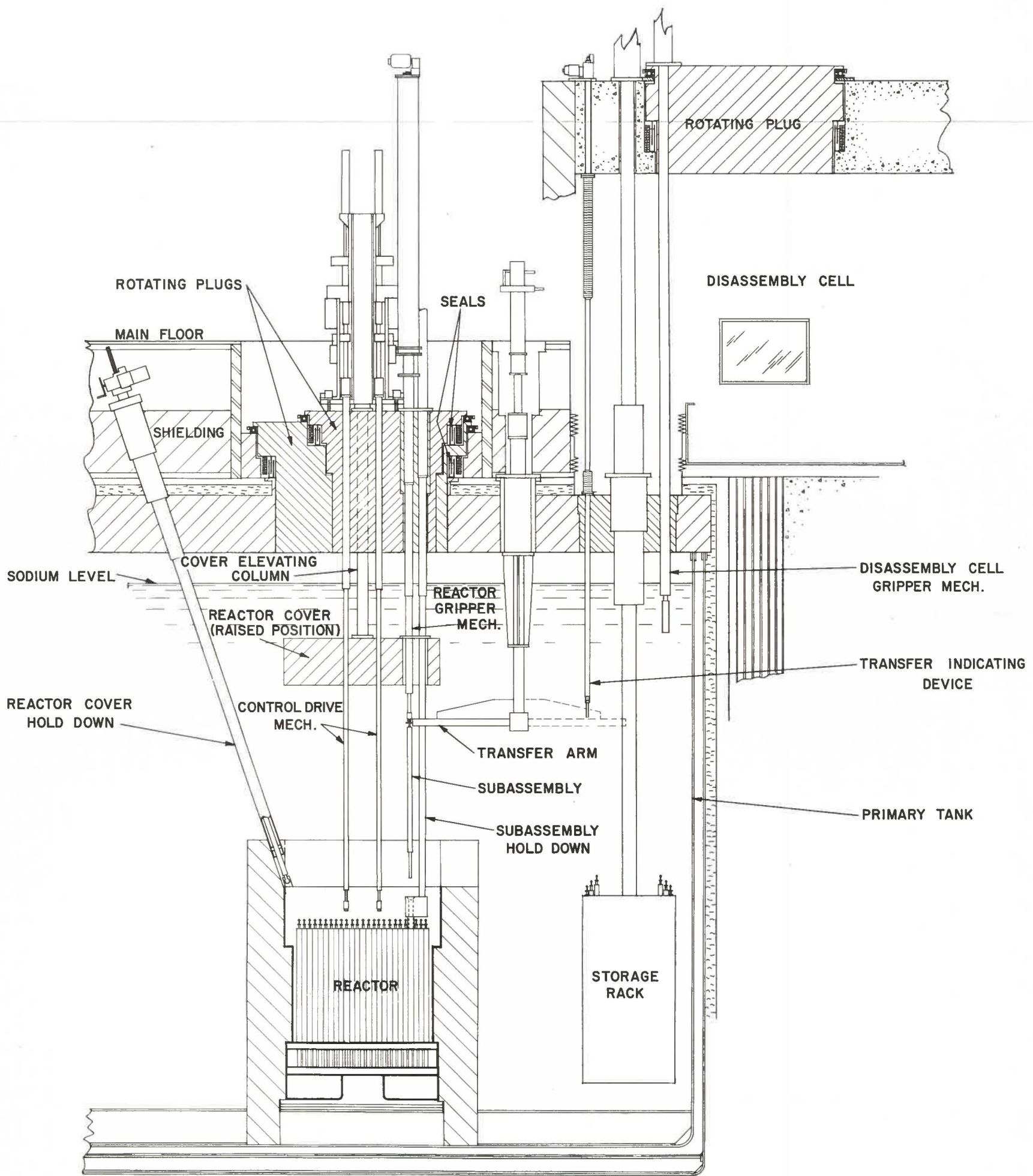


FIG. 28  
E B R II FUEL HANDLING SYSTEM

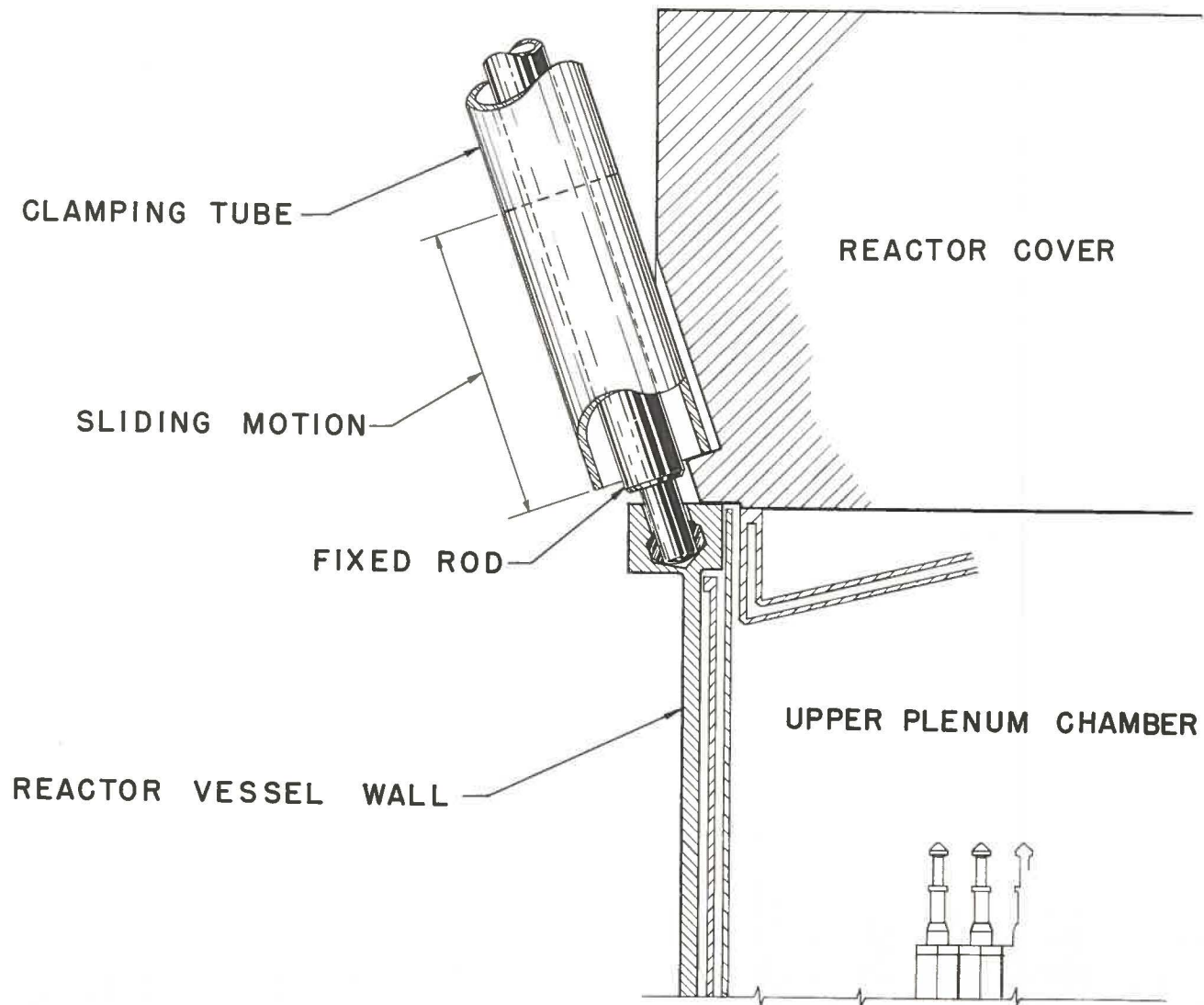


FIG.29  
 REACTOR COVER HOLD DOWN

RE-8-20092-C

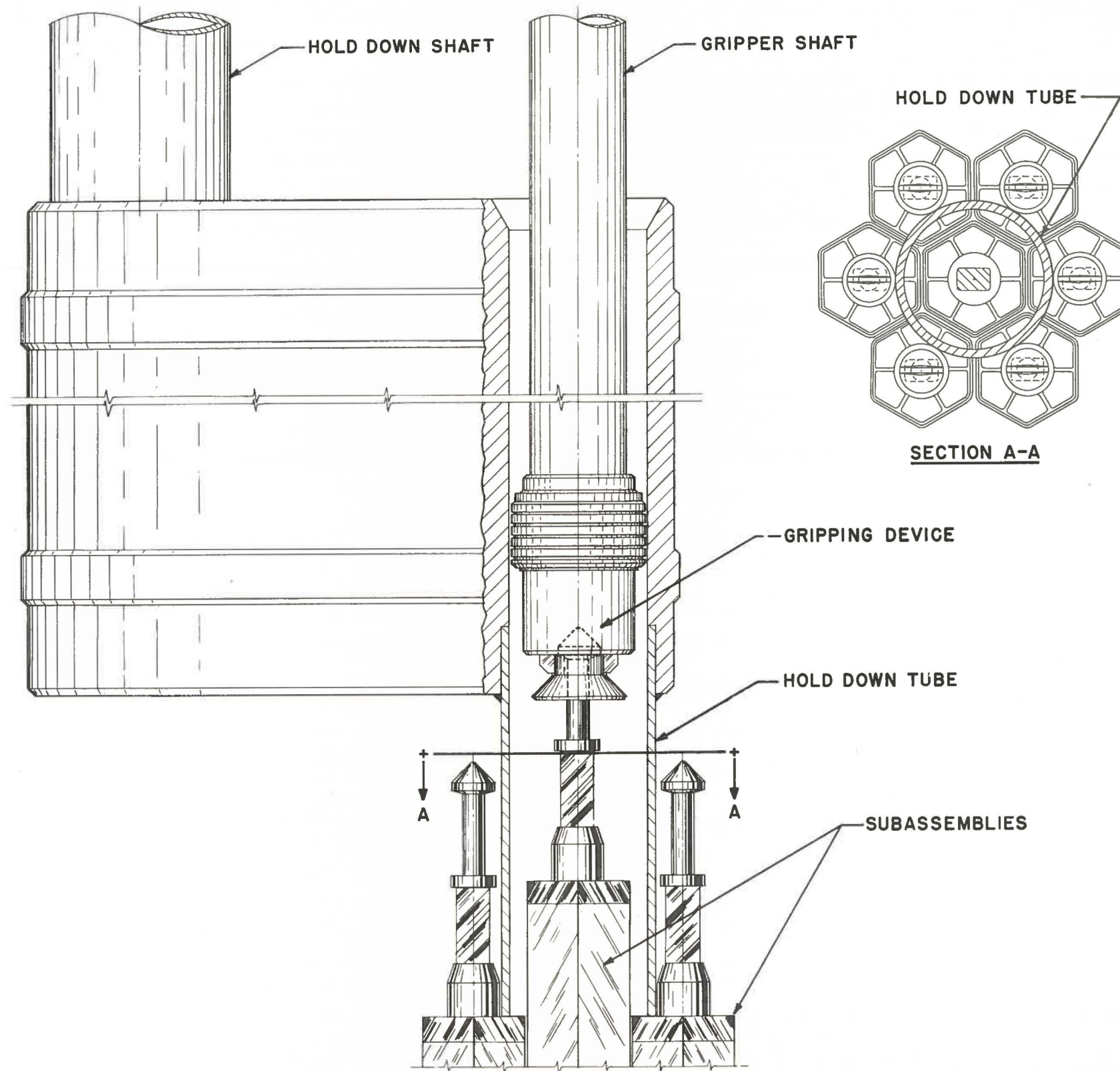
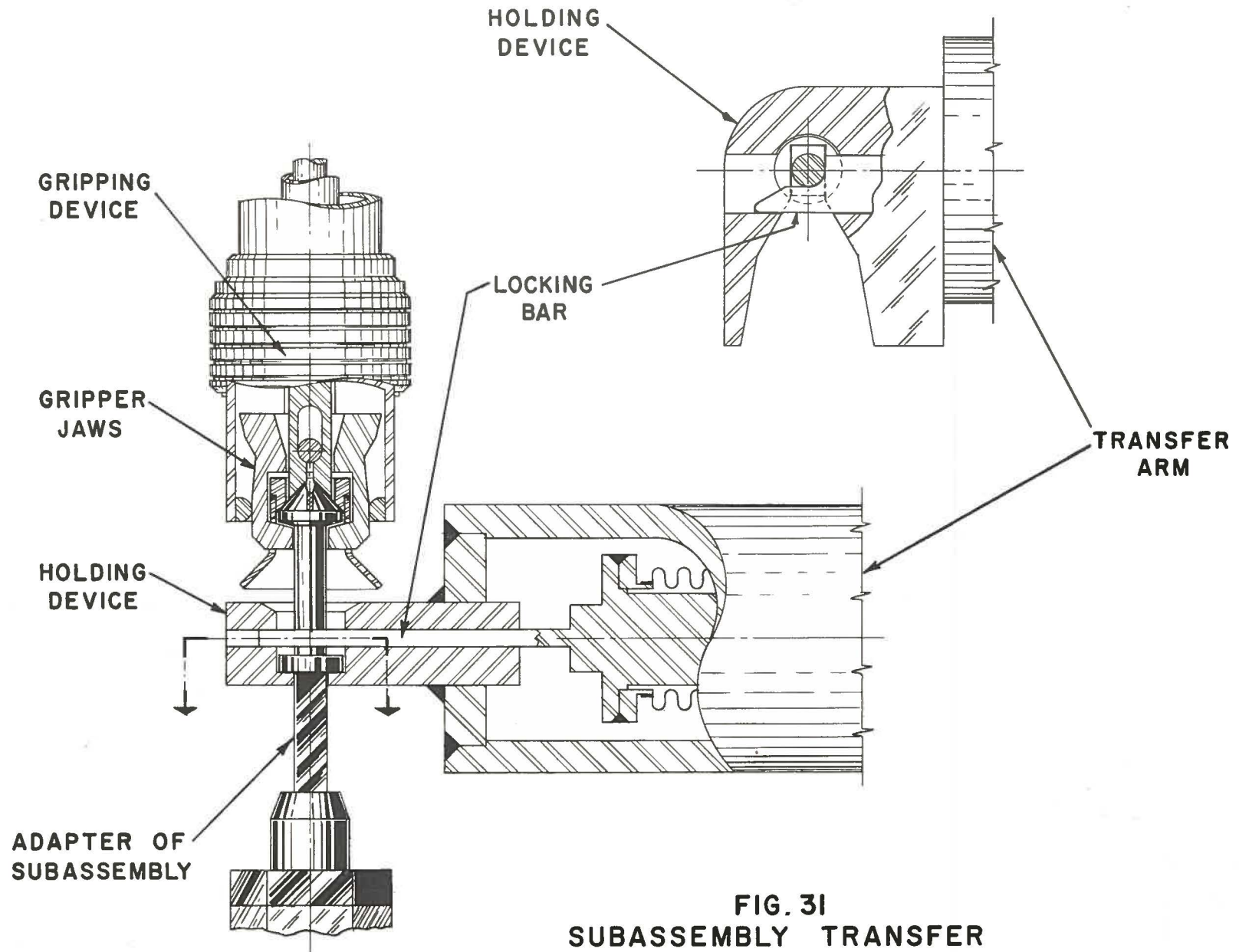


FIG. 30  
SUBASSEMBLY TRANSFER



**FIG. 31**  
**SUBASSEMBLY TRANSFER**

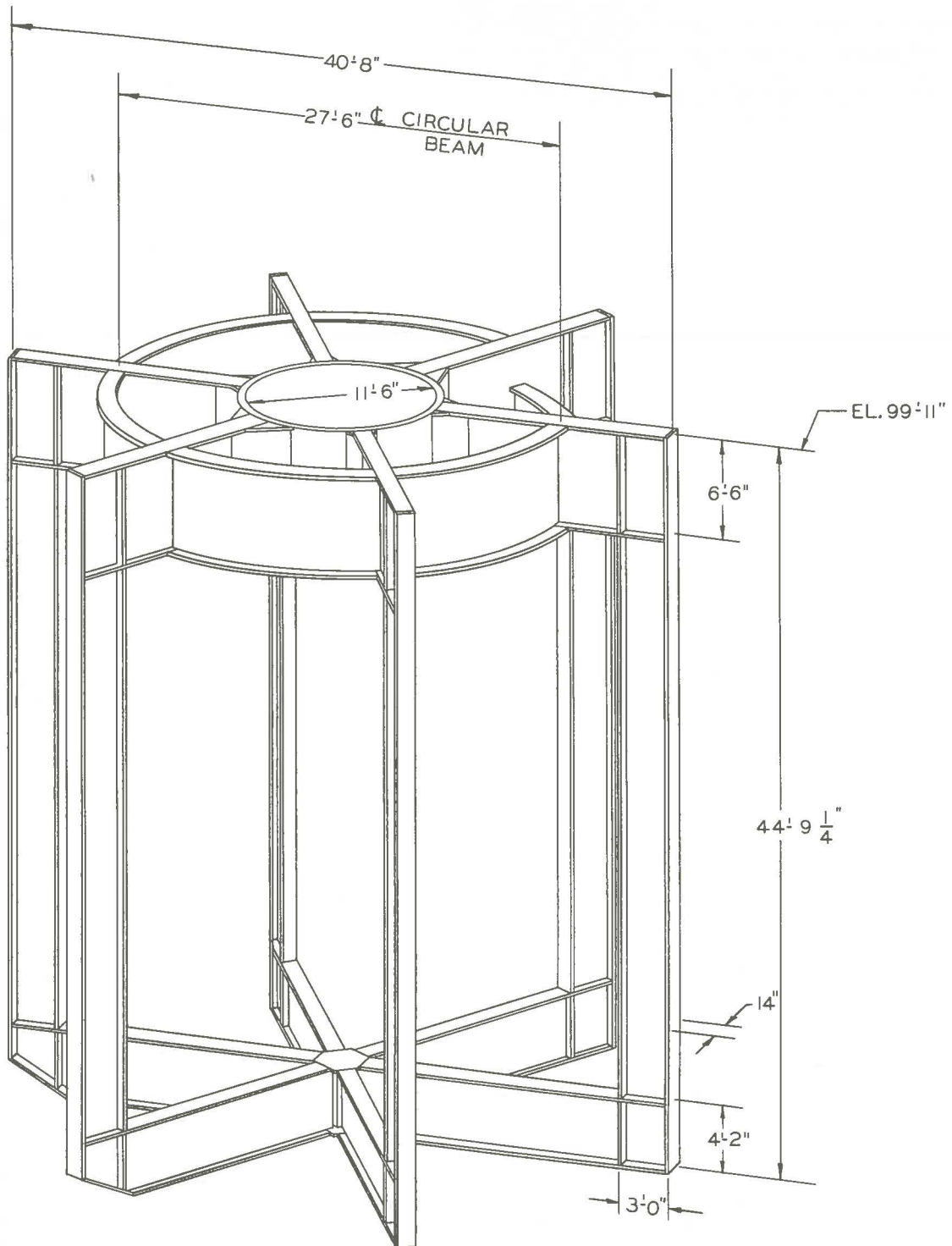


FIG. 32  
PRIMARY TANK SUPPORT STRUCTURE

RE-6-19561-A

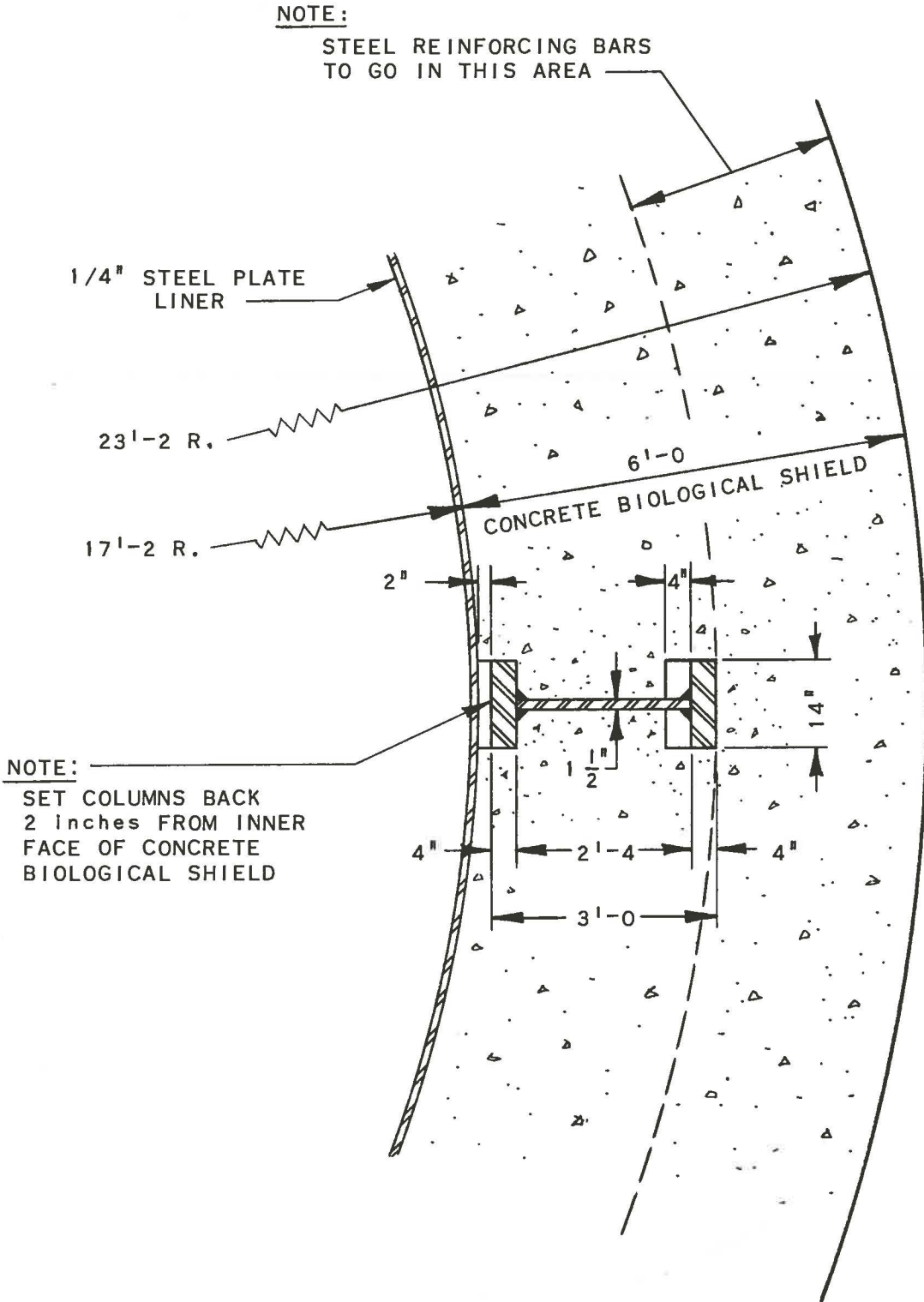


FIG. 33  
TYPICAL COLUMN DETAIL FOR EBR-II  
PRIMARY SYSTEM SUPPORT STRUCTURE

RE-6-20056-B  
R. SEIDENSTICKER: L. K., 3-28-57

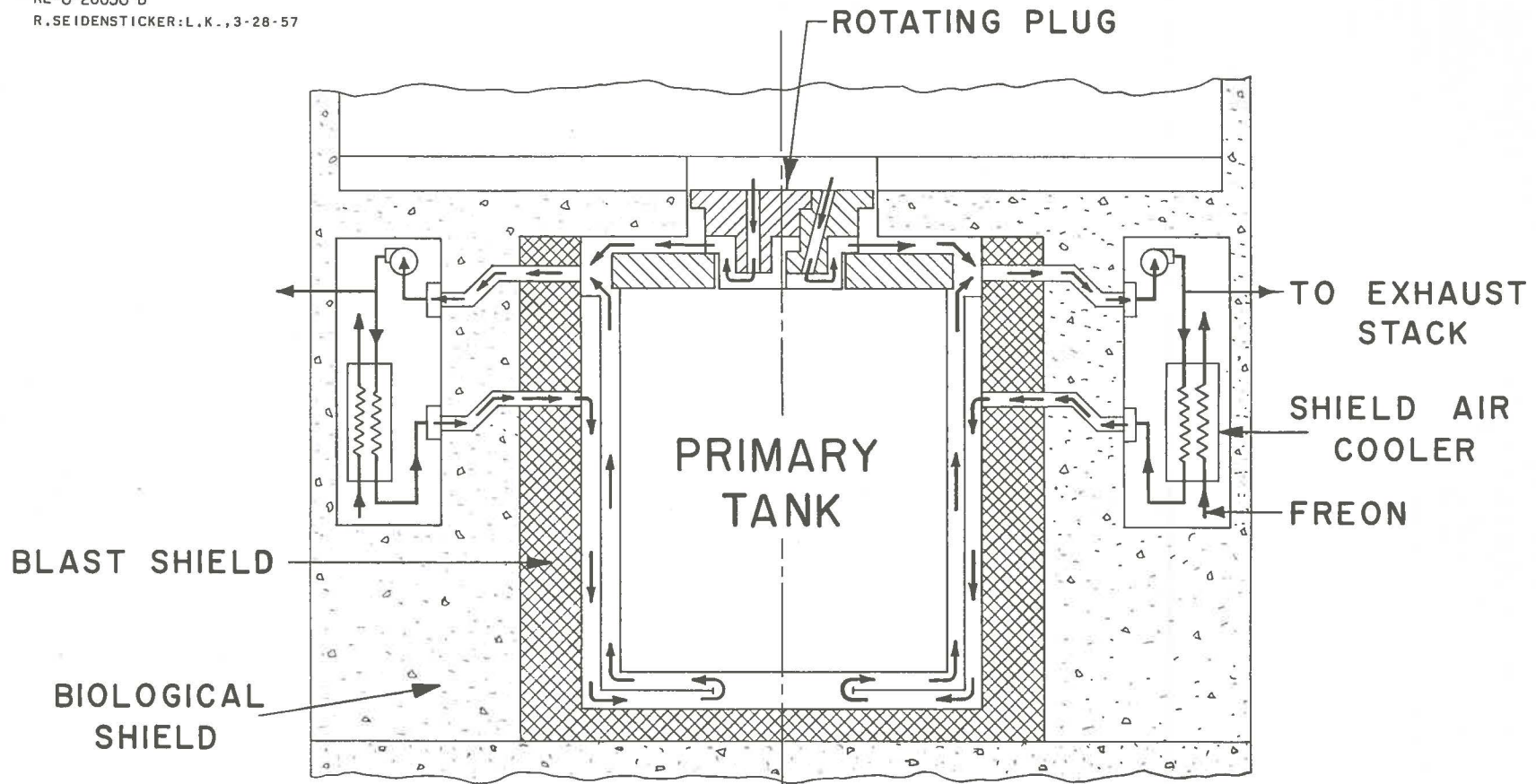


FIG. 34  
SHIELD COOLING AIR SYSTEM  
SCHEMATIC DIAGRAM

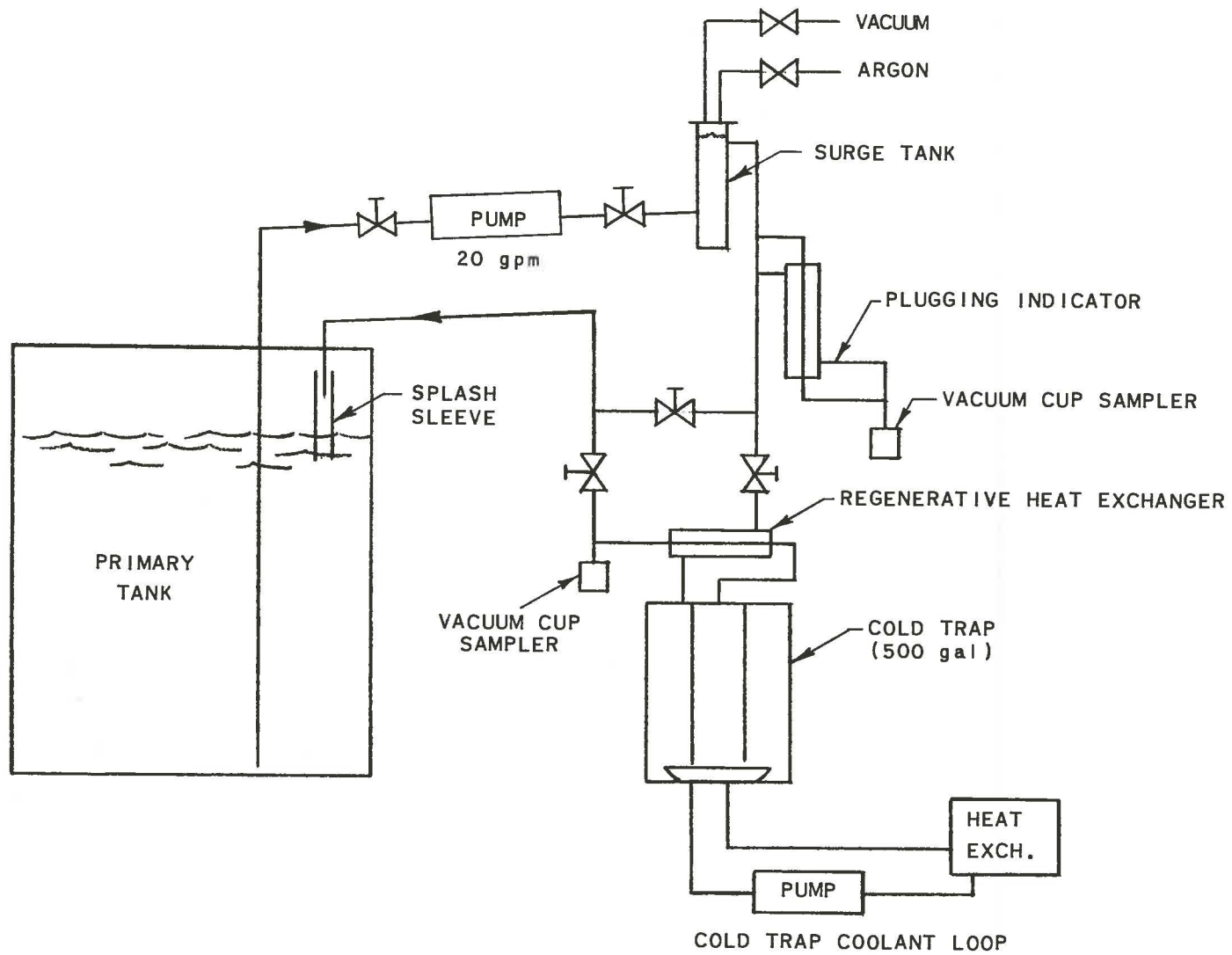


FIG. 35  
SODIUM CLEANUP SYSTEM FLOW DIAGRAM

RE-8-19773-A

RE-B-19781-C  
 J.R. HUMPHREYS, O.O., 2-26-57

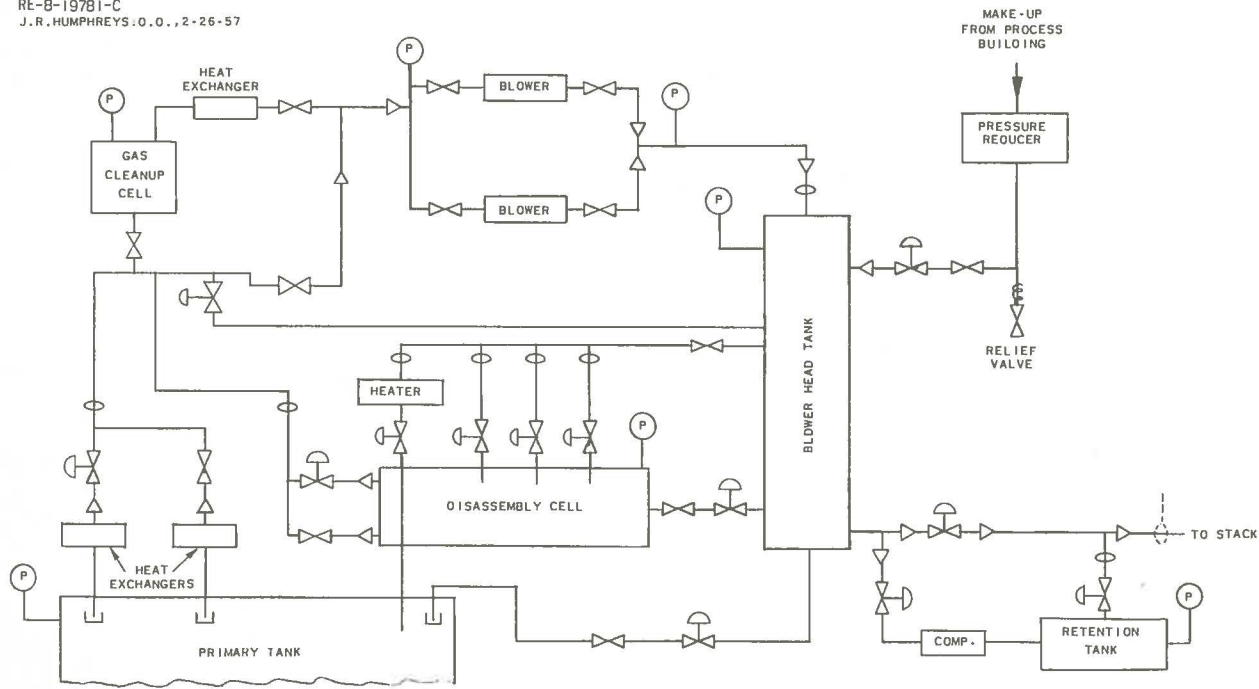


FIG. 36  
 PRIMARY INERT GAS SYSTEM FLOW SHEET

LEGEND

-  PROPORTIONING CONTROL VALVES
-  ON-OFF VALVES
-  CHECK VALVES
-  INSTRUMENTATION FOR PRESSURE DETECTION.
-  INSTRUMENTATION FOR FLOW MEASUREMENT.
-  RADIATION LEVEL CONTROLLER.

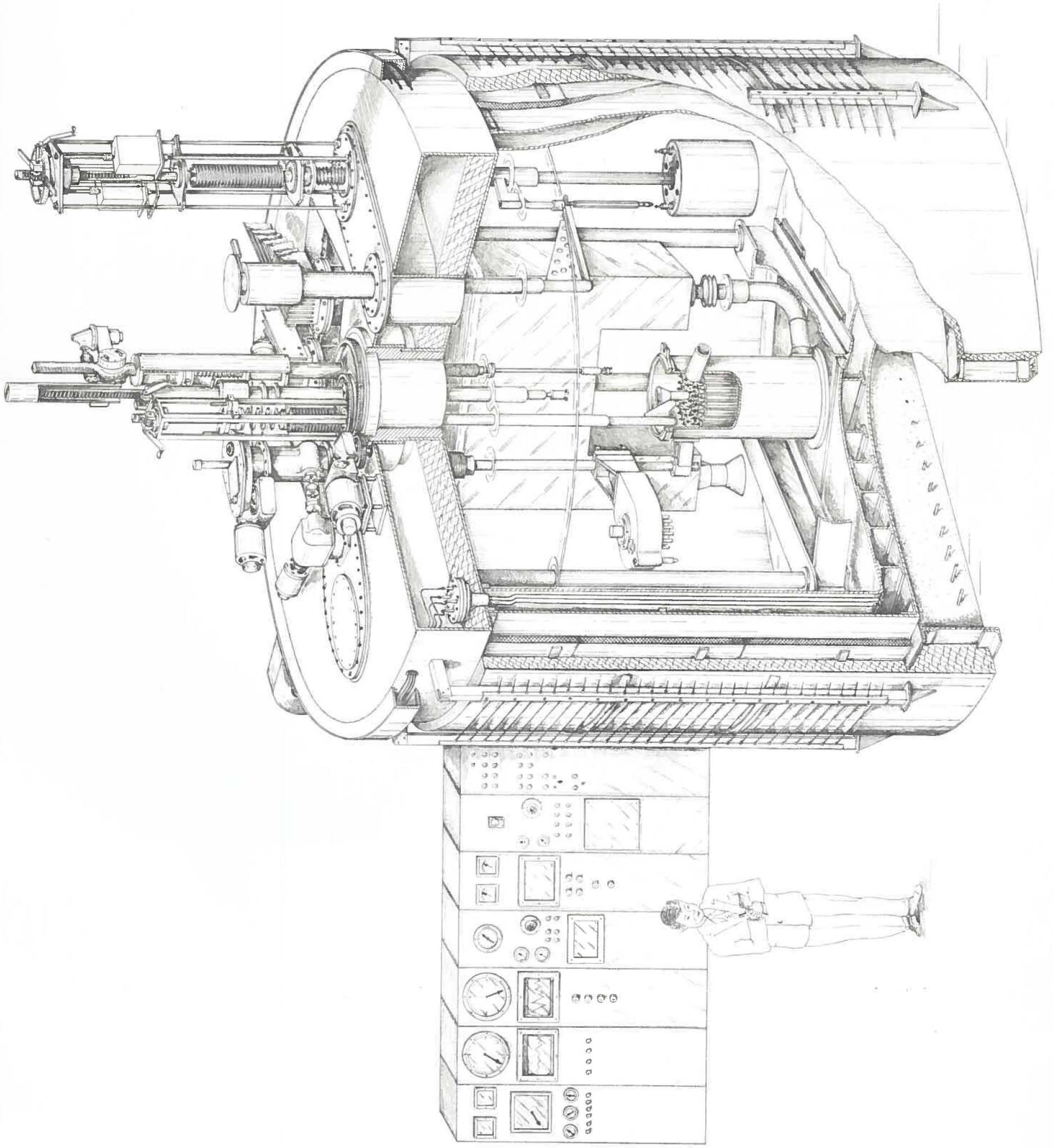
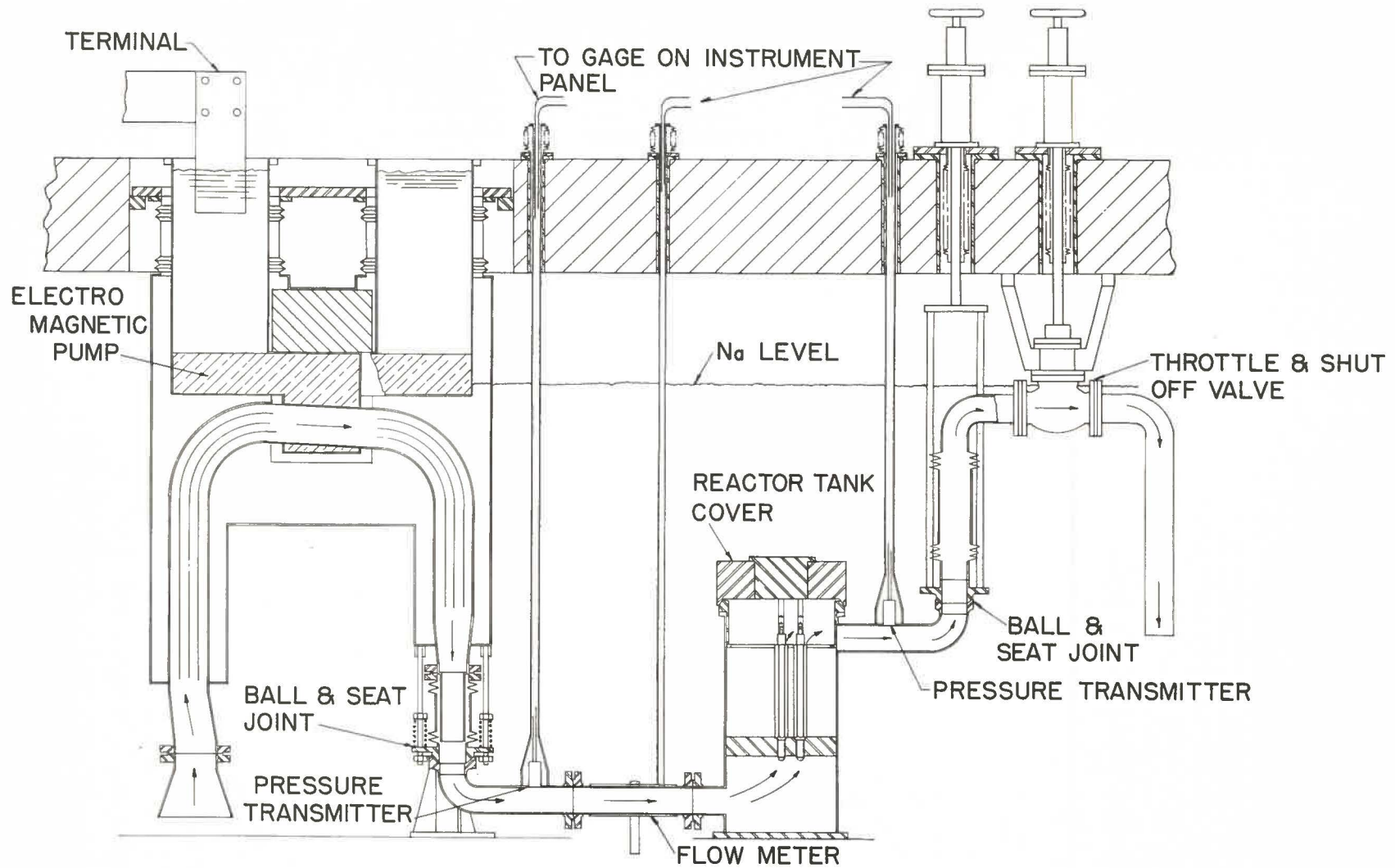


FIG. 37  
E BR - II WORKING MODEL



**FIG. 38**  
**PRIMARY SODIUM SYSTEM**  
**EBR-II WORKING MODEL**

RE-6-19950-C  
 T. SPAULDING: L.K.,  
 3-13-57

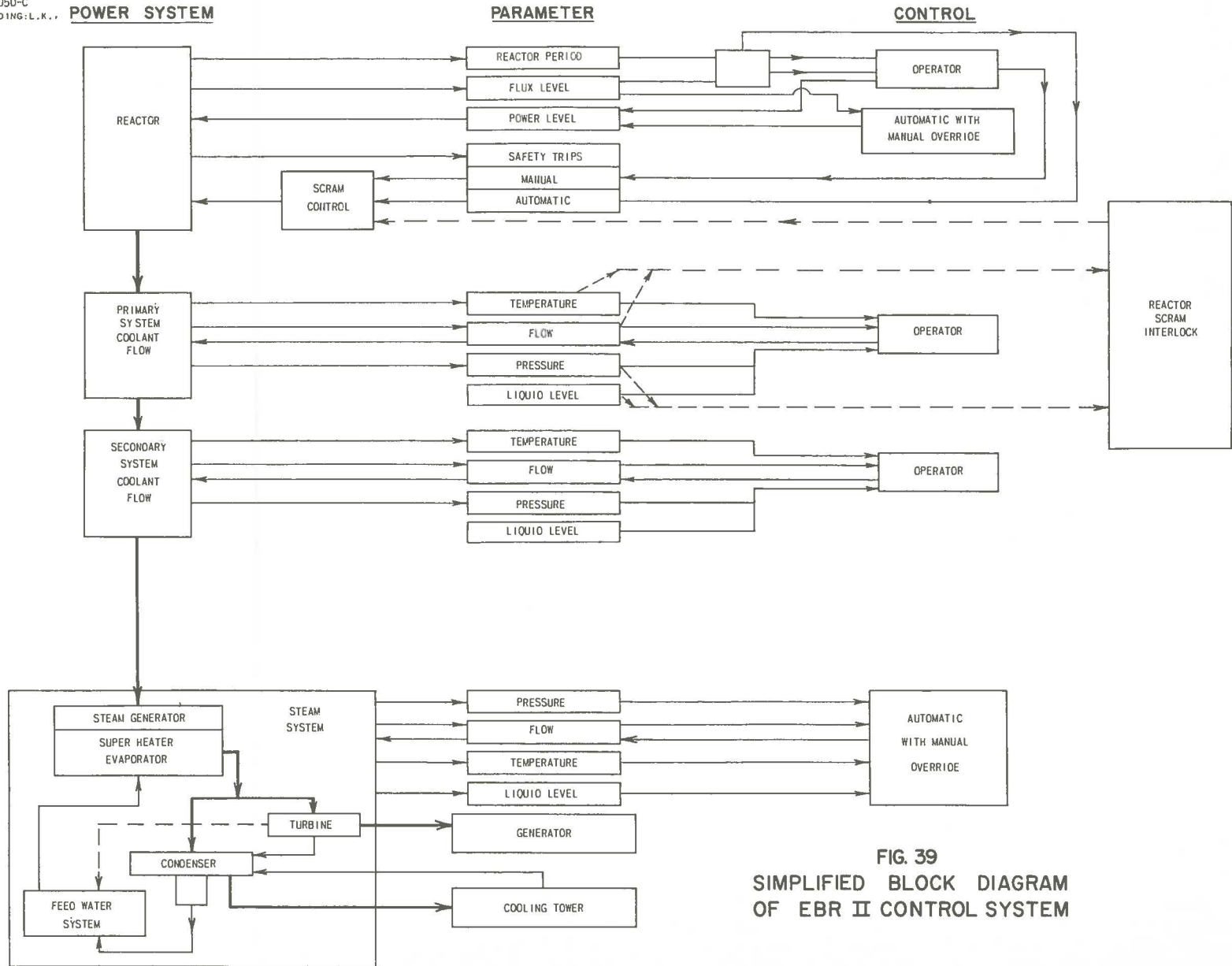


FIG. 39  
 SIMPLIFIED BLOCK DIAGRAM  
 OF EBR II CONTROL SYSTEM

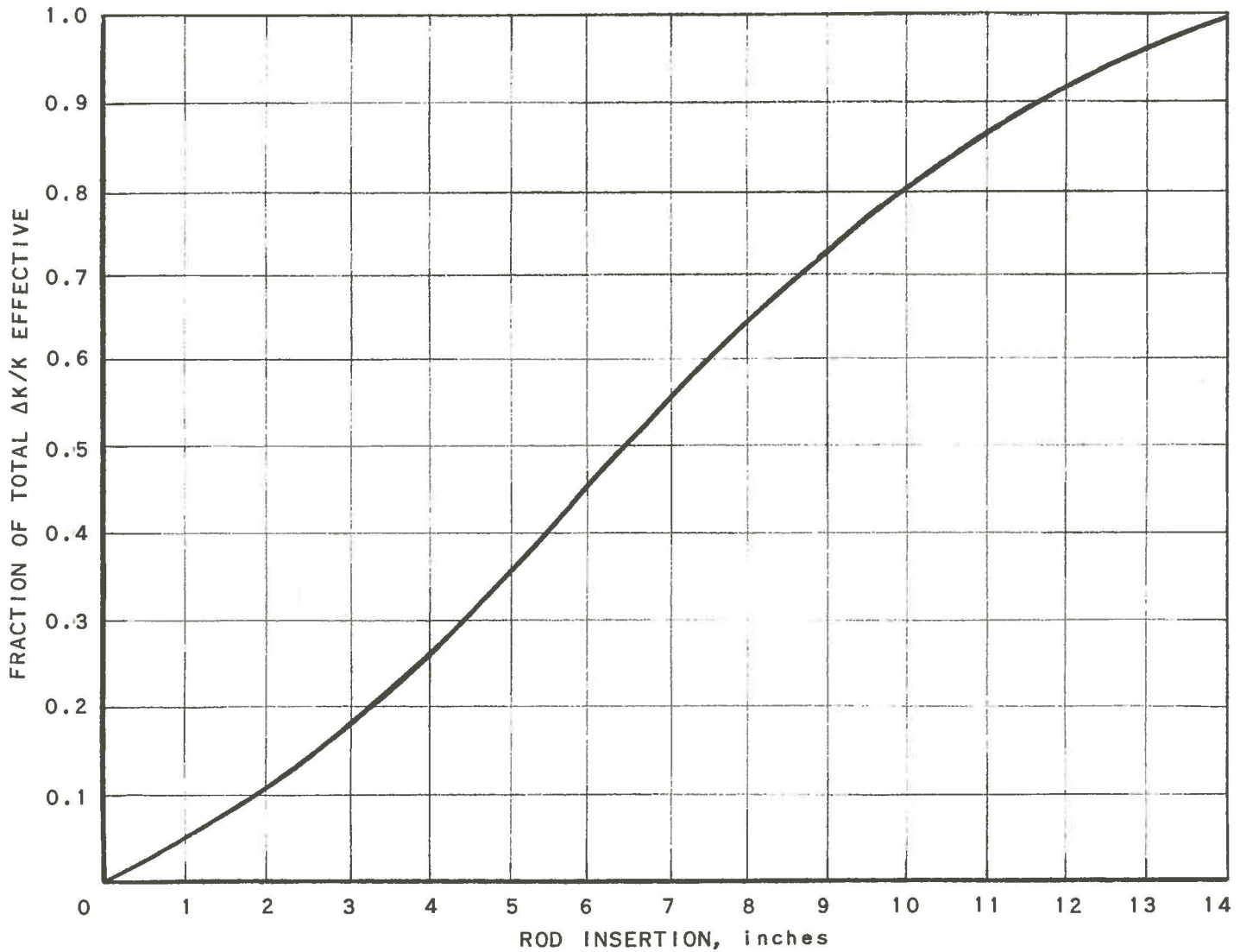


FIG. 40  
ROD INSERTION VS FRACTION OF  
TOTAL ROD WORTH EFFECTIVE

RE-7-20068-A



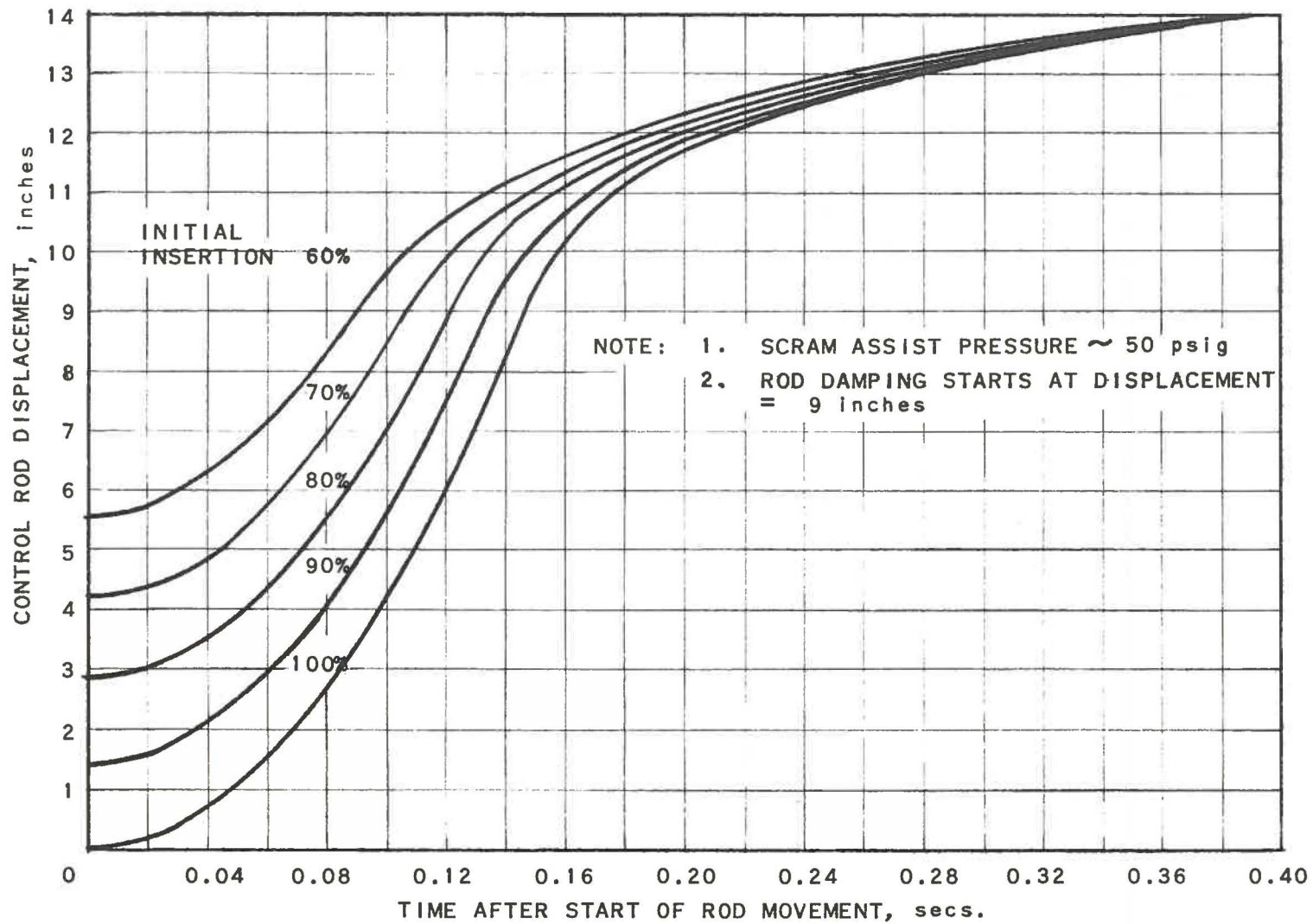


FIG. 41  
CONTROL ROD DISPLACEMENT VS TIME  
AFTER START OF ROD MOVEMENT

RE-7-20076-A

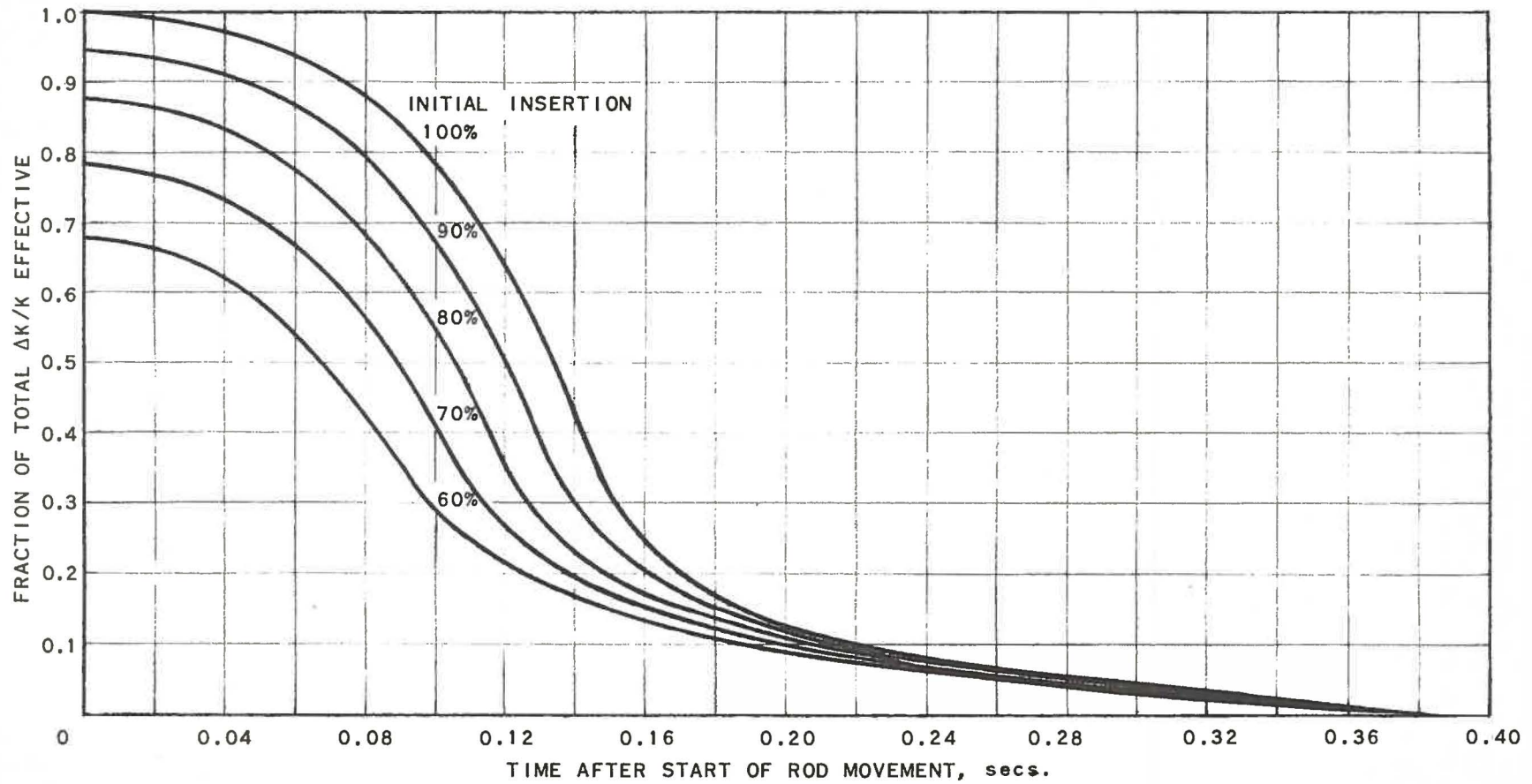


FIG. 42  
FRACTION OF TOTAL CONTROL ROD WORTH EFFECTIVE  
VS TIME AFTER START OF ROD MOVEMENT

RE-7-20075-A

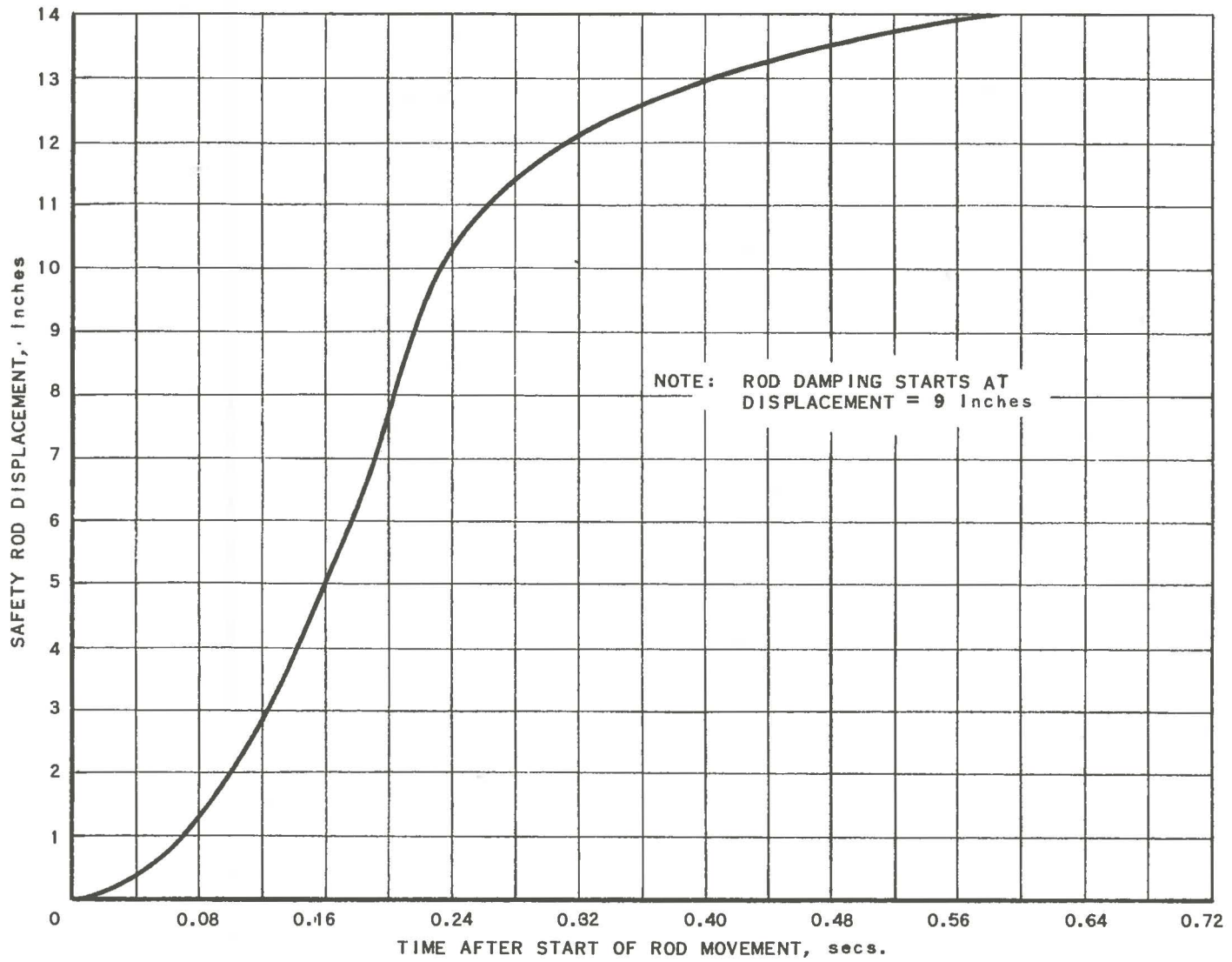


FIG. 43  
 SAFETY ROD DISPLACEMENT VS TIME  
 AFTER START OF ROD MOVEMENT

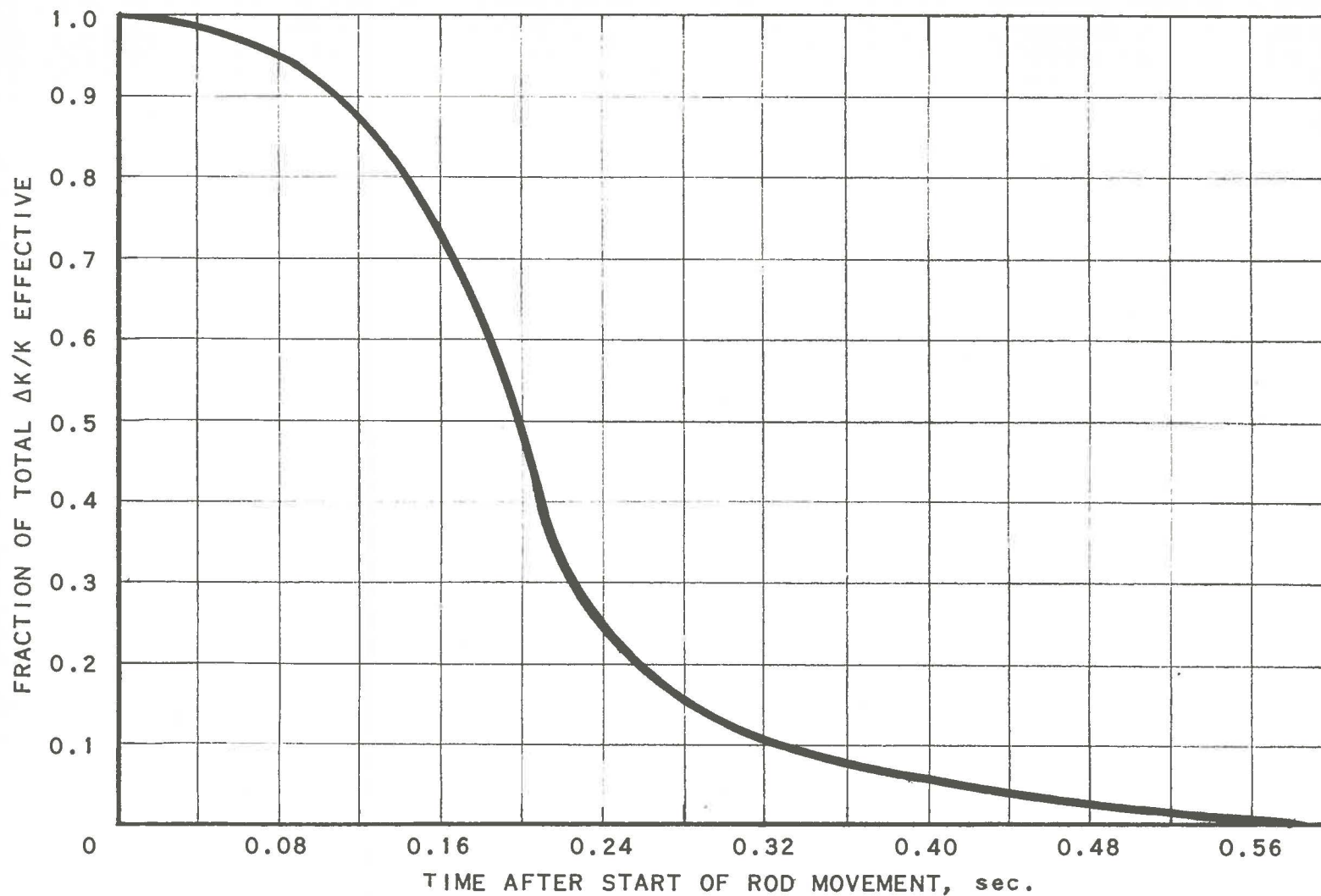


FIG. 44  
FRACTION OF TOTAL SAFETY ROD WORTH EFFECTIVE  
VS TIME AFTER START OF ROD MOVEMENT

RE-7-20069-A

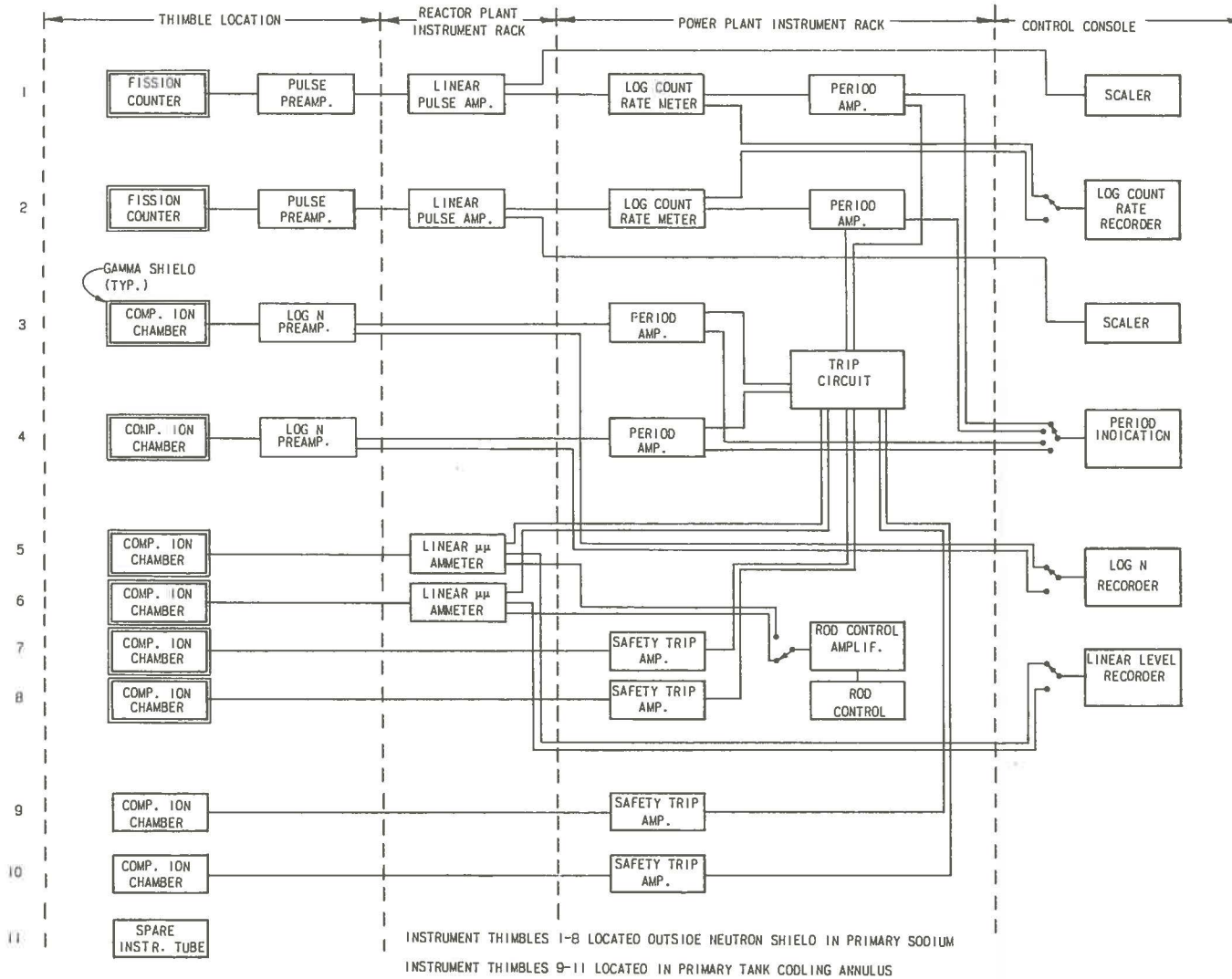


FIG. 45  
EBR II NUCLEAR INSTRUMENT CHANNELS

RE-2-19945-A

R.RAMP:F.T.,3-13-57

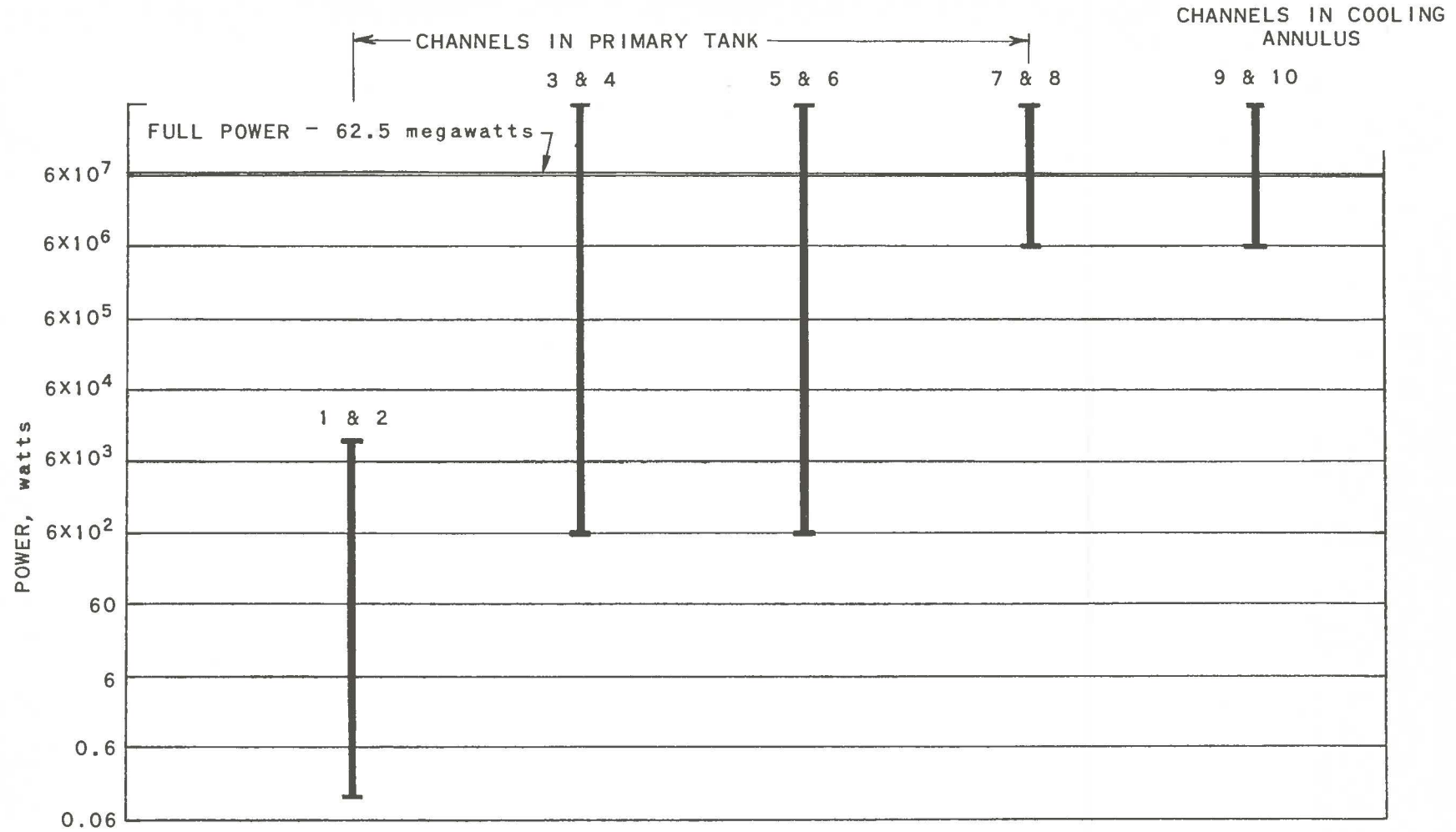


FIG. 46  
EBR-II NUCLEAR INSTRUMENT RANGE

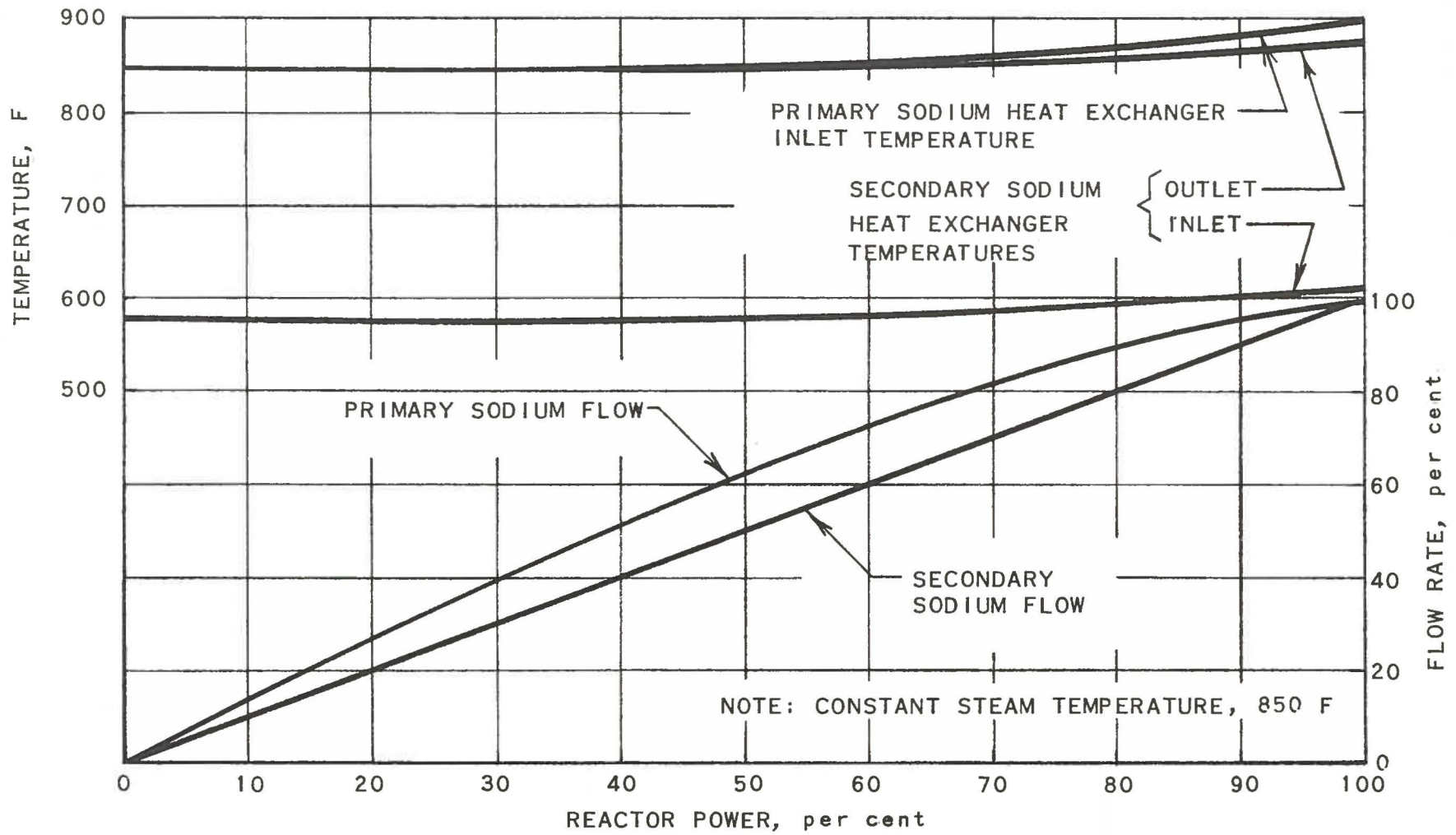


FIG. 47  
 PRIMARY AND SECONDARY SODIUM FLOW RATES  
 AND TEMPERATURES VS REACTOR POWER

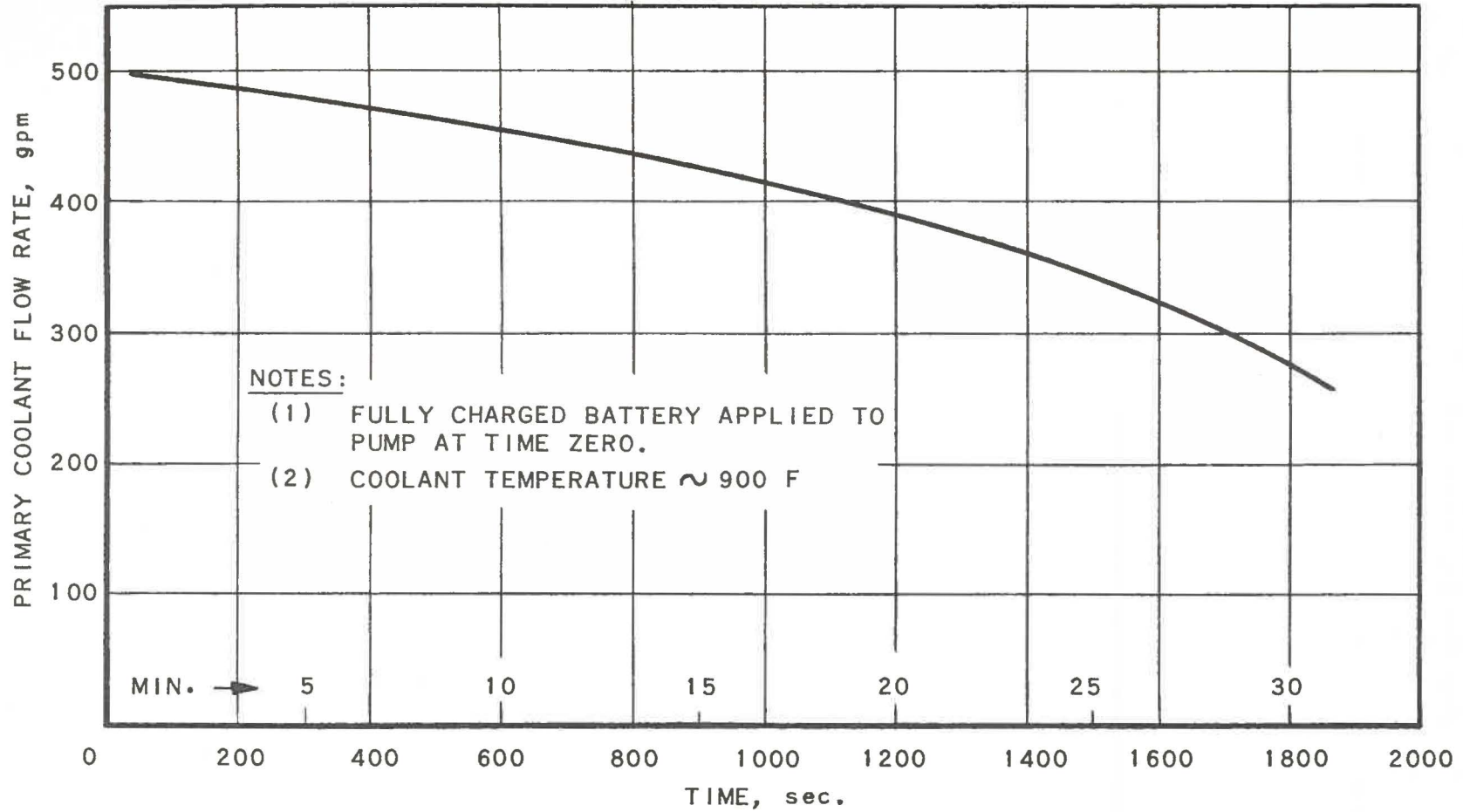
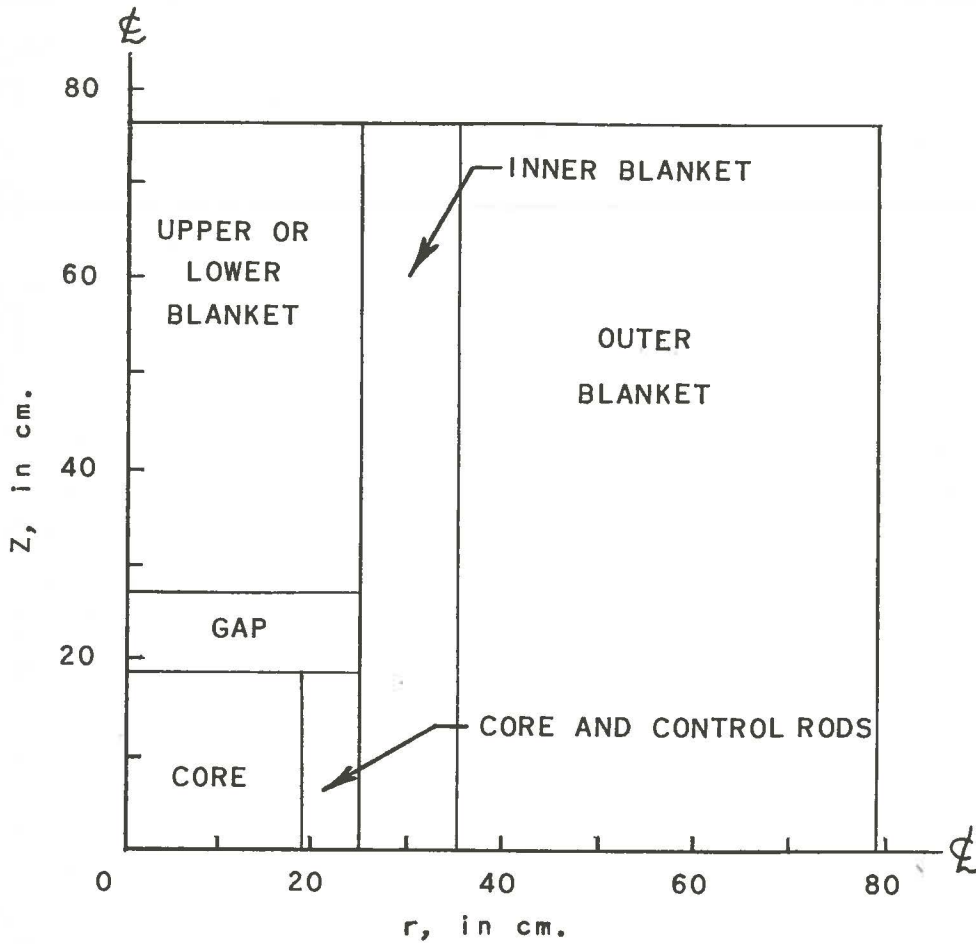


FIG. 48  
PRIMARY COOLANT FLOW RATE VS TIME WITH AUXILIARY  
PUMP ONLY IN OPERATION (ON BATTERY)





Z = 0 IS PLANE OF SYMMETRY  
 r = 0 IS AXIS OF SYMMETRY

FIG. 50  
 REACTOR MODEL FOR TWO-DIMENSIONAL,  
 TWO-GROUP ANALYSIS

RE-7-19990-A

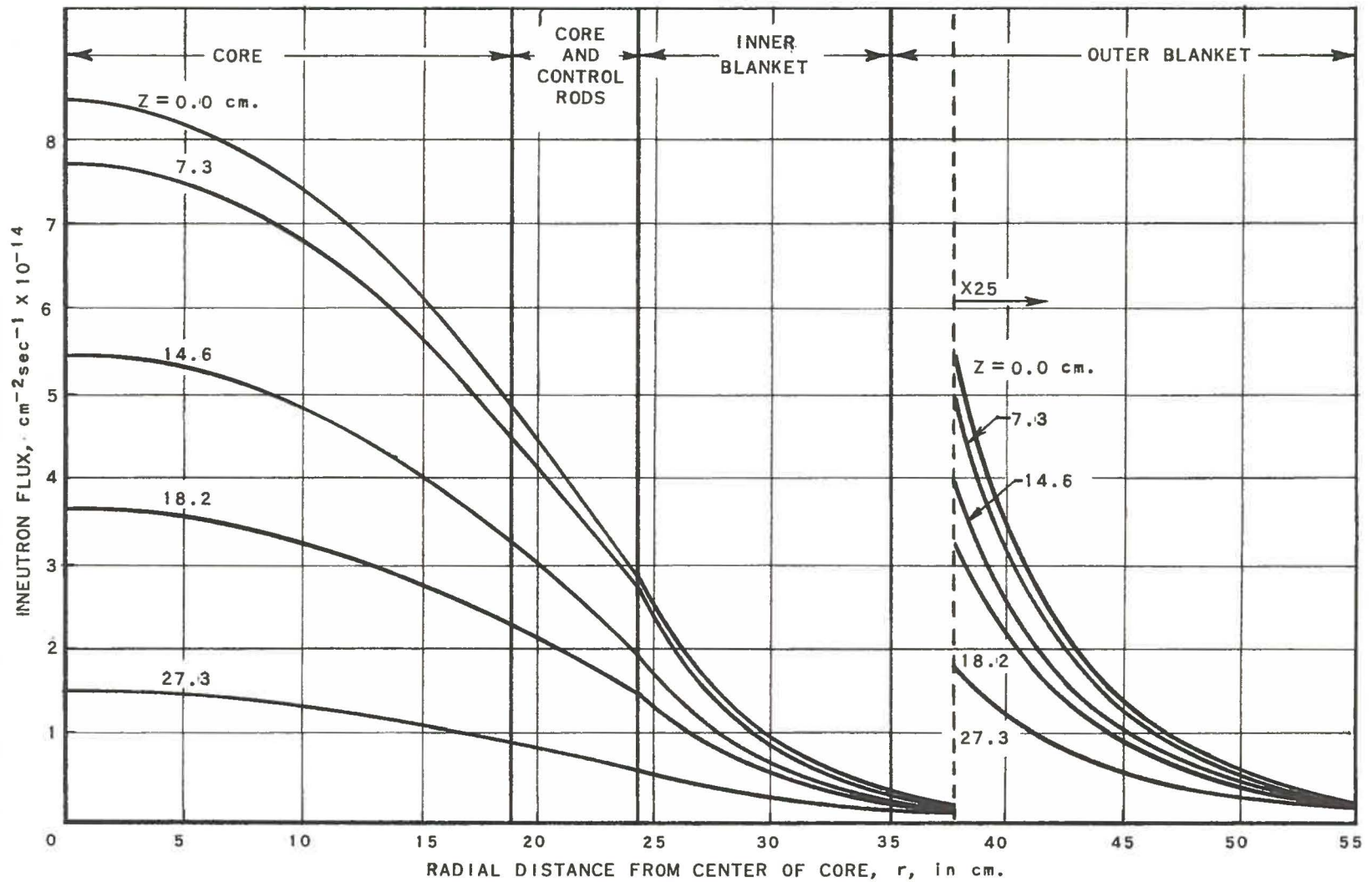


FIG. 51  
 RADIAL GROUP I NEUTRON FLUX DISTRIBUTION  
 (TWO-DIMENSIONAL ANALYSIS)

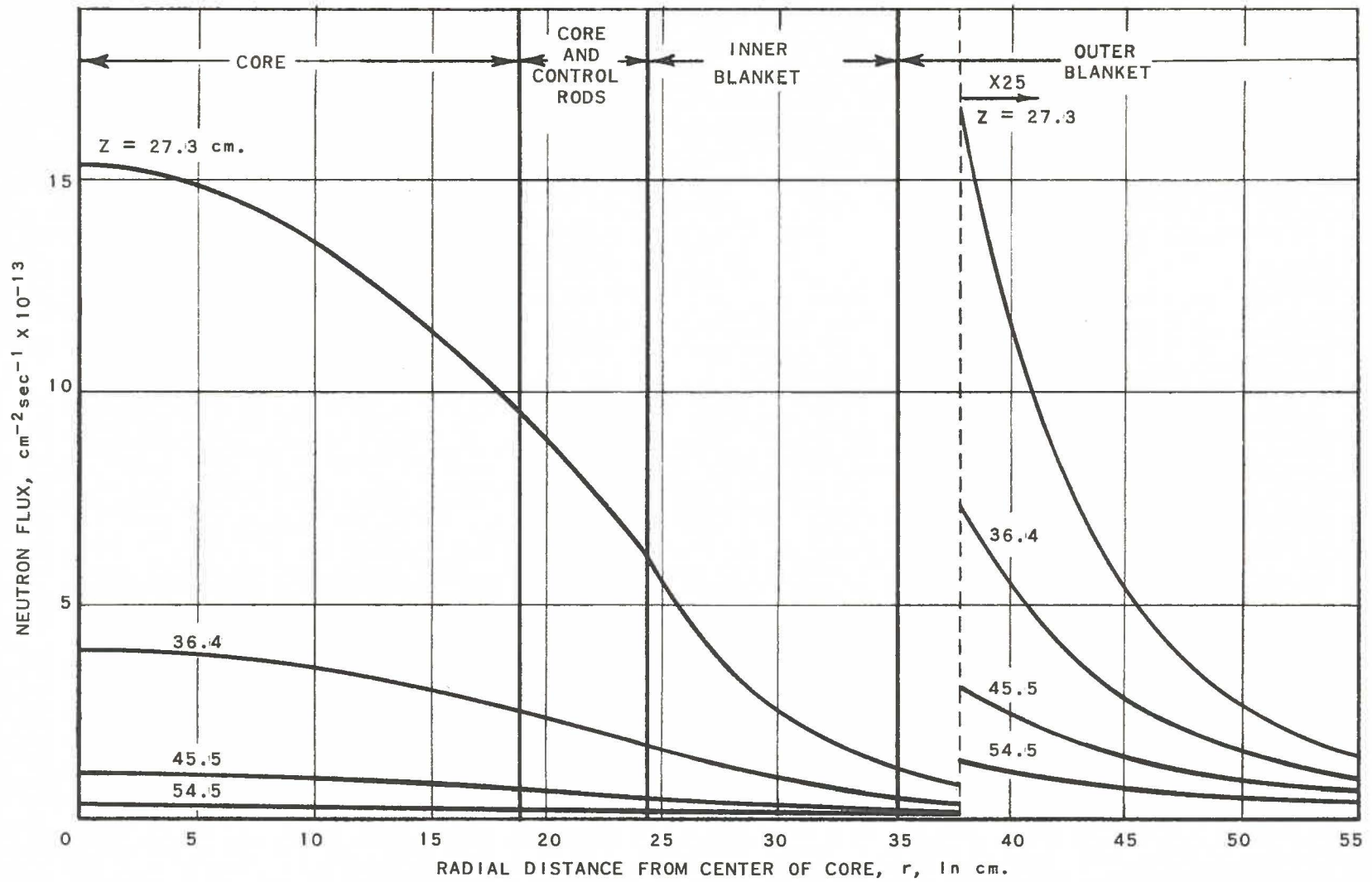


FIG. 52  
 RADIAL GROUP I NEUTRON FLUX DISTRIBUTION  
 (TWO-DIMENSIONAL ANALYSIS)

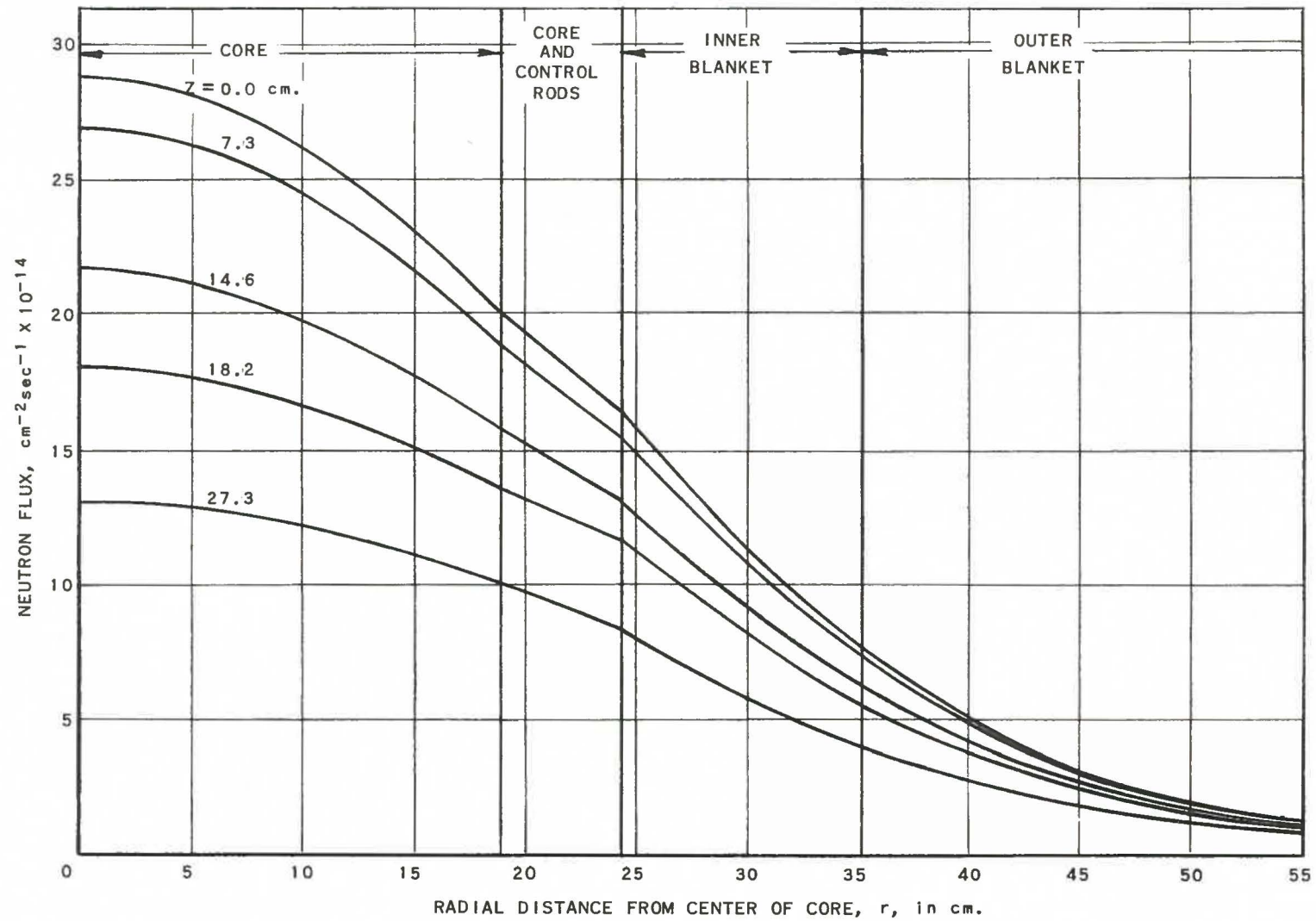


FIG. 53  
 RADIAL GROUP II NEUTRON FLUX DISTRIBUTION  
 (TWO-DIMENSIONAL ANALYSIS)

RE-7-20022-B

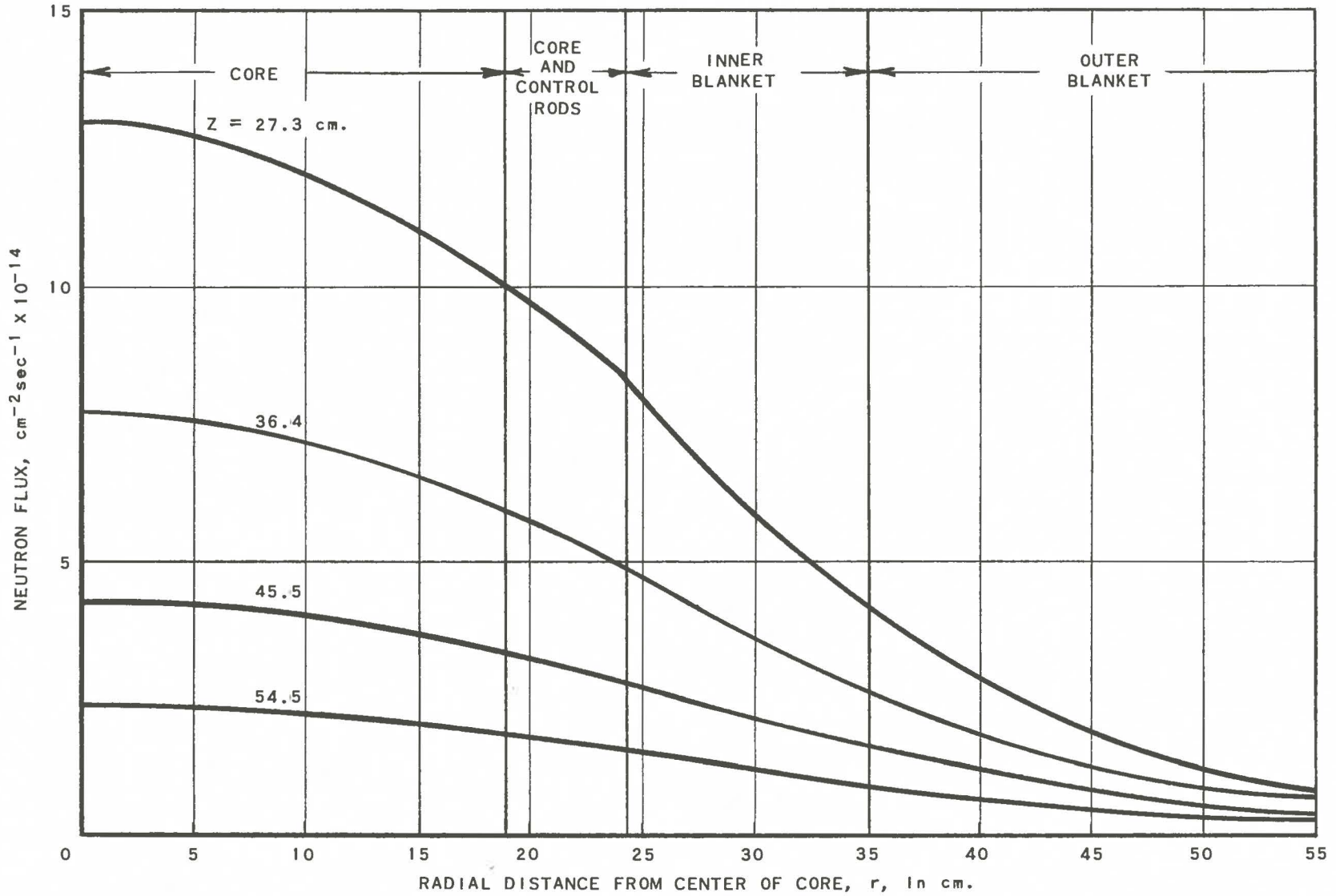


FIG. 54  
RADIAL GROUP II NEUTRON FLUX DISTRIBUTION  
(TWO-DIMENSIONAL ANALYSIS)

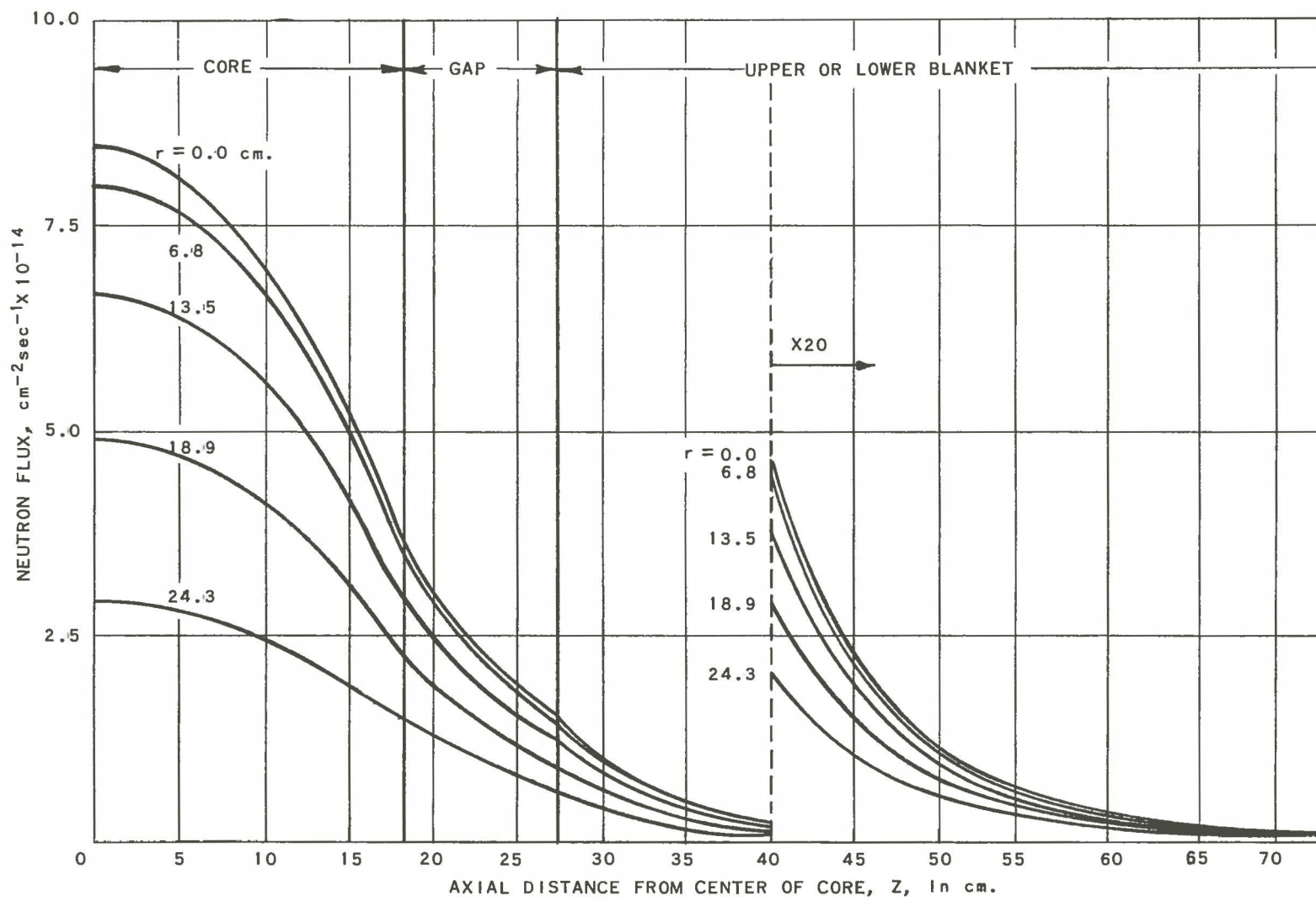


FIG. 55  
 AXIAL GROUP I NEUTRON FLUX DISTRIBUTION  
 (TWO-DIMENSIONAL ANALYSIS)

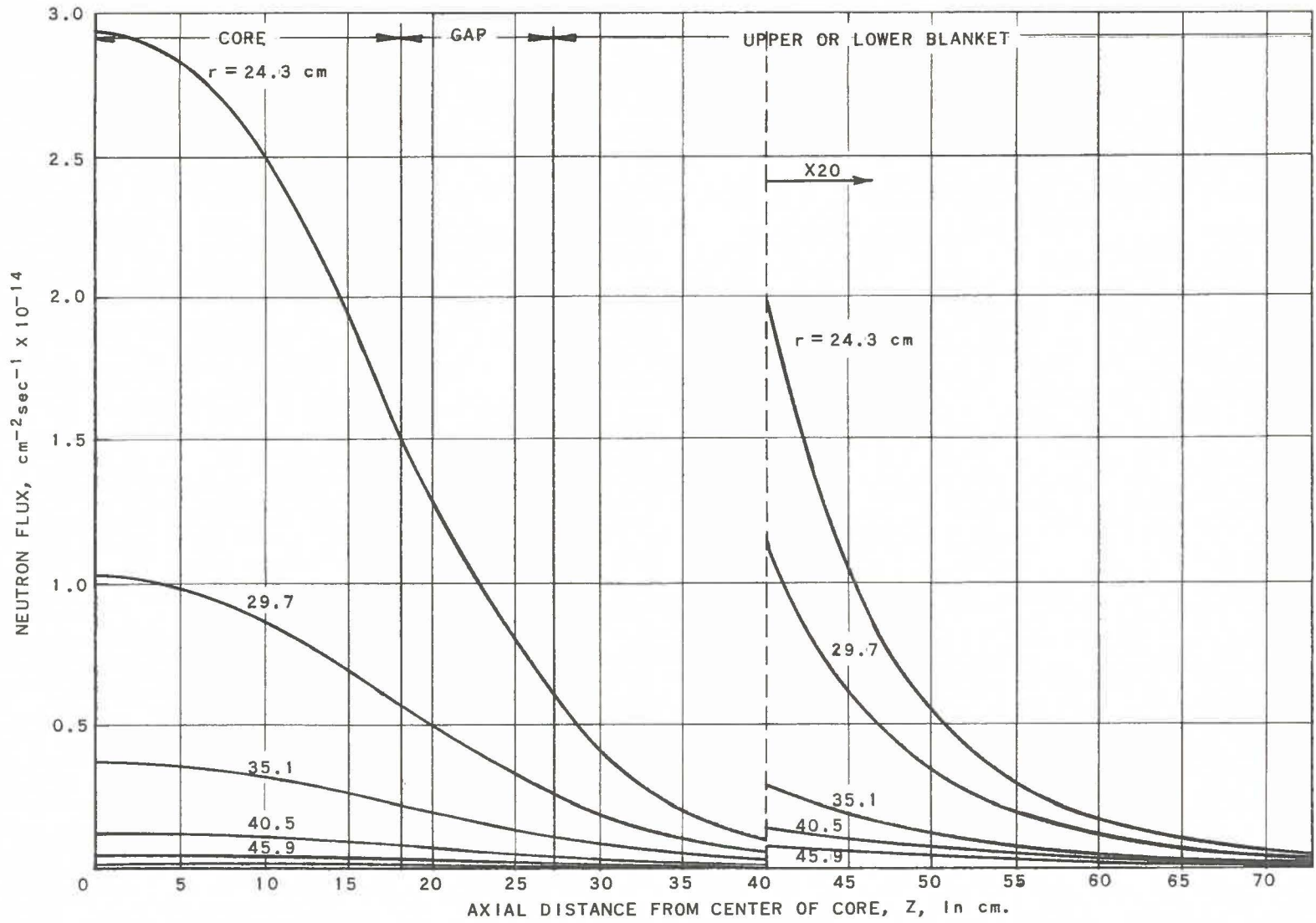


FIG. 56  
 AXIAL GROUP I NEUTRON FLUX DISTRIBUTION  
 (TWO-DIMENSIONAL ANALYSIS)

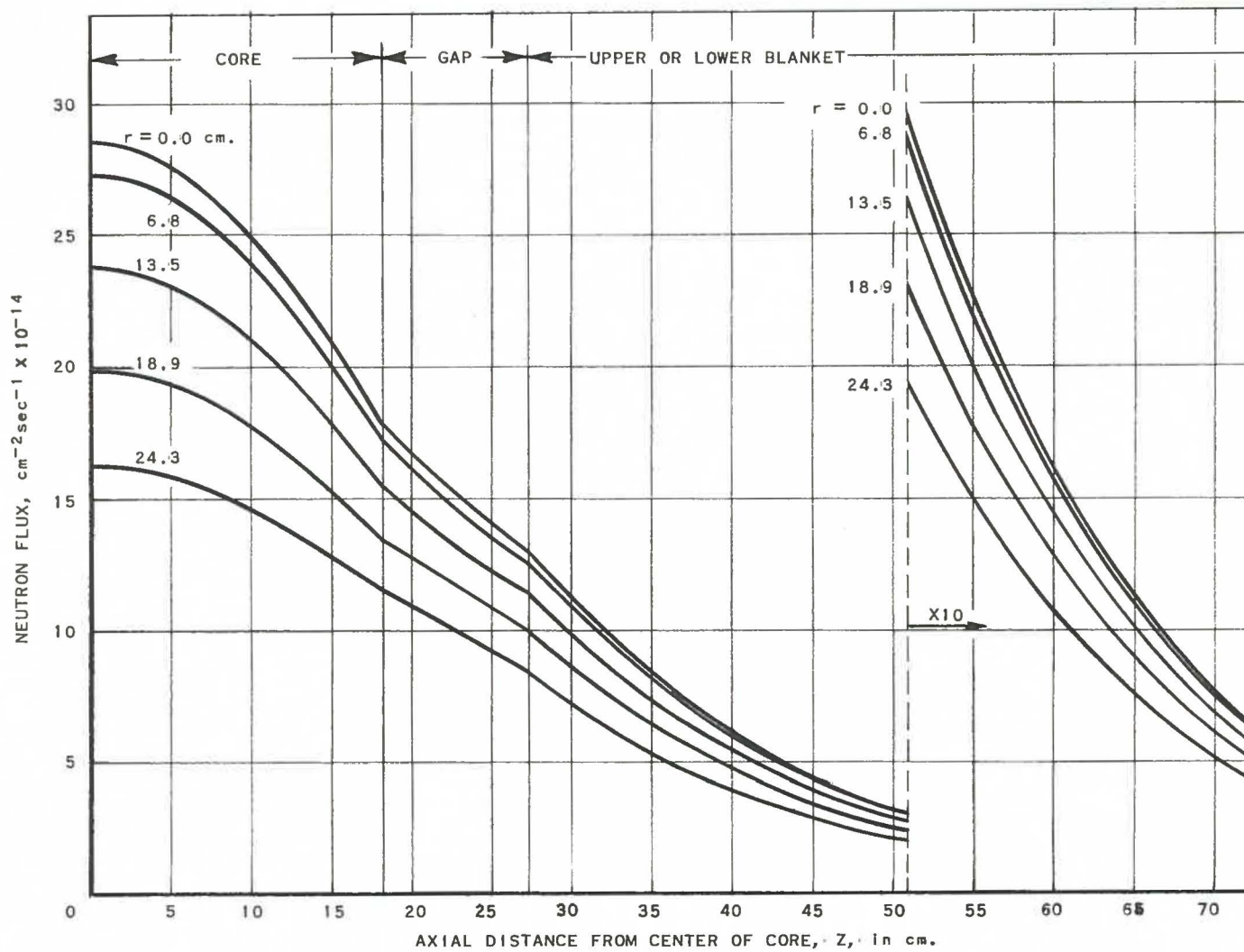


FIG. 57  
 AXIAL GROUP II NEUTRON FLUX DISTRIBUTION  
 (TWO-DIMENSIONAL ANALYSIS)

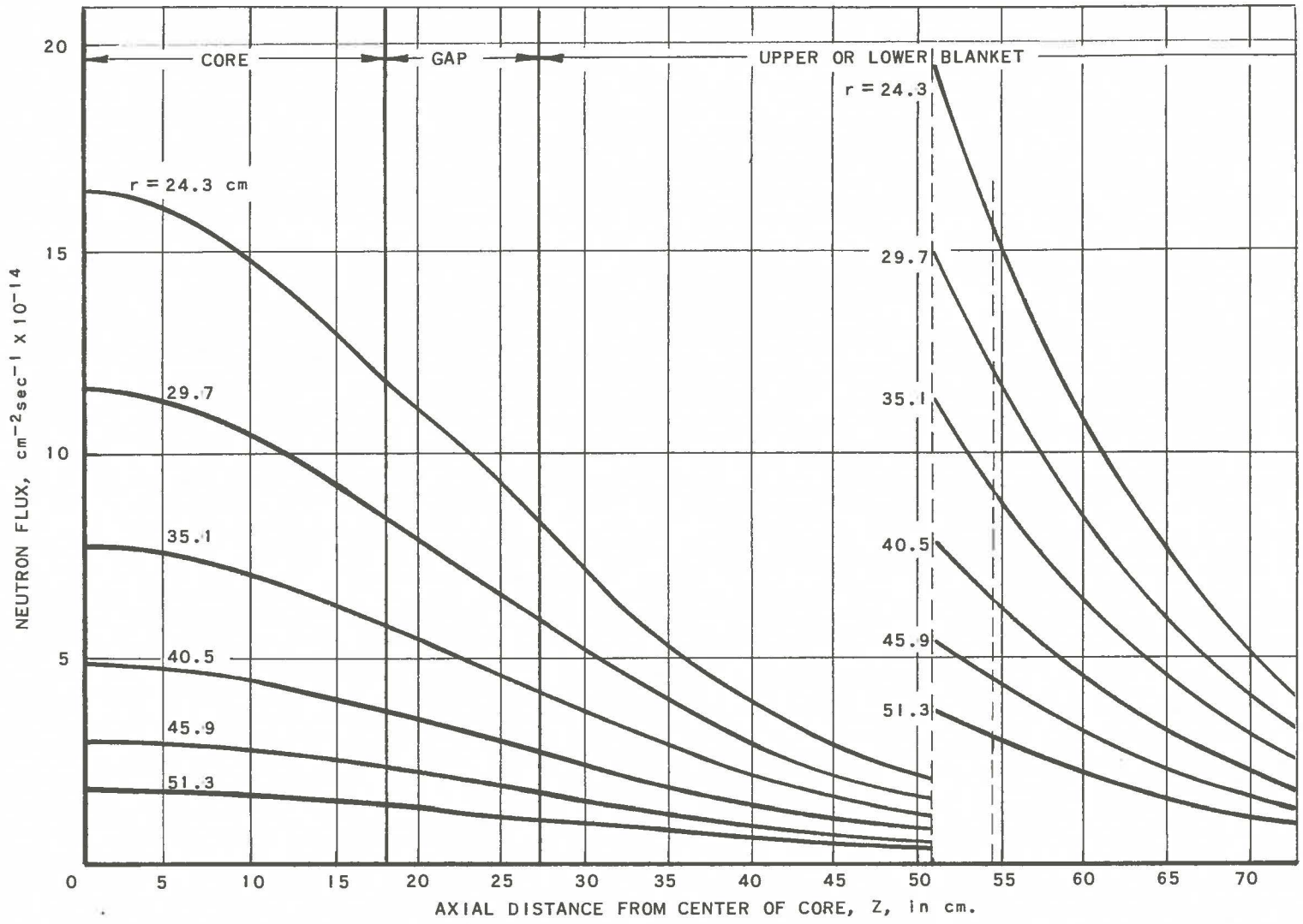


FIG. 58  
AXIAL GROUP II NEUTRON FLUX DISTRIBUTION  
(TWO-DIMENSIONAL ANALYSIS)

RE-7-20021-B

NOTE: LINE  $r = 0$  IS  
AXIS OF SYMMETRY

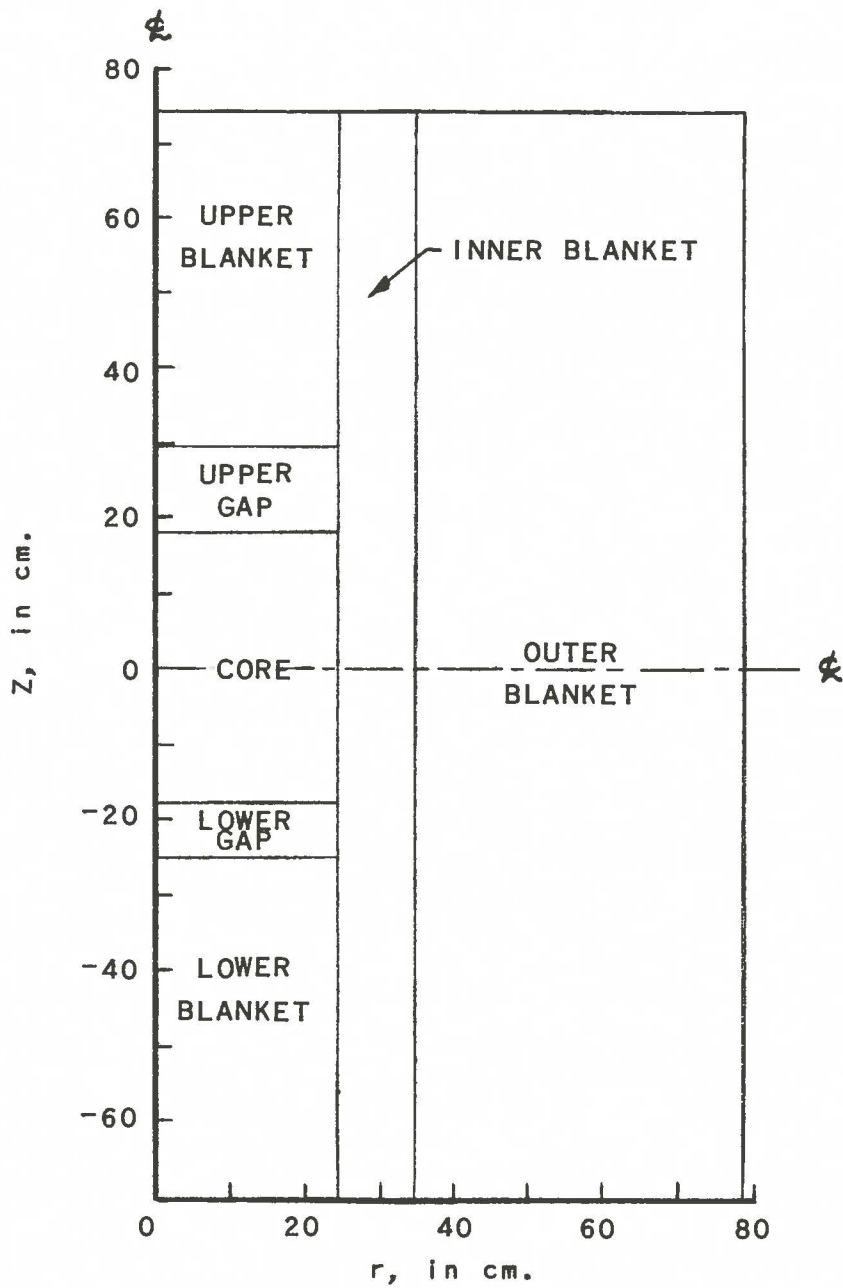


FIG. 59  
REACTOR MODEL FOR ONE-DIMENSIONAL,  
TEN GROUP ANALYSIS

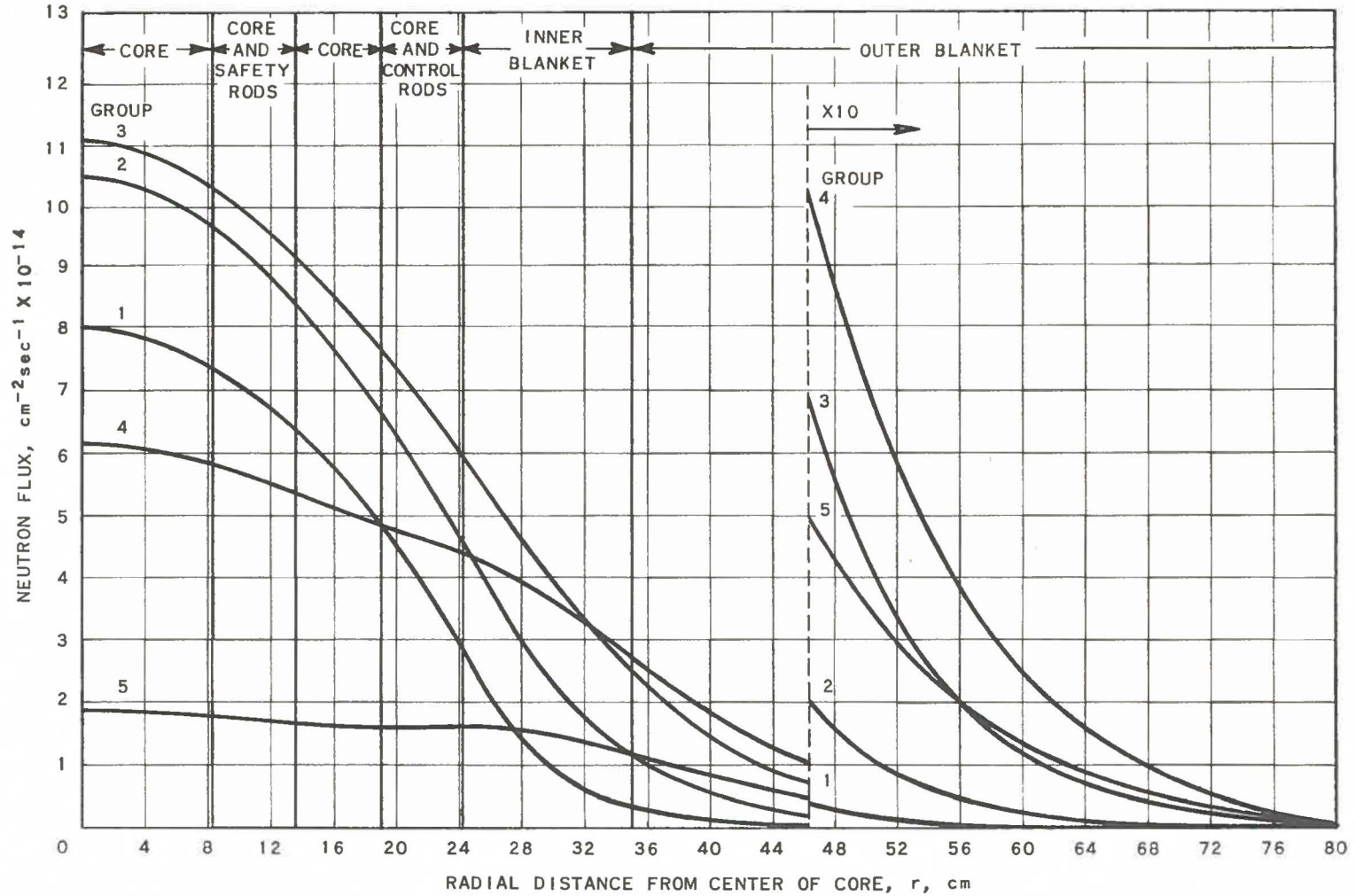


FIG. 60  
 RADIAL NEUTRON FLUX DISTRIBUTIONS IN  $Z = 0$  PLANE  
 (ONE-DIMENSIONAL ANALYSIS)

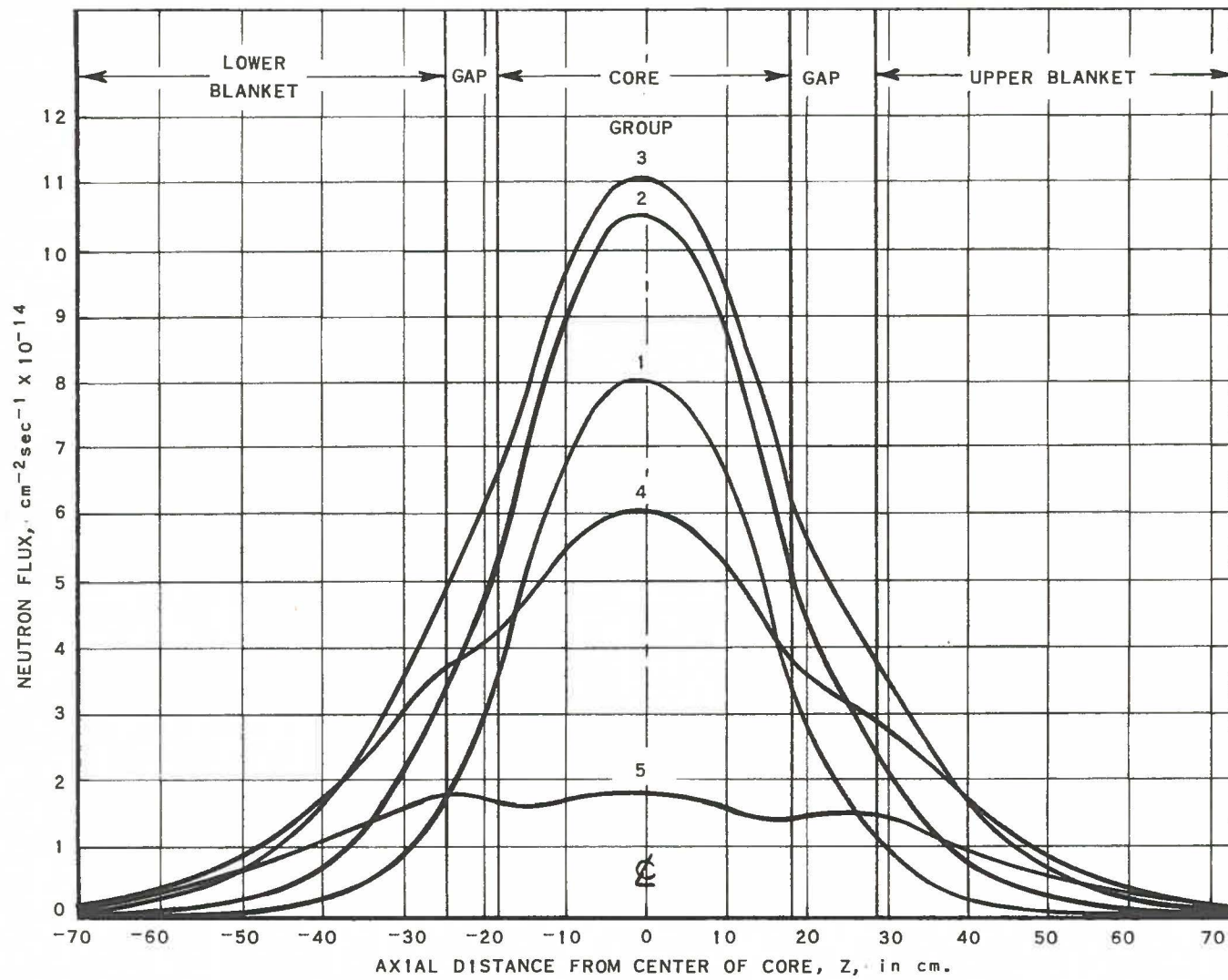


FIG. 61  
 AXIAL NEUTRON FLUX DISTRIBUTIONS AT  $r = 0$   
 (ONE-DIMENSIONAL ANALYSIS)

RE-7-20015-C  
 J. BURELBACH: L. B. 13-26-57

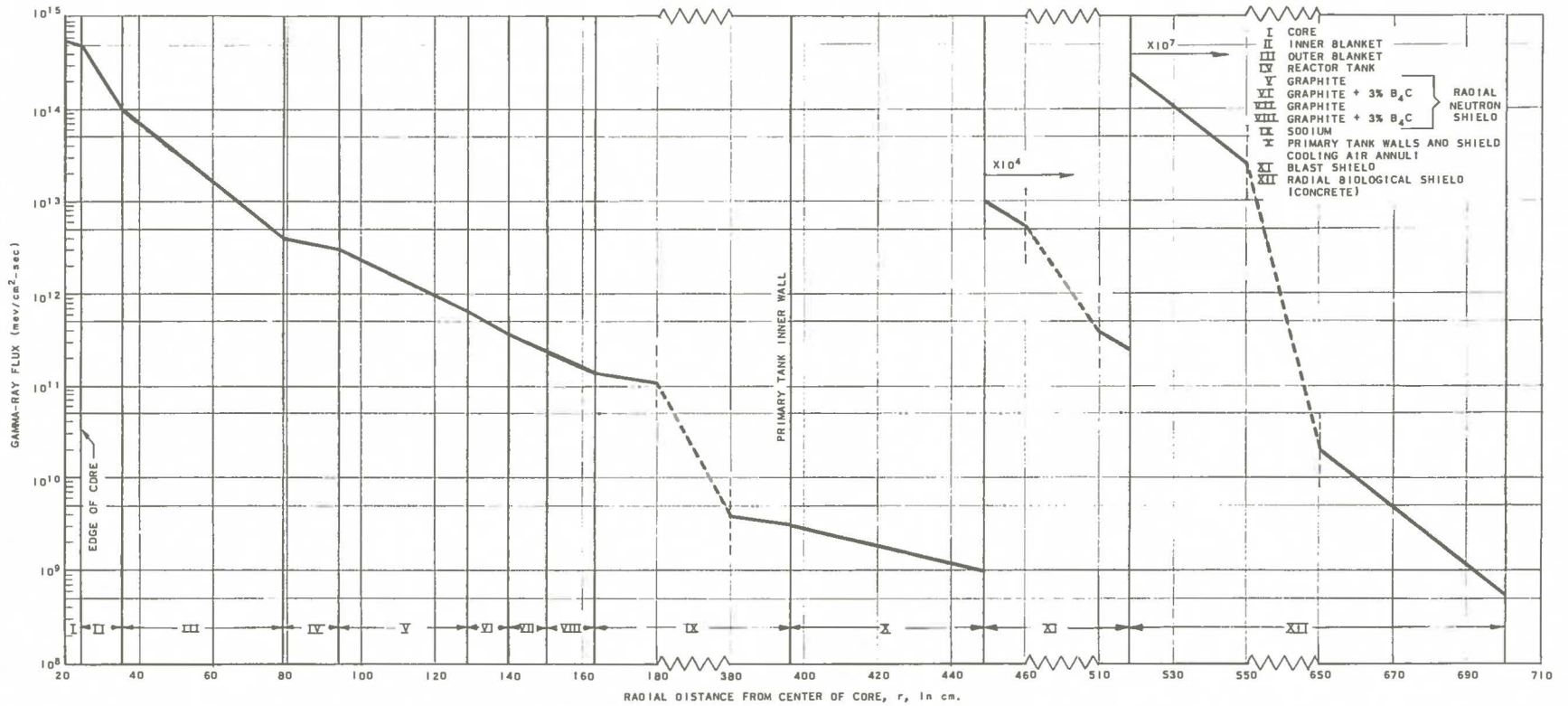


FIG. 62  
 RADIAL GAMMA FLUX DISTRIBUTION IN Z = 0 PLANE

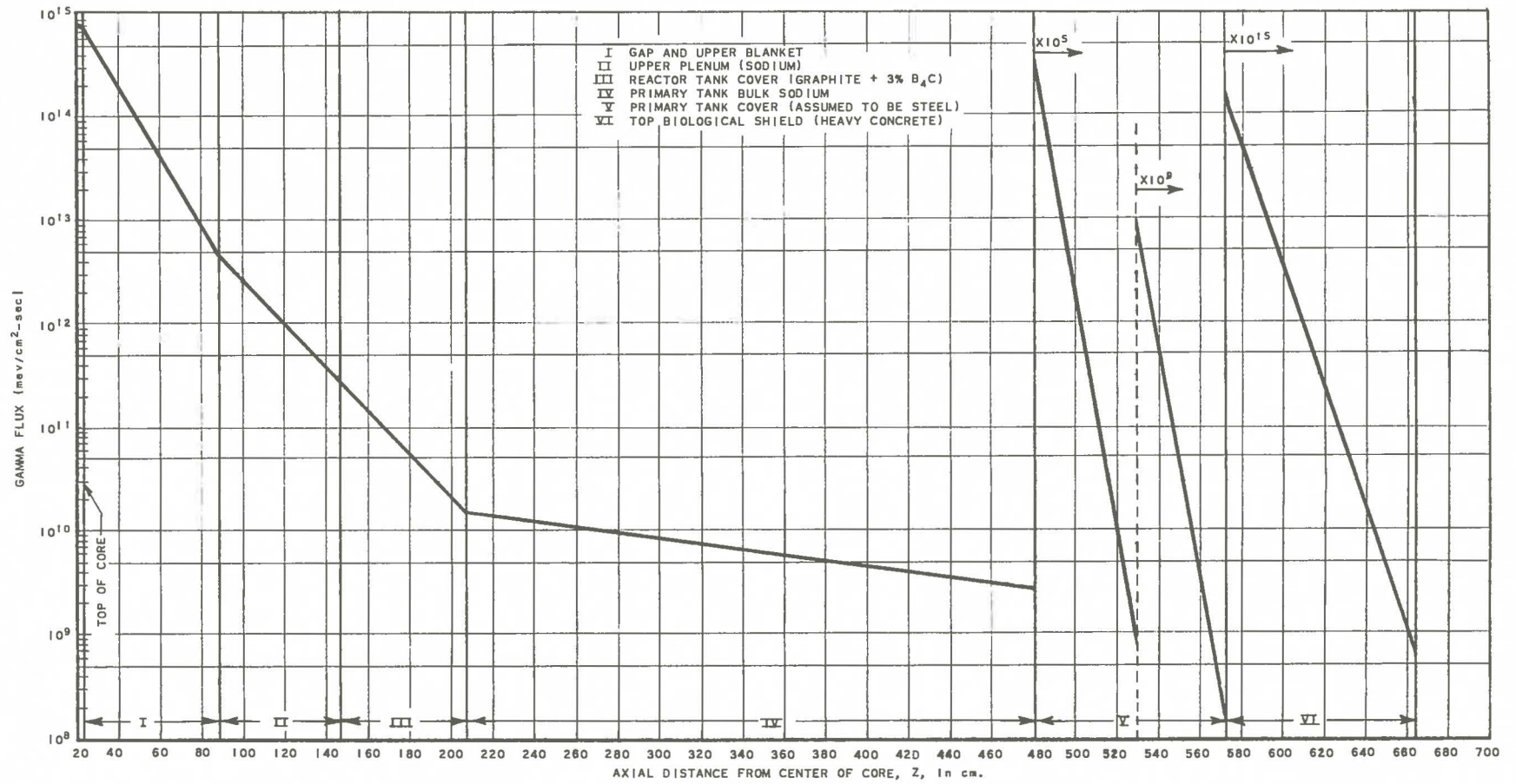


FIG. 63  
 AXIAL GAMMA FLUX DISTRIBUTION (UPWARD) AT  $r = 0$

RE-7-19687-B  
 W. SIMMONS:G.K., 2-15-57

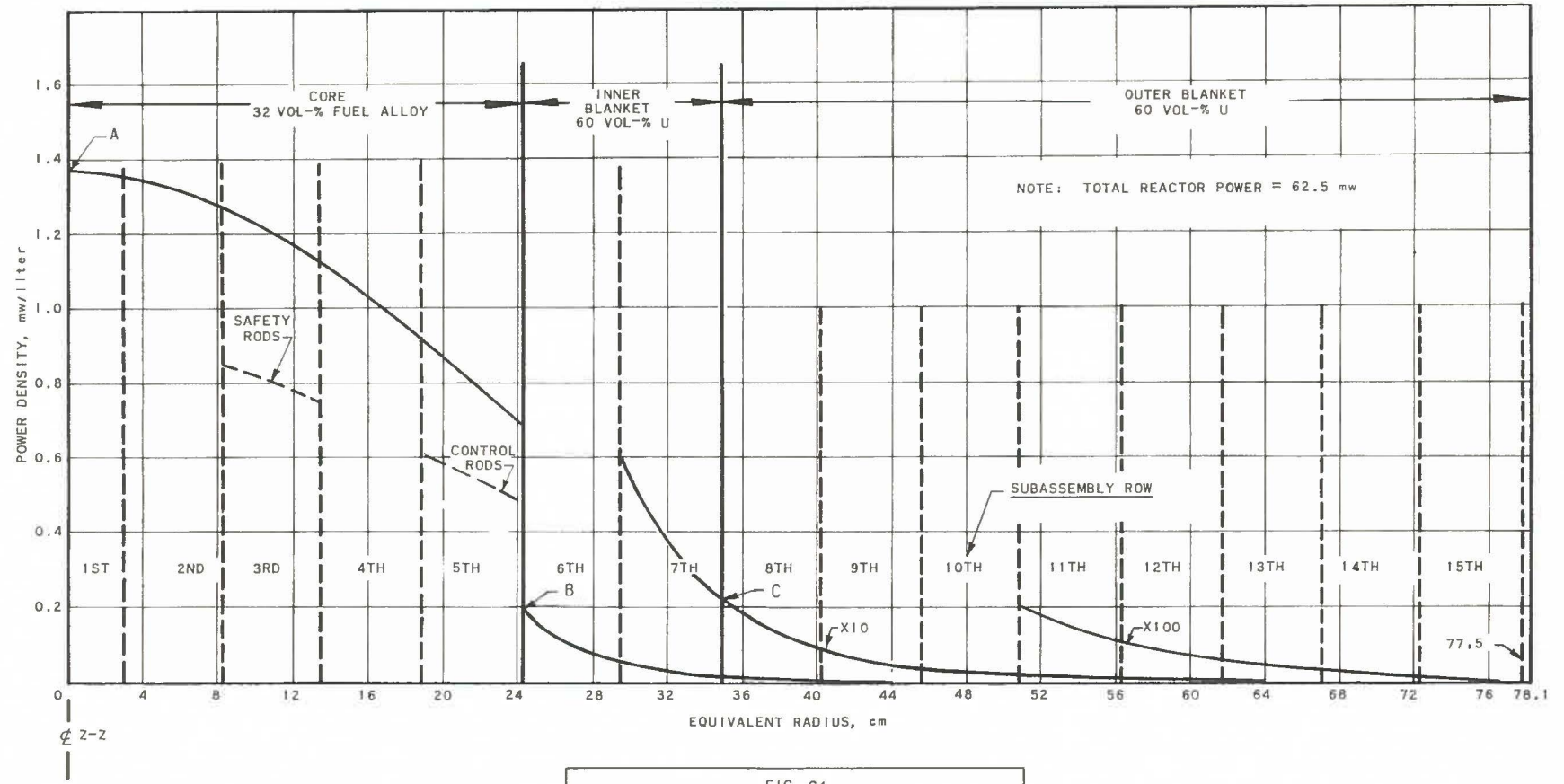


FIG. 64  
 RADIAL POWER DENSITY DISTRIBUTION AT CENTER  
 PLANE OF CLEAN REACTOR (Z = 0)

RE-7-19686-B  
 W. SIMMONS:G.K., 2-15-57

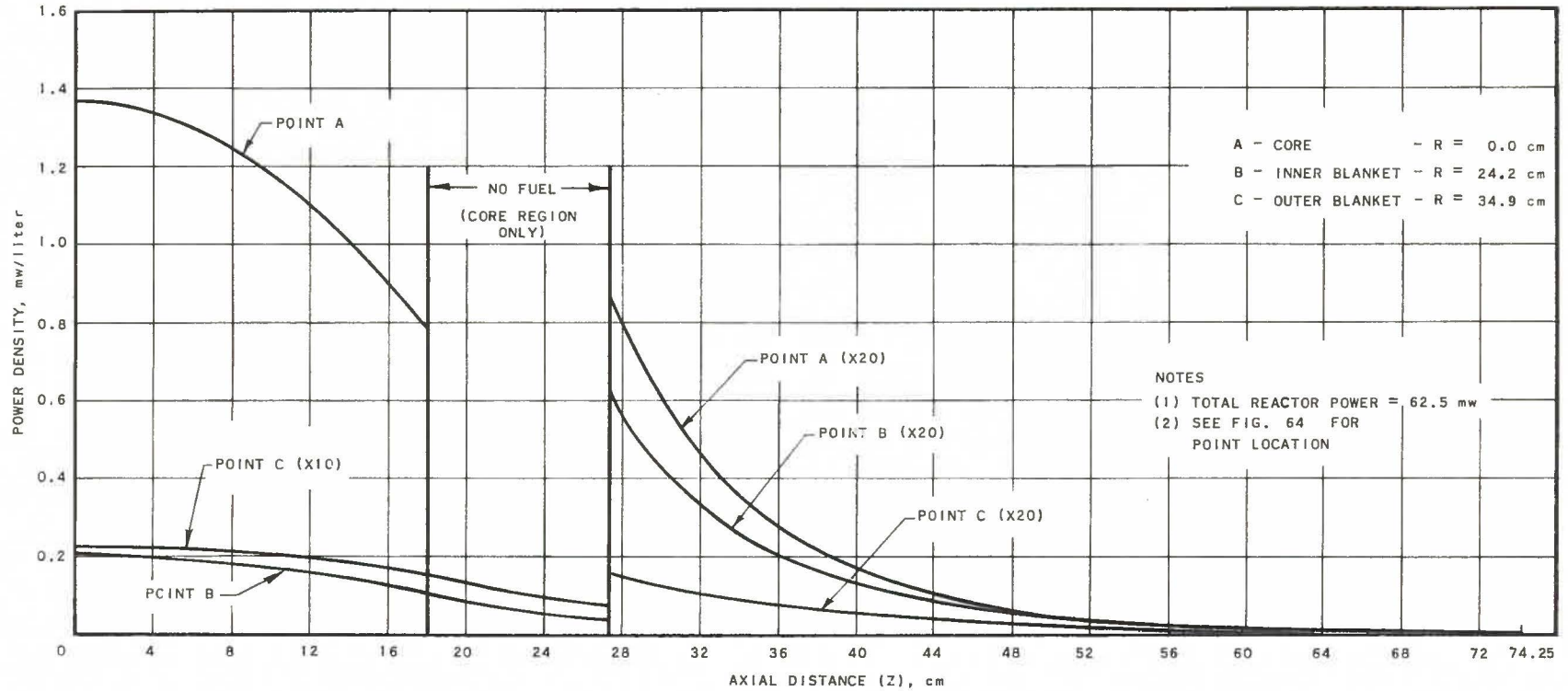


FIG. 65  
 AXIAL POWER DENSITY DISTRIBUTIONS OF CLEAN REACTOR

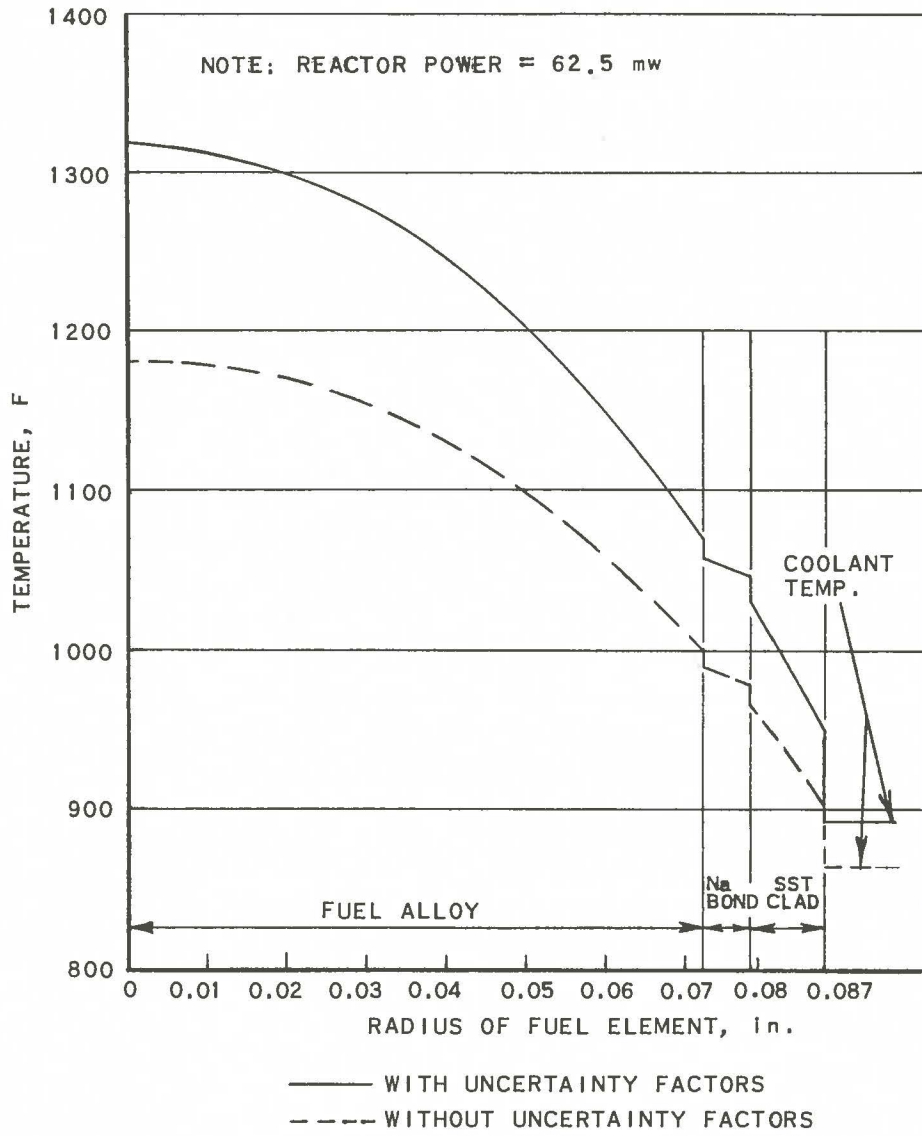
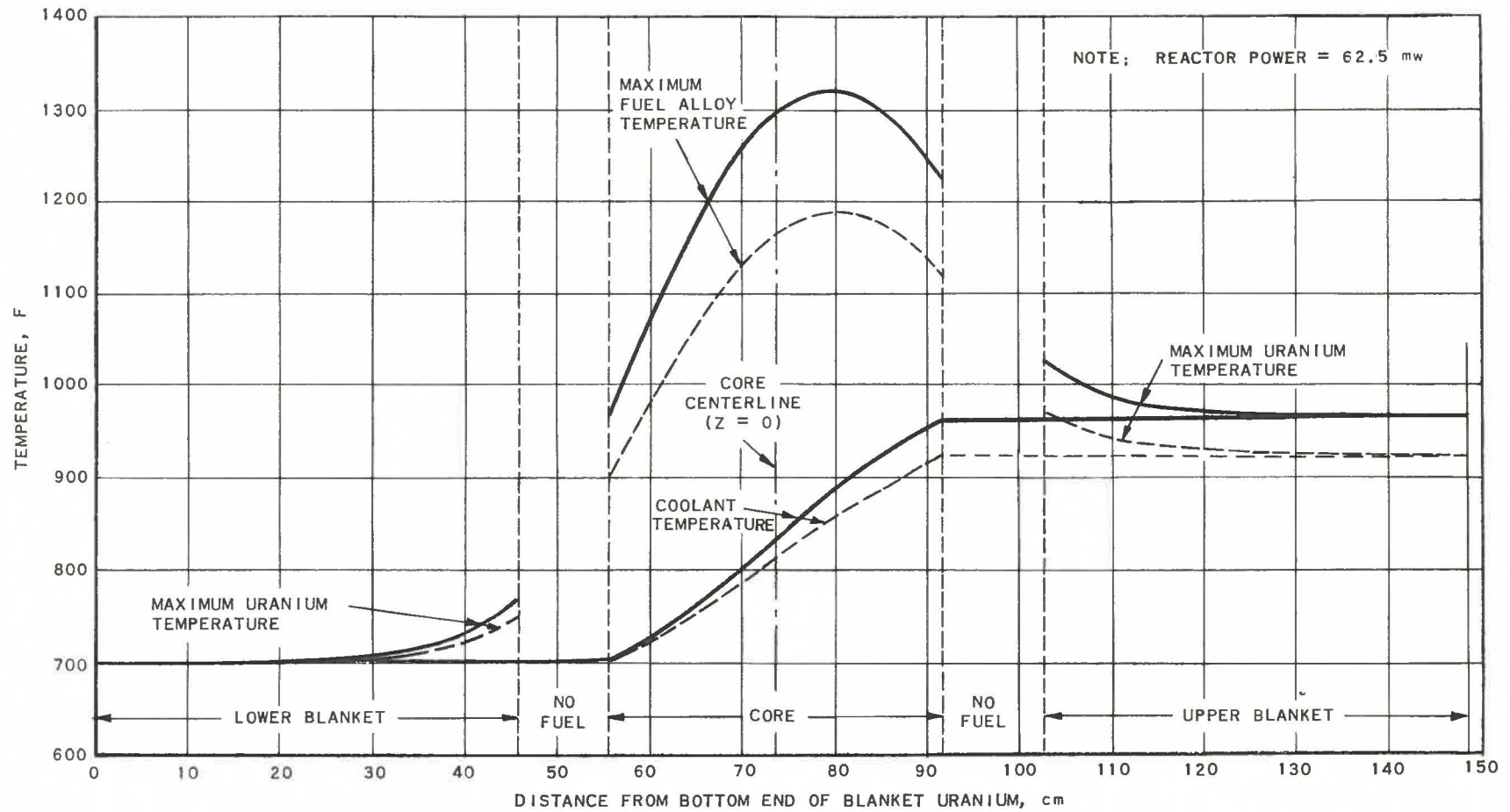


FIG. 66  
RADIAL TEMPERATURE DISTRIBUTION THROUGH A FUEL ELEMENT  
AT POINT OF MAXIMUM FUEL TEMPERATURE

RE-7-19725-A  
W. S. SIMMONS: D. Q., 2-25-57



— WITH UNCERTAINTY FACTORS  
 - - - WITHOUT UNCERTAINTY FACTORS

FIG. 67  
 AXIAL TEMPERATURE DISTRIBUTIONS OF  
 FUEL ALLOY AND COOLANT  
 (POINT A: R = 0 cm)

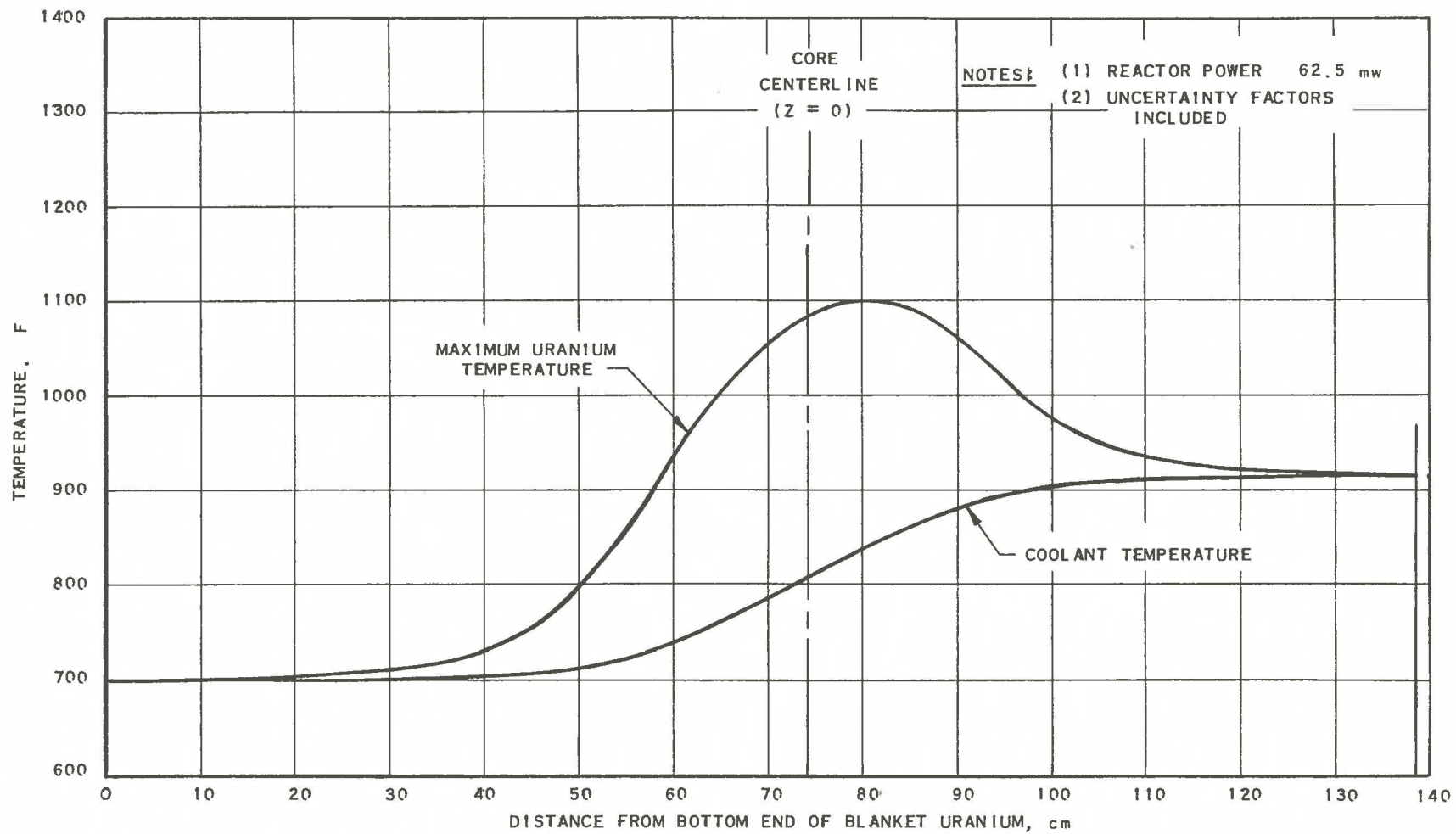


FIG. 68  
AXIAL TEMPERATURE DISTRIBUTIONS OF  
BLANKET URANIUM AND COOLANT  
(POINT B; R = 24.2 cm)

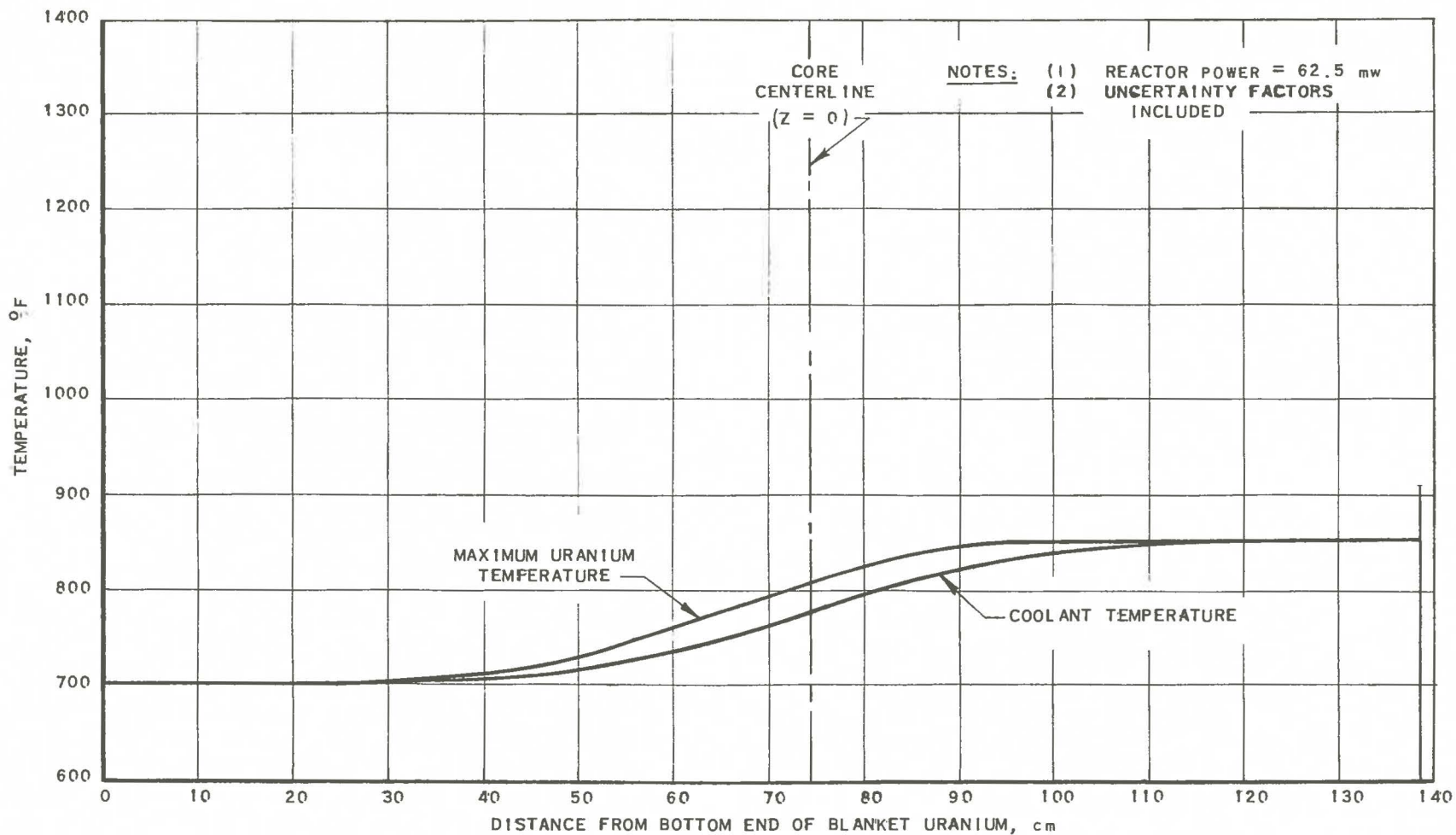


FIG. 69  
AXIAL TEMPERATURE DISTRIBUTIONS OF  
BLANKET URANIUM AND COOLANT  
(POINT C:  $R = 34.9$  cm)

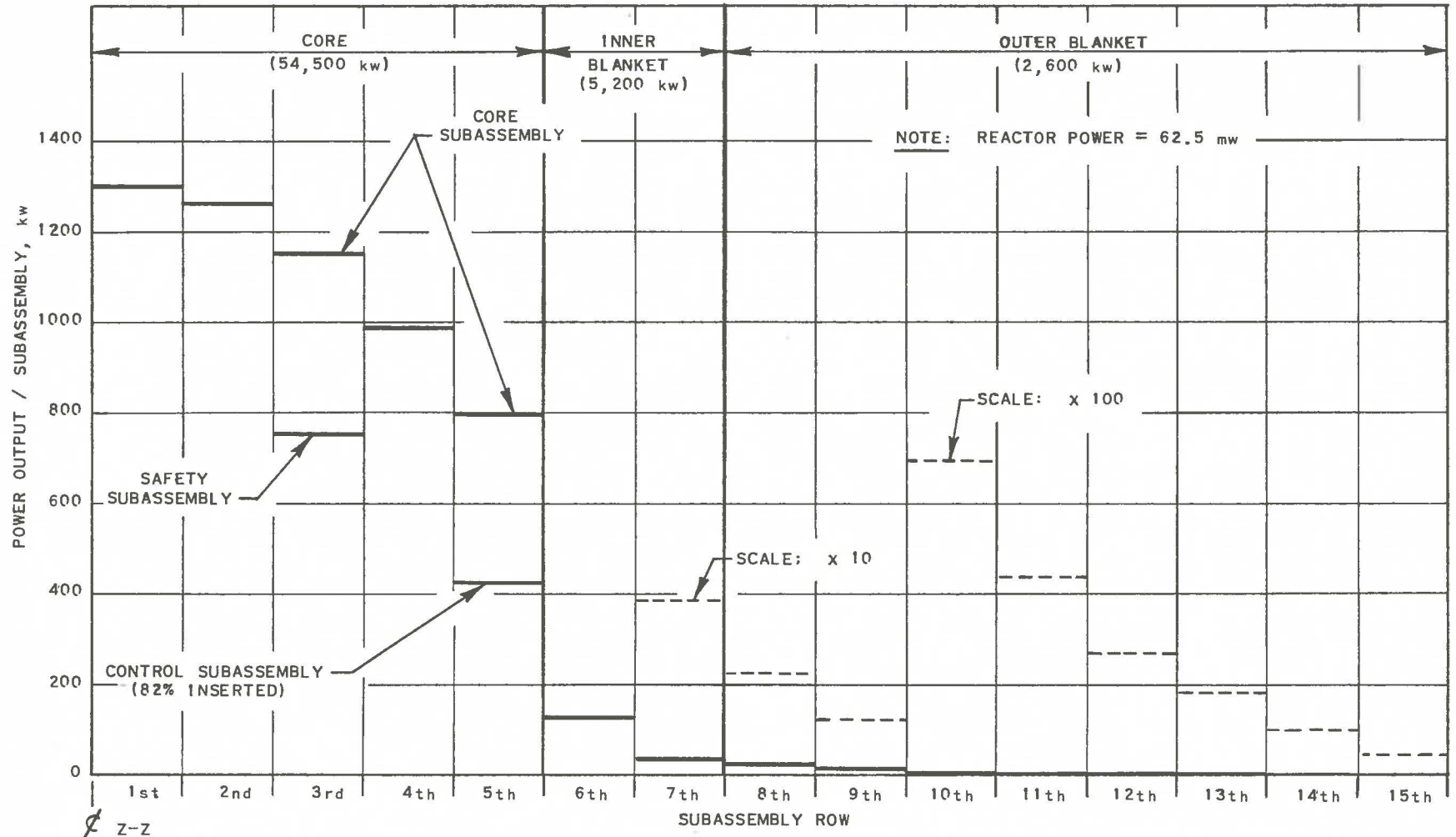


FIG. 70  
POWER OUTPUT PER SUBASSEMBLY  
FOR CLEAN REACTOR

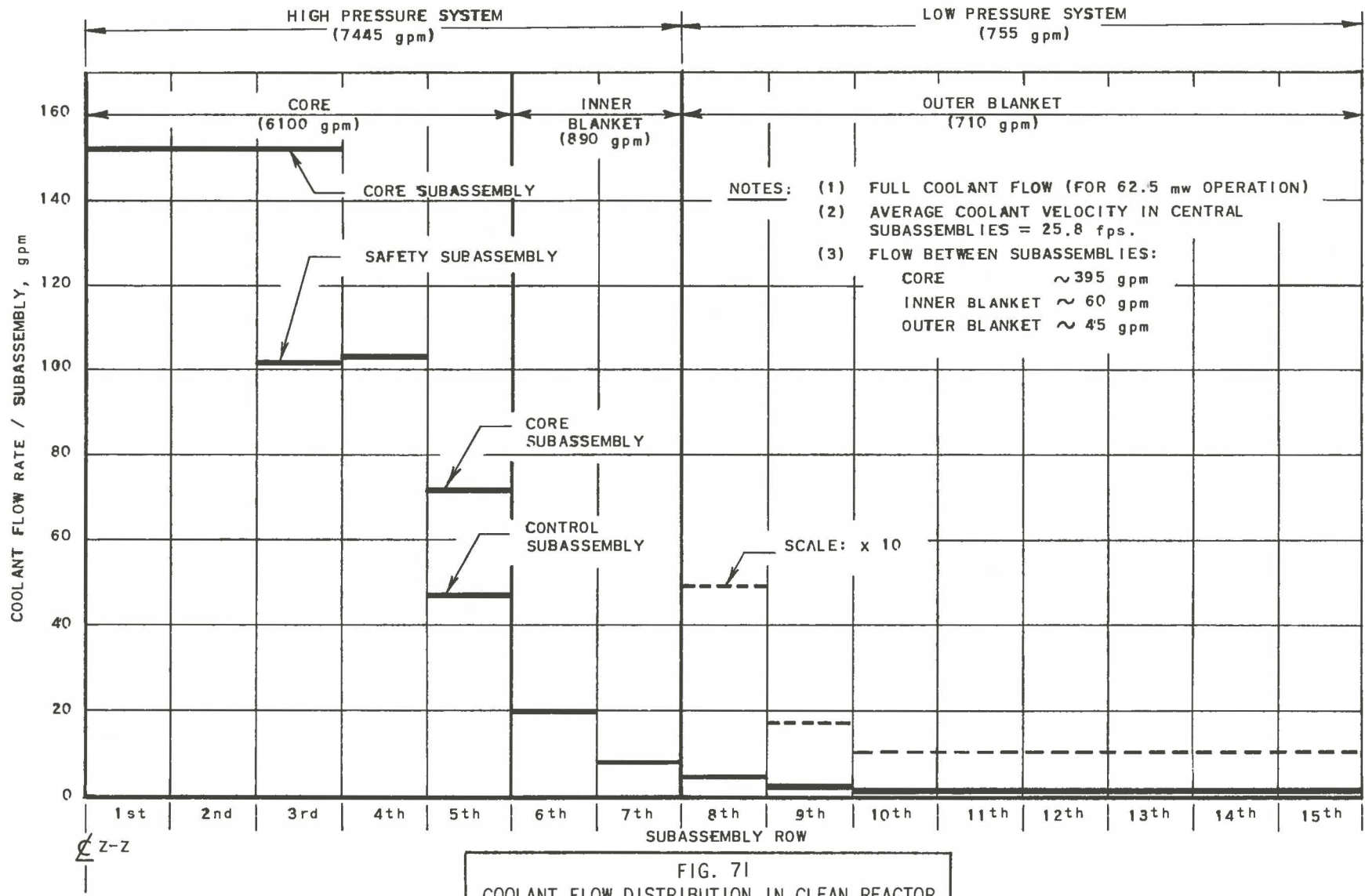


FIG. 71  
COOLANT FLOW DISTRIBUTION IN CLEAN REACTOR

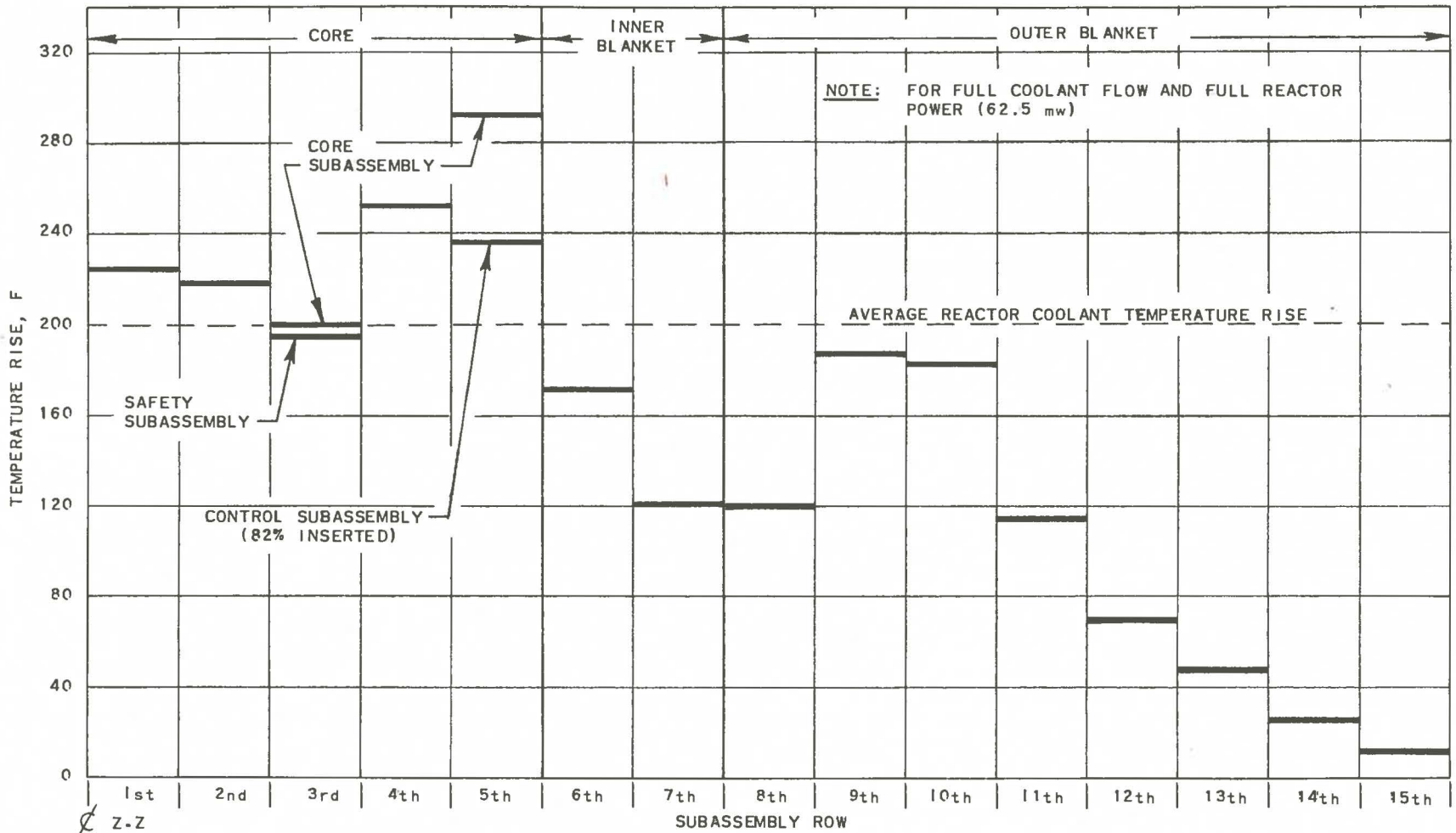


FIG. 72  
AVERAGE COOLANT TEMPERATURE RISE  
THROUGH EACH SUBASSEMBLY

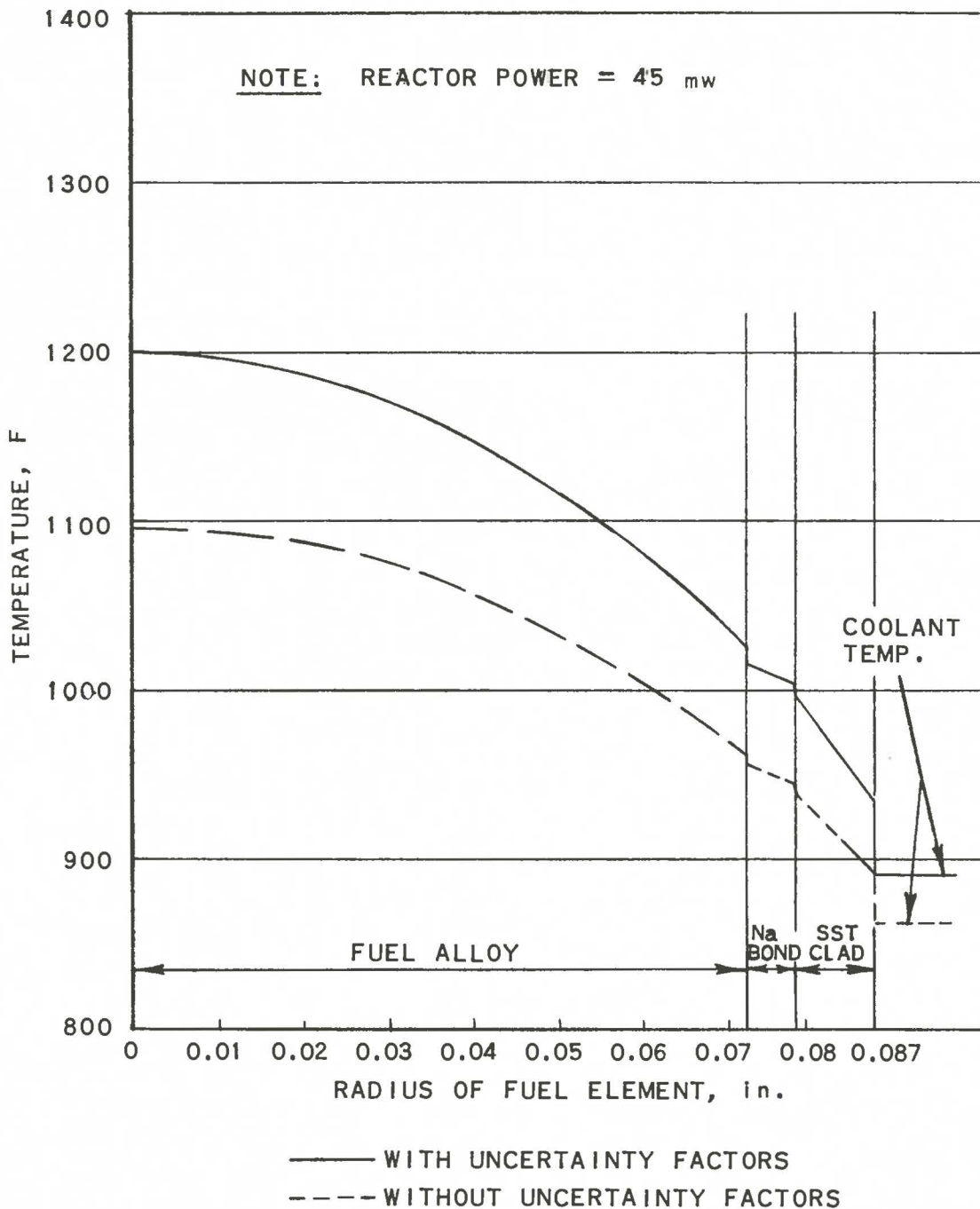


FIG. 73  
 RADIAL TEMPERATURE DISTRIBUTION THROUGH A FUEL ELEMENT  
 AT POINT OF MAXIMUM FUEL TEMPERATURE

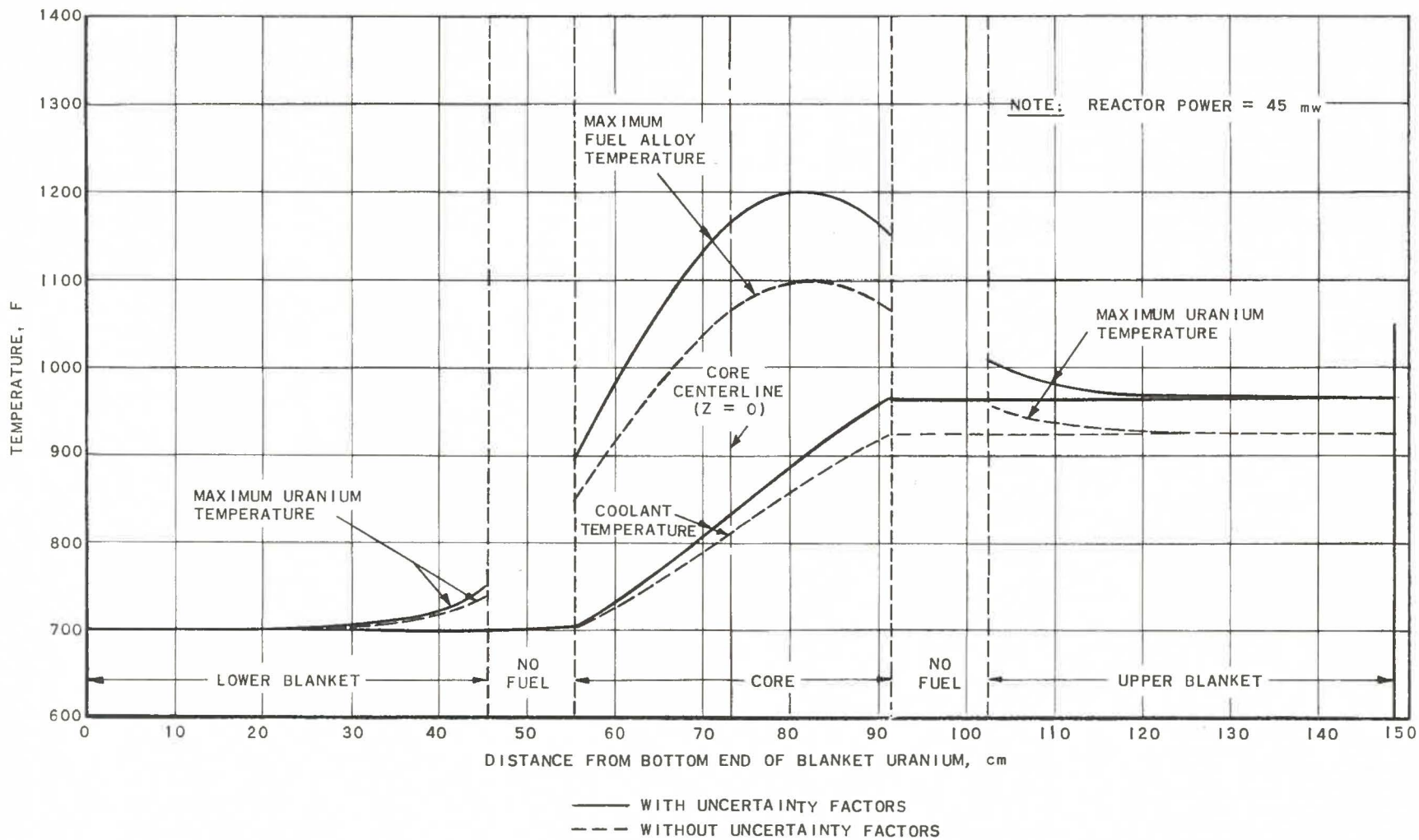


FIG. 74  
 AXIAL TEMPERATURE DISTRIBUTIONS OF  
 FUEL ALLOY AND COOLANT  
 (POINT A: R = 0 cm.)

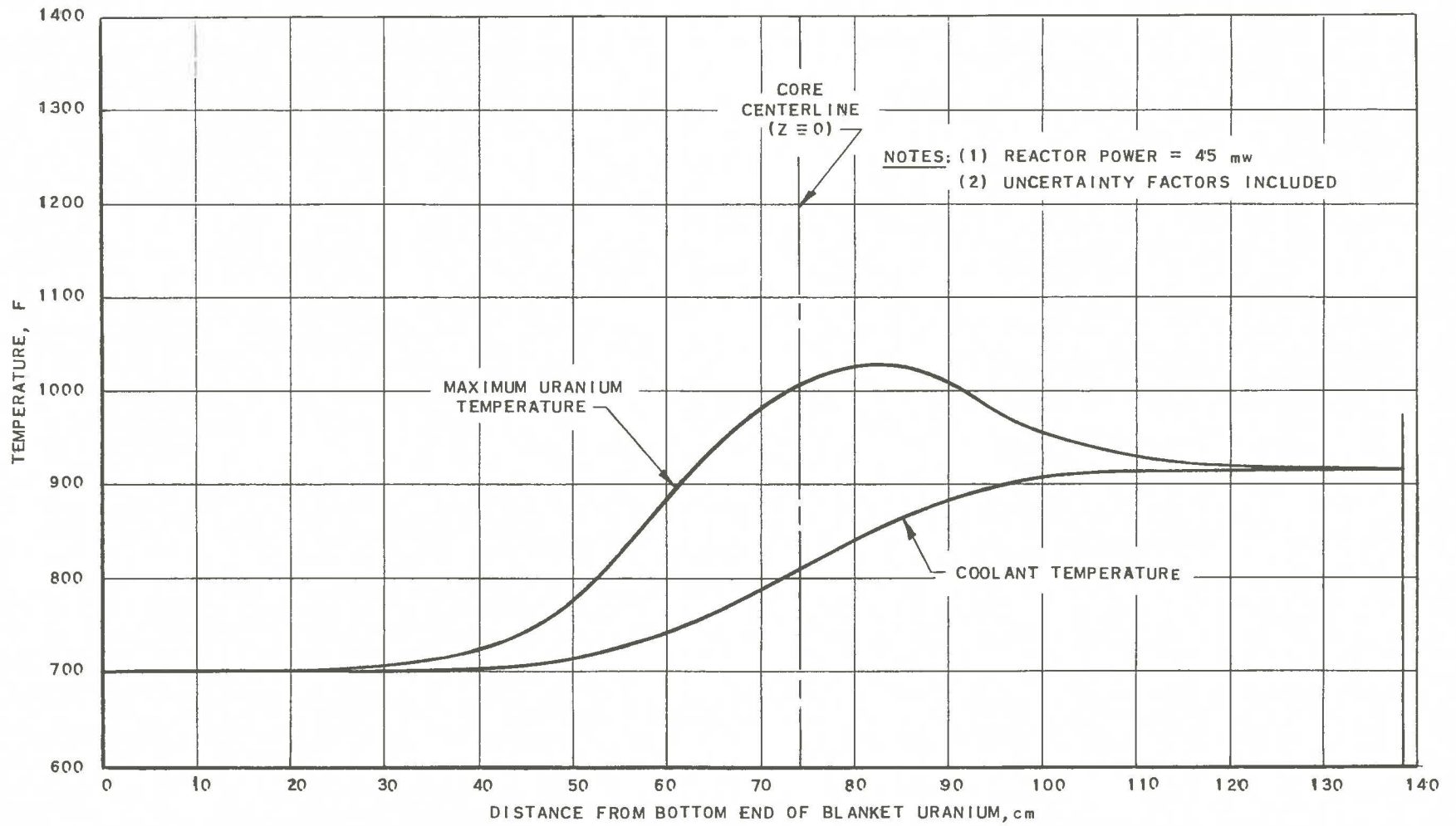


FIG. 75  
 AXIAL TEMPERATURE DISTRIBUTIONS OF  
 BLANKET URANIUM AND COOLANT  
 (POINT B: R = 24.2 cm)

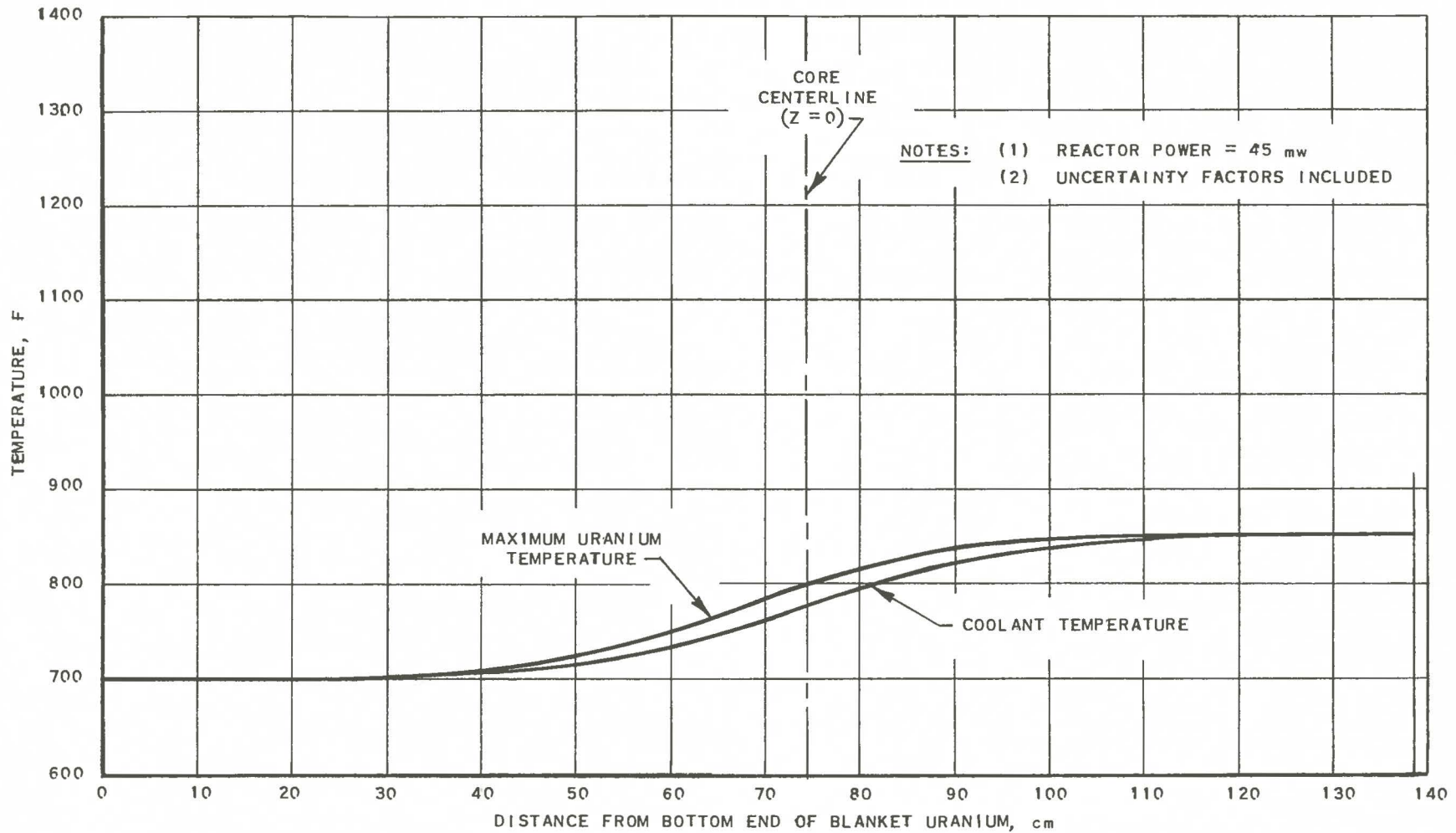


FIG. 76  
AXIAL TEMPERATURE DISTRIBUTIONS OF  
BLANKET URANIUM AND COOLANT  
(POINT C: R = 34.9 cm)

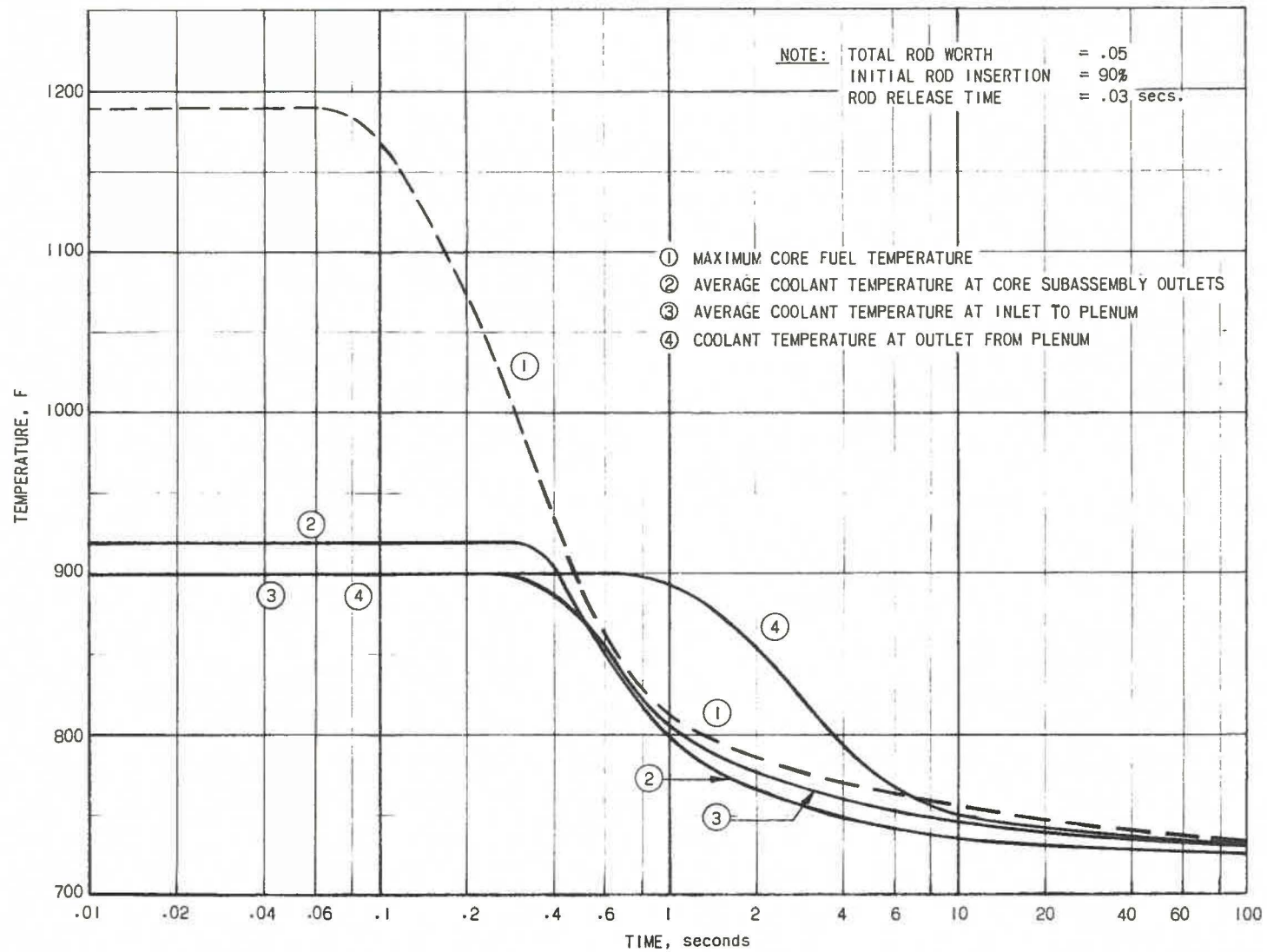
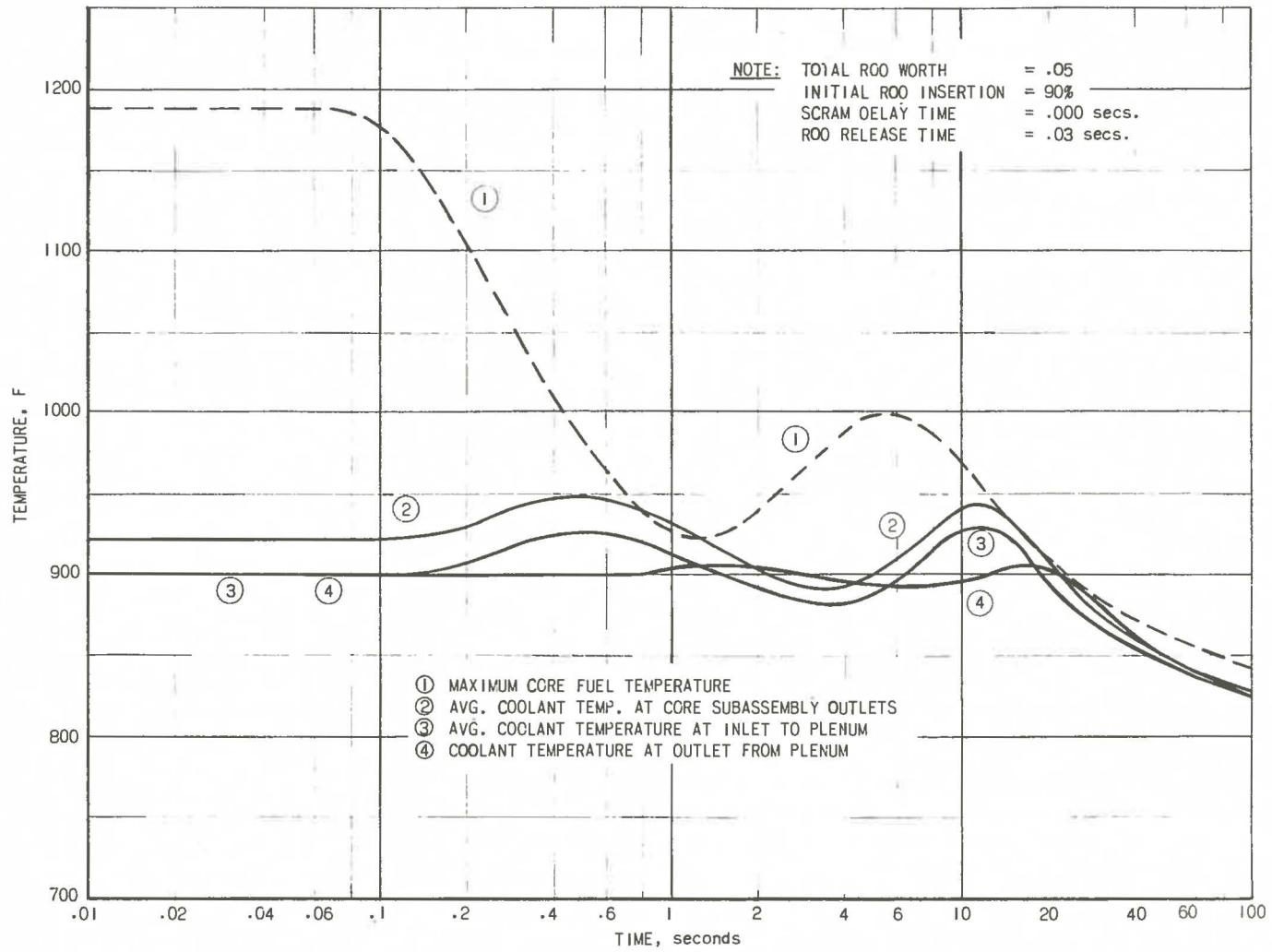


FIG. 77  
 VARIOUS REACTOR TEMPERATURES DURING SCRAM VS.  
 TIME AFTER SCRAM SIGNAL REACHES CONTROL RODS  
 (ALL PUMPS REMAIN IN OPERATION)



**FIG. 78**  
**VARIOUS REACTOR TEMPERATURES DURING**  
**SCRAM VS TIME AFTER FAILURE OF BOTH**  
**MAIN PUMPS (AUXILIARY PUMP CONTINUES**  
**IN OPERATION).**

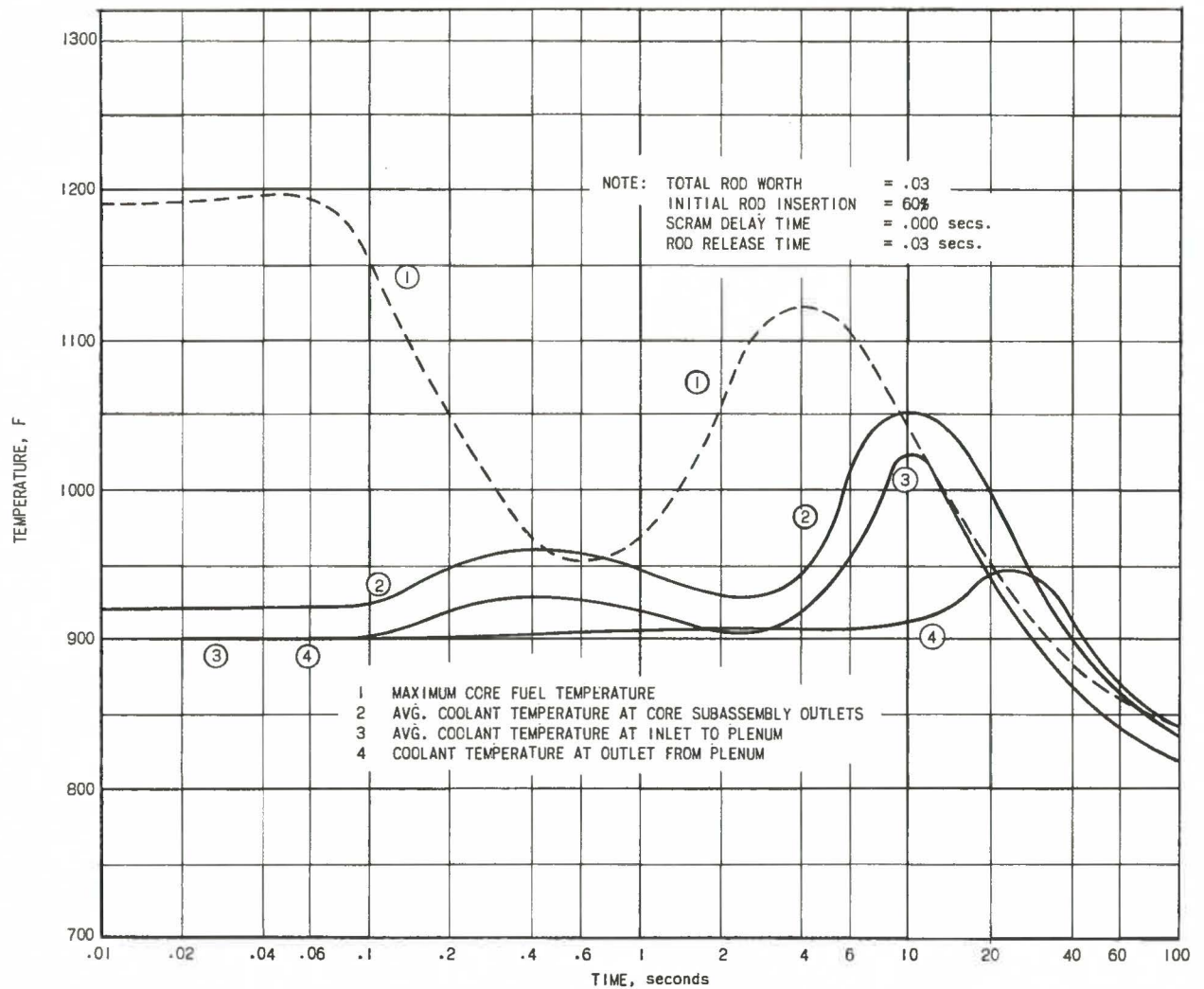


FIG. 79  
 VARIOUS REACTOR TEMPERATURES DURING  
 SCRAM VS TIME AFTER FAILURE OF BOTH  
 MAIN PUMPS (AUXILIARY PUMP CONTINUES  
 IN OPERATION).

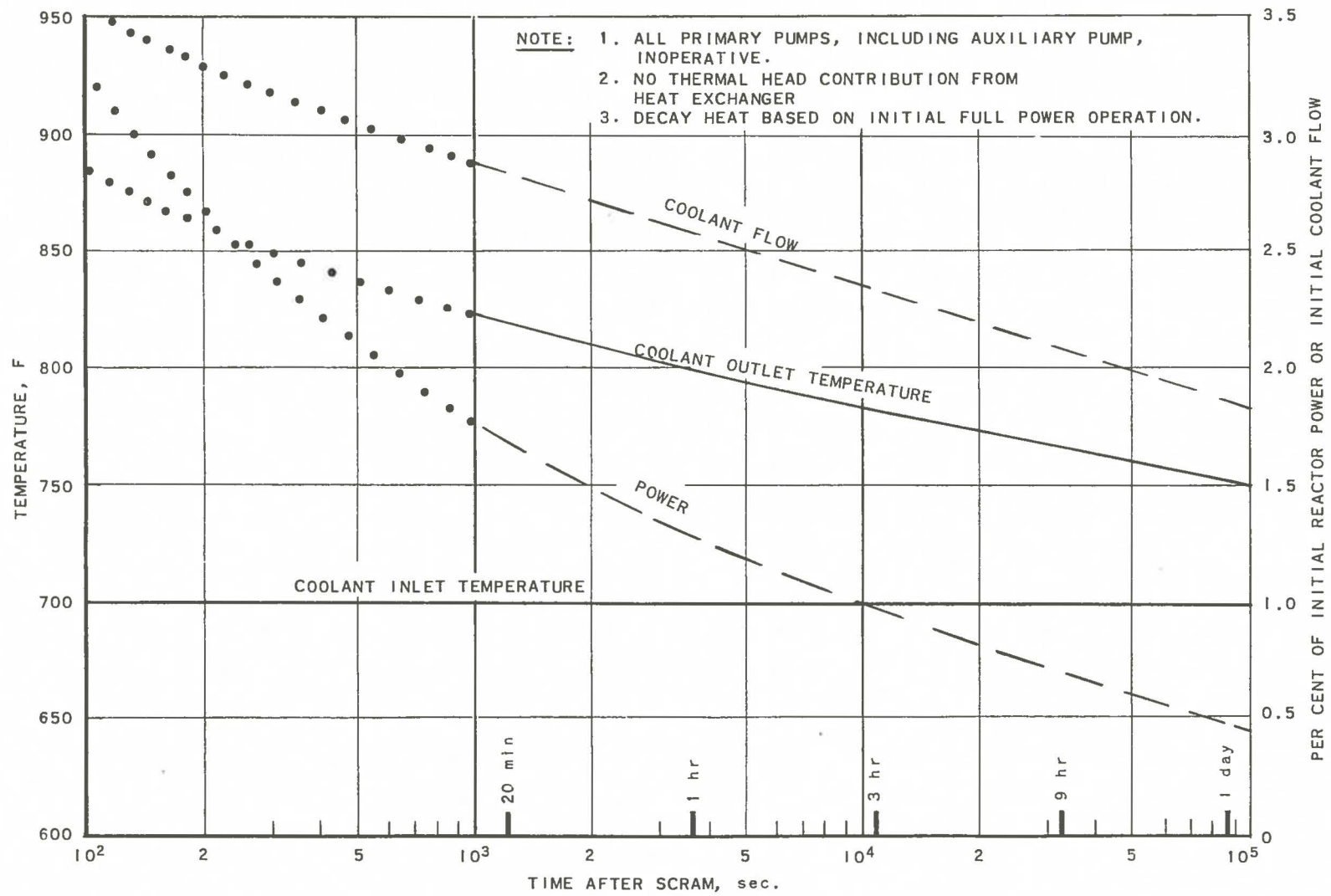


FIG. 80  
APPROXIMATE REACTOR CONDITIONS DURING THE LONG-TERM (NATURAL CONVECTION) COOLING PROCESS

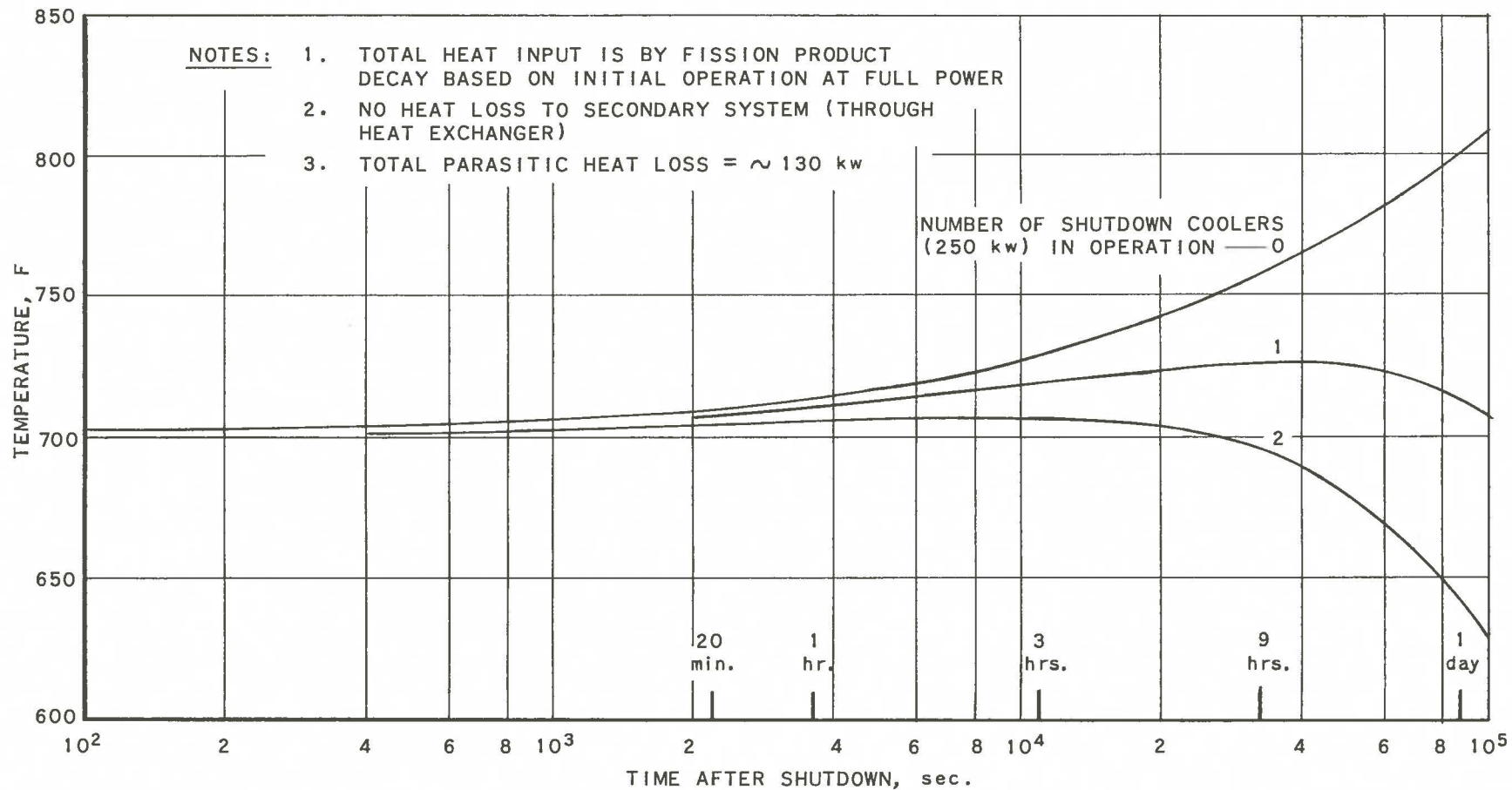


FIG. 81  
 PRIMARY TANK BULK SODIUM  
 TEMPERATURE VS TIME AFTER SHUTDOWN

1  
2  
3  
4  
5  
6  
7  
8  
9  
10  
11  
12  
13  
14  
15  
16  
17  
18  
19  
20  
21  
22  
23  
24  
25  
26  
27  
28  
29  
30  
31  
32  
33  
34  
35  
36  
37  
38  
39  
40  
41  
42  
43  
44  
45  
46  
47  
48  
49  
50  
51  
52  
53  
54  
55  
56  
57  
58  
59  
60  
61  
62  
63  
64  
65  
66  
67  
68  
69  
70  
71  
72  
73  
74  
75  
76  
77  
78  
79  
80  
81  
82  
83  
84  
85  
86  
87  
88  
89  
90  
91  
92  
93  
94  
95  
96  
97  
98  
99  
100

## APPENDIX A

EFFECTS OF OPERATIONAL ABNORMALITIES

The subject matter discussed in this Appendix has been grouped into three major subdivisions. In the first section, a series of hypothetical accidents are discussed in which reactivity is added to the reactor in an uncontrolled fashion. In the second section, the effect of pump failure upon the integrity of the core is examined. In the third section, the expected bowing characteristics of the core subassemblies are treated, and the reactivity effect of bowing in the worst possible configuration is calculated.

1. Nuclear Accidentsa. Reactivity Coefficients

Multigroup diffusion theory has been used to calculate the basic reactivity coefficients which determine the reactivity feedback resulting from heating part or all of the reactor. In general, the one-dimensional spherical model has been used for the calculation, and an extrapolation added to allow for the deviations of the reactor geometry from spherical symmetry. Considerable uncertainty must be ascribed to these coefficients until detailed experiments and improved calculation methods are available.

The reactivity coefficients have been calculated in terms of simple changes in material density or reactor geometry. For example, in Table A-I the reactivity change corresponding to a density change of sodium in the core is given as

$$\Delta k/k = 0.03 \Delta\rho/\rho \quad .$$

In this calculation only the sodium density in the core has been assumed to change, with no change in core dimensions. Also listed is the reactivity effect associated with a change in reactor dimension, where the composition of each region has been maintained. By converting power distributions to temperature distributions, and these in turn to changes in density and dimensions, the reactivity feedback coefficients for a particular transient can be ascertained.

To evaluate the inherent safety characteristics of the reactor, several cases of reactor mismanagement and malfunction have been assumed, and the effects thereof on the reactor calculated. The accidents may be divided into those involving a low rate of reactivity addition and a high rate.

Table A-I

REACTIVITY EFFECTS OF CHANGES IN MATERIAL DENSITY(in units of  $\frac{\Delta k}{k} / \frac{\Delta \rho}{\rho}$ )

	<u>Uranium Density</u>	<u>Sodium Density</u>	<u>Iron Density</u>
Core	0.55	0.03	0.028
Inner Blanket	0.047	0.007	0.016
Outer Blanket	0.01	0.0006	0.0021
Structural Gap	-	0.013	0.026
Upper plus Lower Blanket	0.017	0.0074	0.015

For Axial Core Expansion into Structural Gaps:  $\Delta k/k \sim 0.27 \left( \frac{\Delta L}{L} \right)$

Case 1: Assume the reactor is at delayed critical and at zero power conditions (~8 watts and 600F) with the shutdown safety rods out. These rods are then inserted into the core at their normal speed of 2 in./min.

Case 2: Assume the reactor is at delayed critical and zero power conditions with the central fuel element removed. This element is then loaded at regular speed of 6 in./min for the last 24 in. of travel.

Case 3: Assume the reactor is at delayed critical and zero power conditions and a single control rod is driven in at 5 in./min.

Case 4: Same as Case 3 except we begin excursion at operating power and full flow.

Case 5: Assume the reactor is at delayed critical and zero power conditions with the central fuel element being loaded. It is dropped and falls into the reactor. This is an accident where reactivity is added rapidly. Two cases are considered, first where the element is dropped from just above the core, and second, where the element falls the full length of the reactor.

Case 6: Same as Case 2 but the fuel element is driven all the way in at high speed (72 in./min).

b. Kinetic Behavior Prompted by Slow Rates of Reactivity Insertion

The kinetic behavior of the fast neutron system has been investigated by applying the one-group, space-independent model. The major objective in this analysis is to obtain information concerning the time variation of neutron flux, should the various mechanisms malfunction.

In all of these analyses it is assumed that the reactivity is inserted at rates consistent with normal rod drive speeds. The drive speeds are nonvarying and the rates of insertion of reactivity are quite small, though actually not constant. However, for simplicity of calculation, it has been assumed that the rates of insertion are constant.

The kinetics of the system, including the effect of the delayed neutrons, depend on three basic parameters. The first of these is the prompt neutron lifetime of the system. This is obtained on the basis of multigroup diffusion theory. For the EBR-II-type reactor this is calculated to be about  $0.8 \times 10^{-7}$  sec. The method of calculation has given results in good agreement with experimental measurements on Rossi-Alpha at ZPR-III.

The other two parameters are concerned with the rate of introducing reactivity and the mechanism for shutting the system down due to thermal expansion of the materials in the system.

The analytical approach taken here has been to do a parametric study, considering both insertion rate and reactivity feedback as parameters. The results of these studies will be presented first; then, they will be applied to the specific accidents previously enumerated.

(1) The Parametric Study

Let us first consider  $k_{ex} = k_{eff} - 1 = f(n,t)$ .

A portion of  $f(n,t)$  can be represented by the form  $At$  where  $A$  is a constant describing the rate of inserting reactivity. If the shutdown mechanism is related to the expansion of the system and hence the temperature change, another part of  $f(n,t)$  must be related to the energy stored in the system. This is directly proportional to  $\int_0^t n(t)dt$ , the constant of proportionality being given as  $B$ . The latter must be precisely defined.

The information in Table A-I is sufficient to give information concerning the reactivity changes associated with perturbations of the system. It is then possible to relate a given perturbation with a particular temperature change by suitable application of thermal data. Knowing this

relationship it is then necessary to obtain the representative temperature change of a given time-dependent situation. In its simplest form, this is simply the ratio of the energy produced per unit volume to the heat capacity per unit volume. Appropriate factors must be introduced to account for heat removal by coolant and for varying temperatures throughout the system.

The energy produced per unit volume is given by  $\Sigma_f V \int_0^t n dt$  where  $\Sigma_f$  is the average macroscopic fission cross section and  $V$  is the appropriate average neutron velocity. It is possible to obtain the product  $\Sigma_f V$  directly from the one-group relationship  $\ell = 1/\nu \Sigma_f V$  where  $\ell$  is the prompt neutron lifetime and  $\nu$  the number of neutrons per fission.

In summary, the excess reactivity as a function of time in its simplest form may be given as:

$$k_{ex}(t) = At - B \int_0^t n dt + Bn_0t$$

$B$  consists of a product of several terms which may be given as:

$$B \int n dt = \left( \frac{dk}{dq} \right) \left( \frac{dq}{dt} \right) \Delta T = \left( \frac{dk}{dq} \right) \left( \frac{dq}{dt} \right) \left( \frac{\Sigma_f V \int_0^t n dt}{S_v} \right)$$

$\frac{dk}{dq}$  = reactivity change corresponding to perturbation

$\frac{dq}{dt}$  = perturbation corresponding to given temperature change

$\Delta T$  = temperature change

$S_v$  = heat capacity per unit volume

$\Sigma_f V \int_0^t n dt$  = heat produced per unit volume

The results of the parametric study are presented in Figs. A-1 to A-6. The calculations have been done, assuming the flux  $n = 1$  at  $t = 0$ . The power can therefore be considered arbitrary until application is made to a specific accident, employing a pre-assigned temperature feedback. In Figs. A-1 to A-3, for several values of  $B$  and a fixed  $A$ ,  $n$ ,  $k_{ex}$  and  $\int_0^t n dt$  plotted against time. In Figs. A-4 to A-6, for several values of  $A$  and a fixed  $B$ , again we have  $n$ ,  $k_{ex}$  and  $\int_0^t n dt$  plotted against time.

From Fig. A-1 we see that reducing the feedback by a factor of ten, for a fixed insertion rate, raises the maximum flux by the same factor, ten. The effect on the integral of the flux, as shown in Fig. A-3, is the same.

(2) The Application to Specific Accidents(a) Low Initial PowerCase 1: Safety rods driven into critical reactor.

Consider the situation where the system is at source power, barely subcritical with the fuel sections of the safety rods located just below the core. Then, somehow the fuel sections of the safety rods move into the core at a speed of 2 in./min. No coolant is flowing. Essentially all of the heat generated is retained by the core and coolant. Some loss of heat occurs due to convection.

Each of the safety rods has been calculated to be worth about 1% in reactivity. Hence a total  $\Delta k$  of 2% is moving into the system. We will assume  $\Delta k$  to be a linear function of position. Hence, for a 14-in. stroke, we will be adding  $.02/7 \times 60 = 0.00048 \Delta k/\text{sec} \approx 5 \times 10^{-5} \Delta k/\text{sec} = A$ .

We now need to assign a value to the temperature feedback coefficient, B. The assumption that initially the system is at source power with no coolant flow simplifies the analysis. Since the rate of insertion is slow, it may be assumed that the average coolant, fuel and clad temperatures are equal in any region, though varying in time.<sup>1</sup> Thus the heat capacity per unit volume can be expressed as  $S_v = \sum V_i^F S_{vi}$  where  $V_i^F$  represents the volume fraction of material i in the core and  $S_{vi}$  represents the heat capacity per unit volume of the pure material i.

To calculate the reactivity change associated with a given temperature change it is necessary to calculate  $\frac{\Delta k}{\Delta T} = \sum \frac{\Delta k}{\Delta q_i} \frac{\Delta q_i}{\Delta T}$  where  $q_i$  represents the perturbations. For core effects only this has been calculated to give  $\frac{\Delta k}{\Delta T} \approx -1.28 \times 10^{-5}/\text{C}$  using the data of Table A-I.

In Fig. A-7, the pertinent results of this analysis are summarized. The energy generated, divided by the fractional increase in fuel element length is plotted versus period for the assumption of an exponential power rise. For periods greater than one second, we see the curve is flat, indicating essentially an equilibrium distribution of temperature. For shorter periods the ratio decreases, indicating more and more heat is staying in the uranium. However, for periods shorter than  $10^{-3}$  seconds, the curve starts bending up sharply, as inertial effects begin to take over.

<sup>1</sup>T. R. Bump and R. W. Seidensticker "Reactor Temperatures and Fuel Alloy Expansions Resulting from Exponential Power Excursions in EBR-II." ANL report in preparation. See also paper by Bump and Seidensticker, First Winter Meeting of American Nuclear Society.

We can write for the core:

$$\frac{\Delta k}{k} = \left( \frac{\Delta k}{k} \right)_{\text{density changes}} + \left( \frac{\Delta k}{k} \right)_{\text{dimension changes}} + \left( \frac{\Delta k}{k} \right)_{\text{other}}$$

The category "other" includes Doppler effect, to which we have assigned a coefficient (see Appendix B), and bowing, which is likely to be very small (see Section III) and is neglected here. Assuming a linear expansion coefficient of expansion equal to  $14 \times 10^{-6}$  in./in./C for steel and uranium, and a density coefficient of  $2.9 \times 10^{-4}$ /C for sodium, we have for a one-degree change in temperature,

$$\begin{aligned} \frac{\Delta k}{k} = & [ (-0.55 - 0.028) (14 \times 10^{-6}) - 0.03 (2.9 \times 10^{-4}) ]_{\text{density}} \\ & + [ (0.27) (14 \times 10^{-6}) + (0.2 \times 10^{-6}) ]_{\text{Doppler}} \end{aligned}$$

where the Doppler coefficient is an average coefficient between 300C and 1100C obtained (by using the  $-T^{3/2}$  relation). Thus we obtain for a one-degree change in temperature,

$$\frac{\Delta k}{k} = -1.28 \times 10^{-5}/C$$

This coefficient is subject to considerable uncertainty. The sodium density effect, which contributes more than half the total coefficient, is particularly doubtful. The measurements made at ZPR-III to date are not completely reproducible and agreement between experiment and theory is only fair.

We have neglected one minor effect which may possibly give a small positive contribution. The uranium also expands radially within its jacket, forcing some sodium from the core into the upper gap area above the core, where the worth of coolant conceivably may be slightly greater. In addition, the effects of coolant convection during an incident have also been neglected.

We have not permitted the core to expand radially, over-all, since the bottom structure, which determines fuel element location, will change dimensions only as the bulk sodium changes temperature.

Of course, some heat will be generated in the blanket regions. For the conditions of no coolant flow, it appears reasonable to take the temperature rise distribution through the reactor proportional to the energy distribution during the accident. The reactivity contribution

from the blanket areas per degree temperature rise in the core will be the blanket coefficient per degree multiplied by the relative temperature rise.

The following coefficients have been calculated for the various regions:

$$\left. \frac{\Delta k}{\Delta T} \right|_{\text{inner blanket}} = -0.30 \times 10^{-5}/C$$

$$\left. \frac{\Delta k}{\Delta T} \right|_{\text{outer blanket}} = -0.03 \times 10^{-5}/C$$

$$\left. \frac{\Delta k}{\Delta T} \right|_{\substack{\text{upper blanket plus} \\ \text{lower blanket}}} = -0.26 \times 10^{-5}/C$$

$$\left. \frac{\Delta k}{\Delta T} \right|_{\text{gaps}} = -0.42 \times 10^{-5}/C$$

The temperature rise in each region per degree rise in the core is a function of the power distribution and the heat capacities. We calculate, per degree rise in the core

$$\Delta T_{\text{inner blanket}} = 0.045$$

$$\Delta T_{\text{outer blanket}} = 0.01$$

$$\Delta T_{\substack{\text{upper and lower} \\ \text{blanket}}} = 0.02$$

$$\Delta T_{\text{gap}} = 0 \text{ (neglecting convection and conduction)}$$

resulting in an over-all feedback effect of

$$\left( \frac{\Delta k}{\Delta T} \right)_{\text{total}} = -1.3 \times 10^{-5}/C$$

for the slow excursion with no coolant flow.

Knowing  $\left. \frac{\Delta k}{\Delta T} \right|_{\text{total}}$ , it is then necessary to calculate the

core temperature change as a function of time. This will simply be the ratio of the heat absorbed per unit core volume to the specific heat per unit core volume.

The latter has been calculated to be such that

$$S_v = 0.534 \text{ cal}/(\text{cm}^3)(\text{C})$$

The heat absorbed per unit volume can be represented by

$$\gamma \Sigma_f \int_0^t \phi dt = \gamma \Sigma_f v \int_0^t n dt$$

It is possible to obtain

$$\Sigma_f v$$

directly for a particular system from the expression

$$l \sim \frac{\left(\frac{1}{v}\right)}{(\nu \Sigma_f)}$$

where the brackets indicate proper weighting of fluxes and adjoints. The prompt neutron lifetime,  $l$ , is known to be about  $0.8 \times 10^{-7}$  sec, and  $\nu$  is known to be about 2.5. Hence

$$\Sigma_f v \approx 5 \times 10^6 \text{ sec}^{-1}$$

Since each fission liberates approximately  $0.76 \times 10^{-11}$  calories, we have

$$\gamma \Sigma_f v = (.76) (10^{-11}) (5) (10^6) = 0.38 \times 10^{-4}$$

Thus

$$\begin{aligned} \Delta T &= \frac{\gamma \Sigma_f v \int_0^t n dt}{S_v} = \frac{0.38 \times 10^{-4}}{.534} \int_0^t n dt \\ &= 0.71 \times 10^{-4} \int_0^t n dt * \end{aligned}$$

and the feedback is given by

$$\begin{aligned} \frac{\Delta k}{k}(t) &= \left(\frac{\Delta k}{\Delta T}\right) (\Delta T) = B \int_0^t n dt \\ &= -(1.3 \times 10^{-5}) (0.71 \times 10^{-4}) \int_0^t n dt \\ &= 0.92 \times 10^{-9} \int_0^t n dt \end{aligned}$$

---

\*Since  $n$  is taken as unity at  $t = 0$ , we have a source power of  $-1.9 \text{ cal/sec}$  or 8 watts.

We are now ready to examine the consequences of this accident. The temperature of the system while loading operations are underway should be about 600F or 315C. If the melting point of the fuel is 1130C, a  $\Delta T$  of 815C on the average will melt the fuel pins. Since there is a maximum to average power generation of about 1.5, an average  $\Delta T$  of  $\frac{815}{1.5} = 545C$  will see melting begin at the hot point. Hence

$$\int_0^t n dt = \frac{\Delta T}{7.1 \times 10^{-5}} = \frac{545}{7.1 \times 10^{-5}} = 7.7 \times 10^6$$

when melting begins. From Fig. A-6, for a B of  $1.22 \times 10^{-9}$  and  $A = 5 \times 10^{-5}$ , we find that a flux integral of  $7.7 \times 10^6$  is just reached at the end of the first pulse. However, this feedback coefficient is about 30% too large. From Fig. A-3 we have seen the integral is inversely proportional to B for fixed A. Hence, we can expect the flux integral for our case to reach roughly  $10 \times 10^6$ , and that melting would begin about 120 sec after the beginning of the excursion, should no scrams be operative. The reactivity would be small or possibly negative at this time. The future course of the incident would depend on what new reactivity mechanisms began to take part.

Should a period scram have been operative, with a scram setting of 5 sec, ( $\Delta k/k = 0.0037$ ), Fig. A-5 tells us the signal would have been given at about  $t = 75$  sec, while the power was still very low. The incident would be terminated with no damage. If a power level trip were the shut down mechanism, its time of action would depend on the scram setting. A level of 1000 watts would be reached at approximately  $t = 70$  sec, as indicated in Fig. A-4. If the setting were 65 megawatts, however, the signal would never have been given, before melting began.

While the net bowing effect is expected to be small, an initial decrease in core radius is considered possible as the power rises if the most pessimistic assumptions are made. The maximum inward displacement (about 0.014 in.) would occur when the burst energy reached 8 megawatt-seconds, corresponding to a  $\Delta T$  of roughly 75C. The reactivity gain associated with this bowing would be about  $0.001 \Delta k/k$ , the same as would be lost from other temperature effects. Hence, under the worst conditions there would be no feedback during the first 75C temperature rise. However, during the next 75C the bowing effect would reverse itself and thereafter continue negative so the net contribution of bowing over the entire excursion would be to raise the feedback coefficient and diminish the burst strength.

#### Case 2: Central fuel element driven in at 6 in./min.

If we take an approximate  $\Delta k$  of 2% for a central fuel element, we will get a reactivity insertion rate three times as high as that of Case 1, or an  $A = 1.5 \times 10^{-4} \Delta k/\text{sec}$ . From Fig. A-6, we now have a

maximum  $\int n dt$  greater than  $2 \times 10^7$ , and we can expect to begin melting of the core to begin before  $t = 55$  sec, since  $B$  is really  $0.92 \times 10^{-9}$ . From Fig. A-5, we see the reactivity should again be negative at melting time, however.

Again a period scram would have been effective, giving a signal at  $t = 25$  sec, when the energy release was still low. Even if the loading mechanism continued driving in the fuel element, the safety rods should leave the core within a second after the signal is given, shutting off the incident.

A power level trip in the neighborhood of a kilowatt would also have been effective, producing a scram at about  $t = 31$  sec, while a trip set at 1.2 times maximum rated power would never be affected.

Case 3: A single control rod is driven in at 5 in./min.

Since the rod is worth about 0.5%  $k$ , and the stroke is 14 in., we obtain an average insertion rate of  $A = 3 \times 10^{-5}$ . Again a shut-down coefficient of  $B = 0.92 \times 10^{-9}$  is appropriate. A special calculation has been run for this incident, wherein the reactivity insertion is terminated when  $0.005 \Delta k/k$  has been introduced linearly. The reactor, after being shut down by the feedback term, was followed for some time after so that the total energy developed could be readily ascertained. The results are presented in Figs. A-8 to A-10. The dashed line represents the results of a second calculation in which the reactivity insertion rate is maintained, instead of being dropped to zero at  $t = 166$  sec. From Fig. A-9 we see the peak reactivity reached is only  $\Delta k = 0.0038$ , while from Fig. A-8 we find a peak power of about two megawatts. Four minutes after the beginning of the incident, we find  $\int n dt = 9.4 \times 10^6$  which corresponds to a temperature rise of 670C on the average. This might not produce melting, even though the peak temperature rise would be considerably larger. The reasons are: (1) there would be considerable time for conduction and convection of heat away from hot spots; and (2) as the uranium temperature neared the melting point, that of the sodium should exceed its boiling point, with a subsequent removal of both heat and reactivity.

The comparison of the two calculations in Figs. A-8 to A-10 shows the results are fairly insensitive to the exact reactivity in the rod.

(b) High Initial Power

Case 4: Control rod driven in, starting at full power and full flow.

The calculation of the reactivity feedback in such an incident is complicated particularly by the change in the rate of heat removal by the flowing coolant as the power changes. However, for such

slow rates of reactivity insertion, and at such high powers, where a small percentage change in power produces an immediate temperature effect, some simple estimates are adequate.

If we make the rough assumption that the core and blanket temperatures vary by the same amount on this excursion, we obtain a reactivity feedback of  $2 \times 10^{-5}/C$ . Then, if we add reactivity at the rate of  $3 \times 10^{-5}/\text{sec}$ , we will get a temperature rise of  $1.5C/\text{sec}$ . For full rod insertion, (a total reactivity addition of  $0.005 \Delta k/k$ ), we should get a temperature rise of nearly  $750C$  by the time all the reactivity is inserted. This is more than enough to melt the fuel pins, since they would start the excursion with a temperature of about  $600C$ . Hence, the incident would change its course before the end of the insertion.

No period scram would result, even if these circuits were operative. The reactivity feedback is so prompt, the reactor can go only slightly above critical. However, a power level trip, set at 1.25 times rated power would be effective. For the coolant exit temperatures to rise several hundred degrees, a power considerably greater than this would be required, and a scram would be triggered early in the excursion. A thermocouple-triggered scram on exit coolant temperature would also be effective.

c. Kinetic Behavior Prompted by Rapid Rates of Reactivity Insertion

Case 5: Dropping a Fuel Element during Loading

Ordinarily, should a fuel element be dropped during loading, and should it continue under the force of gravity into position in the core, no nuclear incident would occur. The reactor will be shut down by approximately  $4\% \Delta k/k$  due to withdrawal of the control rods, plus an amount equal to the worth of the fuel element being inserted. Only by some gross mismanagement could the reactor be nearly critical at the time the fuel element was accidentally dropped. Nevertheless, to study the consequences of this highly improbable situation, some calculations have been made of such an accident. Two cases are considered, first where the fuel element is just above the core when dropped (the tube-shaped end having engaged with its guide) and second, where the fuel element has just entered the reactor.

(1) Fuel Element Just Above the Core

The excursion considered here is visualized as resulting from an accidental drop of a fuel subassembly at a time when its fuel region is just above the core. The core is assumed to be critical at the beginning of the drop and at source power; the fuel element is assumed to be worth  $2\%$  or  $\$2.65$ . To obtain reasonable values of reactivity addition

rates it was assumed that

$$\frac{\Delta k_{ex}}{\Delta x} = A \sin^2 \left( \frac{\pi x}{L} \right)$$

where

$$A = \frac{2w}{L}$$

w is total worth of rod,

L is core length

so that

$$\int_0^L \frac{\Delta k_{ex}}{\Delta x} dx = w$$

The instantaneous rate of addition of  $k_{ex}$  as a function of position is

$$\sqrt{2gx} \frac{2w}{L} \sin^2 \left( \frac{\pi x}{L} \right)$$

assuming free fall of the element. An average rate for  $k_{ex} \leq \beta$  was obtained by determining the time required for  $k_{ex}$  to equal  $\beta$  and dividing  $\beta$  by this time. This gave a reactivity addition rate ( $R_0$ ) up to prompt critical of  $.06 \text{ sec}^{-1}$ . For a rate above prompt critical the maximum value of the expression

$$\sqrt{2gx} \frac{2w}{L} \sin^2 \left( \frac{\pi x}{L} \right)$$

was used and this gave a rate above prompt critical ( $R_1$ ) of  $0.2 \text{ sec}^{-1}$ .

An estimate of the value of  $n/(dn/dt)$  where  $n$  is the neutron density indicated that at the time sensible heating occurred, the power level would be rising so fast that essentially all the heat would remain in the fuel during the excursion. One can then estimate the change in reactivity with metal temperature as follows:

$$\begin{aligned} \frac{\Delta k}{k} &= -0.55 \frac{\Delta \rho_u}{\rho_u} + 0.27 \frac{\Delta L_u}{L_u} \\ &= -0.55 \frac{\Delta L_u}{L_u} + 0.27 \frac{\Delta L_u}{L_u} \\ &= -0.28 \frac{\Delta L}{L} \end{aligned}$$

Let us take a linear coefficient of expansion for the fuel pin of  $\Delta L/L = 14 \times 10^{-6} \text{ in./in.}(C)$ . We must consider the influence of inertial effects on the reactivity feedback before applying the expansion. In this hypothetical accident, the reactivity insertion rate is sufficiently high that the reactor will go through and past prompt critical before much heating occurs. Based on previous calculations, a maximum reactivity insertion of approximately 0.0085 is expected, which will lead to a minimum reactor period of approximately  $10^{-4}$  sec, for a prompt neutron lifetime of  $8 \times 10^{-8}$  sec. In the first power burst we expect inertial effects will inhibit the longitudinal expansion of the fuel pins, and diminish the effective reactivity feedback. From the work of Bump and Seidensticker,<sup>1</sup> we can estimate that the expansion rate will be reduced roughly by a factor of three (see Fig. A-7); hence we have

$$\frac{\Delta k}{\Delta T} \approx -0.28 \times \frac{14}{3} \times 10^{-6} = -1.3 \times 10^{-6}/C. *$$

Since the kinetics calculations are made in terms of an arbitrary flux normalization, beginning with a source power of  $n = 1$ , a determination of the appropriate constant of multiplication must be made. Let us assume the following:

Specific heat of uranium\*  $0.71 \text{ cal}/(\text{cm}^3) (C)$

Volume fraction of uranium =  $0.32 \text{ cm}^3/\text{cm}^3$  of core

1 watt second = 0.24 calories

Source power =  $8 \text{ watts}/50 \text{ liters} = 1.6 \times 10^{-4} \text{ watts}/\text{cm}^3$   
 $= 3.8 \times 10^{-5} \text{ cal}/\text{cm}^3$

Then, if  $n = 1$  corresponds to  $3.8 \times 10^{-5} \text{ cal}/(\text{cm}^3)(\text{sec})$ :

$$\Delta T (t) = \frac{3.8 \times 10^{-5} \text{ cal}/\text{cm}^3}{(.32) (.71) \text{ cal}/(\text{cm}^3) (C)} \int_0^t \text{ndt}$$

$$\Delta T (t) = 1.68 \times 10^{-4} \int_0^t \text{ndt}$$

and the feedback reactivity

$$\begin{aligned} \Delta k (t) &= \frac{\Delta k}{\Delta T} \Delta T (t) = 1.3 \times 10^{-6} (1.68 \times 10^{-4}) \int_0^t \text{ndt} \\ &= 2.2 \times 10^{-10} \int_0^t \text{ndt} \end{aligned}$$

The space-independent kinetics equations were solved, taking a source power of 8 watts, with the feedback coefficient rounded off to  $-2 \times 10^{-10}$ . The feedback was assumed to maintain this form independent

\*Doppler effect has been ignored herein

of power level. Then, for the fuel element drop described above, the kinetics equations take the form

$$k_{\text{ex}}(t) = 0.06 t \quad t \leq 0.1254$$

$$k_{\text{ex}}(t) = 0.2 t - 2 \times 10^{-10} \int_0^t n dt \quad t > 0.1254$$

The results of this calculation are presented as the solid lines in Figs. A-11 to A-16. For purposes of orientation the calculations were also done, assuming a feedback ten times greater, and these results have been plotted as dashed lines.

In Fig. A-11 is plotted the  $\int_0^t n dt$  versus time, also the average fuel element temperature rise,  $\Delta T$ . In Figs. A-12 and A-13,  $n$  (also the power) is plotted versus time. In Fig. A-14  $k_{\text{ex}} = k_{\text{eff}} - 1$  is plotted, while in Figs. A-15 and A-16  $n/\overset{\circ}{n}$  is plotted versus time.

From Fig. A-11, we see that if no scrams are operative,  $\Delta T$  reaches 840C when  $t = 0.12995$  sec, while the maximum rise is about 1300C. Since the reactor temperature at loading should be about 600F, the  $\Delta T$  of 840C should be sufficient to melt most of the core fuel elements. At the core center melting would begin a little earlier, at the edge it would not be quite molten. From Fig. A-14 we see that by  $t = 0.12995$ ,  $k_{\text{ex}}$  is down to 0.0073 and is falling further below prompt critical.

The future course of such an accident is difficult to predict. The melting would halt the loss of reactivity due to fuel rod expansion, but sodium boiling and fuel element failure would introduce new reactivity mechanisms.

Suppose the power level scram were operative. Let us assume a 10-millisecond delay in the relay plus an additional 8-millisecond delay in the collapse of the electromagnetic field. Then, if the scram were set at 1 kilowatt, from Fig. A-12 we see the scram signal would be given at  $t = 0.1259$  sec.

Eighteen milliseconds later, at  $t = 0.1439$  sec the two safety rods would start moving - if the reactor had not melted or blown itself up, since at  $t = 0.12995$  sec, melting temperatures were already reached. From Fig. A-14, we see that at  $t = 0.1259$  sec, the reactor was already super prompt critical, hence there really was no time for control rod motion to prevent the first burst. To be effective in this accident, the power level trip would have to be set at a much lower power.

Suppose the period scram were operative. From Fig. A-15 we see that the apparent reactor period would be shorter than 5 sec immediately. If there were a 25-millisecond delay before safety rod motion

began, this would leave 95 milliseconds before prompt critical was reached on present study. From Fig. A-15 we see that the safety rods would move about  $1\frac{3}{4}$  in. in this time, reducing reactivity by perhaps  $0.001 \Delta k/k$ . This would provide additional time for the safeties to act. Their maximum reactivity withdrawal rate is about  $0.1 \Delta k/\text{sec}$ , about half the maximum insertion calculated for the accident. This latter is a peak value, however, which falls off sharply with time. Hence, while the detailed course of the accident depends on specific circumstances, it is likely that this one would not reach prompt critical and furthermore would do no damage, should the period scrams work.

## (2) Fuel Element Drops from Above Reactor

If one considers the excursion to result from a drop of a fuel subassembly at a time when it is just entering the reactor, only minor modifications are necessary. The instantaneous rate is now given by

$$\sqrt{2g(x+h)} \frac{2w}{L} \sin^2\left(\frac{\pi x}{L}\right)$$

where  $h$  is the length of the fuel subassembly and the other quantities are as before. This yields a rate

$$R_0 = .5 \text{ sec}^{-1} \text{ for } k_{\text{ex}} < \beta$$

and

$$R_1 = 1 \text{ sec}^{-1} \text{ for } k_{\text{ex}} \geq \beta.$$

In evaluating  $\Delta k/\Delta T$  the only change is that the factor introduced due to inertial effects is changed from 3 to 5 so for this case

$$\frac{k_{\text{ex}}}{\Delta T} = -.784 \times 10^{-6} \text{ C}^{-1}$$

or

$$k_{\text{ex}} = -1.33 \times 10^{-10} \int_0^t \text{ndt} \dots$$

The kinetics equations were solved again, this time assuming the following form for  $k_{\text{ex}}$

$$k_{\text{ex}}(t) = 0.5 t \quad t \leq 0.015$$

$$k_{\text{ex}}(t) = t - 1.33 \times 10^{-10} \int_0^t \text{ndt} \quad t > 0.015$$

The source power had to be chosen large, due to scaling limitations of the computing machine program. An initial power of 120 watts was used in this calculation. Thus:

$$\Delta T(t) = 15 (1.68 \times 10^{-4}) \int_0^t \text{ndt} = 2.5 \times 10^{-3} \int_0^t \text{ndt}$$

In Fig. A-17, the  $\int_0^t n dt$ , also the average fuel element temperature are plotted versus time for this excursion. In Fig. A-18,  $k_{ex}$  is plotted, while in Fig. A-19  $n/\bar{n}$  (also the power) is plotted against time.

Since this is a more violent accident, the conclusions of the first case will hold, only more strongly. A  $\Delta T$  of 840C should occur at  $t = 0.16827$ , according to Fig. A-17. At this time,  $k_{ex} = 0.00894$ , well above prompt critical, so the future course of the excursion is in doubt. New mechanisms of shutdown presumably must take over, unless the mechanical inertia of the expanding fuel rod continues the axial growth beyond melting temperatures for the next few milliseconds.

Once again, the effect of a possible period scram depends on details of the incident. In any event, it is clear that an accident of this nature must be avoided, less major damage very likely result to the reactor. (See Appendix C)

#### Case 6: Central fuel element driven in at 72 in./min.

In Case 2 we saw that for 1/12 this speed, an average insertion rate of  $1.5 \times 10^{-4} \Delta k/\text{sec}$  was appropriate. Hence, for this accident, an insertion rate in the neighborhood of  $1.8 \times 10^{-3} \Delta k/\text{sec}$  would apply. The feedback coefficient may not be the same as that of the slow accident, since the reactor period during the major power response may well be shorter than one second. Nevertheless, a kinetics calculation has been done for an  $A = 1.7 \times 10^{-3}$ , and a  $B = 0.92 \times 10^{-9}$ , starting with unit flux (corresponding to 8 watts). The results are given in Figs. A-20 to A-22. We find that in the calculation, the power peaked at  $t = 4.5$  sec, and the reactivity peaked at 0.00753, just under prompt critical. The major energy input occurred for excess reactivities above 0.007  $\Delta k$ . The minimum period reached was about 0.015 sec.

Now, from our previous calculation of a feedback coefficient for slow excursions, we found that about a third of the coefficient came from fuel expansion. Here, there will be little time for heat flow, and all the coefficient must come from this source. Hence, one might expect a smaller feedback. However, the uranium gets hotter for the same power input. From Fig. A-7, we see that only about one third of the heat input is required to get the same expansion at an  $\alpha$  of  $10^{-3}$  sec as at the long periods. Thus the feedback should be approximately the same for both cases, and we may well expect about little change in coefficient between these two points. Hence, the assumption of  $B = 0.92 \times 10^{-9}$  is fairly reasonable and the results of the calculation should be applicable.

Since more of the heat remains in the uranium during the burst, we need less power to produce melting. From Case 1, we found an  $\int_0^t n dt = 7.7 \times 10^6$  was needed for melting to begin at the hot point. If we

rather arbitrarily assume half of this is needed to begin melting, we find from Fig. A-22, that melting will begin at about  $t = 5.3$  sec, shortly after the peak power has been reached. At  $t = 6.6$  sec the  $\int_0^t n dt$  reaches  $7.7 \times 10^6$ , so the difference is not large. Again the course of the excursion really becomes uncertain after this point.

If a period scram set at 5 sec had been operative, a scram signal would have resulted almost immediately, halting the insertion and terminating the accident without incident. A power level trip set at a kilowatt would have scrammed the reactor at  $t = 4.05$  sec, with  $k_{ex} = 0.00688$ . Assuming that the rod insertion stopped at that instant and that there were no feedbacks, the power would have risen exponentially on something like a  $1/5$  sec period. Feedback would, of course, lower this rise rate. In addition, the safety rods would start moving out of the reactor. Within 160 milliseconds, the reactor should be subcritical, and the power could do little more than double in this time. Hence, there would be no appreciable consequences of the accident.

If the fuel element did not stop, but continued in at 72 in./min, it would take 400 milliseconds to reach peak reactivity in the original excursion. Well before this, the safety rods would be mostly out of the core, bringing the reactor below subcritical and keeping it there.

If the power level trip were set at 1.2 times rated power, however, it would not be affected by the first burst, since the peak power reached is about 50 megawatts.

## 2. Failure of All Primary System Pumps

One type of operational abnormality is represented by the sudden cessation of all primary system pumping power. The objective in this section is to indicate the time-dependent temperature distributions obtaining within the reactor as a result of three assumed modes of losing all pumping power.

The following cases are considered:

- (1) Loss of all pumping power occurs; reactor scram follows immediately.
- (2) Reactor scram occurs; loss of all pumping power occurs soon (seconds) afterward.
- (3) Loss of all pumping power occurs; all control rods remain fixed in their initial positions.

Three pumps are provided in the primary system: two large "main" pumps, and one small "auxiliary" pump. Each main pump is supplied independently with electrical power from a rectifier operating on the building

power supply (which may or may not be interconnected with the EBR-II generator). The auxiliary pump is powered by a third rectifier operating on building power, but is backed up by a floating battery power supply. Thus, for all primary system pumping power to be lost, either: (1) simultaneous mechanical failure of all three pumps must occur; or, (2) both building power supply and auxiliary pump battery supply must be lost simultaneously.

a. Case 1.

Reactor scram is assumed to follow immediately after cessation of pumping power. The scram signal is derived either from sensing loss of electrical power to one or more pumps or from sensing the abnormal reduction in primary system coolant flow rate. Under any condition, the scram delay time, or time between initiation of reduction in coolant flow rate and receipt of scram signal at the control rods, is equal to or less than 0.2 sec.

The temperature distribution transients within the reactor after scram derive from a varying mismatch between coolant flow rate and reactor power, and from the effects of stored thermal energy. The coolant flow rate initially decays in accordance with the momentum and flow resistance characteristics of the system, decreasing at a progressively lower rate as momentum is dissipated. However, since the system is designed to cool the reactor (at very low power) by natural convection, momentum is gradually replaced as the source of driving force by a thermal head effected in the flow system downstream from the core. In Fig. A-23, the solid curve indicates the approximate coolant flow rate versus time based on momentum alone; the dotted curve indicates the approximate flow rate sustained by natural convection alone; and, the two dashed curves illustrate typical flow rate decay curves within the region of transition from momentum flow to natural convection flow. The manner of decay of reactor power during the transient varies widely with the particular circumstances of the scram and is discussed later.

The major factors entering into determination of the temperature distributions within the reactor after scram are the initial reactor power level, initial internal temperature distributions, total worth of the control rods, degree of initial insertion of the rods, rod release time, scram delay time, and the time-displacement characteristic of the rods during scram.

The following assumptions have been made:

- (1) Initial reactor power equals 62.5 mw (full power).
- (2) Initial reactor temperature distributions are those actually expected to obtain (without uncertainty factors).
- (3) Control rod release time equals 0.030 sec.
- (4) The time-displacement characteristic of the control rods is as indicated in Fig. A-24.

If effects of uncertainty factors should alter the assumed initial temperature distributions, deviations in the general shapes of the transient coolant temperature distributions from those presented will be small; however, the initial maximum core fuel temperature and the maximum core fuel temperature realized during the transient might be higher than those presented by as much as approximately 140F and 100F (estimated), respectively. The control rod release time assumed is considerably longer than the actual release time, which has been experimentally determined to be 0.008 second or less. The assumed time-displacement characteristic of the rods is based upon employment of sufficiently high air pressure in the scram assist cylinder to effect rod acceleration of about 3 g. The actual pressure to be employed is somewhat lower, but this discrepancy is not expected to alter significantly the results discussed below. Assumed values of the remaining variables are indicated in the following discussions of each of the four sub-cases examined.

(1) Case 1.1

This case is the most pessimistic considered, the specific assumptions being:

- (1) Total rod worth, from full in to full out, equals  $0.03 \Delta k/k$ .
- (2) Degree of initial rod insertion equals 60%.
- (3) Scram delay time equals 0.000 sec.

The low value of total rod worth assumed may be viewed in two ways: (1) as an arbitrary value representing a considerably lower total rod worth than expected ( $0.04$  to  $0.06 \Delta k/k$ ); or, (2) as an effective value based upon the assumption that a large fraction ( $1/4$  to  $1/2$ ) of the rods fail to function. The degree of initial rod insertion assumed is also low, since insertion of at least 80% is contemplated.

Figure A-25 indicates the resulting total reactor power (fission heat plus fission product decay heat) as a function of time after start of rod movement. Also shown (although not used here), are four similar curves for various values of total rod worth greater than  $0.03 \Delta k/k$ . In Fig. A-26 are shown four significant reactor temperature versus time curves for the transient. Curve 1 indicates the maximum core fuel temperature. This temperature is seen to start at approximately 1180F at time zero, decrease to about 950F within the first one-half second, and then rise within about 10 sec to a maximum temperature approximately 120F higher than the maximum temperature obtaining during normal full power operation. Following this, the fuel temperature decreases to about 900F, where power generation is due to fission product decay heat only and cooling is by natural convection. Although the maximum fuel temperature attained during this excursion is somewhat higher than desired, it is

not considered to constitute a safety problem. Curves 2 and 3 indicate the average coolant temperature at outlet from the core subassemblies and average coolant temperature at outlet of all subassemblies (or at inlet to the upper plenum), respectively. The maximum temperatures or rates of rise of temperature indicated by these curves do not represent serious thermal shock problems, since the coolant merges and mixes with the large volume of sodium within the upper plenum before coming into contact with either the reactor tank walls or the reactor tank cover lower surface. The temperature of the sodium coolant emerging from the reactor tank via the upper plenum outlet nozzle is shown by Curve 4; obviously, thermal shock of the nozzle or the pipe leading from reactor outlet to heat exchanger inlet is not great. In addition, to minimize further any tendency toward thermal shock, thermal barriers have been provided on the outlet nozzle and the subject surfaces of the upper plenum.

(2) Case 1.2

This case is similar to Case 1.1, except that a scram delay time of 0.200 sec is assumed.

This reactor power versus time after start of rod movement curve is the same as for Case 1.1 (Fig. A-25). Temperature versus time curves for the transient are shown in Fig. A-27. It is seen that the longer scram delay time (0.200 sec as compared to 0.000 sec in Case 1.1) mitigates very slightly the maximum temperatures attained during the excursion.

(3) Case 1.3

This case, as well as Case 1.4, employs assumptions representative of the conditions actually expected to obtain. The assumptions for this case are:

- (1) Total rod worth equals  $0.05 \Delta k/k$ .
- (2) Initial rod insertion equals 90%.
- (3) Scram delay time equals 0.000 sec.

Fig. A-28 indicates the resulting total reactor power as a function of time after start of rod movement. Again, although not necessary to the present discussion, there also are shown four additional curves for various values of total rod worth larger and smaller than  $0.05 \Delta k/k$ . The temperature versus time curves for Case 1.3 are shown in Fig. A-29. The various temperature maxima and the maximum rates of temperature rise are seen to be modest. The maximum core fuel temperature during the excursion is approximately 100F lower than that existing during full power operation.

(4) Case 1.4

This case is similar to Case 1.3 except that a scram delay time of 0.200 sec is assumed.

The reactor power versus time after start of rod movement curve is the same as for Case 1.3 (Fig. A-28). Temperature versus time curves for the transient are shown in Fig. A-30. The curves are, for practical purposes, the same as those for Case 1.3.

b. Case 2

Case 2 employs a series of assumptions considered to lie barely within the realm of possibility. It is assumed that an abnormality occurs somewhere within the system which occasions reactor scram, but that the pumps initially remain in operation (since reactor scram does not call for reduction of pumping power); and, that after a time interval measured in seconds, all three pumps fail simultaneously. Because the reactor power decreases rapidly upon scram, the high pumping rate quickly fills the primary flow system downstream from the reactor core with low temperature coolant and essentially eliminates the thermal driving head necessary to natural convection flow. When the pumping power suddenly ceases, the combination of very rapid decrease in flow rate and low reactor power generation tends to prevent sufficiently rapid establishment of thermal head by a sweeping out of the low temperature coolant and replacement with high temperature coolant within the "hot leg" portion of the flow system. Depending upon the time delay between reactor scram and loss of pumping power, conceivably there could exist the possibility of the core overheating. If the delay time is extremely short, the temperature excursions are obviously similar to those of Case 1, above; only if the incident is accompanied by failure of one-fourth to one-half of the control rods does maximum fuel temperature exceed normal full power operating temperature (then, by about 120F). If the delay time is very long, the reactor power level is sufficiently low that no overheating can occur. Possibility of reaching extremely high temperature, therefore, is restricted to cases of intermediate delay times.

Figure A-31 indicates the maximum fuel temperature attained during the transient as a function of delay time for two different assumed control rod conditions. One condition (total rod worth of  $0.05 \Delta k/k$  and 90% initial insertion) is representative of the expected normal condition; the other (worth of  $0.03 \Delta k/k$  and 60% insertion) is representative of failure of one-fourth to one-half of the control rods combined with an abnormally low initial degree of insertion. Initial reactor power of 62.5 mw and initial reactor temperature distributions actually expected to obtain at full power (without uncertainty factors) are assumed.

For delay times of from about one to ten sec, maximum fuel temperature attained with the expected rod condition is less than the normal full power operating temperature; with the pessimistic rod condition, however, it exceeds this temperature by about 150F. For delay times greater than about ten sec, maximum fuel temperature attained with either rod condition is equal to or lower than the maxima attained under Case 1 conditions. For delay times greater than about 30 sec, maximum fuel temperature reached during the transient, even for the pessimistic rod condition, is less than the normal full power operating temperature. Figures A-32 and A-33 show various transient reactor temperatures, including maximum fuel temperatures, as a function of time after cessation of all pumping power for delay time equal to 30 sec.

c. Case 3

Case 3 employs a combination of assumptions felt to be academic; it is assumed that pumping power of all three pumps is suddenly lost, and that in some manner all 12 control rods are simultaneously rendered completely inoperative, so that they remain fixed in their initial positions. Resulting reactor temperatures as a function of time based on these conditions are indicated in Fig. A-34. Fuel alloy temperature of the hottest elements is seen to reach the melting point in about 3 sec.

3. Bowing

The bowing of fuel elements is examined in this section. Bowing is of importance because of the resulting change in effective core radius, and, therefore, in reactivity. Results of a study are described which indicate the magnitude of changes in effective core radius to be expected under various circumstances, and the approximate manner in which these changes are incurred.

a. General

Because the fuel elements are tightly packed within core subassemblies (with zero nominal clearance), fuel element bowing may be considered essentially synonymous with core subassembly bowing. In this study, therefore, treatment is based upon the subassembly as the bowing unit.

Bowing of a subassembly is caused by existence of a temperature differential across its opposite sides (referred to as opposite "flats"). The temperature differential is effected primarily as a result of the non-uniform radial distribution of heat generation within the subassembly, and secondarily, by the unequal rates of heat transfer from the opposite flats of the subassembly under consideration to the subassemblies of the adjacent rows. Axial distribution of the temperature differential along

subassembly length is non-uniform; its shape is dependent upon the coolant flow condition, and is significant (under all circumstances) only within the core section and/or the lower portion of the upper blanket section. The sign of the temperature differential normally is such as to tend to produce convex curvature of the subassembly as viewed from the core center. The comparative magnitudes of the temperature differentials effected in subassemblies of various core rows are such that the amount of curvature tends to become progressively greater with increase in row number, or distance from the core center.

In order best to describe the quantitative bowing determinations, a qualitative picture of the general mechanism of bowing first is presented. It is necessary to precede this with a brief discussion of the subassembly dimensions and the physical arrangement and method of support of the subassemblies within the reactor.

b. Subassembly Physical Characteristics and Method of Support

A general description of the core subassemblies and their arrangement in the reactor is given in Section III-A-1-a., b., and c.

All core subassemblies are identical in size and shape (hexagonal). The dimension across outside flats of each subassembly is 2.290 in. The center-to-center spacing of the subassemblies is 2.320 in. The resulting nominal clearance between flats of adjacent subassemblies is 0.030 in. Each core subassembly, as well as each inner blanket subassembly, is provided with a "button" on each of its six flats; the buttons are positioned so that they lie in a horizontal plane 1.00 in. above the core (fuel) center line. These buttons protrude a nominal 0.014 in. from the subassembly flat. The button flats are 0.375 in. in diameter. The dimension across opposite button flats of each subassembly is held to  $2.318 \pm 0.002$  in. The resulting nominal clearance between button flats of adjacent subassemblies is 0.002 in.

The subassemblies are positioned and supported in the reactor by their lower adaptors, the ends of which pass through holes in the upper plate of the support grid and engage in the axially aligned holes in the lower plate. The portion of the adaptor which rests on the upper plate is of the shape of a truncated sphere; the upper edge of the plate hole, on which the adaptor rests, is chamfered conically. This arrangement provides a continuous line contact for subassembly support. It has been established experimentally that lateral movement of the upper part of the subassembly (or of the lower end of the adaptor) is accommodated by pivoting of the subassembly about this area of contact; that is, lateral movement of the subassembly in the region of contact with the upper plate does not occur unless a very large force is applied. The reason for this is that the latter movement can take place only in accompaniment with an upward shifting of

the entire subassembly, due to the conical shape of the support seat. Consequently, application of lateral force in or above the region of the core section produces only a pivoting of the subassembly until the lower end of the adaptor closes the lower plate hole clearance (0.0042 in. radially), and, thereafter, results in bending of the subassembly. Lateral movement of the top end is unrestricted up to nominal displacement of 0.030 in., when contact with the adjacent subassembly is made; if the adjacent subassembly also undergoes displacement, restriction is not effected until after correspondingly greater displacement.

c. Qualitative Description of Bowing

Consider a group of five core subassemblies, one in each subassembly row from the first (center of the core) to the fifth (outermost row of the core), and aligned radially. Upon inception of reactor conditions which give rise to radial temperature differentials, a temperature difference appears across the flats of each of the five subassemblies. Magnitude of the  $\Delta T$  across each subassembly, however, increases with distance of the subassembly from the core center (not necessarily proportionally). Consequently, while all subassemblies bow in the same direction, they bow in varying degree. The fifth row subassembly tends to bow the most. In considering the effect upon core radius, therefore, it is reasonable to base all bowing analysis on the action of the fifth row subassembly only.

Qualitatively, bowing of a fifth row subassembly takes place as described below. Note should be taken of the typical axial  $\Delta T$  profiles effected in EBR-II subassemblies as indicated in Figs. A-39 and A-42. For convenience in discussion, the effective  $\Delta T$  magnitude is indicated in terms of maximum  $\Delta T$ , or  $\Delta T_M$ .

As a small  $\Delta T_M$  is effected across the subassembly, all of the subassembly above the lower part of the core section starts to bow radially outward, thus increasing the effective core radius. As the  $\Delta T_M$  is increased, the amount of outward displacement increases until the top end of the subassembly contacts the top of the adjacent subassembly in the inner blanket (displacement at the location of the button being insufficient to produce button contact, as a result of the axial distribution of the  $\Delta T$ ). Further increase in  $\Delta T_M$  results in additional bowing, but because the top end of the subassembly is now prevented from moving outward, this bowing effects a radially inward movement of the core section; at the same time, the subassembly proceeds to pivot, causing the lower end of the adaptor to move outward until it closes the lower plate hole clearance. As the increase in  $\Delta T_M$  continues, the inward movement of the core section continues until the subassembly button contacts the button of the subassembly in the next (fourth) row. Bowing during this period obviously tends to decrease the effective core radius. Additional increase in  $\Delta T_M$  beyond this point continues to increase the bowing,

but does not move the core section further inward because of the button restriction. In fact, since an increasing  $\Delta T_M$  is accompanied by increasing subassembly temperature in the button region, radial thermal expansion of the subassembly, or increase in distance across button flats, results in an outward movement of the core section. To summarize the action, then: as  $\Delta T_M$  is continuously increased from zero, change in effective core radius is initially positive (outward), then negative (inward), and finally, positive again.

#### d. Quantitative Bowing Analysis

Change in effective core radius produced by bowing is dependent upon the axial distribution of  $\Delta T$  across opposite flats of the subassemblies and upon the details of the initial disposition of the subassemblies.

##### (1) Axial Distribution of $\Delta T$

The axial distribution of  $\Delta T$  is a function of coolant flow condition. With coolant flow, the distribution is approximately as indicated in Fig. A-39. The exact amount of coolant flow is not of importance, as long as it is sufficient to preclude appreciable axial heat conduction. The  $\Delta T$  increases approximately linearly from zero at the bottom of the core to a maximum at the top of the core; it is assumed to decrease linearly from the top of the core down to zero within a distance of 9 in. The decrease occurs as a result of coolant mixing during passage through the upper gap and the lower portion of the upper blanket.

For convenience, the effective magnitude of  $\Delta T$  is expressed in terms of maximum value,  $\Delta T_M$ . At full coolant flow and full reactor power,  $\Delta T_M$  across the flats of a fifth row subassembly is about 100F. For other flow and/or power conditions at steady state,  $\Delta T_M$  is inversely proportional to flow and directly proportional to power. Figure A-35 shows variation of  $\Delta T_M$  with time during reactor power excursions at constant periods of from  $10^{-2}$  to  $10^2$  sec for initial conditions of normal full power operation. Also shown in this figure are the times at which a maximum fuel temperature of 2000F (the approximate melting temperature) is reached.

With no coolant flow, the  $\Delta T$  distribution is approximately as indicated in Fig. A-42. In this case, the distribution is represented by a chopped cosine curve which reflects the axial power density distribution. Again, the effective magnitude of  $\Delta T$  is expressed in terms of the maximum value,  $\Delta T_M$ . Figure A-36 shows variation of  $\Delta T_M$  with time during reactor power excursion at constant periods of from  $10^{-2}$  to  $10^2$  sec for initial conditions of no flow, isothermal reactor temperature of 600F and "zero" (1 watt) reactor power. Also shown in this figure are the times at which a maximum fuel temperature of 2000F is reached.

## (2) Initial Disposition of Subassemblies

The initial disposition of the subassemblies within the reactor can only be estimated. Two general arrangements of initial positions are assumed for analysis which are thought to bracket all cases of importance. One represents an extremely conservative case and is termed the "most pessimistic initial position." The other is based on nominal, design subassembly positions and represents the effective disposition thought most likely to obtain. This is termed the "most probable initial position."

The assumed most pessimistic initial position of core subassemblies is indicated in Fig. A-37. This disposition is based on the following major assumptions:

- (a) All core subassemblies are splayed outward; that is, each subassembly (except the center one) is pivoted from its normal, upright position as far as the nominal clearance of the lower plate holes will permit.
- (b) The dimension across opposite button flats of each subassembly is 0.002 in. less than the design nominal, and the minimum within fabrication tolerance.
- (c) The upper and lower plate holes of the fifth row are located at a radius 0.002 in. greater than the design radius, and the maximum radius within fabrication tolerance.
- (d) An isothermal condition exists.
- (e) The subassemblies are straight.

As shown in Fig. A-37, these assumptions result in an initial total clearance between subassembly buttons of 0.026 in. Consequently, there exists 0.026 in. of radial gap potentially available for reduction of core radius (in the plane of the buttons); the actual maximum reduction in radius achievable by bowing, however, necessarily is less than this.

The initial position of core subassemblies considered "most probable" is indicated in Fig. A-38. For this disposition, the following major assumptions are made:

- (a) The core subassemblies are vertical (in their design positions).
- (b) The dimension across opposite button flats of each subassembly is the design nominal dimension.
- (c) The upper and lower plate holes of the fifth row are located at the design radius.

- (d) An isothermal condition exists.
- (e) The subassemblies are straight.

These assumptions result in an initial total clearance between subassembly buttons of 0.008 in. Again, although this much gap is potentially available for reduction of core radius in the plane of the buttons, the maximum reduction achievable by bowing is actually less than this.

### (3) Bowing Results

Four general bowing cases are considered: (1) with coolant flow, and most pessimistic initial disposition; (2) with no coolant flow, and most pessimistic initial disposition; (3) with coolant flow, and most probable initial disposition; and, (4) with no coolant flow, and most probable initial disposition.

#### (a) Case 1

This case assumes the existence of flow and the most pessimistic initial subassembly disposition. The manner of bowing, as discussed earlier, is affected by the amount of outward displacement the top end of the subassembly can undergo before becoming restricted by contact with the top end of the adjacent subassembly in the next row. The nominal clearance available (0.030 in.) will be affected by manufacturing tolerances, subassembly warping due to inadvertent stress relieving, initial position of the adjacent subassembly, etc. Probably the largest effect under any circumstance, however, is that of outward movement of the top end of the adjacent subassembly due to its own bowing. (The bowing of sixth row inner blanket subassemblies is expected to be greater than that of core subassemblies.) Because all of these factors cannot be accurately accounted for, two subcases are investigated; in one, the maximum free displacement (average for all fifth row subassemblies) is conservatively taken as 0.022 in.; in the other, 0.090 in. is assumed.

Figure A-39 depicts the progression of bowing with increase in  $\Delta T_M$  for the 0.022 free displacement condition. Figure A-40 gives the same information for the 0.090 free displacement condition.

By weighting in accordance with the square of the local neutron flux (power density) the local radial displacement from its initial position of every point in the core section, an equivalent change in core radius (in respect to reactivity effect) can be determined for every value of  $\Delta T_M$ . This equivalent change in core radius represents that axially uniform change in core radius which would produce (approximately) the same change in reactivity as the non-uniform change effected by bowing.

Figure A-41 shows the equivalent change in core radius as a function of  $\Delta T_M$  for both the 0.022 and the 0.090 in. free displacement conditions.

(b) Case 2

This case assumes no coolant flow and the most pessimistic initial subassembly disposition. Two subcases are investigated, representing the same two free displacement conditions as assumed in Case 1, above.

Figure A-42 shows the progression of bowing with increase in  $\Delta T_M$  for the 0.022 in. free displacement condition, and Fig. A-43 gives the same information for the 0.090 in. free displacement condition.

Figure A-44 shows the equivalent change in core radius as a function of  $\Delta T_M$  for both subcases.

(c) Case 3

This case assumes the existence of coolant flow and the most probable initial subassembly disposition. The maximum free displacement of the top end of the subassemblies is conservatively taken as the nominal clearance between subassemblies, 0.030 in.

Figure A-45 shows the progression of bowing with increase in  $\Delta T_M$ . Figure A-46 indicates the equivalent change in core radius as a function of  $\Delta T_M$ .

(d) Case 4

This case assumes no coolant flow and the most probable initial subassembly disposition. The assumed maximum free displacement of the top end of the subassemblies is the same as that for Case 3, above.

Figure A-47 shows the progression of bowing with increase in  $\Delta T_M$ . Figure A-48 indicates the equivalent change in core radius as a function of  $\Delta T_M$ .

(4) Conclusions

There exist a number of factors not discussed earlier (and not taken into account in the present analysis) which directly or indirectly affect both the progression of bowing and the maximum magnitude of equivalent core radius reduction effected by bowing. Thought to be the principal factors among these are the following:

(a) Since an annular space filled only with static sodium is incorporated between fuel pin and steel tube of each fuel element, the fuel pin may bow (inside the tube) to a slightly greater extent than does the

subassembly as a whole. As an estimate, this internal bowing might increase the magnitude of maximum effective core radius reduction, under certain circumstances, by as much as 0.002 in.

(b) Because of the shape of the radial power density distribution through the core and the effects of coolant orificing, the effective magnitude of bowing within radial core shells (or subassembly rows) is not proportional to distance from center of the core. Consequently, change in effective core radius produced by bowing is not distributed evenly radially, and conversion of the amount of bowing of fifth row subassemblies only to equivalent change in core radius (in respect to reactivity effect) is not precise. Since the bowing of the fifth row subassemblies is considerably greater than for the other core subassemblies, the indicated results should be conservative in this respect.

(c) Analysis of bowing of fifth row subassemblies is based on core-type subassemblies. Actually, one-half the subassemblies in this row are control subassemblies, and their bowing characteristics are necessarily somewhat different. Because of the clearance required between the control rod and the control subassembly hex can, the rod is free to bow to a greater extent than is a core subassembly. However, the corresponding  $\Delta T$  across flats which produces the bowing is less, because the rods are not fully inserted and because some coolant flows in the clearance space between rod and hex can, thus helping to reduce the  $\Delta T$ . In addition, a given amount of bowing of the control rods exhibits considerably less effect on reactivity than the same amount of bowing of the core subassemblies, since the mass of fissionable material involved in the former is only about 55% of that associated with the latter.

(d) Although the button loads are small, the flats of the subassemblies may deflect slightly in the region of the buttons when the core is in the compacted condition, thus increasing (probably not significantly) the maximum magnitude of equivalent core radius reduction.

(e) Calculation of the axial  $\Delta T$  distribution along the subassemblies, which directly influences the bowing, is obviously subject to a certain amount of error. It is felt that the assumed distributions are conservative.

(f) Since the effects under consideration are minute in magnitude, it is possible that anomalous effects, even though small in scale, might exert some influence on the results.

Because of the above considerations and the relatively wide variation in possible assumptions noted earlier, there exists doubt as to the exact progression of bowing (or progression of the equivalent change in core radius) under a given set of reactor conditions. The progressions

presented herein (in Figs. A-39, A-40, A-42, A-43, A-45, and A-47), however, are considered to be qualitatively correct, and probably may be considered for many purposes to be approximately quantitatively correct. The nature of the progressions is such that, under all circumstances, increasing from zero the effective  $\Delta T$  across subassembly walls initially results in slightly increasing, then decreasing, and finally, increasing again the effective core radius.

The important quantitative conclusions which may be drawn are associated with the maximum magnitudes of equivalent core radius reduction which can be effected by bowing. These may be stated as follows:

(a) With or without coolant flow, the maximum possible (or "credible") reduction in equivalent core radius during heating of the reactor is approximately 0.019 in.

(b) With or without coolant flow, the maximum reduction in equivalent core radius actually expected during heating of the reactor is of the order of 0.004 in.

RE-7-19707-B

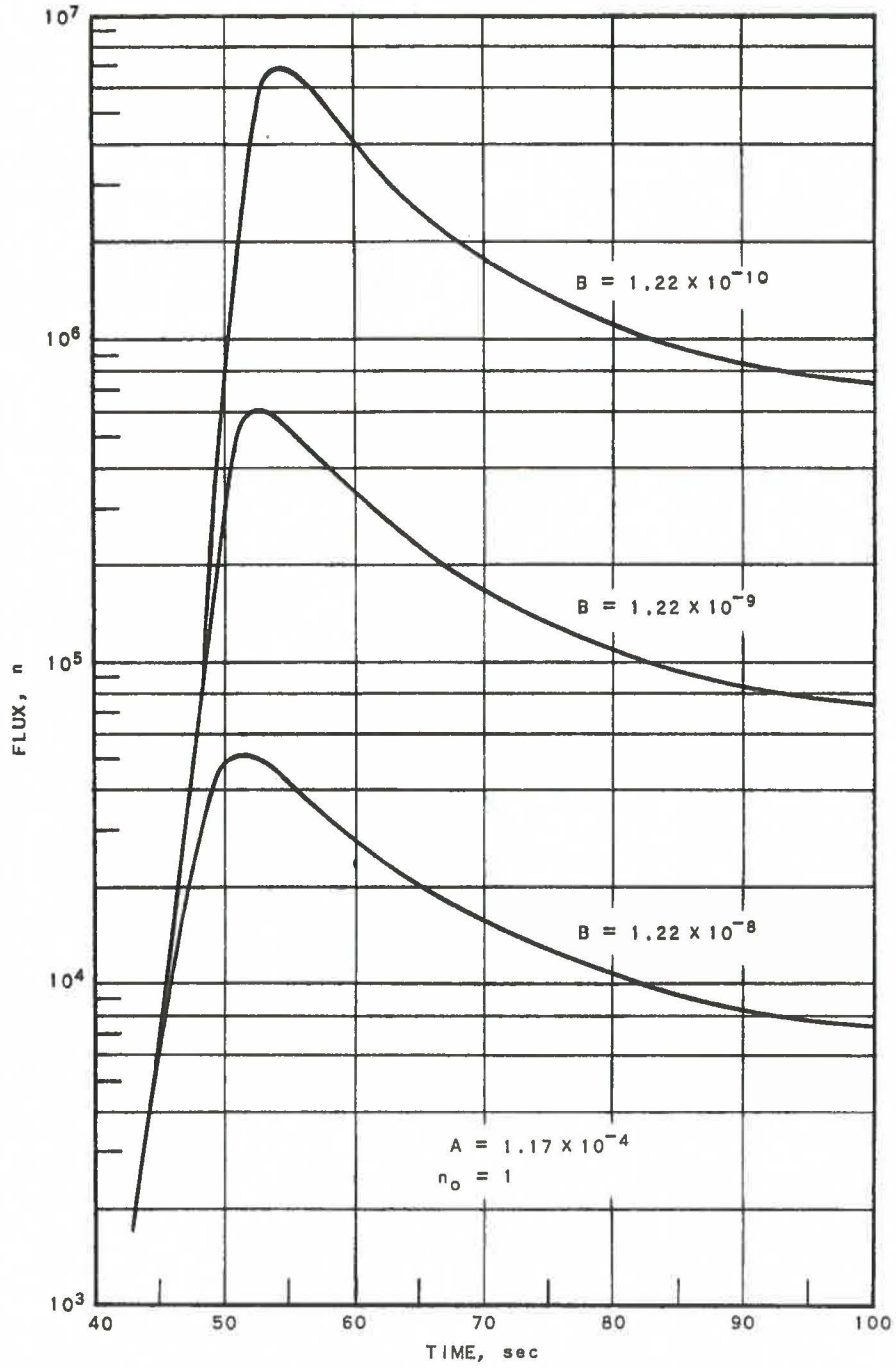


FIG. A-1  
FLUX VS TIME FOR SEVERAL FEEDBACK  
COEFFICIENTS AND FIXED INSERTION RATE

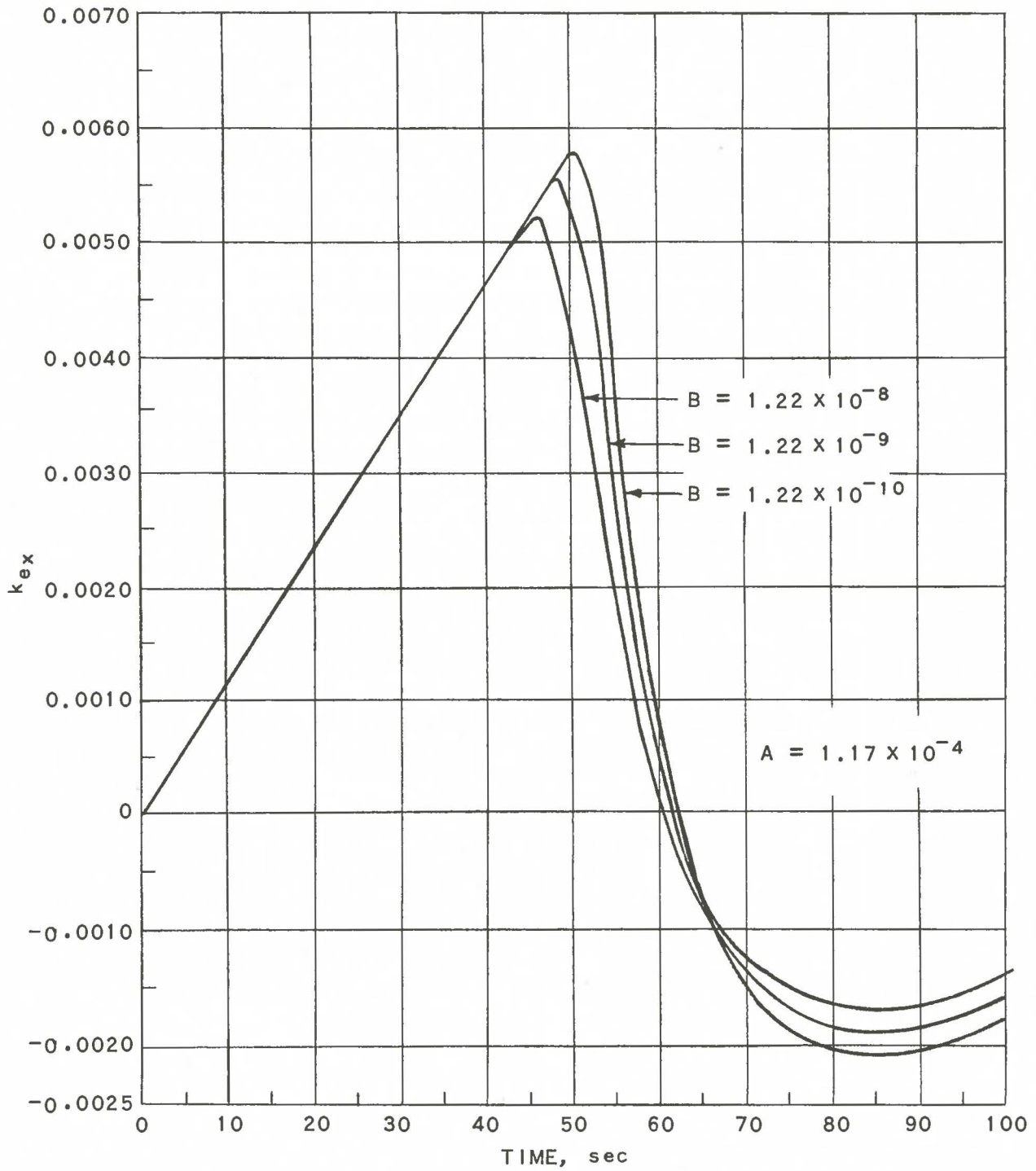


FIG. A-2  
EXCESS REACTIVITY VS TIME FOR SEVERAL  
FEEDBACK COEFFICIENTS AND FIXED INSERTION RATE

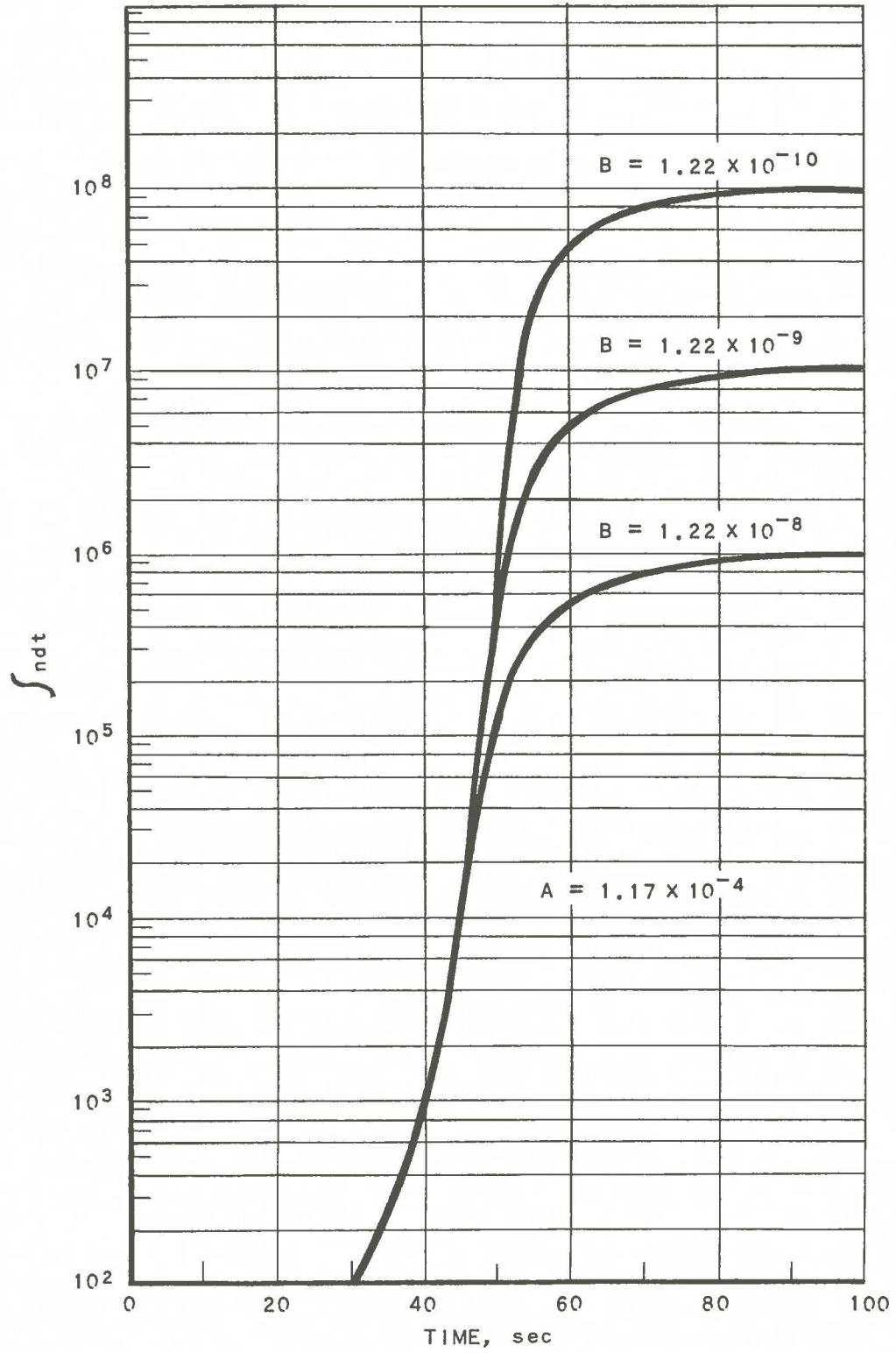


FIG. A-3  
FLUX INTEGRAL VS TIME FOR SEVERAL  
FEEDBACK COEFFICIENTS AND FIXED INSERTION RATE

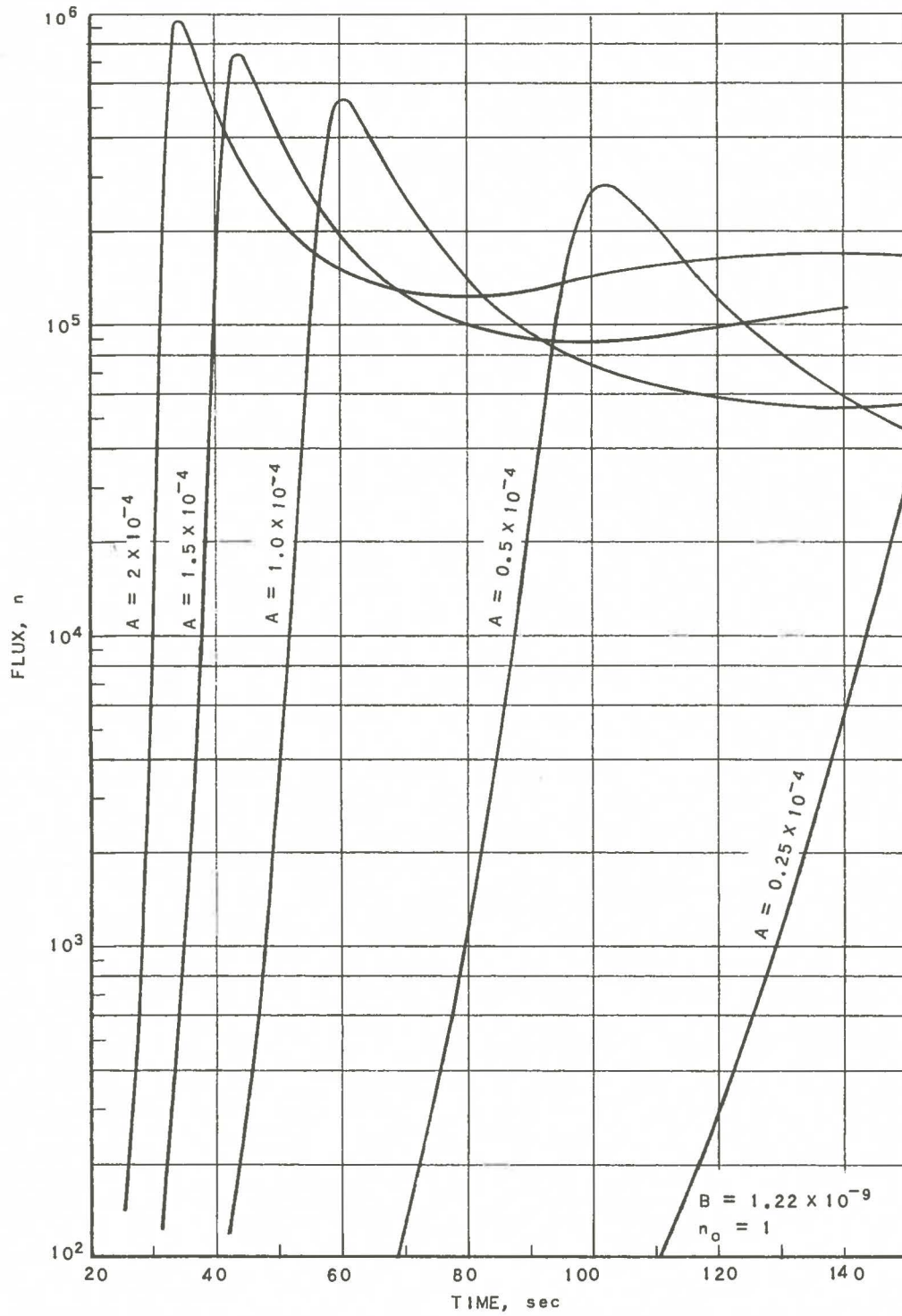


FIG. A-4  
 FLUX VS TIME FOR SEVERAL INSERTION  
 RATES AND FIXED FEEDBACK

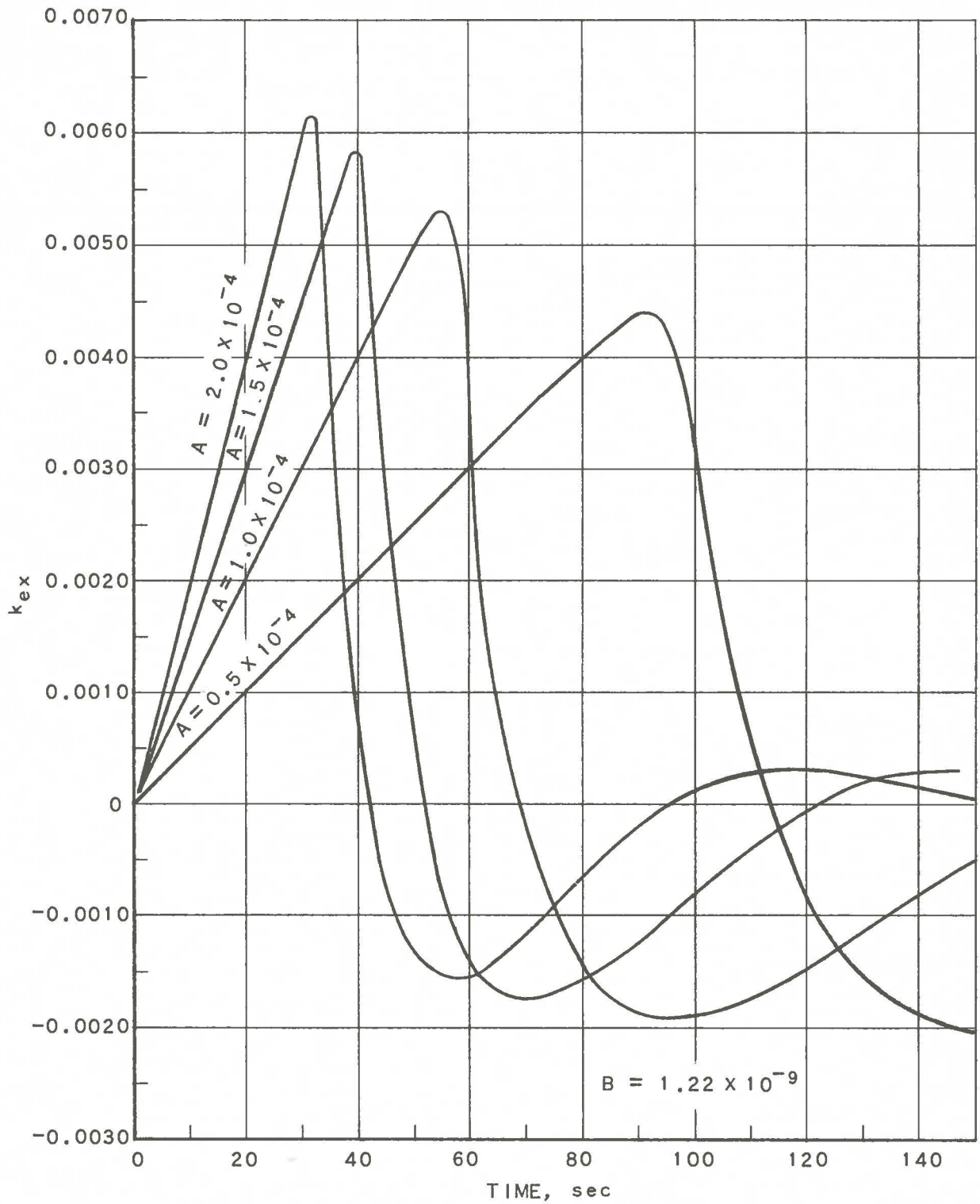


FIG. A-5  
EXCESS REACTIVITY VS TIME FOR SEVERAL  
INSERTION RATES AND FIXED FEEDBACK

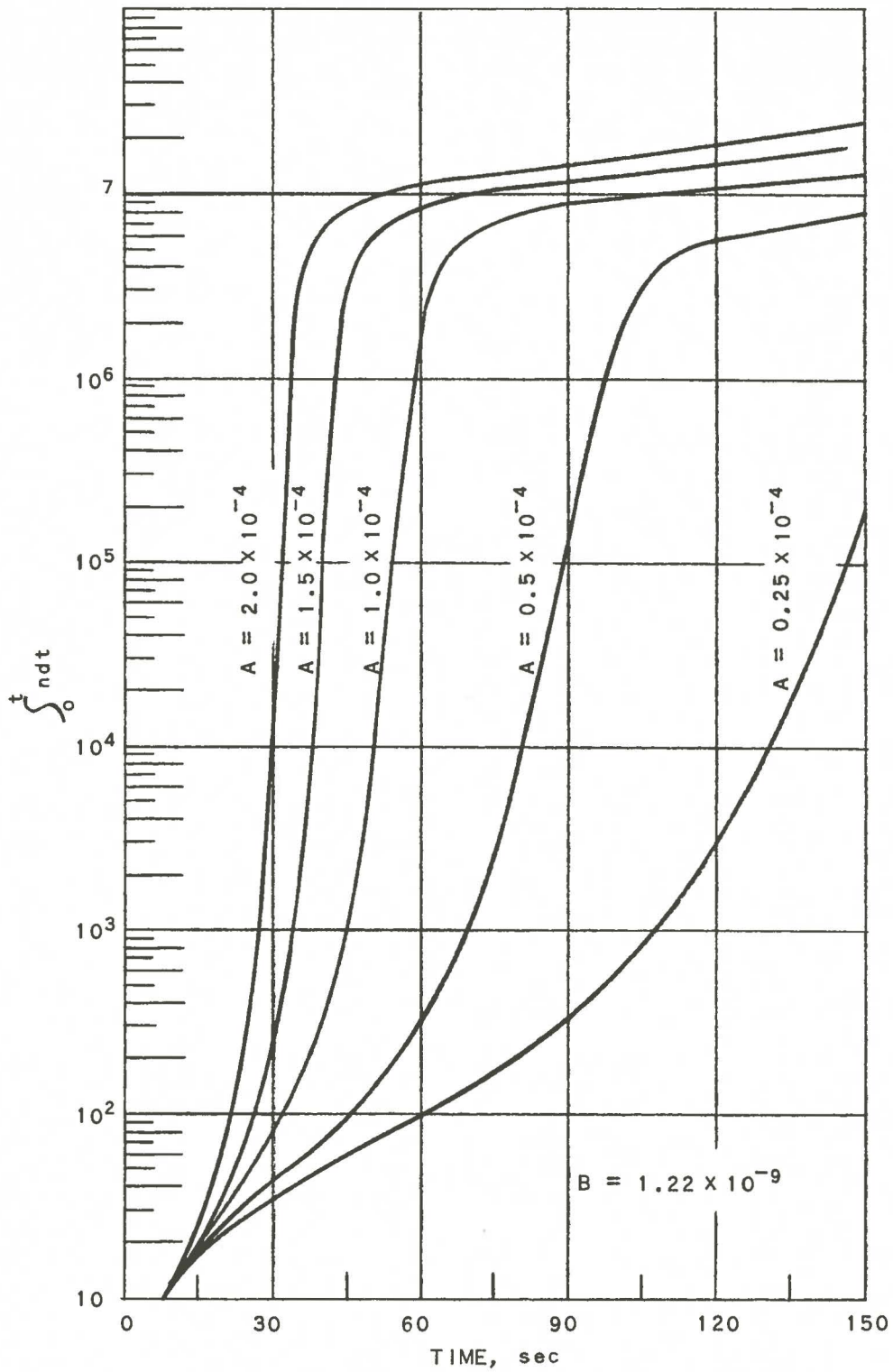


FIG. A-6  
 FLUX INTEGRAL VS TIME FOR SEVERAL  
 INSERTION RATES AND FIXED FEEDBACK

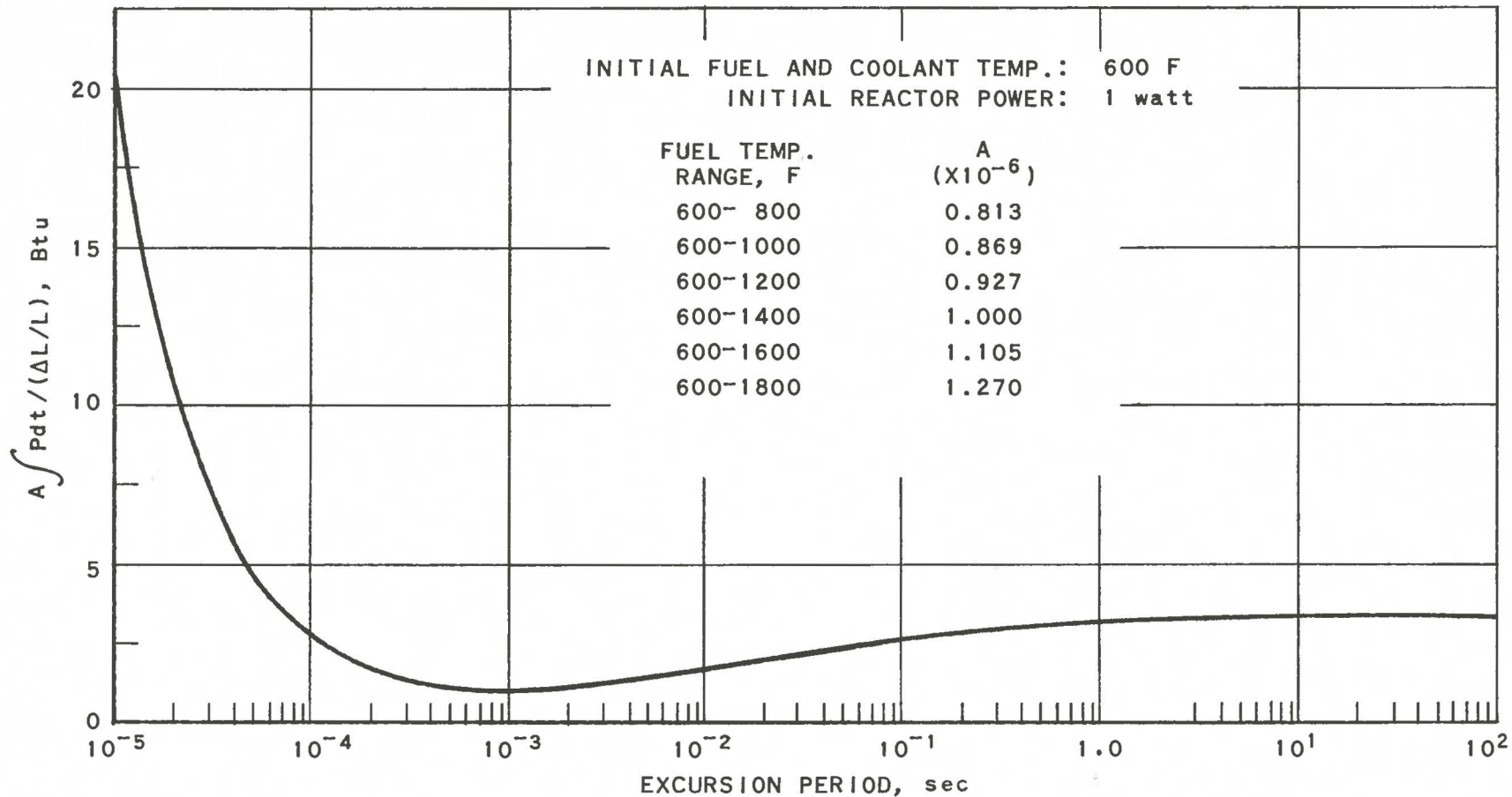


FIG. A-7  
RATIO OF INTEGRATED POWER TO FRACTIONAL CHANGE IN FUEL LENGTH AS A FUNCTION OF REACTOR PERIOD WITH NO COOLANT FLOW

RE-7-19639-A

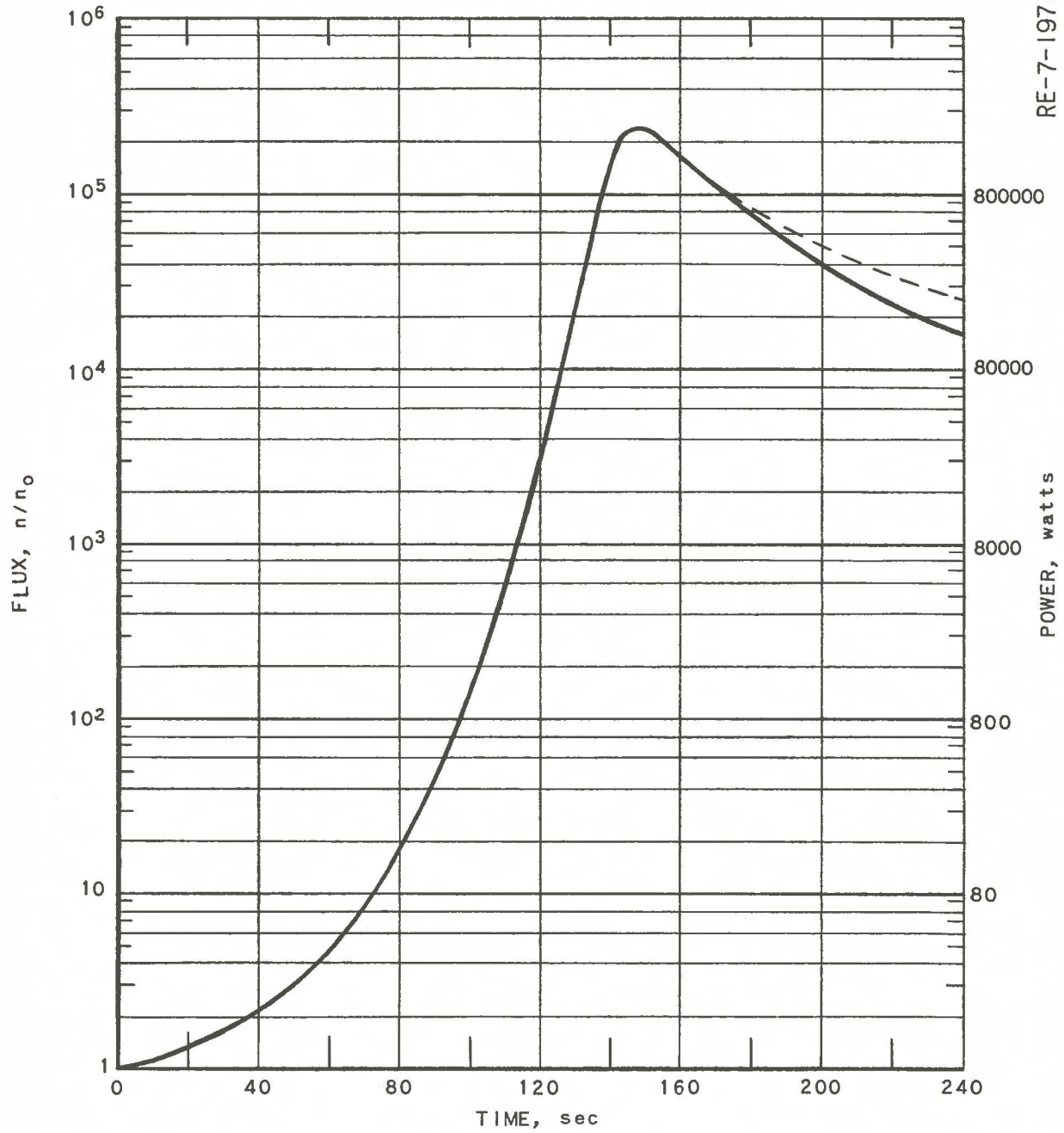


FIG. A-8  
FLUX AND POWER VS TIME FOR  
SINGLE CONTROL ROD INSERTION

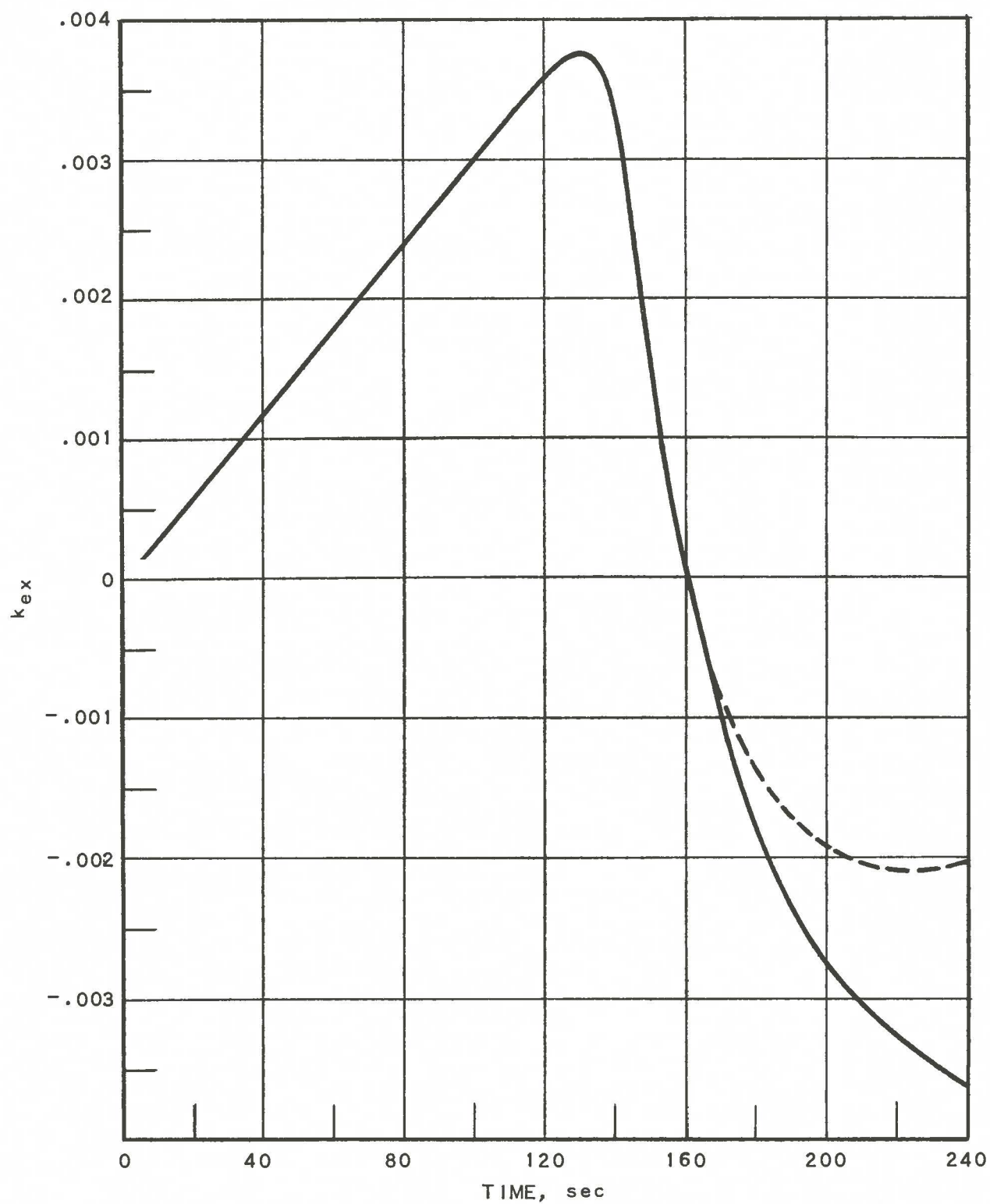


FIG. A-9  
EXCESS REACTIVITY VS TIME  
FOR SINGLE ROD INSERTION

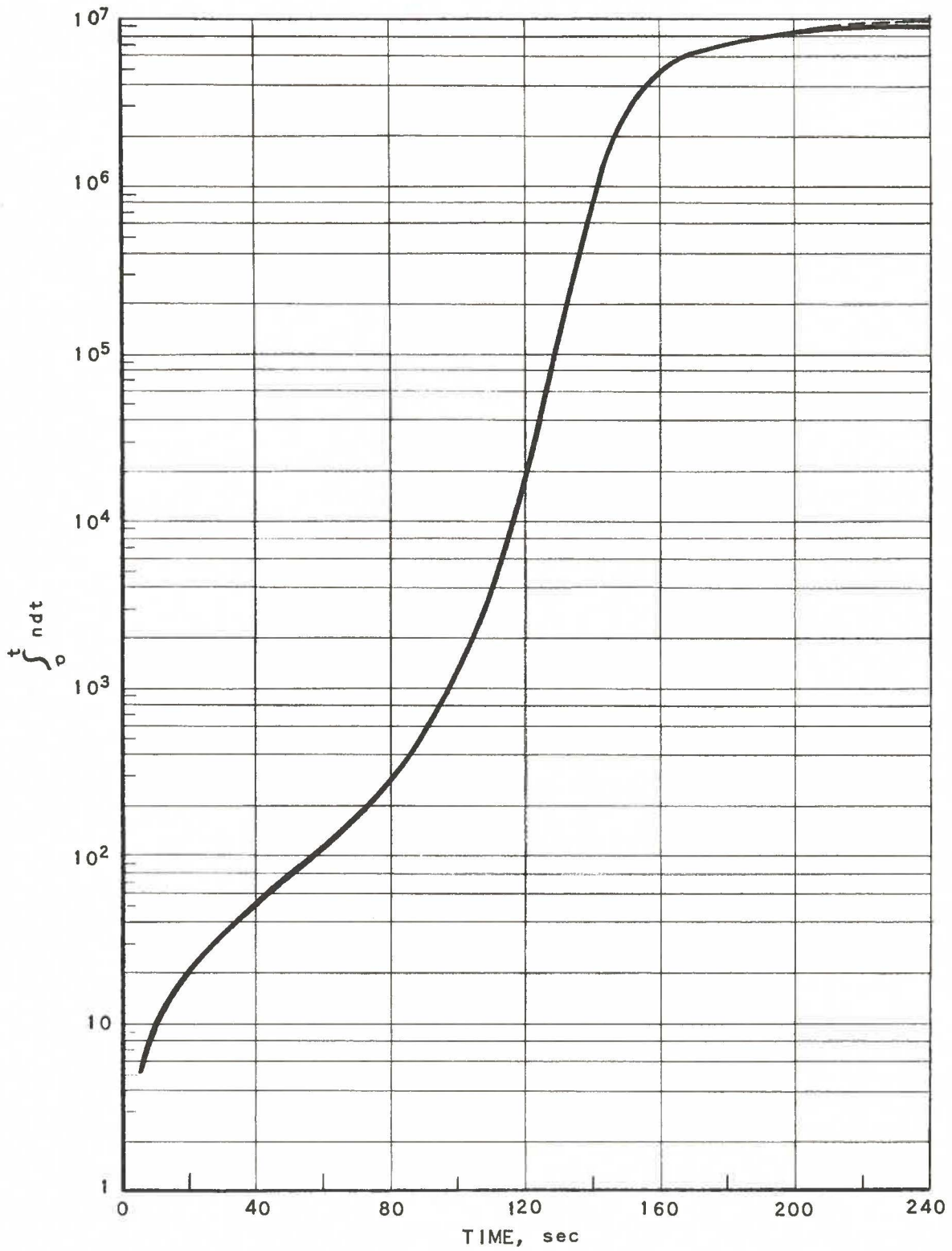
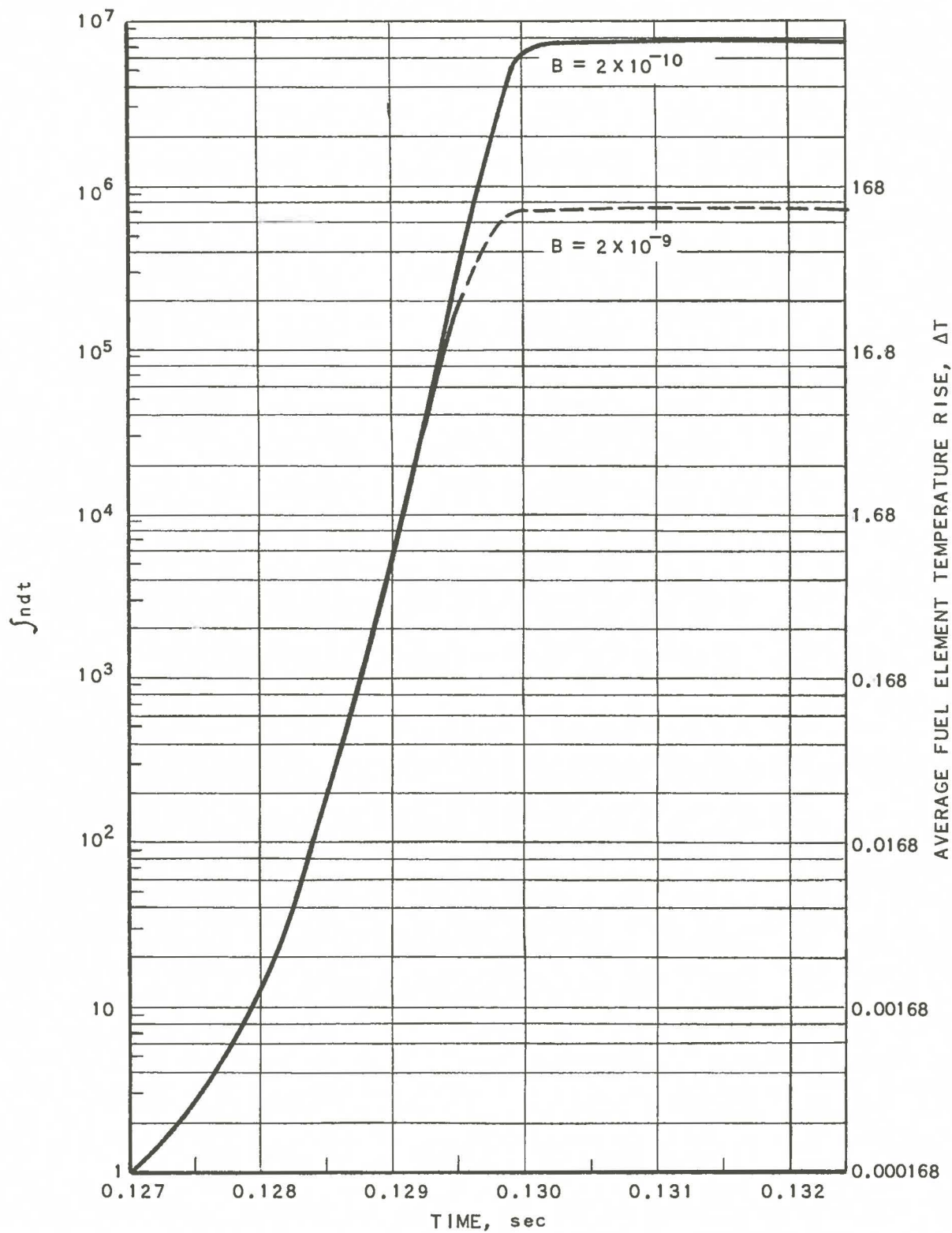
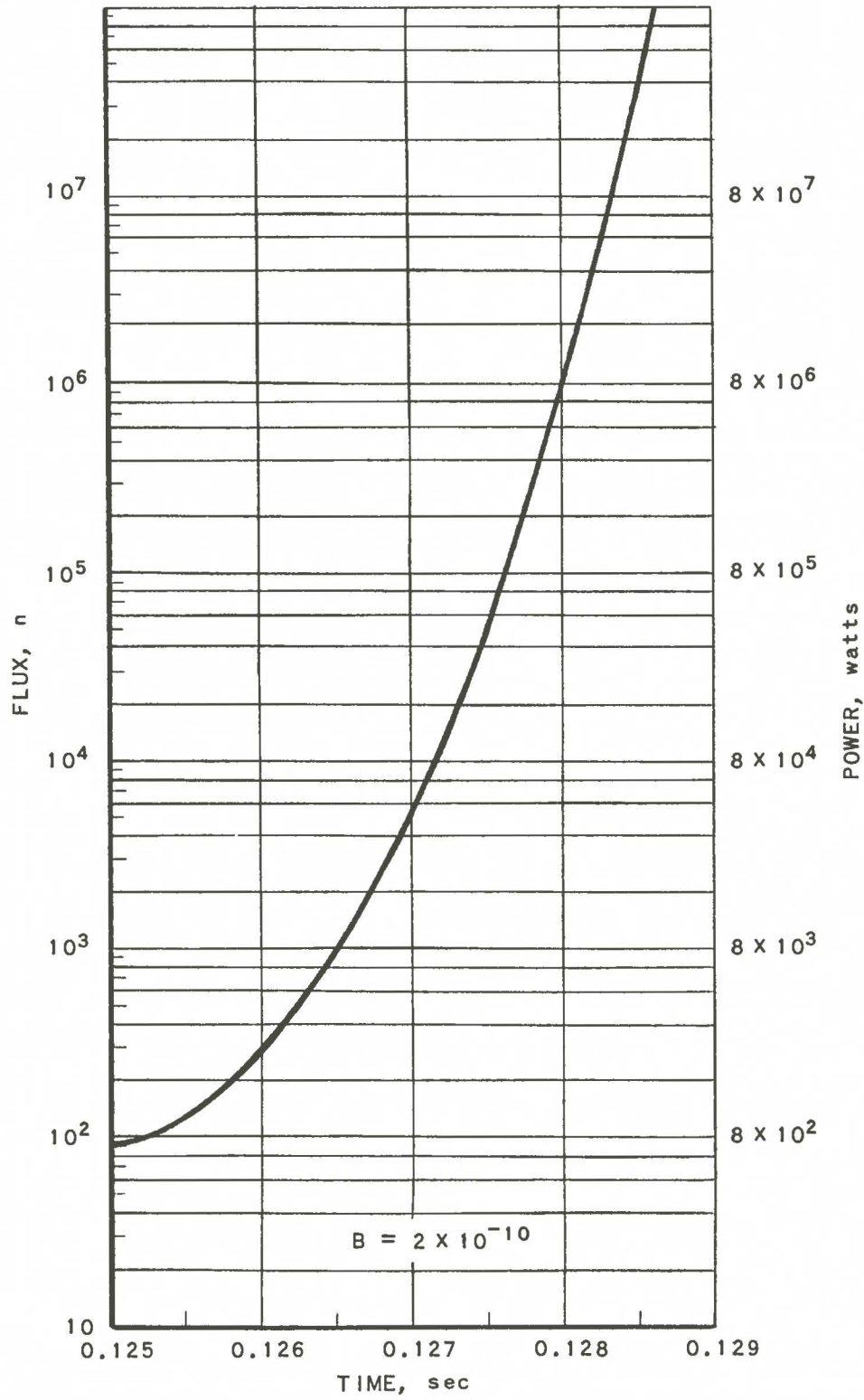


FIG. A-10  
 $\int_0^t n dt$  VS TIME FOR SINGLE ROD INSERTION



RE-7-19714-A

FIG. A-11  
FLUX INTEGRAL AND FUEL ELEMENT  
TEMPERATURE RISE VS TIME



RE-7-19715-A

FIG. A-12  
FLUX AND POWER VS TIME

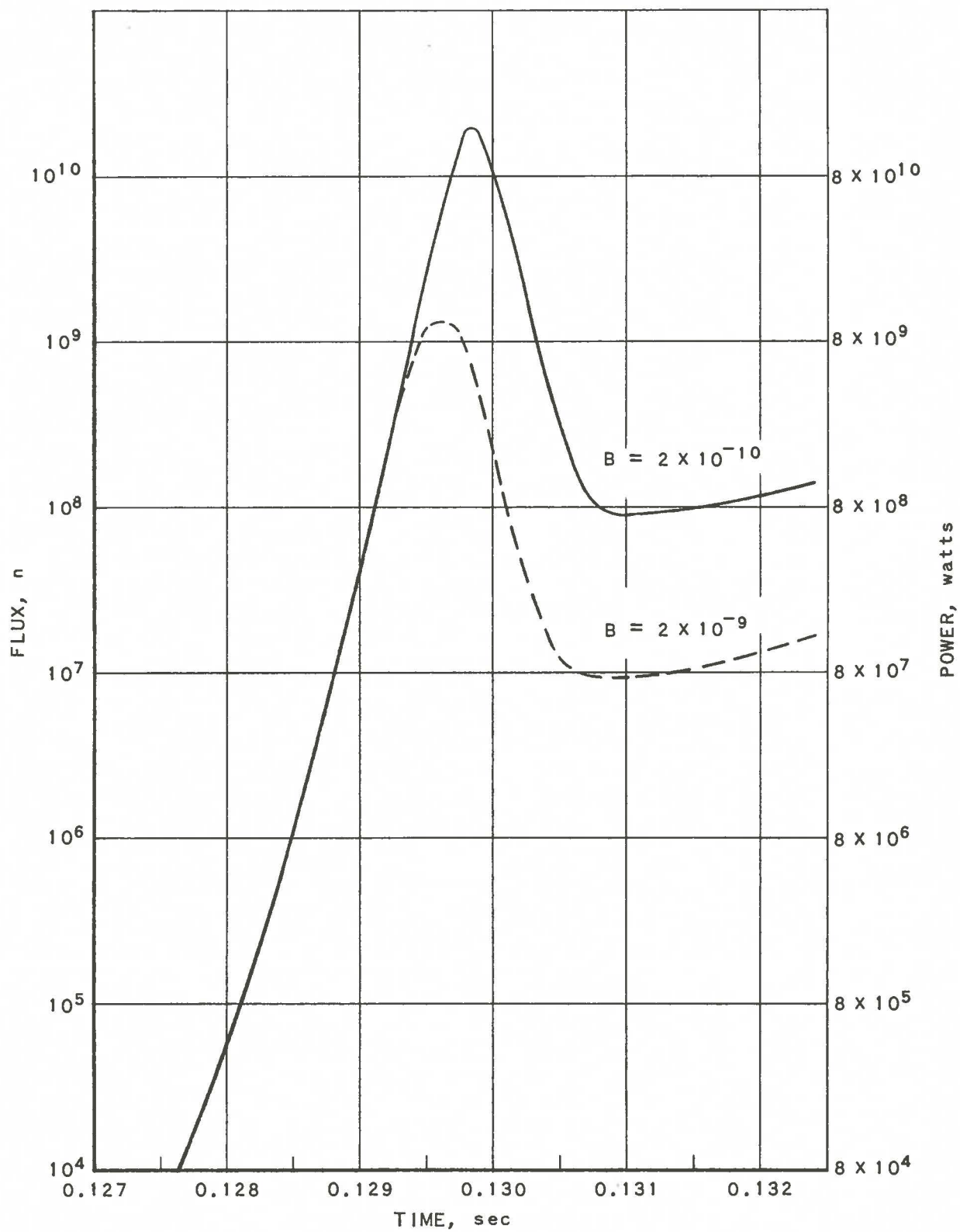


FIG. A-13  
FLUX AND POWER VS TIME

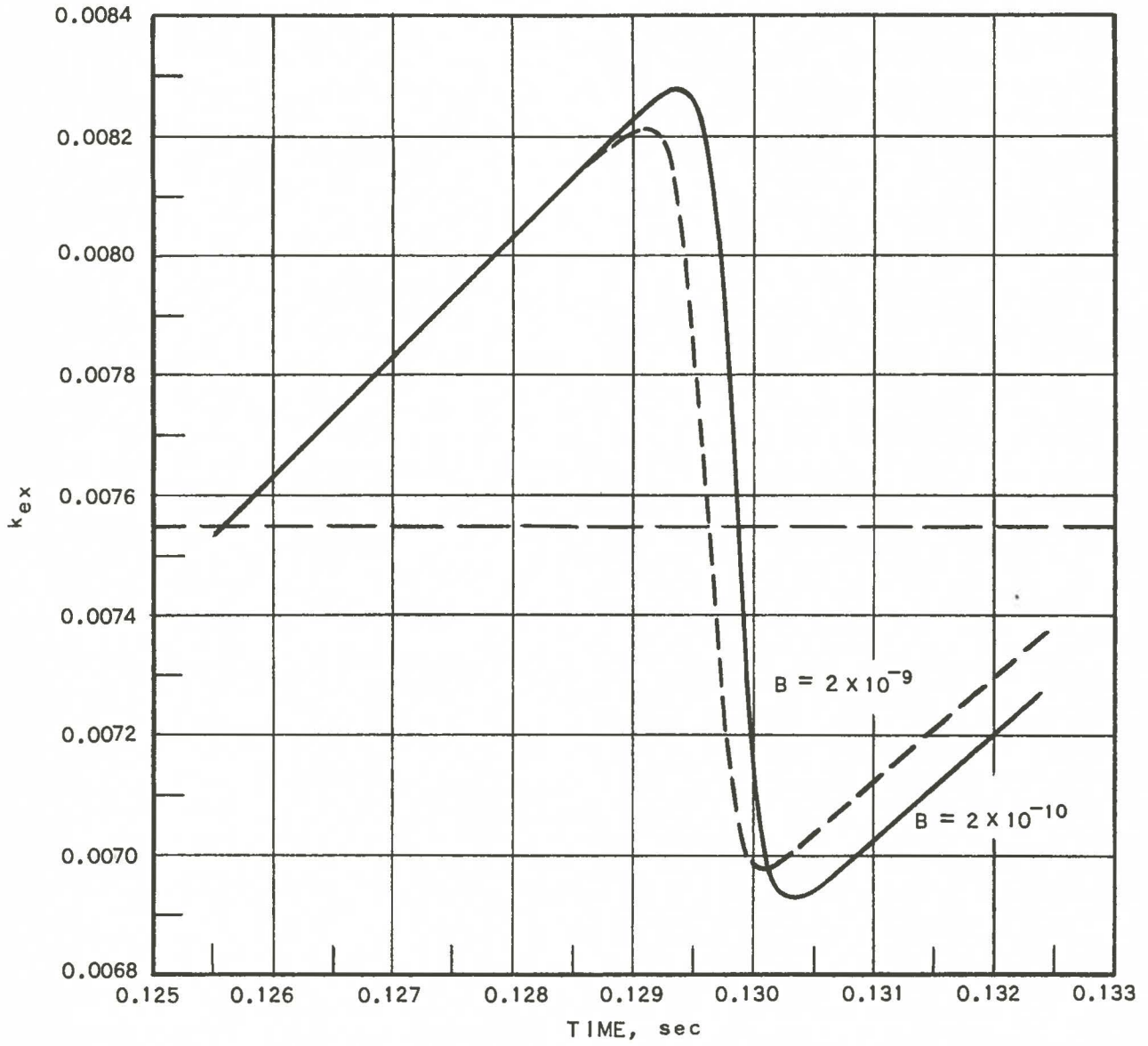


FIG. A-14  
EXCESS REACTIVITY VS TIME

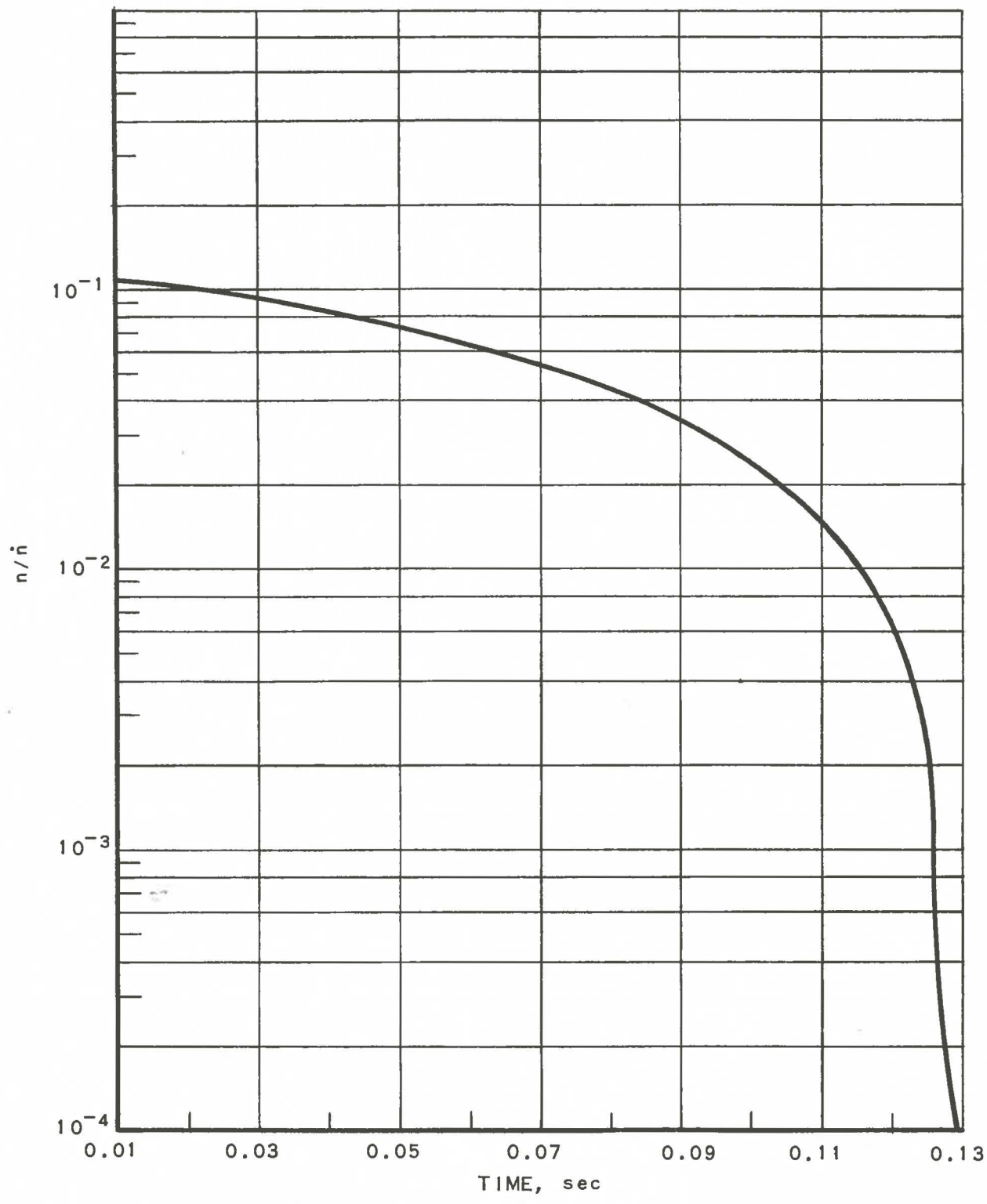


FIG. A-15  
 $n/\bar{n}$  VS TIME

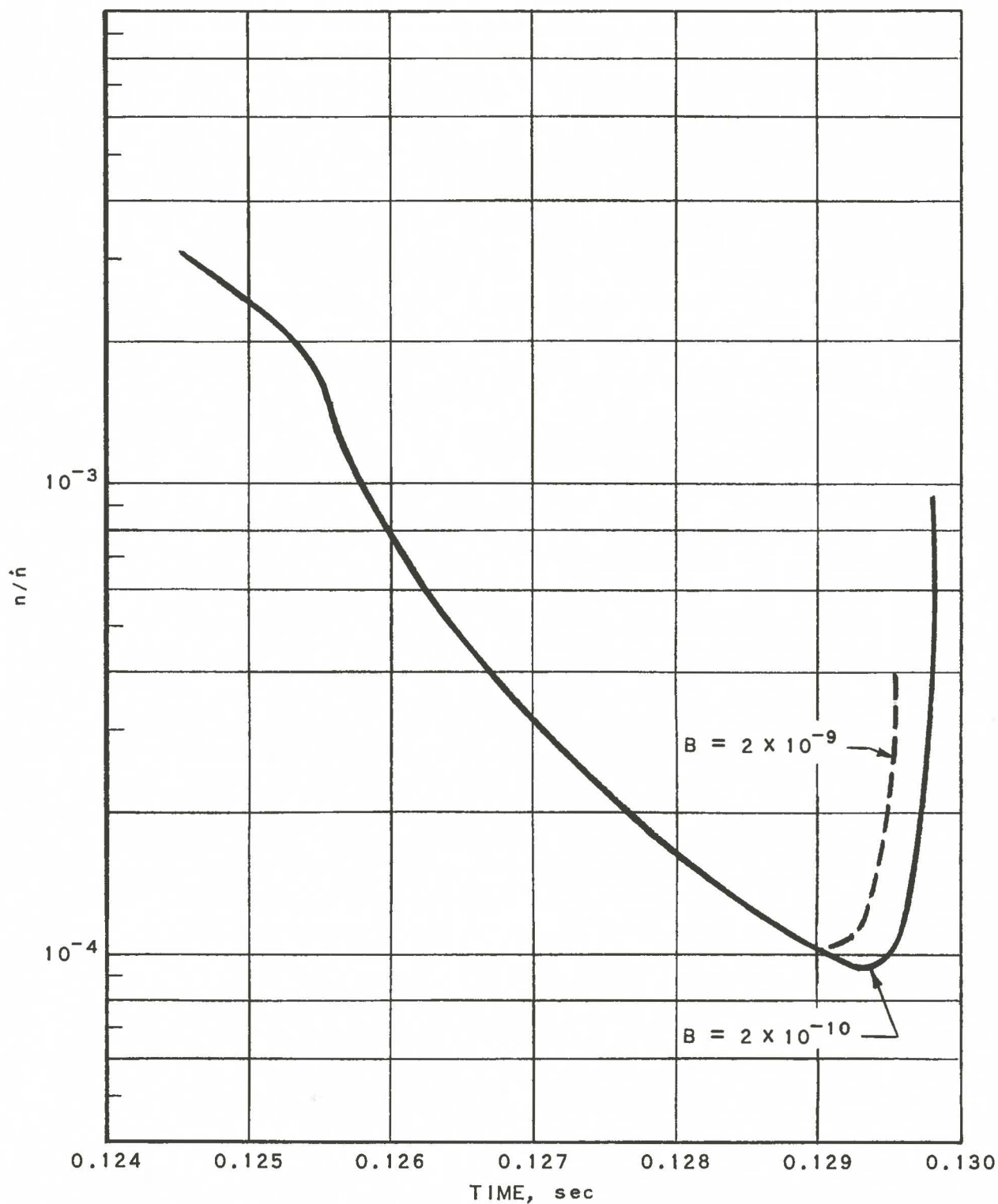


FIG. A-16  
 $n/\dot{n}$  VS TIME

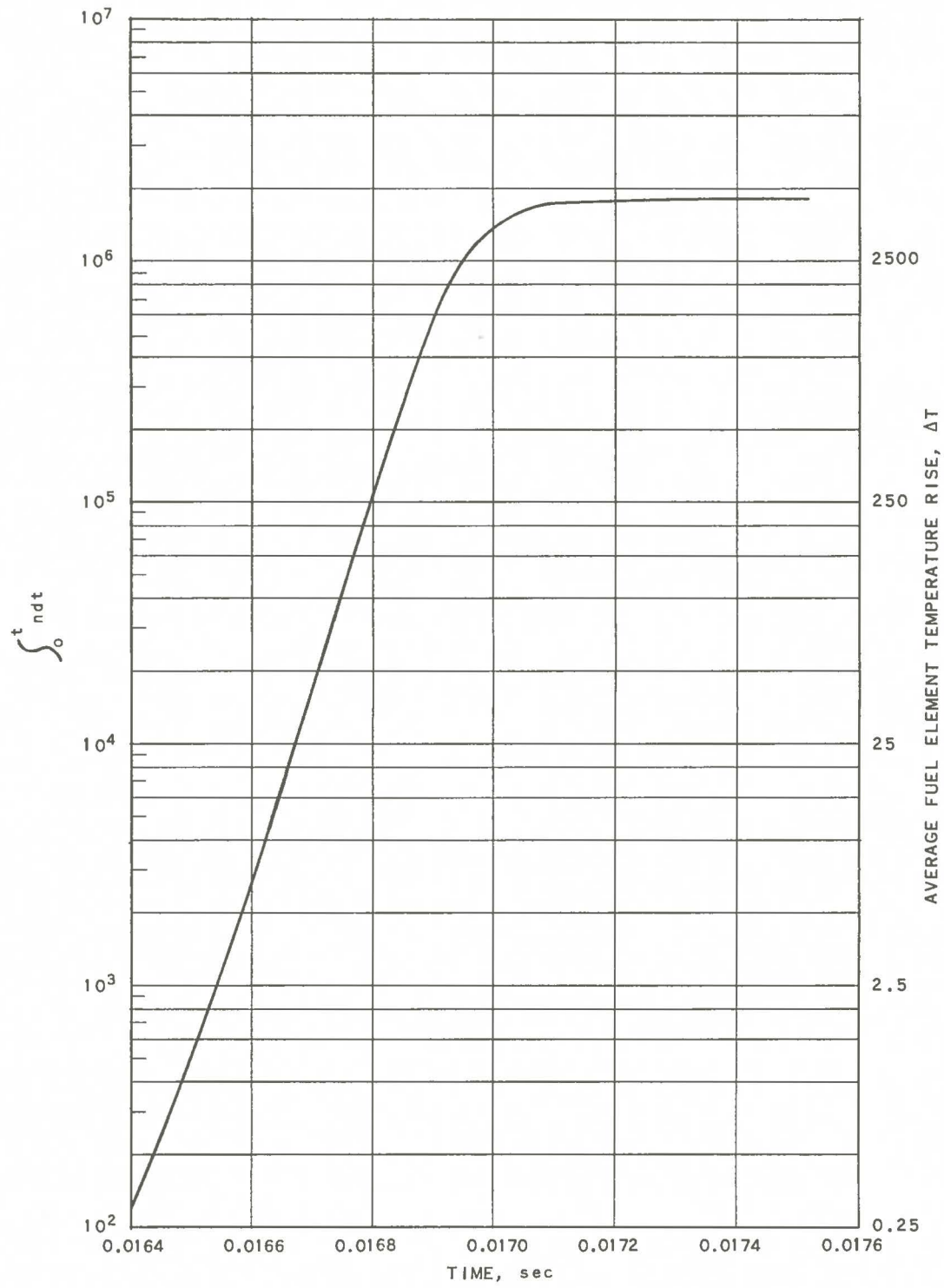


FIG. A-17  
 FLUX INTEGRAL AND FUEL ELEMENT  
 TEMPERATURE RISE VS TIME

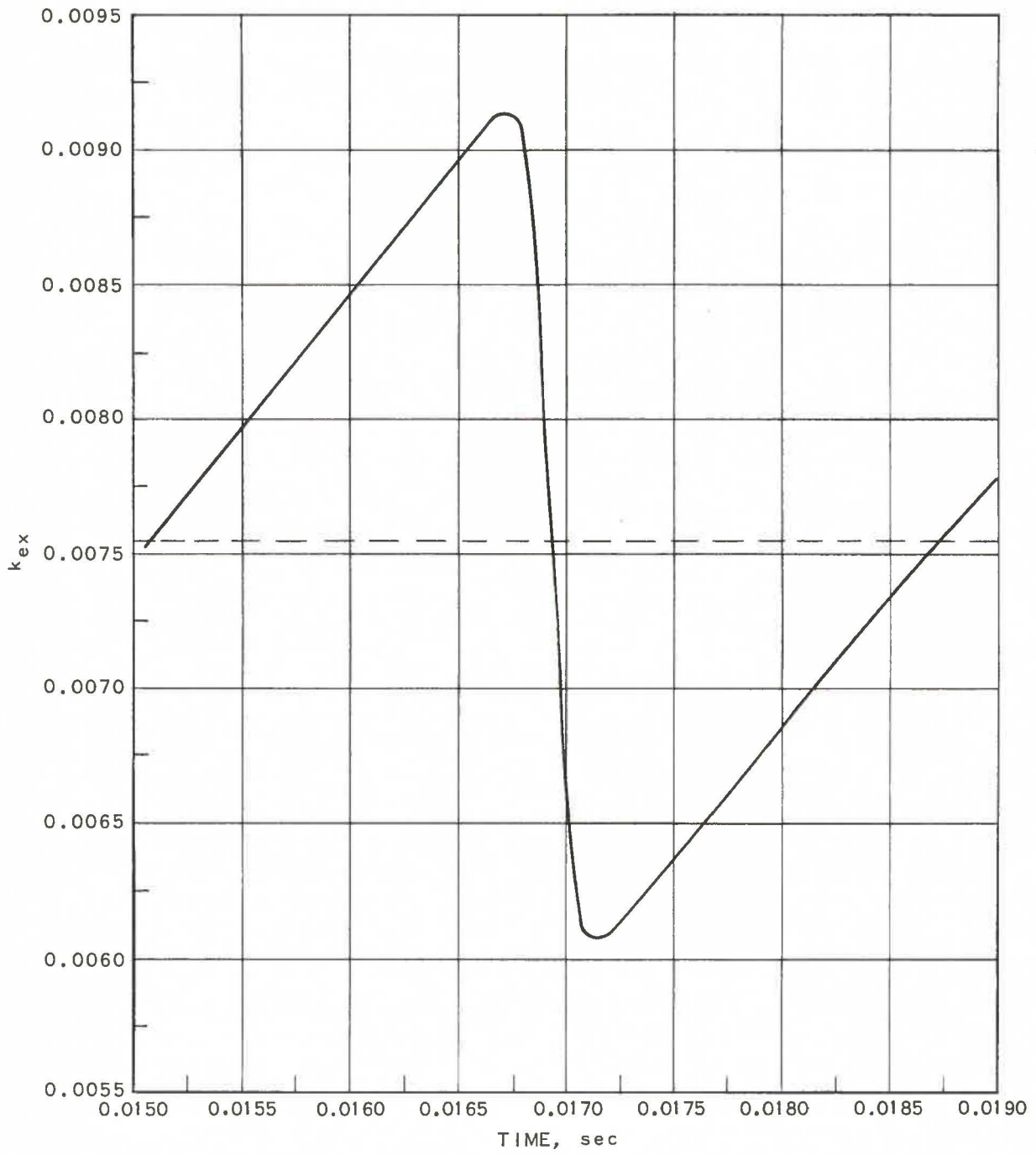


FIG.A-18  
EXCESS REACTIVITY VS TIME

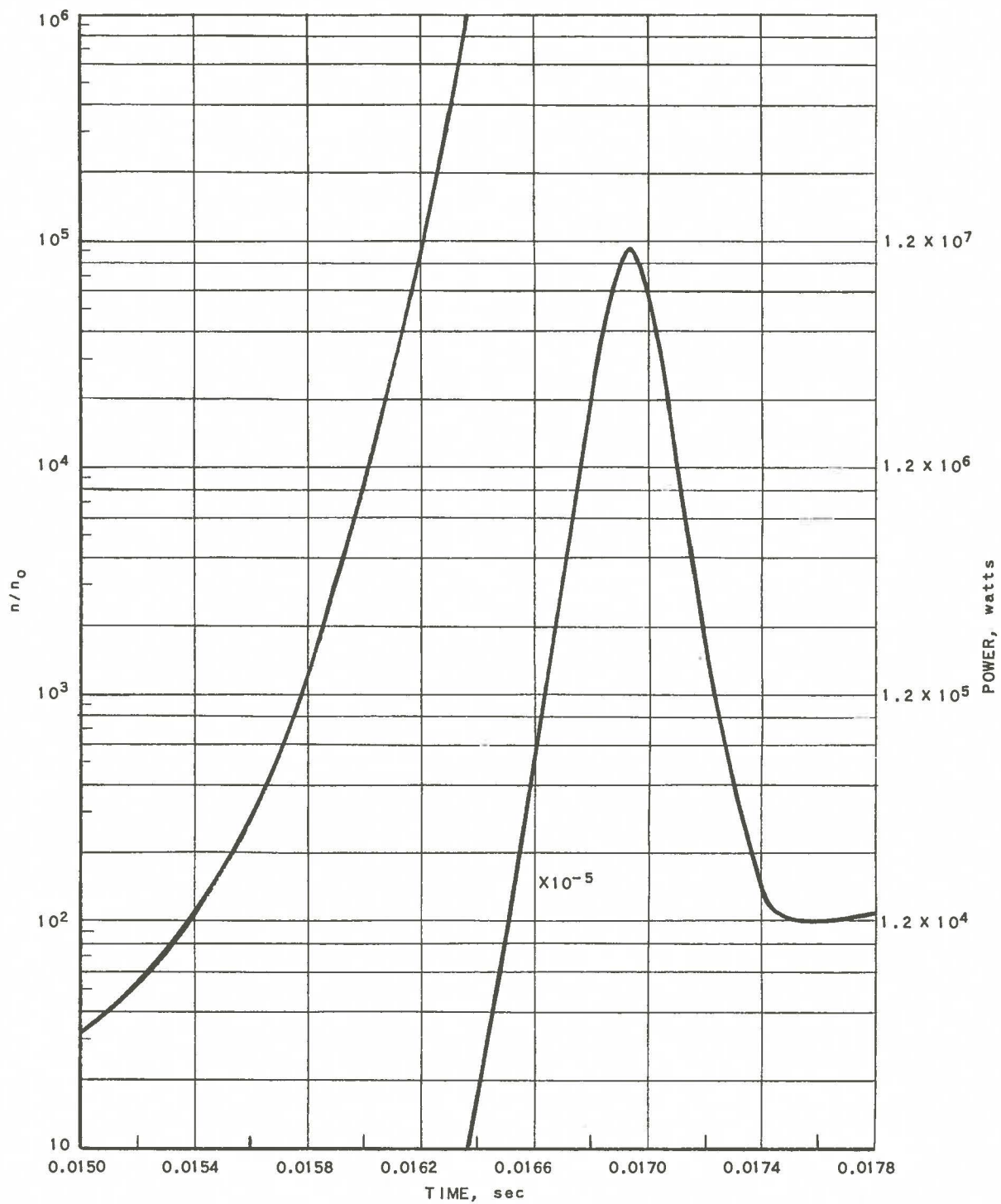
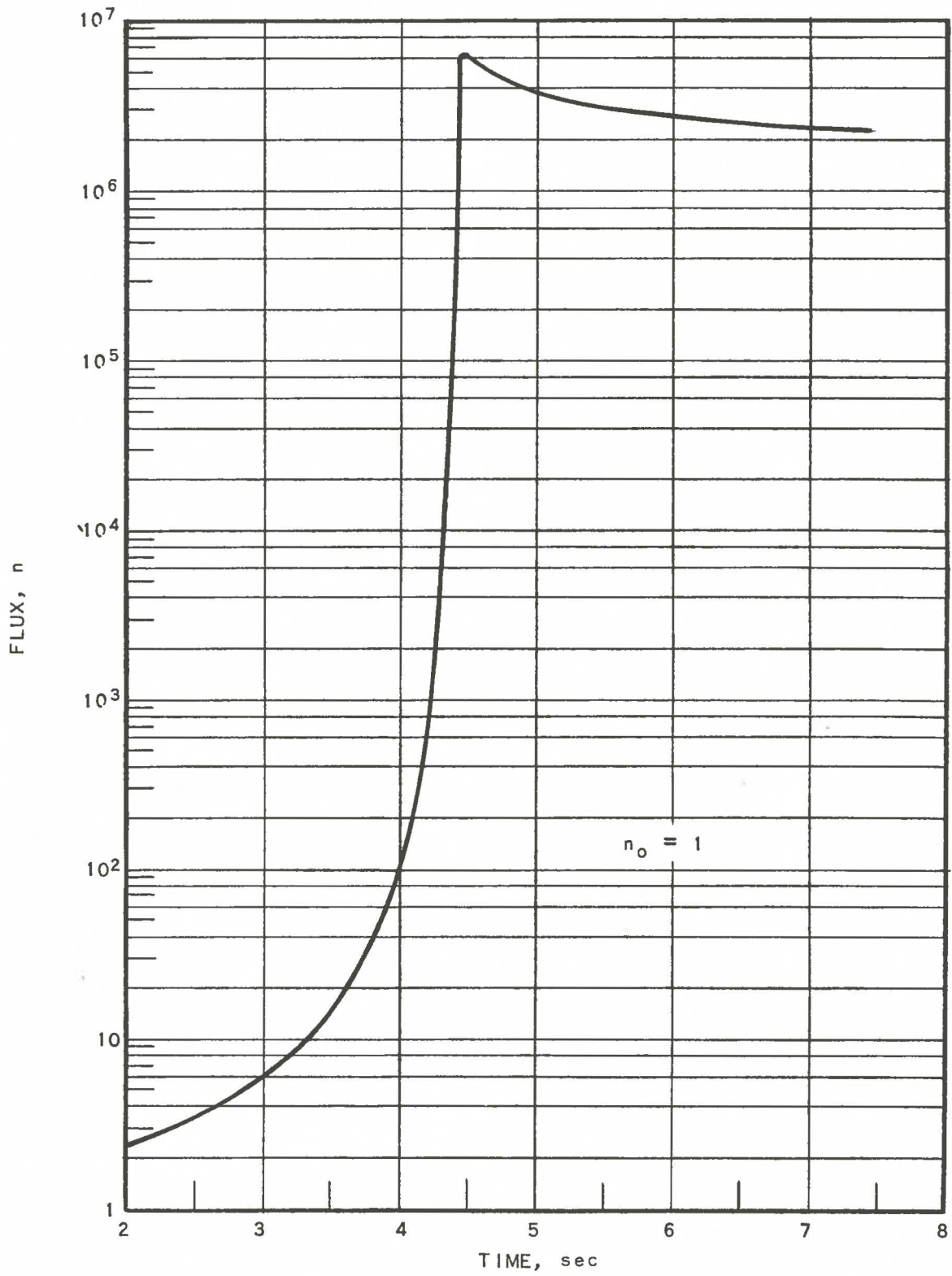


FIG. A-19  
 $n/n_0$ , ALSO POWER, VS TIME



RE-7 - 19720-A

FIG.A-20  
FLUX VS TIME

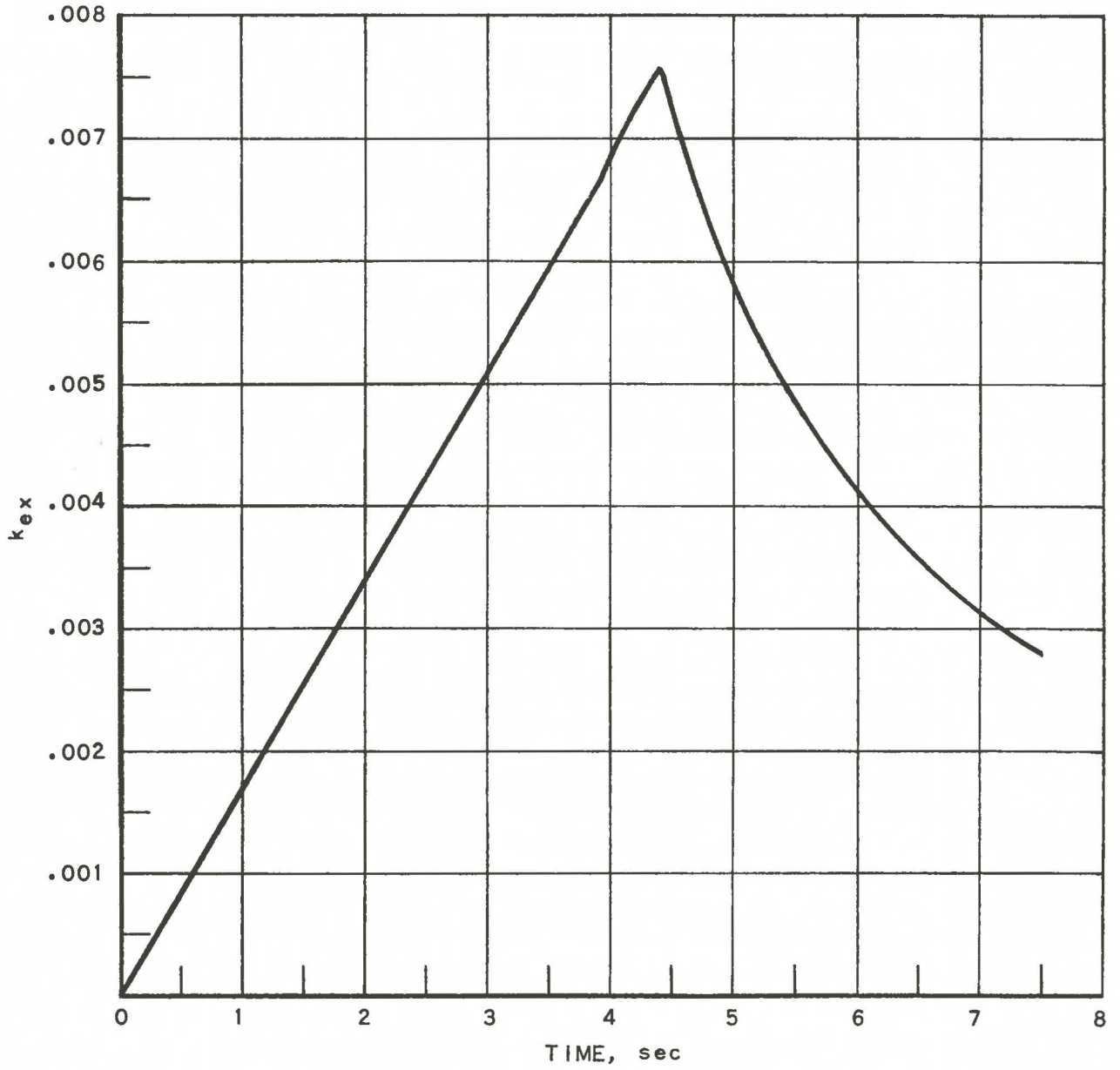
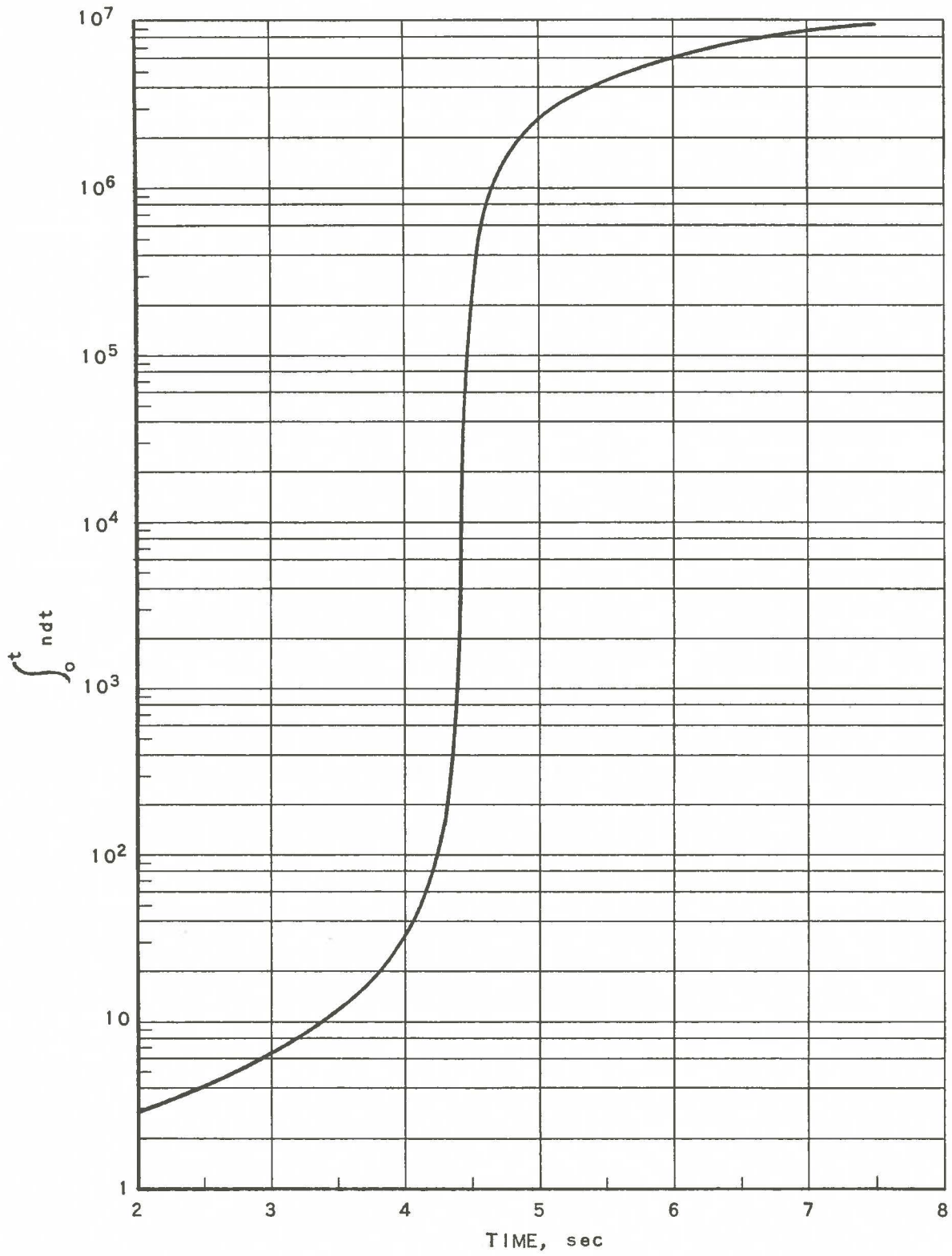


FIG. A-21  
EXCESS REACTIVITY VS TIME



RE-7-19722-A

$\int_0^t n dt$  VS TIME  
FIG.A-22

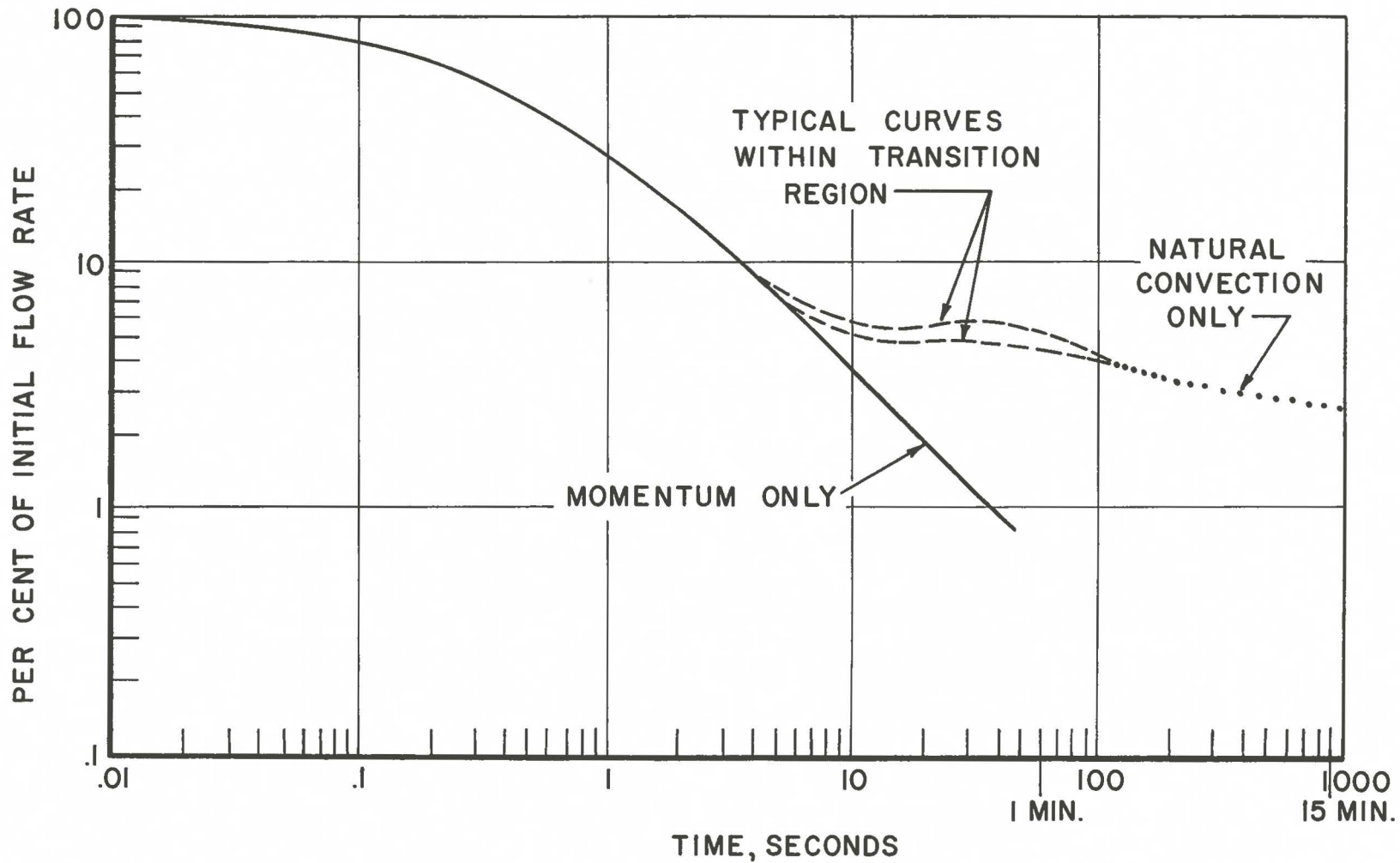


FIG. A-23  
 PRIMARY SYSTEM COOLANT FLOW RATE VS TIME AFTER  
 CESSATION OF ALL PUMPING POWER (BASED ON 100%  
 INITIAL REACTOR POWER AND COOLANT FLOW RATE)

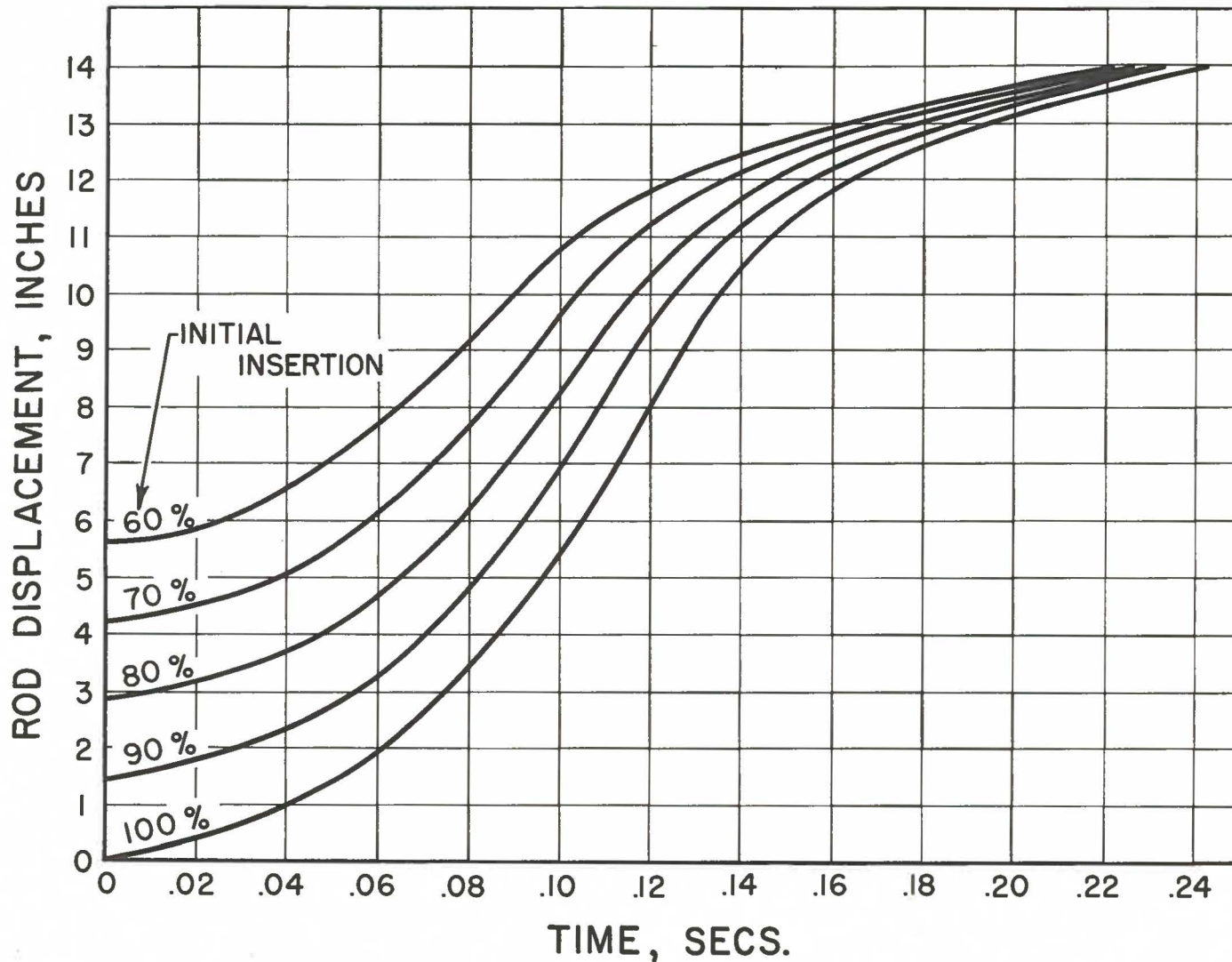


FIG. A-24

CONTROL ROD DISPLACEMENT VS. TIME AFTER START OF ROD MOVEMENT (BASED ON HIGH SCRAM ASSIST PRESSURE, ~ 100 PSI)

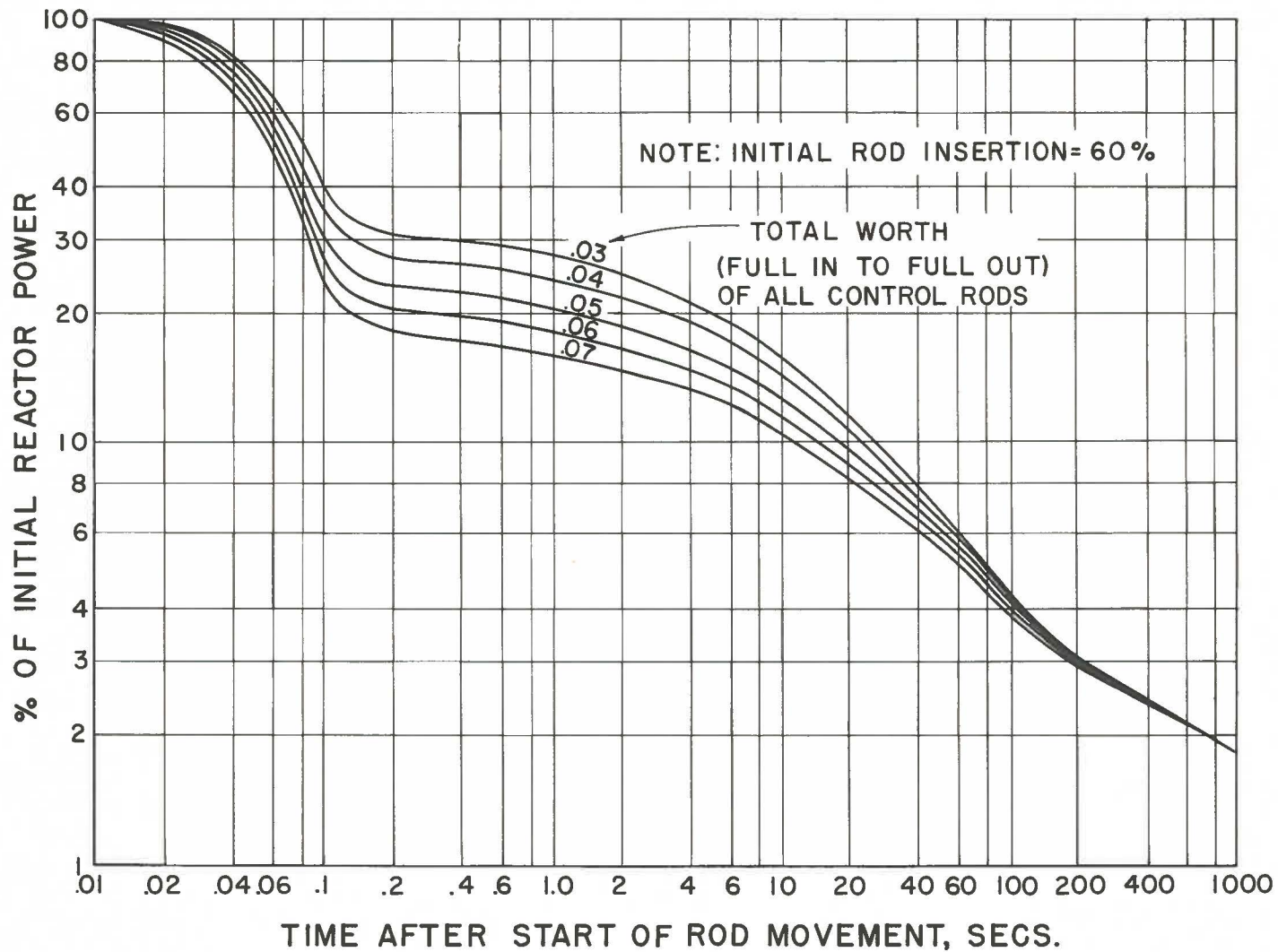


FIG. A-25  
 TOTAL REACTOR POWER VS. TIME AFTER  
 START OF ROD MOVEMENT DURING SCRAM

RE-7-19984-C

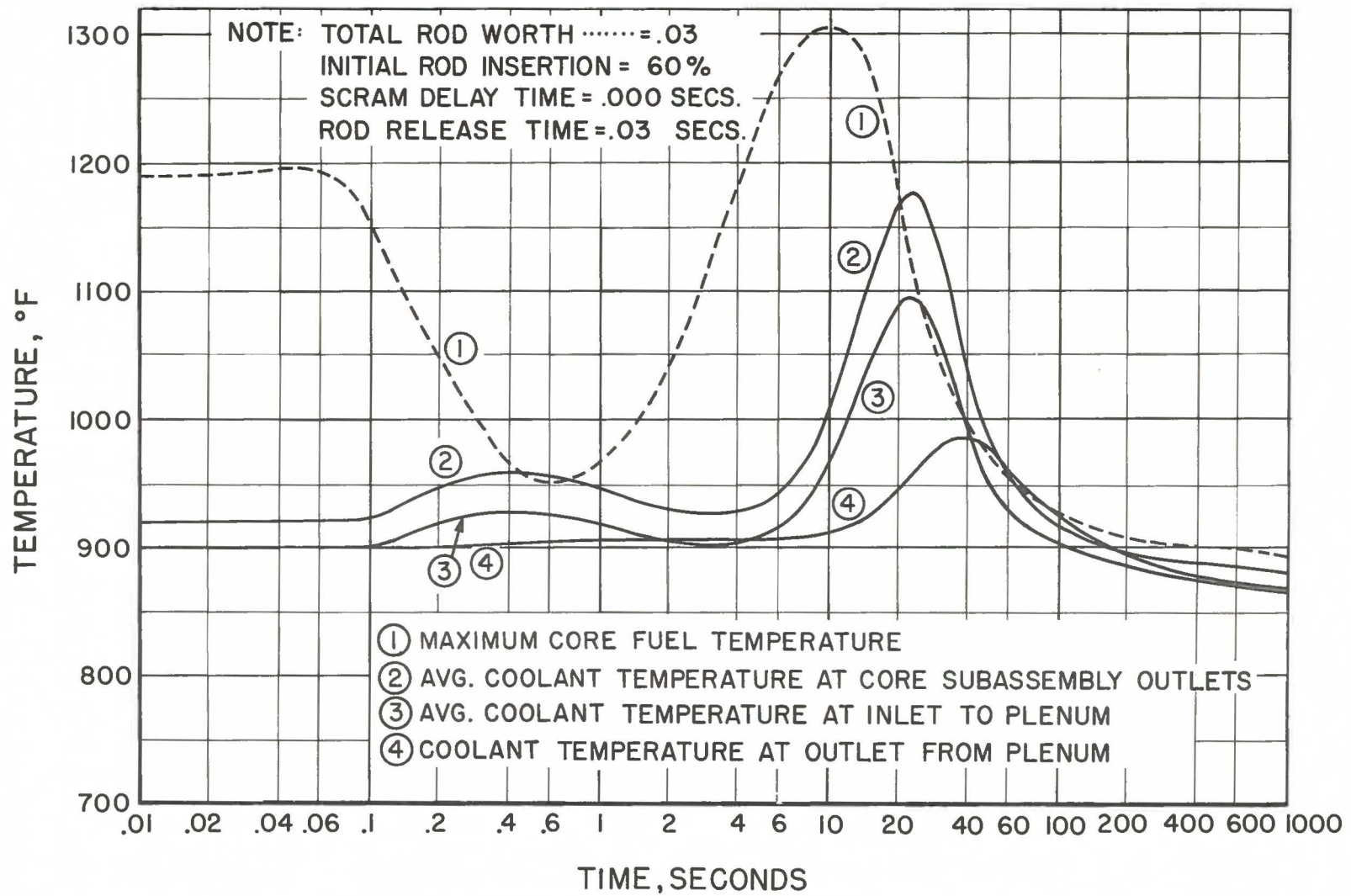


FIG. A-26  
 VARIOUS REACTOR TEMPERATURES DURING SCRAM VS TIME  
 AFTER CESSATION OF ALL PUMPING POWER

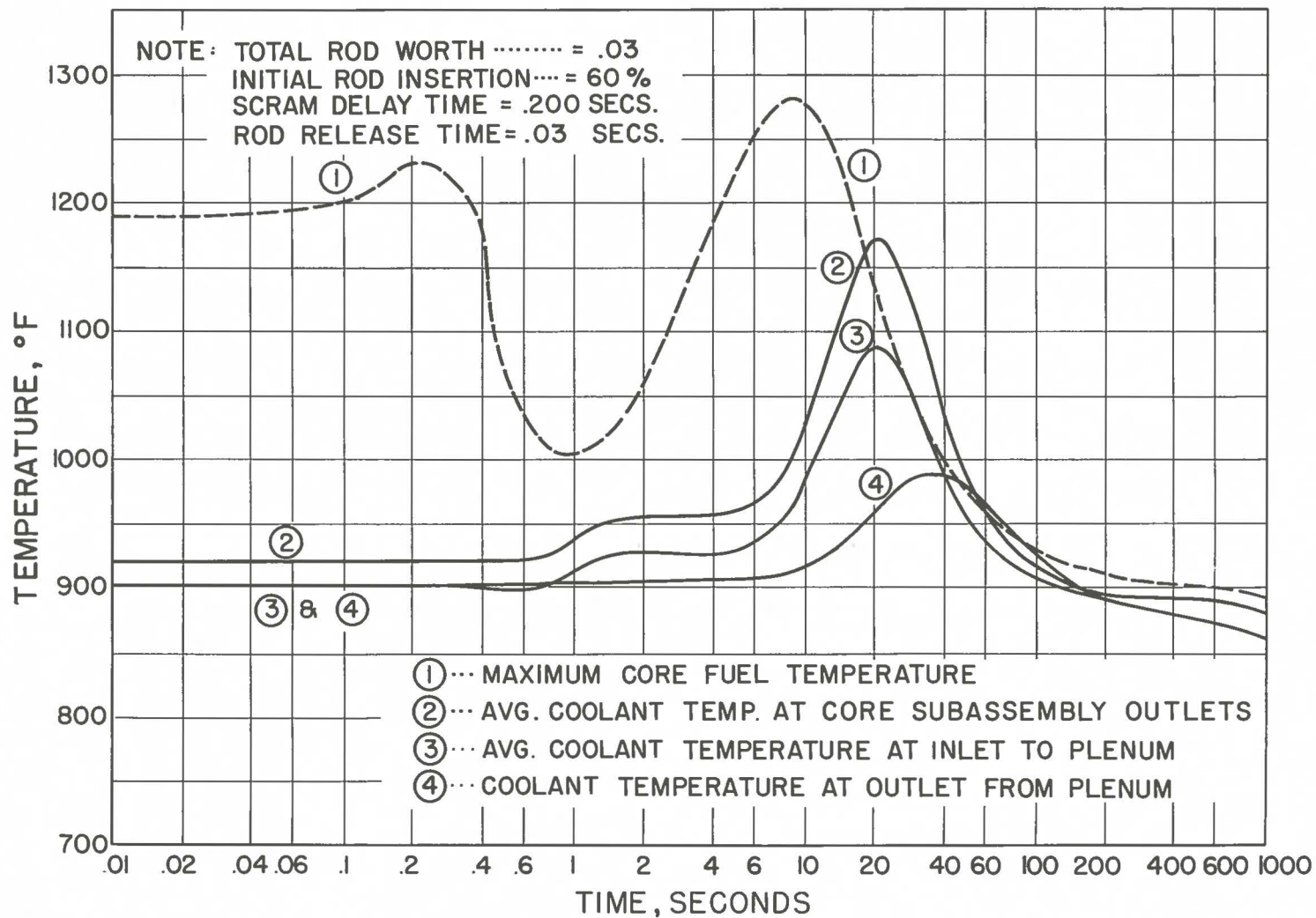


FIG. A-27  
 VARIOUS REACTOR TEMPERATURES DURING SCRAM VS TIME  
 AFTER CESSATION OF ALL PUMPING POWER

RE-7-18076-C

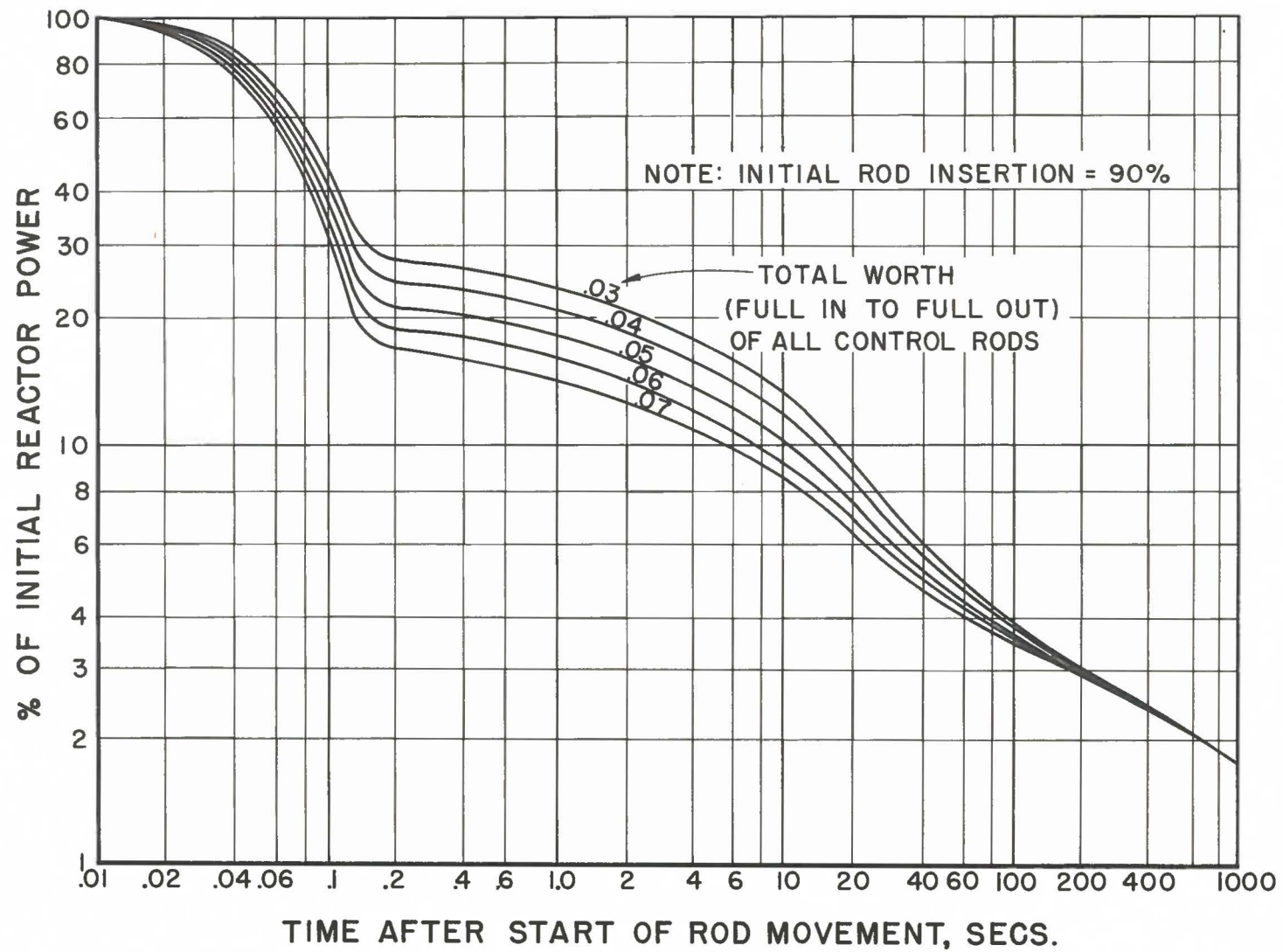


FIG. A-28  
TOTAL REACTOR POWER VS. TIME AFTER  
START OF ROD MOVEMENT DURING SCRAM

RE-7-18073-C

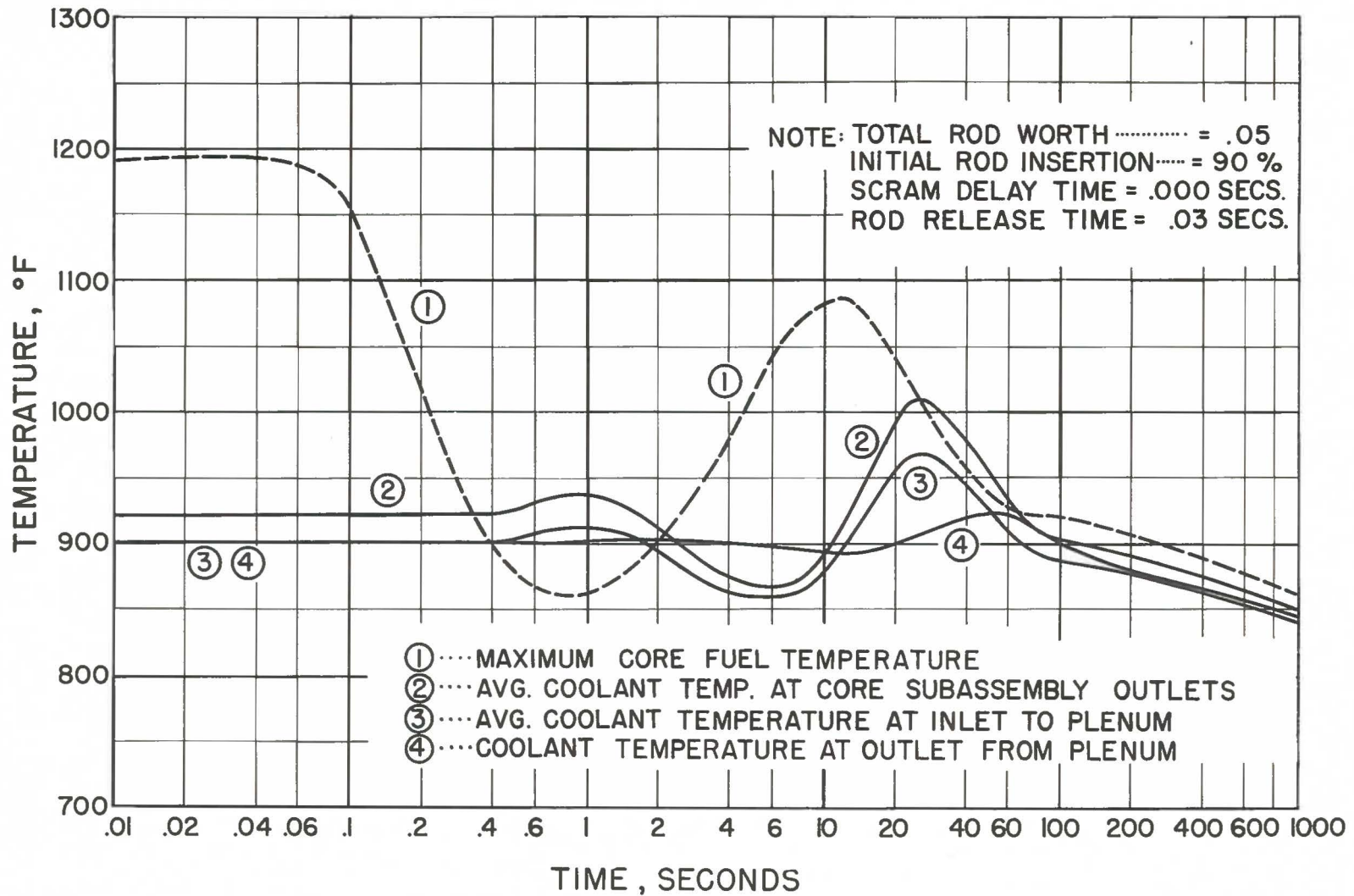


FIG.A-29  
 VARIOUS REACTOR TEMPERATURES DURING SCRAM VS TIME  
 AFTER CESSATION OF ALL PUMPING POWER

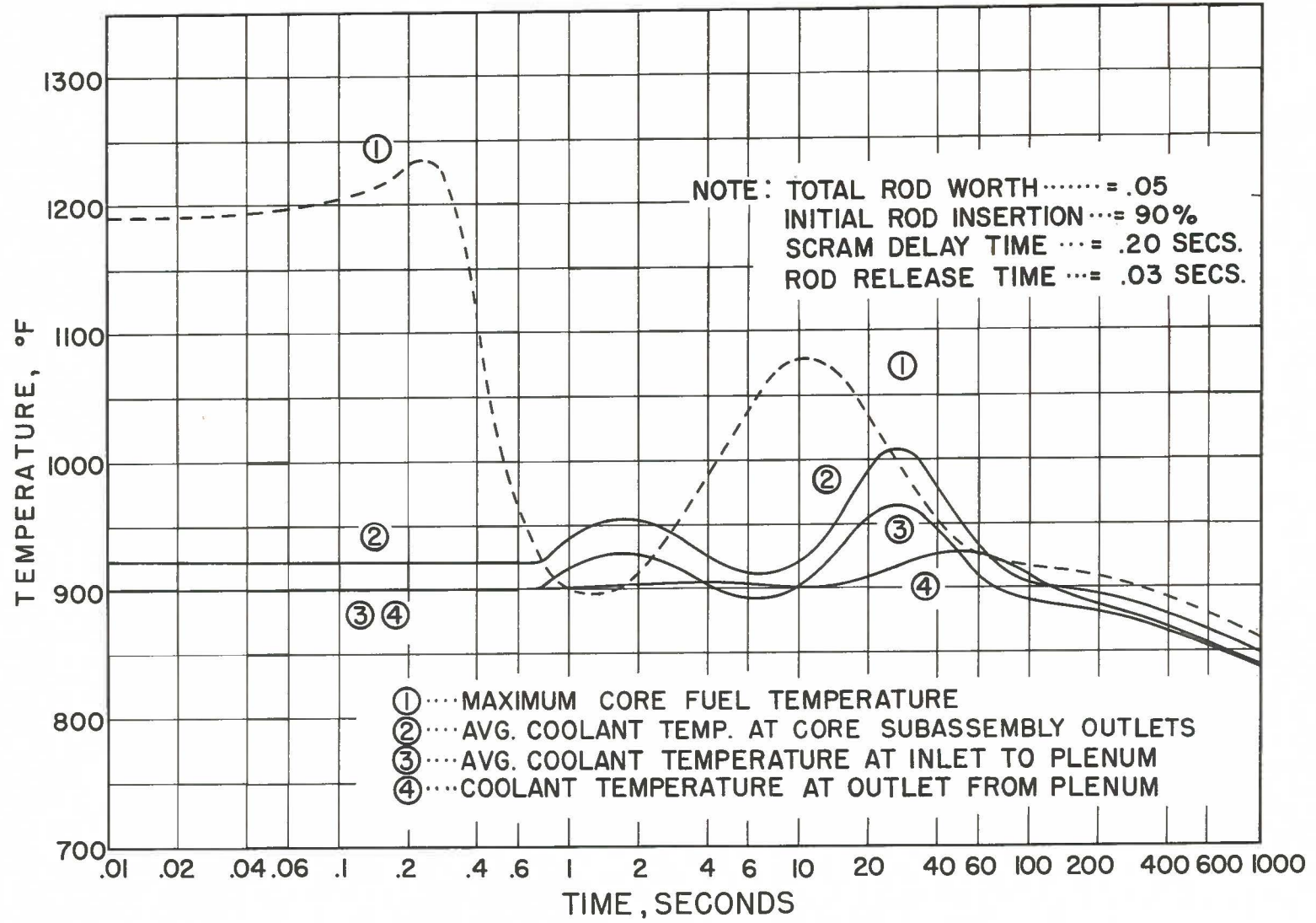


FIG. A-30  
 VARIOUS REACTOR TEMPERATURES DURING SCRAM VS TIME  
 AFTER CESSATION OF ALL PUMPING POWER

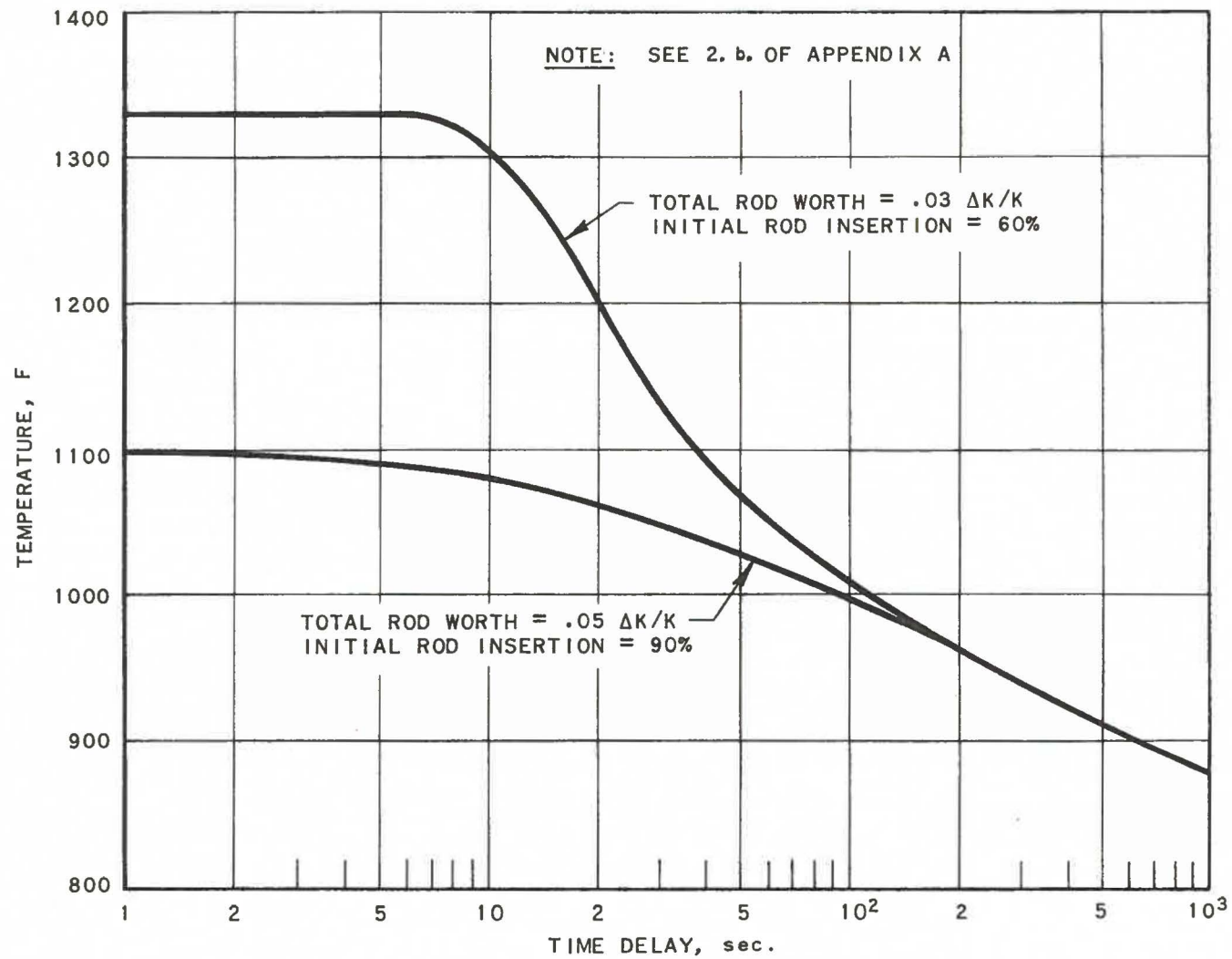


FIG. A-31  
 MAXIMUM FUEL TEMPERATURE OCCURRING DURING  
 TRANSIENT VS TIME DELAY BETWEEN START OF  
 SCRAM AND CESSATION OF ALL PUMPING POWER

RE-7-20176-A

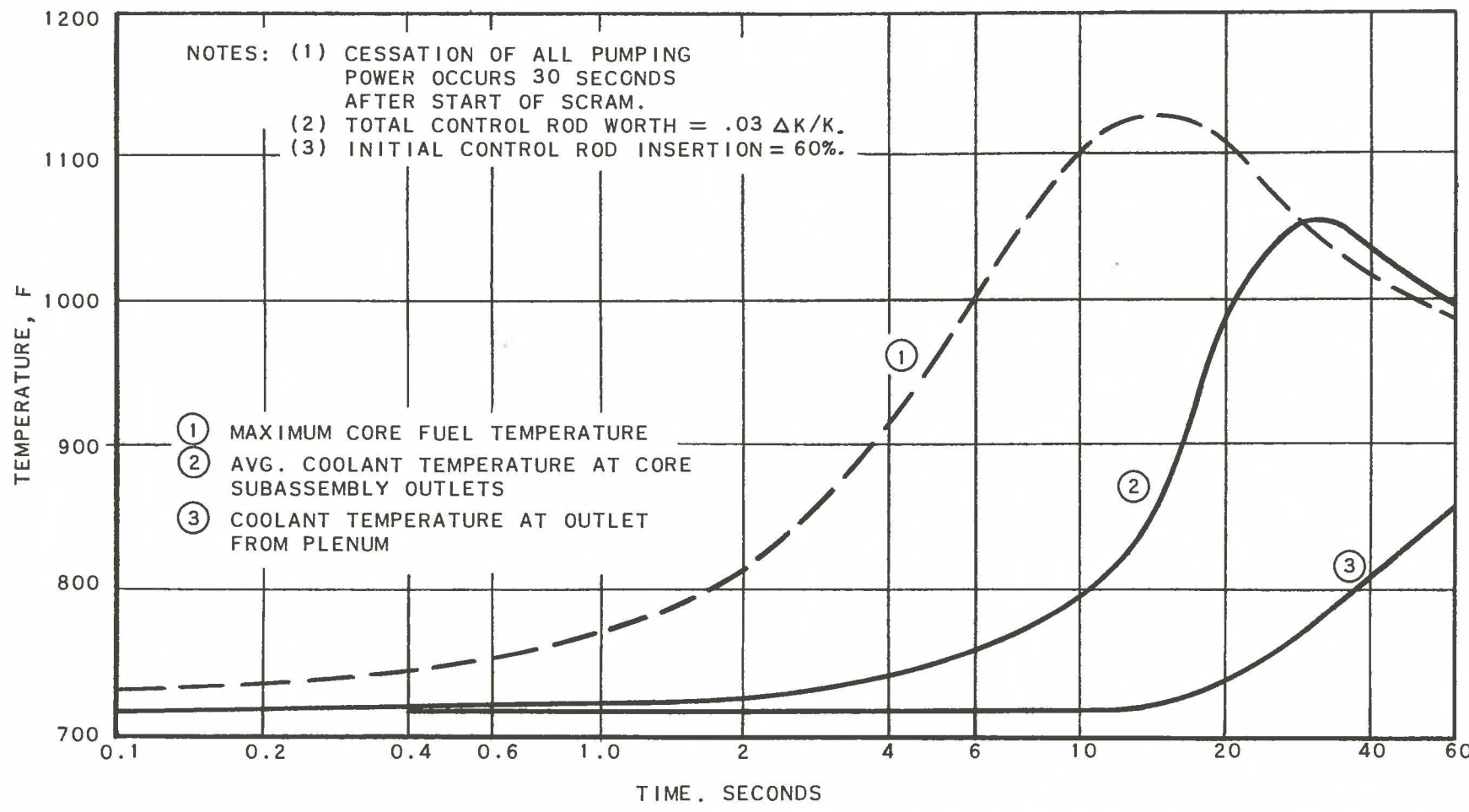


FIG. A-32  
 VARIOUS REACTOR TEMPERATURES VS TIME  
 AFTER CESSATION OF ALL PUMPING POWER  
 SUBSEQUENT TO SCRAM

RE-7-20181-A

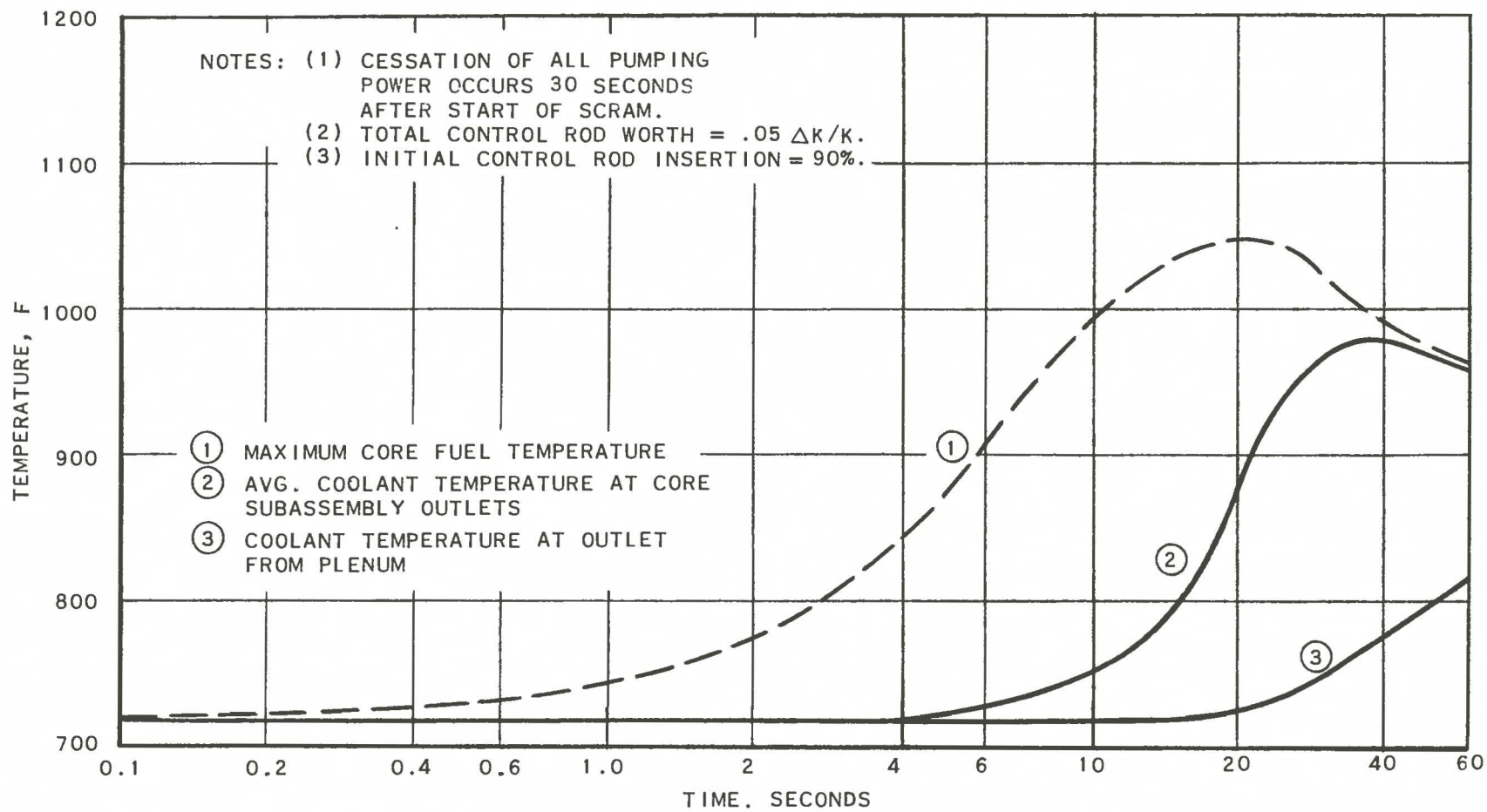


FIG. A-33  
 VARIOUS REACTOR TEMPERATURES VS TIME  
 AFTER CESSATION OF ALL PUMPING POWER  
 SUBSEQUENT TO SCRAM

RE-7-20180-A

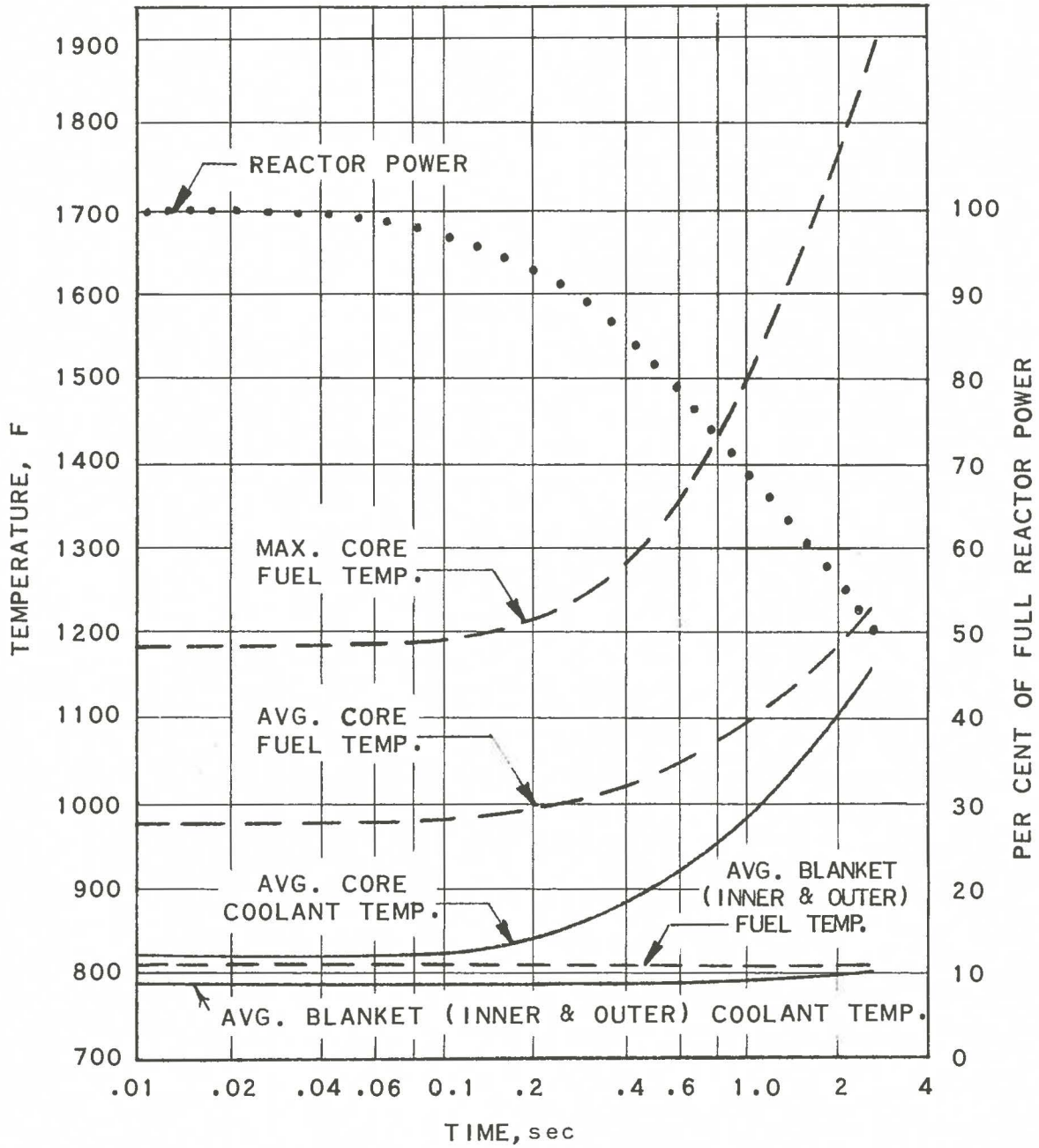


FIG. A-34  
 REACTOR TEMPERATURES VS TIME AFTER  
 LOSS OF ALL PUMPING POWER (WITHOUT SCRAM)

- ASSUMPTIONS: (1) CONSTANT REACTOR PERIOD  
 (2) INITIAL REACTOR POWER=62.5 MW  
 (3) COOLANT VELOCITY = 12.2 FT/SEC.  
 (4) COOLANT INLET TEMPERATURE = 700 °F

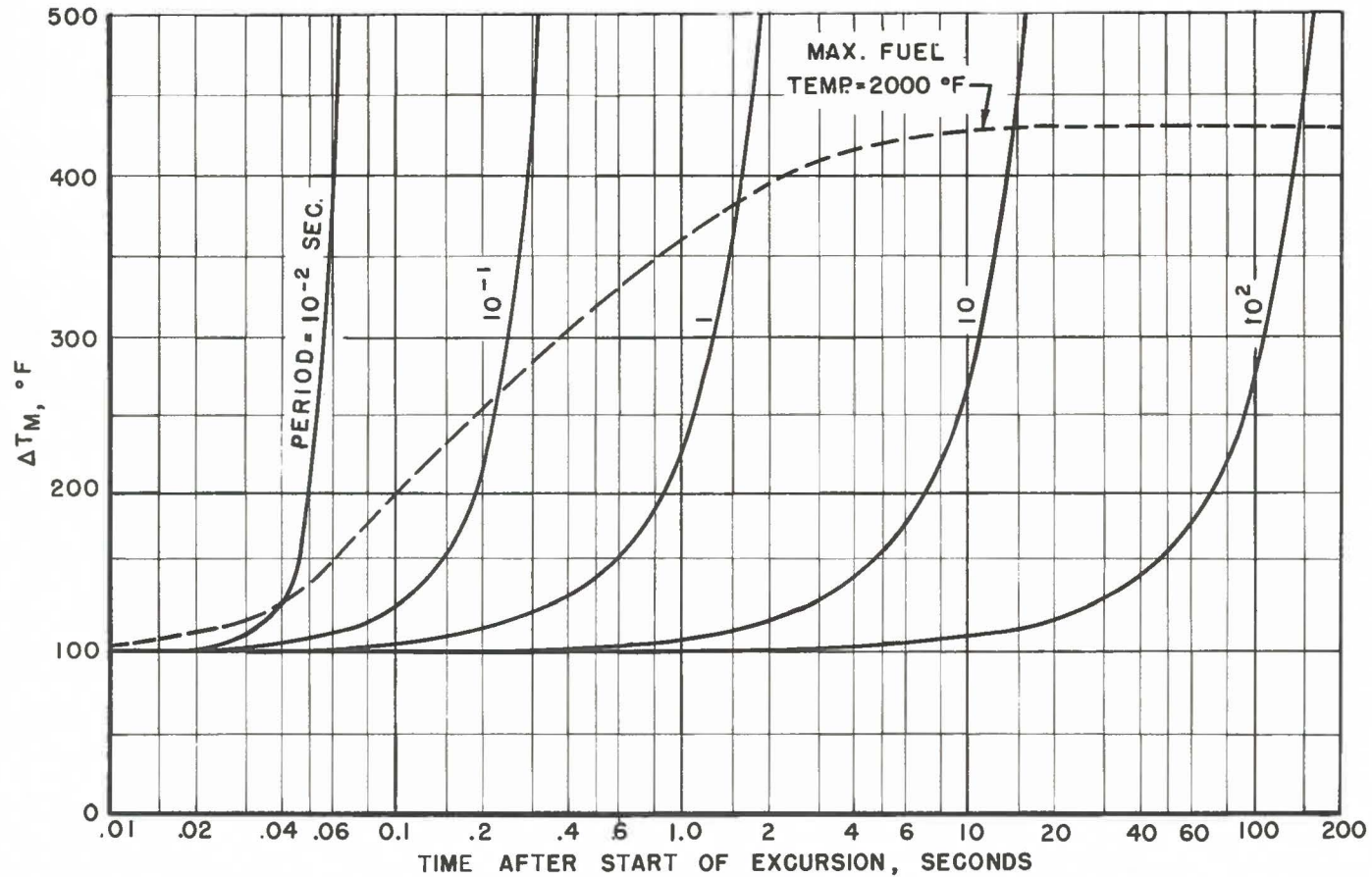


FIG. A-35  
 MAXIMUM TEMPERATURE DIFFERENCE ( $\Delta T_M$ )  
 ACROSS OPPOSITE FLATS OF A FIFTH ROW SUBASSEMBLY DURING A POWER EXCURSION  
 (FOR THE CASE OF FULL COOLANT FLOW)

ASSUMPTIONS: (1) CONSTANT REACTOR PERIOD  
 (2) INITIAL REACTOR POWER = 1 WATT  
 (3) INITIAL REACTOR TEMPERATURE = 600 F

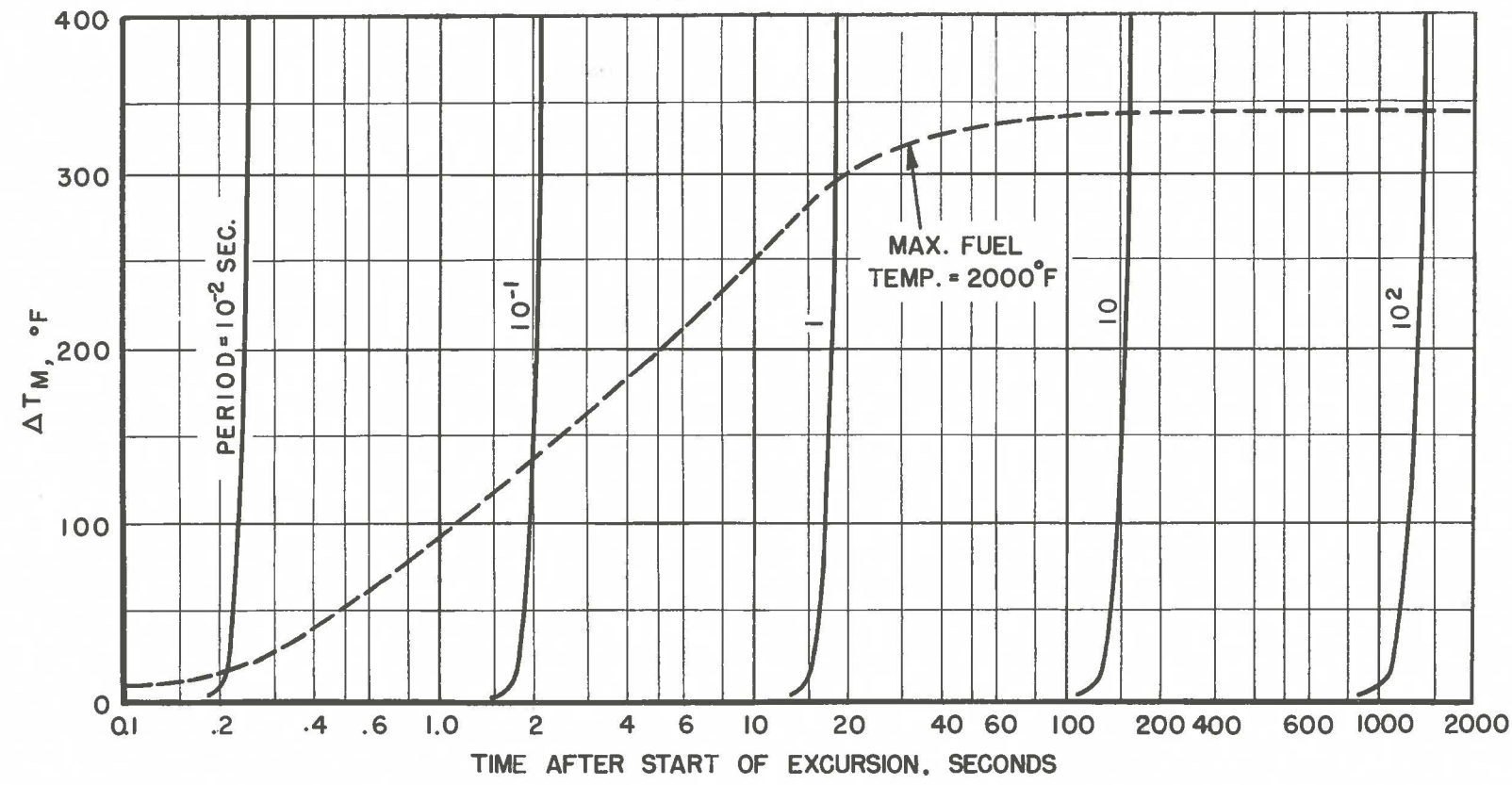


FIG. A-36

MAXIMUM TEMPERATURE DIFFERENCE ( $\Delta T_M$ )  
 ACROSS OPPOSITE FLATS OF A FIFTH ROW SUBASSEMBLY DURING A POWER EXCURSION  
 (FOR THE CASE OF NO COOLANT FLOW)

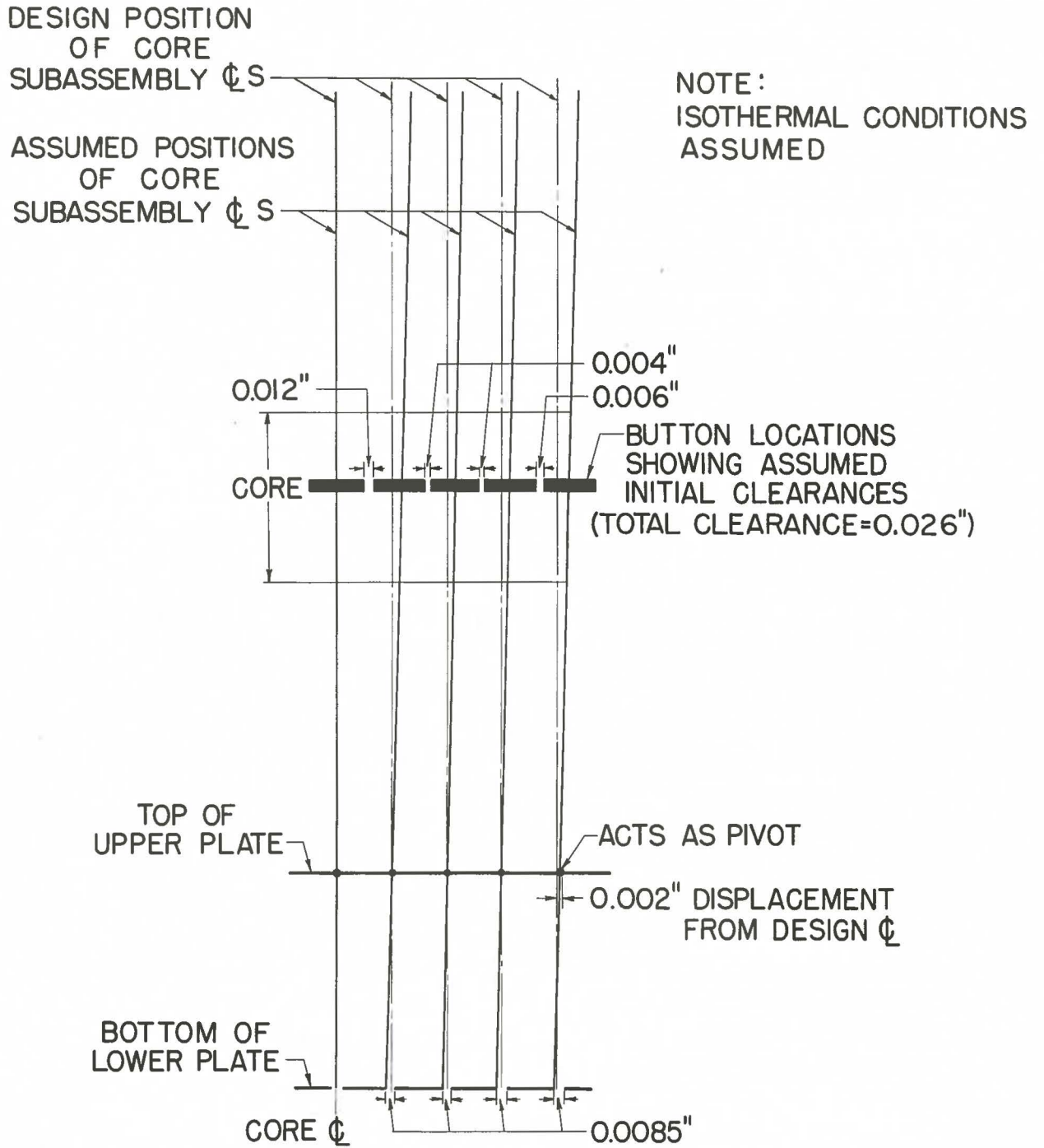


FIG. A-37  
ASSUMED INITIAL POSITION OF CORE SUBASSEMBLIES  
(MOST PESSIMISTIC CASE)

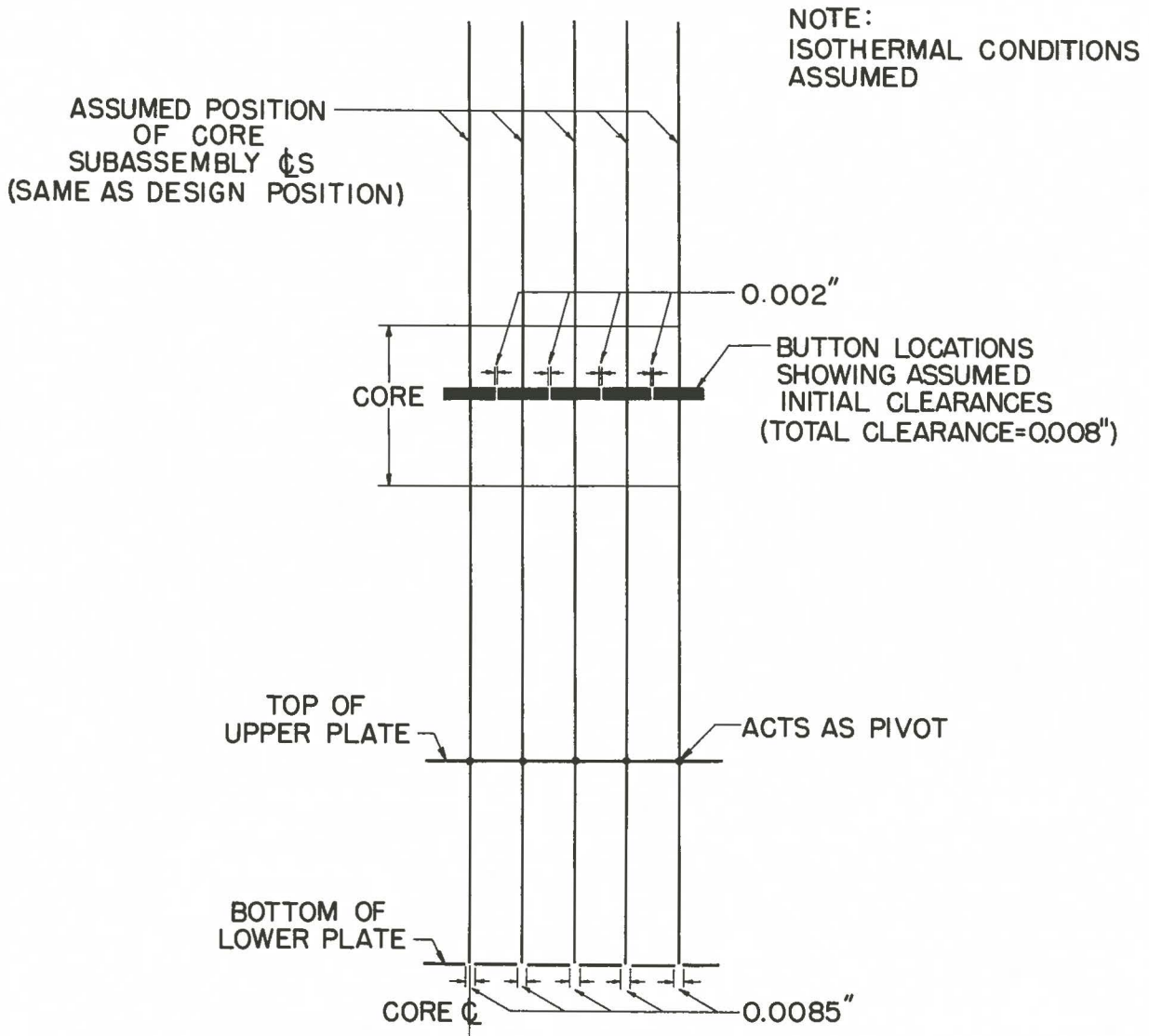


FIG. A-38  
ASSUMED INITIAL POSITION OF CORE SUBASSEMBLIES  
(MOST PROBABLE CASE)

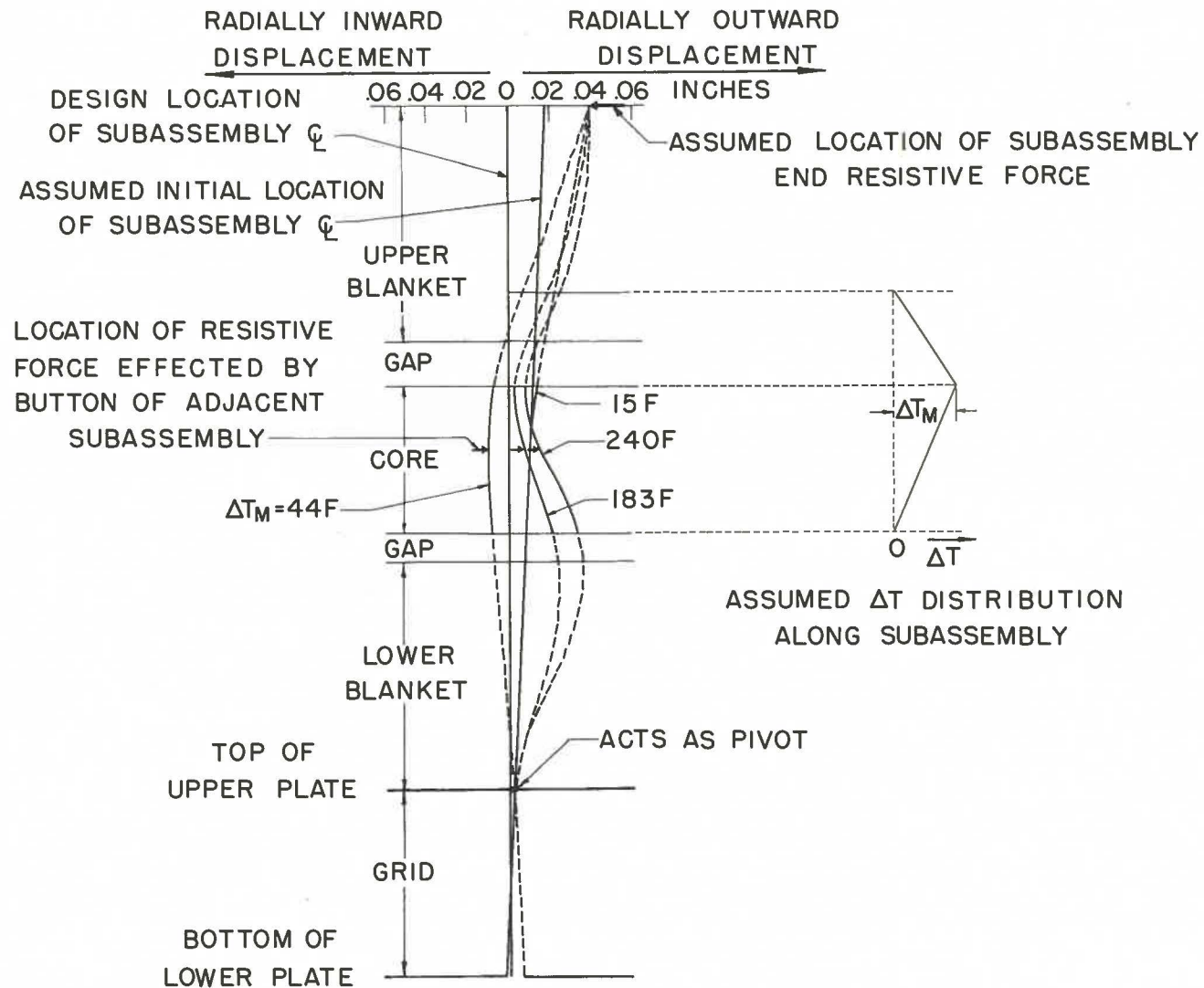


FIG. A-39  
 BOWING OF A FIFTH ROW SUBASSEMBLY  
 (WITH COOLANT FLOW AND MOST PESSIMISTIC INITIAL POSITION)

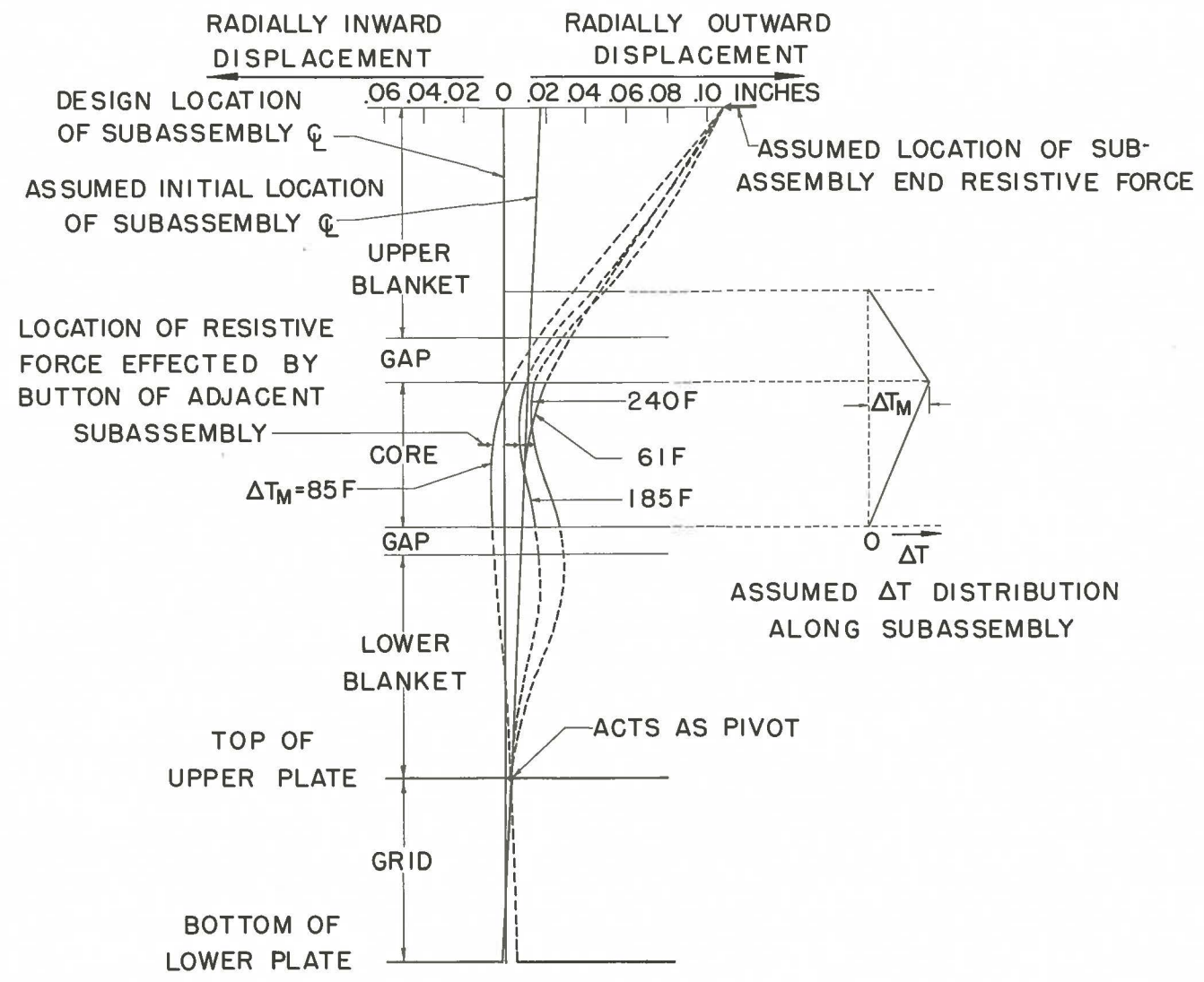


FIG. A-40  
 BOWING OF A FIFTH ROW SUBASSEMBLY  
 (WITH COOLANT FLOW AND MOST PESSIMISTIC INITIAL POSITION)

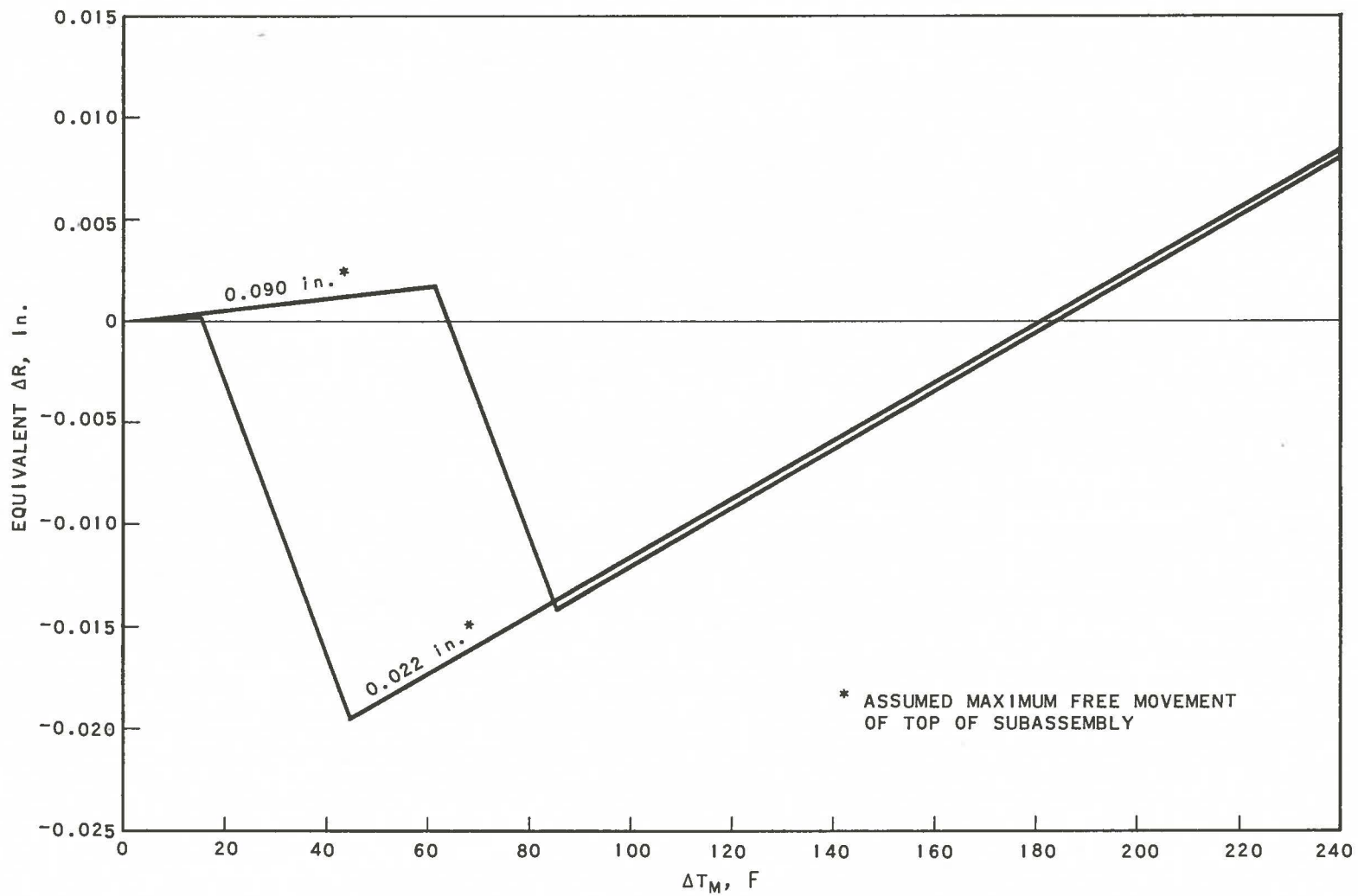


FIG. A-41  
 EQUIVALENT CHANGE IN CORE RADIUS VS MAXIMUM TEMPERATURE  
 DIFFERENCE ACROSS OPPOSITE FLATS OF A FIFTH ROW SUBASSEMBLY  
 (WITH COOLANT FLOW AND MOST PESSIMISTIC INITIAL POSITION)



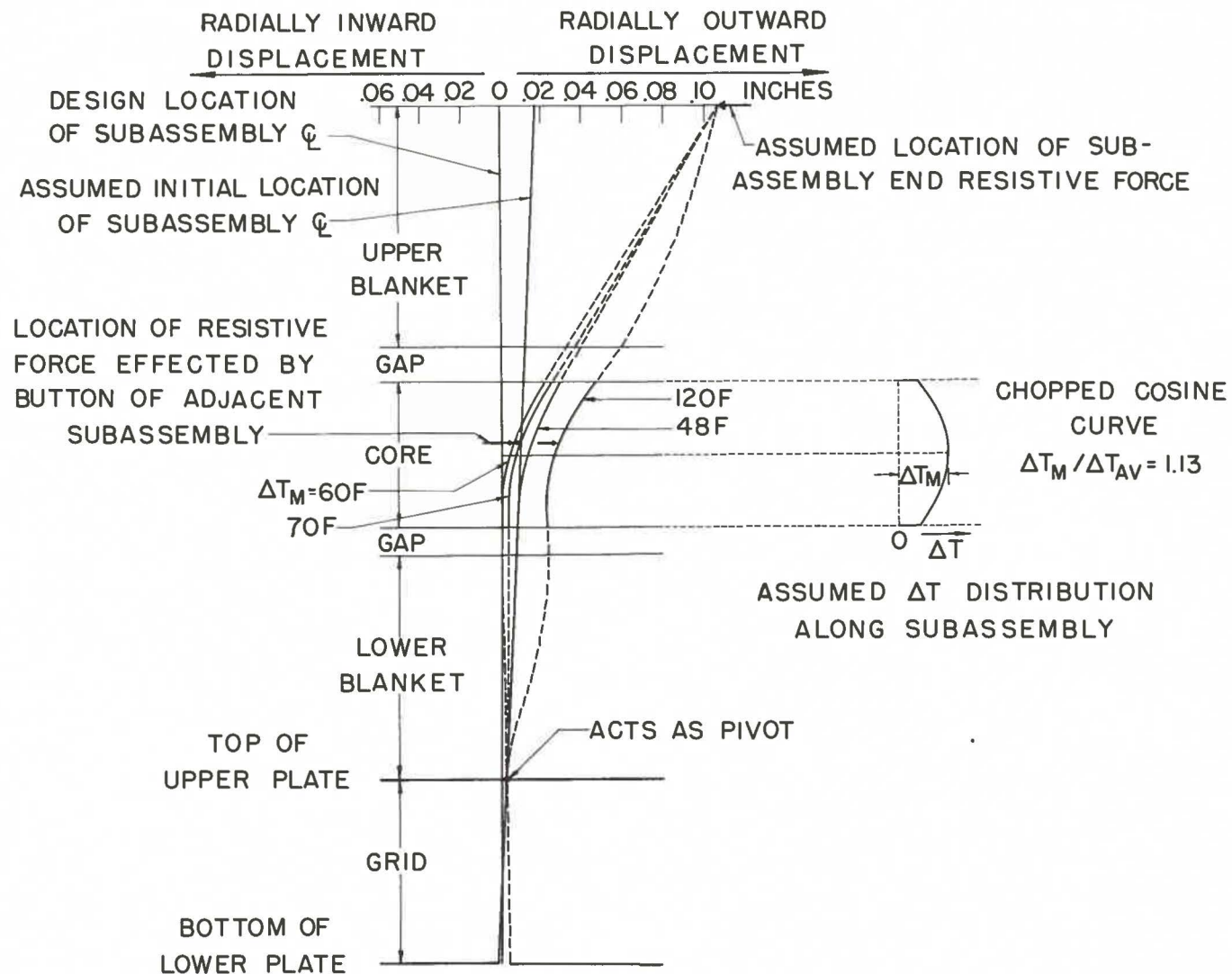
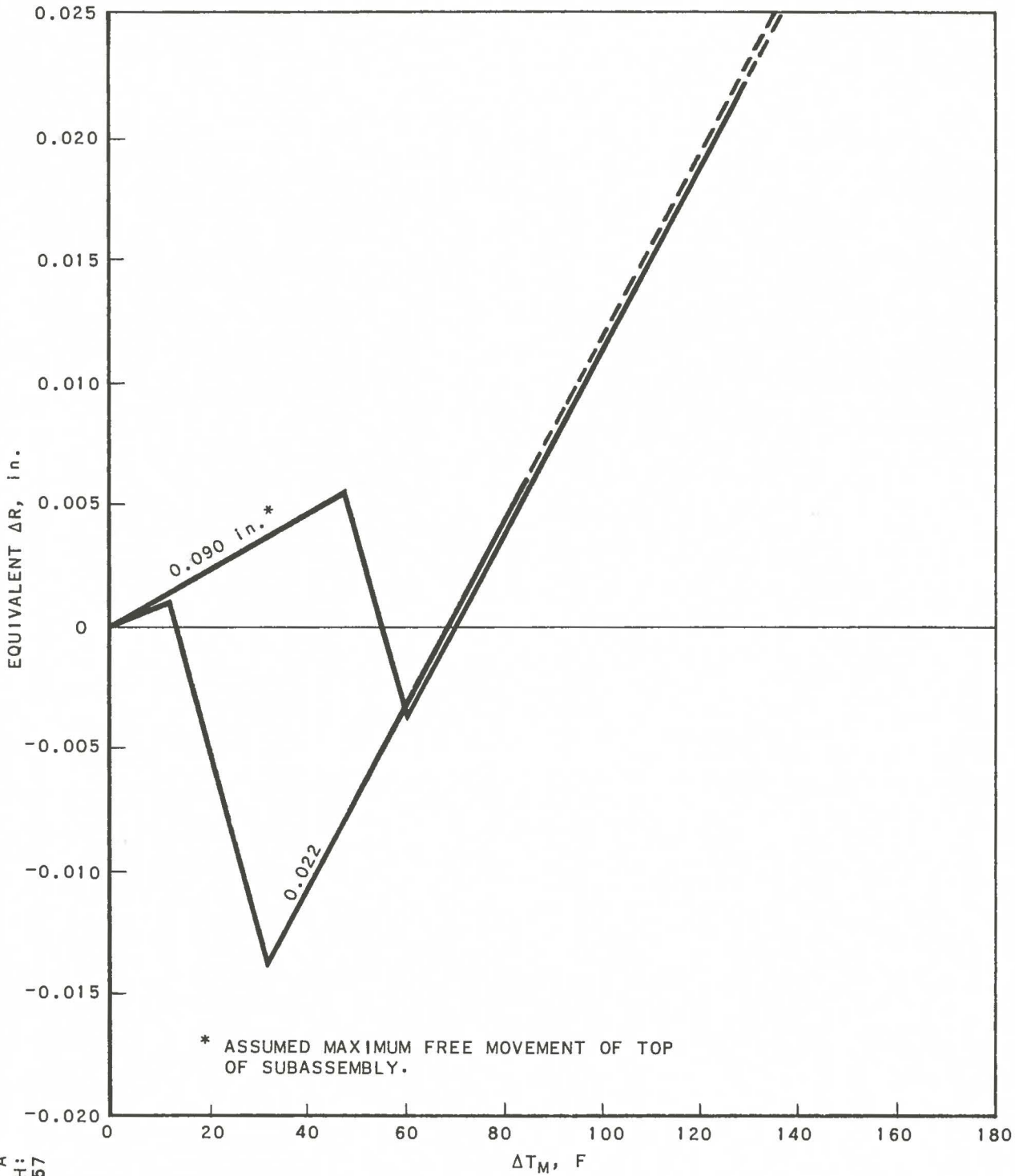


FIG.A-43  
 BOWING OF A FIFTH ROW SUBASSEMBLY  
 (WITH NO COOLANT FLOW AND MOST PESSIMISTIC INITIAL POSITION)



\* ASSUMED MAXIMUM FREE MOVEMENT OF TOP OF SUBASSEMBLY.

RE-7-19981-A  
 J. BURELBACH:  
 S.K., 3-20-57

FIG. A-44  
 EQUIVALENT CHANGE IN CORE RADIUS VS MAXIMUM TEMPERATURE DIFFERENCE ACROSS OPPOSITE FLATS OF A FIFTH ROW SUBASSEMBLY (WITH NO COOLANT FLOW AND MOST PESSIMISTIC INITIAL POSITION)



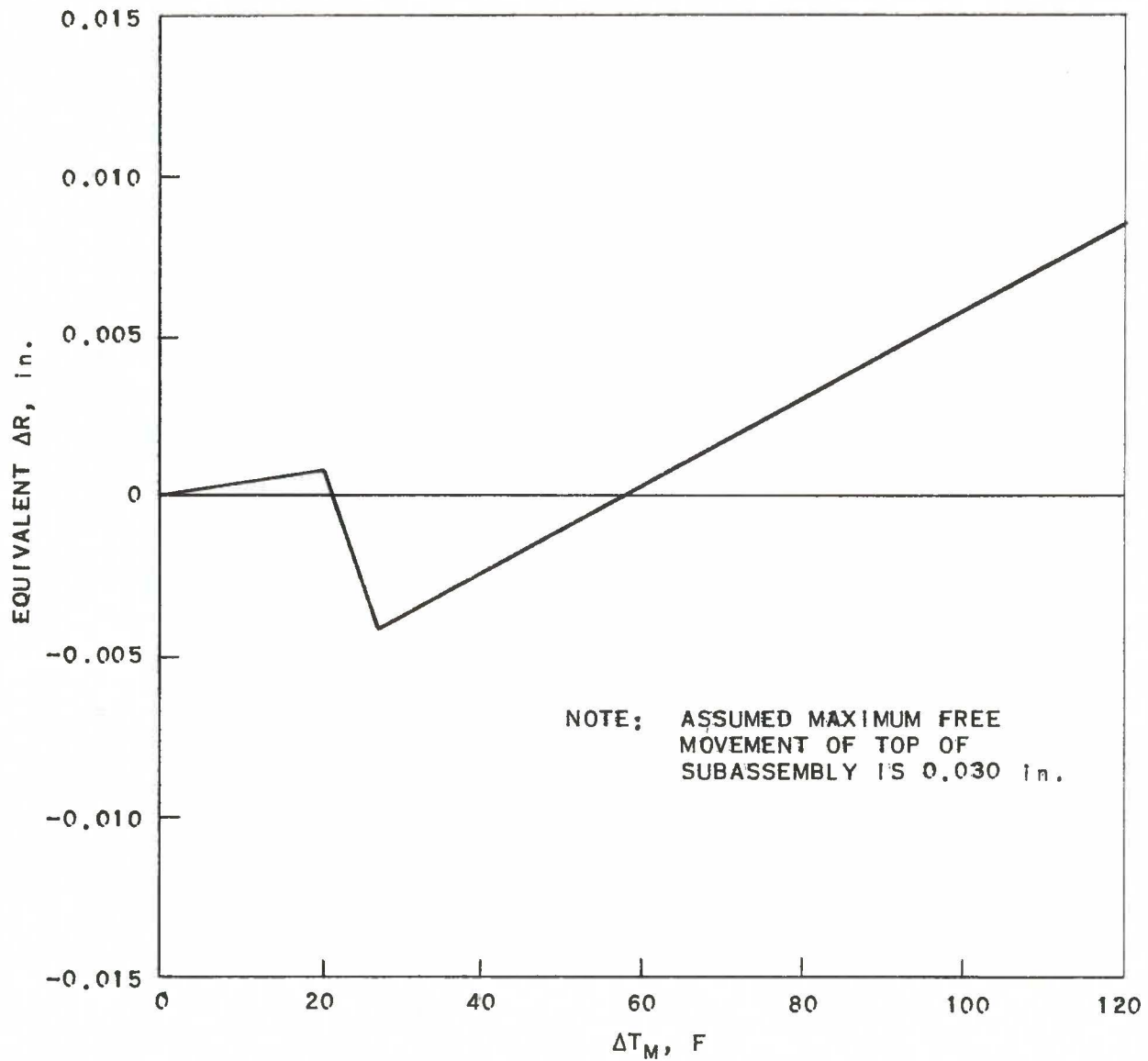


FIG. A - 46  
EQUIVALENT CHANGE IN CORE RADIUS VS MAXIMUM TEMPERATURE DIFFERENCE ACROSS OPPOSITE FLATS OF A FIFTH ROW SUBASSEMBLY (WITH COOLANT FLOW AND MOST PROBABLE INITIAL POSITION)

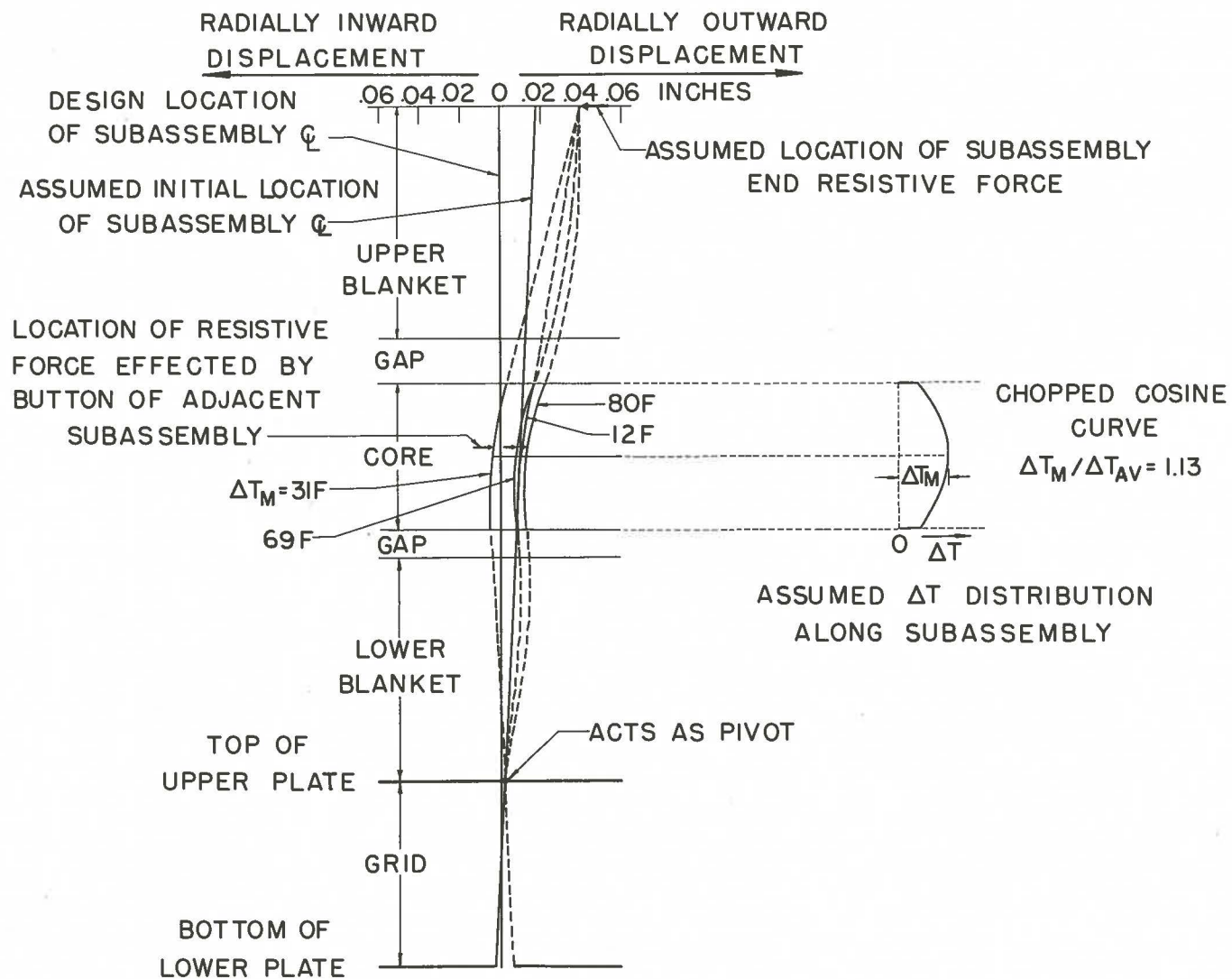


FIG. A-47  
 BOWING OF A FIFTH ROW SUBASSEMBLY  
 (WITH NO COOLANT FLOW AND MOST PESSIMISTIC INITIAL POSITION)

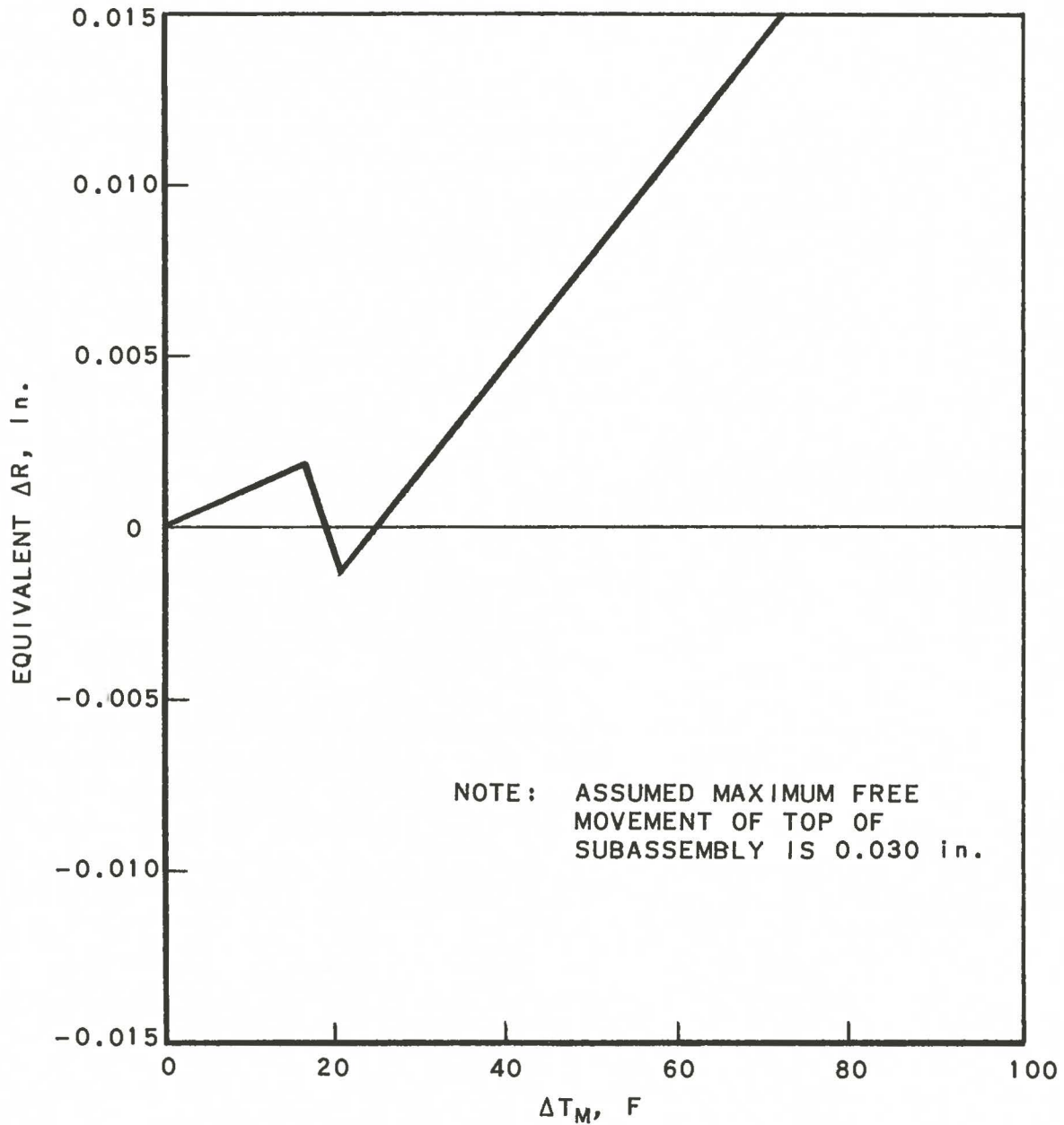


FIG. A-48  
EQUIVALENT CHANGE IN CORE RADIUS VS MAXIMUM TEMPERATURE DIFFERENCE ACROSS OPPOSITE FLATS OF A FIFTH ROW SUBASSEMBLY (WITH NO COOLANT FLOW AND MOST PROBABLE INITIAL POSITION)

## APPENDIX B

DOPPLER EFFECT

Several experiments have been performed in Argonne's fast critical facility, ZPR-III, which shed considerable light on the Doppler effect, and which permit the estimate of a coefficient for EBR-II with some degree of reasonableness.

1. Over-all Temperature Coefficients in Assemblies 2, 2A and 3<sup>1</sup>

Assembly 2 had a cylindrical core of approximately EBR-II composition, surrounded by a thick, high-density, depleted uranium blanket. The core composition (in vol-%), was as follows:

U <sup>235</sup>	14.1
U <sup>238</sup>	16.0
Al	31.5
Stainless Steel	12.4
Void	26.0

The temperature coefficient of reactivity was measured by turning off the heat one cold winter night and allowing the assembly room temperature to drop about 15C. The change in reactivity was measured. The room was allowed to warm up, and the associated reverse reactivity effects were observed. The result was a considerable spread in measured temperature coefficients,  $-4.1 \times 10^{-5} \Delta k/C$  measured cooling down, and  $-1.5 \times 10^{-5} \Delta k/C$  measured warming up. Both measurements were automatically subject to considerable error, due to the small  $\Delta T$  involved. Furthermore, nonuniform temperatures existed in the assembly, also the low temperatures produced some change in alignment of the two halves upon assembly.

Nevertheless, the results were both negative, and average to about  $-2.7 \times 10^{-5} \Delta k/C$ . Calculations were made, using reasonable assumptions on the expansion of the fuel axially, and of the steel matrix laterally, with a resulting coefficient of  $-2.1 \times 10^{-5} \Delta k/C$ . No Doppler effect was included in the calculation.

In assembly 2A, stainless steel was substituted for the depleted uranium in the core. A small increase in critical mass resulted. The core composition was as follows:

U <sup>235</sup>	14.0
U <sup>238</sup>	1.0
Al	31.4
Stainless Steel	27.5
Void	26.1

---

<sup>1</sup>Private communication from C. Branyan, J. K. Long and R. E. Rice.

The measured temperature coefficient was  $-3.3 \times 10^{-5} \Delta k/C$ , with a total  $\Delta T$  of only 10 degrees. The calculation gave  $-2.4 \times 10^{-5} \Delta k/C$  again with no Doppler effect.

While the experimental results for Assemblies 2 and 2A are subject to considerable error, they strongly suggest that a very strong positive Doppler effect in  $U^{235}$  could not have been exactly cancelled out by a very strong negative effect in  $U^{238}$ , in Assembly 2. Or otherwise, the temperature coefficient in 2A would have zero or positive.

Another temperature coefficient was obtained in Assembly 3. Assembly 3 was similar to Assembly 2 in core composition but included a central blanket of medium density, depleted uranium. The increase in critical mass was considerable.

The average neutron energy spectrum in the core was somewhat softer than that of Assembly 2, which might conceivably enhance any Doppler effect. The measured temperature coefficient of reactivity, however, was  $-4.1 \times 10^{-5} \Delta k/C$ .

## 2. First Direct Measurement of Doppler Effect<sup>2</sup>

An experiment was run in Assembly 3 to determine the Doppler effect of  $U^{235}$  in a fast spectrum. Eighty-nine grams of  $U^{235}$  were thermal cycled between 800C and 300C in an assembly having a critical mass of roughly 180 kg of  $U^{235}$ . No effect was seen, but the experiment lacked sufficient sensitivity to say more than that any Doppler effect which may have been present was less than  $9 \times 10^{-11}/C/\text{gram}$  of  $U^{235}$ . This is still about a factor of three greater than has currently been predicted theoretically.<sup>3,4</sup>

## 3. Core Temperature Coefficient in Mock-up of EBR-I<sup>5</sup>

The Doppler effect had remained a possible explanation of the positive prompt coefficient in EBR-I, even though bowing of the fuel elements also appeared as a contributor to this effect. It was decided to mock up EBR-I in ZPR-III, using the regular fuel plates, steel plates, depleted uranium plates, etc., of normal ZPR operation. Aluminum was substituted for NaK. Electric heaters in the core, plus insulation and a cooling air stream between core and blanket, allowed the heating of the core alone. Of course, no bowing, such as might have occurred in EBR-I, was possible; but if a Doppler effect existed, it would carry over.

<sup>2</sup>Personal communication from W. Y. Kato and D. K. Butler.

<sup>3</sup>H. Yamauchi and J. DeFelice. "Doppler Temperature Coefficients of Reactivity in Fast Reactors," NDA-14-82, June 17, 1955

<sup>4</sup>G. Goertzel and C. Klahr, "Interpretation of an Experiment to Measure Doppler Effect," NDA-14-127, June 29, 1956.

<sup>5</sup>Personal communication from J. K. Long.

The axial displacement of the fuel underheating was calculated, using a measured linear coefficient of expansion of  $18 \times 10^{-6}$  in./in./C. This is believed to be a fairly accurate representation, if the springs were truly holding fuel plates at the drawer fronts. The lateral displacement of the core under heating is not subject to calculation, due to the method of construction. An attempt was made to measure the horizontal growth of the core, by means of a pair of probes. The results were not completely reproducible. Furthermore, the measurements varied depending on whether the probe touched matrix tube or fuel plate.

The results of the best experimental run were as follows:

$\Delta k/C$	$1.07 \times 10^{-5}$
Lateral expansion, in/C	$1.10 \times 10^{-4}$ (probe on fuel plate)
	$0.77 \times 10^{-4}$ (probe on matrix tube)
	$0.94 \times 10^{-4}$ average

If we assume the same expansion vertically or horizontally, for a core of length 8.08 in., and equivalent radius 3.42 in., we get the following percent change in volume for heating of 100 degrees.

$$\begin{aligned} \text{Old volume} &= \pi(3.42)^2 8.08 = 296.7517 \\ \text{New volume} &= \pi(3.4247)^2 8.08(1.0018) = 298.1035 \end{aligned}$$

Hence

$$\frac{V_{\text{new}}}{V_{\text{old}}} = 1.00456,$$

and

$$\frac{\Delta V}{V} = 0.00456.$$

From UNIVAC problems 17545 and 17546, we calculate that the relationship  $\frac{\Delta k}{k} = 0.3 \frac{\Delta V}{V}$  for the case of core expansion only in this assembly (#7). Hence, theoretically we predict a core temperature coefficient of approximately  $-(0.3)(0.00456) \times 100 = -1.37 \times 10^{-5} \Delta k/C$ , with an uncertainty of at least 25%. If we took as true the values  $-1.37 \times 10^{-5}$  (calculated without Doppler Effect) and  $-1.07 \times 10^{-5}$  (measured), we might guess the difference of  $+0.30 \times 10^{-5} \Delta k/C$  was due to a small positive Doppler effect. This is slightly less than the predicted theoretical value for EBR-I.

Hence, the experiment strongly indicates that the Doppler effect was not the primary cause of the much larger positive prompt coefficient in EBR-I. Also, the experimental results are in best agreement with theory if a Doppler effect equal to or less than theory is used.

#### 4. Second Measurement of Doppler Effect<sup>6</sup>

A more sensitive measurement of the Doppler effect for  $U^{235}$  has been completed in Assembly 7 at ZPR-III. A helical element was thermal cycled in the center of this mock-up of EBR-I, and the resulting flux changes observed. The element was a 41-turn nickel clad, fully enriched uranium helix containing 506 grams of  $U^{235}$ . The element was made of a 1/8 in. diameter rod, wound into the form of a helix or spring of 1 in. ID with a length between 6 and 7 $\frac{1}{2}$  in. It was mounted on a porous frit filter which was fused to pyrex tubing (1 in. dia.). This was then mounted inside vycor tubing (2 in. OD) so that it would fit into one of the openings of the ZPR-III matrix. The element was heated electrically by passing a current through the helix. It was cooled by flowing chilled helium past the turns of the helix through the porous frit filter.

The experiment was conducted in two parts. The helical element was first thermal cycled in an EBR-I type mock-up with  $U^{235}$  as the fuel. The assembly was then reloaded with plutonium as fuel, maintaining approximately the same geometry, as the element was thermal cycled again. The purpose of thermal cycling the uranium helix in the plutonium fueled assembly was to obtain an estimate of the effect of motion on reactivity. In this experiment two principal effects can produce a small but measurable reactivity change. The Doppler effect of the uranium resonances of the element interacting with the uranium resonances of the core, and small motions of the element due to expansion as a result of heating can each produce a reactivity change. In order to obtain a true Doppler effect measurement it is necessary to correct the observed reactivity change upon thermal cycling for the effect due to this motion.

Expansion of the uranium rod resulted principally in an increase of the diameter of the helix. The expansion of the turns of the helix was measured using a traveling microscope. The average measured radial expansion compared very well with the theoretically calculated expansion. This, together with the measured effects on reactivity of  $U^{235}$  displacement, allowed an estimate of the reactivity change from the expansion motion of the helix. This estimate was checked by the reactivity change observed when the  $U^{235}$  helix was thermal cycled in the plutonium fueled assembly, where any Doppler effect should be very sharply reduced in magnitude.

The small reactivity change was measured by observing the change in neutron flux using four boron coated and  $BF_3$ -filled ion chambers. The signal was observed using a resonant amplifier tuned to the thermal cycling frequency. It was necessary to use the pile oscillation technique to observe

---

<sup>6</sup>W. Y. Kato and D. K. Butler, "Measurement of the Uranium Doppler Temperature Effect in a Fast Assembly," First Winter Meeting (Dec. 10-12, 1956) American Nuclear Society.

the change in neutron flux because the Doppler effect produces only a very small change in reactivity, since only a small fraction of the critical mass of the assembly was thermal cycled. Reactivity changes,  $\frac{\Delta k}{k}$ , of the order of  $10^{-6}$  and  $10^{-7}$  were expected.

Preliminary results are described below:

(a) Enriched uranium helix in  $U^{235}$ -fueled assembly (506 gm  $U^{235}$ ). Effective temperature cycle  $\sim 50 - 169C$ ;  $\Delta T = 119C$ .

$$\begin{aligned} \text{Observed } \frac{\Delta k}{k} &= 1.1 \times 10^{-6} / 506 \text{ gm } U^{235} / 119C \\ &= 1.8 \times 10^{-11} / \text{gm } U^{235} / C \end{aligned}$$

(b) Enriched uranium helix in Pu-fueled assembly (506 gm  $U^{235}$ ). Effective temperature cycle  $\sim 94 - 236C$ ;  $\Delta T = 142 C$

$$\begin{aligned} \text{Observed } \frac{\Delta k}{k} &= 0.42 \times 10^{-6} / 506 \text{ gm } U^{235} / 142C \\ &= 0.58 \times 10^{-11} / \text{gm } U^{235} / C \end{aligned}$$

This reactivity effect should be due principally to the motion of the helix.

(c) Calculated reactivity effect for the radial motion. Based on the radial expansion of  $3.4 \times 10^{-3}$  in. for each turn.

$$\begin{aligned} \frac{\Delta k}{k} &\sim 0.7 \times 10^{-6} / 506 \text{ gm } U^{235} / 119C \\ &\sim 1.2 \times 10^{-11} / \text{gm } U^{235} / C \end{aligned}$$

If we take the measured effect in Pu as a rough lower limit on the motion effect, we get

$$\frac{\Delta k}{k} \text{ (Doppler effect)} \leq + 1.2 \times 10^{-11} / \text{gm } U^{235} / C$$

for the temperature range involved. This neglects the relative importance of the sample, compared to the average position - an effect which is expected to be small in this particular experiment.

This experiment may be compared with the predictions of theory, using the treatment of Goertzel and Klahr.<sup>4</sup> We have that

$$\frac{\Delta \tilde{\mu}_a \text{ unheated}}{\Delta \tilde{\mu}_a \text{ heated}} = \frac{\sqrt{\frac{2 T_0}{T_0 + T_a}} - \sqrt{\frac{2 T_0}{T_0 + T_b}}}{\sqrt{\frac{T_0}{T_a}} - \sqrt{\frac{T_0}{T_b}}}$$

where  $T_0 = 293\text{C}$   
 $T_a = 323\text{C}$   
 $T_b = 442\text{C}$  .

This ratio equals 0.6. Thus, for a critical mass ~ 60 kg, we have;

$$\frac{(\Delta k)_{\text{experiment}}}{(\Delta k)_{\text{heated reactor}}} = \frac{0.506}{60} (0.6) = 4.8 \times 10^{-3}$$

Hence, had we heated the entire reactor from 50 to 169C, we would have obtained

$$\frac{(1.1 - 0.42) \times 10^{-6}}{4.8 \times 10^{-3}} = 0.00014 \Delta k/k \text{ increase in reactivity.}$$

Yamauchi and DeFelice<sup>3</sup> obtain Doppler reactivity coefficients of 6.0, 5.4 and  $4.8 \times 10^{-6}$  ( $\Delta k/k$ )/C at 20C for three different assumptions of resonance level distributions for  $U^{235}$ . If we take  $5 \times 10^{-6}$  as representative of this calculation, we find that for the same temperature range, a reactivity increase of  $0.0004 \Delta k/k$  is predicted, or a factor of three higher than experiment.

It is noted that more recent theoretical work<sup>7,8</sup> suggests that the calculated values should be smaller, perhaps only 1/6 the earlier theoretical results. It must also be noted that some uncertainties still exist in the latest experiment, and that the results should be considered to give order of magnitude only.

## 5. Conclusion

As a result of these experiments it is considered reasonable at the present time to assume a Doppler coefficient for EBR-II equal to half that calculated in NDA-14-82, namely  $1.5 \times 10^{-6}$  ( $\Delta k/k$ )/C at 20C. It is recognized that considerable uncertainties still exist in the coefficient for EBR-I, let alone EBR-II, which remains to be measured; hence a larger fraction of theory than was measured for EBR-I has been assigned to be conservative.

---

<sup>7</sup>A. M. Lane, J. E. Lynn, J. S. Story, "An Estimation of the Doppler Effect in Fast Neutron Reactors," AERE T/M 133

<sup>8</sup>Private communication, H. A. Bethe.

## APPENDIX C

MAXIMUM CREDIBLE NUCLEAR ACCIDENTS

The reactor core design is such that so long as it holds its basic shape, namely solid fuel and blanket elements, no serious nuclear accidents are believed to be possible (see Appendix A). Assuming that the core has melted, in part or in its entirety, however, the situation becomes less straightforward. While it is difficult to demonstrate with assurance that any particular prompt critical configuration will result, it is equally difficult to prove that none will occur. It is even more difficult to estimate with what reactivity addition rate the assembly would pass through prompt critical.

In this appendix, therefore, we will not calculate any particular accident and label it as "the" maximum accident. Instead, we shall estimate some sort of upper limit on the reactivity addition rate possible from gravity, assuming a strictly hypothetical set of circumstances and coincidences. Then for a wide range of reactivity addition rates, we shall calculate the strength of the nuclear explosion for a melting core. The method of analysis used is a modified Bethe-Tait<sup>1</sup> calculation, and it will be described in some detail.

In the accidents considered here, it is assumed the core has lost its general structure, and heating of its components by a rise in power produces no reactivity effect similar to that of expansion in the solid core. Until the material reaches very high temperatures, so that some boiling of uranium has taken place, the expansion is considered to be local, filling in voids, but not enlarging the core radius. The reactivity insertion rates are large, and the reactor goes beyond prompt critical, before a sudden surge of power produces high pressures and a violent disassembly.

Actually, the events can be divided conveniently into three stages: reactivity insertion, reactivity reduction by outward motion of core and possibly a blanket, and subsequent expansion to release the high pressures. In the first stage reactivity is being inserted mechanically, by the fall of a part of the fissionable material into the remainder. Mechanisms of reactivity reduction are assumed to be negligible during this period. When the critical temperature is reached, however, the time rate of reactivity reduction increases very sharply, resulting in a sharp division between the first and second stage. Due to this fact, also, the second stage lasts a very short time, usually less than two e-folding times. During this stage we can neglect mechanical reactivity insertion entirely.

After the reactivity drops below prompt critical, there is little additional heat being generated, but the expansion proceeds until the pressures developed in the interior of the reactor are relieved.

---

<sup>1</sup>H. A. Bethe and J. H. Tait, "An Estimate of the Order of Magnitude of the Explosion When the Core of a Fast Reactor Collapses." RHM(56)/113.

## 1. Reactivity Insertion Rates

To estimate the maximum reactivity insertion rates conceivably resulting from the forces of gravity, the following pessimistic set of hypotheses were made.

- a. The sodium has boiled away from the center of the reactor.
- b. The uranium from the middle of the core has trickled down into the lower part of the core and is retained there, producing a region abnormally dense in enriched uranium at the core bottom, with a large gap at the core center.
- c. At the worst possible moment, the upper portion of the core falls as a single unit, producing a prompt critical configuration at the highest possible insertion rate.

While the middle part of the core is being lost to the bottom part, reactivity decreases for awhile, since fissionable material is being transferred from a position of greater importance to one of lesser importance. If this fuel is retained at the bottom, the density there can rise sufficiently to reverse the reactivity trend and start raising the multiplication of the system as a whole.

Multigroup slab calculations done on the UNIVAC have given the minimum  $k_{\text{eff}}$  as resulting when 17% of the middle of the core has melted out and is distributed uniformly in the bottom part. The reactivity loss associated with this reorientation is calculated to be 12% in  $k$ .

If the upper part of the reactor is then disturbed so that it starts to fall, it has a fairly long distance to cover before the assembly reaches prompt critical. The speed of the fall being greater the longer the distance of the fall, we expect the maximum rate of reactivity insertion in the cases when the fall starts with the reactor as much below critical as possible. However, the reactivity increase for a motion of the upper part of 1 cm is smaller when the gap is large and when a smaller remaining upper mass of fissionable material is moved. Thus the maximum rate of reactivity insertion at prompt critical has been found to occur when only 10% of the middle part has been melted out. UNIVAC calculations (17737 to 17757) have shown that the maximum rate of reactivity insertion reaches 600\$/sec in this case and that the maximum is quite flat. Thus the probability of being in the vicinity of this high rate of reactivity insertion is quite large; provided, of course, that the whole of the upper part falls down at the same time, and that all the other assumptions also hold.

Actually, even this high insertion rate is not truly an upper hypothetical limit. If for some reason the reactor is more highly subcritical when the upper portion falls as a unit, it has a longer distance to fall, hence

produces a critical configuration at a still higher insertion rate. For example, if the control rods had been withdrawn at the beginning of the meltdown, the entire process would have begun with the reactor some 6% below critical. It is possible to calculate reactivity insertion rates in this case as high as 800 or 1000\$ /sec.

It must be reiterated, it is not claimed that these are realistic insertion rates. It seems unlikely that rates a tenth as large could occur, in view of the severe conditions required to accomplish the high values.

## 2. Method of Calculation

### a. Total Reactivity Insertion Before Disassembly

In the following it will be assumed that the accident starts when the reactor is at a very low power level, so that there is no appreciable heating for a while. The amount of heat developed increases extremely rapidly, however, (Eq. 2), and the shutdown rate is sharply dependent upon the amount of heat developed. Thus, from a rough guess of total energy developed,  $Q^1$ , one can determine fairly accurately the maximum reactivity reached.

If  $\frac{dk}{dt}$  is the rate of reactivity insertion and  $\tau$  is the prompt generation time then the change in multiplication rate  $\lambda$  is

$$\mu = \frac{d\lambda}{dt} = \frac{1}{\tau} \frac{dk}{dt} \quad (1)$$

The time rate of change in power,  $n$ , if no reactivity reduction mechanism is operative, is

$$\dot{n} = \mu t n$$

Thus the power at time  $t$  after prompt critical is

$$n(t) = n(0) \exp\left(\frac{1}{2} \mu t^2\right)$$

The amount of heat developed is

$$\begin{aligned} Q(t) &= \int n dt = n(0) \int_0^t \exp\left(\frac{1}{2} \mu t^2\right) dt \\ &\approx \frac{n(0)}{\mu t} \exp\left(\frac{1}{2} \mu t^2\right) \left[1 + \frac{1}{\mu t^2} + \dots\right] \end{aligned} \quad (2)$$

From this expression we find that the time,  $t$ , at which the amount of heat developed reaches  $Q^1$  is given by

$$\mu t_1^2 = 2 \ln \frac{Q^1 \mu^{\frac{1}{2}}}{n(0)} + \ln \left[ 2 \ln \frac{Q^1 \mu^{\frac{1}{2}}}{n(0)} \right] + \dots \quad (3)$$

The reactivity reached at this time is

$$\rho = t_1 \frac{dk}{dt} = \sqrt{\mu t_1^2} \cdot \sqrt{\tau \frac{dk}{dt}} \quad (4)$$

where  $\mu t_1^2$  is given by (Eq. 3). Thus the maximum reactivity reached depends very little on maximum energy reached, when the excursion is very large

$$2 \ln \frac{Q^1 \mu^{\frac{1}{2}}}{n(0)} \gg 1$$

Assuming that the final energy developed is  $Q^1 = 1.1 \times 10^3$  joules/gram of  $U^{235}$ , and that the initial power at prompt critical is  $n(0) = 3.3 \times 10^{-4}$  watts/gram of  $U^{235}$ , also that the reactivity insertion rate varies from  $10^1$  to  $1000^{\dagger}$  \$/sec, we find that  $\frac{Q^1 \mu^{\frac{1}{2}}}{n(0)}$  lies between 48.2 and 52.8. For this range  $\sqrt{\mu t_1^2}$  lies between 7.2 and 7.5, and a factor of  $e = 2.718$  in  $Q^1$  or  $n(0)$  changes  $\sqrt{\mu t_1^2}$  by 2%. The same factor of  $e$  in either  $\tau$  or  $dk/dt$  changes  $\sqrt{\mu t_1^2}$  by only 1%.

#### b. Reactivity Reduction During Violent Disassembly

We have assumed that the reactor has lost its structure and that the sodium has been boiled away from the reactor center. Hence preliminary heating and expansion of the core materials only tends to fill the voids and does not produce an over-all core expansion and resulting loss of reactivity. Not until the energy density reaches some critical value  $Q^*$  do we assume that a pressure begins to build up and produce motion. The critical value  $Q^*$  is reached first in the center of the reactor and the expansion starts there with the outer parts of the core still at rest. Gradually the energy density  $Q^*$  is reached by the outer parts of the reactor core, while the middle part continues to expand.

Outward motion of the fissionable material causes a reduction in reactivity. It can be demonstrated that the displacement ( $u$ ) of reactor material is equivalent to the increase of the diffusion coefficient, and the change in reactivity can be found by first order perturbation theory. Assuming that the reactor is spherical the diffusion equation before expansion is

$$\frac{1}{r^2} \frac{d}{dr} \left( \frac{1}{3\Sigma_{tr}} r^2 \frac{d\Phi}{dr} \right) + (\nu_0 - 1) \Sigma_f \Phi - \Sigma_c \Phi = 0 \quad (5)$$

After the expansion has taken place the element of the reactor with a coordinate  $r$  has moved into the position  $R = r + u$  and the density of the material has increased by factor  $\theta$ , causing the increase of all macroscopic cross section also by factor  $\theta$ . Thus the diffusion equation after the expansion is:

$$\frac{1}{\theta} \frac{1}{R^2} \frac{d}{dR} \left( \frac{1}{3\theta \Sigma_{tr}} R^2 \frac{d\Phi^1}{dR} \right) + (\nu - 1) \Sigma_f \Phi^1 - \Sigma_c \Phi^1 = 0 \quad .$$

Because the amount of the material is conserved,

$$\theta R^2 dR = r^2 dr \quad .$$

We can rewrite the previous equation in the form:

$$\frac{1}{r^2} \frac{d}{dr} \left( \frac{1}{3\Sigma_{tr}} \frac{R^4}{r^4} r^2 \frac{d\Phi^1}{dr} \right) + (\nu - 1) \Sigma_f \Phi^1 - \Sigma_c \Phi^1 = 0$$

or approximately:

$$\frac{1}{r^2} \frac{d}{dr} \left[ \frac{1}{3\Sigma_{tr}} \left( 1 + 4 \frac{u}{r} \right) r^2 \frac{d\Phi^1}{dr} \right] + (\nu - 1) \Sigma_f \Phi^1 - \Sigma_c \Phi^1 = 0 \quad (6)$$

Comparing this equation with (Eq. 5) we see that only the diffusion coefficient,  $\frac{1}{3\Sigma_{tr}}$ , has been altered. And by the first order perturbation theory we can say that the change in reactivity is:

$$\rho = \frac{\Delta\nu}{\nu} = - \frac{\int \frac{4u}{r} \frac{\Sigma_{tr}}{3} \left( \frac{1}{\Sigma_{tr}} \frac{d\Phi}{dr} \right)^2 r^2 dr}{\int \nu_0 \Sigma_f \Phi^2 r^2 dr} \quad (7)$$

The denominator in this expression does not depend on the displacement ( $u$ ) and can be estimated if the cross sections and flux distributions are known. Bethe-Tait<sup>1</sup> make an underestimate obtaining for (Eq. 7):

$$\rho = - \frac{\int 4 u \left( \frac{d\Phi}{dr} \right)^2 r dr}{(2.54 \times 0.8)(b)(q)^{-\frac{1}{2}}} \quad , \quad \dots \quad (8)$$

where  $b$  is the radius of the core of the reactor and  $(1 - q)$  is the flux at the edge of the core. The flux ( $\Phi$ ) is here normalized to yield  $\Phi(r=0) = 1$  at the center.

To obtain the displacement ( $u$ ) for our case we have to solve a forced wave equation:<sup>2</sup>

$$\frac{\partial^2 u}{\partial t^2} - C^2 \left( \frac{\partial^2 u}{\partial r^2} + \frac{2}{r} \frac{\partial u}{\partial r} - \frac{2}{r^2} u \right) = - \frac{1}{s} \frac{\partial p}{\partial r} \quad (9)$$

where  $C$  is the wave velocity,  $p$  is the pressure and  $s$  is density of core material, fuel, and diluent. However the velocity of wave propagation is small compared with the speed at which the thermal shock wave travels in the case of fast accidents. Thus neglecting the wave term we have a simple equation of motion:

$$\ddot{u} = - \frac{1}{s} \frac{\partial p}{\partial r} = - (\gamma - 1) \frac{\partial E}{\partial r} \quad (10)$$

if we assume that:

$$p = (\gamma - 1) (E - Q^*) s \quad (11)$$

For smaller amounts of excess reactivity and consequently slower rates of propagation of the thermal shock wave, it will be shown in the addendum that the displacement ( $u$ ) is altered appreciably by the propagation of the wave, however the reduction in reactivity (Eq. 8) is not influenced by the wave part of (Eq. 9) if  $\frac{\partial \Phi}{\partial r} \propto r$ , as it will be assumed in this calculation. We will also assume that the energy density developed conserves its spatial shape at all times:

$$E(r,t) = Q(t) N_0(r) \quad (12)$$

Also, as we have already mentioned, pressures start being generated only after energy density reaches  $Q^*$ . Thus equation of motion (Eq. 10) can be rewritten in more explicit form as

$$\ddot{u} \begin{cases} = 0 & \text{if } t < t_0(r) \\ = (\gamma - 1) Q(t) \left( - \frac{dN_0}{dr} \right), & \text{if } t > t_0(r) \end{cases} \quad (13)$$

where  $t_0(r)$  is the time at which the energy density reaches  $Q^*$  at  $r$ ,

$$E(r,t_0) = Q^* = Q(t_0) N_0(r) \quad (12a)$$

---

<sup>2</sup>Compare G. E. Hansen, "Burst Characteristics Associated With Slow Assembly of Fissionable Materials," LA-1441, Eq. II-10.

Differentiating Eq.(8) twice with time and substituting Eq. (13) we see that:

$$\begin{aligned} \frac{d^2\rho}{dt^2} &= - \frac{5}{2.54} \frac{\sqrt{q}}{b} \int \ddot{u} \left( \frac{d\Phi}{dr} \right)^2 r dr \\ &= - \frac{5}{2.54} \frac{\sqrt{q}}{b} (\gamma - 1) Q(t) \int_0^{r_1} \left( -\frac{dN_0}{dr} \right) \left( \frac{d\Phi}{dr} \right)^2 r dr \end{aligned} \quad (14)$$

where  $r_1$  is the radius of expansion front at time  $t$ :

$$Q^* = Q(t) N_0(r_1) . \quad (12b)$$

Given power and flux distributions, e.g.,

$$N_0(r) = \Phi(r) = 1 - \frac{q r^2}{b^2} \quad (15)$$

from Eq.(14) and Eq. (12b) we obtain an explicit expression for the reactivity as a function of time.

$$\frac{d^2\rho}{dt^2} = - \frac{8}{2.54} \frac{q}{b^2} (\gamma - 1) Q(t) \left[ 1 - \frac{Q^*}{Q(t)} \right]^{\frac{5}{2}} \quad (14a)$$

This equation together with definition of reactivity above prompt critical:

$$\rho = \tau \frac{d}{dt} \ln \dot{Q} , \quad (16)$$

forms our kinetic equations.

Now the reactivity reduction is very small initially but rises very rapidly. Thus with a fair approximation we can assume that heat developed increases exponentially:

$$Q(t) = Q^* e^{\lambda t} \quad (17)$$

where

$$\lambda = \rho/\tau$$

and find the reactivity reduction directly from Eq.(14a). Substituting Eq.(17) into Eq. (14a), expanding in a power series, and performing integrations we have for large  $\lambda t$

$$\begin{aligned} \rho = - \frac{8}{2.54} \cdot (\gamma - 1) Q^* \frac{q}{b^2 \lambda^2} \left\{ e^{\lambda t} - 1.25(\lambda t)^2 + 0.7009 \lambda t \right. \\ \left. - 2.7915 + 1.875 e^{-\lambda t} - 0.078125 e^{-2\lambda t} - \dots \right\} \end{aligned} \quad (18a)$$

While for very small  $\lambda t$  the integration gives

$$\rho = -\frac{8}{2.54} \cdot \frac{4}{63} (\gamma - 1) Q^* \frac{q}{b^2 \lambda^2} \left(\frac{qr_1^2}{b^2}\right)^{\frac{9}{2}} \left\{ 1 + 2.0909 \left(\frac{qr_1^2}{b^2}\right) + 3.0909 \left(\frac{qr_1^2}{b^2}\right)^2 + 3.9711 \left(\frac{qr_1^2}{b^2}\right)^3 + \dots \right\}, \quad (18b)$$

a slowly converging expression equivalent to (5.18) of Bethe-Tait.<sup>1</sup> Our reactivity reduction Eq. (18a) vs. time has been illustrated by a solid line in Fig. C-1.

For very large amounts of excess reactivity the expansion will reach the edge of the core before shutdown occurs. Then for quite a while there is no expansion inside the blanket since the energy density developed there is too low to burst hex tubes. The core, however, continues to expand.

It seems obvious that a lower limit for reactivity reduction will be obtained if we consider only the expansion inside the core, using core radius,  $b$ , as an upper limit of the integral in Eq. (14) instead of  $r_1$ .

A better estimate of reactivity reduction could be obtained assuming that Eq. (14) holds also for the cases when the expansion continues into the blanket. An "upper" limit of reactivity reduction can be obtained assuming that the power in the blanket is negligible and

$$-\frac{dN}{dr} \begin{cases} = 2q \frac{r}{b^2} & \text{for } r < b \\ = \frac{(1-q)}{\epsilon} & \text{for } b < r < b + \epsilon \end{cases} \quad (19)$$

where  $\epsilon$  is a very small quantity, so that there is a fairly abrupt power drop in the blanket.

Equations (14) and (17) give for the lower limit:

$$\left(\frac{d^2\rho}{dt^2}\right)_l = -\frac{8}{2.54} \frac{q^{7/2}}{1-q} \frac{1}{b^2} (\gamma-1) Q^* e^{(\lambda t - \lambda t_c)} = \rho_l'' e^{(\lambda t - \lambda t_c)} \quad (20)$$

and for the upper limit:

$$\left(\frac{d^2\rho}{dt^2}\right)_u = \rho_u'' \left\{ e^{(\lambda t - \lambda t_c)} + \frac{5}{2} \frac{1-q}{q} \left( e^{(\lambda t - \lambda t_c)} - 1 \right) \right\} \quad (21)$$

Integrating these expressions twice with time we obtain

$$\rho_{\ell} = \rho_c + \frac{\rho'_c}{\lambda} (\lambda t - \lambda t_c) + \frac{\rho''_{\ell}}{\lambda^2} \left[ e^{(\lambda t - \lambda t_c)} - 1 - (\lambda t - \lambda t_c) \right]$$

and

$$\rho_u = \rho_{\ell} + \frac{5}{2} \frac{1-q}{q} \frac{\rho''_{\ell}}{\lambda^2} \left[ e^{(\lambda t - \lambda t_c)} - 1 - (\lambda t - \lambda t_c) - \frac{1}{2} (\lambda t - \lambda t_c)^2 \right]$$

where  $t_c$  is the time the expansion wave reaches the edge of the core;  $\rho_c$  and  $\rho'_c$  are the reactivity reduction and time rate of it at this time;

$$\rho_c = \rho(t=t_c) \text{ and } \rho'_c = \left( \frac{d\rho}{dt} \right)_{t=t_c} .$$

Both  $\rho_{\ell}$  and  $\rho_u$  have been plotted as dashed curves in Fig. C-1 for two values of  $q$  (or  $\lambda t_c$ ):  $q = 0.3935, 0.6321$ , (or  $\lambda t_c = 0.5, 1$ ).

We shall now show that the "upper limit" just calculated should be close to the true physical condition. At the edge of the core a pressure

$$\begin{aligned} p_c &= (\gamma-1) Q^* s (e^{\lambda t - \lambda t_c} - 1) \\ &\approx (\gamma-1) Q^* s (\lambda t - \lambda t_c) \end{aligned}$$

is generated after the impact according to our picture. This pressure is exerted upon the blanket (where no significant back pressure is generated), causing the blanket to recede, and resulting in a rarefaction moving inward from the core boundary. The pressure acting at the interface has to drop to some value  $p$ , such that the particle velocity in the core is the same as that in the blanket at the boundary. The blanket velocity is given by

$$\dot{u}_b = \frac{p}{s_b C_b}$$

where  $s_b$  is the blanket density,  $C_b$  is the speed of sound. In the core we have

$$\dot{u}_c = \frac{p_c - p}{sC} .$$

Thus the pressure at the interface is

$$p = \frac{p_c s_b C_b}{sC + s_b C_b} \quad (22)$$

and the corresponding velocity is

$$\begin{aligned}\dot{u}_b &= \dot{u}_c = p_c / (sC + s_b C_b) \\ &\approx (\gamma-1) Q^* s (\lambda t - \lambda t_c) / (sC + s_b C_b)\end{aligned}$$

so that

$$\ddot{u}_b = \ddot{u}_c = (\gamma-1) Q^* \lambda s / (sC + s_b C_b) \quad . \quad (23)$$

Assuming now that the microscopic transport cross section is the same in the core and in the blanket, the reactivity reduction in (7) is

$$\rho = - \frac{5}{2.54} \frac{\sqrt{q}}{b} s \sigma_{tr} \int (us) \sigma_{tr} \left( \frac{1}{\Sigma_{tr}} \frac{d\Phi}{dr} \right)^2 r dr \quad .$$

Then for the contributions due to the compression wave in the blanket and the rarefaction wave in the core we obtain that

$$\begin{aligned}\frac{d^2 \rho}{dt^2} &= - \frac{5}{2.54} \frac{\sqrt{q}}{b} s \sigma_{tr} \int (\ddot{u}s) \sigma_{tr} \left( \frac{1}{\Sigma_{tr}} \frac{d\Phi}{dr} \right)^2 r dr \\ &= - \frac{5}{2.54} \frac{\sqrt{q}}{b} s \sigma_{tr} [(\ddot{u}_c s) C (t-t_c) + (\ddot{u}_b s_b) c_b (t-t_c)] \\ &\quad \cdot \sigma_{tr} \left( \frac{1}{s \sigma_{tr}} \frac{2q}{b} \right)^2 b\end{aligned}$$

if the time interval  $(t-t_c)$  is small. Substituting here the value for the accelerations from (23) we see that

$$\begin{aligned}\frac{d^2 \rho}{dt^2} &= - \frac{20}{2.54} (\gamma-1) Q^* q^{5/2} b^{-2} \lambda (t-t_c) \\ &= \frac{5}{2} \frac{1-q}{q} \rho''_{\ell} (\lambda t - \lambda t_c) \quad .\end{aligned}$$

So (for a short interval of time) the reactivity reduction brought on by compression and rarefaction waves at the interface is the same as the reactivity decrease,  $\left( \frac{d^2 \rho}{dt^2} \right)_u - \left( \frac{d^2 \rho}{dt^2} \right)_\ell$ , obtained in (21) by a formal procedure. Thus in further calculation we have used (21) to compute reactivity reduction.

c. Energy Yield

Since the reactivity reduction rate increases very sharply starting from negligible values, the reactivity drops very sharply. We can obtain an adequate estimate of energy developed assuming that power increases exponentially until reactivity reduction given in Eq. (18a) becomes equal to maximum reactivity inserted as calculated by Eq. (4). The time,  $t^1$ , at which this occurs can be read out from Fig. C-1 and the energy developed in the core at that time is

$$E^1 = \int_0^b Q^* e^{\lambda t^1} (1 - qr^2/b^2) 4\pi r^2 dr s = (1 - 0.6q) e^{\lambda t^1} Q^* \frac{4\pi}{3} b^3 s$$

That is, the average energy developed in the core per gram of uranium is

$$\epsilon = (1 - 0.6q) e^{\lambda t^1} Q^* \quad (24)$$

This energy ( $\epsilon$ ) is plotted vs. maximum reactivity ( $\rho_{\max}$ ) in the Fig. C-2. The dashed curves (for  $q = 0.3935$  and  $q = 0.6321$ ) give energy development when the reactivity inserted is so large that the expansion reaches the edge of the core.

Assuming initial power  $n(0) = 3.3 \times 10^{-4}$  watt/gm of  $U^{235}$ , a numerical calculation has been performed in this fashion for reactivity insertion rates varying between 10 and 1000  $\$/\text{sec}$ . To simulate EBR-II, the core radius has been taken as  $b = 23$  cm; the prompt generation time  $\tau = 10^{-7}$  sec; critical energy density  $Q^* = 1.1 \times 10^3$  joule/gm of U. Then  $[(8/2.54)q(\gamma-1) Q^* \tau^2 b^{-2}]^{-1/3} = 157.1$ , and the numerical values for the maximum reactivity reached and energy density developed have been tabulated for different insertion rates in Table C-I. It is seen that energy-density developed in the explosion is only a few times the energy density,  $Q^*$ , necessary to start reactivity reduction mechanism.

Table C-I

MAXIMUM REACTIVITY RISE AND AVERAGE ENERGY DEVELOPED FOR VARIOUS REACTIVITY INSERTION RATES IN EBR-II

$dk/dt$ in $\$/\text{sec}$	$\rho_{\max} \times 10^3$	$\lambda t^1$	$\epsilon/Q^*$
10	0.63	0.40	1.14
50	1.42	0.69	1.53
100	2.03	0.88	1.85
200	2.88	1.14	2.39
400	4.10	1.49	3.38
600	5.05	1.73	4.33
800	5.84	1.94	5.32
1000	6.54	2.10	6.26

Assuming 350 kg of uranium in the core, we find that the energy to raise the entire core to  $Q^* = 1.1 \times 10^3 \times 350 \times 10^3 = 3.85 \times 10^8$  joules. Crudely speaking,  $(\epsilon/Q^* - 1)$  multiplied by this quantity is indicative of the energy developed in the explosive portion of the accident and is representative of the pressures available for damage to the reactor plant.

No allowance for Doppler effect has been made in this calculation. It is believed to be a small effect (as a result of recent experiments), but in an explosion of this sort it might still contribute somewhat. If, as we postulate, there is no reactivity loss due to expansion until  $Q^*$  is reached, a positive Doppler effect worth several cents of reactivity between melting temperatures and 10,000 K could increase the energy yield of an accident. On the other hand, if the effect were slightly negative, it could reduce the yields. Any additional reactivity brought into the system would simply increase  $\rho_{\max}$  and the corresponding energy yield. The dependence of the yield on  $\rho_{\max}$  may be seen in Table C-I or Fig. C-II.

It is perhaps worth noting that in the cases considered here, the time between the pressure wave reaching the core boundary and shutdown ( $t^1 - t_c$ ) has a flat maximum as we go from low rates of reactivity insertion to very high rates. Assuming that the wave velocity  $C = 2 \times 10^5$  cm/sec, the rarefaction wave travels less than 5 cm into the core before shutdown occurs.

#### Addendum on Wave Propagation

Calculating  $u$  from Eq. (13) we obtain

$$u = (\gamma - 1)Q^* \frac{1}{\lambda^2} \frac{2q}{b^2} r \left[ \frac{1 - qr^2/b^2}{1 - qr_1^2/b^2} - 1 - \ln \frac{1 - qr^2/b^2}{1 - qr_1^2/b^2} \right] \quad (1A)$$

Substituting this value into the wave term of Eq. (9) we have

$$\begin{aligned} C^2 \left( \frac{\partial^2}{\partial r^2} + \frac{2}{r} \frac{\partial}{\partial r} - \frac{2}{r^2} \right) u \\ = (\gamma - 1)Q^* \frac{2qr}{b^2} \left( \frac{C}{\lambda b} \right)^2 10q \left[ -e^{\lambda t} + \frac{1 - 0.6qr^2/b^2}{(1 - qr^2/b^2)^2} \right] \end{aligned} \quad (2A)$$

as a first order correction to the Eq. (13). This is the force caused by wave propagation that has to be added to the right side of Eq. (13):

$$(\gamma - 1)Q^* \frac{2qr}{b^2} e^{\lambda t} .$$

Because of the factor 10 in Eq. (2A) the correction may be appreciable even for fairly high values of  $\lambda$ . This additional force is partly positive partly negative, depending upon time and position. Calculating the influence of this force upon the rate of reactivity reduction given by Eq. (14) we find zero contribution.

It can be shown easily that the vanishing of the contribution due to the part representing the wave propagation is not limited to the first order (in terms of  $C^2$ ) only, neither is it affected by the particular form of driving force  $\left(-\frac{1}{s} \frac{\partial p}{\partial r}\right)$  chosen in Eq. (13). This term gives vanishing contribution to the reactivity because we have chosen  $\frac{\partial \Phi}{\partial r} \propto r$  in Eq. (14). We can see that by taking the integral in Eq. (14), substituting

$$C^2 \left( \frac{\partial^2}{\partial r^2} + \frac{2}{r} \frac{\partial}{\partial r} - \frac{2}{r^2} \right) u$$

instead of  $-\left(\frac{\partial N_0}{\partial r}\right)$  and integrating by parts. Then we have

$$\begin{aligned} & \int_0^{r_1} C^2 \left\{ \left( \frac{\partial^2}{\partial r^2} + \frac{2}{r} \frac{\partial}{\partial r} - \frac{2}{r^2} \right) u \right\} \left[ \frac{1}{r} \left( \frac{d\Phi}{dr} \right)^2 \right] r^2 dr \\ &= \int_0^{r_1} C^2 u \left\{ \left( \frac{\partial^2}{\partial r^2} + \frac{2}{r} \frac{\partial}{\partial r} - \frac{2}{r^2} \right) \left[ \frac{1}{r} \left( \frac{d\Phi}{dr} \right)^2 \right] \right\} r^2 dr \\ &= \left[ C^2 r^2 u \frac{1}{r} \left( \frac{d\Phi}{dr} \right)^2 \frac{d}{dr} \ln \frac{1}{u} \left( \frac{d\Phi}{dr} \right)^2 \right]_{r_1}^0 \end{aligned}$$

Now if

$$\frac{1}{r} \left( \frac{d\Phi}{dr} \right)^2 \propto r$$

the integrand on the right vanishes. The term free of integral vanishes since both  $u$  and  $du/dr$  vanish at  $r_1$ , the front of the shock wave. This demonstration assumes however, that velocity of wave propagation,  $C$ , in the core does not depend upon the position. Actually this is not strictly true, since parts of the core have varying temperature.

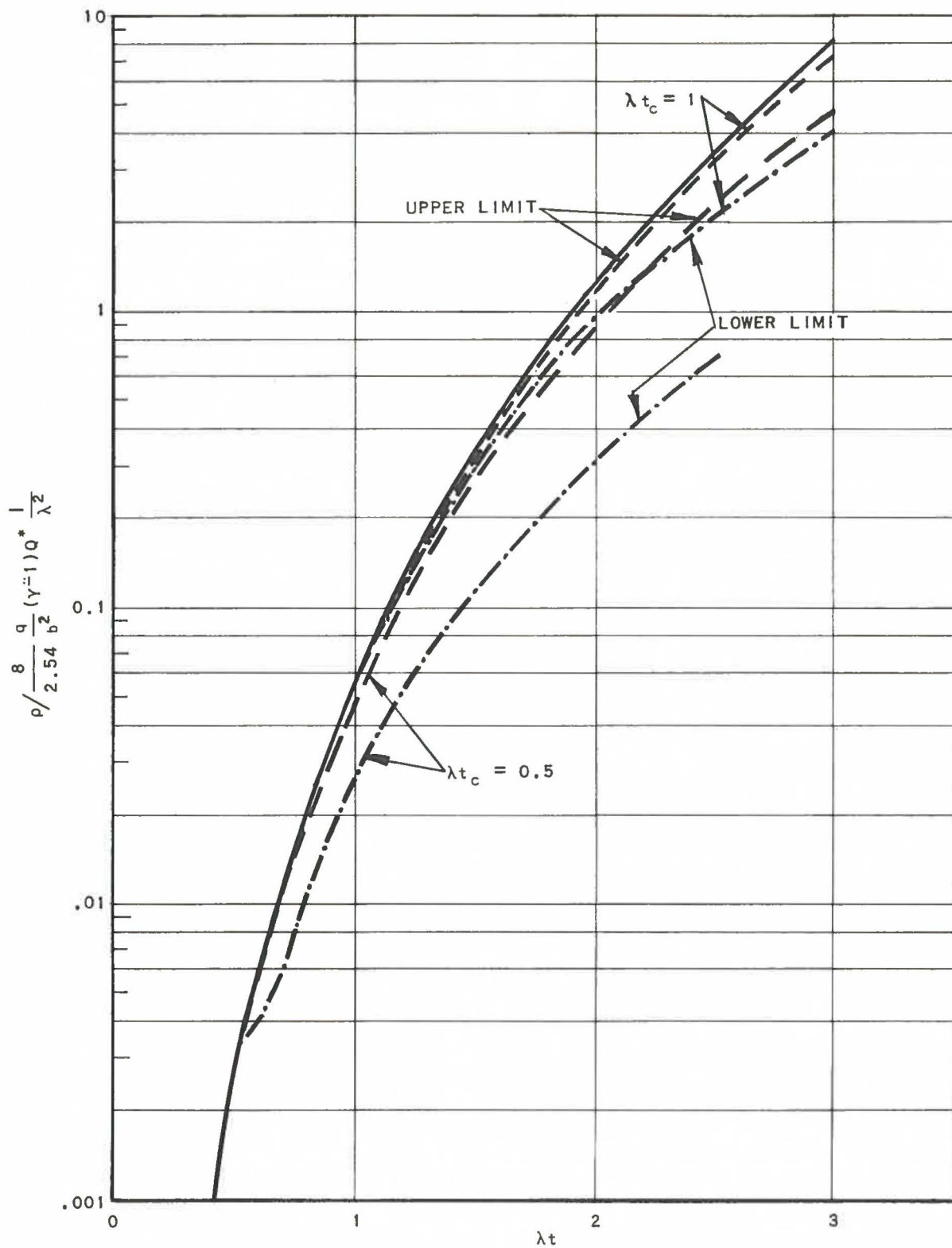


FIG. C-1  
REACTIVITY REDUCTION vs TIME

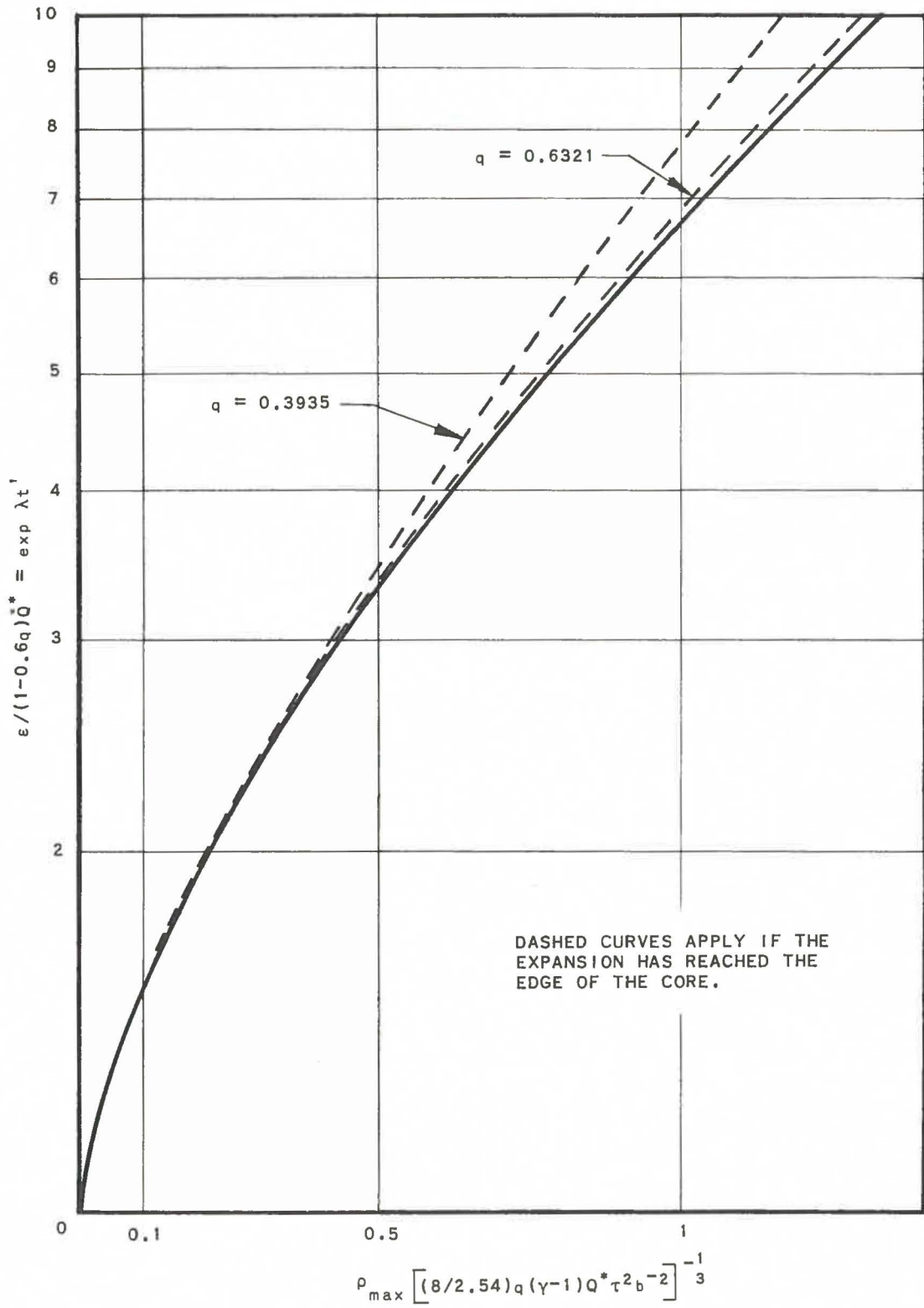


FIG. C-2  
ENERGY DEVELOPED FOR GIVEN EXCESS REACTIVITY



## APPENDIX D

POSSIBLE SODIUM CHEMICAL REACTIONS1. Introduction

In the event of a severe nuclear accident or of equipment failure, it is possible that high-temperature sodium may be discharged from one of the sodium systems within the reactor building. The potential severity of the resulting chemical reactions of this sodium with materials within the building is discussed herein.

Water or other highly reactive material will not be permitted within the reactor building in sufficient quantity to constitute a potential hazard. Therefore, combustion of the sodium in the building atmosphere is the only significant reaction which can occur. The two reaction effects of importance are the maximum pressures and the maximum temperatures generated within the building.

In analyzing the potential hazards associated with a sodium-air reaction, it is necessary to consider the effects of various types of accidents involving the release of sodium into the building atmosphere. Sodium exposure to the atmosphere could occur in three broad categories: stagnant pool, pressurized spray, and as an explosive ejection.

a. Stagnant Pool Exposure

The stagnant pool exposure could occur by low-pressure equipment failure, by spillage, or by opening sodium-containing tanks or lines, and represents the least serious of the three types of accidents. The rate of combustion of a clean sodium surface has been theoretically estimated<sup>1</sup> at 4 lb/(sq ft)(hr) at 500C. However, the oxide buildup effected at the surface of the sodium in any actual case would materially reduce this figure. Even with the theoretical rate of reaction, it would require many hours for all oxygen in the building to be reacted. Consequently, most of the heat generated by the combustion is dissipated to the relatively cold material in the reactor building or is lost by convection and conduction through the building wall and is not available to increase the atmosphere temperature and pressure.

b. Spray Exposure

Sodium release as a pressurized spray leads to much faster reaction rates and consequently develops higher building pressures than those resulting from stagnant pool exposure. An accidental discharge of

<sup>1</sup>Gott, H. H.; "The Dounreay Sphere, Part I, Criteria of Design," RHM(56)129 "Confidential"; U.S.-U.K. Reactor Hazard Meeting, 1956

this type might result from rupture or other failure of equipment or pipes containing sodium under pressure. The resulting sodium-air reaction would occur primarily while the sodium is in flight. Thus, the heat of reaction would be transferred directly to the atmosphere with little energy initially being lost to structures or the building wall. The heat of this reaction is therefore almost completely utilized (initially) in raising the temperature and pressure of the building atmosphere.

An experimental evaluation of the maximum pressures resulting from the sodium spray-air reaction was conducted by Hines and Kelley<sup>2</sup> of the Detroit Edison Company. In these tests, 850F sodium was sprayed through a nozzle into a 532-liter steel vessel (approximately 29 in. dia. by 49 in. high). The pressures resulting from the sodium-air reactions were measured as a function of time. The maximum pressure developed in these tests was 38 psig, when one pound of sodium under 360 psig pressure was forced through the spray nozzle into the reaction vessel atmosphere in 20 sec. This maximum pressure was reached 6 sec after the start of sodium addition. The pressure dropped continuously during the remainder of the addition time. Within 10 minutes, the oxygen in the reaction vessel was completely consumed.

A theoretical study of the sodium spray-air reaction by Gemant<sup>3</sup> of Detroit Edison Company agreed reasonably well with the Hines and Kelley experimental data.

### c. Explosive Ejection Exposure

The third and, potentially, the most severe of the accidental sodium exposure types is that in which sodium is explosively ejected into the building atmosphere. This is a condition which, in the EBR-II, could result only from a serious nuclear excursion. Here, as in the sodium spray condition, reaction primarily occurs while the sodium is in flight. The only effective difference between explosive ejection and high-pressure spray discharge of sodium is that of the resulting reaction rate. Under given temperature conditions, the rate of reaction depends upon the mass rate and distribution within the building of the sodium discharge, and upon the velocity and size of the sodium particles. It is obvious that only in the case of a highly energetic ejection of a very large mass of efficiently dispersed sodium could the optimum conditions for the most severe (maximum theoretical) reaction rate be approached.

---

<sup>2</sup>Hines, Edward and Kelley, J. K.; "Determination of the Maximum Pressures Attained During the Reaction of Sodium with Air in Closed Systems"; Eng. Lab. Res. Dept. Report 55C80, The Detroit Edison Co., Feb. 15, 1956.

<sup>3</sup>Gemant, Andrew; "Calculations on the Sodium Air Reaction"; Eng. Lab. Res. Dept. Report P.55C80-B, The Detroit Edison Co., Jan. 30, 1956.

It is believed that a thermodynamic analysis of the pressure and temperature effects of explosively-mixing sodium and air cannot be conclusive, due to the many assumptions inherent in such an analysis. For this reason, an experimental program has been conducted to obtain data on this type of reaction. Results of this program are described below.

## 2. Description of Equipment

The equipment is designed to permit the explosive ejection of a variable quantity of 750F sodium into a sealed reaction vessel containing air. The resulting internal pressures and temperatures are measured as a function of time. The sodium is ejected from an external reservoir into the reaction vessel by the detonation of a hydrogen-oxygen gas mixture.

### a. Reaction Vessel

The reaction vessel (Fig. D-1) consists of a steel tank 3 ft in diameter and 10 ft high with a wall thickness of  $1/4$  in. The top and bottom plates are of 1 in. steel, each having a 14 in. diameter flanged access port. Numerous sandbags and six stiffening rings (6 in. wide,  $3/4$  in. deep) are added to reduce the effects of vessel wall vibration on the pressure transducers.

### b. Sodium Ejection Equipment

The ejection equipment, or mortar, is located at the bottom center of the vessel and consists of a heated sodium reservoir and a hydrogen-oxygen ignition chamber. The reservoir is positioned above the ignition chamber and is separated from it by a thin stainless steel rupture disc. The top of the reservoir, in turn, is separated from the reaction vessel atmosphere by a second stainless steel rupture disc. Three sizes and shapes of reservoirs and two sizes of ignition chambers are used in the various combinations indicated in Fig. D-2.

### c. Instrumentation

The primary variable measured in the reaction vessel is internal pressure. Certain temperature measurements are also made.

#### (1) Pressure

Three independent pressure measuring systems are used: two high-speed systems to measure the initial fast pressure transients; and one bourdon tube recorder to measure longer term pressure characteristics.

The first of the two high-speed pressure systems consist of two Hathaway Model PS-14A, 0-250 psig resistance strain gage-type pressure transducers used in conjunction with a Hathaway Model MRC-16C strain gage control unit, and a Hathaway Model S14E optical oscillograph. With this system it is possible to record transducer signals of up to 1500 cps with a reproducibility of  $\pm 1/4\%$  of full scale. The first transducer is flush mounted on the top plate of the reaction vessel; the second transducer is mounted on the vessel wall near the top. For some experiments, the second Hathaway transducer is mounted flush with the wall and for others it is connected to the vessel through a length of  $1/4$  in. tubing (1 ft).

The second of the two high-speed systems consists of an Electroproducts Pressuregraph, Model #3700C and a variable capacitance Electroproducts pressure transducer, Model #3709C. The modulated carrier transient response in the Pressuregraph is better than one-tenth of one millisecond and is capable of reproducing sharp wave fronts and instantaneous peak pressures. The amplified transducer signal is transmitted to an oscilloscope and photographed. Pressure profiles of a duration up to 9 sec can be obtained. For all experiments, the pressure transducer in this system is mounted flush with the wall near the top of the pressure vessel.

A Minneapolis-Honeywell bellows-actuated, circular chart recorder Model 702X6N-X-74V1, is used to measure the longer term system pressure characteristics. The instrument is calibrated for the range 0 - 150 psi and the chart speed is one revolution per 75 sec. The bourdon tube sensing element for the circular chart recorder is connected to the tank wall at the bottom through 4 ft of  $1/4$  in. copper tubing.

Figure D-3 is a photograph showing the high-speed pressure recording instrumentation. Locations of two pressure sensing points are evident in Fig. D-1.

The transducers in both the Hathaway and the Electroproducts systems are sensitive to vibration. Even after stiffening the vessel by welding on the vessel stiffening rings and bottom plate bracing beams, vibration was severe enough in a few of the experiments to mask the pressure traces from one or more of the pressure transducers. In most instances, however, the magnitude of the vibration component of the signal did not prevent accurate interpretation.

The circular chart recorder, being connected to the tank through 4 ft of copper tubing, is unaffected by vibration. This long tubing connection results in a slower system and makes peak pressure recording with this system less accurate than with the others.

## (2) Temperature

Thermocouples are used to monitor the outside wall temperatures of the tank. Also, one specially built thermocouple penetrates the tank wall and is arranged for exposure to the same conditions as the inside wall of the reaction vessel. This thermocouple is specifically designed to have low heat capacity, as well as fast thermal response, and is used to indicate the temperature of the material deposited on the wall during the reaction. A sketch of this thermocouple and its mounting plug is shown in Fig. D-4. A Sanborn amplifier and recorder are used to record the signal from this element. No attempt is made to measure temperature of the vessel gas because of the difficulty of shielding a thermocouple from reaction products and unreacted sodium. Instead, the gas temperature is calculated from the measured value of pressure.

## 3. Test Procedure and Data

Twenty-four experiments are reported in which sodium is explosively ejected into the test vessel atmosphere. In all cases, sodium is introduced at 750F, and the initial reaction vessel atmosphere is at normal atmospheric pressure, temperature, and oxygen concentration (with the exception of two argon atmosphere tests). The tests include variations in quantity of sodium, distribution, force of ejection, and water vapor content of the atmosphere.

In conducting these experiments, the test quantity of sodium is sealed in the sodium reservoir section of the mortar assembly and brought to a temperature of 750F. After purging with hydrogen, stoichiometric mixtures of hydrogen and oxygen gases are added to the ignition chamber in the desired amount (from 3 to 9 atmospheres pressure). When this hydrogen-oxygen mixture is detonated by a spark, the contents of the sodium reservoir are explosively ejected into the reactor vessel atmosphere. Resulting pressures and temperatures are monitored as a function of time. Gas samples of the reaction vessel atmosphere are taken two minutes after sodium addition and are analyzed for residual oxygen. After opening the tank, reaction product fall-out samples are taken for chemical analysis.

The results from these experiments are given in Table D-I. The Na/O column indicates the ratio of number of atoms of sodium ejected to number of atoms of oxygen originally present in the reaction vessel. A ratio of 1.00 represents the ejection of a stoichiometric quantity of sodium for reaction with the vessel oxygen to form sodium peroxide.

The Ejection Energy columns list the energy released by the hydrogen-oxygen ejection reaction, both as total kilocalories and as calories per gram of sodium ejected. The sodium ejection times are of the order of 3 to 10 milliseconds.

Table II-1

## ANL EXPERIMENTAL DATA

Run No.	Amount of Sodium Ejected, gm	Na/O Ratio	Ejection Assembly Configuration	Ejection Energy		Total Amount of Water, gm	$\Delta H$ of NaOH Formation, kcal	$\Delta H$ of $\text{Na}_2\text{O}_2$ Formation, kcal	Consumption of Initial Oxygen, %	Oxygen Content of Final Gas Mixture, Vol-%	Maximum Pressure Rise		Approx. Maximum Temperature (Calculated from Measured Pressure), F <sup>(6)</sup>	Measured Maximum Temperatures			
				kcal	cal/gm Na						psi	At Time, sec		Reaction Products on Wall		Outer Surface of Wall	
														F	At Time, sec	F	At Time, sec
1	200	0.26	1	6.34	31.7	25.3	120	-	-	17 ± 3	.2	-	-	-	-	-	
2	200	0.26	1	6.34	31.7	31.8	150	280	14	24 ± 2	.03	1000	-	-	-	-	
3	400	0.52	1	6.34	15.9	25.7	121	-	-	21 ± 3	.05	-	-	-	-	-	
4	400	0.52	1	6.34	15.9	23.9	113	-	-	44 ± 5 <sup>(5)</sup>	-	-	-	-	-	-	
5	400	0.52	1	6.34	15.9	24.3	115	710	35	37 ± 3	.06	1550	-	-	-	-	
6	600	0.78	1	6.34	10.6	26.5	125	-	-	52 ± 2	.07	-	-	-	-	-	
7	600	0.78	1	12.7	21.2	28.4	134	1070	53	50 ± 2	.05	2250	-	-	-	-	
8	800	1.04	1	6.34	7.9	-	-	-	-	48 ± 1	.17	-	-	-	-	-	
9	800	1.04	1	6.34	7.9	30.0	142	950	47	47 ± 3	.13	2050	-	-	-	-	
10	800	1.04	1	12.7	15.9	32.3	152	1290	64	50 ± 3	.08	2200	-	-	-	-	
11	1200	1.57	11	12.7	10.6	20.6	97	2000	99	79 ± 4	.12	3850	-	-	-	-	
12	1600	2.10	11	8.45	5.3	15.1	71	160	8	10 ± 1	-	450	-	-	116	66	
13	1600	2.10	11	8.45	5.3	13.4	63	730	36	43 ± 3	-	1800	-	-	120	120	
14	1600	2.10	11	12.7	8.0	29.7	140	1960	97	75 ± 4	.12	3600	-	-	-	-	
15	1600	2.10	11	15.8	9.9	32.0	151	1620	80	74 ± 3	.10	3400	-	-	160	-	
16	1600	2.10	11	15.8	9.9	22.8	108	1620	80	58 ± 2	-	2800	-	-	169	98	
17 <sup>(1)</sup>	1600	2.10	11	19.0	12.0	-	-	1880	93	67 ± 5 <sup>(5)</sup>	-	3200	-	-	-	-	
18 <sup>(1)</sup>	1600	2.10	11	19.0	12.0	-	-	1840	91	71 ± 5 <sup>(5)</sup>	-	3400	-	-	-	-	
19	1600	2.10	111	22.1	13.8	22.4	106	-	92	-	-	-	1244	.2	182	108	
20 <sup>(2)</sup>	1600	2.10	111	22.1	13.8	-	-	-	-	47 ± 1	.13	-	885	.3	145	90	
21 <sup>(3)</sup>	1600	2.10	11	12.7	7.9	3.9	18	1190	59	50 ± 2	.25	2250	-	-	150	165	
22 <sup>(3)</sup>	1600	2.10	111	22.1	13.8	6.8	32	1980	98	65 ± 5	-	3200	1135	.2	175	75	
23 <sup>(4)</sup>	600	-	1	6.34	10.6	2.0	9	0	-	5 ± 1	.13	260	-	-	-	-	
24 <sup>(4)</sup>	600	-	1	12.7	21.2	3.9	18	0	-	10 ± 2	.05	450	-	-	-	-	

(1) Ignition accidentally occurred before completion of  $\text{H}_2\text{-O}_2$  charging;

(2) 3/4 in. diameter open hole in vessel wall during run;

(3) Dry atmosphere run;

(4) Inert atmosphere calibration run;

(5) Circular chart reading;

(6) Uncorrected for deviation from ideal gas law.

Total water exposed to reaction is calculated by adding the water vapor content of the vessel atmosphere to the mass of water formed by the hydrogen-oxygen ejection reaction. In calculating the heat of formation of sodium hydroxide as a result of presence of this water, the following reactions are assumed to proceed to completion:



Thus, the reaction of one mole of water (in the presence of excess sodium peroxide) results in the formation of two moles of sodium hydroxide with the release of approximately 85 kilocalories of energy.

#### 4. Discussion of Test Results

##### a. General Nature of the Reaction

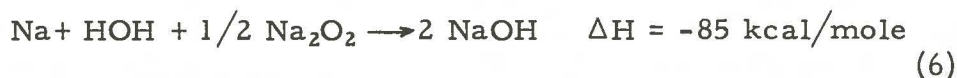
The predominant reaction that occurs when high-temperature molten sodium in a finely divided state is mixed with air, is oxidation of the sodium to form sodium peroxide:



Reaction (4) appears to proceed until all oxygen is combined before additional sodium reduces the sodium peroxide to sodium monoxide:



The presence of water vapor in the initial phase of the reaction results in the formation of sodium hydroxide:



Based on the energy derived from these reactions, the theoretically resulting atmospheric pressures and temperatures for contained sodium-air reaction have been calculated and are shown in Fig. D-5. These curves show the theoretical maximum temperature and maximum pressure obtained as a function of quantity of sodium ejected into the experimental reaction vessel, assuming 100% reaction (of sodium or oxygen, whichever is limiting) and no heat loss to the vessel wall.

There are three reaction zones indicated in Fig. D-5. Zone I represents the condition where the peroxide reaction predominates and where the heat of reaction is distributed between nitrogen, sodium peroxide, and residual oxygen. Zone II represents the region of peroxide reduction by additional sodium, with this additional heat of reaction distributed between the nitrogen and the reaction products sodium peroxide and sodium monoxide. Zone III represents the region where all oxygen has been converted to sodium monoxide and where additional sodium remains unreacted. In this zone, the heat capacity of the excess sodium is effective in reducing the over-all system temperature.

Postulation of the intermediate sodium peroxide step in the formations of sodium monoxide is principally reflected in the temperature values within Zone I. It means that initially, in the oxygen excess system, the oxidation of a given quantity of sodium results in higher temperatures than would be experienced by the direct monoxide formations:



It is seen that the maximum system temperature occurs when 1500 gm of sodium are reacted. This represents the stoichiometric equivalent of sodium and oxygen in sodium monoxide. The addition of either more or less sodium results in lower system temperatures.

It is emphasized that the curves presented in Fig. D-5 are those for an ideal system of zero reaction time, and as such represent a theoretical upper limit for conditions encountered in a real system. In a real system, a discrete time interval is required for mixing and reaction to occur. During this reaction period, the atmospheric temperature becomes sufficiently high for appreciable heat loss to the cold vessel surfaces to occur. Further heat loss, in the actual case, results from the incomplete reaction of sodium while in the air. The unreacted sodium not only absorbs heat, but upon impingement on the vessel wall helps to transfer heat from the atmosphere to the wall. Thus, an actual system maximum temperature would be less than the theoretical value by an amount dependent upon the magnitude of these heat losses. The mixing and reaction processes in the actual case are too complex to permit complete analysis; the necessary information is lacking on the details of the ejection process and the sodium-air reaction rates. Therefore, realistic estimates of maximum temperatures and pressures attainable in practice can be obtained only through experimental testing. The test program under discussion employs reaction conditions considerably nearer the optimum than could be expected in the event of sodium expulsion into the reactor building by a nuclear accident in EBR-II.

The experimental test results obtained are plotted in Fig. D-5 for comparison with the theoretical curves.

## b. Measured Values of Pressure

The data in Table D-I show a wide variation in the maximum pressures developed in the experimental sodium-air reactions. In all cases, the maximum pressures attained are substantially lower than those theoretically possible. This is attributed to a combination of incomplete sodium combustion and system heat losses, as discussed above. Unreacted sodium was found impinged on the reaction vessel walls and the vessel top plate in all runs, even those in which oxygen was present in large excess. The reactions required 0.03 to 0.17 second for completion, and during this interval, heat was lost to the reaction vessel surfaces before theoretical maximum pressure could be developed.

### (1) Maximum Peak Pressures

The maximum peak pressure observed during these experiments was  $79 \pm 4$  psig, which occurred in run 11. Three other runs (14, 15 and 18) were recorded in which peak pressures were about 75 psig. Some associated data for these runs are shown below.

Run No.	Peak Pressure, psig	Theoretical Peak Pressure, psig	O <sub>2</sub> Consumed, %	Ratio of Na Ejected in % of Stoichiometric
11	$79 \pm 4$	109	99	78
14	$75 \pm 4$	120	97	105
15	$74 \pm 8$	120	80	105
18	$71 \pm 5$	120	91	105

These data give a comparison of the experimental peak pressures with those theoretically possible under ideal reaction conditions. The nearest approach to the theoretical value was in run 11, where almost 75% of the potential peak pressure was achieved. In this run, 78% of the required sodium for stoichiometric formation of sodium monoxide was ejected into the vessel. Upon complete reaction, this would result in a reaction product mixture of 56% sodium monoxide and 44% sodium peroxide. In the other three runs listed, sufficient sodium was ejected for complete reduction of sodium peroxide to sodium monoxide. It is interesting to note that the oxygen burnup was essentially complete only in runs 11 and 14, and that a significant quantity of oxygen remained unreacted in runs 15 and 18.

### (2) Duration and Characteristics

The peak pressures occurred within 30 to 200 milliseconds from start of ejection and were immediately followed by a rapid pressure reduction. Normally, the reaction vessel pressure would drop to 0 psig

within three minutes of sodium injection. Typical pressure profiles are shown in Fig. D-6. In all runs, the pressure profiles are similar in shape. The initial pressure rise is associated with the time-in-flight of the ejected sodium. While the sodium is in flight, the entire heat of combustion is absorbed by the reaction products, the atmospheric gases in the reaction vessel, and unreacted sodium. Unreacted sodium impinging on the reaction vessel surfaces quickly becomes covered with a coat of reaction products which effectively inhibits further reaction with the oxygen-depleted atmosphere. A rapid pressure drop follows as heat is lost to the cold reaction vessel surfaces, becoming slower as the difference between gas temperature and wall temperature decreases.

### (3) Effects of Sodium-Oxygen Ratio Variation

The pressure rise per unit weight of sodium reacted decreases with increasing sodium-oxygen molar ratios up to the stoichiometric value required for sodium monoxide. Referring to Fig. D-5, it can be seen that the slopes of the theoretical pressure and temperature curves within Zone I decrease with increasing sodium reaction. This is due to the initial high energy sodium peroxide formation reaction, and to an increasing nitrogen heat capacity with temperature. In Zone II, each added unit of reacted sodium reacts in the lower energy sodium peroxide reduction reaction, and the slopes of the curves become still smaller. In any actual case, another factor enters to reduce the slopes further (in both Zone I and Zone II); as the reaction progresses, the oxygen concentration decreases and the reaction rate, therefore, decreases, permitting a longer time for system heat loss before completion of the reaction.

In the tests, the ratio of ejected sodium to initial oxygen is varied by injecting different quantities of sodium into the system while keeping the original atmospheric oxygen concentration constant. The data in Table D-II give a comparison of representative runs for various sodium to oxygen ratios.

The initial oxygen volume for these runs is such that 750 gm of sodium are required for stoichiometric conversion to  $\text{Na}_2\text{O}_2$ , and an additional 750 gm of sodium are necessary for the total reduction of this  $\text{Na}_2\text{O}_2$  to  $\text{Na}_2\text{O}$ . The data indicate a decreasing influence of additional sodium on the peak pressures, as expected; as can be seen, when the quantity of sodium ejected is increased by a factor of 8 (from 200 to 1600 gm), the maximum pressure realized increases by a factor of approximately 3.

The oxygen consumption values indicate sodium reaction efficiencies of 40 to 60% for ejections up to 800 gm (approximately the stoichiometric amount). Runs 11 (1200 gm) and 14 (1600 gm) consumed substantially all of the atmospheric oxygen, while in runs 15 (1600 gm) and 16 (1600 gm) an appreciable fraction of the oxygen remained unreacted.

Table D-II

TEST DATA FOR SODIUM TO OXYGEN RATIO VARIATION

Run No.	Sodium Ejected, gm.	Na/O. Ratio	O <sub>2</sub> Consumption, %	Maximum Pressure, psig	At time, sec
2	200	0.26	11.3	24 ± 2	0.03
5	400	0.52	30.8	37 ± 3	.06
7	600	0.78	47.1	50 ± 2	.05
9	800	1.04	41.6	47 ± 3	.13
10	800	1.04	58.3	50 ± 3	.08
11	1200	1.57	98.7	79 ± 4	.12
14	1600	2.10	96.6	75 ± 4	.12
15	1600	2.10	76.5	74 ± 8	.10
16	1600	2.10	75.5	58 ± 2	-

Reaction times also appear shorter with the smaller sodium ejections. Peak pressures were achieved within 60 milliseconds in the 200, 400 and 600 gm runs, while for larger quantities of sodium, an average of 110 milliseconds was required.

#### (4) Effects of Ejection Variables

The magnitudes of pressure and temperature developed are affected by the initial sodium particle size and the sodium distribution, or dispersion within the vessel. Variations in these factors were accomplished experimentally by varying the hydrogen-oxygen loadings of the ejection mortar and by employing different geometries of sodium reservoir.

As the force of the ejection reaction is increased with a given quantity of sodium, the initial particle size decreases, resulting in higher surface to volume ratios for the ejected sodium. This increases the initial rate of reaction, which is directly proportional to the exposed sodium surface area. Table D-I lists the energy of the hydrogen-oxygen ejection reactions as total energy and as energy per gram of discharged sodium. These ejection energies range from 5.3 to 31.7 cal/gm.

Figure D-2 shows the various mortar assembly configurations used in these tests. Configuration I, with tapering sodium reservoir walls, gives a wider dispersion cone than the vertical walled configurations II and III. The tapered geometry also results in better initial mixing in the immediate reaction zone directly over the mortar assembly. The very high ejection-energy system, configuration III, was used only in the 1600-gm runs 19, 20 and 22.

Very little effect of ejection energy variation is noticeable in comparing runs 6 and 7 and runs 8, 9 and 10, all of which were made with mortar configuration I. In runs 6 and 7, where the ejection energies were 10.6 and 21.2 cal/gm, respectively, the peak pressures were both approximately 50 psig. Additionally, no significant peak pressure differences were noted in runs 8, 9, and 10, with ejection energy variations between 8 and 16 cal/gm.

The insensitivity of these runs to variations in ejection energy suggests the importance of a secondary dispersion mechanism. The explosive ejection of finely divided sodium into a large atmospheric volume leads to an intense local heating of the zone immediately above the mortar. This results in a violently expanding turbulent gas zone within which a large portion of the ejected sodium is trapped. This secondary dispersion phenomenon has the characteristic of a mild explosion ignited by the initial sodium reaction. Once initiated, the thermal expansion dispersion mechanism is progressive. As the larger sodium particles are broken apart, the resulting increase in reaction rate supplies additional energy to the expanding gas zone, thus promoting further breakdown and dispersion of the entrapped sodium particles.

It appears that in the runs cited above, this secondary dispersion mechanism was sufficient to override differences in the magnitude of the hydrogen-oxygen ejection reactions. The effect of secondary dispersion can be seen in the different results obtained in the duplicate runs 12 and 13. An ejection energy of 5.3 cal/gm was used in both runs, and yet the peak pressure for run 12 was only 10 psig while that for run 13 was 43 psig. The ejection energy used in these runs was the lowest in the 1600 gm test series and resulted in the poorest sodium dispersion characteristics. It is thought that the reaction rate resulting from the original mortar dispersion in run 12 was too slow to trigger the secondary dispersion mechanism. This led to poor reaction efficiency, which resulted in the small system pressure rise. In contrast, the data indicate that the secondary dispersion did occur in run 13. In run 13, this supplementary dispersion effect increased the sodium air reaction efficiency by a factor of more than four times that experienced in run 12. All controllable test conditions were the same for both runs; the probable explanation for the difference in results is that there adventitiously resulted in the one case a local dispersion of very fine sodium particles which initiated the secondary dispersion process.

The difference in peak pressures between runs 21 and 22 appear to be due, at least in part, to the difference in the effectiveness of the secondary expansion caused by the difference in ejection energies used (7.9 and 13.8 cal/gm, respectively). Peak pressures for the two runs were 50 and 65 psig. The higher ejection energy in run 22 produced better initial dispersion and more finely divided particles than did the 7.9 cal/gm for

run 21. This resulted in more immediate activation of potential expansion centers, entrapping a larger quantity of sodium in the resulting secondary expansion zone.

Similarly, the difference between peak pressures obtained in run 13 and runs 14 - 16 seems to be partly due to the difference in ejection energy employed, with the resulting effect upon secondary dispersion.

#### (5) Effects of Water Vapor

The total system water listed in Table D-I includes both water vapor present as atmospheric humidity and as reaction product from the hydrogen-oxygen ejection reaction. Of these two sources, atmospheric humidity was the most significant, contributing an average of 80% of the total. The energy realized from the sodium-water vapor reaction is small, amounting to less than 5% of that potentially available from the sodium peroxide reaction. However, the water vapor reaction differs from the sodium-oxygen reaction in one important respect. Water vapor reacts with both sodium and its oxides, whereas sodium oxide barriers inhibit further oxygen reaction. This results in the fast, complete reaction of all water vapor in the system. Therefore, while the direct energy contribution of the water vapor reaction is small, it represents a substantial fraction of the immediate reaction preceding the secondary dispersion process, and conceivably might influence both initiation and propagation of this process.

Runs 21 and 22 were "dry atmosphere" runs in which water vapor was removed from the reaction vessel atmosphere by recirculation through Drierite. The peak pressures of 65 and 50 psig obtained were somewhat lower than the 60 to 75 psig obtained in comparable 1600 gm runs using natural humidity atmosphere. The secondary dispersion process was more effective in run 22, where the ejection energy was 13.8 cal/gm (6.8 gm water) than in run 21 with 7.9 cal/gm (3.9 gm water). The difference in pressures effected, therefore, is attributed to a combination of better initial dispersion and to the presence of additional water vapor in the initial reaction zone in run 22.

In an attempt to determine the magnitude of the initial reaction of the hydrogen-oxygen reaction water vapor with sodium, two inert atmosphere runs were made to eliminate the effects of the sodium-air reaction. The reaction vessel was completely filled with dry argon gas before sodium ejection. Two 600-gm runs were made with this inert atmosphere using ejection energies of 10.6 cal/gm (2.0 gm water) and 21.2 cal/gm (3.9 gm water). The resulting peak pressures were 5 and 10 psig, respectively. The energy transferred to the argon from the sodium in flight comes from two sources: the initial heat content of the 600 gm of sodium at 750F; and, the heat of reaction of the water vapor and sodium. The difference in

peak pressures for the two inert atmosphere runs cannot be accountable completely to the difference in amounts of hydrogen-oxygen reaction water, but must be partially due to the better heat transfer characteristics of the finer sodium dispersion in the 10-psig run.

c. Fallout and Distribution of Reaction Products

A characteristic distribution of sodium and its reaction products was observed in these experiments. The unreacted sodium impinges upon the vessel walls and top, adhering to the surface in a definite spray pattern. Here thin oxide films are quickly formed by the action of remaining oxygen.

Essentially all of the reaction products come to rest on the bottom plate of the reaction vessel as a very light, fluffy powder. This deposit was normally between one-half and one inch in thickness. Figure D-7 shows two photographs of reaction product deposit on the bottom flange of the reaction vessel. One view shows the bottom flange with the deposit as it occurred with the gasket still in place. The other view shows the same deposit with the gasket removed and with grooves scraped in the material.

The rate of reaction product fallout is an important factor in the determination of the pressure-time characteristic of the system following a sodium-air reaction. In these experiments it is estimated that well over half of the airborne reaction products had settled to the reaction vessel floor within one minute from the time of sodium ejection. This rapid fallout serves to remove a large component of the gas phase heat capacity. This reduced gas phase heat capacity greatly increases the sensitivity of the temperature in the reaction vessel atmosphere to heat losses to the cold vessel wall. The net effect of the removal of particulate material from the atmosphere is an increase in the rate of pressure drop as heat is lost from the system.

d. Analysis of Reaction Products

Reaction product fallout samples were taken for chemical analysis in five of the runs. The results of these analyses are given in Table D-III.

The column titled "Other" includes all reaction products for which no direct analysis was made, such as NaOH, NaH, and Na<sub>2</sub>O. The total Na deposit values represent the quantities of combined sodium in the reaction products on the bottom plate of the reaction vessel. The presence of carbonate is attributed to contamination of the samples by atmospheric carbon dioxide.

Table D-III

REACTION PRODUCT DATA

Run No.	Peak Pressure, psig	O <sub>2</sub> Consumed, %	Na Ejected, gm	Total Na Deposit, gm	Deposit Composition, wt-%			
					Na <sub>2</sub> O <sub>2</sub>	Na <sub>2</sub> CO <sub>3</sub>	Other	Total Na
18	71	91	1600	-	62.9	9.8	27.3	57.1
19	-	92	1600	500	87.3	8.4	4.3	57.5
20	47	-	1600	-	84.3	9.0	6.7	56.3
21	50	59	1600	-	84.7	4.7	10.6	55.8
22	65	98	1600	660	71.1	7.8	21.1	60.6

5. Extrapolation of Experimental Data to EBR-IIa. Peak Pressure

The manner of sodium ejection, the range of quantity of sodium ejected, and the range of ejection energy employed in the investigation correspond to explosive ejection of from 2,900 to 23,000 lb of 750F sodium with ejection energies of from  $4.1 \times 10^4$  to  $14 \times 10^4$  kcal (equivalent to 90 to 310 lb of TNT) into a vessel of EBR-II reactor building size. In Fig. D-8 the theoretical maximum pressure and maximum temperature curves for the reactor building are shown. These curves indicate the theoretical maximum pressure and maximum temperature attainable as a function of quantity of sodium ejected into the building, assuming 100% reaction (of sodium or oxygen, whichever is limiting) and no heat loss to the building wall. The three reaction zones shown are the same as those discussed under Section D-1. Also plotted are all the experimental pressure and temperature data points (except for inert atmosphere runs 23 and 24), the "amount of sodium ejected" coordinate being scaled up in accordance with the ratio of reactor building volume to experimental vessel volume. The experimental pressures and temperatures obviously appear much lower than the theoretical maxima.

The validity of the above transposition of the experimental vessel data to the reactor building on the basis of volume ratio (or oxygen ratio) alone is perhaps questionable. Because of the much larger mean diameter of the reactor building, the effective heat transfer rate to the wall during the pressure buildup period (effected principally by unreacted sodium and reaction product transport) might be comparatively lower, and the peak pressure, therefore, somewhat higher. It is thought, however, that any such peak pressure effect probably is minor.

It is felt that the peak pressure achievable within the EBR-II reactor building by means of sodium-air reaction should not be considered to approach the maximum values obtained experimentally. Firstly, the design objective of the EBR-II primary containment system (which surrounds the primary tank in which the reactor and almost all of the building sodium are situated) is to contain the effects of a nuclear accident without breaching, and any small amounts of sodium which might escape into the building atmosphere could be of little significance. Secondly, even if the primary containment system were to breach, explosive ejection of enormously large amounts of sodium (of the order of 14,000 to 23,000 lb) with extremely great ejection energies (equivalent to 180 to 310 lb of TNT) would be required. Thirdly, an efficiency of distribution and dispersion of the ejected sodium throughout the reactor building comparable to that achieved in the experimental vessel could not be realized (because of a number of readily apparent factors, including the large contributions to building volume represented by the basement, the sub-basement, and the volume above the top missile shield, most of which would not be readily accessible to the ejected sodium).

b. Pressure Fall-Off

The rate of pressure fall-off in the reactor building would be considerably lower than in the experimental vessel. This is true because the ratio of surface area available for cooling to gas volume is much smaller in comparison, and because the building surface heat capacity is comparatively smaller.

The steel in the experimental reaction vessel has a total heat capacity of 72 kcal/F, which means that the entire heat of reaction of all oxygen in the system could be absorbed with less than 50F average temperature rise. This large heat capacity contributed greatly to the rapid rate of system pressure reduction observed immediately after establishment of peak pressure (the pressure normally returning to atmospheric within three minutes from the time of sodium ejection). Comparison of effects of vessel heat capacities of different systems for comparable degrees of reaction may be made by relating the absolute heat capacities to their respective system volumes. On this basis, the relative heat capacity of the experimental reaction vessel is about 12 times that of the EBR-II reactor building (assuming effective heat absorption only by the innermost two-inch thickness of concrete of the missile shielding, which is somewhat pessimistic). Accordingly, higher average wall temperature would be produced in the reactor building (perhaps 325F rise in the most pessimistic case), with correspondingly reduced heat transfer rates, and would mean that pressure fall-off would be considerably slower than in the experimental vessel.

e. Reaction Product Fallout

One possibly beneficial effect of reaction product fallout in addition to that of increasing the rate of pressure fall-off from the peak value attained, as discussed in Section D-3, probably should be noted. If an EBR-II nuclear accident of sufficiently large magnitude to effect ejection of significant amounts of sodium were to occur, the building atmosphere could be expected to include fission products and plutonium, as well as activated sodium. It is probable that upon conclusion of fallout, the atmosphere would consist essentially only of nitrogen and volatile or gaseous fission products, the major portion of the nonvolatile fission product particles having been swept down by the falling reaction products. As a result, it would seem that any assumed gas escape from the reactor building thereafter likely would involve only relatively small fractions of the radioactive material originally introduced.

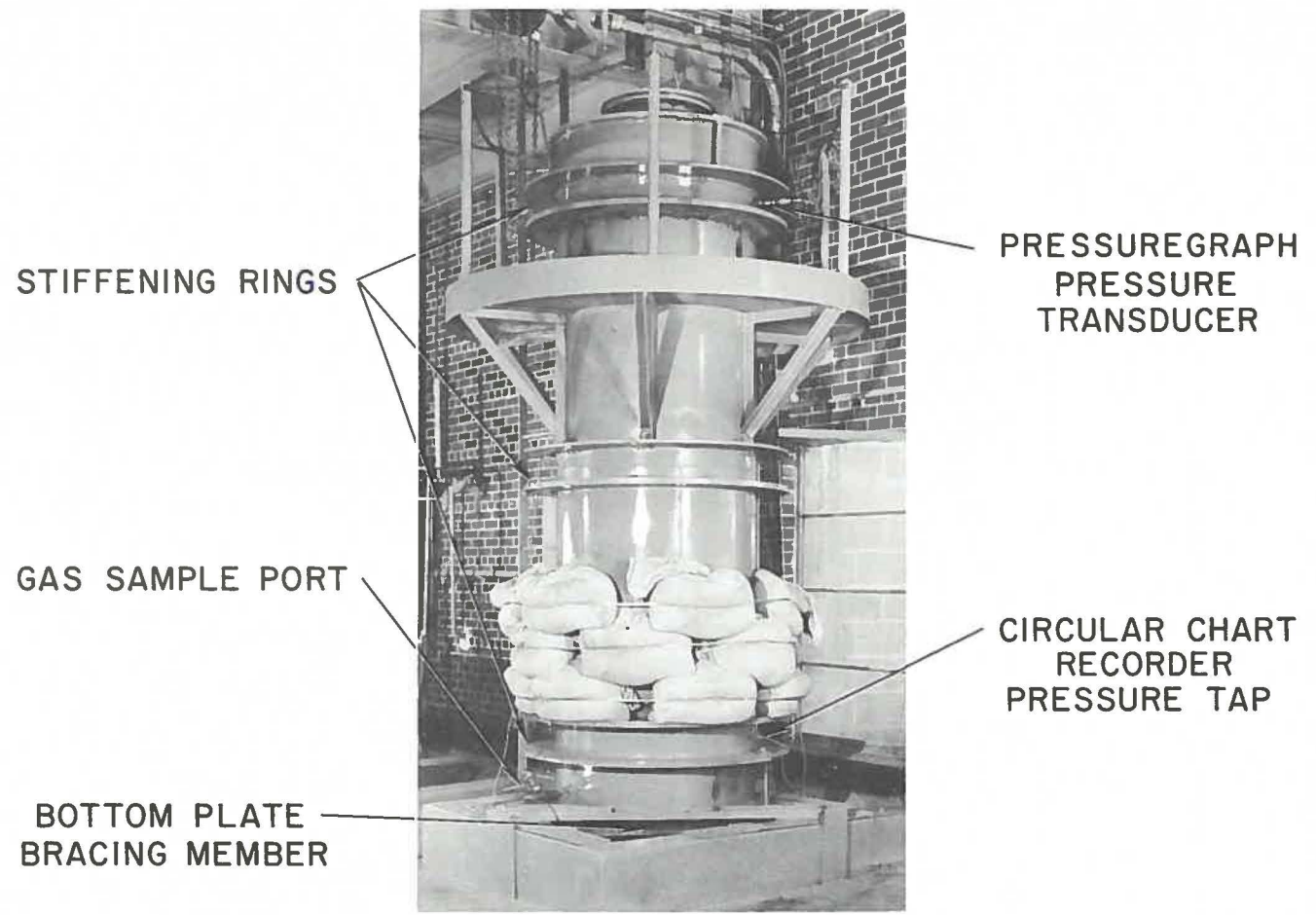


FIG. D-1  
PHOTOGRAPH OF EXPERIMENTAL  
REACTION VESSEL

COMBINATION I - RUNS UP TO 800 g. Na  
 COMBINATION II - RUNS OVER 800 g. Na  
 COMBINATION III - HIGH ENERGY EJECTION GEOMETRY

COMBINATION	VOL. ml.		
	I	II	III
IGNITION CHAMBER	1350	1350	2350
SODIUM RESERVOIR	1000	2000	2400

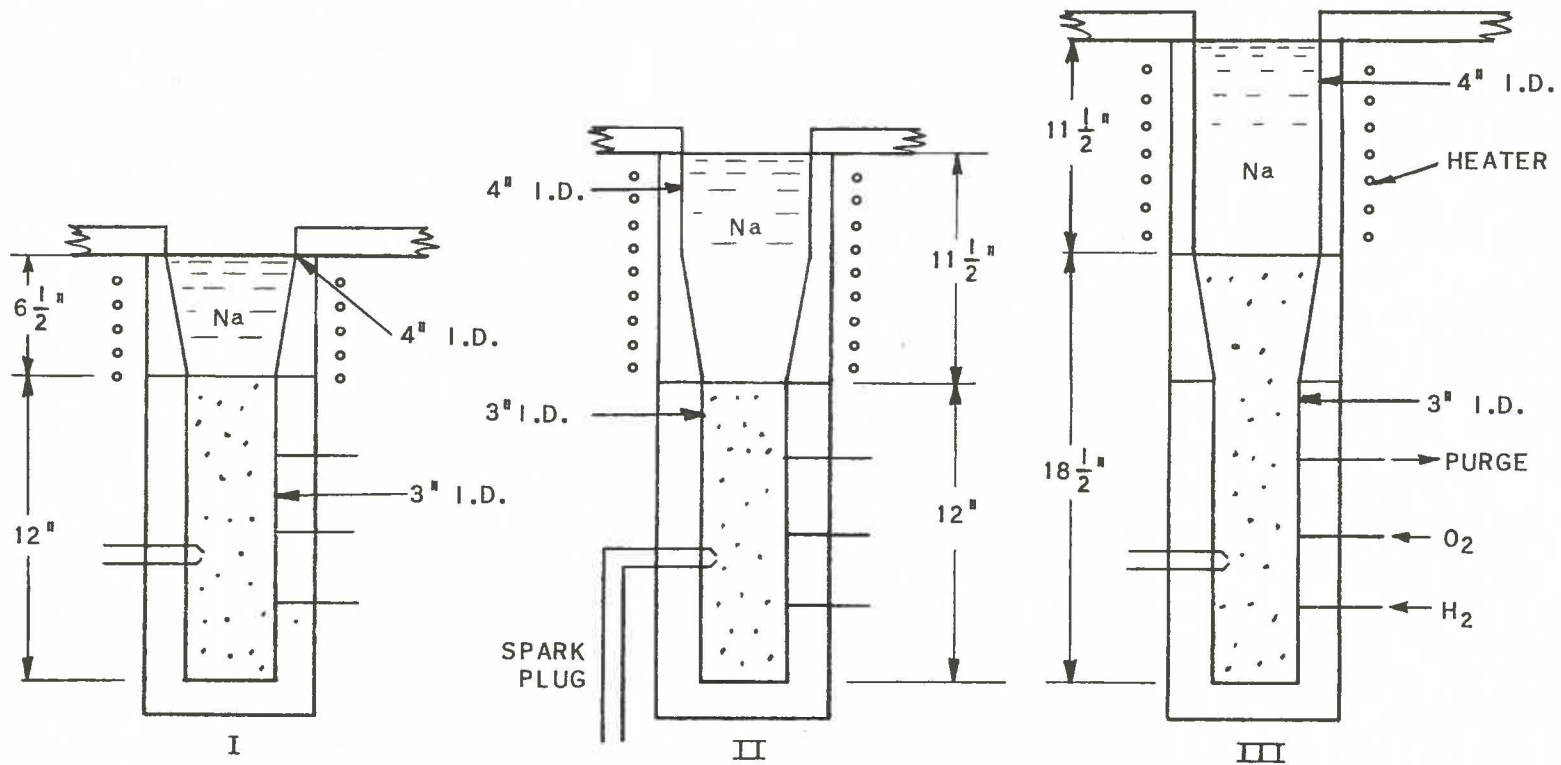
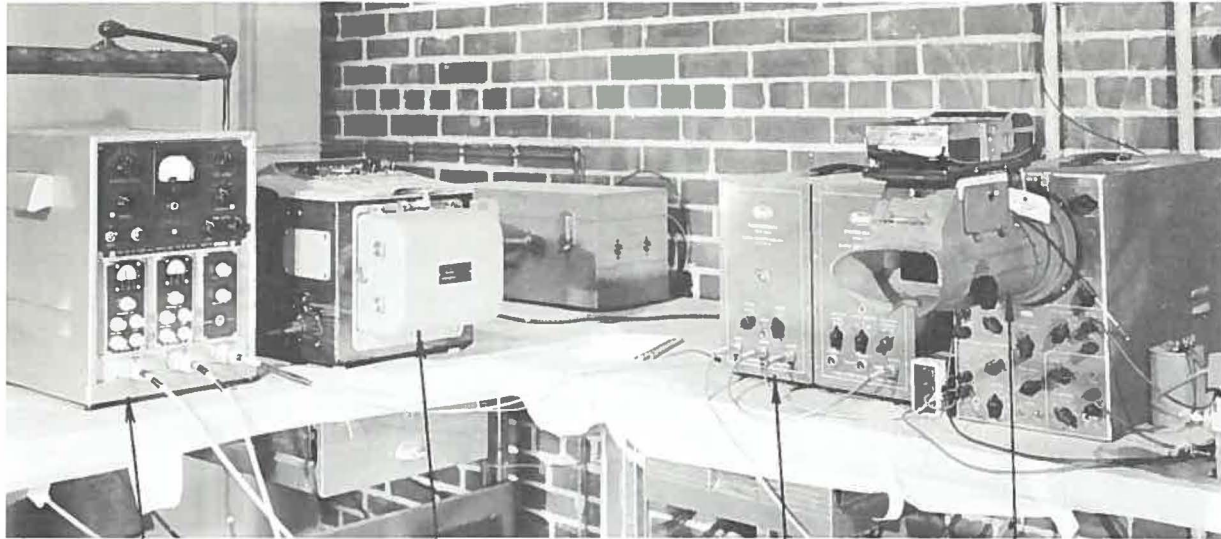


FIG. D-2  
 COMBINATIONS OF EJECTION EQUIPMENT  
 RESERVOIRS AND IGNITION CHAMBERS



STRAIN GAGE  
CONTROL UNIT

OSCILLOGRAPH

CAMERA AND  
OSCILLOSCOPE

HATHAWAY

PRESSUREGRAPH

FIG. D-3  
PHOTOGRAPH OF HIGH SPEED PRESSURE  
RECORDING INSTRUMENTATION

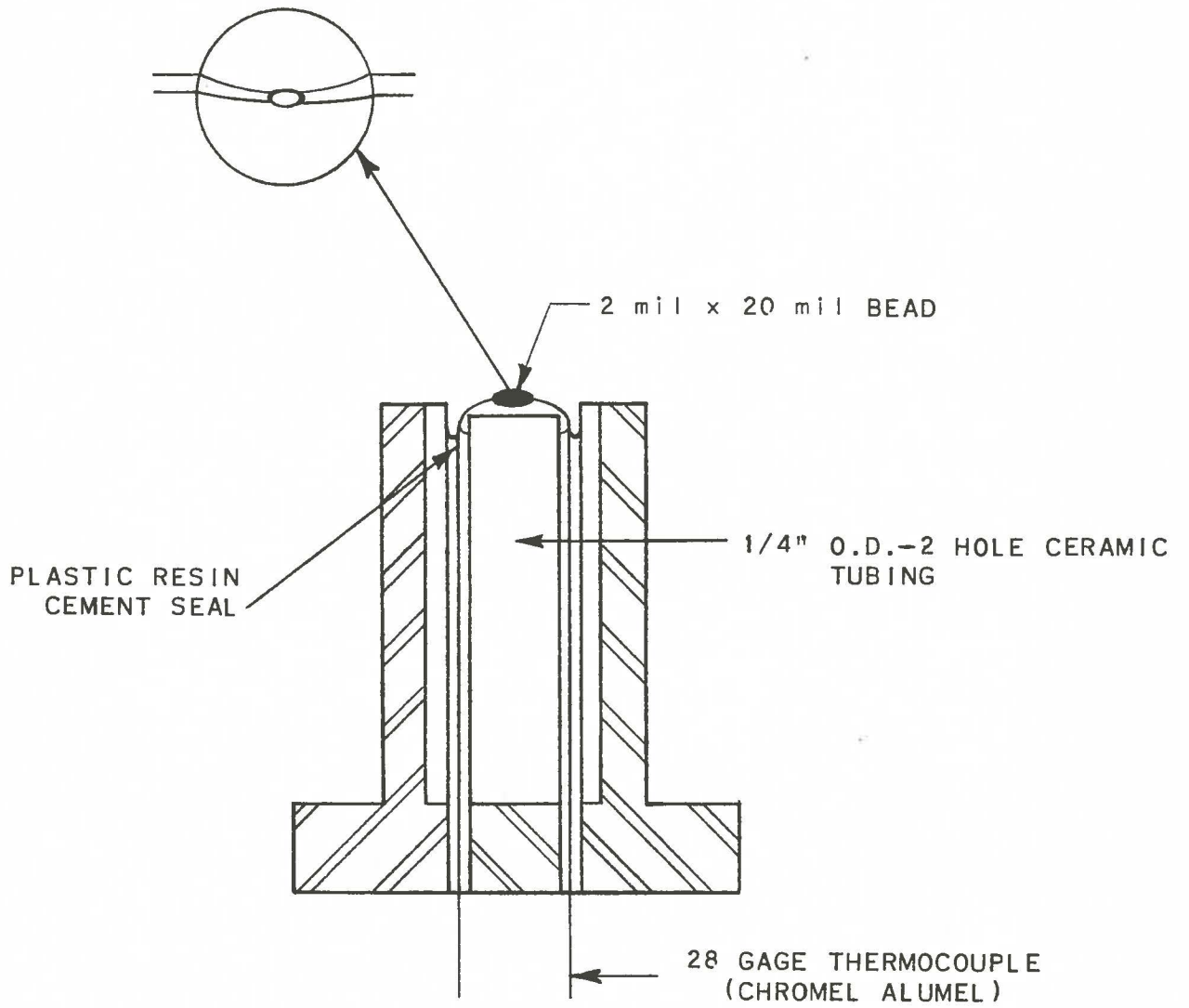
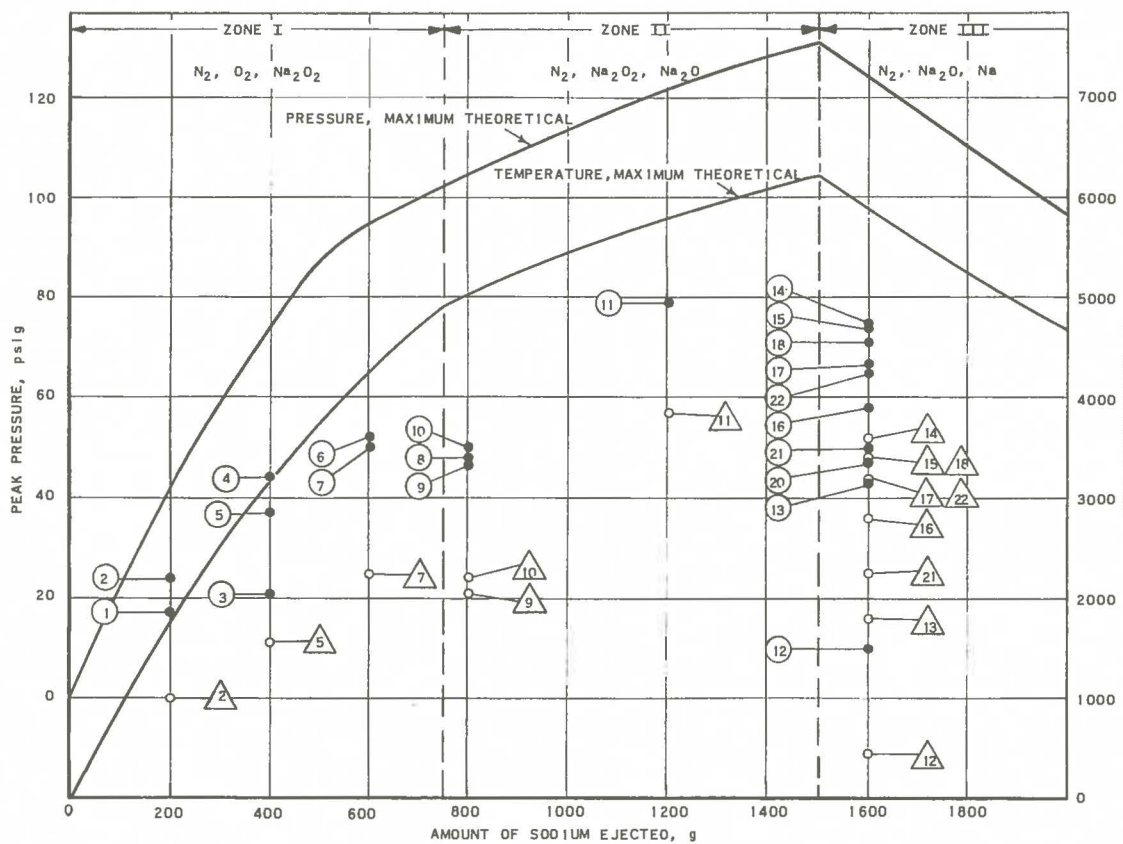


FIG. D-4  
SKETCH OF THERMOCOUPLE USED TO MEASURE  
TEMPERATURE OF WALL DEPOSITS



## NOTES:

1. CURVES INDICATE MAXIMUM POSSIBLE PEAK PRESSURES AND TEMPERATURES BASED ON:

(a) 100% REACTION OF SODIUM OR OXYGEN, WHICHEVER IS LIMITING.

(b) INSTANTANEOUS REACTION (WHICH IMPLIES NO HEAT LOSS; OR, PERFECT DISTRIBUTION, INFINITE PARTICLE VELOCITY, AND INFINITESIMAL PARTICLE SIZE OF THE SODIUM).

(c) THE FOLLOWING AVERAGE SPECIFIC HEATS ARE ASSUMED:

$$C_v(N_2) = 4.82 + 3.3 \times 10^{-4}t - 4.7 \times 10^{-8}t^2 \text{ cal/mole}^\circ\text{C}$$

$$C_p(Na_2O_2) = 0.31 \text{ cal/g } ^\circ\text{C}$$

$$C_p(Na_2O) = 0.31 \text{ cal/g } ^\circ\text{C}$$

$$C_p(Na) = 0.31 \text{ cal/g } ^\circ\text{C}$$

2. EXPERIMENTAL DATA ARE INDICATED AS FOLLOWS:

(A) = EXPERIMENTAL PEAK PRESSURE (MEASURED), RUN A.

(A) = EXPERIMENTAL PEAK TEMPERATURE (CALCULATED FROM MEASURED PEAK PRESSURE), RUN A.

FIG. 0-5  
PEAK PRESSURE AND TEMPERATURE VS QUANTITY OF  
SODIUM EXPLOSIVELY EJECTED INTO EXPERIMENTAL REACTION VESSEL

RE-7-20080-B

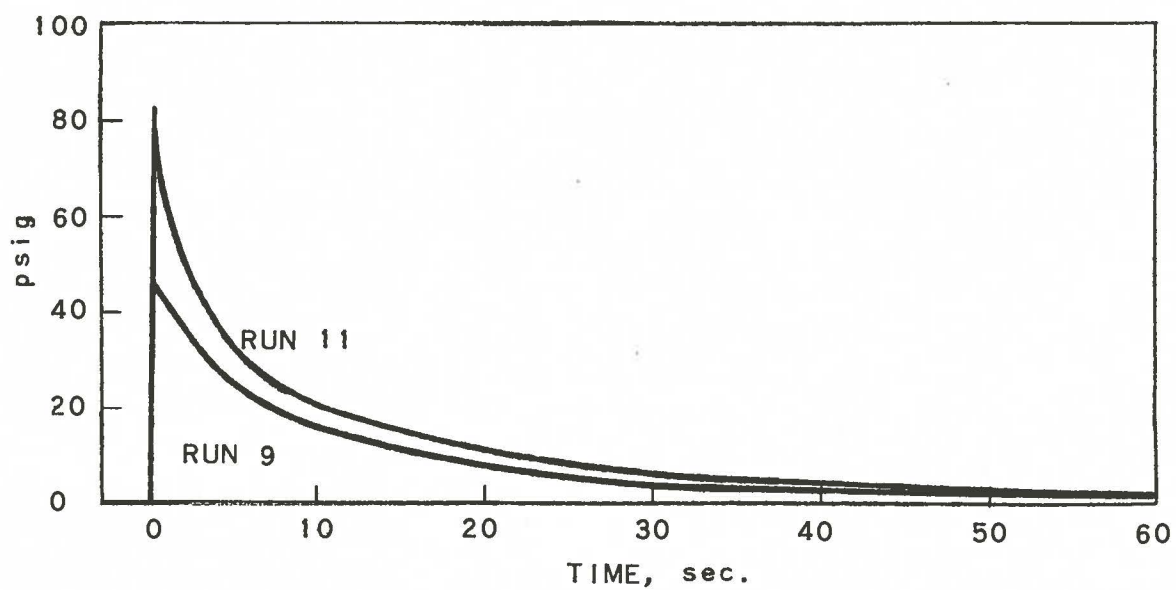
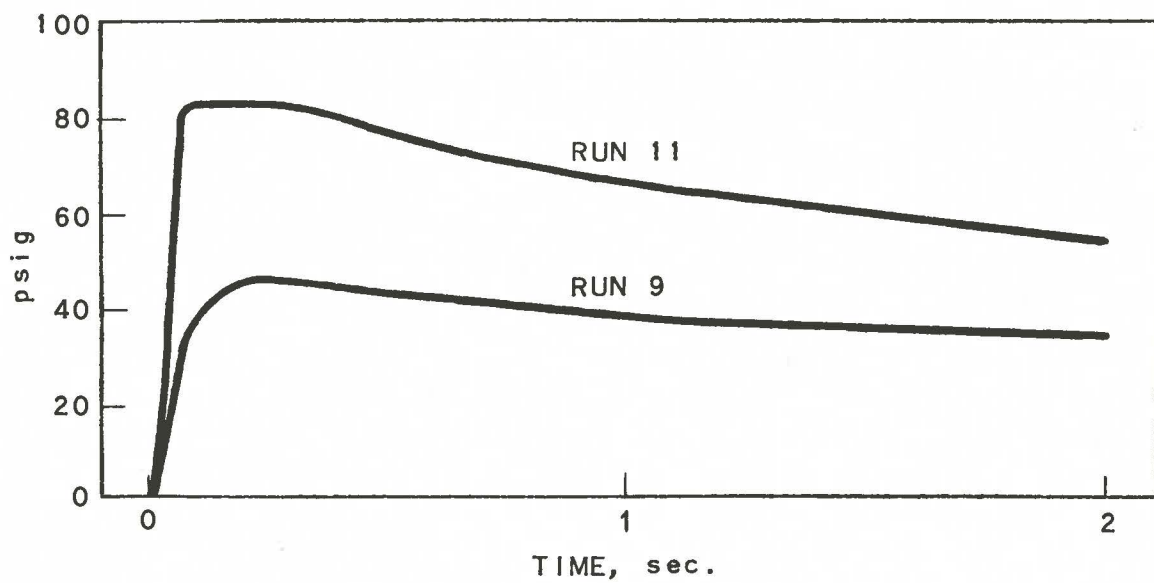
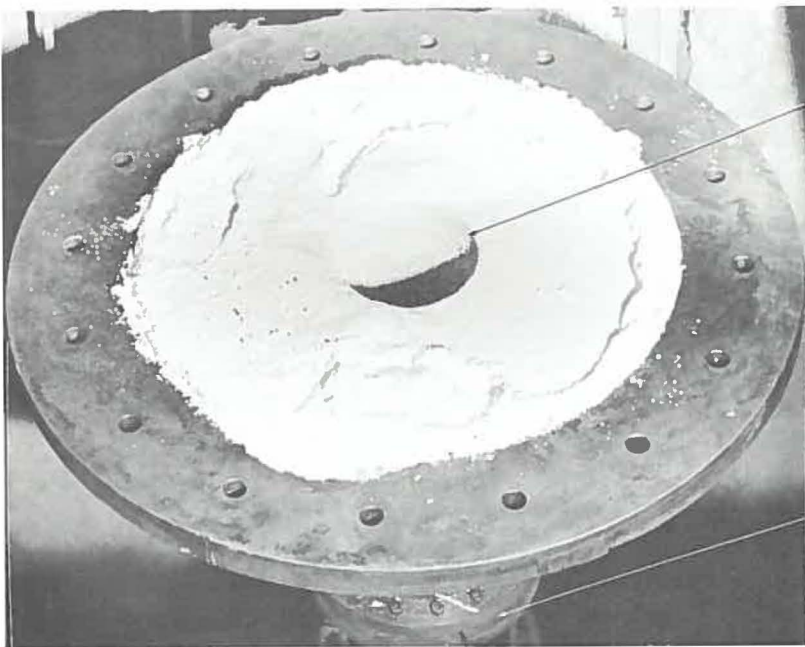


FIG. D-6  
TYPICAL EXPERIMENTAL PRESSURE PROFILES



GASKET

BLOWN TOP RUPTURE  
DISC



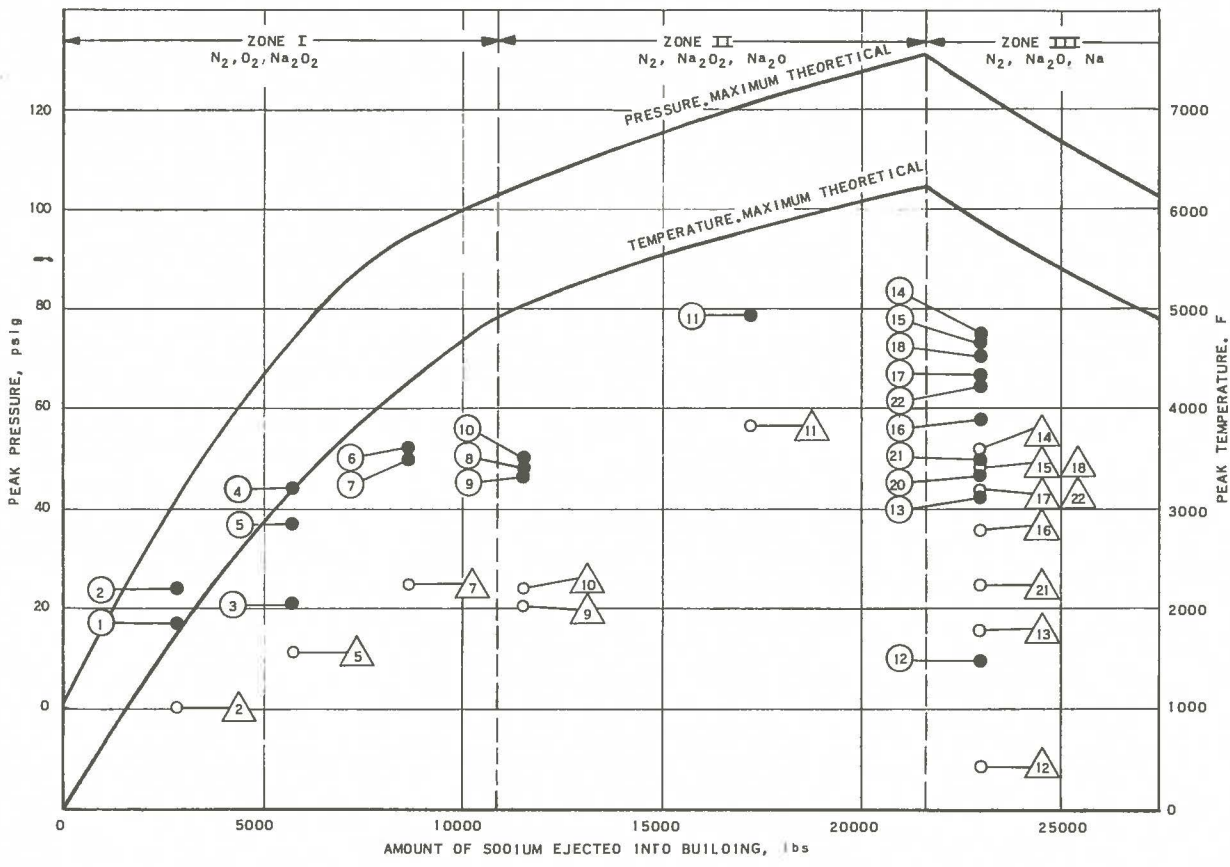
SODIUM EJECTION  
PORT

REACTION VESSEL  
BOTTOM FLANGE

BOTTOM FLANGE OF  
SODIUM RESERVOIR

20"

FIG. D-7  
PHOTOGRAPHS OF REACTION PRODUCT  
FALLOUT ON VESSEL BOTTOM FLANGE



- NOTES:**
- CURVES INDICATE MAXIMUM POSSIBLE PEAK PRESSURES AND TEMPERATURES BASED ON:
    - 100% REACTION OF SODIUM OR OXYGEN, WHICHEVER IS LIMITING.
    - INSTANTANEOUS REACTION (WHICH IMPLIES NO HEAT LOSS; OR, PERFECT DISTRIBUTION, INFINITE PARTICLE VELOCITY, AND INFINITESIMAL PARTICLE SIZE OF THE SODIUM).
    - THE FOLLOWING AVERAGE SPECIFIC HEATS ARE ASSUMED:
      - $C_p(N_2) = 4.82 + 3.3 \times 10^{-4}t - 4.7 \times 10^{-8}t^2$  cal/mole °C
      - $C_p(Na_2O_2) = 0.31$  cal/g °C
      - $C_p(Na_2O) = 0.31$  cal/g °C
      - $C_p(Na) = 0.31$  cal/g °C
  - PLOTTE POINTS REPRESENT TRANSPOSITION OF EXPERIMENTAL DATA IN ACCORDANCE WITH THE RATIO OF REACTOR BUILDING VOLUME TO EXPERIMENTAL REACTION VESSEL VOLUME:
    - = EXPERIMENTAL PEAK PRESSURE (MEASURED), RUN A.
    - △ = EXPERIMENTAL PEAK TEMPERATURE (CALCULATED FROM MEASURED PEAK PRESSURE), RUN A.

FIG. D-8  
 PEAK PRESSURE AND TEMPERATURE VS QUANTITY OF  
 SODIUM EXPLOSIVELY EJECTED INTO EBR-II REACTOR BUILDING

RE-7-20081-B

Handwritten text along the right edge of the page, possibly bleed-through from the reverse side. The text is mostly illegible but appears to be a list or series of entries.

## APPENDIX E

CONTAINMENT OF POSSIBLE ACCIDENTS

Containment of the EBR-II is provided to preclude release of fission products and/or plutonium from the Reactor Plant in the unlikely event of a major nuclear accident. Two echelons of containment are incorporated. The first, termed the "primary containment system," surrounds the primary tank in which the reactor is submerged. Its function is to contain the effects of the nuclear energy release without breaching. The second, termed the "building containment system," surrounds both the primary containment system and the remainder of the Reactor Plant. The function of this system is to localize within the reactor building the effects of a possible sodium-air reaction energy release.

1. Primary Containment Systema. Design

The primary containment system consists primarily of a cylindrically shaped "pressure vessel" which surrounds the primary tank. Figure E-1 gives an over-all view of the design of this vessel. The wall of the vessel is formed by the specially reinforced radial biological shield. The top closure is formed by the top structure of the primary tank support structure, together with the additional structure required for support of the primary system component plugs, and the top biological shielding. The bottom closure is formed by a reinforced concrete structure which employs for its main beams the bottom structure of the primary tank support structure. Top and bottom closures are tied together by six peripherally positioned columns. Figure 32 shows the assembly of the main beams of both closures, together with the six tie columns. Both the vessel wall and the bottom closure are lined on their inner surfaces with a "blast shield."

(1) Vessel Wall

A plan view of the vessel wall is shown in Figs. E-1 and 33. The only penetrations of the wall are those of the shield cooling air ducts, a series of pipes (8 in. dia.) extending approximately radially through the wall in a horizontal plane immediately below the bottom surface of the vessel top closure. These ducts are indicated in Figs. 7 and 34.

Wall material is ordinary density concrete of 2000 psi ultimate compressive strength at 28 days. Nominal wall thickness is 6 ft, with the columns of the support structure positioned within the innermost three feet. The columns are not considered to be part of the vessel wall; they are radially recessed 2 in. into the concrete with clearance provided between the columns and surrounding concrete. Isolation of the columns permits

considerable outward movement of the vessel wall without imposition of lateral loading on the columns (lateral loading being undesirable from the standpoint that it decreases the strength of the columns in respect to hold-down of the vessel top closure). Even though no movement of the vessel wall is contemplated, this arrangement has been incorporated as an added safety feature with the justification that it can be provided easily and at negligible cost.

The major concrete reinforcement is located within the outermost three feet of wall thickness and employs intermediate grade billet-steel bars for which an allowable stress of 20,000 psi is assumed. Design of the reinforcement is based on an internal wall pressure of 75 psig, with no credit taken for strength of the concrete. The concrete strength probably represents an additional 10 to 15 psig permissible internal pressure.

## (2) Top Closure

The main structure of the vessel top closure consists of six radial beams tying into a central ring (12 ft dia.) for accommodation of the large rotating plug, and a reinforcement ring ( $27\frac{1}{2}$  ft dia.). This structure is criss-crossed with numerous additional beams which provide support for the many primary system components hung from, or penetrating through, the structure. A continuous steel plate (1 in. thick) is incorporated across the bottom of the structure. A sectionalized, removable steel plate is provided across the top.

The lower 3 ft of the closure is filled with heavy concrete to form part of the top biological shield. The upper  $3\frac{1}{2}$  ft is utilized for passage of pipes and lines, and for additional shielding. Numerous vertically positioned plugs extend through the closure. A locking arrangement is provided for each of these plugs which securely locks the plug either to the closure structure or to the primary tank cover, except when deliberately unlocked for plug removal. The heat exchanger plug, which contains two 12-in. diameter sodium-carrying pipes, is provided with appropriate void space at its lower end to enable sodium pressure relief through local rupturing of the pipes within the plug (to prevent bursting of the pipe externally to the top closure).

The depth ( $6\frac{1}{2}$  ft) of the top closure is dictated by biological shielding and structure stiffness requirements, rather than by strength requirements based on vessel internal pressure. The design strength of the closure is greater than that which would be required for a vessel internal pressure of 75 psig.

The top closure is tied to the bottom closure by the six columns located about its periphery. These columns, as well as all the beams of the top (and bottom) closure are of Carilloy T-1, for which an allowable stress of 45,000 psi is assumed. The columns are designed to hold down the top closure against a vessel internal pressure of 75 psig.

### (3) Bottom Closure

The bottom closure of the vessel consists of six radial beams (4 ft deep) tying into a central post, the entire structure being imbedded in highly reinforced concrete. The reinforcement bar and concrete specifications are the same as those for the vessel wall, or biological shield. The closure is backed up by the building shell, the shell concrete pad, and the lava rock bed on which the building rests. The arrangement is shown in Figs. E-1 and 32. The bottom closure also is designed for 75 psig internal vessel pressure.

### (4) Blast Shield

The vessel wall is lined on its inner surface with a blast shield, 2 ft thick. The purposes of this shield are to protect the wall from shock wave and to enable absorption of an appreciably large fraction of the total nuclear energy release. Final design of the shield is not resolved; however, it is certain that the effectiveness of the shield as constructed will not be less than that of the shield as presently conceived. The present design consists of four 4 in. thicknesses of porous, 25% normal density concrete alternated with 1/2 in. thick steel plates, followed by two 3 $\frac{5}{8}$  in. thicknesses of glass wool alternated with 1/2 in. thick steel plates.

No blast shield is provided for the top closure, since analysis indicates (as discussed later) that effective shock wave protection is afforded by the 18 in. depth of gas blanket over the primary tank bulk sodium.

To gain additional energy absorption, the bottom closure also is lined with a blast shield; this shield is composed of two tiers of porous concrete and steel plate, and is 1 ft thick.

### (5) Missile Protection

Missile protection is provided as a part of the primary containment system. More than adequate protection from missiles originating within the reactor, all of which would be of low velocity, is afforded by the wall and top and bottom closures of the pressure vessel. Only missiles which conceivably could originate within the top closure require consideration. Protection against the latter is provided by a missile shield (14 in. thick) of reinforced concrete which lines the cylindrical section of the building shell from the operating floor up, and a false ceiling (missile shield) of the same construction which joins the former and completes the enclosure.

b. Evaluation

(1) Analysis

An evaluation of the EBR-II primary containment system has been made by Armour Research Foundation of Illinois Institute of Technology. This study arbitrarily was based on a total energy release within the reactor core equivalent to detonation of 300 lb of TNT. The rate of energy release assumed was that which calculations indicate to be the worst possible from the viewpoint of containment by this particular system (time of energy release equal to about 0.0018 sec). An energy release time either longer or shorter than this would be expected to produce less hazardous conditions.

The major results of this study may be summarized as follows:

(a) The maximum pressure exerted on the bottom surface of the top closure is not more than 24 psig, and this maximum pressure is effective only for about 0.002 sec.

(b) The maximum pressure exerted on the inner surface of the vessel wall, or biological shield, is not more than a few psig (because of the effectiveness of the blast shield).

(c) The steady-state pressure eventually reached within the vessel (assuming no heat loss and no pressure relief through the shield air cooling ducts) is not more than 3.4 psig.

(d) The void space available in the heat exchanger plug is ample to assure that a final plug design can be achieved which will effect pressure relief of the sodium pipes entirely within the plug, without rupture of the pipes externally to the pressure vessel.

The above results are reported in ARF Progress Report No. 2 and a supplementary letter, both of which are reproduced herein as an addendum.

Additional studies have been conducted by Armour Research Foundation, but have not yet been officially reported. The indicated results from these and ANL studies, however, are as follows:

(e) Components wholly submerged in the primary tank bulk sodium, such as blanket subassemblies, reactor tank cover, and pump magnets, are not potential missiles. The maximum possible velocities acquired by these components are a function of component size and other factors, but are in all cases negligibly low. As examples, a cube of

steel one centimeter on a side could acquire a velocity of only about 10 fps, and a cube 50 centimeters on a side, roughly 1 fps. These velocities are negligible in view of the obvious stopping power of the pressure vessel wall and top and bottom closures.

(f) The upward thrust acting on any plug derives from one or both of the following: a gas pressure on the inner plug surface of not more than 24 psig over a period of less than 0.002 sec; a sodium pressure on mechanisms or pipes fastened to the plug and extending through the primary tank gas blanket into the bulk sodium of about 10,000 psig over a similar period of time. Because of the low magnitude and short duration of the maximum gas pressure, and the very small areas and short time over which the maximum sodium pressure acts, no difficulty is anticipated in arranging plug to structure locking devices of ample strength to prevent plug ejection.

(g) Because all sodium pipes make a right angle turn to a horizontal run inside the top closure and are covered with up to three feet of heavy shielding, it seems evident that no pipe which might be torn loose from its plug could be ejected through the top of the closure as a missile.

(h) It is scarcely possible that any of the control or fuel-handling mechanisms could be ejected through the top closure as a missile. All of these mechanisms are of a very long, slender configuration and would require essentially perfect axial alignment of thrust to preclude bending. They pass through at least seven feet of top closure and primary tank cover with only small clearances; a relatively small amount of bending would most surely produce binding during any attempted ejection. The control and safety rod drives also pass through more than two and one-half feet of reactor tank cover, so that any appreciable tipping of this cover, which probably would occur early in the accident, also would tend to bind these particular mechanisms.

(i) Ejection of a portion of a control or fuel-handling mechanism through the top closure is considered to be the most pessimistic assumption which can be made in respect to determination of required missile protection. The maximum possible velocity of such a missile is not more than 200 fps (the maximum sodium velocity in the primary tank, as indicated in the addendum). As examples of the stopping power of reinforced concrete, blunt-nosed projectiles of 6 in. diameter, 200 lb weight and 1,000 fps velocity, or of 2.5 in. diameter, 30 lb weight, and 1,500 fps velocity, penetrate only to a depth of about 11 in. Accordingly, the 14 in. thick missile shield provided, as described earlier, appears to be more than adequate.

(2) Conclusions

(a) For Energy Release of 300 lb TNT Equivalent

The EBR-II primary containment system is capable of withstanding, without breaching, a nuclear energy release within the reactor core equivalent to the detonation of 300 lb of TNT. Although production of missiles of significant energy is improbable, the reinforced concrete missile shielding readily stops the most highly energetic missile possible. Small amounts of sodium vapor escape into the building from the "pressure vessel;" escape occurs through the shield air cooling ducts, and possibly, from ruptured sodium pipes within the top closure (also, through the rotating plug seals, if the accident occurs with the seals in the molten condition).

(b) For Energy Release Greater Than 300 lb TNT Equivalent

It is evident that the primary containment system is adequate to contain nuclear energy releases greater than 300 lb of TNT equivalent. Some pertinent considerations follow:

1) Vessel Wall: An allowable tensile stress of 20,000 psi for the wall reinforcement bars was used in design. Since the ultimate tensile strength of the bars is 60,000 psi, an ultimate safety factor of three is indicated, even without taking credit for the strength of the concrete. Further, the assumed pressure on the inner wall surface was 75 psig, whereas analysis indicates the expected pressure to be only a few, say 5, psig. The latter suggests a safety factor of 15, so that the total safety factor becomes approximately 45. In view of this, the blast shield is being redesigned to reduce its cost (if possible), and, at the same time, to exhibit highest efficiency at energy releases considerably greater than that employed in the present analysis. The final design will be such that the maximum pressure exerted on the vessel wall will be not greater than 25 to 30 psig for any assumed energy release up to at least a few times the present, arbitrary value. The total safety factor then will be in the neighborhood of 7.

2) Top Closure: An allowable stress of 45,000 psi for the main structure (Carillo T-1) was used. Since the ultimate strength of T-1 is 105,000 psi, an ultimate safety factor of at least 2.3 is indicated. In addition, the assumed pressure on the bottom surface of the closure was (more than) 75 psig, whereas analysis indicates the expected pressure to be only 24 psig. The latter ratio is 3.1, so that the total safety factor becomes at least 7.2. The same total factor applies to the columns which hold down the top closure.

3) Bottom Closure: Similarly to the top closure, the total safety factor for the bottom structure is at least 7.2.

4) It can easily be shown that within the range of interest, the maximum gas pressure exerted on the top closure is proportional to less than the one-half power of the magnitude of the energy release. An energy release of 1500 lb TNT equivalence, for example, would be expected to produce a gas pressure of less than 50 psig. The duration of maximum pressure would not be appreciably changed.

5) Similarly, the velocities acquired by submerged components, the sodium pressure exerted on components or mechanisms protruding through the gas blanket into the bulk sodium, and the velocities acquired by mechanisms assumed ejected from the top closure as missiles, all would increase approximately as the square root of the magnitude of the energy release. Again using 1500 lb TNT equivalence as an example, the magnitudes of these variables would be increased only by a factor of about 2.3.

In view of the very large design safety factors employed and the non-linearity of pressure (and velocity) generation, as discussed above, it seems probable that the EBR-II primary containment system is adequate to contain nuclear energy releases several times larger than 300 lb TNT equivalent.

## 2. Building Containment System

### a. Design

The building containment system consists of a steel "building shell" enclosing the primary containment system and the remainder of the Reactor Plant.

#### (1) Shell

The shell is cylindrical, with a hemispherical top closure and a semi-ellipsoidal bottom closure. Inside diameter is 80 ft; total height is approximately 146 ft, 48 ft of which is below grade. Figure 5 gives an over-all view of the shell design. The shell material is ASTM 201 Grade B Fire Box Quality carbon steel. Thickness of the cylindrical section is one inch, and thickness of the closures is commensurate with this in respect to strength. All joints are double butt welded, except joints between subassemblies of double-welded plates of the bottom closure which, of necessity, are single butt welded (with backing strips). Radiographic examination of 10% of weld length is made, including all weld intersections. Stress relieving of the shell as a whole is not contemplated. The shell is to be pneumatically pressure tested at 30 psig.

Based on internal pressure of 24 psig, maximum shell stress is 15,000 psi.

## (2) Openings

A large number of openings through the shell are required for personnel, equipment, sodium pipe, electrical conductor, ventilating air, and other access. All openings are located approximately at grade line elevation. All openings employ gastight seals, either of the metal-to-metal type or of an organic type suitably protected from high-temperature building gas. All openings are designed so as not to detract from the strength of the building shell and so as to be capable of sustaining the same building pressure as the maximum containable by the shell itself. Reinforced shell openings, and all shell plates in the proximity of air locks, are stress relieved. The major openings are briefly discussed below.

The personnel air lock incorporates two vertical door openings each 3 ft wide by 6 ft high. Both doors swing inward toward the Reactor Building. Each door forms a gastight closure. Both doors are provided with motor operation and manual operation. Door operation is such as to permit personnel access to and from the Reactor Building with maintenance of shell gastightness at all times; positive interlocks are provided to permit only one door to be open at a time. The air lock cylinder and the door frames are of the same grade steel as used for the shell. Missile protection is afforded by a 14 in. thick wall of reinforced concrete positioned in front of the air lock opening.

The equipment air lock incorporates two horizontal, circular openings (5 ft dia.). Each door for these openings forms a gastight closure. Both doors are provided with motor operation and manual operation. Door operation is such as to permit access of coffins and other equipment to and from the Reactor Building with maintenance of shell gas tightness at all times; positive interlocks are included to permit only one door to be open at a time. The air lock cylinder and the door frames are of the same grade steel as used for the shell. No missile protection is required, since this air lock is below floor level.

The freight door opening is 7 ft wide by 9 ft high. It is not an air lock, and will be opened only when the plant is shut down. It is gastight, and employs a bolted, gasketed closure. A "hinged" door with roller support is used. Missile protection for the opening is provided by a steel plate of such thickness as to give protection equivalent to that from a 14 in. thick wall of reinforced concrete.

Two openings are provided for the secondary system sodium pipes (12 in. dia.). The sealing of these (and all other) pipes is such as to preclude stressing of the shell. Four openings are required for the primary system shutdown cooler pipes (4 in. dia.), which carry NaK. Eight openings are required for rectifier and main primary pump bus cooling pipes; these pipes (4 in. dia.) carry Dow Corning silicone fluid. Several shell penetrations

are required for pipes serving the building air and shield cooling air coolers; these pipes carry ammonia or silicone fluid. A fast-acting valve is provided in each of the above pipes to maintain building leak tightness in event of an accident.

The ventilation system requires four large (16 in. dia.) pipe openings for air inlet and exhaust. A fast-acting valve is incorporated in each pipe to maintain building leak integrity in event of an accident. Normally, two of these valves are locked in the closed position; they are opened only for occasional purging of the building.

Numerous openings are provided for accommodation of electrical conductors. Design of these openings is such as to permit pressure and leak testing of major portions of the assemblies prior to installation in the building shell and similar testing of the complete sealing assembly, without requiring pressurization of the entire building, after final installation in the building shell.

A compressed nitrogen line penetrates the shell. The purpose of this line is to provide automatic bleed-in of nitrogen to prevent excessive reduction in building pressure due to consumption of oxygen in the event of a major sodium-air reaction. The system is designed to maintain building pressure at not more than 1 psi below atmospheric.

### (3) Tightness

The building shell, complete with "openings," is to be gas-tight. At final acceptance, total building leakage rate with internal pressure of 20 psig will be not more than 1000 cu ft/day.

### (4) Insulation

Insulation over the entire inner surface of the building shell is provided to protect the shell from the high gas temperatures which conceivably could be produced in the event of a significant sodium-air reaction. Except for a portion of the shell top closure, insulation is effected by a minimum thickness of concrete (either structural or missile shield) of 14 in. The remainder of the top closure is protected by high temperature (>1200F) insulation (6 in. thick) lined on its inner surface with sheet steel.

## b. Evaluation

### (1) Without Breaching of Primary Containment System

As discussed earlier, the design objective of the primary containment system is to withstand a nuclear accident without breaching. If breaching does not occur, it is apparent that only small amounts of sodium can escape into the reactor building atmosphere. It is clear from

the discussions of Appendix D that these small amounts could not produce significant pressure rise within the building and that, on this basis, the building containment system as designed is more than adequate.

(2) With Breaching of Primary Containment System

There of course exists some assumed magnitude of nuclear energy release sufficiently large to effect breaching of the primary containment system. With this assumption, appreciable amounts of sodium could be ejected into to building atmosphere.

From Appendix D, it appears that ejection of some 14,000 to 23,000 lb of 750F sodium with ejection energy approximately equivalent to 180 to 310 lb of TNT would be required to produce a building pressure as high as 75 to 80 psig. However, such pressures could be achieved only if the distribution and dispersion of the ejected sodium were as highly efficient as that achieved (with considerable difficulty) in the experimental work described.

The ultimate strength of the building shell steel is 60,000 psi. As noted earlier, the maximum shell stress incurred with building pressure of 24 psig is only 15,000 psi. For this pressure, then, a safety factor of about 4 is indicated. It therefore would appear very possible that, unless metal temperature became too high, the containment system as designed could successfully withstand pressures of 75 or 80 psig. The gas temperature associated with such pressure, however, is of the order of 3900F. Although a temperature of this magnitude would exist for only a very short time, the effect on the concrete and top closure insulation cannot be predicted accurately, and maximum local temperatures of the shell which might be realized become difficult to estimate. As an indication, a maximum possible average temperature of the shell for such an incident can be determined. The total thermal energy released is  $1.3 \times 10^7$  kcal, equivalent to 29,000 lb of TNT. Approximately 50% of the total energy is initially retained by the reaction products; after fallout, a large part of this energy is transferred to the building floor and is not available for heating the shell. A very conservative estimate of average shell temperature might be based, then, on the following assumptions: none of the available energy is absorbed by the missile shield; all available energy is absorbed by that portion of the building shell above the operating floor level, only; and, the available energy amounts to 75% of the total energy released. The thermal capacity of the above portion of the shell is  $3.0 \times 10^4$  kcal/F. Accordingly, the resulting average temperature rise of the shell, based on these pessimistic assumptions, is 325F and the nominal, final average shell temperature is about 400F. As a result (since the shell steel retains its room temperature strength up to 650F), there probably exists at least a possibility that the building containment system could withstand even the most severe sodium-air reaction hypothesized.

In view of the very large amounts of ejected sodium required to produce pressure approaching 75 to 80 psig, and the virtual certainty that the efficiency of dispersion could not equal that obtained experimentally, it seems safe to assume that the peak pressure achievable within the EBR-II reactor building would not reach this very high value, even with relatively major breaching of the primary containment system.

Again from information presented in Appendix D, it can be estimated that ejection of some 3,000 lb of sodium with highly efficient dispersion, or considerably larger amounts with a more realistic degree of dispersion, would be required to produce a building pressure in the vicinity of 25 psig (and gas temperature of about 1200F). Sodium ejection of this order perhaps represents a reasonably realistic possibility. The building containment system, designed for maximum stress of 15,000 psi at 24 psig internal pressure, easily contains such pressure (gas temperature being no problem, since the allowable stress remains constant up to 650F and the maximum shell temperature realized would obviously be considerably lower than this value). After sufficient reduction in gas temperature occurs, the building pressure tends to fall below atmospheric; however, the automatic nitrogen bleed-in system maintains the maximum pressure differential at less than 1 psi, which is also within the design strength of the shell.

**ARMOUR RESEARCH FOUNDATION OF ILLINOIS INSTITUTE OF TECHNOLOGY**

TECHNOLOGY CENTER · 10 WEST 35TH STREET · CHICAGO 16, ILLINOIS · CALUMet 5-9600

PROPULSION AND FLUID MECHANICS  
RESEARCH DEPARTMENT  
3422 SOUTH DEARBORN STREET

IN REPLY REFER TO:

February 20, 1957

Mr. H. O. Monson  
Project Engineer  
EBR-II  
Argonne National Laboratory  
Lemont, IllinoisSubject: "Design Evaluation of EBR-II in Regard to  
Internal Explosion"  
Contract No. 31-109-38-576  
ARF Project No. D090  
Progress Report No. 2

Dear Mr. Monson:

This letter will present an estimate of the pressure time profiles on the top of the primary tank, due to an explosion on the centerline of the tank 8 feet from the bottom. It will also present the Foundation's conclusion that the top of the primary tank is safe if designed to a static pressure of 75 lb/in.<sup>2</sup>.

Details of Analysis

The explosion is considered to be equal in energy to that from 300 lb of TNT. This quantity of TNT yields

$$300 \text{ lb} (453 \text{ g/lb}) 10^3 \text{ cal/g} = 1.36 \times 10^8 \text{ cal}$$

The primary tank is 13 feet = 3.97 m in radius and the sodium is 24.8 ft = 7.56 m deep, hence there are

$$\pi(3.97)^2 7.56 = 375 \text{ m}^3 \text{ of sodium.}$$

At 750°F = 400°C the density of sodium (Ref. 1, page 370) is 0.857 g/cm<sup>3</sup>, hence there are

$$375(0.857) 10^6 = 3.21 \times 10^8 \text{ g of sodium}$$

in the tank.

Mr. H. O. Monson

- 2 -

February 20, 1957

If we assume that the total energy is imparted to the sodium by a shock wave, then the energy will be equally divided between pressure and kinetic energy. If we further assume that the entire tank is at a uniform high pressure when the shock wave strikes the side walls, we can calculate this pressure, if we assume that the sodium behaves as an elastic material.

From Ref. 2

$$\frac{E}{2} = \frac{p^2 V_o^2}{c^2}$$

where  $E$  is now the energy per gram of sodium.

$E = 0.424 \text{ cal/g} (4.18) \text{ joules/cal} 10^7 \text{ ergs/joule} = 1.77 \times 10^7 \text{ ergs/g}$ ,  
 $V_o$  is the specific volume  $1.17 \text{ cm}^3/\text{g}$ ,  $c$  is the speed of sound in sodium  
 $2.75 \times 10^5 \text{ cm/sec}$  while  $p$  the pressure behind the shock wave in  
 $\text{dynes/cm}^2$ . Solving this equation for  $p$  we obtain

$$p^2 = \frac{Ec^2}{2V_o^2} = \frac{1.77 \times 10^7 \text{ ergs} (2.75)^2 \times 10^{10} \text{ cm}^2 \text{g}^2}{2(1.17)^2 \text{ cm}^6 \text{ sec}^2}$$

$$p = 7.07 \times 10^8 \text{ dynes/cm}^2 = 700 \text{ atm}$$

Now the flow velocity behind this shock wave will be given by

$$\begin{aligned} \mu &= \frac{7 \times 10^8 \text{ } 1.17 \text{ g cm cm}^3 \text{ sec}}{2.75 \times 10^5 \text{ sec}^2 \text{ g cm cm}^2} \\ &= 2.98 (10^3) \text{ cm/sec} \cong 100 \text{ ft/sec} \end{aligned}$$

Since the side walls of the tank cannot withstand 700 atm, they will start to move out at this velocity the instant the shock wave strikes them.

The shock wave moving toward the top of the tank travels at about the acoustic velocity and covers the  $16.8 \text{ ft} = 5.12 \text{ m}$  from the presumed center of the explosion to the argon in

$$t = \frac{5.12 \text{ m sec}}{2750 \text{ m}} = 0.00186 \text{ sec}$$

Now the sodium, which was immediately behind the shock wave, moving at  $29.8 \text{ m/sec}$  doubles its velocity and moves into the argon at  $59.6 \text{ m/sec}$ .

We now assume that an expansion wave starts from the center of the tank at the instant the shock breaks the sodium surface. To calculate the

distance required for this expansion wave to catch the moving sodium, we note that in time  $t_1$  from the start of the explosion, the interface will move a distance

$$\left( t_1 - \frac{5.12}{2750} \right) 59.6 = d$$

while the expansion wave will move a distance  $d + 5.12$  m in time

$$t_1 - \frac{5.12}{2750}, \text{ hence}$$

$$\frac{d + 5.12}{2750} = t_1 - \frac{5.12}{2750}$$

We solve for  $d$  easily by substitution for  $t_1$  between these two equations as

$$\left( \frac{d}{2750} + \frac{5.12}{2750} \right) 59.6 = d,$$

which yields  $d \cong 0.113 \text{ m} = 0.372 \text{ ft}$ .

From this we see that the sodium never reaches the top of the tank except as a spray, since it is broken up when the expansion wave catches it.

A shock wave will be produced in the argon by the sodium as it moves upward. The speed of sound in argon at  $400^\circ\text{C}$  is about  $1390 \text{ ft/sec} = 425 \text{ m sec}$ . Hence,

$$\frac{\mu}{a} = \frac{59.6}{425} = 0.140$$

Now from any table of shock wave properties in argon, such as Ref. 3, we see that the shock Mach No. is 1.09 under these conditions, and the pressure ratio across the shock is  $(p_1/p_0) = 1.23$ . This was obtained by using

$$\frac{p_1}{p_0} = \frac{2\gamma M_1^2 - (\gamma - 1)}{\gamma + 1} \quad (\text{Ref. 4})$$

where  $\gamma$  = specific heat ratio 1.66 for argon. This shock wave reflects from the top of the tank and the pressure behind this reflected wave will rise to  $(p_2/p_0) = 2.6$ .

This pressure will last until the expansion wave from the sodium travels through the argon and relieves it. The initial shock wave in the argon travels at  $3200 \text{ ft/sec} = 976 \text{ m sec}$ , and therefore, strikes the top of the tank in a time

Mr. H. O. Monson

- 4 -

February 20, 1957

$$0.00186 + \frac{0.366}{976} = 0.00223 \text{ sec}$$

after the initial explosion. The expansion wave comes to relieve this pressure in roughly

$$\frac{0.250 \text{ m sec}}{672 \text{ m}} = 0.000372 \text{ sec} + 0.00372 \text{ sec}$$

for a total time of 0.00409 sec from the instant of explosion. Hence, this pressure lasts 0.00409 - 0.00223 sec for a total of 0.00186 sec before relief.

At time  $t_1$  the sodium starts to fall back in the tank and oscillates to its final equilibrium pressure. The final equilibrium pressure in the tank may be calculated as follows on the conservative assumption that no leakage of gas or sodium occurs from the inner tank.

When equilibrium has been established, the temperature of the argon and the sodium will be the same. If both were at the same temperature initially, i. e., 750°F or 400°C, we can write the first law of thermodynamics as

$$E = (c_{P_{Na}} M_{Na} + c_{P_A} M_A)(T - 673^\circ\text{K})$$

where  $E = 1.36 \times 10^8 \text{ cal}$ ,  $c_{P_{Na}} = 0.32 \text{ cal/g}$ ,  $M_{Na} = 3.21 \times 10^8 \text{ g}$ .

$$c_{P_A} = 0.26 \text{ cal/g} \quad M_A = 475 \text{ g.}$$

Note: The mass of argon is obtained by taking the volume of a tank 7.56 m in radius and 0.366 m high and multiplying by 0.000724 g/cm<sup>3</sup>, the density of argon at 1 atm pressure and 673°K.

Solving the above for T we obtain  $T = 674.3^\circ\text{K}$ . The temperature increase is less than two degrees Kelvin. Under these circumstances, the pressure increase due to the temperature increase can be at most 3.4 psi for a final pressure of 18.1 psi.

#### Final Results and Conclusions

A proposed pressure time curve for design purposes is given as Fig. E-2. It is apparent from Fig. E-2 that if the top of the tank is designed for a static pressure of say 75 lb/in.<sup>2</sup>, then no danger need be anticipated from internal explosions under the assumed conditions.

Mr. H. O. Monson

- 5 -

February 20, 1957

It must be noted that this analysis does not account for pipes which might go down through the argon into the sodium. These pipes will be exposed to pressures like 700 atm and must be analyzed later when the basic designs are further completed.

For convenience, a distance-time diagram showing the sodium argon motion and the shock and expansion waves is attached as Fig.E-3. It is hoped that this letter provides the necessary data for design purposes. Further letter reports will be presented as data is generated.

Respectfully submitted,

ARMOUR RESEARCH FOUNDATION OF  
ILLINOIS INSTITUTE OF TECHNOLOGY

*S. A. Hoenig*

S. A. Hoenig, Associate Engineer

#### REFERENCES

1. Sodium, Marshall Sittig, Reinhold Publishing Corporation, New York, 1956.
2. B. E. R. Report, pages 1-11.
3. Resler, Lin and Kantrowitz, Journal of Applied Physics, Vol. 23, No. 12, December 1952, pages 1390-99.
4. NACA TN 1135, 1953.

**ARMOUR RESEARCH FOUNDATION OF ILLINOIS INSTITUTE OF TECHNOLOGY**

TECHNOLOGY CENTER · 10 WEST 35TH STREET · CHICAGO 16, ILLINOIS · CAIumet 5-9600

PROPULSION AND FLUID MECHANICS  
RESEARCH DEPARTMENT  
3422 SOUTH DEARBORN STREET

March 22, 1957

IN REPLY REFER TO:

Mr. Harry Monson  
Reactor Design Division  
Argonne National Laboratories  
Lemont, Illinois

Dear Mr. Monson:

This letter may be considered an extension or modification of our letter report No. 2 of February 20, 1957.

With regard to the bottom of the structure, beneath the Sodium tank, no problems need be anticipated. The concrete and steel structure will be adequate to prevent any damage to the main containment shell.

In answer to your question about the biological shield I think we can be sure that the blast shield will reduce the pressures on the biological shield to a few PSIA above normal. Similarly, because of the Argon layer above the Sodium, the top structure will be subjected to pressures no greater than 38.2 PSIA for a time of no more than about 2 M.S.

In the case of the vertical pipes carrying Sodium from the heat exchanger, as long as the present space in the top cover (some 4-1/2 feet in diameter) is available, the bursting pipes will be able to relieve themselves completely inside the top cover.

The time of energy release was chosen as that value which would result in the entire volume of Sodium being raised to the same high pressure by the shock wave. This would delay pressure relief until the last possible moment and result in the most conservative design. For this reason it is our opinion that this rate of energy release represents the worst possible case.

It is hoped that this letter will be of assistance to you.

Yours truly,

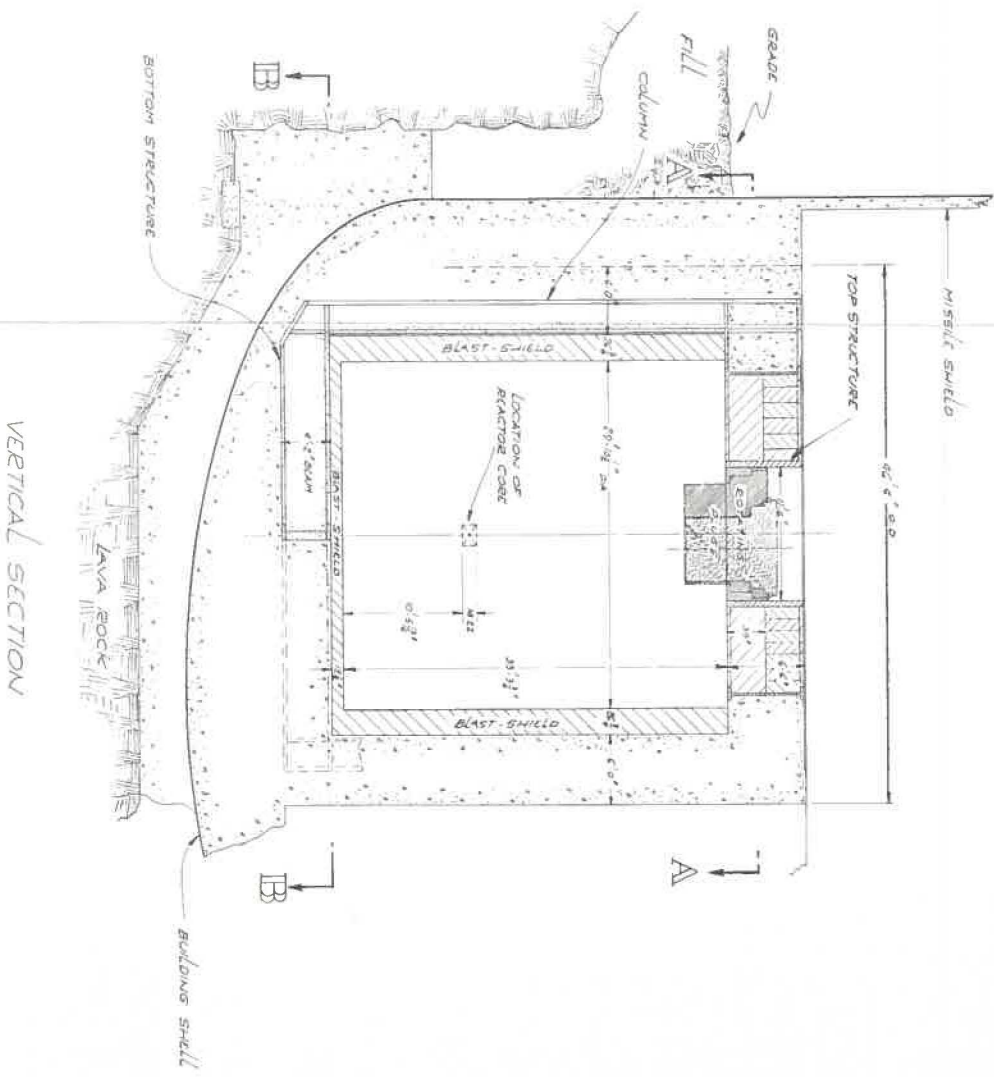
*S. Hoenig*  
S. Hoenig  
Associate Engineer

FILE \_\_\_\_\_  
DCV \_\_\_\_\_

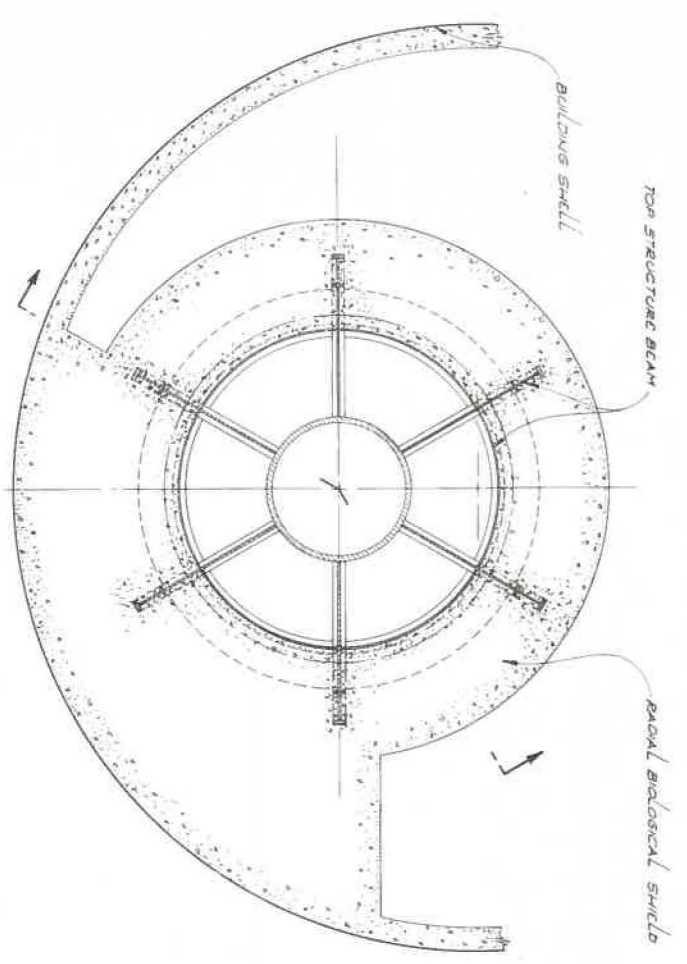
MAR 25 1957

H. O. MONSON  
REACTOR ENGINEERING DIV.

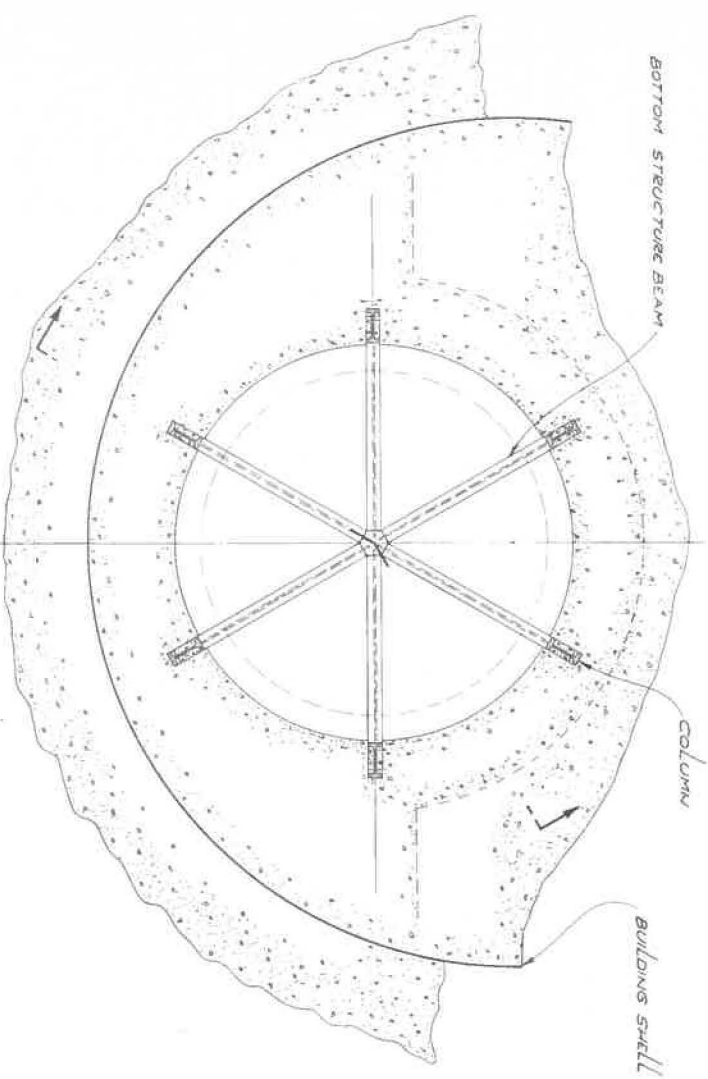
ACTION \_\_\_\_\_



VERTICAL SECTION



SECTION A-A



SECTION B-B

FIG. E-1  
PRIMARY CONTAINMENT SYSTEM "PRESSURE VESSEL"

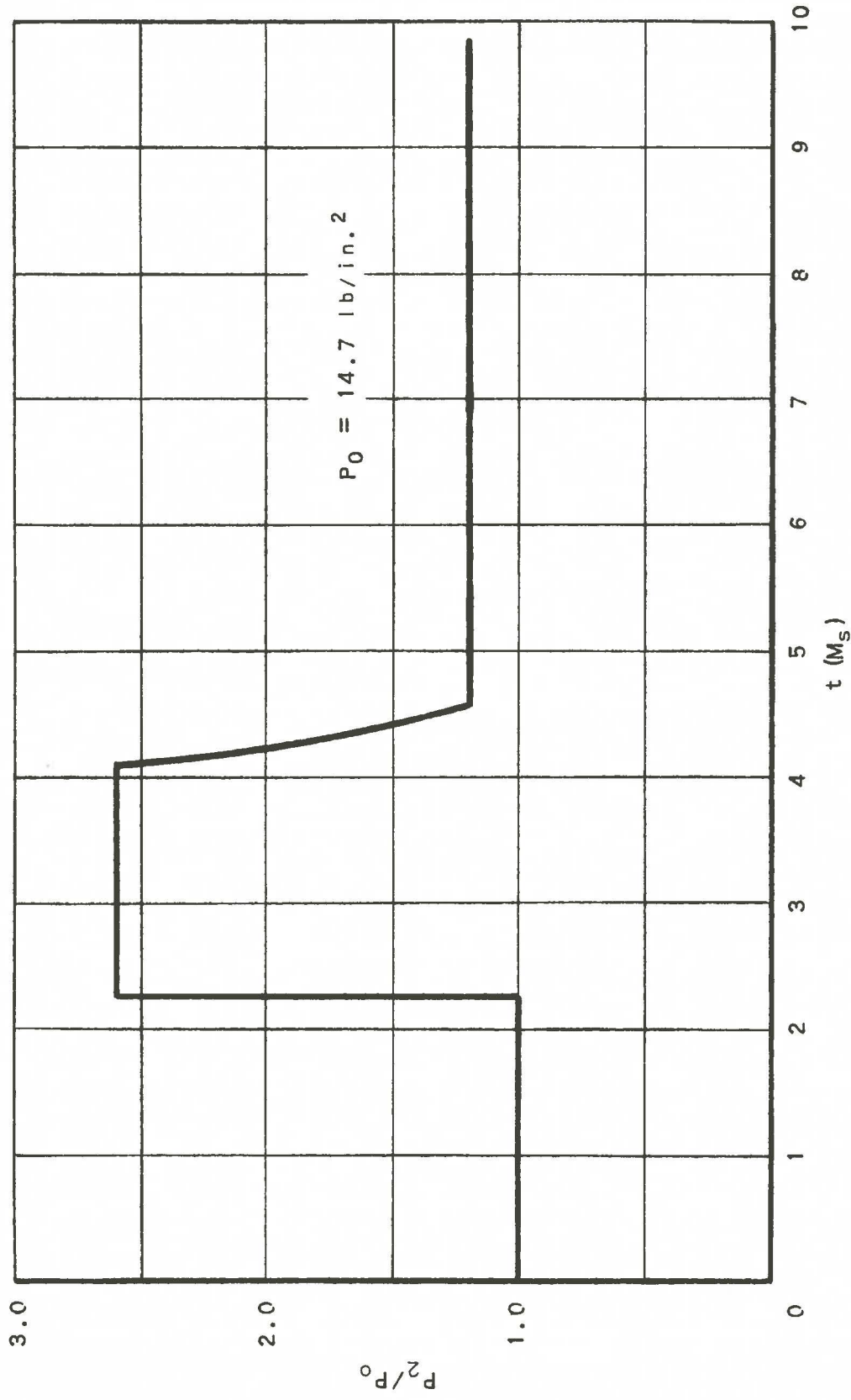


FIG. E-2  
PRESSURE TIME PLOT FOR TOP OF TANK

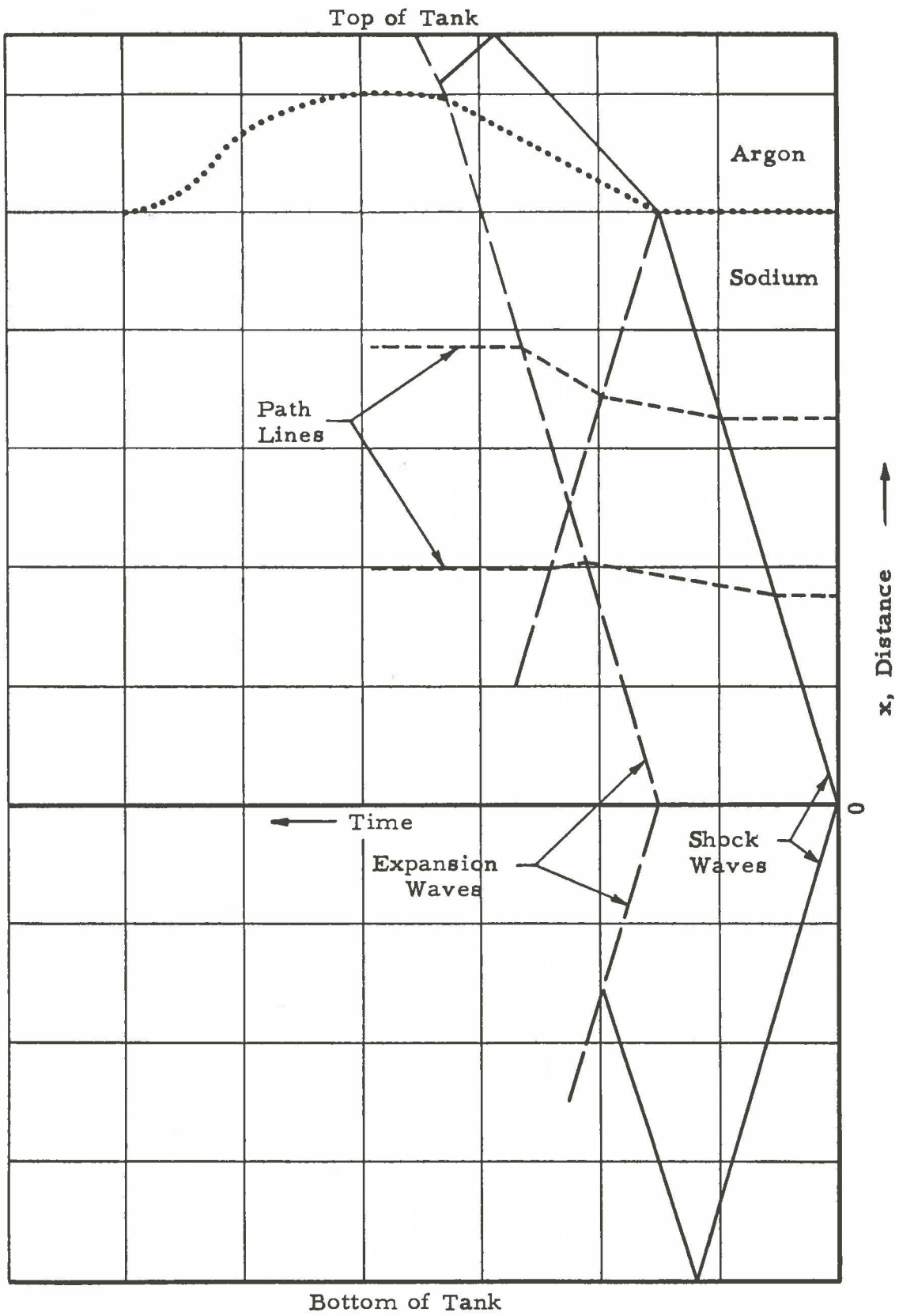


Fig. E-3 Distance Time Diagram for Primary Tank

## APPENDIX F.

THE RADIATION HAZARD TO THE SURROUNDING AREA FROM A  
HYPOTHETICAL REACTOR DISASTER

In the following hazard estimates, it has been arbitrarily assumed that a reactor operates continuously at a steady power of 60 megawatts. At the end of 135 days of such operation, a hypothetical reactor disaster occurs which consists of  $10^{20}$  fissions in one millisecond and which ruptures the containment shell. The steady operation and the disaster depend primarily upon the fission of  $U^{235}$  by fast neutrons. It has also been arbitrarily assumed that at the time of the disaster, the reactor core contains 125 kg of  $Pu^{239}$ .

The energy liberated instantaneously by the disaster will be about 185 Mev/fission or about  $7.1 \times 10^8$  calories for  $10^{20}$  fissions.

The pessimistic assumption has been made that 50% of the fission product activity contained in the reactor (and 50% of the  $Pu^{239}$ ) is released to the atmosphere by the disaster. It has been further assumed that there is no fallout of the activity released to the atmosphere except in the case of washout which is considered separately. This causes the estimated radiation doses more than several miles downwind to be on the high side since there will be a certain amount of fallout. Similarly, the estimated radiation doses within several miles of the hypothetical disaster will be on the low side; however, with the exception of the staff at the reactor site, there are no people within several miles of the reactor building.

So far as gross beta and gamma activity are concerned, that resulting from the steady power period of operation is roughly equal to the activity resulting from the  $10^{20}$  fissions at about 12 seconds after the disaster. For times greater than two minutes after the disaster, the activity built up during steady power operation is more than 10 times the activity from the  $10^{20}$  fissions. For times greater than 25 minutes after the disaster, the activity built up during steady power operation is more than 100 times the activity from the  $10^{20}$  fissions. Hence, only the effects of the long term fission product buildup were considered in the following estimates. For purposes of estimating the internal radiation hazards, the 125 kg of Pu and those fission products generated during the long-term operation, having half-lives greater than a day, were taken into account. Again the contribution of the  $10^{20}$  fissions is negligible, steady state operation having produced 1000 times as much activity.

For a power reactor which has been operating at a steady power of P kilowatts for  $t_0$  sec before shutdown (here, by a disaster), the gamma source strength of the fission products can be approximated by

$$2.3 \times 10^{14} P \left[ t^{-0.21} - (t_0 + t)^{-0.21} \right] \text{ Mev/sec}$$

where  $t$  is the time after shutdown in seconds, the beta source strength can also be approximated by the same expression (ref. 1, pp 107, 157). Therefore, in the following hazard estimates, the gamma and the beta source strengths have been taken as

$$6.9 \times 10^{18} \left[ t^{-0.21} - (t_0 + t)^{-0.21} \right] \text{ Mev/sec .}$$

In estimating the external radiation hazard from airborne activity, the quantity in brackets has been approximated by  $t^{-0.21}$ ; this overestimates the source strength by 20% to 50% in the period 1/2 hour to 24 hours.

The seriousness of the estimated external radiation doses may be gauged by comparison to several numbers. One such number is a total exposure of 300 r over the whole body (about 15% mortality). This exposure is the limiting dose used by the Reactor Safeguard Committee in defining the exclusion radius for a power reactor (ref. 2). Another such number is a total exposure of 25 r (measured in air) over the whole body. This is the "once in a lifetime" dose defined in the National Bureau of Standards Handbook 59 (ref. 3). The "once in a lifetime" dose is supposed to produce no detectable clinical effects; it is assumed that an exposure of 25 r will have no effect upon the radiation tolerance status of the observer.

Estimates of the internal radiation doses downwind have been made using the values given in Table F-I. Column 2 of Table F-I has been taken from Table IX of ANL-5334, Estimation of Fission Product Spectra in Fuel Elements Discharged From The Power Breeder Reactor And The Experimental Breeder Reactor No. 2, I. G. Dillon and Leslie Burris, Jr., October, 1954. Column 3 of Table F-I is derived from column 2. Columns 4 through 10 have been taken from Tables C.IV, C.V, and C.VIII of Supplement No. 6 to the British Journal of Radiology, Recommendations Of The International Commission On Radiological Protection, revised December 1, 1954. The radioisotopes for which internal hazard estimates have been made are those isotopes listed in ANL-5334 for which values are given in Supplement No. 6.

Column 2 of Table F-I gives the number of atoms of each radioisotope per 100 atoms fissioned ( $U^{235}$  by 1-Mev neutrons) after 135 days of steady operation and no cooling time. Steady operation at 60 mw for 135 days results in a total of  $2.184 \times 10^{25}$  fissions. Thus the number of atoms of each radioisotope present in the reactor at the time of the hypothetical disaster is  $2.184 \times 10^{23} \times$  (value in column 2). The number of atoms of each radioisotope has been expressed in microcuries, multiplied by 50%, and listed in column 3. The 125 kg of  $Pu^{239}$  has an activity of  $7.66 \times 10^9$  microcuries; 50% of this activity has been listed in column 3. The values in column 3 have been arbitrarily taken as the amounts of the radioisotopes which escape from the reactor building and travel downwind as a result of the hypothetical reactor disaster.

The most serious inhalation or external radiation hazard will exist during the time the radioactive cloud or plume is passing by the observer; more indirect ways of getting an internal radiation dose, such as breathing radioactive dust caused by fallout, have not been considered here. In general, the hazard due to a cloud or plume will be serious only for one or possibly two days after a hypothetical disaster. The half lives of the radioisotopes considered here are long enough that the decay of the activity from the time of the disaster to the time of inhalation has been neglected. The hazard estimates for  $\text{Mo}^{99}$  will be a little on the high side because  $\text{Mo}^{99}$  has a 2.8 day half-life. The amounts of  $\text{La}^{140}$  and  $\text{Pm}^{147}$  build up during the first 30 days following the reactor shutdown so that estimates of the inhalation hazard will be a little on the low side (ref. 4).

The seriousness of the estimated internal radiation dose due to inhalation of specific radioisotopes may be gauged by comparing the amounts of the radioisotopes accumulated to the maximum permissible body burdens as given by column 5 of Table F-I. For the internal radiation dose due to ingestion of specific radioisotopes, the drinking water concentration of the various activities may be compared to the maximum permissible concentration as given in column 8 of Table F-I. As explained in Supplement No. 6, "The...values of maximum permissible body burden and maximum permissible concentration in air and water...are developed on the premise that the maximum permissible concentration in air or water is that which will permit the accumulation of a burden of the radioisotope in the critical body organ, so that it will receive an average dose-rate of 0.3 rem/week after the contaminated air or water has been used exclusively for a time that is much longer than the effective half-life of the radioisotope in the critical body organ, but not greater than 70 years in any case." (ref. 5, p. 42). The maximum permissible body burden and concentrations in air and water for  $\text{Pu}^{239}$  are obtained from a comparison with radium for which there is a long established maximum permissible body burden. "Permissible dose is a dose of ionizing radiation that, in the light of present knowledge, is not expected to cause appreciable bodily injury to a person at any time during his lifetime. As used here, 'appreciable bodily injury' means any bodily injury or effect that a person would regard as being objectionable and/or competent medical authorities would regard as being deleterious to the health and well-being of the individual." (ref. 5, p. 15).

The choice of the critical organ for which hazard estimates have been made (column 4 of Table F-I) is somewhat arbitrary and limited. Except for  $\text{Pu}^{239}$ , only the hazards resulting from soluble compounds of the various radioisotopes have been considered. For insoluble compounds, the lungs or the gastrointestinal tract are usually the critical organ. Similarly, for soluble compounds of the radioisotopes, the gastrointestinal tract is usually the critical organ during the period of ingestion or inhalation. However, other organs (column 4 of Table F-I) become the critical organs when the intake of the radioisotope is discontinued (ref. 5, p. 27). Despite the

limited consideration of the internal radiation hazards, it is felt that the estimates that have been made should be sufficient to indicate the order of magnitude of the internal radiation hazard.

For the parent-daughter radioisotopes listed in Table F-I, the values tabulated refer to the parent, not the daughter; e.g., the maximum permissible body burden is 98 microcuries of  $\text{Cs}^{137}$ , not 98 microcuries of  $\text{Cs}^{137} + \text{Ba}^{137}$ . Similarly, the effective half-life of  $\text{Cs}^{137}$  is 17 days, etc. "It is assumed in these cases that the appropriate fraction of equilibrium of the daughter is reached with the parent element after fixation of the parent takes place in the critical body organ. It is further assumed that the daughter element remains in the critical organ after its birth for a length of time determined by its biological and radioactive half-life, and, consequently, contributes to the total dose." (ref. 5, p. 56). In the case of the inhalation hazard, the radioisotope is essentially taken into the body in one shot, not continuously. Thus the comparison of the amount of  $\text{Zr}^{95} + \text{Nb}^{95}$  accumulated by inhalation to the maximum permissible body burden will make the hazard look somewhat worse than it is because it takes between 100 and 200 days for the  $\text{Nb}^{95}$  to reach equilibrium with the  $\text{Zr}^{95}$ , whereas the effective half-life of  $\text{Zr}^{95}$  in the body is about 48 days. For the other parent-daughter radioisotopes, the time required to reach equilibrium is short compared to the effective half-life of the parent; thus an equilibrium state is reached before the body burden of the parent has decreased to any extent (say, to 0.7 of its original amount).

Of the radioisotopes listed in Table F-I,  $\text{Ag}^{111}$ ,  $\text{Te}^{127}$ ,  $\text{Sr}^{89}$ ,  $\text{Y}^{91}$ , and  $\text{Nb}^{95}$  have isomeric states. The values taken from ANL-5334 and from Supplement No. 6 refer to the long-lived isomer. The hazard due to the inhalation or ingestion of the short-lived isomer should be negligible by comparison.

The radioactive half-lives given in Table F-I are those taken from Supplement No. 6. A few of these half-lives differ by as much as 20% or 30% from the half-lives used in ANL-5334 and from more recently measured half-lives. However this discrepancy is not important in the present considerations.

## 1. The Spread of the Activity

### a. Atmospheric Diffusion Formulae

In the unlikely event of a reactor disaster and the release to the atmosphere of large quantities of radioactive debris, there are various ways in which a downwind observer could receive a radiation dose. Some of these ways which seem to present the most serious hazards are outlined below:

### External Radiation Dose

From gaseous and small particulate airborne activity  
 Beta radiation dose (TID/Q)  
 Gamma radiation dose (nomograph)  
 From activity deposited on the ground by precipitation  
 (w/Q).

### Internal Radiation Dose

Inhalation dose from gaseous and small particulate air-  
 borne activity (TID/Q).  
 Ingestion dose from activity deposited on the ground by  
 precipitation (w/Q).

The external beta radiation dose and the internal inhalation dose from airborne activity depend upon the time integral of the concentration of activity at the observer; that is, upon the total integrated dose (TID). The external radiation dose and the internal ingestion dose from activity deposited upon the ground depend upon the ground concentration of activity (w). The external gamma radiation dose from airborne activity depends upon the distribution of activity in a large part of the cloud or plume and is most conveniently estimated by use of a special nomograph.

The following expressions were used to calculate the values of TID/Q and w/Q which are given in Table F-II (for a discussion of these expressions, cf. ref. 1, Chapters 4, 7):

$$\text{TID}/Q = \frac{2 \exp [-h^2/(C^2D^{2-n})]}{\pi \bar{u} C^2 D^{2-n}}$$

$$\text{TID}/Q \text{ (fumigation conditions)} = \frac{1}{\sqrt{\pi} C_y H \bar{u} D^{(2-n)/2}}$$

$$\text{w}/Q \text{ (Washout at "optimum" scavenging rate)} = \frac{1}{e \sqrt{\pi} C_y D^{2-(n/2)}}$$

$$\text{w}/Q \text{ (Total instantaneous washout)} = \frac{1}{\pi C^2 D^{2-n}}$$

where TID/Q = the time integral of the activity concentration at the observer for a unit source (sec/meter<sup>3</sup>)

w/Q = The concentration of activity on the ground at the observer for a unit source (meters<sup>-2</sup>)

Q = Source strength (microcuries, Mev/sec, etc.)

$D$  = The distance of the observer downwind (meters).

$\bar{u}$  = The mean wind speed (meters/sec)

$h$  = The height of the center of the cloud puff or of the axis of the plume above the ground (meters)

$H$  = The height of the lapse layer under fumigation conditions (meters)

$n$  = Sutton's stability parameter (non-dimensional)

$C$  = The generalized diffusion coefficient for isotropic turbulence (meters) <sup>$n/2$</sup>

These expressions are all based upon O. G. Sutton's formula for the diffusion of an atmospheric contaminant from an instantaneous elevated point source. (ref. 1, p. 45). In the expressions given above, it has been assumed that the diffusion is isotropic; this is currently thought to be a good assumption for source heights greater than 100 ft. (Ref. 1, p. 23).

In using the expression for TID/Q, it has been assumed that any radioactive cloud or plume which escapes from the reactor building can be considered as originating from a point source directly above the reactor at the assumed cloud or plume height; this is a good approximation since the primary interest is in the hazards which might exist miles from the disaster. Furthermore, it has been assumed that the crosswind distance of the observer is zero; i.e., the observer stands directly under the path of the cloud's center or directly under the axis of the plume. Finally, it has been assumed that the observer stands under the cloud or plume until all of the activity which escapes has passed overhead. Then it is not necessary to specify the leak rate of the activity out of the reactor building in the case of the slow release of activity, resulting in a radioactive plume. Moreover, the same TID/Q expression can be used for a cloud or a plume since the plume can be considered as a series of cloud puffs.

Fumigation conditions occur when there are two layers of the atmosphere with different stability conditions (specifically, lapse below, inversion aloft) and therefore a modified expression for the TID/Q must be used. Here, again, it has been assumed that the cloud or plume originates from a point source directly above the reactor, that the crosswind distance of the observer is zero, and that the observer remains under the cloud or plume until all of the activity has passed by him.

At distances of several miles or more from the hypothetical reactor disaster, the largest ground concentrations of activity will result from precipitation rather than from dry deposition (fallout). If it rains at

a steady rate from the time of the disaster until some time after the cloud or plume has passed by the observer, there will be a certain "optimum" scavenging rate which produces the maximum deposition at the observer's position. Radiation hazards from activity deposited on the ground have been estimated for the case of washout at the "optimum" scavenging rate where the crosswind distance of the observer is again zero. The total instantaneous washout expression provides an upper limit to the possible ground concentrations of activity (except for fallout close to the reactor). In this case it has been assumed that a radioactive cloud is instantaneously emitted from a point source directly above the reactor building and that the entire radioactive content of the cloud is deposited instantaneously on the ground by precipitation when the center of the cloud is directly above the observer.

The TID/Q expression is not particularly applicable in calculating the external gamma radiation dose from airborne activity. The observer will get a considerable fraction of whatever dose he might get from parts of the cloud or plume not in his immediate vicinity because of the long range of the fission product gamma rays (nominally, about 300 meters in air). The external gamma radiation hazard has been estimated by using a nomograph prepared by J. Z. Holland (ref. 1, p. 108). This nomograph takes into account the decay of the radioactivity, the gradual spread of the cloud, the spatial distribution of material in the cloud, and the absorption and scattering of the radiation by the air. The maximum error in the nomograph is believed to be about  $\pm 20\%$ .

#### b. Meteorological Parameters

The most important smaller-scale meteorological elements for consideration in diffusion problems are winds and air stability (as measured by the vertical temperature gradient) in the lower few hundred feet of the atmosphere. Values of TID/Q are given in Table F-II for the following conditions:

Daytime conditions, average windspeed;  $n = 0.20$ ,  
 $\bar{u} = 4$  meters/sec.

Daytime conditions, low windspeed;  $n = 0.20$ ,  $\bar{u} = 1$  meter/sec

Nocturnal conditions, average windspeed;  $n = 0.50$ ,  $\bar{u} = 1, 3, 5$   
 meters/sec depending upon cloud or plume height.

Transition from nocturnal to daytime conditions, average  
 windspeed;  $n = 0.50$ ,  $\bar{u} = 2$  meters/sec.

The condition,  $n = 0.20$ ,  $\bar{u} = 4$  meters/sec, is supposed to represent the average daytime diffusion condition at the NRTS. There are strong negative vertical temperature gradients (strong lapse for superadiabatic lapse rates) resulting in unstable atmospheric conditions which favor the rapid vertical (and horizontal) mixing of atmospheric contaminants. The vertical distribution of windspeed (in terms of which

O. G. Sutton defines  $n$ ) is correlated with the vertical temperature gradient and therefore with the stability conditions of the atmosphere. Because the hazards due to the airborne long-lived activity built up in a power reactor increase with decreasing windspeed, the condition  $n = 0.20$ ,  $\bar{u} = 1$  meter/sec has also been considered. Winds less than one meter/sec have not been considered because it is not likely that a low wind speed coupled with a constant wind direction will persist for many hours. Moreover, the long travel time associated with a low windspeed allows time to warn and evacuate (if necessary) downwind communities; e.g., with a windspeed of one meter/sec or less, one has three hours or more in which to alert communities more than seven miles downwind.

The condition,  $n = 0.50$ ,  $\bar{u} = 1, 3, 5$  meters/sec (for heights of 10, 70, and 500 meters, respectively), is supposed to represent the average nocturnal diffusion condition at the NRTS. There are strong positive vertical temperature gradients (temperature inversions) resulting in very stable atmospheric conditions which do not favor the vertical (and horizontal) mixing of atmospheric contaminants. Radiation doses significantly larger than those for average daytime conditions may result when the diffusion of any hypothetical reactor disaster debris takes place under stable atmospheric conditions or during the transition from stable to unstable conditions. Here again the increased hazard due to very light winds has not been considered because the longer time of travel tends to mitigate the hazard. In the case of fumigation conditions (a particularly undesirable type of transition from stable to unstable conditions) the choice of  $n = 0.50$  implies that the radioactivity traveled downwind under stable conditions and that the fumigation set in just as the activity reached the observer; this should give the maximum hazard. Two meters/sec is supposed to represent the average windspeed during a fumigation.

Values of  $w/Q$  are given in Table F-II for the following conditions:

Total instantaneous washout:  $n = 0.20$ ,  $\bar{u} = 4$  meters/sec  
 Washout at the "optimum" scavenging rate;  $n = 0.25$ ,  
 $\bar{u} = 4$  meters/sec.

These parameters are supposed to represent the average conditions existing at the NRTS during the precipitation conditions considered.

The stabilization height of a cloud puff or the height of rise of a plume can range between the height of release (building height) and several thousand feet, depending upon the atmospheric diffusion conditions and upon the temperature, density, and composition of the cloud puff or plume. Because of the uncertainties about the manner of release of the fission product activity to the atmosphere and the uncertainty in estimating the height of rise of a postulated cloud puff, the  $TID/Q$  has been given in

Table F-II for three cloud heights to indicate the range of exposures which an observer might receive. Values in Table F-II for  $h = 10$  meters are supposed to indicate the hazard due to a plume leaking out of the building without appreciable rise. Values for  $h = 500$  meters are supposed to indicate the hazard due to a cloud puff released by a mild explosion and/or released under stable conditions. Seventy meters is simply a conveniently interpolated height. A hypothetical disaster involving  $10^{20}$  fissions and occurring during average daytime diffusion conditions might well result in a cloud puff which rises to a stabilization height of 2000 to 3000 meters above the terrain at the NRTS. (Ref. 1, p. 83). Here a cloud height of 500 meters is clearly on the pessimistic side. A disaster involving less than  $10^{20}$  fissions may very well result in a cloud or plume at less than 500 meters height, especially under stable atmospheric conditions. Then it is likely that the assumption that 50% of the fission product activity escapes into the atmosphere is rather pessimistic.

The values of the generalized diffusion coefficient,  $C$ , were taken from a nomograph (ref. 1, p. 117) which gives the diffusion coefficient as a function of atmospheric stability (for  $n = 0.20$ ,  $n = 0.25$ , and  $n = 0.33$ ), windspeed (1 to 15 meters/sec), and cloud or plume height (10 to 1000 meters). This nomograph is based upon a recomputation and an extension by Barad & Hilst of some values for  $n$ ,  $\bar{u}$ , and  $C$  suggested by O. G. Sutton, (ref. 9). For calculations involving a value of  $n = 0.50$ , the corresponding generalized diffusion coefficients were somewhat arbitrarily taken to be those given by the nomograph for  $n = 0.33$ . The use of the values of  $C$  given by the nomograph (which are derived from values suggested by Sutton) is somewhat justified by the agreement between Sutton's suggested values for  $n$  and the values of  $n$  measured at the NRTS, (ref. 7, p. 50, 51).

The use of Sutton's theory of atmospheric diffusion in stable conditions (nocturnal or fumigation conditions) is open to question: (ref. 1, p. 49, 60) the theory gives the most reliable results for lapse conditions ( $n = 0.25$ ). In stable atmospheres, the assumption of isotropy is probably in error; a value of 3 has been suggested for the ratio of the horizontal diffusion coefficient to the vertical diffusion coefficient (ref. 1, p. 61). Then too, the choice of the parameters  $n$ ,  $\bar{u}$ , and  $C$  is somewhat arbitrary. Nevertheless, it is felt that the values of  $TID/Q$  and  $w/Q$  in Table F-II provide a reasonable estimate of the radiation hazard associated with average daytime conditions and they give a reasonable picture of the extent to which these hazards could increase as the atmospheric diffusion conditions become bad.

#### c. Atmospheric Diffusion Conditions at the NRTS

The following remarks which have been abstracted from IDO-10016, IDO-10020, and IDO-10021 (refs. 6, 7, 8) may serve to make the choice of diffusion parameters seem less arbitrary and to indicate the

frequency of occurrence of the various atmospheric diffusion conditions. The geographic features of the Snake River Plain are such that there is a large diurnal range of temperature near the ground. This results in strong negative vertical temperature gradients (lapse or unstable conditions) in the daytime and strong positive vertical temperature gradients (inversion or stable conditions) at night. Strong winds and cloudy skies interfere with the daily regime of the vertical gradient, the interference being greatest in the winter and least in the summer. However, the diurnal effect is so strong that it is only rarely hidden entirely.

The types of atmospheric stability conditions at the NRTS have been divided into five classes (A, B, etc.), these being selected as the types that are most likely to persist for periods of one to several hours. Though slight variations may occur in each category, these types will suffice to describe the diffusion conditions that occur in practice. Table F-III, taken from IDO-10016, gives a two-year summary of the frequency of occurrence of the five classes of diffusion conditions at various times during the day. O. G. Sutton has suggested some values of  $n$  corresponding to the types of stability conditions and meteorological data taken at the NRTS are in agreement with these values:

Type A, strong lapse (looping)	$n = 0.20$
Type B, weak lapse (coning)	$n = 0.25$
Type C, moderate inversion (fanning)	$n = 0.33$
Type C, large inversion (fanning)	$n = 0.50$
Type D, (lapse aloft, ) (lofting)	( $n = 0.20$ or $0.25$ )
(inversion below)	( $n = 0.33$ or $0.50$ )
Type E, (inversion aloft,)	( $n = 0.33$ or $0.50$ )
(lapse below, ) (fumigation)	( $n = 0.20$ or $0.25$ )

*Strongly  
fanned*  
The most frequent daytime conditions during all but the winter months is southwesterly winds with type A conditions. During such conditions, the wind speed at the 250-ft level will most frequently exceed 8 miles/hour; a constant wind direction and a windspeed averaging 2 miles/hour or less for eight consecutive hours is not likely to occur. Usually type B conditions occur for a few minutes just before the formation of the nocturnal inversion, and with cloudy weather, and cannot be considered as the "average" atmospheric diffusion condition.

Type C conditions are the predominant nocturnal conditions. However, during the winter months the nocturnal inversion (type C or stable conditions) may not break until after the working day has started. For example, in January and February, data taken at the NRTS shows that the effect of the nocturnal inversion is still present as late as 1100 MST. Most commonly the winds are light and variable with inversion conditions; this is especially true of the long periods of stagnant inversion conditions (lasting several days) that occur during the winter months.

Type D conditions are usually associated with the transition from lapse to inversion conditions (type A to type C) near sunset and last from one to three hours on the average. With moderate to strong winds, type D conditions may also occur during the transition from inversion to lapse conditions in the morning. In general, type D conditions are the most favorable conditions in which to have a reactor disaster and will not be considered any further.

Type E conditions occur at the time that the nocturnal inversion is being dissipated by the heat from the morning sun. Type E conditions last only about one to two hours except in winter when they have been found to persist for as long as nine hours. The average windspeed during a type E inversion break is about five miles per hour with calms existing for 20% of such breaks, as compared with an average windspeed of 15 miles/hour and no calms for the other types of inversion breaks. Observations of stack gas at the NRTS show that the fumigation conditions accompanying type E conditions almost always occur to the southwest of the stack.

The annual amount of precipitation is about 7 in., with roughly half of the precipitation in the form of snow. Almost all precipitation occurring in the winter months is snowfall. Calms are not frequent, occurring mostly with winter snowfall. The rains that fall are usually in the form of localized instability showers during the warmer months, the stability conditions being type A or type B. On a particular day, parts of the NRTS may have moderately heavy showers, while other parts may receive no rain. The rain from a single shower may exceed considerably the average rainfall for the month in which the shower occurs. The normal or average rainfall for a warmer month must be obtained from the more or less random effects of showers, and showers may pass directly over a particular station or miss it entirely. Since the number of occasions when showers occur are relatively few, the total rainfall for a month is greatly affected by whether or not a shower directly crosses a station.

## 2. Estimates of the Radiation Hazard Downwind

### a. The External Radiation Hazard

Tables F-IV and F-V give estimates of the maximum external radiation doses which a downwind observer might receive under the atmospheric diffusion conditions given at the tops of the columns. Table F-IV gives the estimated maximum doses due to airborne activity for the slow or rapid escape of the activity in nonprecipitating weather. Table F-V gives estimated maximum doses and dose rates due to activity deposited upon the ground by washout. Among other reasons, the doses given are maximum doses because any motion crosswind will lower the dose and

because the assumption that 50% of the activity in the reactor escapes from the building and travels downwind is rather pessimistic. All of the beta doses in tables F-IV and F-V (which are tabulated separately or added to the gamma doses and tabulated) have arbitrarily been divided by ten to account for the shielding effect of clothing.

Under the variety of good and bad diffusion conditions considered, the estimated maximum external dose is less than the 300 r exclusion radius dose at distances greater than 11 miles. The maximum external dose is less than 100 r at distances greater than 35 miles. During average daytime diffusion conditions, the maximum external dose is less than 200 r for all distances greater than 0.6 mile. With the exception of Atomic City and the staff at the reactor site, there are no population groups closer than 11 miles to the reactor. The other sites at the NRTS are more than 12 miles distant. With the exception of Arco and a few other communities with populations of the order of 100, the surrounding communities are more than 35 miles distant. Moreover, the prevailing winds under inversion conditions (nocturnal conditions or fumigation conditions) are such as to direct a concentrated cloud away from the nearest centers of heavy population (ref. 7, p. 33). Then too, it is not likely that a large dose would be received more than 30 miles from the reactor site under inversion or fumigation conditions. The average daily length of inversion conditions is about 12 hours (ref. 7, p. 30). Then comes an inversion break, possibly a fumigation, followed by unstable diffusion conditions. For the low windspeeds which usually accompany inversion conditions, the cloud or plume can only travel zero to, say, 30 miles (at 2 meters/sec) under inversion conditions.

During precipitation conditions the estimated maximum external radiation hazard increases greatly. Columns 3 and 4 of Table F-V give the estimated maximum external (beta + gamma) dose rate in rep/hour at the observer's position at the time the activity is deposited. The dose rates will be less in the case of a plume which is deposited by total instantaneous washout or in the case of a plume which is washed out at the "optimum" scavenging rate. Columns 5 and 6 of Table F-V give the maximum external (beta + gamma) dose in rep received during the first three hours after the disaster for a windspeed of 4 meters/sec. For higher windspeeds, the time of travel is reduced and the doses during the first three hours after the disaster at greater distances will be greater. Columns 7 and 8 of Table F-V give the maximum external (beta + gamma) dose received during the first three hours after the disaster for a windspeed of 12 meters/sec (the same TID/Q values were used for the 12 meter/sec windspeed as for the 4 meter/sec windspeed). For distances of 56,000 and 100,000 meters downwind, the values in columns 5 and 6 are zero because the travel time of the activity is more than three hours. Column 9 of Table F-V gives the radius of the contaminated area for the case of total instantaneous washout

of a cloud coming from an instantaneous point source. The radius is defined as the distance from the center of the ground concentration at which the concentration has fallen off to  $1/e$  of the value at the center. The distances in column 9 give some indication of the distance crosswind which the observer must move in order to leave the highly contaminated area.

There are a number of mitigating conditions which would tend to reduce the doses and dose rates given in Table F-V, possibly by a factor of ten or more. The top soil and the underlying lava in the Snake River Plain are so porous that most of the rain is drained by percolation into the ground water supply. It seems likely that some of the activity which is soluble or very finely divided would be washed into the top few millimeters of the soil with the rainwater. This would greatly reduce the doses and dose rates, because 10/11 of the doses and dose rates is due to beta activity which could be stopped by a few millimeters of top soil. Then too, the probability that a shower occurs over a community at the same instant that a radioactive plume or cloud from a hypothetical reactor disaster is directly overhead is quite small. The prevailing winds under precipitation conditions are such as to direct a radioactive cloud or plume away from the nearest centers of heavy population. The assumption that 50% of the reactor fission products escape to the atmosphere and travel downwind without fallout is rather pessimistic. Finally, the observer would not have to move more than a few miles crosswind to reduce the dose rate and the dose by a factor of ten. Because the nearest surrounding communities are rather small, evacuation of a contaminated area would be facilitated.

The gamma doses in Table F-IV were obtained from J. Z. Holland's nomograph (ref. 1, p. 108). The nomograph gives the gamma dose in roentgens for 100% escape of the fission products of a reactor operating at a previous steady power of 1 kw. For the release of 50% of the fission products of a reactor operating at a previous steady power of 60 mw, the dose given by the nomograph must be multiplied by  $3 \times 10^4$ .

The beta doses from airborne activity were calculated using the expression

$$\text{Beta dose} = \left( \frac{\text{TID}}{Q} \right) \text{QKG where } Q = 6.9 \times 10^{18} t^{-0.21} \text{ Mev/sec}$$

The values of  $\text{TID}/Q$  were taken from Table F-II. The time "t" was set equal to the time of travel of the activity from the reactor building to the observer, i.e., to  $D/u$ . G is a geometry factor equal to  $(0.5)(0.64) = (0.32)$ . The factor 0.5 arises because the beta flux at the surface of the skin is one-half that in free air. The factor 0.64 arises because the earth's surface reduces the free air radiation flux by a factor of  $1/2$  at ground to one at heights greater than the range of the beta radiation; Taylor has computed 0.64 to be an average reduction factor for a man 1.8 meters tall (ref. 1, p. 100). K is a conversion factor equal to  $1 \text{ rep}/(6.8 \times 10^{10} \text{ Mev/meter}^3)$ . The value of the conversion factor K is based upon the

assumption that at the observer's position, the fission product energy absorbed per unit volume of air per sec is equal to the fission product energy given off per unit volume per second. The absorption (and by assumption, the emission) of  $6.8 \times 10^{10}$  Mev/meter<sup>3</sup> of air at standard conditions at the observer's position corresponds to a dose to a small volume element of tissue of 1 rep (ref. 1, p. 157). (The difference between the density of air at sea level and at the NRTS has been neglected.) In the case of the beta activity, this assumption is good since the concentration of fission product activity should be reasonably constant within 5 ft of the observer (the range of the beta rays). (The gamma doses under fumigation conditions were calculated using the same expression as that for the beta dose due to airborne activity except that G is equal to 0.5 (due to the presence of the earth's surface). Here the assumption of radiative equilibrium will cause the gamma dose to be overestimated considerably because the nominal range of the gamma range is about 300 meters, while the cloud radius (just prior to the onset of fumigation conditions) will not exceed 300 meters until the downwind distance is greater than 100,000 meters (62 miles) under stable conditions ( $n = 0.5$ ).

Columns 3 and 4 of Table F-V were calculated using the expression (gamma + beta) dose rate =  $Q(w/Q) (E_\gamma + E_\beta/10)$  where the values of  $(w/Q)$  were taken from Table F-II. The time "t" was set equal to the travel time of the activity; i.e., to  $D/\bar{u}$ .  $E_\gamma$  and  $E_\beta$  are conversion factors which give the beta and gamma dosage rates per unit ground concentration of beta and gamma activity; the values used are those given in Wash III.  $E_\gamma = 1.51 \times 10^{-13}$  (r/sec) for a ground concentration of one Mev of gamma activity per sec per meter<sup>2</sup>.  $E_\beta = 1.51 \times 10^{-11}$  (r/sec) for a ground concentration of one Mev of beta activity per sec per meter<sup>2</sup>. Columns 5, 6, 7, and 8 were obtained by integrating the dose rate from  $t = D/\bar{u}$  to  $t = 3$  hours. Column 6 is essentially the radius of a cloud puff coming from an instantaneous point source; i.e., radius =  $C D (z-n)^{1/2}$ .

### 3. Internal Radiation Hazard

Tables F-VI and F-VII give estimates of the maximum amount of the radioisotopes listed in Table F-I which a downwind observer could accumulate in the critical organ by inhalation under two different atmospheric diffusion conditions. Table F-VI gives the estimated maximum amounts accumulated for average daytime conditions with average windspeed ( $n = 0.20$ ,  $\bar{u} = 4$  meters/sec,  $h = 70$ ). Table F-VII gives the estimated maximum amounts accumulated for very stable conditions (nocturnal conditions) with average windspeed ( $n = 0.50$ ,  $\bar{u} = 3$  meters/sec,  $h = 70$ ). These two conditions should indicate the range of the inhalation hazard for distances greater than about 6 miles from the disaster. For fumigation conditions or for distances less than 6 miles, the inhalation hazard could be a factor of 10 or even 100 greater.

The inhalation hazard for atmospheric diffusion conditions other than the two considered here can be estimated by comparing the TID/Q values since the inhalation hazard is proportional to the TID/Q values. (The TID/Q values for the conditions considered range from about  $10^{-5}$  to about  $10^{-9}$ ).

Some indication of the seriousness of the inhalation hazard may be obtained by comparing the amounts of radioisotope accumulated in the critical organ (as given in Tables F-VI and F-VII) with the maximum permissible amounts of radioisotope in the critical organ (column 3 of Tables F-VI and F-VII). Column 3 is simply the product of columns 5 and 6 of Table F-I. Consider, for example, the inhalation hazard under stable nocturnal diffusion conditions ( $n = 0.5$ ,  $\bar{u} = 3$  meters/sec,  $h = 70$  meters) at 100,000 meters downwind (62 miles); of the 17 radioisotopes for which the hazard is estimated, the observer could accumulate a maximum amount of each of 12 radioisotopes which exceeds the maximum permissible amount of that radioisotope considerably.

The seriousness of the inhalation hazard may also be ascertained by calculating the dose in rem to the critical organ during some time interval, say one week, or for a very long time (infinity). Table F-VIII gives the dose in rem to the critical organ during the first week after inhalation of the activity for several downwind distances for the two atmospheric diffusion conditions considered in Tables F-VI and F-VII. The distances were chosen to give a range of TID/Q values; the doses given in Table F-VIII may be compared to the doses which would be received under different atmospheric diffusion conditions and/or at different distances downwind by comparing the TID/Q values.

The total doses for the first week following the inhalation of the activity, as given in Table F-VIII, are quite large. For example, at 62 miles distance from the hypothetical disaster, the dose received during the first week after the inhalation of the activity under nocturnal conditions ( $n = 0.50$ ,  $\bar{u} = 3$  meters/sec,  $h = 70$  meters) would be about 190 rem to the thyroid, 0.4 rem to the kidneys, and about 150 rem to the bone. This compares to an external (beta + gamma) dose of 25 rep under the same conditions of exposure. Similarly, for the other conditions of exposure the internal inhalation dose received during the first week is considerably larger than the external radiation dose. Furthermore, in the example considered the observer will receive another 190 rem dose in his thyroid in the next 12 weeks; similarly, he will continue to be irradiated appreciably by  $\text{Sr}^{89}$ ,  $\text{Sr}^{90} + \text{Y}^{90}$ ,  $\text{Y}^{91}$ ,  $\text{Ba}^{140} + \text{La}^{140}$ , etc. as can be inferred from columns 8 and 9 of Table F-VIII. It must be remembered, however, that the internal radiation doses given in Table F-VIII are maximum doses. The same discussion applies here that was given for the estimated maximum external radiation doses. That is, any crosswind movement will reduce the amount of activity inhaled; the assumption that 50% of the fission products escape and travel downwind

without fallout is rather pessimistic; the prevailing winds under inversion conditions (which afford the most serious hazards) are such as to direct a concentrated cloud or plume away from the nearest centers of heavy population; it is not likely that large concentrations of activity will travel more than 30 miles from the disaster under inversion conditions.

The values in Tables F-VI and F-VII were obtained by using the expression

$$\left[ \begin{array}{l} \text{Amount of radioisotope} \\ \text{accumulated in critical} \\ \text{organ} \end{array} \right] = A = (\text{TID}/Q) Q B f$$

where the values of TID/Q were taken from Table F-II, the values of Q were taken from Table F-I (Q is the amount of radioisotope in microcuries which escapes from the reactor building and travels downwind), B is the breathing rate ( $1 \times 10^7$  cc in 8 hours or  $3.48 \times 10^{-4}$  meters<sup>3</sup>/sec), and f is the fraction of the inhaled radioisotope which goes to the critical organ (given in Table F-I).

The values in Table F-VIII were calculated using the expression

$$\left[ \begin{array}{l} \text{Dose to critical organ} \\ \text{in rem during time in-} \\ \text{terval T after the} \\ \text{hypothetical disaster} \end{array} \right] = \int_0^T \left( \frac{0.3 \text{ rem/day}}{7 \text{ MPA}} \right) A \exp(-0.693 t/T_{\frac{1}{2}}) dt$$

where  $T_{\frac{1}{2}}$  is the effective half-life of the radioisotope in days, A is the amount of radioisotope accumulated in the critical organ in microcuries. The assumption has been made that the maximum permissible amount of the radioisotope in the critical organ corresponds to a dose rate to the critical organ of 0.3 rem per week. In the case of Pu<sup>239</sup>, this is not the case, since the maximum permissible amount of Pu<sup>239</sup> has been fixed by comparison to radium, but the assumption should serve to give some indication of the hazard due to Pu<sup>239</sup>.

Table F-IX gives some indication of the seriousness of the ingestion hazard from activity which gets into the drinking water supply due to washout. Columns 4 and 5 give the estimated maximum ground concentrations of the various radioisotopes in microcuries per meter<sup>2</sup> from total instantaneous washout at 20 miles downwind, and washout at the "optimum" scavenging rate at 62 miles downwind. The values in columns 4 and 5 are simply the product of Q and w/Q where Q was taken from column 3 of Table F-I and w/Q was taken from Table F-II. It was arbitrarily assumed that the activity was deposited upon an open water supply 10 feet deep. Then, the maximum concentration of each radioisotope in the water was

calculated and divided by the maximum permissible concentration in water as given by column 8 of Table F-I. This ratio of estimated concentration to maximum permissible concentration has been tabulated in columns 6 and 7 of Table F-IX. The ground concentrations at other distances can be found by comparing  $(w/Q)$  values in Table F-II.

For distances of twenty miles or greater, the concentrations of fission product activity in water which one might expect in the unlikely event of a reactor disaster should be considerably less than the concentrations given in column 6 of Table F-IX. As has been pointed out before, the assumption that 50% of the reactor's fission product activity escapes to the atmosphere and travels downwind without fallout is rather pessimistic. Then, too, the total instantaneous washout formula does not necessarily provide a good description of the scavenging action of a summer shower or a winter snowstorm at the NRTS; it is simply a convenient expression for an upper limit which one uses in the absence of any data on the scavenging effect of rain and snow at the NRTS. It is not unlikely that the concentration of activity given by the formula for washout at the "optimum" scavenging rate might be somewhat more realistic, this concentration being less by a factor of ten than that for total instantaneous washout (compare the  $w/Q$  values given in columns 13 and 14 of Table F-II). The concentrations of activity given in column 6 of Table F-IX are for a downwind distance of 20 miles; for a distance of 35 miles, the concentrations would be about 36% of those at 20 miles; for a distance of 62 miles downwind, the concentrations of activities would be about 13% of those at 20 miles.

It is estimated that the ground water moves through the area (the Snake River Plain) at the rate of one-half mile per year (about 7 ft per day) (ref. 11); commonly the horizontal permeability exceeds the vertical permeability (ref. 6). Thus it would take at least several days for the activity to enter even the shallowest of wells. Some of the wells at the NRTS are about 600 ft deep (ref. 6); in this case it would take more than 85 days for the activity to enter the well. Several days should be sufficient time in which to start monitoring (and, possibly, halt the use of) the well water in any populated region where washout of a radioactive cloud may have occurred.

If the activity is deposited more than, say, 5 miles from the Snake River, then it should take more than 10 years for the activity to move with the ground water into the river (at one-half mile per year). In this time, the  $I^{131}$ ,  $Sr^{89}$ ,  $Nb^{95}$ , and  $Ba^{140} + La^{140}$  will have decayed out, leaving only the  $Sr^{90}$ ,  $Y^{90}$  and  $Pu^{239}$  which should be diluted considerably in moving five miles or more underground.

The greatest concentration of activity in the Snake River would occur if a sudden, heavy shower occurred directly over some part of the river at the same time that a radioactive cloud from a reactor disaster is

directly above the same place. It is rather unlikely that a sudden, heavy shower will occur over a given region at a specified time because of the localized, sporadic nature of the precipitation occurring in the Snake River Plain. Then, too, the nearest part of the Snake River is more than 25 miles from the reactor. With a windspeed of 4 meters/sec. (9 miles per hr), the travel time of the activity would be more than 2.8 hrs; with a windspeed of 12 meters/sec. (27 miles per hr) the travel time of the activity would be more than 0.9 hr. Thus, in the unlikely event that some part of the Snake River should become contaminated, one should have more than one hr from the time of the disaster in which to contact communities downstream from the area where the washout took place. Also, any activity deposited in the Snake River above American Falls should be diluted considerably by the water in American Falls Reservoir. Then too, a large quantity of the Snake River water enters the lava flows before it reaches the reservoir at American Falls. This water comes out in springs down river from the dam (ref. 11). Any delay in the motion of the activity downstream, such as being held up in the reservoir above American Falls or moving slowly through the lava flows, should allow more time in which to warn communities downstream from the American Falls and should lead to a greater dilution of the activity by ground water, water in the reservoir, etc. During precipitation conditions at the NRTS, the winds would be such as to allow deposition of activity in the Snake River below the American Falls somewhat less than 20% of the time (ref. 6).

REFERENCES

1. Meteorology and Atomic Energy, Supt. of Documents, Washington, D. C. (1955)
2. Summary Report of the Reactor Safeguard Committee (WASH III)
3. Permissible Dose From External Sources of Ionizing Radiation, National Bureau of Standards Handbook 59, Supt. of Documents, Washington, D. C. (1954)
4. Dillon, I. G., and Burris, Leslie Jr., Estimation of Fission Product Spectra in Fuel Elements Discharged from the Power Breeder Reactor and the Experimental Breeder Reactor No. 2, ANL-5334, Argonne National Laboratory, Lemont, Illinois (1954).
5. Recommendations of the International Commission on Radiological Protection, (Revised December 1, 1954), Supplement No. 6 to the British Journal of Radiology, British Institute of Radiology, London (1955).
6. Humphrey, P. A., and Wilkins, E. M., Environmental Aspects of the MTR Operation (IDO-10016), U. S. Atomic Energy Commission, Idaho Operations Office, Idaho Falls, Idaho (1952).
7. Humphrey, P. A., and Wilkins, E. W., The Climatology of Stack Gas Diffusion at the NRTS (IDO-10020), U. S. Atomic Energy Commission, Idaho Operations Office, Idaho Falls, Idaho (1952).
8. Humphrey, P. A., and Wilkins, E. W., Engineering Climatology of the ANP Site at the NRTS (IDO-10021), U. S. Atomic Energy Commission, Idaho Operations Office, Idaho Falls, Idaho (1953).
9. Barad, M. L., and Hilst, G. R., A Recomputation and Extension of Parameters Involved in Sutton's Diffusion Hypothesis (HW-21415), General Electric Company, Hanford Works, Richland, Washington (1951).
10. Hunter, H. F., and Ballou, N. E., Simultaneous Slow Neutron Fission of U<sup>235</sup> Atoms. I. Individual and Total Rates of Decay of the Fission Products (ADC-65), Naval Radiological Defense Laboratory, San Francisco Naval Shipyard, San Francisco 24, California (1949)
11. (Secret) WAPD-70, Reactor Hazards Associated with Operation of the Mark I Submarine Thermal Reactor, Westinghouse Electric Corp., Atomic Power Division, P. O. Box 1468, Bettis Field, Pittsburgh 30, Pennsylvania (November 20, 1952).

Table F-I

Radioisotope	Number of atoms per 100 atoms fissioned; 0 days cooling time	Q = amount of activity which escapes from reactor building (microcuries)	Critical organ	Maximum permissible amount of radioisotope in total body (microcuries)	Fraction in critical organ of that in total body	Fraction reaching critical organ by inhalation	Maximum permissible concentration of radioisotope in water (microcuries/cubic centimeter)	Radioactive half-life (days)	Effective half-life (days)
Ag <sup>111</sup>	0.054	1.71(11)	Liver	39	0.1	2(-3)	5	7.5	2.1
I <sup>131</sup>	0.270	8.00(11)	Thyroid	0.6	0.2	0.15	6(-5)	8	7.5
Cs <sup>137</sup> + Ba <sup>137</sup>	6.190	1.21(10)	Muscle	98	0.45	0.36	2(-3)	1.2(4)	17
Ru <sup>106</sup> + Rh <sup>106</sup>	0.416	2.70(10)	Kidneys	4	0.04	0.01	0.1	365	19
Te <sup>127</sup>	0.028	5.77(9)	Kidneys	4	0.2	0.02	3(-2)	90.4	13
Sr <sup>89</sup>	1.955	8.57(11)	Bone	2	0.7	0.22	7(-5)	53	52
Sr <sup>90</sup> + Y <sup>90</sup>	4.410	1.44(10)	Bone	1	0.7	0.22	8(-7)	9.1(3)	2.7(3)
Y <sup>91</sup>	2.715	1.05(12)	Bone	3	0.65	0.14	4(-2)	57	51
Zr <sup>95</sup> + Nb <sup>95</sup>	3.595	1.31(12)	Bone	10	0.62	0.058	0.4	65	48
Mo <sup>99</sup>	0.190	1.61(12)	Bone	17	0.5	2(-4)	5	2.85	2.8
Nb <sup>95</sup>	2.470	1.67(12)	Bone	44	0.4	0.12	2(-3)	35	21
Ba <sup>140</sup> + La <sup>140</sup>	0.788	1.46(12)	Bone	1	0.96	0.2	5(-4)	12.8	12
La <sup>140</sup>	0.012	1.70(11)	Bone	7	0.3	0.1	0.3	1.67	1.6
Ce <sup>144</sup> + Pr <sup>144</sup>	3.990	3.35(11)	Bone	1	0.8	0.1	8(-3)	275	180
Pr <sup>143</sup>	0.755	1.31(12)	Bone	6	0.6	0.063	8(-2)	13.8	11
Pm <sup>147</sup>	2.755	6.87(10)	Bone	25	0.7	0.09	0.2	1.46(3)	140
Pu <sup>239</sup> (sol.)	-	3.83(9)	Bone	0.04	0.75	0.18	6(-6)	8.8(6)	4.3(4)
Pu <sup>239</sup> (insol.)	-	3.83(9)	Lungs	0.02	1.0	0.12	-	8.8(6)	360

The numbers in parentheses indicate the powers of ten by which the tabulated values are to be multiplied.

Table F-II

Distance downwind		$\frac{TID}{Q} \equiv \frac{\text{Total Integrated Dose}}{\text{Source Strength}} \left( \frac{\text{seconds}}{\text{meter}^3} \right)$										$\frac{W}{Q} \equiv \left( \frac{\text{relative ground concentration}}{\left( \frac{1}{\text{meters}^2} \right)} \right)$	
		n = 0.20; strong lapse, daytime conditions						n = 0.50; large inversion, nocturnal conditions			Fumigation conditions n = 0.50 $\bar{u} = 2$ H = 70 C = 0.050	Total instantaneous washout n = 0.20 $C^2 = 0.027$ h = 500 $\bar{u} = 4$	Washout at "optimum" scavenging rate n = 0.25 C = 0.080 h = 500 $\bar{u} = 4$
		$\bar{u} = 4$ ; average windspeed			$\bar{u} = 1$ ; low windspeed			Average windspeed					
Meters	Miles	h = 10 $C^2 = .088$	h = 70 $C^2 = .053$	h = 500 $C^2 = .027$	h = 10 $C^2 = .110$	h = 70 $C^2 = .070$	h = 500 $C^2 = .035$	h = 10 $\bar{u} = 1$ $C^2 = .0060$	h = 70 $\bar{u} = 3$ $C^2 = .0025$	h = 500 $\bar{u} = 5$ $C^2 = .0010$			
560	0.35	2.02(-5)	1.20(-5)	(-49)	6.47(-5)	4.67(-5)	(-40)	2.27(-3)	(-67)	0	7.0(-4)	1.33(-4)	1.82(-5)
1,000	0.62	7.18(-6)	8.23(-6)	(-21)	2.29(-5)	2.74(-5)	(-17)	1.98(-3)	(-30)	0	4.5(-4)	4.69(-5)	6.15(-6)
1,800	1.12	2.50(-6)	3.65(-6)	2(-11)	7.98(-6)	1.14(-5)	1.30(-9)	1.12(-3)	(-15)	0	2.9(-4)	1.63(-5)	2.04(-6)
3,200	1.99	8.88(-7)	1.41(-6)	3.09(-8)	2.84(-6)	4.31(-6)	2.70(-7)	5.34(-4)	9.57(-9)	0	1.9(-4)	5.78(-6)	6.95(-7)
5,600	3.48	3.24(-7)	5.29(-7)	2.01(-7)	1.04(-6)	1.61(-6)	9.06(-7)	2.43(-4)	6.94(-7)	0	1.2(-4)	2.11(-6)	2.43(-7)
10,000	6.21	1.14(-7)	1.88(-7)	2.08(-7)	3.65(-7)	5.72(-7)	7.33(-7)	1.04(-4)	1.20(-5)	0	8.0(-5)	7.44(-7)	8.20(-8)
18,000	11.18	3.96(-8)	6.56(-8)	1.05(-7)	1.27(-7)	1.97(-7)	3.42(-7)	4.36(-5)	1.56(-5)	(-50)	5.2(-5)	2.58(-7)	2.72(-8)
32,000	19.88	1.41(-8)	2.33(-8)	4.26(-8)	4.50(-8)	7.07(-8)	1.34(-7)	1.84(-5)	1.05(-5)	(-24)	3.4(-5)	9.17(-8)	9.26(-9)
56,000	34.80	5.14(-9)	8.52(-9)	1.63(-8)	1.64(-8)	2.58(-8)	5.07(-8)	8.00(-6)	5.53(-6)	(-14)	2.2(-5)	3.35(-8)	3.24(-9)
100,000	62.14	1.81(-9)	3.00(-9)	5.84(-9)	5.79(-9)	9.09(-9)	1.81(-8)	3.35(-6)	2.52(-6)	(-10)	1.4(-5)	1.18(-8)	1.09(-9)
(TID/Q) <sub>maximum</sub>		5.86(-4)	1.20(-5)	2.34(-7)	2.34(-3)	4.78(-5)	9.37(-7)	2.34(-3)	1.59(-5)	1.87(-7)	-	-	-
D <sub>max.</sub> TID/Q <sub>'</sub> (meters)		49.9	571	7380	43.2	493	6380	635	15,600	374,000	-	-	-

The numbers in parentheses indicate the powers of 10 by which the tabulated values are to be multiplied.

Table F- III

ANNUAL SUMMARY OF LOW LEVEL TEMPERATURE SOUNDINGS  
TWO YEAR PERIOD: SEPTEMBER, 1950 THROUGH AUGUST, 1952  
NRTS, IDAHO, CENTRAL FACILITIES

Time of sounding (MST)	0200	0500	0715	0900	1100	1500	1830	2000	2130	All soundings
Total number of soundings made	279	280	282	272	263	241	239	253	268	2377
Number of soundings not taken due to winds in excess of 12 mph (gusts >15 mph) (probably lapse)	23	15	15	24	30	50	47	37	29	270
Per cent of soundings in which inversions were found	88.6	89.4	76.0	30.5	14.7	6.5	46.6	85.5	87.7	59.7
Per cent of soundings:										
Type A	2.6	3.8	13.2	62.3	80.6	87.6	33.2	4.8	3.6	31.2
Type B	8.7	7.0	10.8	7.2	4.6	5.9	20.0	9.7	8.8	9.0
Type C	70.6	73.7	51.0	21.2	8.2	2.6	17.9	41.8	57.4	39.6
Type D	16.8	13.3	11.2	2.0	1.0	0.6	28.2	40.8	28.0	15.6
Type E	1.2	2.4	13.8	7.2	5.6	3.2	0.6	3.0	2.3	4.5
Average temperature difference between 5 ft level and 400 ft level (°F)	+7.4	+7.8	+2.8	-1.8	-4.1	-4.4	+0.2	+3.5	+5.5	1.9

Taken from IDO-10016, "Meteorology of MTR Hazards," P. A. Humphrey and E. M. Wilkins, U.S.W.B. December, 1952

Table F-IV

EXTERNAL  $\beta$ -DOSE (REP) AND  $\gamma$ -DOSE (ROENTGENS) FROM AIRBORNE FISSION PRODUCT ACTIVITY

Distance downwind		Daytime conditions,								Nocturnal conditions,				Fumigation,	
		Average windspeed						Low windspeed		average windspeed				average windspeed	
		h = 10 $\bar{u} = 4$ n = 0.20 $C^2 = .088$		h = 70 $\bar{u} = 4$ n = 0.20 $C^2 = .053$		h = 500 $\bar{u} = 4$ n = 0.20 $C^2 = .027$		h = 10 $\bar{u} = 1$ n = 0.20 $C^2 = .110$		h = 10 $\bar{u} = 1$ n = 0.50 $C^2 = .0060$		h = 70 $\bar{u} = 3$ n = 0.50 $C^2 = .0025$		H = 70 $\bar{u} = 2$ n = 0.50 $C^2 = 0.050$	
Meters	Miles	$\beta$	$\gamma$	$\beta$	$\gamma$	$\beta$	$\gamma$	$\beta$	$\gamma$	$\beta$	$\gamma$	$\beta$	$\gamma$	$\beta$	$\gamma$
560	0.35	23	160	14	140	(-43)	.51	56	360	1.95(3)	3.00(3)	(-61)	250	697	1.09(4)
1,000	0.62	7.3	56	8.4	84	(-15)	.45	17	140	1.51(3)	2.3(3)	(-24)	220	397	6.20(3)
1,800	1.12	2.2	20	3.3	51	2(-5)	.60	5.4	51	754	1.5(3)	(-9)	200	226	3.51(3)
3,200	1.99	.71	8.1	1.1	13	.16	1.1	1.7	19	319	840	7(-3)	170	130	2.01(3)
5,600	3.48	.23	2.7	.38	4.5	.14	1.9	.55	6.6	129	480	.46?	170	76	1.19(3)
10,000	6.21	.07	.90	.12	1.5	.13	1.3	.17	2.0	49	260	7.1	190	44	675
18,000	11.18	.02	.26	.04	.51	.06	.69	.05	.63	18	130	8.2	160	25	386
32,000	19.88	7(-3)		.01	.16	.02	.30	.02		6.8	66	4.9	110	14	222
56,000	34.80	2(-3)		4(-3)		7(-3)		5(-3)		2.6	27	2.3	57	8.3	92
100,000	62.14	7(-4)		1(-3)		2(-3)		2(-3)		.97	11	.92	24	4.8	74

The numbers in parentheses indicate the powers of 10 by which the tabulated values are to be multiplied. All beta doses have been divided by 10 to account for the shielding effect of clothing.

Table F-V

## EXTERNAL RADIATION HAZARD FROM ACTIVITY DEPOSITED ON THE GROUND

Distance downwind		External $\beta + \gamma$ dose rate at time $D/\bar{u}$ in rep/hour		External $\beta + \gamma$ dose during first three hours after the disaster in rep				Radius of contaminated area in meters $n = 0.20$ $C = 0.16$ $\bar{u} = 4$ $h = 500$
		Average windspeed		Average windspeed		High windspeed		
		Total instantaneous washout	Washout at "optimum" scavenging rate	Total instantaneous washout	Washout at "optimum" scavenging rate	Total instantaneous washout	Washout at "optimum" scavenging rate	
Meters	Miles	$n = 0.20$ $C^2 = 0.027$ $\bar{u} = 4$ $h = 500$	$n = 0.25$ $C = 0.080$ $\bar{u} = 4$ $h = 500$	$n = 0.20$ $C^2 = 0.027$ $\bar{u} = 4$ $h = 500$	$n = 0.25$ $C = 0.080$ $\bar{u} = 4$ $h = 500$	$n = 0.20$ $C^2 = 0.027$ $\bar{u} = 12$ $h = 500$	$n = 0.25$ $C = 0.080$ $\bar{u} = 12$ $h = 500$	
560	0.35	1.9 (6)	2.7 (5)	2.9 (6)	3.9 (5)	2.9 (6)	4.0 (5)	46
1,000	0.62	6.0 (5)	7.9 (4)	1.0 (6)	1.3 (5)	1.0 (6)	1.3 (5)	80
1,800	1.12	1.9 (5)	2.3 (4)	3.3 (5)	4.2 (4)	3.5 (5)	4.4 (4)	136
3,200	1.99	5.8 (4)	7.0 (3)	1.1 (5)	1.4 (4)	1.2 (5)	1.5 (3)	228
5,600	3.48	1.9 (4)	2.2 (3)	3.8 (4)	4.3 (3)	4.3 (4)	5.0 (3)	378
10,000	6.21	5.9 (3)	651	1.1 (4)	1.3 (3)	1.4 (4)	1.6 (3)	637
18,000	11.18	1.8 (3)	191	2.9 (3)	304	4.5 (3)	478	1080
32,000	19.88	570	58	436	44	1.4 (3)	139	1810
56,000	34.80	185	18	0	0	362	35	3000
100,000	62.14	58	5.4	0	0	49	4.5	5060

All beta doses have been reduced by a factor of ten to account for the shielding effect of clothing. The numbers in parentheses indicate the powers of ten by which the tabulated values are to be multiplied.

Table F-VI

AMOUNT OF RADIOISOTOPE WHICH COULD BE ACCUMULATED IN CRITICAL ORGAN  
BY INHALATION UNDER DAYTIME CONDITIONS  
(Microcuries)

Radioisotope	Critical organ (C.O.)	Maximum permissible amount in C.O. (microcuries)	Distance Downwind (Meters)									
			560	1,000	1,800	3,200	5,600	10,000	18,000	32,000	56,000	100,000
			Distance Downwind (Miles)									
			0.35	0.62	1.12	1.99	3.48	6.21	11.18	19.88	34.80	62.14
TID/Q for n = 0.2, h = 70, $\bar{u}$ = 4												
			1.20(-5)	8.23(-6)	3.65(-6)	1.41(-6)	5.29(-7)	1.88(-7)	6.56(-8)	2.33(-8)	8.52(-9)	3.00(-9)
Ag <sup>111</sup>	Liver	3.9	1.43(0)	9.79(-1)	4.34(-1)	1.68(-1)	6.30(-2)	2.24(-2)	7.81(-3)	2.77(-3)	1.01(-3)	3.57(-4)
I <sup>131</sup>	Thyroid	.12	5.02(2)	3.44(2)	1.53(2)	5.89(1)	2.21(1)	7.86(0)	2.74(0)	9.74(-1)	3.56(-1)	1.25(-1)
Cs <sup>137</sup> + Ba <sup>137</sup>	Muscle	44.1	1.82(1)	1.25(1)	5.55(0)	2.14(0)	8.04(-1)	2.86(-1)	9.97(-2)	3.54(-2)	1.30(-2)	4.56(-3)
Ru <sup>106</sup> + Rh <sup>106</sup>	Kidneys	.16	1.13(0)	7.74(-1)	3.43(-1)	1.33(-1)	4.97(-2)	1.77(-2)	5.17(-3)	2.19(-3)	8.01(-4)	2.82(-4)
Te <sup>127</sup>	Kidneys	.8	4.82(-1)	3.31(-1)	1.47(-1)	5.67(-2)	2.13(-2)	7.56(-3)	2.64(-3)	9.37(-4)	3.13(-4)	1.21(-4)
Sr <sup>89</sup>	Bone	1.4	7.87(2)	5.40(2)	2.39(2)	9.25(1)	3.47(1)	1.23(1)	4.30(0)	1.53(0)	5.59(-1)	1.97(-1)
Sr <sup>90</sup> + Y <sup>90</sup>	Bone	.7	1.32(1)	9.05(0)	4.02(0)	1.55(0)	5.82(1)	2.07(-1)	7.22(-2)	2.56(-2)	9.37(-3)	3.30(-3)
Y <sup>91</sup>	Bone	1.95	6.14(2)	4.21(2)	1.87(2)	7.22(1)	2.71(1)	9.63(0)	3.36(0)	1.19(0)	4.36(-1)	1.54(-1)
Zr <sup>95</sup> + Nb <sup>95</sup>	Bone	6.2	3.17(2)	2.17(2)	9.64(1)	3.72(1)	1.40(1)	4.96(0)	1.73(0)	6.15(-1)	2.25(-1)	7.92(-2)
Mo <sup>99</sup>	Bone	8.5	1.34(0)	9.22(-1)	4.09(-1)	1.58(-1)	5.92(-2)	2.11(-2)	7.35(-3)	2.61(-3)	9.54(-4)	3.36(-4)
Nb <sup>95</sup>	Bone	17.6	8.36(2)	5.74(2)	2.54(2)	9.83(1)	3.69(1)	1.31(1)	4.57(0)	1.62(0)	5.94(-1)	2.09(-1)
Ba <sup>140</sup> + La <sup>140</sup>	Bone	.96	1.22(3)	8.39(2)	3.72(2)	1.44(2)	5.40(1)	1.92(1)	6.69(0)	2.38(0)	8.69(-1)	3.06(-1)
La <sup>140</sup>	Bone	2.1	7.10(1)	4.87(1)	2.16(1)	8.35(0)	3.13(0)	1.11(0)	3.88(-1)	1.38(-1)	5.04(-2)	1.78(-2)
Ce <sup>144</sup> + Pr <sup>144</sup>	Bone	.8	1.40(2)	9.63(1)	4.27(1)	1.65(1)	6.19(0)	2.20(0)	7.68(-1)	2.73(-1)	9.97(-2)	3.51(-2)
Pr <sup>143</sup>	Bone	3.6	3.44(2)	2.36(2)	1.05(2)	4.05(1)	1.52(1)	5.40(0)	1.88(0)	6.69(-1)	2.45(-1)	8.61(-2)
Pm <sup>147</sup>	Bone	17.5	2.58(1)	1.77(1)	7.85(0)	3.03(0)	1.14(0)	4.04(-1)	1.41(-1)	5.01(-2)	1.83(-2)	6.45(-3)
Pu <sup>239</sup> (sol.)	Bone	.03	2.88(0)	1.98(0)	8.76(-1)	3.38(-1)	1.27(-1)	4.51(-2)	1.57(-2)	5.59(-3)	2.04(-3)	7.20(-4)
Pu <sup>239</sup> (insol.)	Lungs	.02	1.92(0)	1.32(0)	5.84(-1)	2.26(-1)	8.46(-2)	3.01(-2)	1.05(-2)	3.73(-3)	1.36(-3)	4.80(-4)

The numbers in parentheses indicate the powers of 10 by which the tabulated values are to be multiplied.

Table F-VII

AMOUNT OF RADIOISOTOPE WHICH COULD BE ACCUMULATED IN CRITICAL ORGAN  
BY INHALATION UNDER NOCTURNAL CONDITIONS  
(Microcuries)

Radioisotope	Critical organ (C.O.)	Maximum permissible amount in C. O. (microcuries)	Distance Downwind (Meters)									
			560	1,000	1,800	3,200	5,600	10,000	18,000	32,000	56,000	100,000
			Distance Downwind (Miles)									
			0.35	0.62	1.12	1.99	3.48	6.21	11.18	19.88	34.80	62.14
			TID/Q for n = 0.50, h = 70, $\bar{u}$ = 3									
			(-67)	(-30)	(-15)	9.57(-9)	6.94(-7)	1.20(-5)	1.56(-5)	1.05(-5)	5.53(-6)	2.52(-6)
Ag <sup>111</sup>	Liver	3.9	(-62)	(-25)	(-10)	1.14(-3)	8.26(-2)	1.43(0)	1.86(0)	1.25(0)	6.58(-1)	3.00(-1)
I <sup>131</sup>	Thyroid	.12	(-60)	(-23)	(-8)	4.00(-1)	2.90(1)	5.02(2)	6.52(2)	4.39(2)	2.31(2)	1.05(2)
Cs <sup>137</sup> + Ba <sup>137</sup>	Muscle	44.1	(-61)	(-24)	(-9)	1.45(-2)	1.05(0)	1.82(1)	2.37(1)	1.60(1)	8.41(0)	3.83(0)
Ru <sup>106</sup> + Rh <sup>106</sup>	Kidneys	.16	(-63)	(-26)	(-11)	9.00(-4)	6.52(-2)	1.13(0)	1.47(0)	9.87(-1)	5.20(-1)	2.37(-1)
Te <sup>127</sup>	Kidneys	.8	(-63)	(-26)	(-11)	3.85(-4)	2.79(-2)	4.82(-1)	6.27(-1)	4.22(-1)	2.22(-1)	1.01(-1)
Sr <sup>89</sup>	Bone	1.4	(-60)	(-23)	(-8)	6.28(-1)	4.55(1)	7.87(2)	1.02(3)	6.89(2)	3.63(2)	1.65(2)
Sr <sup>90</sup> + Y <sup>90</sup>	Bone	.7	(-61)	(-24)	(-9)	1.05(-2)	7.63(-1)	1.32(1)	1.72(1)	1.16(1)	6.08(0)	2.77(0)
Y <sup>91</sup>	Bone	1.95	(-60)	(-23)	(-8)	4.90(-1)	3.55(1)	6.14(2)	7.99(2)	5.38(2)	2.83(2)	1.29(2)
Zr <sup>95</sup> + Nb <sup>95</sup>	Bone	6.2	(-60)	(-23)	(-8)	2.53(-1)	1.83(1)	3.17(2)	4.12(2)	2.77(2)	1.46(2)	6.65(1)
Mo <sup>99</sup>	Bone	8.5	(-62)	(-25)	(-10)	1.07(-3)	7.77(-2)	1.34(0)	1.75(0)	1.18(0)	6.19(-1)	2.82(-1)
Nb <sup>95</sup>	Bone	17.6	(-60)	(-23)	(-8)	6.67(-1)	4.84(1)	8.36(2)	1.09(3)	7.32(2)	3.85(2)	1.76(2)
Ba <sup>140</sup> + La <sup>140</sup>	Bone	.96	(-59)	(-22)	(-7)	9.76(-1)	7.08(1)	1.22(3)	1.59(3)	1.07(3)	5.64(2)	2.57(2)
La <sup>140</sup>	Bone	2.1	(-61)	(-24)	(-9)	5.67(-2)	4.11(0)	7.10(1)	9.24(1)	6.22(1)	3.27(1)	1.49(1)
Ce <sup>144</sup> + Pr <sup>144</sup>	Bone	.8	(-60)	(-23)	(-8)	1.12(-1)	8.12(0)	1.40(2)	1.83(2)	1.23(2)	6.47(1)	2.95(1)
Pr <sup>143</sup>	Bone	3.6	(-60)	(-23)	(-8)	2.75(-1)	1.99(1)	3.44(2)	4.48(2)	3.01(2)	1.59(2)	7.23(1)
Pm <sup>147</sup>	Bone	17.5	(-61)	(-24)	(-9)	2.06(-2)	1.49(0)	2.58(1)	3.35(1)	2.26(1)	1.19(1)	5.42(0)
Pu <sup>239</sup> (sol.)	Bone	.03	(-62)	(-25)	(-10)	2.30(-3)	1.67(-1)	2.88(0)	3.74(0)	2.52(0)	1.33(0)	6.05(-1)
Pu <sup>239</sup> (insol.)	Lungs	.02	(-62)	(-25)	(-10)	1.53(-3)	1.11(-1)	1.92(0)	2.50(0)	1.68(0)	8.85(-1)	4.03(-1)

The numbers in parentheses indicate the powers of 10 by which the tabulated values are to be multiplied.

Table F-VIII  
RADIATION HAZARD FROM INHALED AIRBORNE ACTIVITY

Radioisotope	Critical Organ	Effective half-life (days)	Maximum total dose (rem) to critical organ during first week				Fraction of dose received in infinitely long time which is received in time T	
			Average daytime conditions n = 0.20, h = 70, $\bar{u} = 4$		Nocturnal conditions n = 0.50, h = 70, $\bar{u} = 3$		T = 7 days	T = 91 days
			D = 56,000 (34.8 miles)	D = 18,000 (11.2 miles)	D = 100,000 (62.1 miles)	D = 32,000 (19.9 miles)		
Ag <sup>111</sup>	Liver	2.1	3.0(-5)	2.3(-4)	9.0(-3)	0.038	0.90	1.00
I <sup>131</sup>	Thyroid	7.5	0.66	5.0	190	810	0.48	1.00
Cs <sup>137</sup> + Ba <sup>137</sup>	Muscle	17	7.7(-5)	5.9(-4)	0.023	0.095	0.25	0.98
Ru <sup>106</sup> + Rh <sup>106</sup>	Kidneys	19	1.3(-3)	0.010	0.39	1.6	0.23	0.96
Te <sup>127</sup>	Kidneys	13	1.1(-4)	8.3(-4)	0.032	0.13	0.31	0.99
Sr <sup>89</sup>	Bone	52	0.11	0.88	34	140	0.089	0.70
Sr <sup>90</sup> + Y <sup>90</sup>	Bone	2.7(3)	4.0(-3)	0.031	1.2	5.0	0.0018	0.023
Y <sup>91</sup>	Bone	51	0.064	0.49	19	79	0.091	0.71
Zr <sup>95</sup> + Nb <sup>95</sup>	Bone	48	0.010	0.080	3.1	13	0.096	0.73
Mo <sup>99</sup>	Bone	2.8	1.6(-5)	1.2(-4)	4.7(-3)	0.020	0.82	1.00
Nb <sup>95</sup>	Bone	21	9.0(-3)	0.070	2.7	11	0.21	0.95
Ba <sup>140</sup> + La <sup>140</sup>	Bone	12	0.22	1.7	66	280	0.33	0.99
La <sup>140</sup>	Bone	1.6	2.3(-3)	0.017	0.67	2.8	0.95	1.00
Ce <sup>144</sup> + Pr <sup>144</sup>	Bone	180	0.037	0.28	11	46	0.027	0.30
Pr <sup>143</sup>	Bone	11	0.016	0.13	4.9	20	0.36	1.00
Pm <sup>147</sup>	Bone	140	3.1(-4)	2.4(-3)	0.091	0.38	0.034	0.36
Pu <sup>239</sup> (sol.)	Bone	4.3(4)	0.020	0.15	5.9	24	0.00011	0.0015
Pu <sup>239</sup> (insol.)	Lungs	360	0.020	0.16	6.0	25	0.013	0.16

The numbers in parentheses indicate the powers of ten by which the tabulated values are to be multiplied.

Table F-IX

## INTERNAL RADIATION HAZARD FROM ACTIVITY DEPOSITED ON THE GROUND

Radioisotope	Critical organ	Maximum permissible concentration of radioisotope in water ( $\mu\text{c}/\text{cc}$ )	Ground concentration of activity in $\mu\text{c}$ per meter <sup>2</sup>		Ratio of estimated concentration in water to maximum permissible concentration (assuming dilution by 10' of water)	
			Total instantaneous washout $n = 0.20$ $C^2 = 0.027$ $\bar{u} = 4$ $D = 32,000$	Washout at "optimum" scavenging rate $n = 0.25$ $C = 0.080$ $\bar{u} = 4$ $D = 100,000$	Total instantaneous washout (from column 4)	Washout at "optimum" scavenging rate (from column 5)
Ag <sup>111</sup>	Liver	5	1.57(4)	186	1.0(-3)	1.2(-5)
I <sup>131</sup>	Thyroid	6(-5)	7.34(4)	872	400	4.8
Cs <sup>137</sup> + Ba <sup>137</sup>	Muscle	2(-3)	1.11(3)	13.2	0.18	2.2(-3)
Ru <sup>106</sup> + Rh <sup>106</sup>	Kidneys	0.1	2.48(3)	29.4	8.1(-3)	9.6(-5)
Te <sup>127</sup>	Kidneys	3(-2)	5.29(2)	6.29	5.8(-3)	6.9(-5)
Sr <sup>89</sup>	Bone	7(-5)	7.86(4)	934	370	4.4
Sr <sup>90</sup> + Y <sup>90</sup>	Bone	8(-7)	1.32(3)	15.7	540	6.4
Y <sup>91</sup>	Bone	4(-2)	9.63(4)	1.14(3)	0.79	9.4(-3)
Zr <sup>95</sup> + Nb <sup>95</sup>	Bone	0.4	1.20(5)	1.43(3)	0.098	1.2(-3)
Mo <sup>99</sup>	Bone	5	1.48(5)	1.75(3)	9.7(-3)	1.2(-4)
Nb <sup>95</sup>	Bone	2(-3)	1.53(5)	1.82(3)	25	0.30
Ba <sup>140</sup> + La <sup>140</sup>	Bone	5(-4)	1.34(5)	1.59(3)	88	1.0
La <sup>140</sup>	Bone	0.3	1.56(4)	185	0.017	2.0(-4)
Ce <sup>144</sup> + Pr <sup>144</sup>	Bone	8(-3)	3.07(4)	365	1.3	0.015
Pr <sup>143</sup>	Bone	8(-2)	1.20(5)	1.43(3)	0.49	5.9(-3)
Pm <sup>147</sup>	Bone	0.2	6.30(3)	74.9	0.010	1.2(-4)
Pu <sup>239</sup> (sol.)	Bone	6(-6)	3.51(2)	4.17	19	0.23
Pu <sup>239</sup> (insol.)	Lungs	-	3.51(2)	4.17	-	-

The numbers in parentheses indicate the powers of 10 by which the tabulated values are to be multiplied.

## APPENDIX G

HYDROLOGY, SEISMOLOGY, AND METEOROLOGY1. Hydrologya. Soil and Sub-Surface Characteristics

The National Reactor Testing Station (NRTS) is located on a level plain at an average elevation of 4,865 ft, ranging from an elevation of 4,788 to 4,965 ft. above sea level.

The surface of much of the plain is covered by waterborne and windborne top soil, under which there is a considerable depth of gravel, ranging in size from fine sand to 3 in. in diameter. At the several locations inspected to date, the gravel lies from approximately 1 ft to 50 ft under the top soil. Lava rock extends below this gravel layer and downward to a considerable depth, ranging at least to the water table. The lava rock is honeycombed with openings of about 1/8 in. in diameter. Frequently, large openings occur, and these range upwards to the size of tunnels, tubes, and caves.

What little surface drainage there is, is toward the Northeast, opposite to the main body of water flow. Normally, surface drainage is small due to the high porosity of the gravel overburden.

b. Drainage

The National Reactor Testing Station overlays a natural underground reservoir of water having an estimated lateral flow of not less than 500 cubic-foot-seconds (323,136,000 gal/day).

The main sources of water for this reservoir are the streams that start in the mountains to the north, and disappear into the porous soils of the NRTS area. These streams include Big Lost River, Little Lost River and Birch Creek.

The path of water flow from the surface to the ground water level is unknown. However, it is expected that the drainage would be rapid. The flow would be very rapid through the gravel overburden, while the drainage pattern through the lava rock would be less rapid but still very high as compared to flow through sands or clays. It is expected that the flow would be around rather than through the claybeds. Therefore, in case of a major accident with loss of a large volume of liquid wastes, the ground water would undoubtedly become contaminated in a very short time.

The estimated rate of flow of the main body of water through the lava is approximately one-half mile per year. Based on this estimate the contaminated water would reach the Snake River Canyon Springs and enter the Snake River in about 120 to 140 years, depending upon the exact location of the Reactor Plant within the Testing Station Area.

## 2. Seismology

The NRTS site is located in a region which "The Pacific Coast Uniform Building Code," 1949, designated as a Zone 2 area, as given by the "Seismic Probability Map of the United States," published by the United States Coast and Geodetic Survey.

Quoting J. Stewart Williams:<sup>1</sup>

"Earthquake risk at this Site (NRTS) is appreciable, but not great. Since isoseismal maps for principal earthquakes have been drawn, beginning in 1925, the isoseismals of only one earthquake reached Cerro Grande. Prior to this time several earthquakes recorded for surrounding areas may have been felt at Cerro Grande. There is no record of a major earthquake originating close to Cerro Grande.

"However, Cerro Grande is surrounded by areas of comparatively high seismic activity. Furthermore, it lies in a region of geologically young faults, any of which must be considered potentially active. For these reasons earthquake risk at the NRTS site should not be dismissed from consideration in planning any structure to be built at the site.

"Cerro Grande is situated within one hundred and fifty miles of several areas of pronounced earthquake activity. Any one of these might produce a shock stronger than it has yet produced with a corresponding greater intensity at Cerro Grande. The earthquake history of 100 years for this area is very short, from the geological point of view. An earthquake might occur any day that would alter substantially our ideas of the distribution of seismic activity in the area about the Snake River Plains.

"Earthquake risk in any area is relative to the type of structure to be built. Reinforced concrete buildings, well constructed in every way, with high factors of safety and incorporating features recommended by engineers acquainted with earthquake-proof design, stand less risk of being damaged. Such buildings, set on the lava bedrock at Cerro Grande, certainly would be reasonably safe from earthquake damage.

---

<sup>1</sup>S. McLain, R. K. Winkleblack, "Hazards of the Materials Testing Reactor," ANL-SM-236, June 15, 1950.

"No traces of recent faults are known by the writer to cross the Snake River Plains. The chances, then of displacement in the ground that would cut water supplies are small enough to be eliminated from consideration.

"In spite of the fact that a Zone 3 area exists both North and South of the Arco area, the distances are so great that Zone 2 has been considered completely safe."

### 3. Meteorology

#### a. Surface Winds

The NRTS area is located to the south and west of the Continental Divide, on a high, gently-rolling plain, surrounded by mountain ranges and skirted by the Snake River.

Measurements of wind speed and direction have been made for a five year period, from June, 1950, to May, 1955. Figure G-1 is an annual wind rose from the Central Facilities Area at the 20-foot level. The length of the bars represents the percent of time winds from the given direction occurred. In Fig. G-2 the percentage distribution of winds is separated into lapse and inversion conditions with a wind rose for each condition. (The winds were divided into lapse and inversion according to the temperature measurements made at the 5-ft and 100-ft levels on the tower at the Central Facilities Area.) Isothermal cases were taken as inversion. The higher percentage of winds between 1 and 5 mph in the inversion wind rose indicates that lighter winds are frequently accompanied by inversion conditions. Note that both northeasterly and southwesterly winds are more frequent with lapse than with inversion conditions.

A summary of temperature inversions for the year August, 1950 to July, 1951, is presented in Table G-I.

A study of the comparison of the frequencies of occurrence of northeasterly and southwesterly winds under lapse and inversion conditions is presented in Fig. G-3. This study is of interest both from the standpoint of frequency and because of the northeast-southwest alignment of the building sites. Southwesterly winds were predominant in every month except July and September. Northwesterly winds coincided most frequently with

lapse conditions, the only exceptions being the summer months. Southwesterly winds were distributed about equally between lapse and inversion conditions except for November, where inversion dominated about two to one. In general, however, pronounced lapse conditions tend to coincide with southwest winds, and pronounced inversion conditions tend to coincide with northeasterly winds. Fig. G-4 shows these relationships for 1500 MST and 0300 MST. The 1500 hour has mostly strong lapse, and the 0300 hour has mostly strong inversion conditions over the year as a whole. Also notable is the absence of winds from the east and southeast at 0300 MST, and the small frequency of calm or light winds at 1500 MST.

Since precipitation is known to capture, or "washout" effluent from an accident, especially particulate matter, thus bringing contaminant to the ground, the frequency distribution of wind directions and speeds during times of precipitation is of particular interest. A precipitation wind rose made from winds tabulated during 539 (hourly) observations of precipitation is shown in Fig. G-5. Very little difference exists between the precipitation winds and the annual wind rose (Fig. G-1). It is noted that calms are less frequent during precipitation periods and the frequency of northeasterly and southwesterly winds increases slightly at the expense of the other directions.

b. The Winds Aloft

Annual lapse and inversion wind roses for the 500-ft and the 5,000 ft. levels are presented in Figs. G-6 and G-7, respectively. The lengths of the arrows now correspond to percent frequency of winds occurring in the given direction rather than percent of time occurring. The most important differences between the lapse and inversion wind roses at the 500-ft level (Fig. G-6) are:

(1) Calms are about twice as frequent with inversion as with lapse conditions, although the frequency of calms is small in either case as compared with the winds at the 20-ft level.

(2) The average speeds are slightly greater with lapse than with inversion conditions. The direction frequencies are very similar, except that west and west-southwest winds are favored more with inversion conditions at the expense of southwest and south-southwest winds.

(3) The average wind speed at this level is 9.4 knots with lapse, and 8.5 knots with inversion conditions.

The 5,000-ft level wind roses (Fig. G-7) are indicative of flow above the level of strong influence of up-valley and down-valley flow. Consequently, the frequency of northeasterly winds is much smaller. Calms occur very seldom at this level. The main difference between lapse and

inversion conditions is that with inversion conditions the frictional influence of the ground is removed so that westerly winds increase in frequency at the expense of southwesterly winds. As in the case of winds at the 500-ft level the southwesterly winds average a little stronger with lapse conditions. The average windspeed for all directions is 13.8 knots with lapse and 11.7 knots with inversion conditions.

Variations of wind direction with height are frequent. This is evident from comparison of wind roses at the different levels. The most frequent case is southwesterly winds near the ground, changing gradually to westerly winds as high as about 5,000-ft above the ground. However, at times there have been very pronounced changes in wind direction between layers of air only a few hundred feet apart. Table G-II summarizes a study made of these cases. Seasonal tabulations of wind shifts are given at levels nearest the midpoint between layers of air that are moving in different directions. A pronounced shift of wind direction with height is defined as a direction change of 90 degrees or more within a height difference of a few hundred feet.

The frequency of direction shifts does not show any particular preference for any one season, but the frequency is about 41% with inversion conditions compared with 29% for lapse conditions. The majority of the direction shifts occurred between 1,500 ft and 2,500 ft with both lapse and inversion conditions. With inversion, however, there was also a maximum near the 500-ft level. Also, 30 of the 49 soundings showing pronounced direction shifts during inversion conditions near 500-ft had a second shift near 1,500 ft. These occurred with a very strong inversion, the top of which could not be reached by the temperature soundings, and was probably near the level of the upper directions shift. In every case a layer of northeasterly winds was "sandwiched" between a light southwesterly surface wind and a southwesterly or westerly wind aloft.

The speed of the winds at all levels was low; in particular, very low wind speeds occurred below about 2,000 ft above the ground. It appears that during very pronounced inversion conditions it is possible that the northeast drainage flow may warm (adiabatically) sufficiently in flowing down the gradual slope of the Plain to be forced aloft over the shallow pool of colder air in the lower elevations of the Valley. The very light southwest wind at the surface must be due to the drainage down the local slope (downward and to the northeast) on the NRTS region.

A zone of shearing winds near stack level is implied by the wind shifts near the ground during strong inversion conditions with light winds. The effect of this condition is that the effluent, which contains airborne contaminants from either normal stack operation or an accident, would be spread out horizontally, thereby resulting in far smaller concentrations at any point in the effluent stream. There are indications

that perhaps a recirculation of effluent over the NRTS region occurs during these circumstances, since a local southwest surface wind could not be maintained inside a broad flow of northeasterly winds in the absence of some sort of closed circulation system.

Table G-I

SUMMARY OF TEMPERATURE INVERSIONS FOR THE YEAR AUGUST, 1950,  
TO JULY, 1951 (NRTS - CENTRAL FACILITIES)

Month	Jan.	Feb.	Mar.	April	May	June	July	Aug.	Sept.	Oct.	Nov.	Dec.	Annual
Number of Nights with Inversion	30	27	30	27	30	30	31	31	28	30	28	28	350
Total Inversion Hours	342	347	340	294	288	322	368	403	363	418	358	320	4163
Percent of Time With Inversion	46	52	46	41	39	45	50	54	50	56	50	43	48%
Average daily number of Inversion Hours Per Inversion Day	11.4	12.9	11.3	10.9	9.6	9.6	11.9	13.1	12.1	13.1	12.8	11.4	11.7
Longest Inversion Period	19	17	15	14	13	13	15	17	18	17	18	18	19
Longest Lapse Period (Hours)	57	57	61	91	48	19	16	13	65	82	57	86	91
Average Daily Maximum (Inversion) Intensity (F/100 ft.)	+7.3	+6.4	+5.6	+8.1	+6.2	+7.6	+10.1	+7.7	+8.9	+7.8	+6.6	+6.7	+7.4
Average Daily Maximum Lapse Intensity (F/100 ft.)	-1.6	-1.7	-2.0	-3.0	-3.5	-3.7	-3.4	-3.3	-2.1	-2.0	-1.9	-1.8	-2.5

Table G-II

NUMBER OF CASES THAT PRONOUNCED WIND DIRECTIONS SHIFTS OCCURRED  
NEAR INDICATED LEVELS - JUNE, 1950 - MAY, 1951

Feet Above Ground	500	1000	1500	2000	2500	3000	3500	4000	4500	5000	5500	6000 7000	Total No. of Shifts	Total No. of Soundings
----------------------	-----	------	------	------	------	------	------	------	------	------	------	--------------	------------------------	---------------------------

DURING LAPSE CONDITIONS

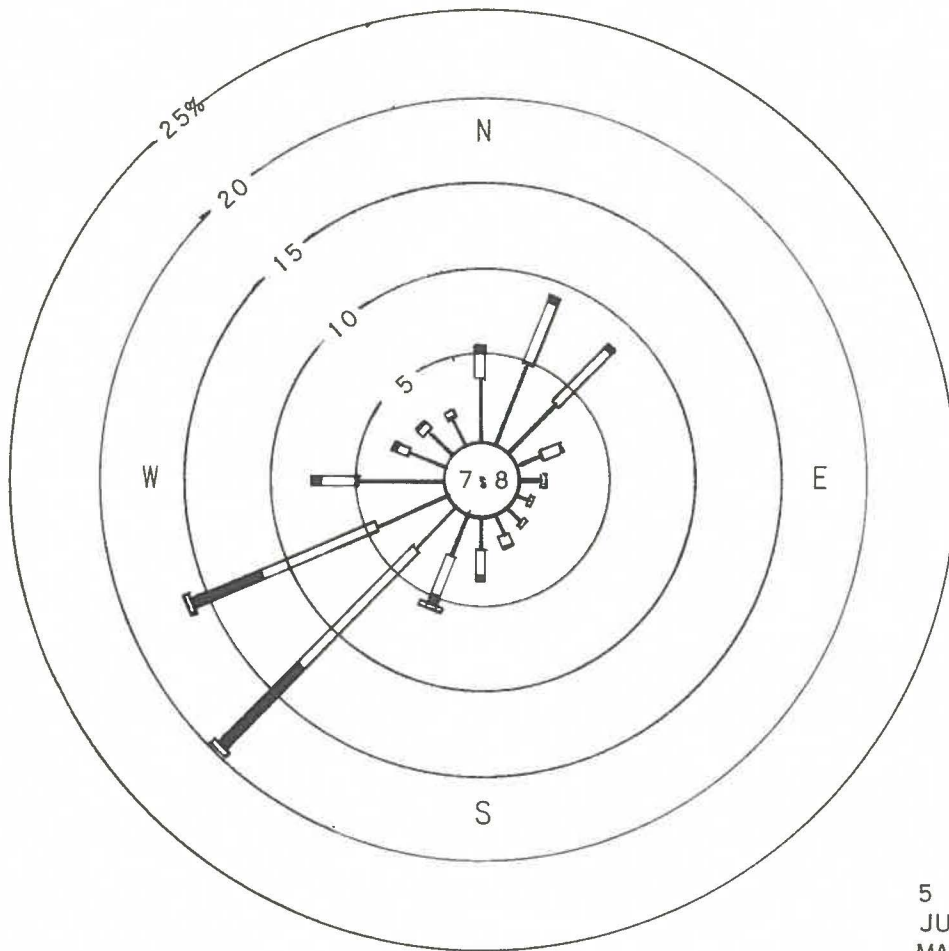
Winter	5	3	14	4	2		1		1				30	92
Spring	6	8	9	7	7	4	2	2	1	3			49	173
Summer	1	3	7	8	7	4	2	3	4	2	2	2	45	165
Fall	4	2	15	4	4	3		4	1	1		1	39	126
TOTAL	16	16	45	23	20	11	5	9	7	6	2	3	163	556

DURING INVERSION CONDITIONS

Winter	16	4	14	11	4	1	2	1					53	115
Spring	14	4	8	10	6	4	2	3	2	1	1		55	119
Summer	8	4	5	8	11	9	3	4	5	5	1	4	67	143
Fall	11	7	15	7	7	3	1	3	3	1			58	162
TOTAL	49	19	42	36	28	17	8	11	10	7	2	4	233	539

U. S WEATHER BUREAU

FIG. G1  
 ANNUAL WIND ROSE FOR THE 20-ft WIND LEVEL  
 CENTRAL FACILITIES (WBO), N.R.T.S., IDAHO



5 YEARS OF RECORD  
 JUNE 1950 THRU  
 MAY 1955.  
 370 hours MISSING

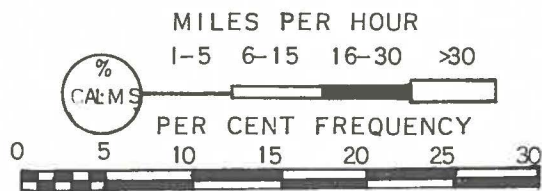
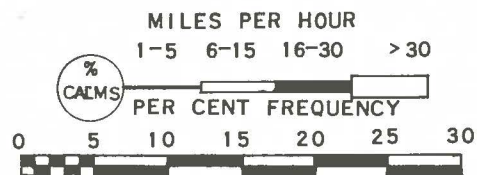
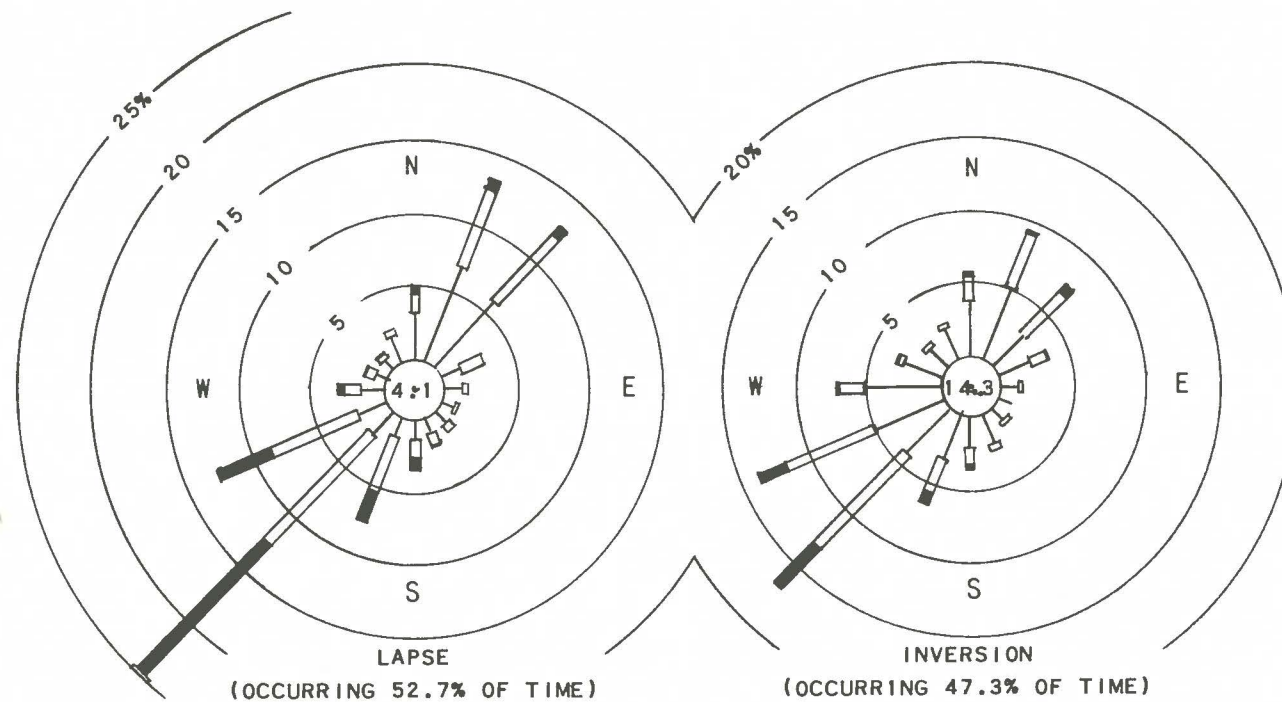


FIG. G2  
 LAPSE AND INVERSION WIND ROSES FOR YEAR JUNE 1950 THRU MAY 1951

WIND AT 20 ft. LEVEL  
 CENTRAL FACILITIES (WBO)



RE-6-20302-A

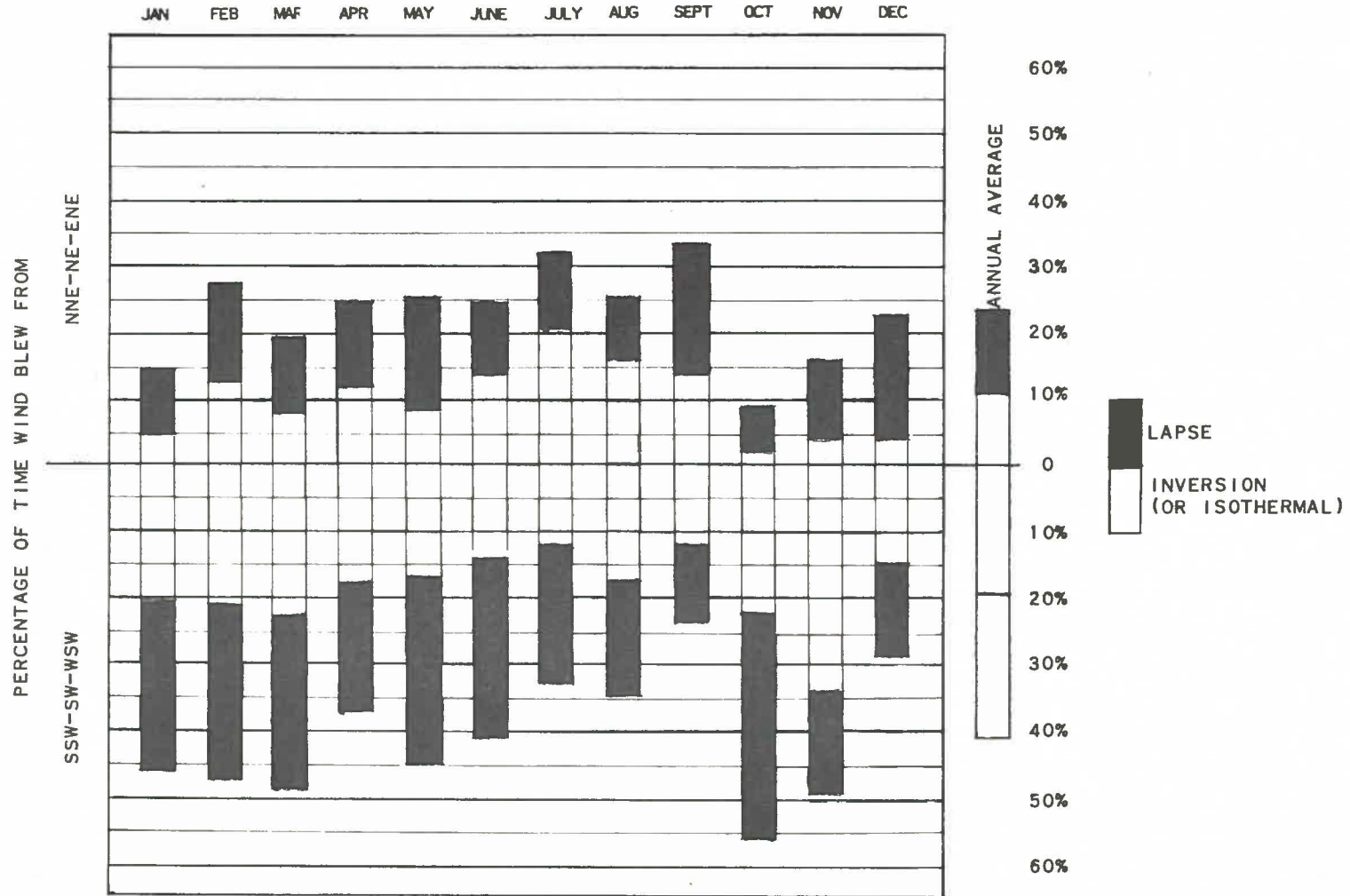
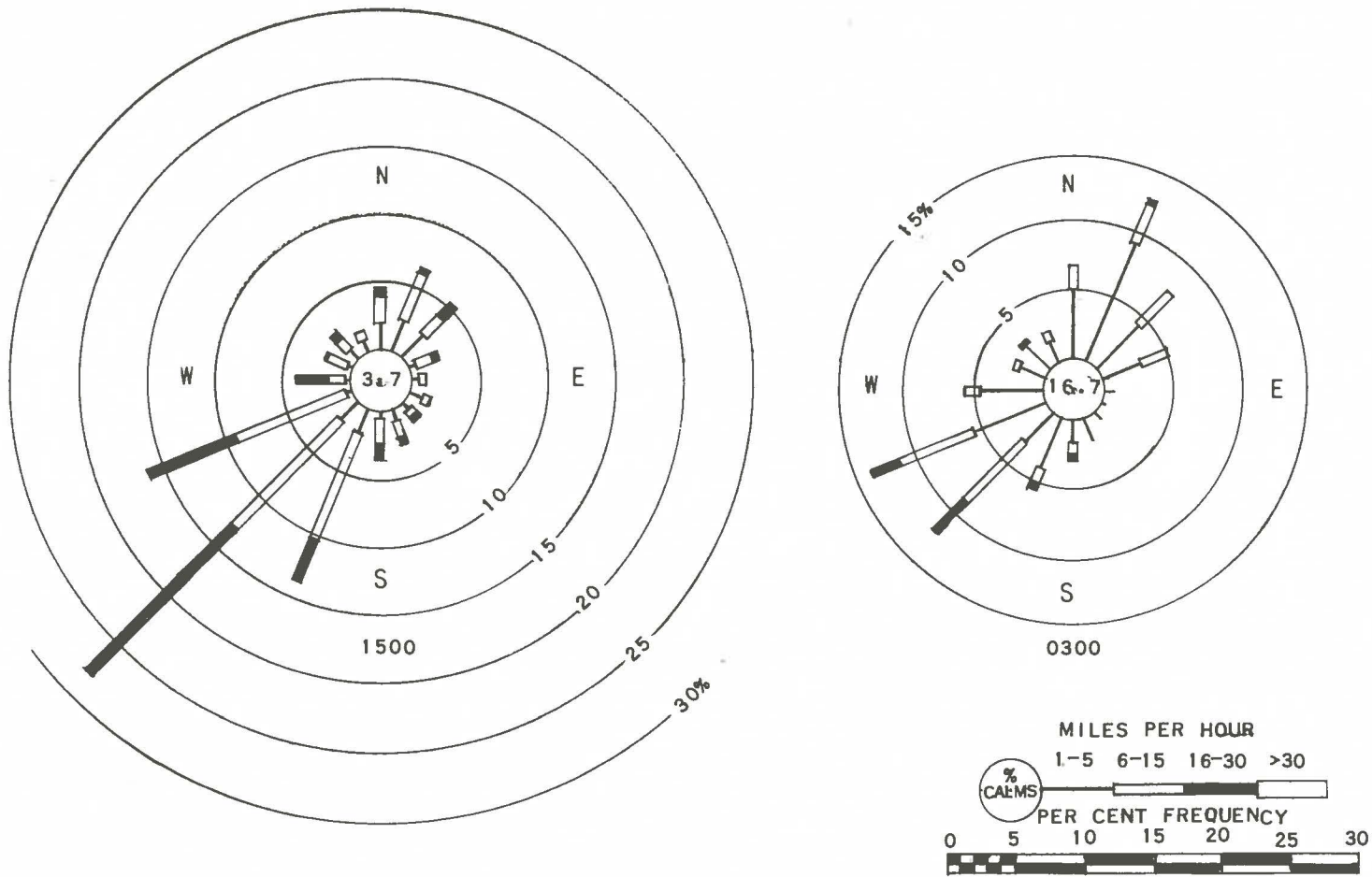


FIG. G3  
 FREQUENCY OF NORTHEASTERLY VERSUS SOUTHWESTERLY WINDS  
 GIVEN IN PER CENT OF TIME OCCURRING (20 ft. LEVEL)  
 DATA FOR YEAR JUNE 1950 THRU MAY 1951

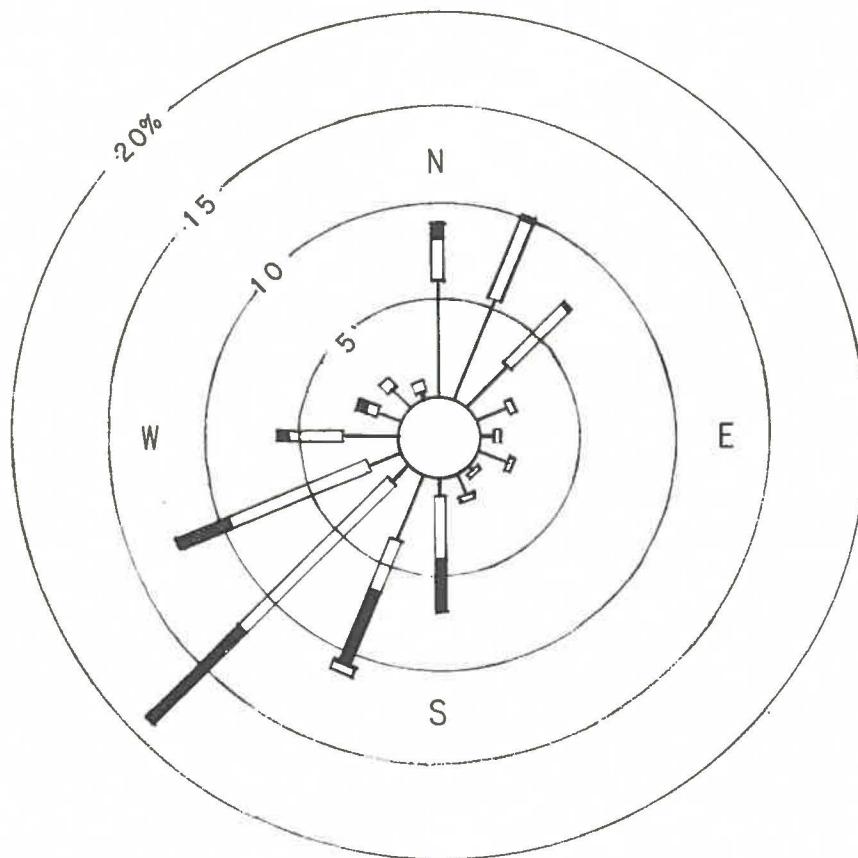
FIG. 64  
 WIND ROSES FOR 0300 AND 1500 hours FOR YEAR MAY 1950 THRU APRIL 1951  
 WIND AT 20 ft. LEVEL  
 CENTRAL FACILITIES (WBO)



RE-6-20304-A

FIG. G5  
 PRECIPITATION WIND ROSE FOR PERIOD MAY 1950 THRU DEC. 1951  
 WIND AT 20 ft. LEVEL  
 CENTRAL FACILITIES (WBO)

RE-6-20305-A



TAKEN FROM 539 OBSERVATIONS OF PRECIPITATION

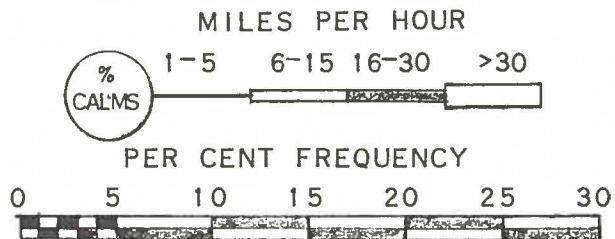
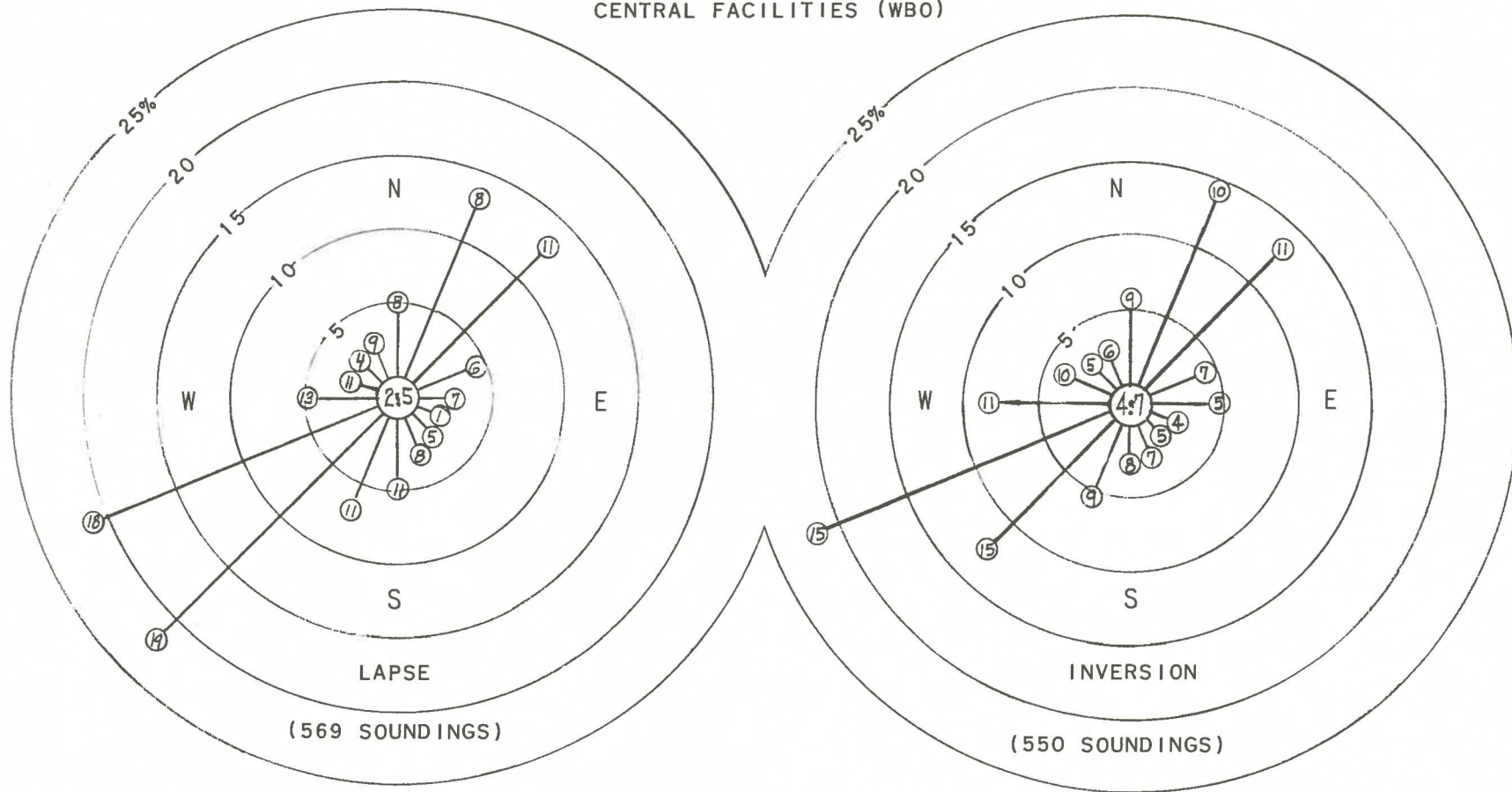


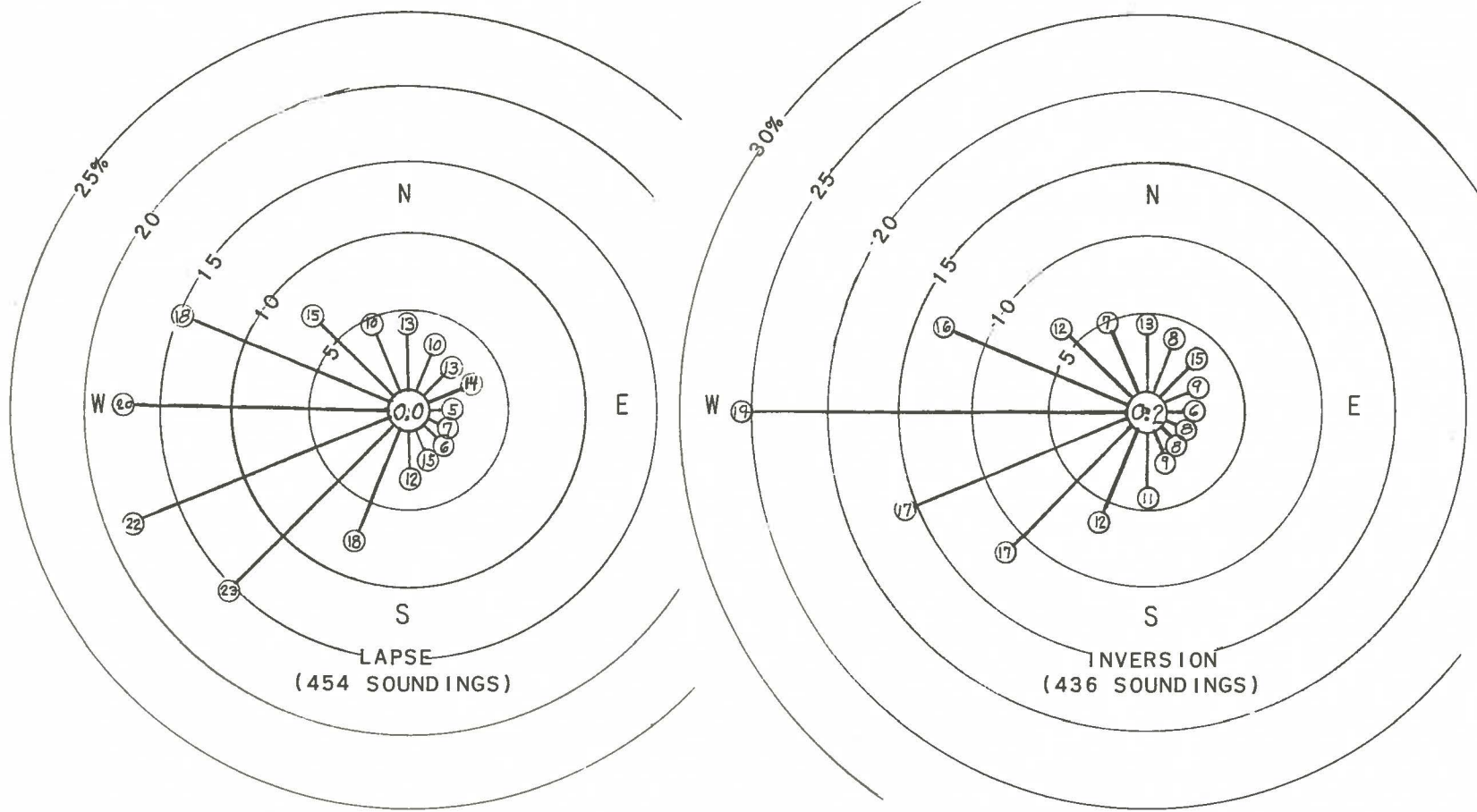
FIG. G6  
 ANNUAL LAPSE AND INVERSION WIND ROSES FOR THE 500-foot LEVEL  
 PILOT BALLOON SOUNDINGS FOR THE YEAR SEPT. 1950 THRU AUG. 1951  
 CENTRAL FACILITIES (WBO)



AVERAGE SPEEDS ARE CIRCLED (KNOTS)  
 PER CENT OF CALMS IN CENTER



FIG. G7  
 ANNUAL LAPSE AND INVERSION WIND ROSES FOR THE 5000-foot LEVEL  
 PILOT BALLOON SOUNDINGS FOR THE YEAR SEPT. 1950 THRU AUG. 1951  
 CENTRAL FACILITIES (WBO)



PER CENT OF CALMS IN CENTER  
 AVERAGE SPEEDS (KNOTS) ARE CIRCLED



RE-6-20307-A

ARGONNE NATIONAL LAB WEST



3 4444 00021043 5

